MECHANISMS OF NI-CATALYSED C–O FUNCTIONALISATION AND CARBOXYLATION REACTIONS

Rosemarie Janet Somerville

UNIVERSITAT ROVIRA i VIRGILI

Mechanisms of Ni-Catalysed C–O Functionalisation and Carboxylation Reactions

Rosemarie Janet Somerville
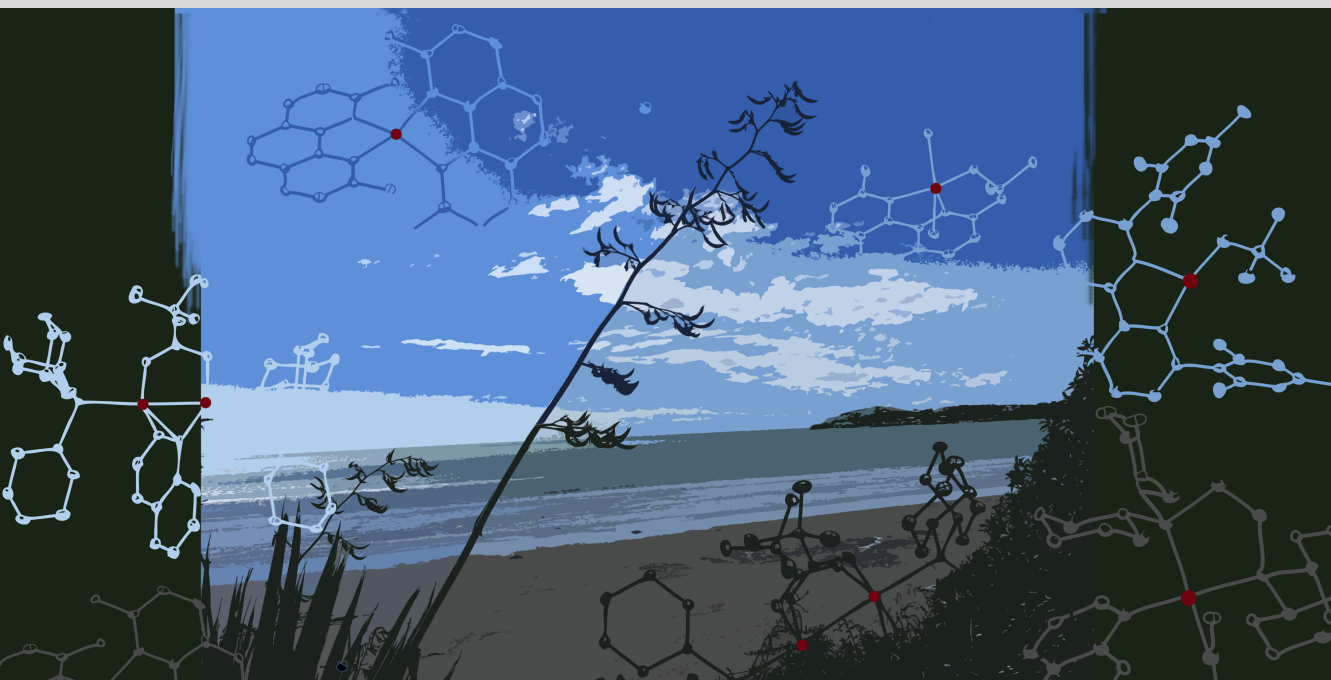
DOCTORAL THESIS
2020

Mechanisms of Ni-Catalysed C–O Functionalisation and Carboxylation Reactions

Rosemarie Janet Somerville

DOCTORAL THESIS
Supervised by Prof. Rubén F. Martín Romo
Institut Català d'Investigació Química (ICIQ)
Universitat Rovira i Virgili (URV)
Department of Analytical Chemistry & Organic Chemistry

UNIVERSITAT ROVIRA i VIRGILI

ICIQ
Institut
Català
d'Investigació
Química

Tarragona 2020

Prof. Rubén Martín Romo, Group Leader at the Institute of Chemical Research of Catalonia (ICIQ) and Research Professor of the Catalan Institution for Research and Advanced Studies (ICREA),

STATES that the present study, entitled "Mechanisms of Ni-Catalysed C–O Functionalisation and Carboxylation Reactions", presented by Rosemarie Janet Somerville for the award of the degree of Doctor, has been carried out under his supervision at the Institute of Chemical Research of Catalonia (ICIQ).

Tarragona, February 2020

Doctoral Thesis Supervisor

Prof. Rubén Martín Romo

List of Publications

At the time of printing, the results reported herein have been published as:

1. Yanagi, T.*; **Somerville, R. J.***; Nogi, K.; Martin, R.; Yorimitsu, H. Ni-Catalyzed Carboxylation of C(sp^2)–S bonds with CO_2: Evidence for the Multifaceted Role of Zn. *ACS Catal.,* **2020**, DOI: 10.1021/acscatal.9b05141.
2. **Somerville, R. J.**; Hale, L. V. A.; Gómez-Bengoa, E.; Burés, J.; Martin, R. Intermediacy of Ni–Ni Species in sp^2 C–O Bond Cleavage of Aryl Esters: Relevance in Catalytic C–Si Bond Formation. *J. Am. Chem. Soc.*, **2018**, 140, 8771–8780. DOI: 10.1021/jacs.8b04479.

The author has also contributed to the following:

3. Sun, S.-Z.*; Duan, Y.*; Mega, R. S.; **Somerville, R. J.**; Martin, R. Site-Selective 1,2-Dicarbofunctionalization of Vinyl Boronates via Dual Catalysis. *Angew. Chem. Int. Ed.* Accepted Author Manuscript. **2020**, DOI:10.1002/anie.201916279
4. **Somerville, R. J.**; Martin, R. Relevance of Ni(I) in Catalytic Carboxylation Reactions. In *Nickel Catalysis in Organic Synthesis;* Ogoshi S. Ed. Wiley Online Library, **2019** pp. 285–330. (Book Chapter). DOI: 10.1002/9783527813827.ch12.
5. **Somerville, R. J.**; Martin, R. Forging C–C bonds Through Decarbonylation of Aryl Ketones. *Angew. Chem., Int. Ed.* **2017**, 56, 6708-6710 (Highlight). DOI: 10.1002/anie.201702188.
6. Zarate, C.*; van Gemmeren, M.*; **Somerville, R. J.**, Martin, R. Phenol Derivatives: Modern Electrophiles in Cross-Coupling Reactions. *Advances in Organometallic Chemistry, Elsevier,* **2016***, 66,* 143-222. (Book Chapter). DOI: 10.1016/bs.adomc.2016.07.001.

* indicates co-authorship

Table of Contents

Acknowledgements

First of all, I'd like to express my appreciation and gratitude to **Prof. Ruben Martin**. These last four years have been one unforgettable journey and I wouldn't have grown so much as a person and a scientist without the amazing opportunities and challenges that being in your group has thrown at me. In particular, you were always there, if not in person then by email at basically all hours, to listen to my doubts and panic moments as well as to celebrate the good moments and breakthroughs. Thanks for trusting me with the "barren terrain" of mechanistic studies in the Martin group and for believing that I could turn it into a thesis.

Second, I would like to thank the members of my committee, **Dr. David Nelson**, **Dr. Amor Rodríguez**, and **Dr. Alex Shafir** for accepting our invitation to read and assess my work.

I would also like to acknowledge the collaborators that I have worked with during the projects summarised in this work: **Dr. Lily Hale**, **Dr. Enrique Gómez-Bengoa**, and **Dr. Jordi Burés**, then **Tomoyuki Yanagi**, **A/Prof. Keisuke Nogi**, and **Prof. Hideki Yorimitsu**, and most recently **Prof. Nilay Hazari**, **A/Prof. Kathrin Hopmann**, **Marc Obst**, and **Carlota Odena**. Appreciation also goes to **Craig Day** and **Carlota** for their willingness to join the group to take on tough mechanistic projects and for their hard work and smart ideas that are already producing wonderful chemistry.

I would also like to thank the "la Caixa" Foundation (ID 100010434) under the agreement LCF/BQ/SO15/52260010 for the PhD fellowship.

I am very grateful to **Ingrid Mateu**, **Miriam Sau**, and **Sergio Sopeña** for all your work over the years taking care of the things that keep the group running. Thanks also for the chats in the office or lab. Without the **ICIQ Research Support Units** many parts of this thesis would have been much much more difficult. Thanks in particular to **Marta**, **Eddy**, **Jordi**, and **Eduardo** from X-ray, **Isra** and **Kerman** from NMR, and **Georgiana** from the MCU. Georgiana, thanks for the wonderful conversation during the hours of running EPR experiments for Chapter 3. I'll visit Romania some day! And **Xavi**, gràcies!

A very special thank you is dedicated to **Dr. Mónica Pérez-Temprano**. Thanks for making time for office chats, lunches, and a few emergency discussions here and there. I am very grateful for the support you have given me over the last 4 years.

Thanks also to **Prof. Nilay Hazari** for the warm welcome at Yale and your support with the Ni(I)-alkyl project. I learnt so much from being in the group and appreciate the time you have taken looking at drafts of the paper and asking sharp questions. I also learnt a lot about Overcooked, 15*, Crystar, and the endless possibilities for a handmade thanksgiving sweater. I'd like to thank **Megan Mohadjer Beromi** for imparting Ni(I) knowledge. I wish you and Brian all the best! And **Amira Dardir**, we've exchanged many emails over the last year and I hope we can stay in touch and see each other many more times in the future (without any civil unrest this time). At some point PhD ends, supposedly!

Thanks to the **past and present members of the Martin group** for making it the place it is. Those Martinis who were there when I first started, including **Masaki**, **Daniel G.**, **Manuel**, and **Xiang-wei**: Thanks for supporting me in the beginning. **Marino**, it has been quite the journey since we started PhD that same day. Thanks for being there in stressful situations with kind words and a reminder that things

will turn out ok, for your advice about CO_2 chemistry, and for our wistful discussions about adventures that we can now do without PhD stress upon us. **Yiting**, I will miss you a lot. Hope we can see each other again!! Getting to know you better in Vienna is a good memory from these PhD times. And **Yangyang**, you are a star. I wish you and Yiting lots of happiness. **Eloisa**, thanks for all the support and for helping me through the twists and turns of the Martin group experience. I hope we can see each other again soon in Biberach. **Raul Martin!** Your friendship means a lot to me. You were a wonderful desk buddy - I will remember our T-rex scream shenanigans, meme laughs, and los catalizadores. I hope the W projects and the final stretch of PhD are super smooth. **Andreu**, you are a very giving person! I appreciate all your help and support over the years. Good luck for the rest of PhD! **Reddy**, I was lucky to have you as my desk buddy for the time I was in 2.12 and miss your sage wisdom and unforgettable sense of humour. **Alberto**, you have a really big heart and I am grateful to have met you and shared a hood with you. **Shang-Zheng**, you're so sweet and caring and have always had encouraging words to share with me. **Bradley**, you've always got amazing chemistry ideas, plentiful memes, and interesting conversation. **Alicia**, you brought your strength and kindness to the group and are a really awesome role model.

It was great to meet so many wonderful visiting students over the years, particularly **Lily**, **Thomas**, **Tomoyuki**, **Tim**, and **Georgios**. Tomoyuki, it was really nice to end up collaborating with you! Tim, we had some great conversations while you were here and it's nice to see what you are getting up to in your new academic work. And Georgios, you are an awesome chemist and amazing personality. I won't forget the Martini Langostinis and the amazing stories that you told about things like mystery floods in your flat and hilarious scenarios about potentially ending up in Zaragoza after too much partying with Marino. **Lily**, in 8 weeks you played a bigger role than you know in me getting to this point. When you arrived, I needed a "coppery boost" and you working with me helped me not just gain momentum to go on with solving the silylation puzzle, but set me on a path of growing confidence in being at ICIQ and being a scientist. I'm really grateful for the friendship that we have grown in both the good times and in the chemistry crises.

To the non-Martin group friends I've made in the last years – **Katia Rintjema (nee Smirnova!)** for taking me to Zumba in the early days and giving me important PhD advice. **Elena** for your friendship and all the swimming at the Sant Pere i Sant Pau swimming pool. **Franzi**, thanks for shaking me out of working too hard to go on adventures and have pie nights and fight the power at ICIQ. **Fedor**, I am very grateful for the support that you gave me during the first years. You helped me adjust to ICIQ and I am very grateful. Thanks for taking the time to discuss the Ni(II) fluoride complex, J Young suppliers, and climbing. **Francesca**, you're a very strong person and I am glad to have met you while you were here. The ICIQ climbers are a particular source of friendship and support. The old-time Slab crews of **Jeroen**, **Sope**, **Cris**, **Marino**, then **Marta**, **Jan H.**, **Jan O.**, and **Ludo**, and now the Monobloc crew of **Pablo**, **Patri**, **Ani**, **Joan**, **Jacob**, **Anna**, **Anna**, et al.. DURAAA. **Cristina**, I am really happy to have met you! I hope that we can stay in touch. I also want to visit the palm trees! The last years would have been much harder without your calm and steady advice, day-brightening post-its, and our chats over tea. **Marta**, you are so active in lots of causes and it's awesome. I hope the last parts of PhD are really smooth. I'll remember our trip to Albarracín! And **Jan**, hope you can be happy and lucky. Don't keep climbing with open wounds! I'd also like to acknowledge the ceramic being that is **Lucky Cow**. Thanks for the X-ray structure of the DMSO adduct. And **Santa Tecla**, I think you played a role in smoothing the path for the X-ray structure of [(**L1**)Ni(neopentyl)].

Thanks to the friends from SCPS that have been in contact in the last 4 years – **Putri, Kris, Lia, Brad, The Joe**, **Thomas**, **Julia**, and of course **Prof. John Spencer**. John, I'm so grateful to have had the chance to try organometallic chemistry. I remember when I told you I was offered a summer fellowship to work in coordination chemistry rather than organic chemistry and you said "oh, you'll be doing proper chemistry then" with a twinkle in your eye. You could indeed be correct! I would also like to acknowledge

the late **Prof. Brian Halton**. Brian, your sure advice, sometimes scathing criticism of writing and university bureaucracy, and depth of knowledge that you loved to pass on are memories that I will keep with me. I also finally figured out what you meant about the order of brackets/parentheses while writing this thesis. **Payal**, our friendship deepened immensely during the last 4 years. I'm really honoured that you consider me your friend. Thank you for being there, for the thousands of messages we've shared, for the videos and songs and book discussions. It's Horizon 2020 now, let's see where we go from here.

To **Mum**, **Dad**, and **David**. This chemistry journey has been very long and you've seen me disappear into my work too many times than is healthy. You've looked after me, fed me, moved stuff from NZ to Spain for me, cheered me up, sent me silly videos and articles, fostered a love of learning, and generally just made this all possible. I love you. And finally, a deep thetanic acknowledgement goes to **Shouhei**. Although we have spent most of this time far from each other you have patiently and lovingly supported me through this rollercoaster.

Preface

The work presented in this thesis has been performed at the Institute of Chemical Research of Catalonia (ICIQ) under the supervision of Professor Ruben Martin. The thesis is divided into five chapters: a general introduction, three research chapters (summarised below), and a summary of the overall conclusions of the Thesis.

In Chapter 1, background literature is presented concerning Ni catalysis as an important and rapidly growing field. The role of mechanistic studies in improving and understanding such reactions is also discussed. Finally, a broad overview of Ni-catalysed C(sp^2)–O functionalisation and Ni-catalysed carboxylation reactions is provided in order to set the scene for the following research chapters.

Chapter 2, "*The mechanism of the Ni-catalysed C(sp^2)–O silylation of aryl esters: Understanding oxidative addition and the role of additives*" describes a mechanistic study into the Ni-catalysed silylation of aryl pivalate esters. In this chapter, the first examples of aryl pivalate oxidative addition complexes bearing monodentate phosphine ligands are demonstrated and an unusual dinickel oxidative addition complex is implicated as an off-cycle species. The role of the additives was also investigated and fluoride, rather than previously proposed Cu, is shown to be important in preventing catalyst deactivation. Variable time normalization kinetic analysis and DFT studies provided data to support the mechanistic proposal. This work was carried out in collaboration with Dr. Lillian V. A. Hale, Dr. Jordi Burés, and Dr. Enrique Gómez-Bengoa.

Chapter 3, "*Understanding Ni(I)–alkyl complexes in reductive carboxylation*" describes the synthesis, characterisation, and CO$_2$ insertion reactivity of Ni(I)–alkyl complexes of substituted phenanthroline ligands. These complexes are invoked in a wide number of Ni-catalysed reactions, including carboxylation and amidation cross-electrophile reactions. The preliminary DFT results reported in this Chapter were carried out by Marc Obst in the group of Associate Professor Kathrin Hopmann. Final experimental studies are being carried out by Carlota Odena. The manuscript is under preparation.

The final research chapter, Chapter 4, "*Ni-catalysed carboxylation of C(sp^2)–S bonds: Mechanistic studies into C–S cleavage and the role of the Zn.*" describes mechanistic details behind the synthesis of carboxylic acids from arylsulfonium salts and CO$_2$. Specifically, this Ni-catalysed methodology employs Zn powder as a reductant and evidence for the formation of arylzinc species during the reaction is presented. The Ni-catalysed methodology was developed by Tomoyuki Yanagi in the group of Professor Hideki Yorimitsu and Assistant Professor Keisuke Nogi.

General conclusions of this Doctoral Thesis are presented in Chapter 5.

Glossary

acac – acetylacetonate

ATR – attenuated total reflection

BDE – bond dissociation energy

bipy – 2,2'-bipyridine

Bpin – 4,4,5,5-tetramethyl-1,2,3-dioxaboronic ester

COD – 1,5-cyclooctadiene

Cp – cyclopentadienyl

CV – cyclic voltammetry

Cy – cyclohexyl

DEMS – $(EtO)_2MeSiH$

DFT – density functional theory

DMA – dimethylacetamide

DMAP-OED – 4-dimethylaminopyridine organic electron donor

DME – dimethoxyethane

DMI – 1,3-dimethyl-2-imidazolidinone

EPR – electron paramagnetic resonance

equiv – equivalents

HMPA – hexamethylphosphoramide

Mes – mesityl

NBO – natural bonding orbital

phen – 1,10-phenanthroline

RPKA – reaction progress kinetic analysis

SCE – saturated calomel electrode

SOMO – singly occupied molecular orbital

SQUID – superconducting quantum interference device

TDAE – tetrakis(dimethylamino)ethylene

TEP – Tolman electronic parameter

THF – tetrahydrofuran

VTNA – variable time normalisation analysis

Abstract

In recent years, homogeneous catalysis with nickel has received considerable research attention and many transformations have been developed to take advantage of its abundance, nucleophilicity, and accessible one-electron redox pathways.[1-3] In broadening the scope of reactivity between the transition metal catalyst and different substrates, the mechanisms of these new Ni-catalysed transformations have diverged from those expected from Pd and are in many cases unexplored.[4]

Two important classes of Ni-catalysed reaction are $C(sp^2)$–O bond functionalisation reactions and cross-electrophile coupling reactions (Scheme 1). In line with the Martin group's continuing interest in these transformations, this Thesis focuses on the mechanistic aspects of the $C(sp^2)$–O functionalisation of aryl esters and the Ni-catalysed reductive carboxylation of alkyl and aryl electrophiles. At the outset of this work, it was unclear whether the mechanistic underpinnings of these reactions would be revealed. However, the studies described herein contribute important and long-sought mechanistic knowledge to these two fields.
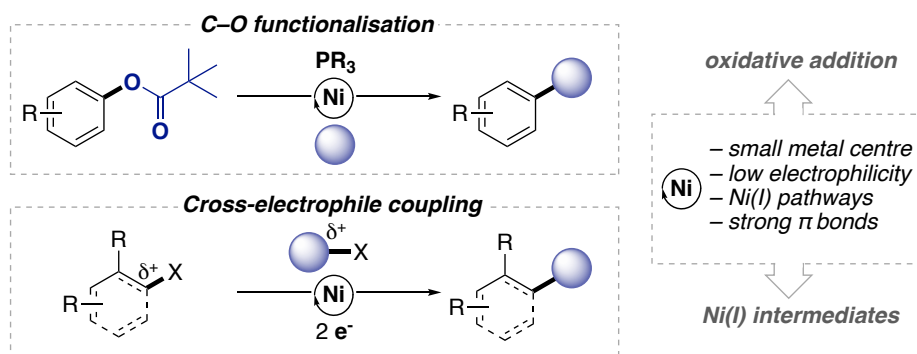
Scheme 1. Ni-catalysed $C(sp^2)$–O functionalisation of aryl esters and cross-electrophile coupling reactions.

The first study is a combined experimental and computational study into the $C(sp^2)$–O silylation of aryl pivalate (OPiv) esters (Scheme 2).[5] This reaction employs a Ni/PCy₃ catalyst that finds widespread use in $C(sp^2)$–O functionalisation. However, no experimental studies had been carried out on any such reactions employing a monodentate phosphine ligand and many mechanistic questions existed. One key question involved $C(sp^2)$–OPiv oxidative addition. Although many aryl halide oxidative addition complexes have been isolated, no $C(sp^2)$–OPiv oxidative addition complexes bearing a monodentate phosphine had been isolated. In this work, the first $C(sp^2)$–OPiv oxidative addition complexes were characterised and located within the catalytic cycle. The role of unusual dinickel oxidative addition complexes as off-cycle sources of mononickel complexes was also uncovered and their disproportionation reactivity probed with trapping experiments. This work also shed light on the role of the CuF₂ and CsF additives that are necessary to obtain high yields of silylated products. Instead of using Cu to transfer a silyl group to the metal as previously proposed,[6] data supported the role of the fluoride anions as scavengers for the Bpin⁻ leaving group. These results will provide a basis for studies of related $C(sp^2)$–O functionalisation reactions and highlight the importance of off-cycle intermediates and additives as a trap

of a deactivating leaving group,[18] which may be relevant to improving the efficiency and generality of other Ni-catalysed reactions.
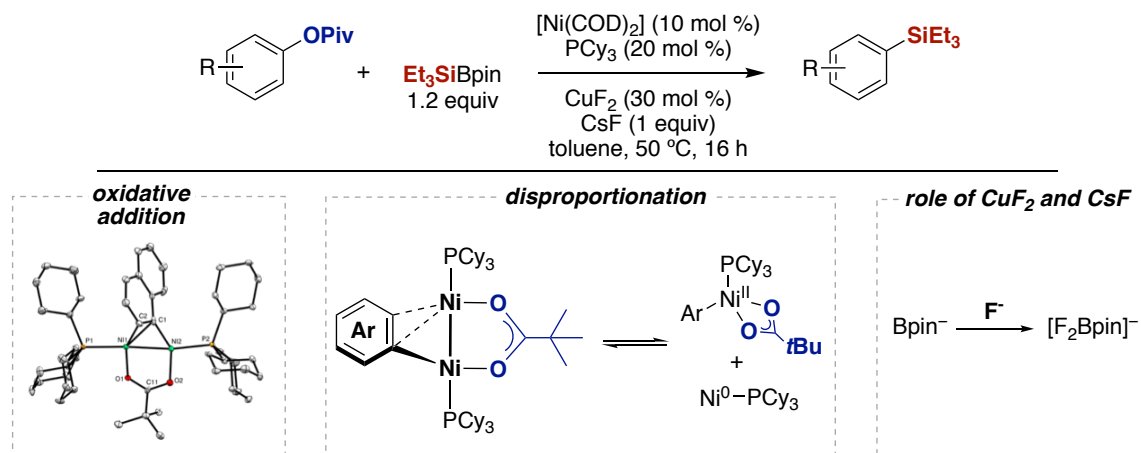
Scheme 2. Mechanistic study of C(sp^2)–O functionalisation of aryl pivalate esters.

The final two chapters of this Thesis are linked by a common theme – Ni-catalysed reductive carboxylation. Over the last 10 years the scope of this cross-electrophile coupling reaction has grown to encompass a wide range of substrates including alkyl and aryl halides.[7]

The second project investigated the role of Ni(I)–alkyl complexes in the Ni-catalysed reductive carboxylation of alkyl halides. Whereas aryl halide carboxylation reactions have received some mechanistic attention, very few studies have addressed the mechanisms of alkyl halide carboxylation reactions.[8,9] This is probably due to the difficulties involved in studying processes that may involve open-shell Ni−alkyl intermediates and heterogeneous reductants. Nickel(I)–alkyl or alkyl complexes are proposed to react with CO_2 during catalysis in lieu of Ni(II) oxidative addition complexes.[10] However, evidence for this step is scarce.[9] Nickel(I)–halide complexes bearing a very bulky phenanthroline ligand and a ligand employed in a reported carboxylation reaction[8] were synthesised in good yields. These were then reacted with a series of alkyl organometallic reagents. The isolation and characterisation by X-ray diffraction of a bulky Ni(I)–neopentyl complex marked the first example of such a complex. This was reacted with CO_2 and extremely rapid insertion occurred to form a carboxylate complex that was characterised by EPR and IR spectroscopy and investigated by DFT calculations. Experimental evidence for this reaction is a large step forward in mechanistic understanding for alkyl carboxylation.
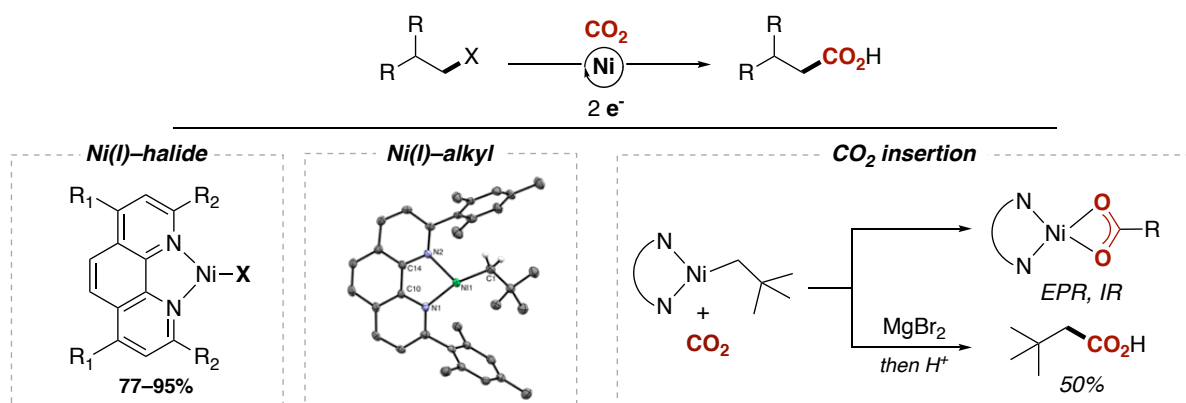
Scheme 3. Investigating Ni(I) species in alkyl carboxylation.

The final chapter of this Doctoral Thesis describes the mechanistic picture of the Ni-catalysed reductive carboxylation of arylsulfonium salts developed by the Yorimitsu group. Organosulfur electrophiles had not been employed in reductive carboxylation, making this the first link between carboxylation and the rich field of organosulfur chemistry. Metal powder reductants employed in such reductive reactions are not just a source of two electrons but are a source of Lewis acids that may aid CO_2 insertion into the Ni–C bond.[11] This study also provided strong evidence for the formation of organozinc species from Ni–aryl species via transmetalation.
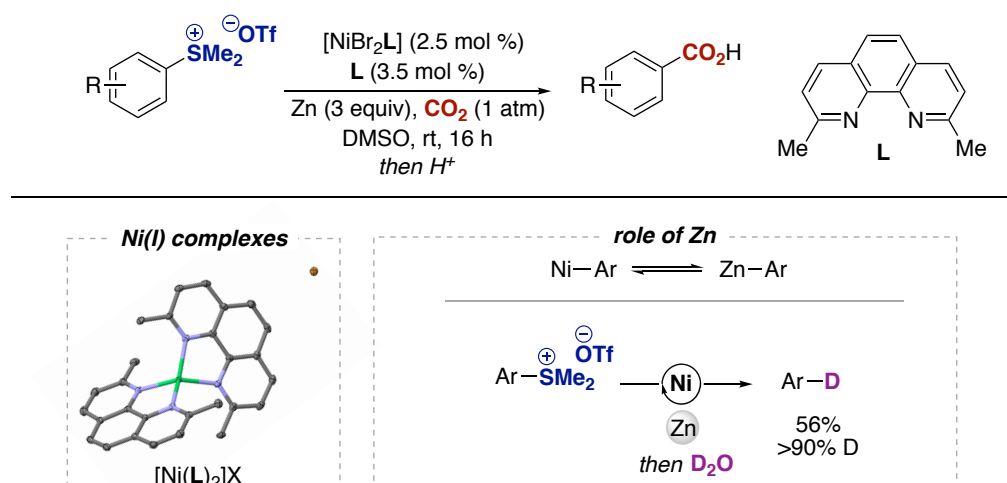
Scheme 4. Ni-catalysed reductive carboxylation of arylsulfonium salts.

In conclusion, this Doctoral Thesis has produced mechanistic insights into a Ni-catalysed C(sp^2)–O silylation reaction and the Ni-catalysed reductive carboxylation reactions of alkyl and aryl halides. Notably, proposed intermediates that had never been isolated – a C(sp^2)–OPiv oxidative addition complex bearing PCy$_3$ and a Ni(I)–alkyl complex bearing a phenanthroline ligand – were isolated and reacted with key components of the reactions. The findings in this work have consequences for further mechanistic studies and for investigations into the fundamental chemistry of these key intermediates.

References:

(1) Tasker, S.; Standley, E.; Jamison, T. Recent Advances in Homogeneous Nickel Catalysis. *Nature* **2014**, *509* (7500), 299–309.

(2) Hazari, N.; Melvin, P. R.; Beromi, M. M. Well-Defined Nickel and Palladium Precatalysts for Cross-Coupling. *Nat. Rev. Chem.* **2017**, *1* (3), 1–17.

(3) Ananikov, V. P. Nickel: The "Spirited Horse" of Transition Metal Catalysis. *ACS Catal.* **2015**, *5* (3), 1964–1971.

(4) Diccianni, J. B.; Diao, T. Mechanisms of Nickel-Catalyzed Cross-Coupling Reactions. *Trends Chem.* **2019**, *1* (9), 830–844.

(5) Somerville, R. J.; Hale, L. V. A.; Gomez-Bengoa, E.; Burés, J.; Martin, R. Intermediacy of Ni–Ni Species in Sp^2 C–O Bond Cleavage of Aryl Esters: Relevance in Catalytic C–Si Bond Formation. *J. Am. Chem. Soc.* **2018**, jacs.8b04479.

(6) Zarate, C.; Martin, R. A Mild Ni/Cu-Catalyzed Silylation via C–O Cleavage. *J. Am. Chem. Soc.* **2014**, *136* (6), 2236–2239.

(7) Tortajada, A.; Juliá-Hernández, F.; Börjesson, M.; Moragas, T.; Martin, R. Transition-Metal-Catalyzed Carboxylation Reactions with Carbon Dioxide. *Angew. Chem. Int. Ed.* **2018**, *57* (49), 15948–15982.

(8) Juliá-Hernández, F.; Moragas, T.; Cornella, J.; Martin, R. Remote Carboxylation of Halogenated Aliphatic Hydrocarbons with Carbon Dioxide. *Nature* **2017**, *545* (7652), 84–88.

(9) Diccianni, J. B.; Hu, C. T.; Diao, T. Insertion of CO_2 Mediated by a (Xantphos)Ni^I–Alkyl Species. *Angew. Chem. Int. Ed.* **2019**, *58* (39), 13865–13868.

(10) Somerville, R. J.; Martin, R. Relevance of Ni(I) in Catalytic Carboxylation Reactions. In *Nickel Catalysis in Organic Synthesis*; Ogoshi, S., Ed.; Wiley Online Library, 2019; pp 285–330.

(11) Charboneau, D. J.; Brudvig, G. W.; Hazari, N.; Lant, H. M. C.; Saydjari, A. K. Development of an Improved System for the Carboxylation of Aryl Halides through Mechanistic Studies. *ACS Catal.* **2019**, *9* (4), 3228–3241.

Chapter 1.

General Introduction

1.1.   Ni-catalysed cross-coupling reactions

The development of transition metal-catalysed cross-coupling reactions is undoubtedly one of the most revolutionary achievements in chemistry in the last 60 years, and the formation of new C–C or C–heteroatom bonds in such a manner is now a cornerstone of organic synthesis. Nickel catalysis in particular has received much attention, with its origins linked to those of the field of homogeneous catalysis itself and with the development of fundamental organonickel chemistry (Scheme 1.1).[1–4] Scheme 1.1 summarises some of the seminal works in Ni catalysis by Sabatier, Mond, and Wilke from the beginning-to-mid 20th century, along with two Ni-catalysed processes used in industry to produce ethylene oligomers and adiponitrile.[4–6] The final part of Scheme 1.1 summarises six rather "simple" organonickel complexes that showcase some of the properties discussed later on in this Chapter: three Ni(0) olefin complexes from the pioneering laboratory of Günther Wilke, a Ni(0)-ate methyl complex reported by Pörschke and colleagues, and two three-coordinate diphosphine alkyl complexes. The first diphosphine complex is a coordinatively unsaturated Ni(II) complex displaying a β-agostic interaction relevant to the SHOP process[7] and the second a rare Ni(I) alkyl complex.[8]
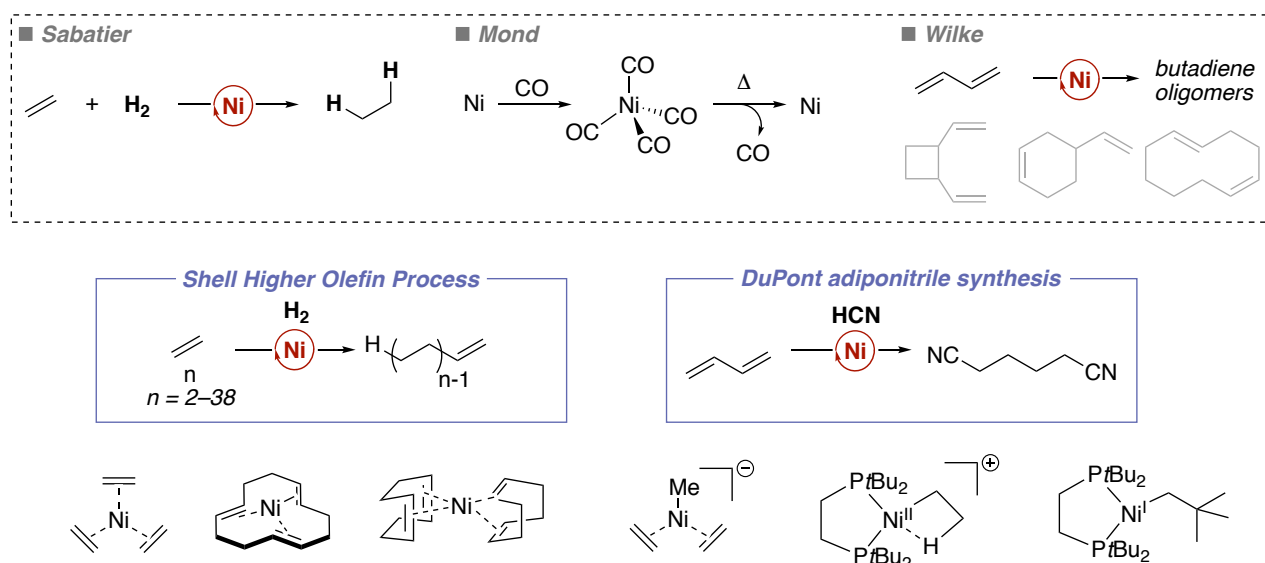
Scheme 1.1. Selected landmarks in the development of Ni catalysis and organonickel chemistry.

1.1.   Characteristics of Ni

Unlike other metals that are commonly employed in homogeneous catalysis, such as palladium, platinum, iridium, and rhodium, nickel is relatively cheap and Earth-abundant. The use and development of Ni-catalysed transformations is also motivated by its chemical properties (Scheme 1.2).[9] Its position on the first row of the periodic table means that it has a smaller energy difference between d orbitals and can therefore more easily access high-spin electron configurations. This means that Ni catalysis can often occur via one-electron pathways, providing more options for the possible transformations at the metal centre. One-electron reactivity can allow for catalytic cycles to operate in one-electron steps alongside

polar Ni(0)/Ni(II) mechanisms.[10] Organonickel complexes also contain comparatively weak Ni–C bonds.[11] This boosts reactivity in catalytic C–C bond formation but has the downside of decreasing the stability of intermediates. Whereas some Pd catalysed reactions are so robust they can be catalysed by "homeopathic" Pd, weak Ni–C bonds and favourable homolytic cleavage pathways may make a Ni-catalysed reaction less robust.[12,13] This can also cause complications for the isolation and/or characterisation of organometallic intermediates that may be key to understanding the mechanism of the transformation.

Regarding activation of the σ bonds of potential substrates, Ni(0) is smaller and more nucleophilic than Pd(0) making it suited to the catalytic coupling of unconventional electrophiles containing strong bonds such as aryl fluorides or aryl esters. Furthermore, the coupling of $C(sp^3)$–X substrates (X = halide or (pseudo)halide) may be more favourable with Ni catalysts as the β-hydride elimination pathway is less favourable. Unsaturated systems bind very strongly to Ni compared to Pd and Pt and π back donation is facilitated by the less electronegative Ni centre.[14,15] This has consequences in chain walking carboxylation reactions and in the substrate scopes of Ni-catalysed methodologies.[16]

In summary, the use of a Ni complex in the development of a new catalytic transformation can result in facilitated oxidative addition, reductive elimination, and coordination of π systems; however, controlling this reactivity can be difficult and often requires careful ligand design.
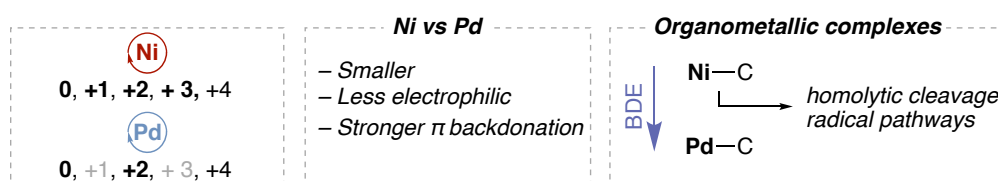
Scheme 1.2. General trends for Ni compared to Pd.

1.1.1. Cross-electrophile coupling reactions

Over the last decade, two classes of Ni-catalysed reaction have risen to some prominence. The first is that of cross-electrophile coupling (Scheme 1.3). Challenging and useful transformations such as the coupling of alkyl halides with $C(sp^2)$–X electrophiles or the coupling of "inert" CO_2 with other electrophiles fall under this umbrella. Such reactions do not require the (pre)formation of a nucleophilic coupling partner and instead harness the ability of Ni to access a range of oxidation states and promote radical reactivity. However, cross-electrophile reactions are more difficult to develop than nucleophile-electrophile coupling reactions due to the similar reactivities of the coupling partners and the selectivity issues that arise from this. The Martin group has investigated a number of cross-electrophile coupling reactions but has focused the majority of its efforts on Ni-catalysed reductive carboxylation reactions (Scheme 1.3).[17] In these transformations, an electrophile such as an aryl or alkyl halide is coupled with electrophilic CO_2. As for cross-electrophile coupling reactions, two electrons are required. These are usually supplied by a metal reductant (Zn or Mn powder). In the last decade, the reductive carboxylation reaction has been extended to a wide variety of substrates.[17] Recent efforts have seen the successful use

of a Ni/photoredox system that avoids the formation of stoichiometric metal waste that is costly to dispose of on a large scale.[18,19]
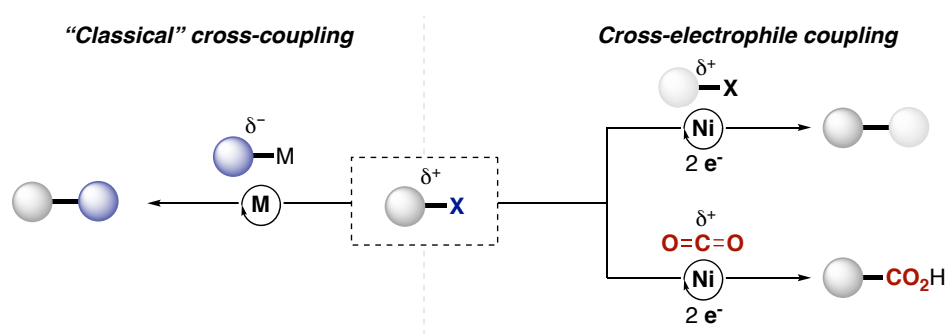
Scheme 1.3. Ni-catalysed cross-electrophile and reductive carboxylation reactions.

1.1.2. C(sp^2)–O functionalisation

The second class of reaction that has been driven by Ni catalysis involves the use of unconventional electrophiles such as aryl esters, aryl ethers, or aryl fluorides. Whereas strong C(sp^2)–F bonds or C(sp^2)–OMe bonds, for example, are inert to cleavage by Pd(0), Ni(0) complexes are able to insert into these and activate the substrate towards a cross-coupling reaction.[20,21] This reactivity has been harnessed to allow a wide range of bonds to become unconventional sites for further functionalisation. In doing so, it has also provided reactions that can be orthogonal to "traditional" Pd-catalysed reactions. One such field is the use of aryl esters as electrophiles in Ni-catalysed C(sp^2)–O to C(sp^2)–C, C(sp^2)–Heteroatom and C(sp^2)–H transformations.[22] Aryl esters are derived from phenols, which are more abundant than aryl halides and can provide routes to cross-coupled products that avoid the formation of halide-containing waste.
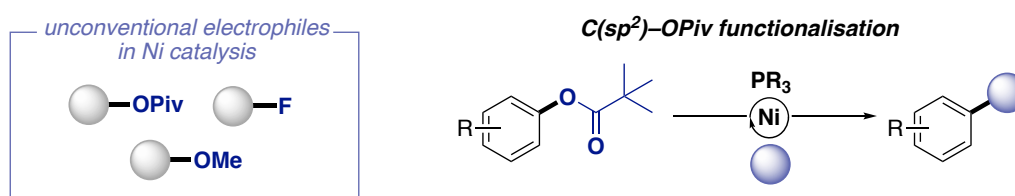
Scheme 1.4. Functionalisation of strong bonds with Ni catalysis.

1.2.   Ligands in Ni catalysis

Many ligands, including the common NHC ligands, phosphines, and α-diimines, are common to both Ni and Pd catalysis (Scheme 1.5). However, as mentioned above, Ni–C bonds are weaker than Pd–C bonds[11] and radical reactivity is common, making ligand choice and ligand tailoring very important in Ni catalysis. Furthermore, the dissociation and ligand-centred reactivity at Ni differs from that of Pd and can have a strong influence on the efficiency of a catalytic reaction. For example, Dixon and co-workers studied the binding energy of PH$_3$ to Ni/Pd(0) and Ni/Pd(II) complexes.[23] They showed that M(PH$_3$)$_2$X$_2$ Ni(II) complexes bind PH$_3$ less tightly than do analogous Pd(II) complexes, which might affect the

stabilisation of square planar oxidative addition complexes. In M(PH$_3$)$_2$ Ni(0) complexes, PH$_3$ was found to bind tighter to the Ni centre than in the analogous Pd complex.

Bulky electron-rich trialkyl phosphines and bipyridine or phenanthroline ligands are frequently employed in C(sp^2)–O functionalisation and reductive carboxylation reactions, respectively (Scheme 1.5). Unlike phosphine ligands, where parameters such as the Tolman electronic parameter, buried volume, cone angle, and dispersion have been well studied,[24] knowledge about substituted phenanthroline and bipyridine ligands in Ni catalysis is less clear.[25,26]
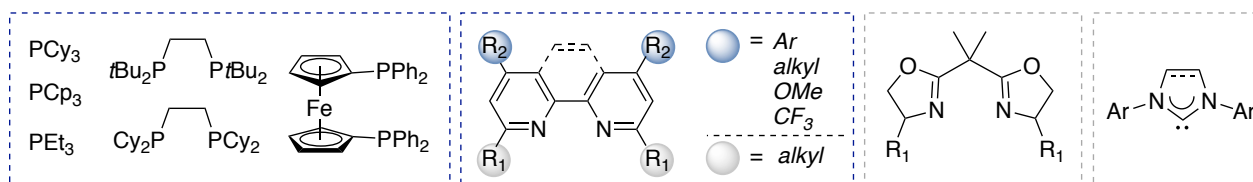
Scheme 1.5. A selection of ligands employed in Ni catalysis, those common in C–O functionalisation and carboxylation highlighted by blue boxes.

Phenanthroline and bipyridine ligands can act as π acceptor ligands and as electron reservoirs due to the overlap between the π^* orbitals of the ligand backbone and metal d orbitals.[27] This is exemplified by common "Ni(0)" sources bearing such ligands: [Ni(**L**)$_2$]. At first glance, [Ni(bpy)$_2$] would seem to be an 18-electron Ni(0) complex with neutral bipyridine ligands. However, spectroscopic studies and analysis of the X-ray structure showed that [Ni(bpy)$_2$] is best represented as [Ni(I)(bpy·−)(bpy)]^0. A related complex bearing **L1** (2,9-dimethylphenanthroline), [Ni(**L1**)$_2$], is best described as [Ni(II)(**L1**·−)$_2$]^0.[28] EPR and magnetic measurements showed that both complexes are diamagnetic due to antiferromagnetic coupling between the unpaired electrons at Ni(I) or Ni(II) and those displaced to the ligand.

As shown in Scheme 1.6, bond distances in such complexes can provide valuable information about the extent of electron transfer between the metal and the ligand. When electron density is moved from Ni to the ligand, the central C–C bond distance will decrease compared to that in a neutral ligand. The C–N bond distance will increase due to its antibonding character.[27]
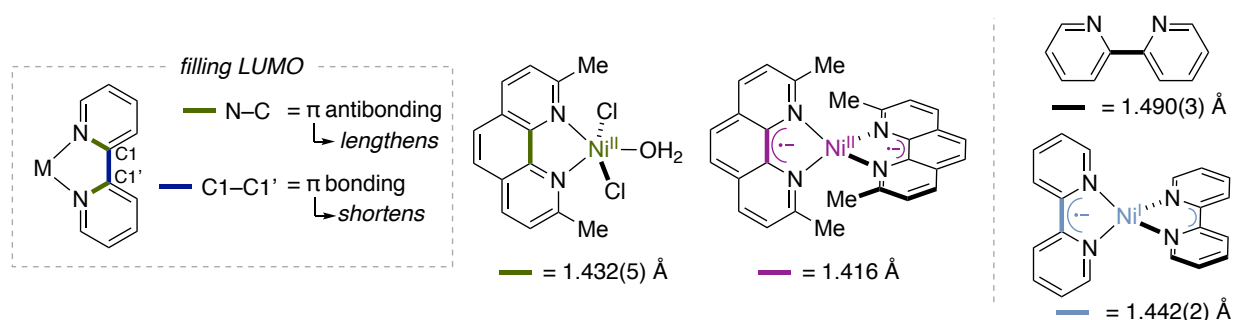
Scheme 1.6. Changes in ligand bond lengths on formation of "Ni(0)" complexes.[28–30]

It is clear from a number of reports that the substituents on the phenanthroline or bipyridine ligand, particularly those in the 2- and 9-positions, influence the yields and selectivities of reactions.[31,32] For example, in the deaminative hydroalkylation reaction summarised in Scheme 1.7-left, *t*Bu substituents in

the 4- and 4'-positions boosted the yield of the product while steric bulk around the metal centre decreased the yield dramatically. In the dicarboxylation reaction summarised in Scheme 1.7-right, addition of a single methyl substituent in the 2-position increased the yield of the dicarboxylic acid by approximately 20%.
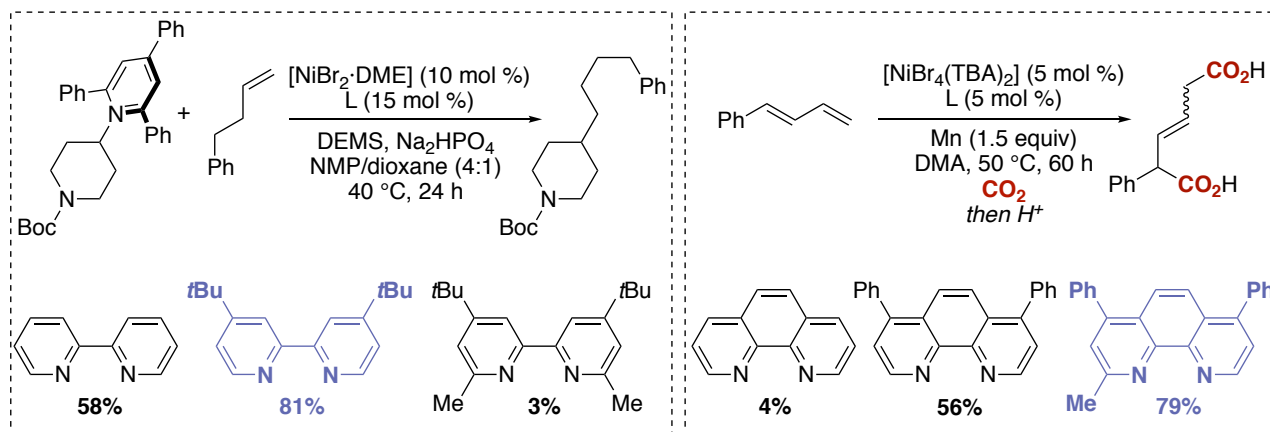
Scheme 1.7. Examples of the effect of bipyridine or phenanthroline substitution on yields of deaminative hydroalkylation (left) and dicarboxylation reactions (right).[31,32]

Although the effects of substitution on the binding affinities of phenanthroline ligands have been studied based on calculations of molecular electrostatic potentials, substitution in the 2- and 9- positions has not been investigated.[25] Therefore, it is worth highlighting a report describing the role of bulky substituents on an *N,N'*-donor diimine ligand.[33] Zimmerman, McNeill, and co-workers carried out a detailed theoretical study on the effect of steric bulk on the transmetalation step of a Ni-catalysed catalyst-transfer polymerisation reaction. Of note is the requirement for the transmetalation step to occur at a high-spin Ni centre – a tetrahedral geometry – followed by further evolution of the catalyst to a low-spin square planar geometry prior to reductive elimination (Scheme 1.8). Although the ligands investigated only differed by a single methyl group, this was enough to perturb preferences for high and low spin states of a key transmetalation intermediate and affect the barriers of transmetalation steps. The Ni(II) dihalide starting material was tetrahedral for both ligands, while the bis(thiophene) product of the two transmetalation steps was low spin square planar. Following the potential energy surface for both electronic structures, the authors determined that transmetalation occurred via a high spin pathway. Although this was favoured by the bulky ligand, the requirement for a spin switch to square planar in the final product meant that the bulky ligand was not optimal for the transformation. Studies such as this shed light on the subtleties behind catalytic reactions that, when unknown, result in much trial and error.
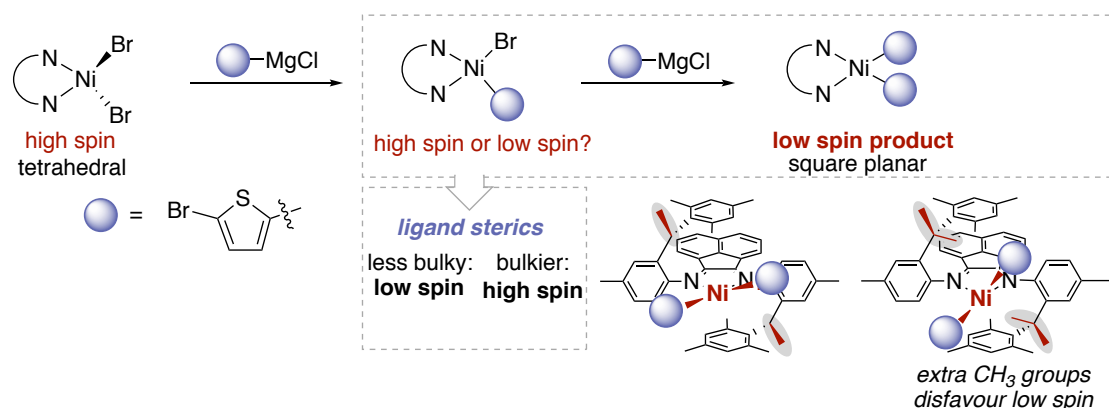
Scheme 1.8. Spin-switching transmetalation is influenced by the steric properties of the ligand.

1.3.   Mechanistic studies

Nickel is able to catalyse many interesting transformations by virtue of the properties mentioned in Section 1.1. However, these also lend a broader scope to the possible mechanisms of Ni-catalysed transformations resulting in a need for mechanistic studies to resolve questions about mechanistic steps and intermediates. Experimental studies of Ni-catalysed reactions often focus on the role of open-shell intermediates and on oxidative addition. These will be discussed in detail below.

Obtaining mechanistic understanding is important for a number of reasons. First, obtaining information about the structure, bonding, and reactivity of intermediates can produce knowledge that will lead to fundamental understanding about the molecules in question. Secondly, one of the main aims of methodology development is the uptake of the new reaction by the wider community. However, if complicated or sensitive ligands, high catalyst loading, toxic solvents, or many additives are required, it is unlikely that the reaction will be embraced by academic and industrial chemists. If the transformation is useful and the need for these undesirable or expensive aspects can be rationalised or minimised, it might be more likely to be used in organic syntheses or scaled up for processes.

1.3.1. Oxidative addition

Oxidative addition is usually the first step in a Ni-catalysed coupling reaction and therefore receives sustained research attention. Broadly, it involves the reaction of a metal complex with a substrate resulting in the cleavage of a bond in the substrate, an increase in the oxidation state of the metal, and the formation of at least one new Ni–element bond.[34] Activation of challenging substrates such as aryl esters and alkyl chlorides by oxidative addition benefits from the small size and lower electrophilicity of Ni and is further facilitated by electron-donating ligands such as trialkyl phosphines and NHCs that stabilise the oxidised complex.

Depending on the substrate and ligands on the metal complex, different oxidative addition pathways are accessible. For aryl halide substrates, the concerted pathway (Scheme 1.9-top) has been calculated for a number of reactions including the concerted oxidative addition of Ni(0) to $C(sp^2)$–O and C–SCF$_3$ electrophiles.[35] Nucleophilic Ni(0) complexes can also carry out S$_N$2 oxidative addition (Scheme 1.9-

bottom).[36] For many substrates, Ni(0) coordinates adjacent to the C(sp^2)–X bond in an η^2 fashion prior to insertion.
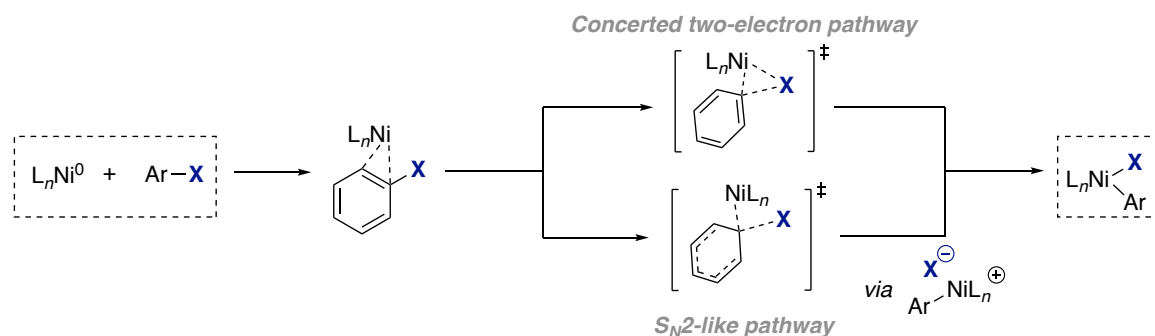
Scheme 1.9. Two-electron oxidative addition mechanisms for aryl halides.

The expanded redox manifold of Ni compared to Pd means that even after a two-electron oxidative addition, Ni(I) complexes can be produced. Nelson, Sproules, and co-workers carried out a systematic study on the rates of oxidative addition of Ni(0) to a range of aryl electrophiles (Ar–X) (Scheme 1.10).[37] The [(dppf)Ni(COD)] complex (**1**) that was employed reacted with aryl electrophiles in an oxidative addition-comproportionation manner leading to Ni(I)–X complexes that were observed by EPR spectroscopy. The second product of this reaction – the Ni(I)–aryl complex – was not isolated or characterised but was proposed to decompose by disproportionation and reductive elimination to form biaryl and **1**.

X =	I	Br	Cl	OTf	OPiv	OMe	F
k_{rel}	10	0.31	0.071	0.011	0.002	$< 2 \times 10^{-5}$	$< 2 \times 10^{-5}$
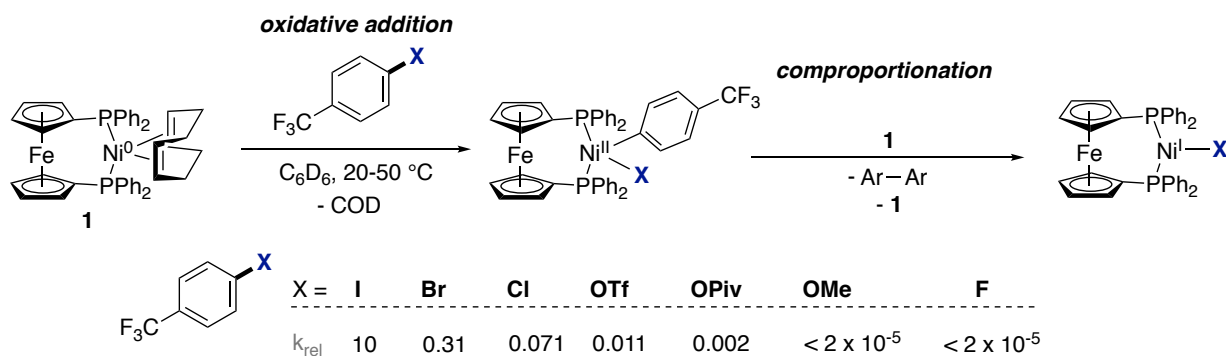
Scheme 1.10. Direct oxidative addition of Ni(0) complex 1 to a range of aryl (pseudo)halides resulting in comproportionation.[37]

Nickel(0) can also take part in one-electron radical oxidative addition pathways. Scheme 1.11-top shows the radical oxidative addition pathway first investigated by Tsou and Kochi.[38] Escape of the aryl radical from the solvent cage followed by hydrogen atom abstraction has also been investigated for a Ni complex bearing a monodentate phosphine ligand.[36] Oxidative addition with a monodentate phosphine complex [Ni(PEt$_3$)$_4$] rather than bidentate phosphine-bearing **1** shows that halide abstraction to form Ni(I) complexes can compete with formation of the Ni(II) oxidative addition complex. Halide abstraction can also be favoured by ligands that are very bulky.[39]

Radical pathway

Halide abstraction
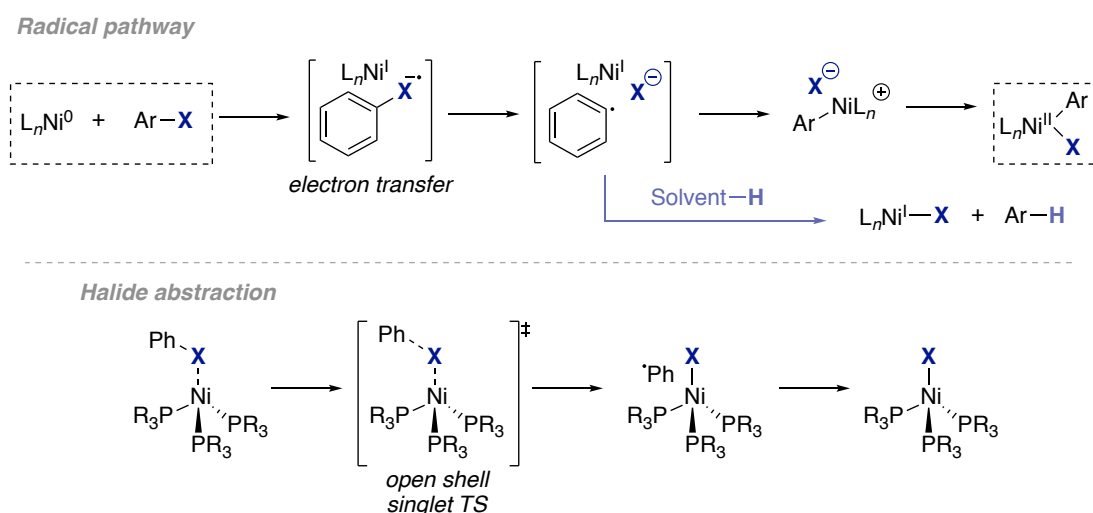
Scheme 1.11. Oxidative addition and halide abstraction via radical species.[36,38]

Oxidative addition of Ni(0) to alkyl substrates occurs through either a concerted, S_N2, or radical pathway (Scheme 1.12). The mechanism that operates is substrate-dependent and can be probed computationally or experimentally by employing specific substrates. One such experiment involves oxidative addition to stereochemically defined α,β-deuterated substrates.[40] If S_N2 oxidative addition is occurring, the transformation of interest will result in inversion at the α-position. For example, an α,β-deuterated primary alkyl bromide underwent inversion of configuration at the α-position when subjected to Ni-catalysed reductive carboxylation conditions.[41] If radical oxidative addition is occurring, scrambling at the α-position will occur due to recombination with Ni(I) from either face. Scrambling was observed when α,β-deuterated primary alkyl chlorides and bromides were subjected to reductive carboxylation and amidation conditions, respectively.[42,43] It is important to note that this experiment assumes no involvement of the β-hydrogen atoms in any Ni-centred processes. Scrambling could also be produced by S_N2 oxidative addition followed by β-hydride elimination, re-coordination of the resulting alkene, and reinsertion of the nickel hydride.

The radical pathway can be further probed using a substrate such as 6-chloro-1-hexene where primary radical formation can lead to recombination with the same Ni centre or escape from the solvent cage and radical rearrangement (in this case 5-exo-trig cyclisation). By changing the concentration of the catalyst and monitoring the ratio of unrearranged to rearranged product, it is possible to determine whether the radical is escaping the solvent cage. If cage escape is occurring then it would be expected that high catalyst concentrations would lower the amount of rearranged product due to there being a higher chance of the radical combining with a Ni centre before rearranging.

■ *Two-electron pathways*
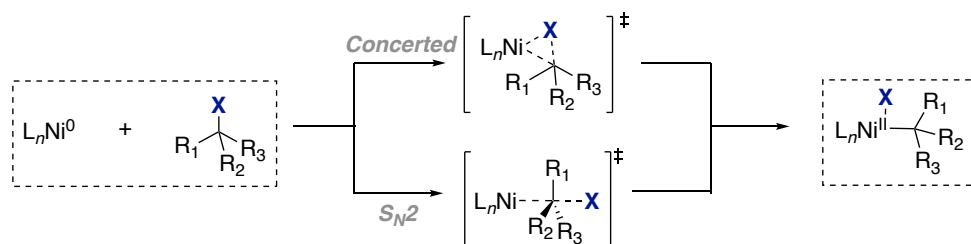
■ *Radical pathway*
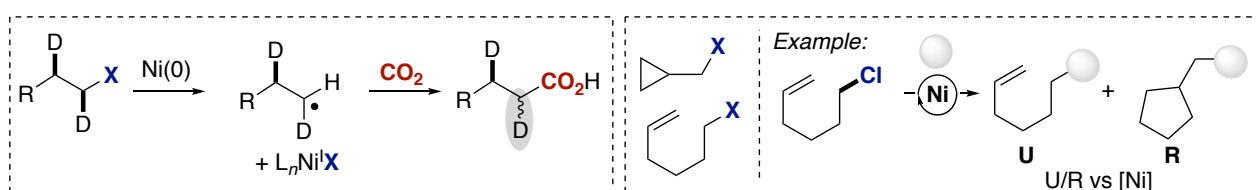
Scheme 1.12. Oxidative addition for alkyl halides.

As for aryl halides, halogen abstraction at alkyl halides can also compete with oxidative addition. Indeed, Diao and colleagues showed that halogen abstraction should not be ruled out as a key mechanism for alkyl bromide activation at Ni(I)–aryl complexes.[44] Two-electron oxidative addition of an aryl or alkyl halide to Ni(I) has also been proposed as an elementary step (Scheme 1.13).[45] Tilley and co-workers reported the first stoichiometric example of this reaction, where oxidative addition of MeI to a Ni(I) bis(amido) complex at −78 °C to form a structurally characterised Ni(III)–CH$_3$ complex. Finally, bimolecular oxidative addition forming two separate Ni species has also been invoked in two Ni-catalysed cross-coupling reactions.[46,47]
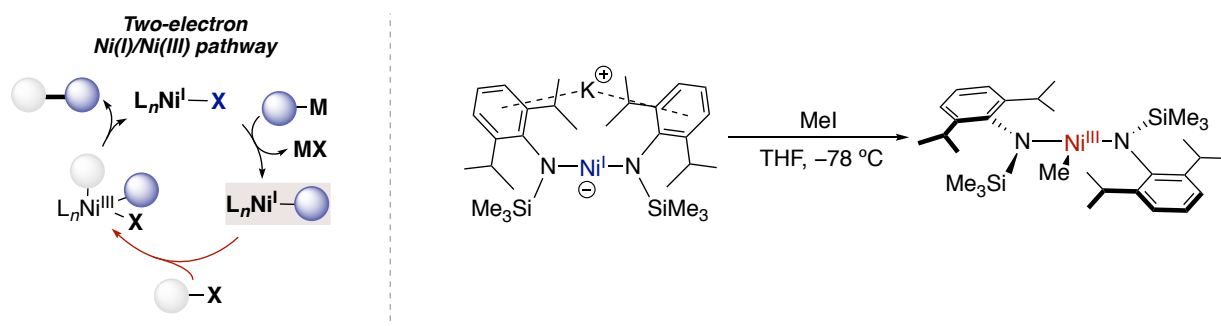
Scheme 1.13. Two-electron oxidative addition to a Ni(I) complex.

1.3.2. Nickel(I) intermediates

The possibility for the formation of intriguing Ni(I) intermediates during Ni-catalysed reactions – rather than perhaps more predictable Ni(II) intermediates – has spurred research into mechanistic studies and into synthetic routes to such complexes. Although approximately 300 Ni(I) complexes have now been reported and characterised,[48] understanding of these complexes, particularly in catalysis, is still in its infancy.[45,48] Nickel(I) alkyl, aryl, and halide complexes have been invoked in numerous Ni-catalysed cross-coupling reactions including cross-electrophile couplings, reductive carboxylation, radical chain and "radical rebound" pathways in the cross-coupling of C(sp^3) electrophiles,[49] reductive diene coupling reactions,[50] and Ni/photoredox dual catalytic transformations.[51–53] Scheme 1.14 demonstrates a selection of such mechanisms with Ni(I) intermediates highlighted in red.[10]
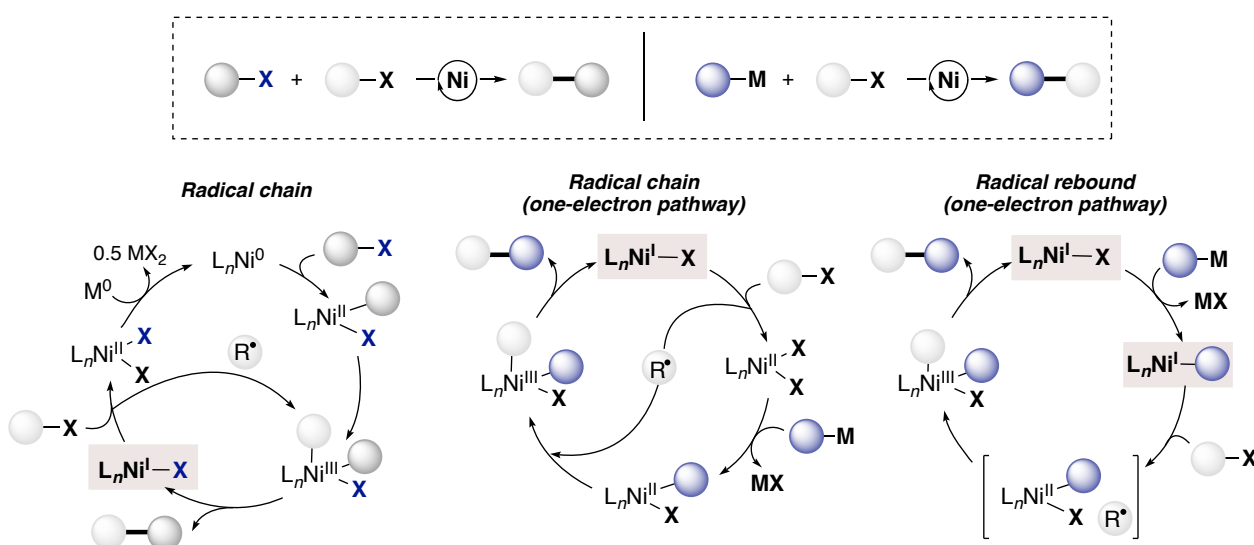
Scheme 1.14. Ni(I) intermediates in for cross-electrophile and nucleophile-electrophile coupling.

The detection of Ni(I) complexes during catalytic reactions by spectroscopic methods is a common method for obtaining knowledge about whether Ni(I) is relevant to a particular reaction. However, the synthesis and characterisation of Ni(I) complexes is also sought in order to confirm the assignment of the signal(s) or to carry out stoichiometric reactions. Such complexes are important to study for numerous reasons. First, there is little direct evidence that they are in fact intermediates as many of the mechanistic proposals have not been studied experimentally. Second, the metal-based radical can have interesting reactivity. Thirdly, they are challenging synthetic targets due to the potential for homolytic cleavage of the Ni–C bond or disproportionation to Ni(0) and Ni(II) complexes.

Scheme 1.15 describes the four synthetic routes that are used to obtain Ni(I) complexes with examples of the syntheses of four Ni(I) complexes that display interesting features or that are useful precursors.[48] The first route – oxidation with an Ag(I) salt – has been employed to synthesise a Ni(I) analogue of [Ni(COD)₂].[54] This might be a useful "ligand-free" source of Ni(I). The second reaction shows another common route to Ni(I) complexes – reduction.[55] Decomposition of Ni(II) complexes can also be a source of Ni(I). This reaction led to the first isolation of the useful NHC–Ni(I) precursor "Sigman's dimer".[56] Comproportionation between a Ni(0) source and a preformed Ni(II) dihalide complex can also produce

Ni(I)–halide complexes in good yields. Such complexes include "Sigman's dimer" and the α-diimine complex reported by Chirik.[56,57] Nickel(I)–halide complexes are useful precursors to Ni(I)–organyl or Ni(I)–silyl[58] complexes via transmetalation.[57]
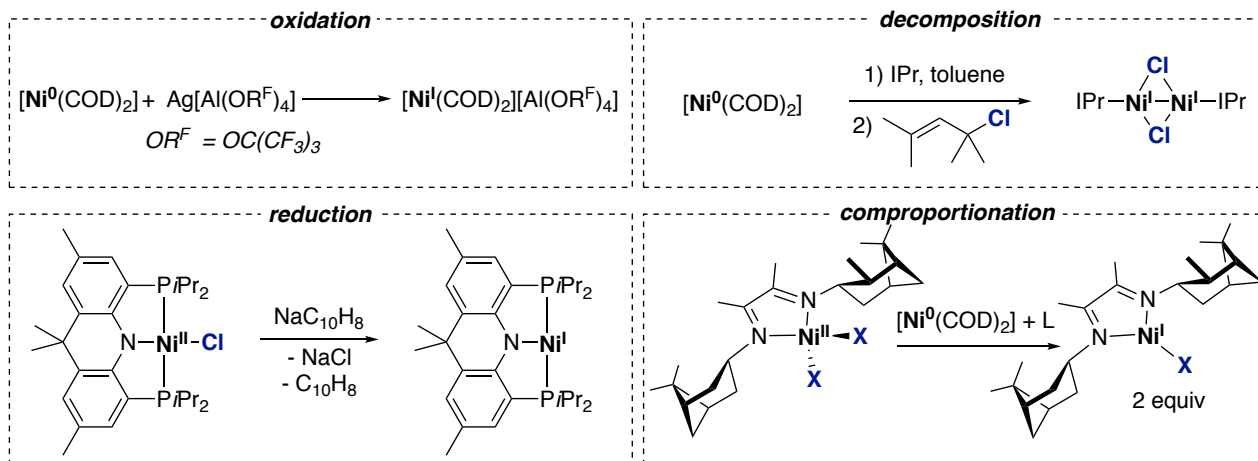
Scheme 1.15. Synthetic routes to Ni(I) complexes with examples of some notable complexes.[54–57]

A range of Ni(I) complexes from two- to six-coordinate have been crystallographically characterised, with three-coordinate Ni(I) complexes being very common. This may be due to the availability of bidentate α-diimine, phosphine, and pincer ligands and the widespread use of such ligands in catalysis. Three-coordinate complexes have an idealised D_{3h} trigonal planar geometry, but are instead found as Y-shaped or T-shaped complexes (Scheme 1.16). Whether the complex is Y- or T-shaped is ligand-dependent. Jahn-Teller distortion favouring the T-shape geometry is one factor that comes into play.[55] The other is whether the frontier molecular orbitals that result on distortion of the particular complex from trigonal planar to a C_s symmetry T-shape are lower in energy than those of the C_{2v} Y-shape.[59] Scheme 1.16 shows selected examples of Y- and T-shaped complexes including two complexes previously mentioned above, a Ni(I)–aryl complex bearing a catalytically relevant 2,9-dimethylphenanthroine ligand,[60] and a lutidine complex bearing an anionic β-diketiminato ligand.[61]
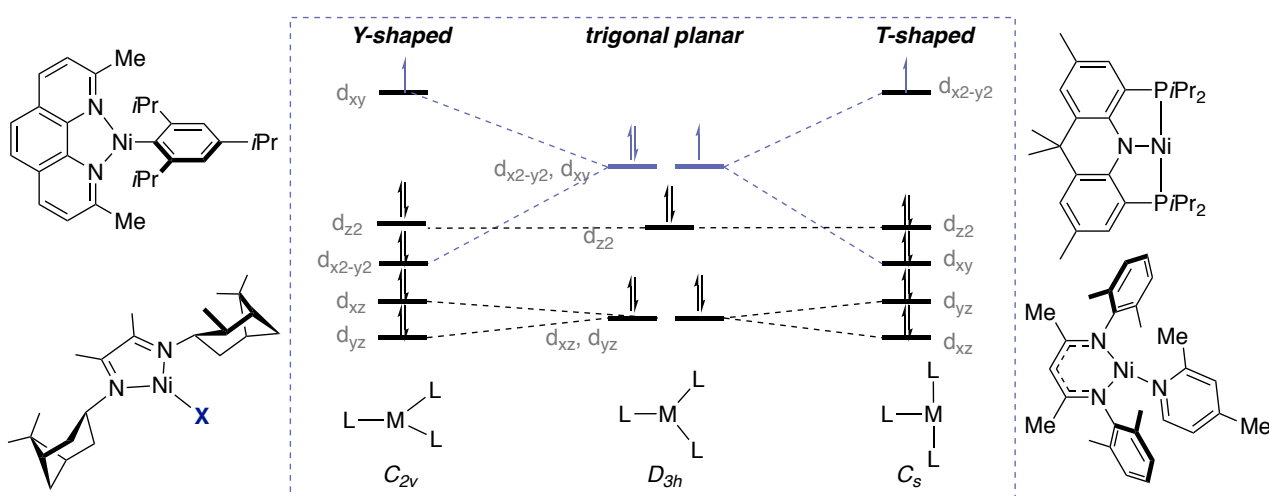
Scheme 1.16. Examples of three-coordinate d⁹ Ni(I) complexes in Y- and T-shape geometries.[55,57,60,61]

1.4.   General objectives of this Thesis

Taking into account the importance of Ni catalysis and organonickel chemistry, especially given the recent resurgence of Ni catalysis, obtaining mechanistic information about Ni-catalysed transformations is invaluable for further development of the field. A number of research lines in the Martin group originate from a central theme – the use of Ni catalysis to enable transformations that are otherwise difficult with another metal catalyst or with a metal-free method. These themes encompass topics including Ni-catalysed reductive carboxylation with CO_2 and the functionalisation of strong $C(sp^2)$–O bonds.

The overall aim of this Doctoral Thesis is to provide mechanistic information about three such reactions: the $C(sp^2)$–O silylation of aryl pivalate esters, the reductive carboxylation of alkyl halides, and the reductive carboxylation of arylsulfonium salts. This main aim was divided into three objectives:

- To carry out a mechanistic study of the $C(sp^2)$–O silylation of aryl pivalate esters with specific emphasis on the oxidative addition step and the role of the additives.
- To synthesise and characterise Ni(I)–alkyl complexes bearing catalytically relevant phenanthroline ligands as proposed intermediates in the reductive carboxylation of aryl halides.
- To develop the Ni-catalysed reductive carboxylation of arylsulfonium salts in collaboration with the Yorimitsu group (University of Kyoto) and obtain a mechanistic picture of the reaction.

Challenges that were expected during these projects included difficulties in isolating sensitive Ni complexes and difficulties in obtaining strong experimental evidence to support a mechanistic proposal based on the numerous pathways that can be envisioned. If these challenges can be overcome, this work will have a broad impact in the field of Ni catalysis.

1.5.   References

(1)   Wilke, G. Contributions to Organo-Nickel Chemistry. *Angew. Chem. Int. Ed. Engl.* **1988**, *27* (1), 185–206.

(2)   Tasker, S.; Standley, E.; Jamison, T. Recent Advances in Homogeneous Nickel Catalysis. *Nature* **2014**, *509* (7500), 299–309.

(3)   Standley, E. A.; Tasker, S. Z.; Jensen, K. L.; Jamison, T. F. Nickel Catalysis: Synergy between Method Development and Total Synthesis. *Acc. Chem. Res.* **2015**, *48* (5), 1503–1514.

(4)   Keim, W. Nickel: An Element with Wide Application in Industrial Homogeneous Catalysis. *Angew. Chem. Int. Ed. Engl.* **1990**, *29*, 235–244.

(5)   *Metal-Catalysis in Industrial Organic Processes*; Chiusoli, G. P., Maitlis, P. M., Eds.; RSC Publishing: Cambridge, 2006.

(6)   Cornils, B.; Herrmann, W. A. Concepts in Homogeneous Catalysis: The Industrial View. *J. Catal.* **2003**, *216* (1–2), 23–31.

(7)   Conroy-Lewis, F. M.; Mole, L.; Redhouse, A. D.; Litster, S. A.; Spencer, J. L. Synthesis of Coordinatively Unsaturated Diphosphine nickel(II) and palladium(II) β-Agostic Ethyl Cations: X-Ray Crystal Structure of [Ni{Bu$^t_2$P(CH$_2$)$_2$PBu$^t_2$}(C$_2$H$_5$)][BF$_4$]. *J. Chem. Soc. Chem. Commun.* **1991**, No. 22, 1601–1603.

(8)   Kitiachvili, K. D.; Mindiola, D. J.; Hillhouse, G. L. Preparation of Stable Alkyl Complexes of Ni(I) and Their One-Electron Oxidation to Ni(II) Complex Cations. *J. Am. Chem. Soc.* **2004**, *126* (34), 10554–10555.

(9)   Jolly, P. W. *The Organic Chemistry of Nickel: Organonickel Complexes*; Elsevier, 2012.

(10)   Diccianni, J. B.; Diao, T. Mechanisms of Nickel-Catalyzed Cross-Coupling Reactions. *Trends Chem.* **2019**, *1* (9), 830–844.

(11)   Macgregor, S. A.; Neave, G. W.; Smith, C. Theoretical Studies on C–heteroatom Bond Formation via Reductive Elimination from Group 10 M(PH$_3$)$_2$(CH$_3$)(X) Species (X=CH$_3$, NH$_2$, OH, SH) and the Determination of metal–X Bond Strengths Using Density Functional Theory. *Faraday Discuss.* **2003**, *124* (1), 111–127.

(12)   Ananikov, V. P. Nickel: The "Spirited Horse" of Transition Metal Catalysis. *ACS Catal.* **2015**, *5* (3), 1964–1971.

(13)   Deraedt, C.; Astruc, D. "Homeopathic" Palladium Nanoparticle Catalysis of Cross Carbon–Carbon Coupling Reactions. *Acc. Chem. Res.* **2014**, *47* (2), 494–503.

(14)   Massera, C.; Frenking, G. Energy Partitioning Analysis of the Bonding in L$_2$TM–C$_2$H$_2$ and L$_2$TM–C$_2$H$_4$ (TM = Ni, Pd, Pt; L$_2$ = (PH$_3$)$_2$, (PMe$_3$)$_2$, H$_2$PCH$_2$PH$_2$, H$_2$P(CH$_2$)$_2$PH$_2$). *Organometallics* **2003**, *22* (13), 2758–2765.

(15)   Nunzi, F.; Sgamellotti, A.; Re, N.; Floriani, C. A Density Functional Study of [M(PH$_3$)$_2$(η^2-C$_2$X$_4$)] Alkene Complexes for the Group 10 Metals Ni, Pd, Pt: The Effect of Electron-Attracting Substituents. *J. Chem. Soc., Dalt. Trans.* **1999**, No. 19, 3487–3491.

(16)   Cooper, A. K.; Leonard, D. K.; Bajo, S.; Burton, P.; Nelson, D. J. Aldehydes and Ketones Influence Reactivity and Selectivity in Nickel-Catalyzed Suzuki-Miyaura Reactions Aldehydes and Ketones Influence Reactivity and Selectivity in Nickel-Catalyzed Suzuki-Miyaura Reactions. *Chem. Sci.* **2020**, DOI: 10.1039/C9SC05444H.

(17)   Tortajada, A.; Juliá-Hernández, F.; Börjesson, M.; Moragas, T.; Martin, R. Transition-Metal-Catalyzed Carboxylation Reactions with Carbon Dioxide. *Angew. Chem. Int. Ed.* **2018**, *57* (49), 15948–15982.

(18)   Sahoo, B.; Bellotti, P.; Juliá-Hernández, F.; Meng, Q. Y.; Crespi, S.; König, B.; Martin, R. Site-Selective, Remote sp^3 C−H Carboxylation Enabled by the Merger of Photoredox and Nickel Catalysis. *Chem. Eur. J.* **2019**, *25* (38), 9001–9005.

(19)   Meng, Q. Y.; Wang, S.; König, B. Carboxylation of Aromatic and Aliphatic Bromides and Triflates with CO$_2$ by Dual Visible-Light–Nickel Catalysis. *Angew. Chem. Int. Ed.* **2017**, *56* (43), 13426–13430.

(20)   Liu, X. W.; Echavarren, J.; Zarate, C.; Martin, R. Ni-Catalyzed Borylation of Aryl Fluorides via C–F Cleavage. *J. Am. Chem. Soc.* **2015**, *137* (39), 12470–12473.

(21)   Álvarez-Bercedo, P.; Martin, R. Ni-Catalyzed Reduction of Inert C–O Bonds: A New Strategy for Using Aryl Ethers as Easily Removable Directing Groups. *J. Am. Chem. Soc.* **2010**, *132* (49), 17352–17353.

(22)   Zarate, C.; van Gemmeren, M.; Somerville, R. J.; Martin, R. Chapter Four-Phenol Derivatives: Modern Electrophiles in Cross-Coupling Reactions. *Adv. Organomet. Chem.* **2016**, *66*, 143–222.

(23)   Craciun, R.; Vincent, A. J.; Shaughnessy, K. H.; Dixon, D. A. Prediction of Reliable Metal–PH$_3$ Bond Energies for Ni, Pd, and Pt in the 0 and +2 Oxidation States. *Inorg. Chem.* **2010**, *49* (12), 5546–5553.

(24)   Durand, D. J.; Fey, N. Computational Ligand Descriptors for Catalyst Design. *Chem. Rev.* **2019**, *119* (11), 6561–6594.

(25)   Remya, G. S.; Suresh, C. H. Assessment of the Electron Donor Properties of Substituted Phenanthroline Ligands in Molybdenum Carbonyl Complexes Using Molecular Electrostatic Potentials. *New J. Chem.* **2018**, *42* (5), 3602–3608.

(26)   Ardizzoia, G. A.; Bea, M.; Brenna, S.; Therrien, B. A Quantitative Description of the σ-Donor and π-Acceptor Properties of Substituted Phenanthrolines. *Eur. J. Inorg. Chem.* **2016**, *2016* (23), 3829–3837.

(27)   Scarborough, C. C.; Wieghardt, K. Electronic Structure of 2,2′-Bipyridine Organotransition-Metal Complexes. Establishing the Ligand Oxidation Level by Density Functional Theoretical Calculations. *Inorg. Chem.* **2011**, *50*

(20), 9773–9793.

(28) Wang, M.; England, J.; Weyhermüller, T.; Wieghardt, K. Electronic Structures of "Low-valent" Neutral Complexes [NiL₂]^0 (S = 0; L = Bpy, Phen, Tpy) – An Experimental and DFT Computational Study. *Eur. J. Inorg. Chem.* **2015**, *2015* (9), 1511–1523.

(29) Ding, C. F.; Miao, Y. F.; Tian, B. Q.; Li, X. M.; Zhang, S. S. Aquadichloro(2,9-Dimethyl-1,10-Phenanthroline-κ^2N,N′)nickel(II). *Acta Crystallogr. Sect. E* **2006**, *62* (5), 1062–1063.

(30) Chisholm, M. H.; Huffman, J. C.; Rothwell, I. P.; Bradley, P. G.; Kress, N.; Woodruff, W. H. Bis(2,2'-bipyridyl)diisopropoxyinolybdenum(ll). Structural and Spectroscopic Evidence for Molybdenum-to-Bipyridyl π^* Bonding. *J. Am. Chem. Soc.* **1981**, *103* (16), 4945–4947.

(31) Sun, S.-Z.; Romano, C.; Martin, R. Site-Selective Catalytic Deaminative Alkylation of Unactivated Olefins. *J. Am. Chem. Soc.* **2019**.

(32) Tortajada, A.; Ninokata, R.; Martin, R. Ni-Catalyzed Site-Selective Dicarboxylation of 1,3-Dienes with CO₂. *J. Am. Chem. Soc.* **2018**, *140* (6), 2050–2053.

(33) Vitek, A. K.; Leone, A. K.; McNeil, A. J.; Zimmerman, P. M. Spin-Switching Transmetalation at Ni Diimine Catalysts. *ACS Catal.* **2018**, *8*, 3655–3666.

(34) Crabtree, R. H. *The Organometallic Chemistry of the Transition Metals*, Sixth.; John Wiley & Sons, 2014.

(35) Dürr, A. B.; Yin, G.; Kalvet, I.; Napoly, F.; Schoenebeck, F. Nickel-Catalyzed Trifluoromethylthiolation of Csp²–O Bonds. *Chem. Sci.* **2016**, *7* (2), 1076–1081.

(36) Funes-Ardoiz, I.; Nelson, D. J.; Maseras, F. Halide Abstraction Competes with Oxidative Addition in the Reactions of Aryl Halides with [Ni(PMeₙPh₍₃₋ₙ₎)₄]. *Chem. Eur. J.* **2017**, *23* (66), 16728–16733.

(37) Bajo, S.; Laidlaw, G.; Kennedy, A. R.; Sproules, S.; Nelson, D. J. Oxidative Addition of Aryl Electrophiles to a Prototypical Nickel(0) Complex: Mechanism and Structure/Reactivity Relationships. *Organometallics* **2017**, *36* (8), 1662–1672.

(38) Tsou, T. T.; Kochi, J. K. Mechanism of Oxidative Addition. Reaction of Nickel(0) Complexes with Aromatic Halides. *J. Am. Chem. Soc.* **1979**, *101* (21), 6319–6332.

(39) Nelson, D. J.; Maseras, F. Steric Effects Determine the Mechanisms of Reactions between bis(N-Heterocyclic Carbene)-nickel(0) Complexes and Aryl Halides. *Chem. Commun.* **2018**, *54* (75), 10646–10649.

(40) Péralez, E.; Négrel, J.-C.; Chanon, M. Further Evidence for the Radical Chain Character of Grignard's Reagent Formation. Use of Free Radical Clock in Conjunction with Changes in Concentration of Active Mg. *Tetrahedron* **1995**, *51* (46), 12601–12610.

(41) Wang, X.; Liu, Y.; Martin, R. Ni-Catalyzed Divergent Cyclization/Carboxylation of Unactivated Primary and Secondary Alkyl Halides with CO₂. *J. Am. Chem. Soc.* **2015**, *137* (20), 6476–6479.

(42) Börjesson, M.; Moragas, T.; Martin, R. Ni-Catalyzed Carboxylation of Unactivated Alkyl Chlorides with CO₂. *J. Am. Chem. Soc.* **2016**, *138* (24), 7504–7507.

(43) Serrano, E.; Martin, R. Nickel-Catalyzed Reductive Amidation of Unactivated Alkyl Bromides. *Angew. Chem. Int. Ed.* **2016**, *55* (37), 11207–11211.

(44) Diccianni, J. B.; Katigbak, J.; Hu, C.; Diao, T. Mechanistic Characterization of (Xantphos)Ni(I)-Mediated Alkyl Bromide Activation: Oxidative Addition, Electron Transfer, or Halogen-Atom Abstraction. *J. Am. Chem. Soc.* **2019**, *141* (4), 1788–1796.

(45) Zimmermann, P.; Limberg, C. Activation of Small Molecules at Nickel(I) Moieties. *J. Am. Chem. Soc.* **2017**, *139* (12), 4233–4242.

(46) Breitenfeld, J.; Wodrich, M. D.; Hu, X. Bimetallic Oxidative Addition in Nickel-Catalyzed Alkyl − Aryl Kumada Coupling Reactions. *Organometallics* **2014**, *33*, 5708–5715.

(47) Lin, Q.; Diao, T. Mechanism of Ni-Catalyzed Reductive 1,2-Dicarbofunctionalization of Alkenes. *J. Am. Chem. Soc.* **2019**, *141* (44), 17937–17948.

(48) Lin, C.-Y.; Power, P. P. Complexes of Ni(I): A "Rare" Oxidation State of Growing Importance. *Chem. Soc. Rev.* **2017**.

(49) Kuang, Y.; Anthony, D.; Katigbak, J.; Marrucci, F.; Humagain, S.; Diao, T. Ni(I)-Catalyzed Reductive Cyclization of 1,6-Dienes: Mechanism-Controlled Trans Selectivity. *Chem* **2017**, *3* (2), 268–280.

(50) Jones, G. D.; Martin, J. L.; McFarland, C.; Allen, O. R.; Hall, R. E.; Haley, A. D.; Brandon, R. J.; Konovalova, T.; Desrochers, P. J.; Pulay, P.; et al. Ligand Redox Effects in the Synthesis, Electronic Structure, and Reactivity of an Alkyl-Alkyl Cross-Coupling Catalyst. *J. Am. Chem. Soc.* **2006**, *128* (40), 13175–13183.

(51) Twilton, J.; Le, C. C.; Zhang, P.; Shaw, M. H.; Evans, R. W.; MacMillan, D. W. C. The Merger of Transition Metal and Photocatalysis. *Nat. Rev. Chem.* **2017**, *1*.

(52) Milligan, J. A.; Phelan, J. P.; Badir, S. O.; Molander, G. A. Alkyl Carbon–Carbon Bond Formation by Nickel/Photoredox Cross-Coupling. *Angew. Chem. Int. Ed.* **2019**, *58* (19), 6152–6163.

(53) Tellis, J. C.; Kelly, C. B.; Primer, D. N.; Jouffroy, M.; Patel, N. R.; Molander, G. A. Single-Electron Transmetalation via Photoredox/Nickel Dual Catalysis: Unlocking a New Paradigm for Sp³-Sp² Cross-Coupling. *Acc. Chem. Res.* **2016**, *49* (7), 1429–1439.

(54)   Schwab, M. M.; Himmel, D.; Kacprzak, S.; Kratzert, D.; Radtke, V.; Weis, P.; Ray, K.; Scheidt, E. W.; Scherer, W.; De Bruin, B.; et al. [Ni(cod)$_2$][Al(OR^F)$_4$], a Source for Naked Nickel(I) Chemistry. *Angew. Chem. Int. Ed.* **2015**, *54* (49), 14706–14709.

(55)   Yoo, C.; Lee, Y. A T-Shaped Nickel(I) Metalloradical Species. *Angew. Chem. Int. Ed.* **2017**, *56* (32), 9502–9506.

(56)   Dible, B. R.; Sigman, M. S.; Arif, A. M. Oxygen-Induced Ligand Dehydrogenation of a Planar Bis-μ-chloronickel(I) Dimer Featuring an NHC Ligand. *Inorg. Chem.* **2005**, *44* (11), 3774–3776.

(57)   Zarate, C.; Yang, H.; Bezdek, M. J.; Hesk, D.; Chirik, P. J. Ni(I)–X Complexes Bearing a Bulky α-Diimine Ligand: Synthesis, Structure, and Superior Catalytic Performance in the Hydrogen Isotope Exchange in Pharmaceuticals. *J. Am. Chem. Soc.* **2019**, *141* (12), 5034–5044.

(58)   Witzke, R. J.; Tilley, T. D. A Two-Coordinate Ni(I) Silyl Complex: CO$_2$ Insertion and Oxidatively-Induced Silyl Migrations. *Chem. Commun.* **2019**, *55* (46), 6559–6562.

(59)   Eckert, N. A.; Dinescu, A.; Cundari, T. R.; Holland, P. L. A T-Shaped Three-Coordinate Nickel(I) Carbonyl Complex and the Geometric Preferences of Three-Coordinate d^9 Complexes. *Inorg. Chem.* **2005**, *44* (22), 7702–7704.

(60)   Mohadjer Beromi, M.; Brudvig, G. W.; Hazari, N.; Lant, H. M. C.; Mercado, B. Q. Synthesis and Reactivity of Paramagnetic Polypyridyl Ni Complexes Relevant to C(sp^2)–C(sp^3) Coupling Reactions. *Angew. Chem. Int. Ed.* **2019**, *58* (18), 6094–6098.

(61)   Kogut, E.; Wiencko, H. L.; Zhang, L.; Cordeau, D. E.; Warren, T. H. A Terminal Ni(III)-Imide with Diverse Reactivity Pathways. *J. Am. Chem. Soc.* **2005**, *127* (32), 11248–11249.

Chapter 2.

The mechanism of the Ni-catalysed C(sp^2)–O silylation of aryl esters: Understanding oxidative addition and the role of additives

2.1.   Introduction

Due to their ease of synthesis, stability, and relatively low cost, phenol-derived C–O electrophiles such as aryl esters have recently found a role as coupling partners in cross-coupling reactions.[1–6] Although activated C–O electrophiles such as aryl sulfonates have long been employed in cross-coupling reactions, it was not until the last decade that the use of aryl ester electrophiles as alternatives to aryl halides received significant attention. Unlike the $C(sp^2)$–O bonds of aryl sulfonates, those of aryl esters are not readily cleaved by Pd catalysts and may therefore have been ignored as potential coupling partners while the field of Pd catalysis grew (Scheme 2.1). Aryl ester $C(sp^2)$–O bond functionalisation instead occurs with Earth-abundant and cheap Ni catalysts due to the small and electron-rich nature of Ni(0) discussed in Chapter 1. The successful development of Ni-catalysed cross-coupling reactions with aryl esters has not only provided a path to the use of alternative electrophiles in cross-coupling, but has also provided an opportunity to develop orthogonal coupling strategies.[7–9] These take advantage of the "inertness" of esters in Pd-catalysed cross-coupling reactions to allow the use of coupling sequences that end with Ni-catalysed aryl ester $C(sp^2)$–O functionalisation.
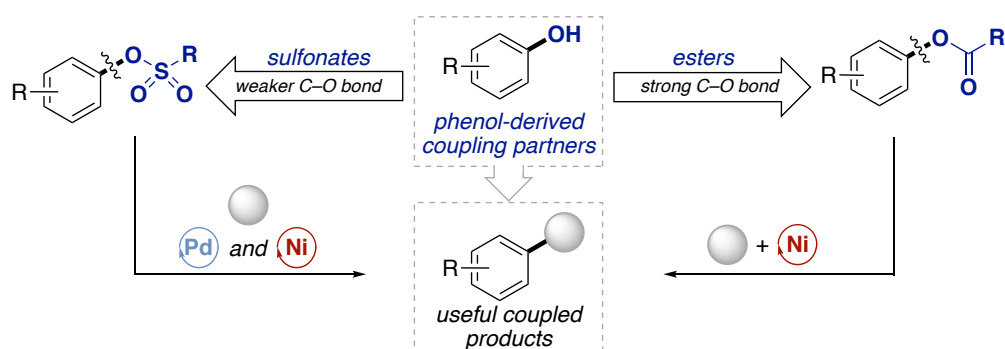
Scheme 2.1. Phenol-derived electrophiles in Ni- or Pd- catalysed C–O functionalisation

Over the last decade, a number of research groups have demonstrated that the Ni-catalysed cross-coupling of aryl esters can be employed with success in $C(sp^2)$–O functionalisation reactions that are not just limited to C–C bond formation but that can be extended to borylation,[10] amination,[11–13] stannylation,[7] phosphorylation,[14,15] and silylation reactions (Figure 2.1).[16]
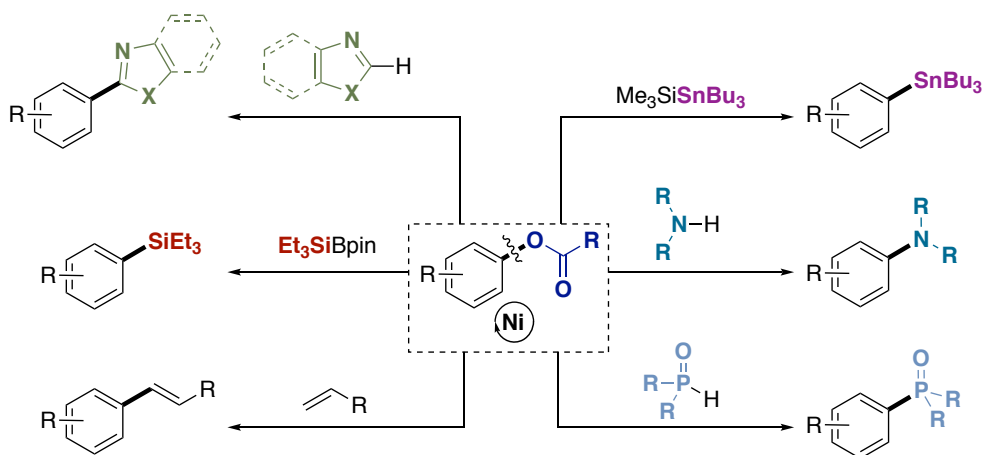
Figure 2.1. Overview of some selected Ni-catalysed C(*sp²*)–O functionalisation methodologies.

These C(*sp²*)–O functionalisation methodologies tend to share key features such as the type of ligand required or the additives involved. For example, a combination of Ni(0) and a phosphine ligand such as PCy₃ or dcype (1,2-bis(dicyclohexylphosphino)ethane) is used in all but one of the methodologies summarised in Figure 2.1. More broadly, the field of C(*sp²*)–O functionalisation relies on this combination of an electron-rich Ni(0) centre and a σ-donating trialkyl phosphine to favour oxidative addition of the strong C(*sp²*)–O bond. That being said, little understanding exists about the mechanistic details that underpin methodologies that employ C(*sp²*)–O electrophiles. This contrasts with that known about methodologies employing the aryl halide electrophiles that are ubiquitous in cross-coupling reactions. For example, whereas aryl halide oxidative addition to Ni(0) or Pd(0) has been studied since the late 1960s – with the first example of oxidative addition to Ni(0) reported by Fahey in 1970 – little work has been carried out on the oxidative addition of C(*sp²*)–O electrophiles such as aryl esters.[17–19] Without a clear understanding of the mechanisms of these reactions, further development and refinement of the field will be difficult.

2.1.1. Oxidative addition

There seems to be a consensus that, like for a classical Pd(0)/Pd(II) cycle involving an aryl halide electrophile, a Ni-catalysed C(*sp²*)–O functionalisation reaction is initiated by oxidative addition to a Ni(0)L$_n$ complex. As mentioned above, however, there are few examples of *isolated* C(*sp²*)–O oxidative addition complexes compared to those of aryl halides. Site-selectivity for the oxidative addition must also be taken into account because there are two C–O bonds in an aryl ester and both can be cleaved by Ni(0) (Scheme 2.2).
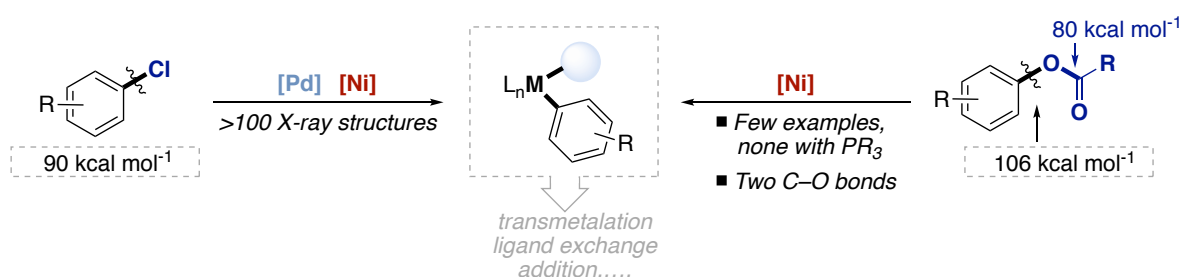
Scheme 2.2. Differences between Ar–Cl and Ar–OPiv oxidative addition.

The first oxidative addition complex derived from direct insertion of Ni(0) into the C(sp^2)–O bond of an aryl pivalate ester was reported by Itami and co-workers (Scheme 2.3, left).[20] This complex, [Ni(σ-2-naphthyl)(κ^1-OPiv)(dcype)] (**1**), was synthesised at 100 °C and required bidentate dcype. When a similar and more rigid ligand, dcypt (3,4-bis(dicyclohexylphosphino)thiophene), was employed, the oxidative addition reaction was found to be faster and the resulting complex isolated after only 2 h.[21] Later, Love et al. showed that a very electron-rich source of Ni(0) – again bearing an electron-rich bidentate ligand – could insert into the C(sp^2)–OAc bond of aryl esters at room temperature (Scheme 2.3, right).[22]
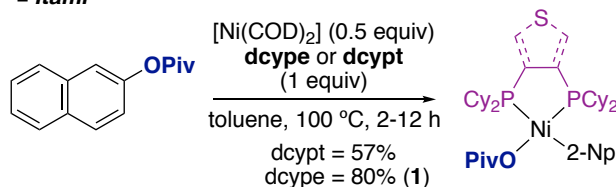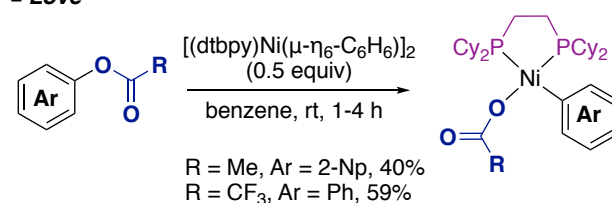
Scheme 2.3. Syntheses of Ni(II) aryl ester oxidative addition complexes via direct oxidative addition.

Successful isolation of an oxidative addition complex from the direct reaction of a Ni(0) complex bearing monodentate phosphine ligands with an aryl ester had not been reported. Although monodentate PCy$_3$ is the most frequently used ligand in Ni-catalysed C(sp^2)–O functionalisation, the only synthetic route to isolable Ni(II) complexes bearing monodentate phosphines was via anion metathesis (Scheme 2.4).[23–26] This is a very common procedure to install a carboxylate ligand at a metal centre yet there are only two examples of this reaction at a Ni complex. First, Kravtsov and co-workers reported the synthesis of four carboxylate complexes via stepwise anion metathesis.[25,26] Cavell and co-workers also employed anion metathesis in the synthesis of a range of N,O-chelated Ni(II) carboxylate complexes.[23,24]
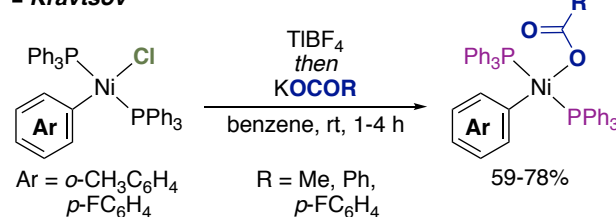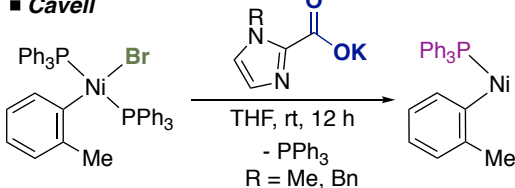
Scheme 2.4. Indirect syntheses of σ-aryl carboxylate complexes.[23–26]

As mentioned in Chapter 1, Nelson, Sproules, and co-workers included a *para*-substituted aryl pivalate in a systematic study of Ni(0) oxidative addition to a range of aryl electrophiles.[27] This direct oxidative addition reaction was found to form Ni(I)–OPiv species via comproportionation.

The dearth of isolated aryl ester oxidative addition complexes supported by monodentate phosphines is likely due to the recent emergence of the field and therefore the lack of studies into this reaction. This is also influenced by the more flexible monodentate ligands and their increased tendency to dissociate to form fluxional intermediates compared with bidentate ligands. Combined with the possibility for comproportionation or disproportionation at Ni, the synthesis and isolation of such intermediates may be difficult. Indeed, Ni(I) species were observed by Nelson et al. in the direct oxidative addition reaction mentioned above, and when Itami attempted to reproduce the successful synthesis of **1** with PCy₃ instead of dcype, 2,2'-binaphthalene was the only product identified.[20]

2.1.2. Mechanistic studies

Few mechanistic studies have been carried out on $C(sp^2)$–OPiv functionalisation reactions and many mechanistic questions come to mind when a $C(sp^2)$–OPiv functionalisation reaction is scrutinised. [20,28–30] The most common questions might be distilled down to the following four: how is selectivity between the *two* C–O bonds achieved? Is Ni(I) formed during oxidative addition or during the catalytic cycle? What is the identity of the oxidative addition intermediate? What is the rate-determining zone of the particular $C(sp^2)$–OPiv functionalisation reaction?[31–33] The following discussion will present what is known about these questions alongside a discussion of what has prevented chemists from fully answering these questions.

Two seminal reports by Yamamoto and co-workers with Ni(0)/PR₃ laid the groundwork for understanding why $C(sp^2)$–O vs O–acyl functionalisation is favoured in the aryl ester functionalisation methodologies developed in the last decade (Scheme 2.5).[34,35] Reactions of Ni(0)/PR₃ were carried out with a range of aryl esters. In all cases, including a case when PCy₃ was employed, cleavage of the O–acyl bond occurred. This led to an oxidative addition complex that was prone to decarbonylation and subsequent dimerisation and β-hydride elimination reactions. Exploring the substituents on the aryl ring showed that electron-withdrawing groups increased reactivity of the ester towards Ni(0).
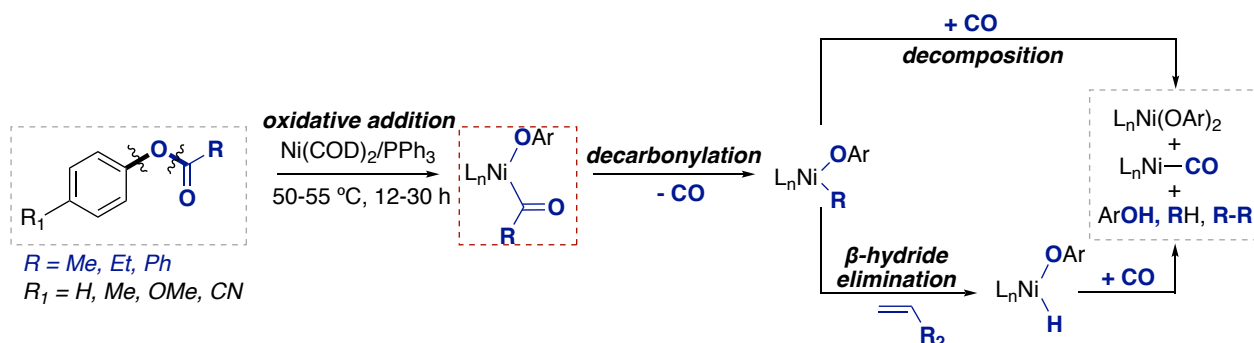
Scheme 2.5. Decomposition pathways for O–acyl cleavage.

These fascinating reports lay dormant until the first catalytic C(sp^2)–OPiv functionalisation methodologies were reported by the Garg and Shi groups (Scheme 2.6).[9,36,37] It should be noted that the successful C(sp^2)–OPiv arylation that was obtained might not be expected based on the work by Yamamoto described above: in that work, Ni(0)/PCy$_3$ preferentially cleaved the weaker O–acyl bond.[34,35]
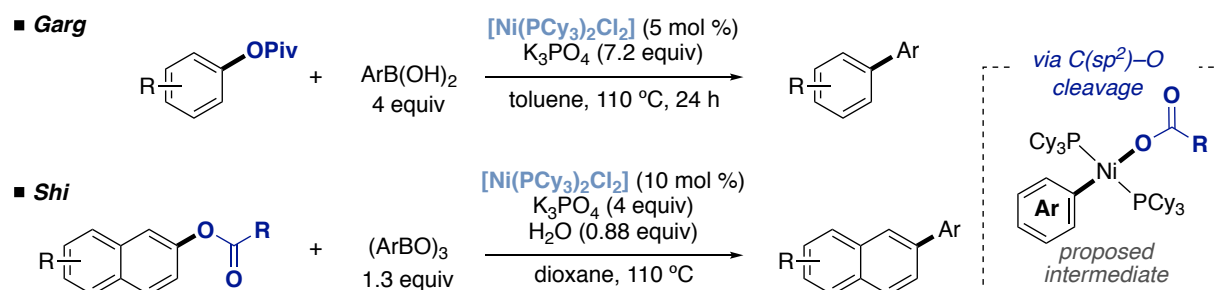
Scheme 2.6. Seminal C(sp^2)–O functionalisation: Ni-catalysed Suzuki-Miyaura reactions.[9,37]

This unexplored and synthetically very appealing selectivity prompted Liu et al. to carry out a theoretical study on the Ni(0)/PCy$_3$-catalysed Suzuki-Miyaura reaction between PhOAc and PhB(OH)$_2$.[28] In this study, Liu et al. developed a full mechanistic proposal for the transformation and demonstrated that a monophosphine pathway, rather than the diphosphine pathway proposed by Shi, is much more energetically favourable.

The calculated mechanism was consistent with the experimental finding that the stronger C(sp^2)–OAc bond is functionalised instead of the weaker O–acyl bond (Scheme 2.7). First, as expected, cleavage of the O–acyl bond was found to have a smaller barrier compared to cleavage of the C(sp^2)–OAc bond (14.2 kcal mol^{-1} vs 22 kcal mol^{-1}). However, the resulting O–acyl cleavage product was much higher in energy than the C(sp^2)–OAc oxidative addition complex [Ni(σ-phenyl)(κ^2-OAc)(PCy$_3$)] (−11.5 kcal mol^{-1} compared to −30.3 kcal mol^{-1}. This meant that O–acyl cleavage could be reversible under the reaction conditions. Furthermore, the ca. 20 kcal mol^{-1} free energy discrepancy between the two C–O oxidative addition intermediates meant that a transmetalation pathway from the O–acyl complex was calculated to pass through intermediates with much greater energies than those of the C(sp^2)–O functionalisation pathway.
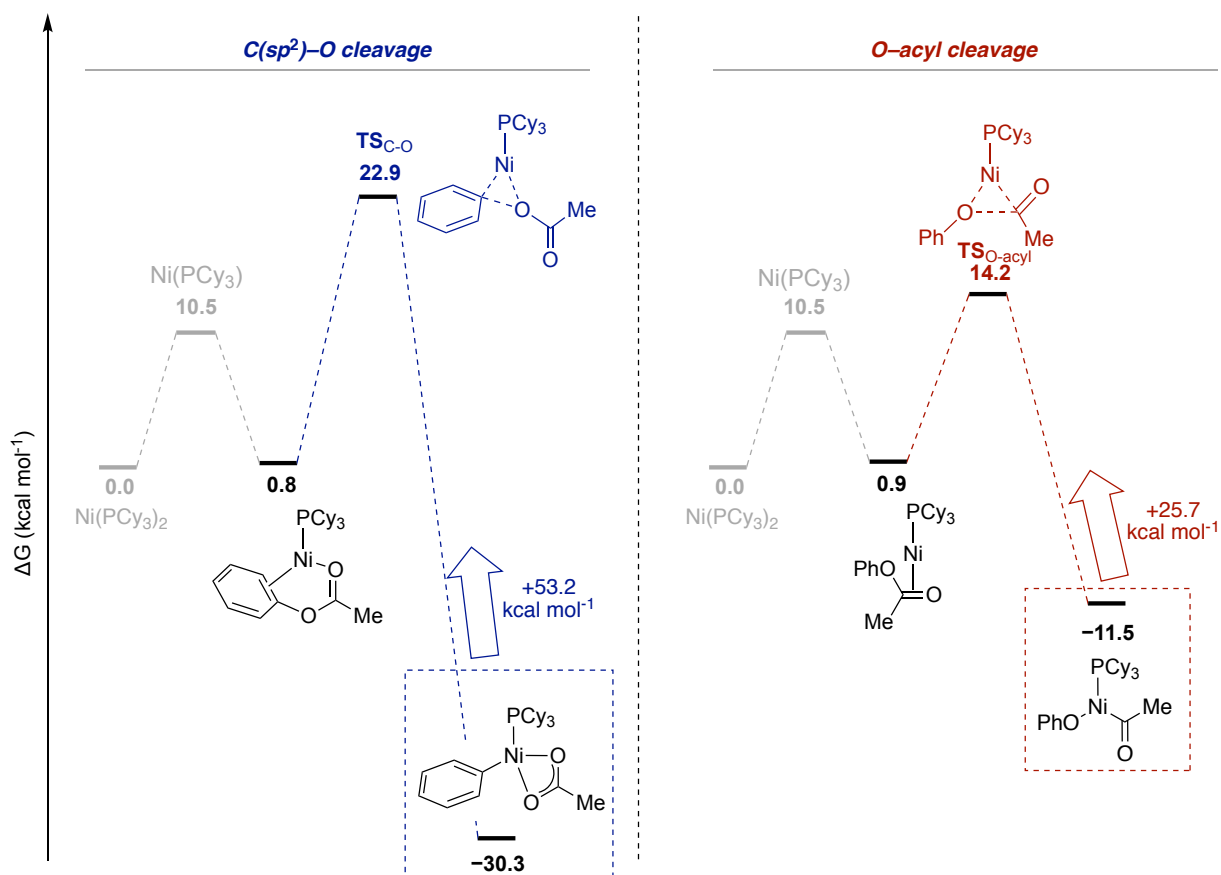
Scheme 2.7. DFT investigation into C(sp²)–O vs O–acyl cleavage by Liu et al.[28]

If the C(*sp²*)–O functionalisation literature is surveyed it is clear that aryl pivalate esters are the most prevalent ester substrates.[1,2] This is not only because they are stable and easy to synthesise and handle; the *t*Bu group does not provide a route to *β*-hydride elimination pathways if undesired C$_{acyl}$–O bond cleavage occurs, and the *t*Bu group cannot easily accept d electrons from the Ni centre (vide infra).[29,34]

The difference in reactivity that can be induced by exchanging an aryl pivalate for an aryl benzoate ester in Ni-catalysed C–O/C–H coupling was investigated by the Itami and Houk groups.[29,30] Itami and co-workers showed that the use of aryl pivalate esters in this coupling reaction led to C(*sp²*)–O functionalisation[38] and that aryl benzoate esters led to functionalisation of the weaker O–acyl bond through a decarbonylative C–H arylation (Scheme 2.8).[30,39,40]
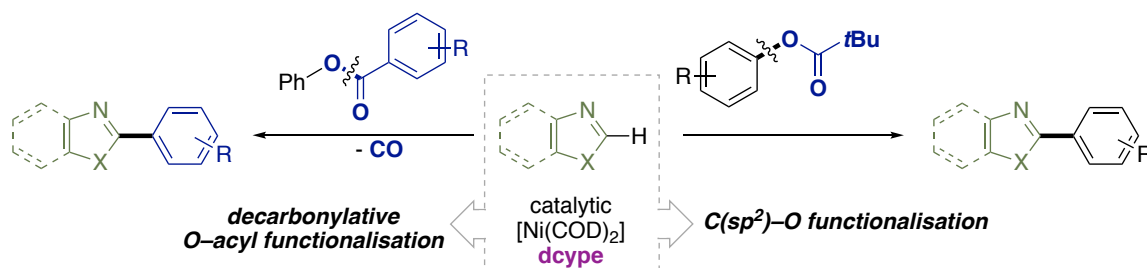
Scheme 2.8. Effect on product selectivity for Ar vs *t*Bu ester in C–O/C–H coupling.

Houk et al. carried out a DFT study that probed the role of the ester substrate and the ligand in determining selectivity between C(sp^2)–O or O–acyl functionalisation (Scheme 2.9).[29] Although the reaction of Ni(0)/dcype with the weaker O–acyl bond was found to be favourable for aryl pivalates and for aryl benzoates, the products of decarbonylation of the resulting O–acyl oxidative addition complexes differed significantly. In the case of the aryl pivalate, the resulting *t*Bu ligand had unfavourable steric interactions with bulky dcype and, as mentioned above, was unable to accept d electrons from Ni. Overall, this made the barriers to coupling via O–acyl cleavage prohibitive and explained why the products of C(sp^2)–O functionalisation were obtained with aryl pivalates and Ni(0)/dcype. In the case of the aryl benzoate, the steric clash was greatly reduced and the π system of the Ph ligand could form a stabilising d-π* interaction with Ni. Overall, this made coupling via O–acyl cleavage feasible for aryl benzoates.
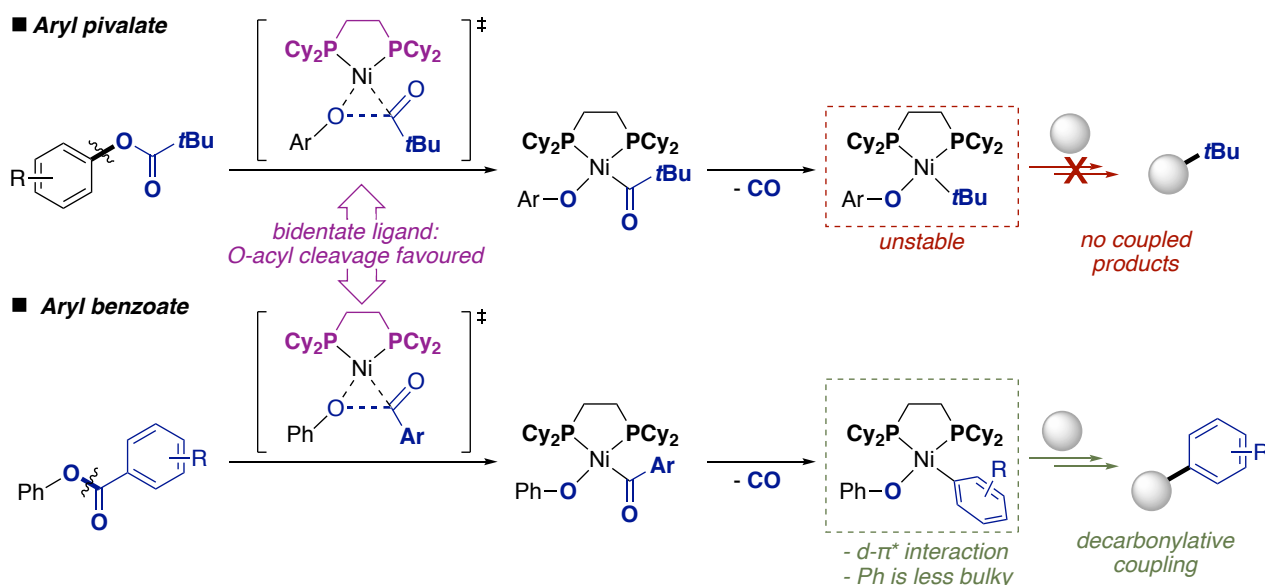
Scheme 2.9. O–acyl vs C(sp^2)–O selectivity for different ester substituents.[29]

The rather in-depth study also discussed the effect of the ligand on C–O selectivity (Scheme 2.10). Although the two methodologies developed by Itami both employ dcype (Scheme 2.8) many functionalisation reactions employ PCy$_3$ to obtain C(sp^2)–O functionalisation.[20,30,38] Unlike the study by Liu discussed above, Houk analysed Ni(0)/PCy$_3$ C–O selectivity with an aryl benzoate ester substrate. When PCy$_3$ was employed with such a substrate, the carbonyl oxygen atom was found to interact with Ni to form a five-membered TS that lowered the barrier to C(sp^2)–O cleavage.
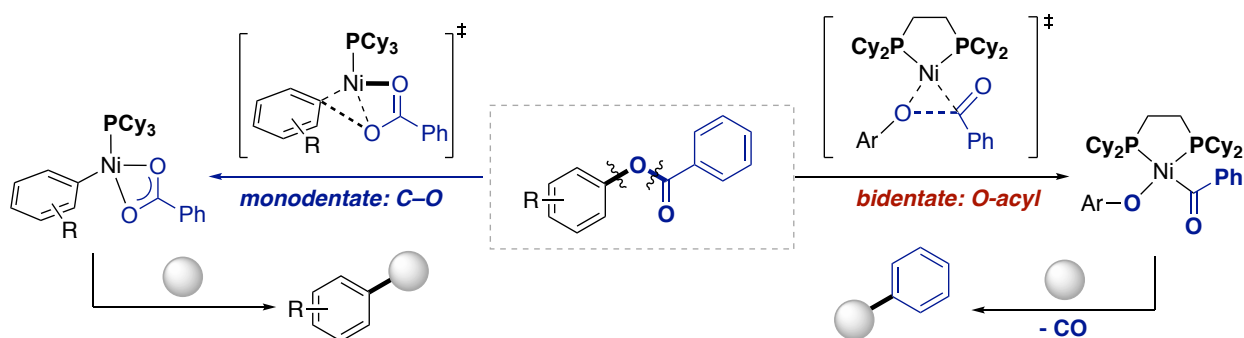
Scheme 2.10. Selectivity between the C–O bonds for PCy₃ vs dcype (aryl benzoate substrate).

The first experimental study of a C(sp^2)–OPiv functionalisation reaction was reported by Itami, Yamaguchi, and Lei (Scheme 2.11).[20] The chosen reaction – a C(sp^2)–O/C–H coupling between aryl pivalates and azoles – employed Ni(0)/dcype and Cs$_2$CO$_3$. Although a mechanism was suggested in the original report, there was no experimental evidence for any of the proposed steps.[38] Thus, attempts were made to understand some of the Ni intermediates and to provide evidence for the mechanistic steps. This study is noteworthy as it was the first time that an oxidative addition complex of an aryl pivalate, complex **1**, was isolated from a direct oxidative addition reaction. This complex reacted with benzoxazole to form the product of C(sp^2)–O/C–H coupling in 32% yield. In addition, kinetic studies that suggested that transmetalation at complex **1** is rate-determining. A later computational study proposed that as well as acting as a base, Cs$_2$CO$_3$ could be forming clusters that interact with the oxidative addition complex to lower the barrier to C–H activation (Scheme 2.11, right).[30] This may explain the increase in reaction rate and yield when the reaction was carried out in the presence of Cs$_2$CO$_3$.
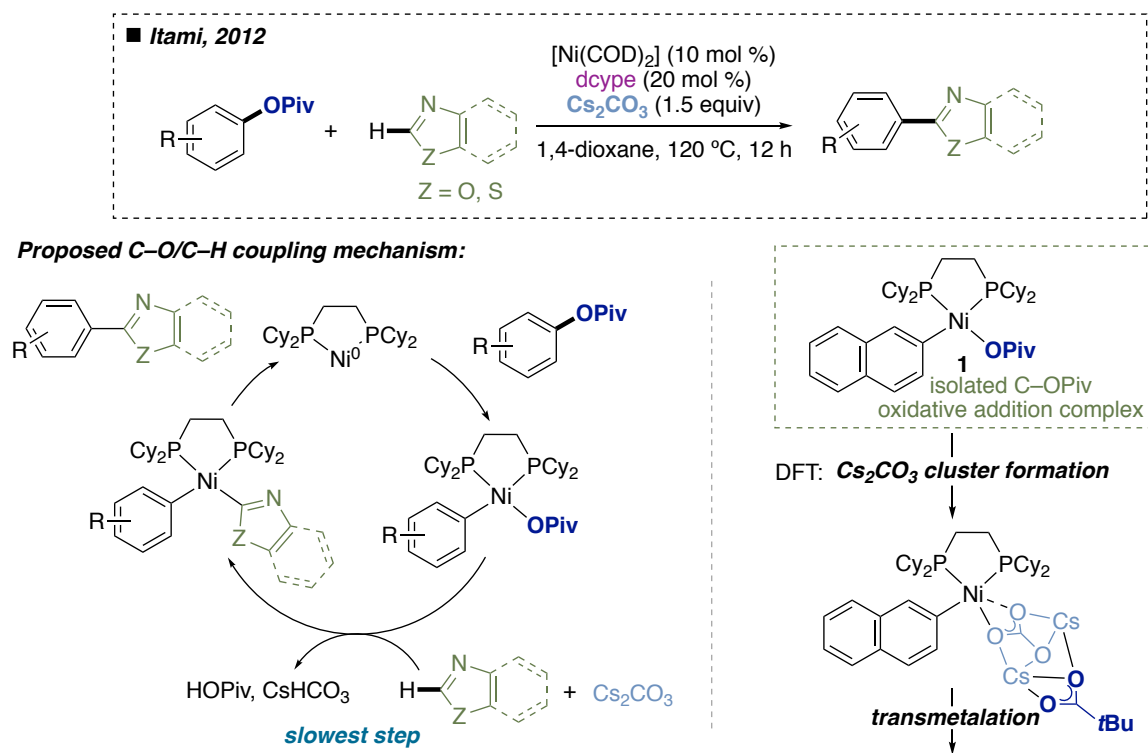
Scheme 2.11. Ni-catalysed C–O/C–H coupling studied experimentally and computationally.

Although monodentate phosphines are employed extensively in C(sp^2)–OPiv functionalisation, no experimental studies had been carried out to study the mechanisms of these methodologies, and no experimental evidence existed to support the identity of the C(sp^2)–OPiv oxidative addition complex as that proposed in computational studies by Liu and Houk. Experimental studies with monodentate phosphines may pose difficulties due to the less rigid coordination of the ligand and greater opportunity for de-coordination and formation of κ^2- or bridged pivalate complexes compared to bidentate ligands such as dcype.[25,26] Furthermore, the investigations carried out by Yamamoto shown in Scheme 2.5 suggest the likelihood of numerous by-products if undesired O–acyl cleavage occurs.[34,35]

2.1.3. Silylation of aryl pivalate esters

Given the lack of mechanistic information about C(sp^2)–OPiv functionalisation with Ni(0)/PR$_3$ and the absence of direct oxidative addition complexes of aryl esters to Ni(0)/PR$_3$, we decided to address this gap in the literature by studying the Ni/PCy$_3$-catalysed silylation of aryl pivalates reported by the Martin group in 2014 (Scheme 2.12).[16]
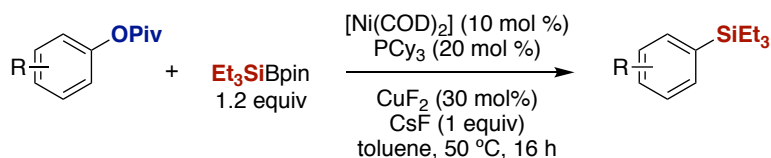
Scheme 2.12. Ni-catalysed silylation of aryl pivalate esters.

Organosilicon compounds are important intermediates in organic synthesis. For example, aryl silanes undergo a variety of transformations including Hiyama and Hiyama-Denmark couplings, *ipso*-halogenation, and *ipso*-borylations.[41] Therefore, the development of a methodology employing catalytic Ni and an abundant phenol-derived electrophile to synthesise useful C(sp^2)–SiR$_3$ compounds provided an appealing alternative to routes such as the reaction of a Grignard reagent with a silyl halide or the Pd-catalysed silylation of aryl halides. While one might argue that rather sophisticated silylboranes such as the Et$_3$SiBpin shown in Scheme 2.13 would find little uptake in silylation techniques, a close inspection into the literature indicates otherwise. Silylboranes have recently emerged as powerful tools for the addition of silyl and/or boryl functional groups via both mono- and difunctionalisation.[42–44] Metal-catalysed methods and transition metal-free methods have been developed and a representative selection of just some of the varied methodologies is shown in Figure 2.2.[16,45–50]
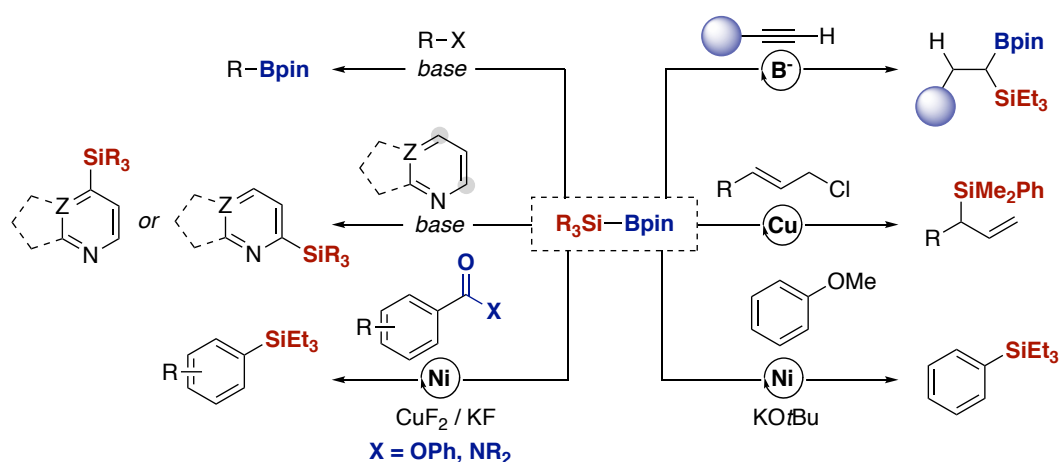
Figure 2.2. Selected examples of functionalisation using a silylborane.[16,45–50]

The first silylborane syntheses were reported by Nöth, wherein a silyl lithium was reacted with a boron electrophile.[51,52] Recognising the interesting properties and synthetic potential of these compounds, Suginome and Hartwig developed two convenient synthetic routes (Scheme 2.13).[53,54] The Et$_3$SiBpin used in the C(sp^2)–O functionalisation under study here is prepared by the Ir-catalysed Si–H borylation method reported by Hartwig.[54] The route developed by Suginome requires the synthesis of the corresponding silyl

lithium, and whereas PhMe₂SiLi can be synthesised from Li metal, Et₃SiLi must be generated by a somewhat less user-friendly Hg–Li exchange.[53,55,56] Undoubtedly, the development of a precious metal-free methodology for the synthesis of Et₃SiBpin would be highly appreciated.
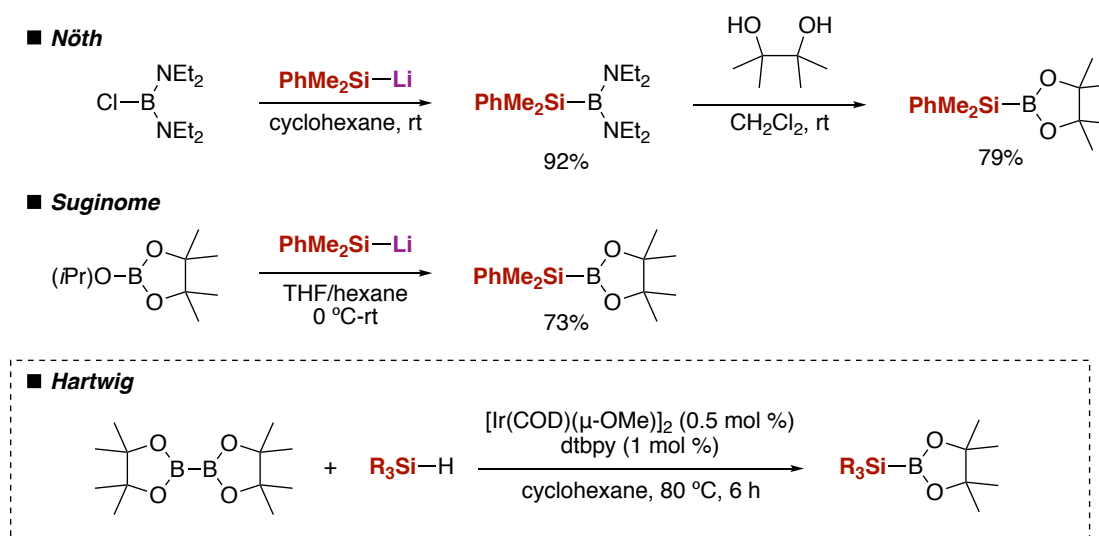
Scheme 2.13. Syntheses of silylboranes.[51–54]

The proposed mechanism for the $C(sp^2)$–OPiv silylation reaction is shown below in Scheme 2.14. It involves the oxidative addition of the $C(sp^2)$–OPiv bond followed by transfer of the silyl group via a Cu cycle.[57] The Si–B bond was proposed to be activated towards reaction with Cu by coordination with CsF. This was based on the very high BDE of a B–F bond of approximately 150 kcal mol⁻¹ [58,59] and on the previous reports by Ito where reaction of methoxide with the Lewis acidic boryl fragment activated the silyl moiety towards further reactivity.[47,60] Oestreich also proposed that during a Cu-catalysed addition of silyl nucleophiles, a Cu(I)–OMe intermediate underwent σ-bond metathesis with Me₂PhSi–Bpin to form the nucleophilic Cu–silyl species.[61]
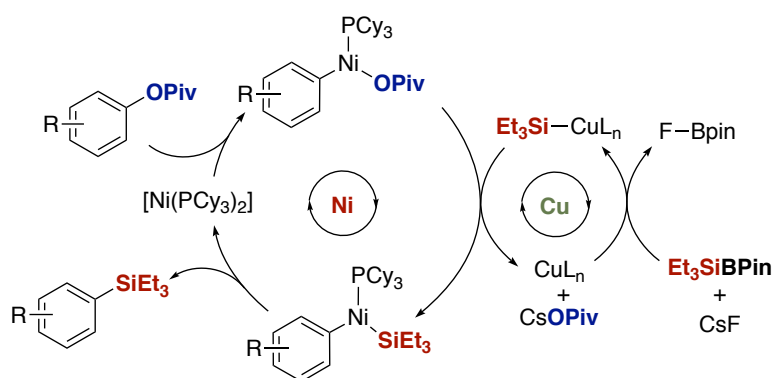
Scheme 2.14. Mechanistic proposal for the Ni/Cu-catalysed $C(sp^2)$–OPiv silylation.

In the years since the Martin group reported the $C(sp^2)$–OPiv silylation reaction, other methodologies have employed similar combinations of Ni catalyst and additive – including substoichiometric Cu(I) or Cu(II) – for related silylation or borylation reactions (Scheme 2.15).[45,62–65]
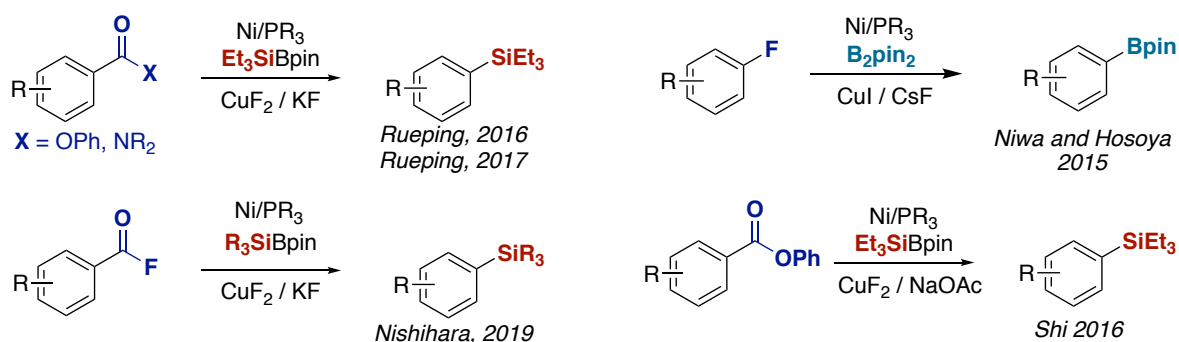
Scheme 2.15. Ni/PCy₃-catalysed methodologies employing a Si–B or B–B reagent alongside CuF₂ and a fluoride salt.[45,62–65]

2.2.   Aims of this project

Prior to our investigations there were many unanswered questions regarding the mechanistic intricacies of C(sp^2)–OPiv functionalisation with Ni(0)/PCy₃. Although Liu and Houk had previously addressed C(sp^2)–OCOR oxidative addition with Ni(0)/PCy₃ computationally (Scheme 2.7), there was no experimental evidence for this step. Furthermore, there was no experimental evidence to support the proposal of a Cu-catalysed silyl transfer cycle. This silylation transformation was therefore employed as a case study for the first mechanistic study on a C(sp^2)–OPiv functionalisation with Ni(0) complexes bearing monodentate PCy₃.

As discussed in Chapter 1, mechanistic studies are important as they facilitate reaction development and refinement. Herein, three experimental sections – oxidative addition, kinetic studies, and stoichiometric experiments are presented with the aim of understanding oxidative addition, the delivery of the SiEt₃ group from Et₃SiBpin to Ni, the role of the CuF₂ and CsF, and, overall, of proposing a mechanism supported by experimental and computational data. The DFT study was carried out by Enrique Gomez-Bengoa at UPV/EHU (San Sebastian).

2.3. Oxidative addition

This study began with an investigation into $C(sp^2)$–OPiv oxidative addition. Oxidative addition was likely to be the first step in the silylation catalytic cycle but oxidative addition intermediates had never been directly confirmed in any Ni(0)/PR$_3$-catalysed $C(sp^2)$–O functionalisation reactions. As mentioned in Section 2.1.1, oxidative addition complexes of aryl esters have only been investigated in a handful of reports. Early reports employed monodentate phosphines but subsequent studies focused exclusively on complexes bearing bidentate phosphines. These recent studies used Ni(0) and direct $C(sp^2)$–O oxidative addition to synthesise the desired complexes,[20–22] whereas early work employed anion metathesis between an Ar–Cl oxidative addition complex and a carboxylate salt.[23–26] During the process of investigating $C(sp^2)$–OPiv oxidation in this work, both synthetic routes were explored. The synthesis of the oxidative addition complex [Ni(σ-1-naphthyl)(κ^1-OPiv)(PCy$_3$)$_2$] (**2**) was initially targeted as 1-naphthyl pivalate is a common model substrate in many $C(sp^2)$–O functionalisation reactions.

2.3.1. Anion metathesis

A stepwise anion metathesis reaction reported by Peregudov and co-workers is the first example of a synthetic route to a σ-aryl carboxylate complex.[25,26] It was therefore chosen as the starting point in efforts towards isolating complex **2** (Scheme 2.16, top). Initial experiments resulted in the disappearance of NMR signals of the [Ni(σ-1-naphthyl)(Cl)(PCy$_3$)$_2$] starting material and the appearance of two broad ^{31}P NMR signals alongside a broadened signal for PCy$_3$. Broadened signals may be attributable to fluxional coordination of the pivalate ligand via either one or both oxygen atoms, so the reaction was tentatively deemed a success. Preliminary assignments of the ^{31}P NMR signals to **2** (δ_P = 8 ppm) and to a monophosphine κ^2-OPiv complex [Ni(σ-1-naphthyl)(κ^2-OPiv)(PCy$_3$)] (**3**) (downfield signal at δ_P = 35 ppm) and were made. Although the evidence for these assignments will be discussed below, the identities of these species were not unambiguously confirmed during the course of this work. The hypotheses discussed in this section became the focus of a project later carried out by Craig Day (PhD student in the Martin group) and were confirmed through the isolation and crystallisation of a range of mononickel κ^1- and κ^2-OPiv complexes.

An alternative route to oxidative addition complexes via the reaction of a Ni–OH complex with a carboxylic acid was next explored.[66] One advantage of this route is that unlike the carboxylate salt the carboxylic acid is completely soluble in THF. This allowed for more flexibility regarding reaction setup (vide infra). The μ$_2$-hydroxo complex [Ni(σ-1-naphthyl)(μ-OH)(PCy$_3$)]$_2$ (**4**) was synthesised following a modified literature procedure then reacted with 1 equivalent of both HOPiv and PCy$_3$ (Scheme 2.16-bottom).[67] An extremely rapid colour change from yellow to orange was observed. The resulting ^{31}P NMR spectrum was compared with that obtained after stepwise anion metathesis and was found to be almost identical (Figure 2.3). This demonstrated that both reaction pathways lead to the same mixture of complexes. As mentioned above, the signals highlighted in grey in both spectra of Figure 2.3 were assigned to the monophosphine κ^2-OPiv complex **3** (δ_P = ca. 34 ppm), free PCy$_3$ (δ_P = 12.8 ppm) and the "classical" square planar diphosphine oxidative addition complex **2** (δ_P = ca. 8 ppm).
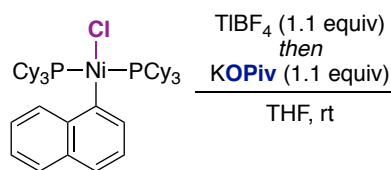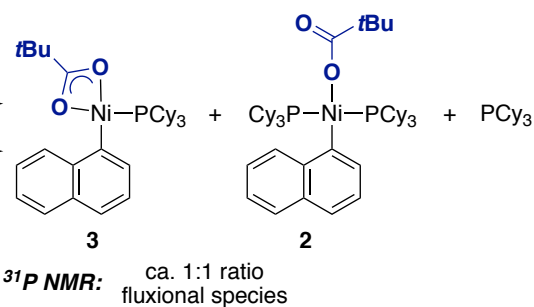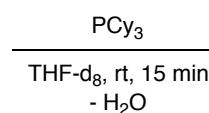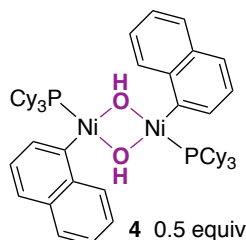
Scheme 2.16. Attempted reactions to form an isolable Ni(II) oxidative addition complex.
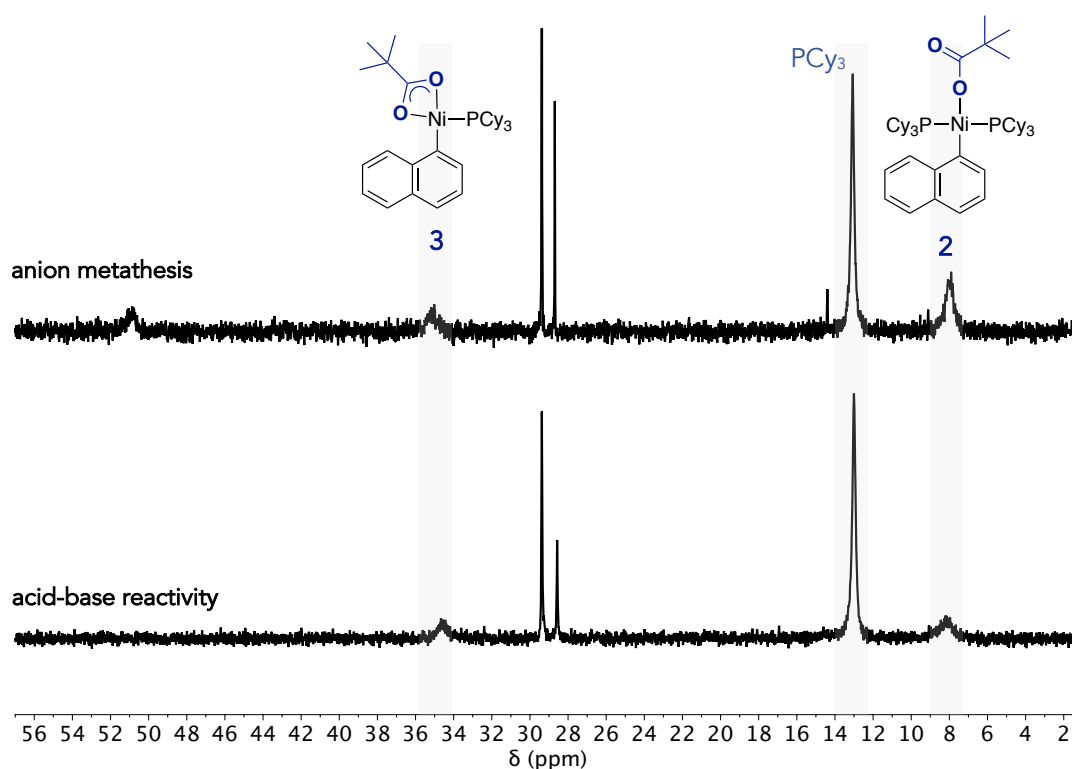
Figure 2.3. Comparisons of ^{31}**P NMR spectra obtained after anion metathesis (top) or after reaction of HOPiv with OH complex 4 (THF-d$_8$) (bottom).**

In order to obtain evidence for this assignment, two experiments were carried out. The first involved the addition of three different carboxylic acids to a solution of **4** and comparison of the resulting ^{31}P NMR spectra with those of Figure 2.3. It was hypothesised that different carboxylic acids would lead to different positions of what was proposed to be an equilibrium between the monophosphine κ^2-carboxylate complex and the diphosphine κ^1-carboxylate. Indeed, different ratios of free PCy$_3$ (δ$_P$ = 12.8 ppm) and ^{31}P NMR

signals in the ranges of 32–36 (κ^2-carboxylate) and 5–10 ppm (κ^1-carboxylate) were observed (Figure 2.4). The hypothesis that the carboxylate ligands were responsible for the different ratios was supported by the observation that the smallest carboxylate ligand – acetate – resulted in a much higher concentration of the presumed κ^1-carboxylate complex ($\delta_P = 8.3$ ppm). The introduction of bulky adamantyl and pivalate ligands both resulted in smaller amounts of the κ^1-carboxylate complex and large amounts of free PCy_3 in comparison. This supported the assignment of the most upfield signals in Figure 2.3 and Figure 2.4.

Strikingly, the addition of trifluoroacetic acid/PCy_3 to **4** showed a single signal at $\delta_P = 9.2$ ppm. Single crystals were directly obtained from this reaction mixture and the formation of the square planar diphosphine κ^1-carboxylate complex [Ni(σ-1-naphthyl)(κ^1-O_2CCF_3)($PCy_3)_2$] (**5**) was confirmed by X-ray diffraction (Figure 2.5). The Ni–κ^1-(O_2CCF_3) bond distance of 1.920(9) Å was comparable to that in **1** (1.919(4) Å). The Ni–naphthyl bond distance (Ni–C1 1.900(7) Å) was slightly longer than those of [Ni(σ-1-naphthyl)(Cl)($PPh_3)_2$] (1.885(4) Å)[68] or [Ni(σ-1-naphthyl)(F)($PCy_3)_2$] (1.8881(16) Å).[69] This complex is the first example of a σ-naphthyl κ^1-carboxylate complex bearing monodentate phosphine ligands and the first new example of a C(sp^2)–O oxidative addition complex bearing monodentate phosphine ligands since the reports by Peregudov et al. in 1988.[25,26]
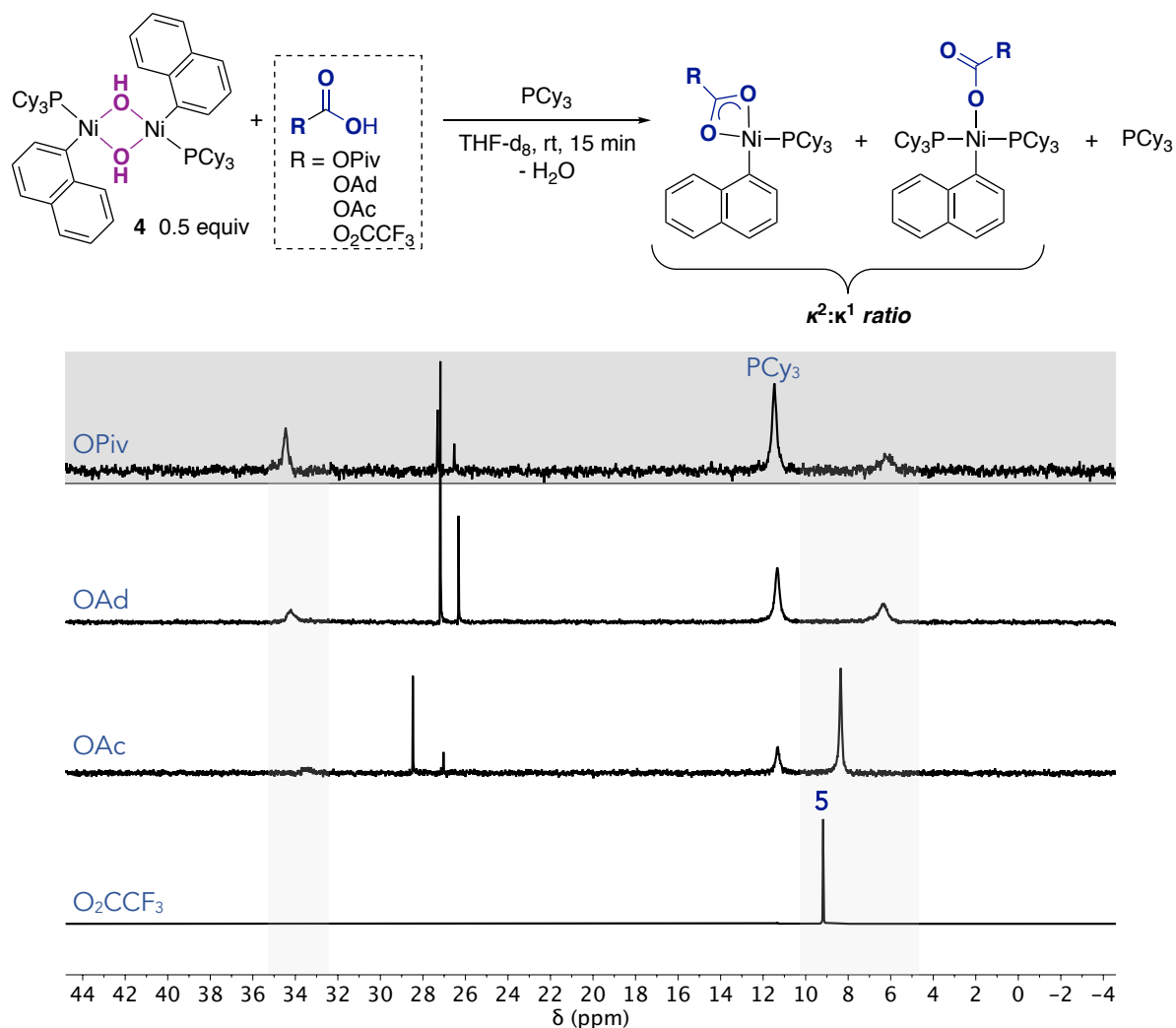
Figure 2.4. ^{31}P NMR spectra resulting from the addition of carboxylic acids to **4**.
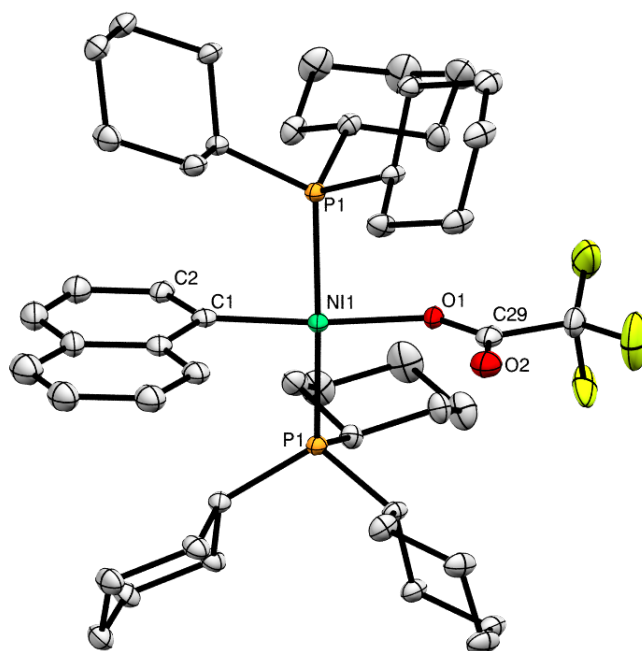
Figure 2.5. X-ray crystal structure of 5 (thermal ellipsoids at the 50% probability level). Hydrogen atoms and a THF molecule have been omitted. The trifluoroacetate, THF, and naphthyl group were disordered.

The ^{31}P NMR spectra of the anion exchange reactions summarised above indicate that, apart from in the synthesis of **5**, at least four Ni complexes are present in the reaction mixtures. Furthermore, analysis of the corresponding ^{1}H NMR spectra showed that small amounts of naphthalene sometimes formed, which hinted that decomposition of the targeted oxidative addition complexes might be occurring. To attempt to control the number of species in solution and slow down decomposition, a low temperature NMR-scale reaction between HOPiv and **4** was carried out. A THF-d_8 solution of **4** and PCy$_3$ (2 equiv) was cooled to below −100 ºC before a solution of HOPiv (2 equiv) was added. The tube was agitated very briefly then the solution analysed by ^{1}H NMR spectroscopy at −80 ºC. Comparison of the resulting ^{1}H NMR and ^{31}P NMR signals with those of naphthyl trifluoroacetate oxidative addition complex **5** showed significant similarities (Figure 2.6). Specifically, the ^{31}P NMR signal of the product of the low temperature reaction at δ_P = 7.56 ppm (−80 ºC), was in the same δ_P = 5–10 ppm range as that of **5**. The aromatic ^{1}H NMR signals of the new complex also closely matched those of **5**. Thus, NMR evidence suggested that **2** can be synthesised at low temperature. Warming of the probe to −10 ºC resulted in the appearance of a broad signal at δ_P = 36 ppm that was assigned to the κ^2-OPiv naphthyl complex **3** by comparison with the spectra in Figure 2.3. By the time the reaction had reached 0 ºC, naphthalene had begun to appear.
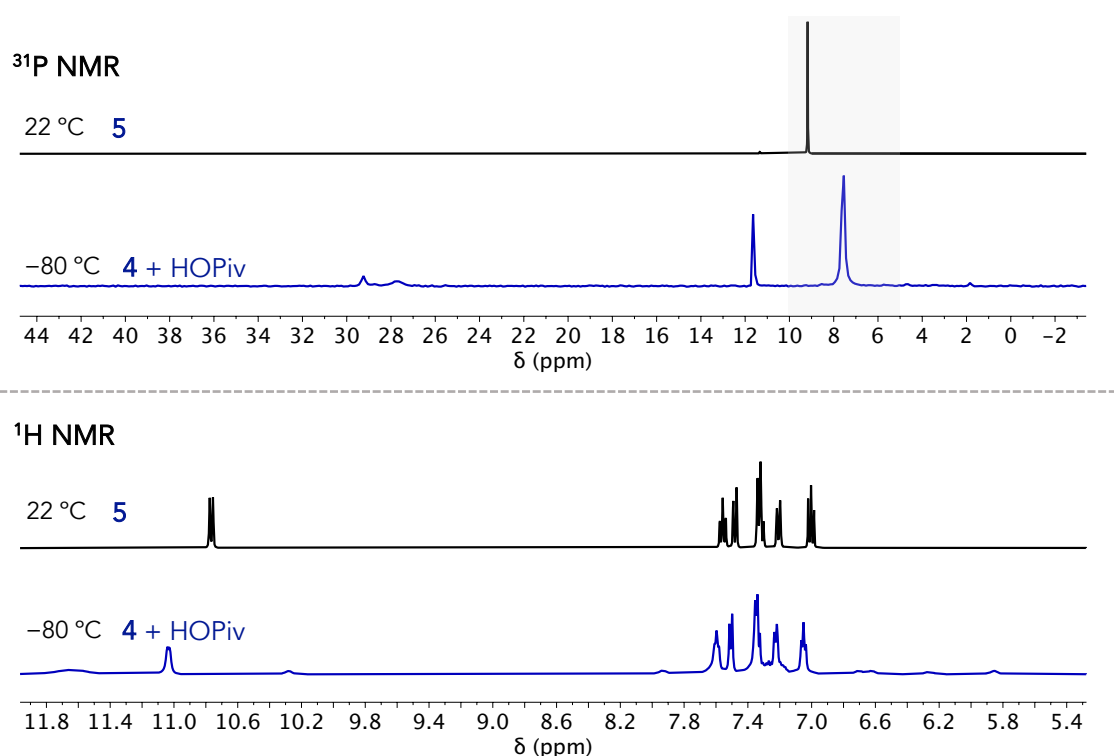
Figure 2.6. Comparison of ¹H NMR (top) and ³¹P NMR (bottom) spectra of 5 (black, room temperature) and low temperature reaction of HOPiv with 4 (blue, −80 °C).

The κ¹-OPiv diphosphine complex **2** was therefore only observed as the major species in this very low temperature reaction. This meant that although the targeted oxidative addition complex had been successfully synthesised, it was very difficult to handle. The tendency for the naphthyl pivalate oxidative addition complex to exist in equilibrium between the κ¹-OPiv and κ²-OPiv forms may be due to the size of the naphthyl and pivalate ligands – loss of one PCy₃ ligand may relieve crowding around Ni.

Overall, none of the syntheses described above resulted in isolated naphthyl pivalate oxidative addition complex. However, the investigation was continued by Craig Day and the choice of different aryl ligands opened up the possibility to isolate and study Ni(II) κ¹-OPiv and κ²-OPiv oxidative addition complexes synthesised in the manners described above.

2.3.2. Direct oxidative addition

Given that the naphthyl carboxylate complexes synthesised via anion metathesis were equilibrium mixtures, hopes that an isolable C(sp^2)–OPiv oxidative addition complex bearing monodentate phosphine ligands might be obtainable were pinned on the direct reaction between a Ni(0) source and an aryl ester. Although equilibrium mixtures might indeed be expected given that the resulting products should be the same as those described in Section 2.3.1, it was important to investigate this synthetic route due to the dearth of information about naphthyl carboxylate complexes and their roles in catalysis. Direct oxidative addition was used by both Itami and Love in the synthesis of oxidative addition complexes bearing bidentate ligands.[20,70] It is worth noting, however, that 2,2'-binaphthyl was obtained by Itami when bidentate dcype was substituted by PCy₃.

Keeping Itami's unsuccessful direct reaction in mind, this investigation began by lowering to ca. 25 ºC the temperature of the reactions between naphthyl pivalate **6a** or **6b** and [Ni(COD)$_2$]/PCy$_3$. Gratifyingly, controllable reactivity *was* observed at this temperature for both substrates and, furthermore, no biaryls or equilibrium mixtures were formed. The reaction between **6a** and [Ni(COD)$_2$]/PCy$_3$ is summarised in Scheme 2.17. After 5 h, 10% conversion of **6a** was observed and a new ^{31}P NMR signal had appeared at δ_P = 24.8 ppm. This was accompanied by new and very distinctive aromatic signals in the ^{1}H NMR spectrum. The ^{1}H NMR signal at δ_H = 10.4 ppm was reminiscent of a signal found for the naphthyl ligand of a square planar Ni(II) oxidative addition complex such as **5** (δ_H = 10.8, THF-d$_8$), [Ni(σ-1-naphthyl)(Cl)(PCy$_3$)$_2$] (δ_H = 10.2, CDCl$_3$)[71] or [Ni (σ-1-naphthyl)(F)(PCy$_3$)$_2$] (δ_H = 9.9, THF-d$_8$).[69] However, the rather upfield aromatic signal at δ_H = 5.6 ppm indicated that unexpected η^2-arene coordination might also be also present.[72,73] The hallmarks of two somewhat disparate modes of interaction might therefore suggest that these signals are part of different Ni complexes. However, a ^{1}H–^{31}P HMBC experiment showed that the two signals at δ_H = 10.4 ppm and δ_H = 5.6 ppm are correlated with the singlet at δ_P = 24.8 ppm. This confirmed the presence of a single, unusual, Cy$_3$P–Ni–naphthyl moiety.
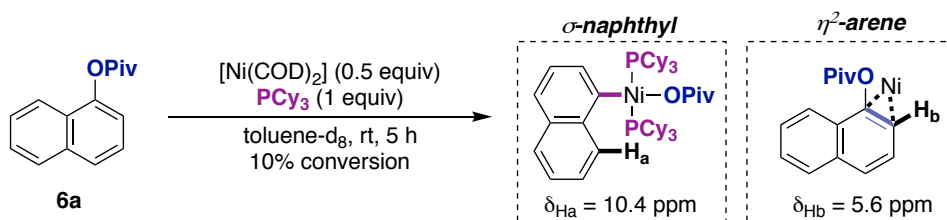
Scheme 2.17. Reaction of 6a with Ni(0)/PCy$_3$ and ^{1}H NMR data supporting a Ni-naphthyl bond.

The reaction was then heated to 50 ºC – the temperature of the catalytic reaction – to try to increase conversion of **6a**. Prolonged heating at this temperature did indeed result in the formation of 1,1'-binaphthalene and by-products that will be discussed below. However, optimisation of the reaction conditions allowed for the successful isolation of an unconventional dinickel oxidative addition complex **7a** in 50% yield (Scheme 2.18). Recrystallisation of the green highly air-sensitive powder from toluene/pentane at −30 ºC provided single crystals of **7a** that were suitable for X-ray diffraction (Figure 2.7). This confirmed that, indeed, both the σ-naphthyl (1.857(6) Å) and η^2 interactions indicated by the ^{1}H NMR shifts were present. The C1–C2 bond distance was lengthened quite significantly from that in **5**. That in **5** is comparable to that in naphthalene (1.377(10) Å vs ca. 1.37 Å),[74] whereas the C1–C2 bond in **7a** was lengthened to 1.409(8) Å due to backdonation from filled d orbitals at Ni into the π^* orbital and donation from the naphthyl π system to the Ni atom.

The Ni–Ni distance of 2.3949(9) Å is consistent with there being a bonding interaction between the two Ni atoms,[75–79] and completing the dinickel complex is a bridging pivalate ligand with Ni1–O1 and Ni2–O2 bond distances that are equivalent within 3σ (1.951(4) and 1.948(4) Å, respectively). In order to determine whether the Ni–Ni bond is polarised, NBO analysis of the optimised structure of **7a** was carried out. This showed a symmetrical distribution of charge at the Ni–Ni core. The two Ni atoms bear similar positive charges (+0.16 and +0.15) and the two oxygen atoms in the bridging pivalate ligand bear comparable negative charges (−0.69 and −0.68).
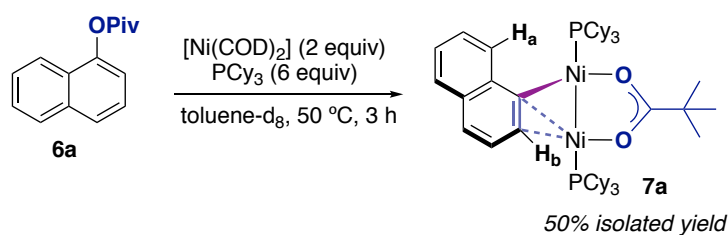
Scheme 2.18. Preparation of dinickel oxidative addition complex 7a.
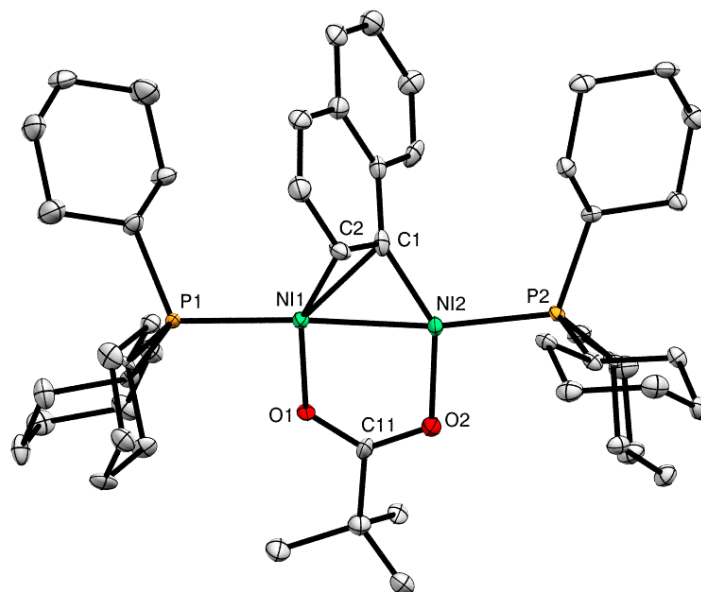
Figure 2.7. X-ray crystal structure of 7a (thermal ellipsoids at the 50% probability level). Hydrogen atoms have been omitted. The *t*Bu group is disordered over two positions (70:30 ratio), with the major orientation shown.

Complex **7a** is the first example of an isolated oxidative addition complex obtained from the direct reaction of Ni(0)/PR₃ with an aryl ester. Additionally, it is a new member of the small class of dinickel complexes that contain a σ-arene ligand that also binds via a π-interaction to another metal centre (Figure 2.8).[75,76,78,80–84] The two dinickel complexes in Figure 2.8 that were reported by the Matsubara group are worth highlighting as alongside the similar (μ-η²-arene) core they have a similar linear L–Ni–Ni–L geometry and Ni–Ni bond distance (2.3954(5) Å) to **7a**.[84] These dinickel NHC complexes were discovered during an investigation into the Ni-catalysed Kumada-Tamao-Corriu cross-coupling of aryl halides and were proposed to be important intermediates within the catalytic cycle.
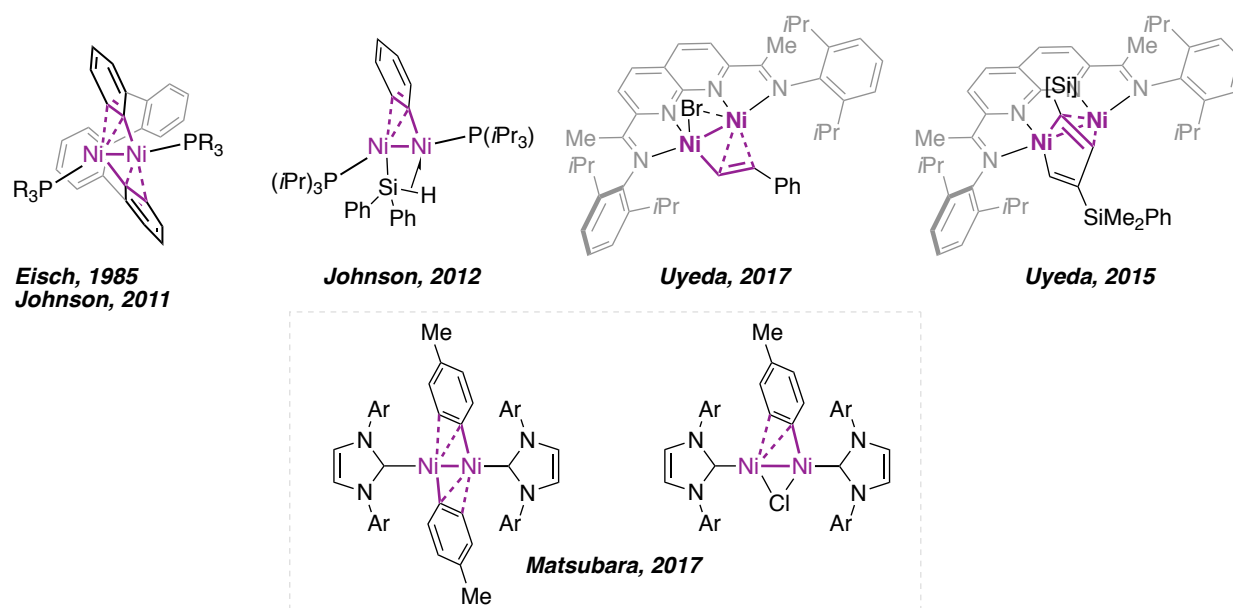
Figure 2.8. Examples of dinickel complexes containing a (μ-η²-arene).[75,76,81–84]

As shown in Figure 2.9, the $^{31}P\{^1H\}$ NMR spectrum of **7a** is temperature-dependent. At room temperature, a singlet is observed. Even though there is no mirror plane perpendicular to the Ni–Ni bond in the X-ray structure, the presence of a singlet was ascribed to rapid exchange of the Ni–naphthyl interactions between the two Ni atoms (Scheme 2.19). With such a process occurring, a PCy₃ ligand coordinated to the Ni atom bearing the σ-arene interaction (shown in red in Scheme 2.19) would not be distinguishable from that coordinated to the second Ni atom.

When the toluene-d₈ solution of **7a** was cooled, the singlet broadened until coalescence occurred near −40 ℃. Two broad signals then appeared at $\delta_P = 33.0$ and $\delta_P = 16.4$ ppm. These sharpened with decreasing temperature, consistent with a slowing of the fluxional behaviour and an approach to the solid-state structure where the two PCy₃ ligands are inequivalent. Between −60 ℃ and −80 ℃ the upfield signal did not sharpen as much as the downfield signal. A possible explanation for this is that the phosphine responsible for this signal is coordinated to the Ni atom that is taking part in the η² interaction: this interaction is likely weaker than the σ-bond and therefore might still take part in a rapid fluxional process at −80 ℃.
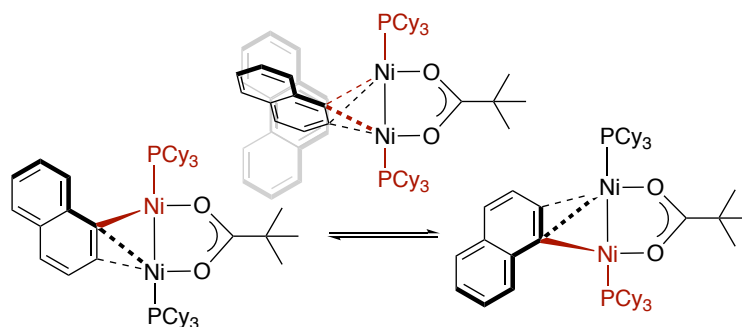
Scheme 2.19. Schematic of fluxional Ni-σ-naphthyl interaction in 7a.
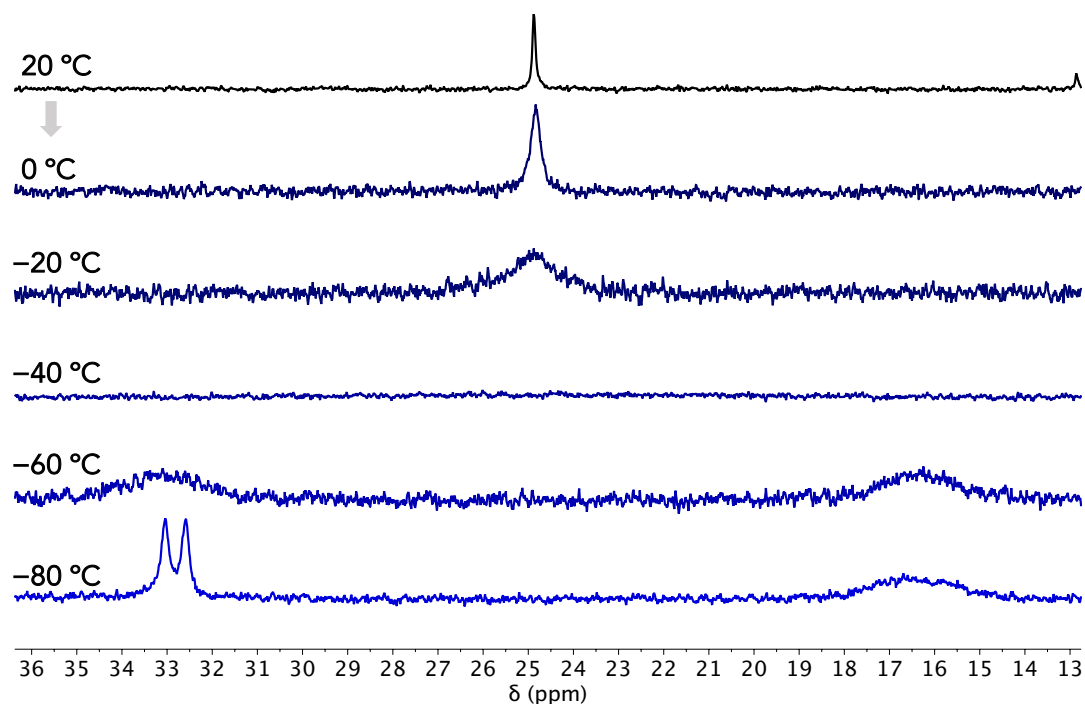
Figure 2.9. Change in the ^{31}P{^{1}H} NMR spectrum when a sample of 7a was cooled from +20 °C (top) to −80 °C (toluene-d$_8$).

Formation of unconventional oxidative addition complex **7a** may be explained by an initial oxidative addition to give a mononickel complex followed by rapid reaction with unreacted Ni(0). Specifically, oxidative addition of the aryl pivalate to Ni(0)/PCy$_3$ – first described computationally by Liu and co-workers[28] – may result in mononickel species **3**. This complex has been proposed to form during the anion metathesis reactions described previously in this Chapter (Section 2.3.1). In close proximity to an electron-rich Ni(0) complex such as [(PCy$_3$)Ni(toluene)][85] or [Ni(0)(PCy$_3$)(**6a**)], electron transfer could then occur to form a Ni–Ni bond. This hypothesis was based on a comproportionation mechanism proposed by Balcells and Hazari for a related reaction at a Ni(II) centre supported by a diphosphine ligand (Scheme 2.20).[86] The calculated mechanism suggested that prior to spin crossover the Ni(0) complex coordinates to one of the aryl substituents of the dppf ligand (dppf = 1,1'-bis(diphenylphosphino)ferrocene). In the case of **7a**, Ni(0) would be coordinated to the σ-naphthyl ligand.

Overall, this mechanistic hypothesis could be tested by the synthesis of a mononickel oxidative addition complex followed by the addition of a Ni(0) complex. Although the choice of a σ-naphthyl ligand only gave mixtures of the κ^2- and κ^1-pivalate complexes **3** and **2** when the synthesis of a mononickel complex was investigated, a different choice of aryl ligand might have resulted in a successful synthesis of an isolable mononickel complex.
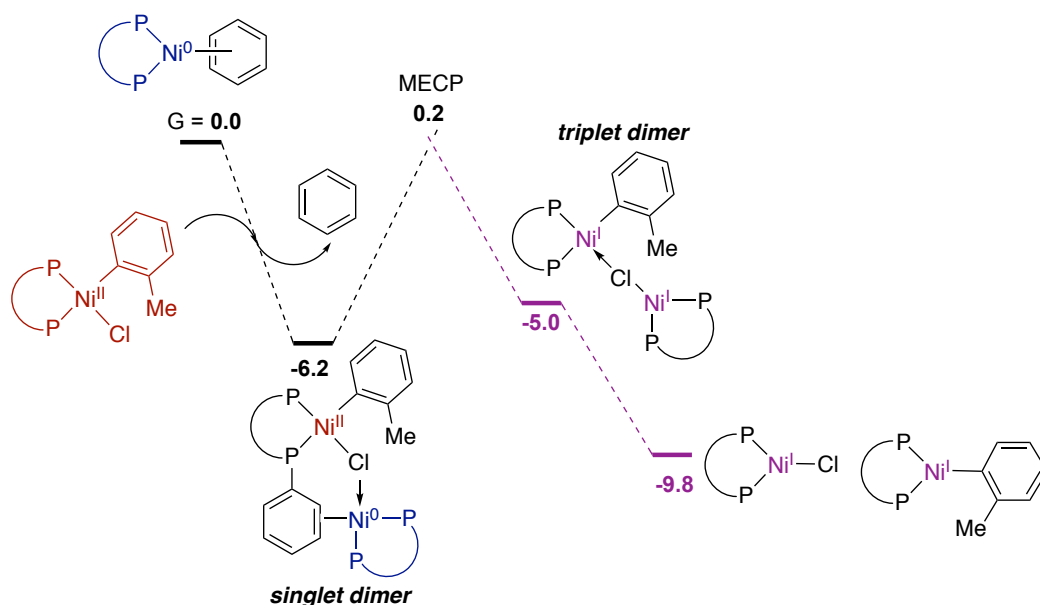
Scheme 2.20. Proposed mechanism for comproportionation between Ni(II) and Ni(0) complexes facilitated by coordination of Ni(0) to dppf. MECP = minimum energy crossing point between singlet and triplet surfaces.[86]

With a synthetic route to **7a** in hand, the Ni(0) precursor was exchanged for COD-free $[Ni(PCy_3)_2]_2N_2$. This precursor acts as a source of $[(PCy_3)Ni(\eta^6\text{-arene})] + PCy_3$ when the reaction is carried out in an arene solvent.[85] The subsequent oxidative addition reaction was much faster as COD dissociation was no longer required: full conversion of **6a** to **7a** was obtained within 15 minutes at room temperature (Scheme 2.21). The reaction was so rapid that when the oxidative addition reaction was monitored by ^1H NMR spectroscopy starting from −40 ºC, **7a** signals began to appear at 0 ºC. This very low temperature C(sp^2)–O cleavage reaction contrasts with the high temperature necessary to synthesise Itami's [Ni(σ-2-naphthyl)(κ^1-OPiv)(dcype)] (**1**).[20] Overall, the reactions summarised above with both $[Ni(COD)_2]$ and $[Ni(PCy_3)_2]_2N_2$ suggest that oxidative addition may not be involved in the rate limiting process(es) of the silylation reaction.
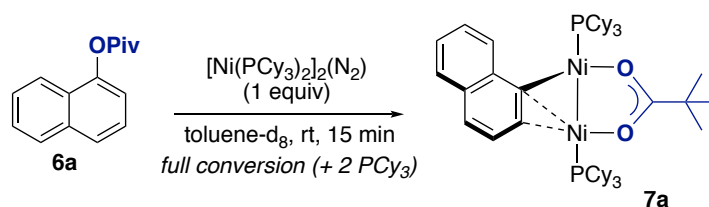
Scheme 2.21. Rapid reaction between 6a and [Ni(PCy₃)₂]₂N₂.

Returning to the optimised synthesis of **7a** summarised in Scheme 2.18, it is important to highlight the moderate yield of 50%. In this synthesis it was not a case of that the yield is reasonably low because it is difficult to isolate the complex; instead, it was found that reactions between **6a** or **6b** and $[Ni(COD)_2]/PCy_3$ do not go to completion. Extended heating at 50 ºC only served to form binaphthalene and increase the intensity of broad signals at $\delta_H = 3.44$, −0.84, and −1.92 ppm (toluene-d_8). A reaction

time of 3 h was chosen as a compromise between obtaining as much conversion of **6a** to **7a** as possible without forming significant amounts of decomposition by-products. After prolonged periods of heating, large green crystals grew from the toluene reaction mixture. These were identified as a nickel(II) paddlewheel complex [Ni₂(μ-OPiv)₄(PCy₃)₂] (**8**) (Scheme 2.22, right). The Ni–Ni distance of 2.7364(2) Å is significantly longer than that in **7a**. Analysis by SQUID magnetometry revealed antiferromagnetic coupling between the high spin square pyramidal nickel centres. The formation of **8** and 1,1'-binaphthalene was also detected by ¹H NMR upon heating **7a** to 100 ºC. It is important to note that silylated product **9a** was obtained in an 18% yield when **8** was used as a precatalyst (10 mol % Ni).
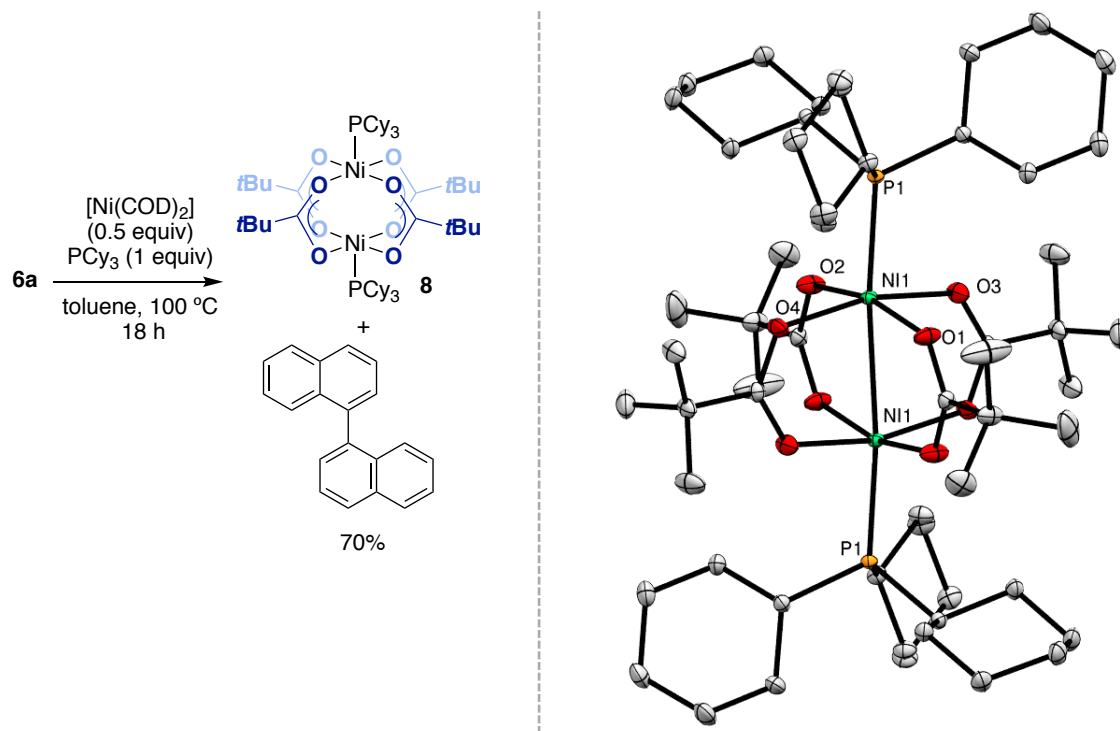
Scheme 2.22. Synthesis and ORTEP diagram of 8 (thermal ellipsoids at the 50% probability level). Hydrogen atoms have been omitted.

In the course of optimising the reaction time to obtain a synthetic route to isolable **7a**, NMR monitoring reactions were carried out. During one such experiment, ¹H NMR signals of 1,3-cyclooctadiene and 1,4-cyclooctadiene were detected alongside the formation of **7a** (Figure 2.10).[87] This is consistent with Yamamoto's observation of 1,5-cyclooctadiene isomers after the reaction between [Ni(COD)₂], a monodentate phosphine, and an aryl ester.[34,35] Isomerisation of the 1,5-cyclooctadiene introduced through the use of [Ni(COD)₂] as the Ni(0) source may therefore be a common off-cycle process (necessarily involving Ni–H intermediates) that should be kept in mind when this precatalyst is used.[88]
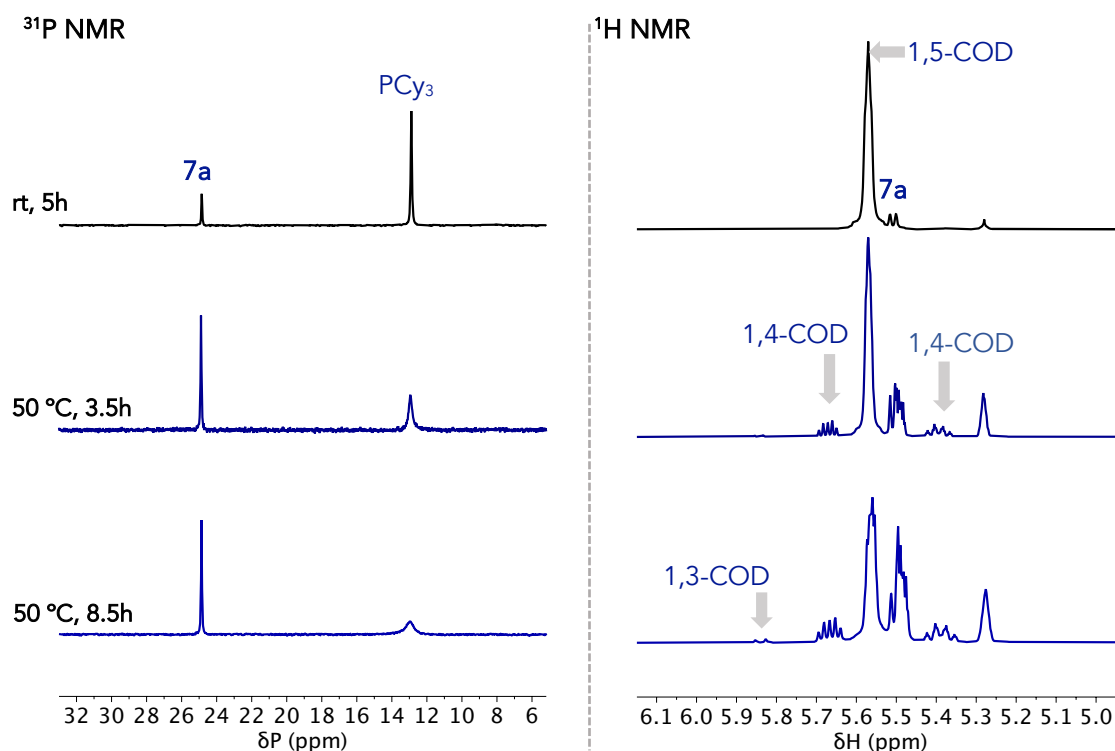
Figure 2.10. Reaction of 6a with [Ni(COD)$_2$]/PCy$_3$ (toluene-d$_8$). ^{31}P NMR and ^{1}H NMR spectra showing conversion to 7a and the appearance of COD isomers.

Alongside COD isomers, binaphthalene, and **8**, traces of products presumably derived from O–acyl bond cleavage were observed. When O–acyl cleavage occurs, the resulting acyl and alkoxide ligands can undergo decomposition. As mentioned previously, this was studied by Yamamoto in early work that laid important groundwork for the Ni-catalysed C–O functionalisation field.[34] One hallmark of Ni–acyl decomposition was found to be the formation of carbonyl complexes. Carbonyl complex [Ni(PCy$_3$)$_2$(CO)] was formed during the synthesis of **7a** and is labelled in Figure 2.11 at δ_P = 37.2 ppm (toluene-d$_8$, lit: δ_P = 37.5[89]). The signal at δ_P = 43.7 ppm was assigned to the unusual Ni cluster [Ni(O)PCy$_3$]$_4$. This complex was first reported by Ogoshi in a reaction between Ni(0) and aldehydes and was later invoked by Love as a possible decomposition product in reactions of Ni(0) with aryl esters.[70,90]
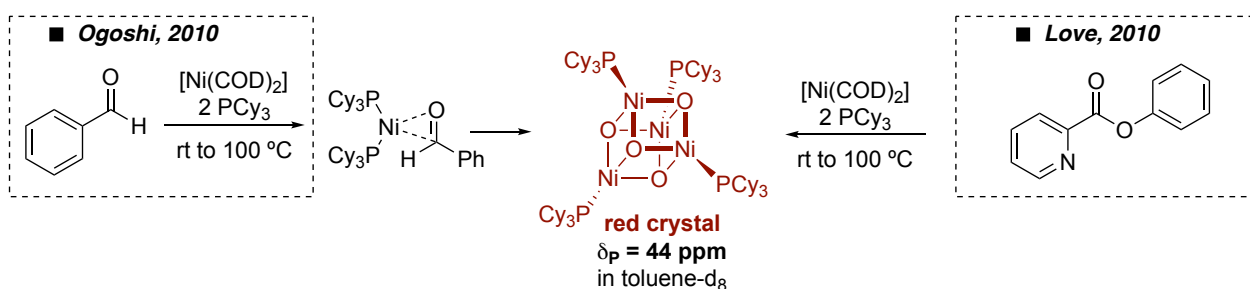
Scheme 2.23. Reported syntheses of unusual C–O cleavage by-product [Ni(O)PCy$_3$]$_4$.[70,90]
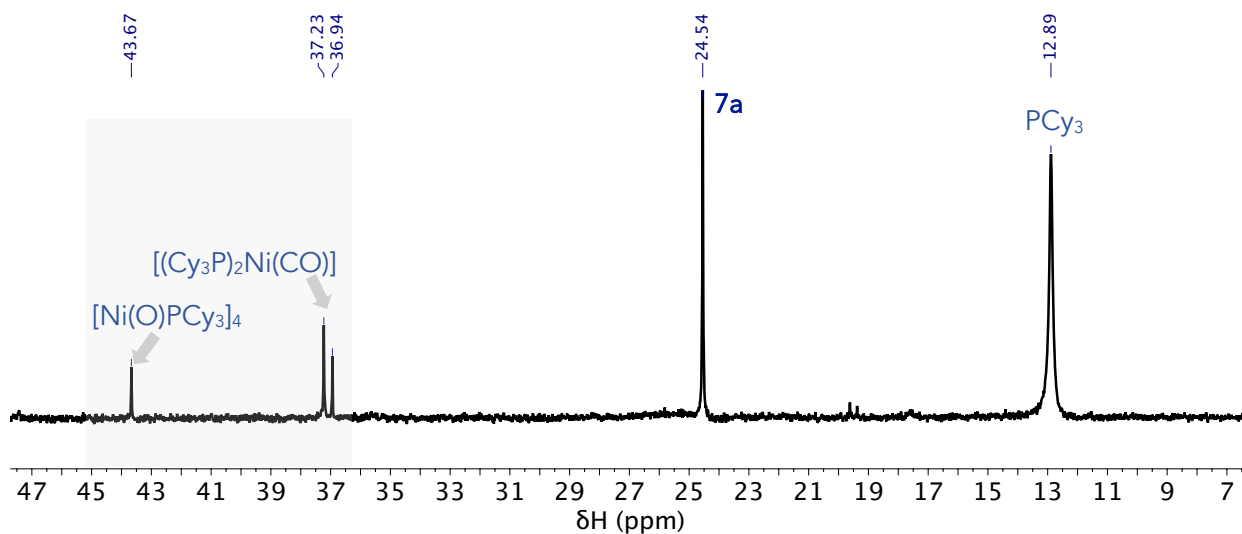
Figure 2.11. Reaction of 6a with Ni(COD)₂/PCy₃ (toluene-d₈, 50 °C) after 15.5 h. O–Acyl cleavage-derived products highlighted in grey.

2.3.3. Other dinickel oxidative addition complexes

Given the smooth synthesis of **7a** shown in Scheme 2.21, [Ni(PCy₃)₂]₂(N₂) was next reacted with naphthyl pivalates **6b–e** (Scheme 2.24). These reactions gave dinickel oxidative addition complexes **7b–e** in good NMR yields. Although no crystals of these complexes were obtained, the presence of the dinickel(μ-η²-arene) core was confirmed by ¹³C{¹H} NMR spectroscopy. The Ni–(σ-naphthyl) *ipso* carbon (δ_C = 143–150 ppm, $^2J_{P\text{-}C}$ triplet) and the carbonyl carbon of the μ-OPiv ligand (δ_C = 195–196 ppm, $^3J_{P\text{-}C}$ triplet) are distinctive to this interaction (Figure 2.12. and Figure 2.13). Without the dinickel(μ-η²-arene) core, the ¹³C chemical shifts and ³¹P–¹³C coupling constants should differ significantly from those of **7a**; instead, they are all within a narrow range. For example, the ¹³C NMR chemical shift of the OPiv carbonyl carbon in each complex is within 1 ppm of that of **7a** (Figure 2.12).

Substrates **6c** and **6d** were not included in the substrate scope of the reported reaction so were subjected to the standard silylation conditions to ensure they are relevant substrates in C(*sp²*)–O silylation. In all cases, the silylated product was obtained. For naphthyl ester **6d**, co-elution of the reduced product during column chromatography precluded isolation of pure **9d** (pentane R_f = 0.73). The C(*sp²*)–O bond is rather hindered, which might slow down transmetalation and allow undesired reactivity to occur.

Substrates **6a–e** are all extended π-systems and are usually more reactive in C(*sp²*)–O functionalisation than phenyl derivatives. It was therefore interesting to test whether phenyl pivalate (**6f**) would also undergo oxidative addition to form a dinickel complex. Reaction of **6f** with [Ni(PCy₃)₂]₂(N₂) was slow, and after 1 h at room temperature, the ³¹P NMR spectrum showed that [(PCy₃)Ni(toluene)] and free PCy₃ were the major species in solution. A broad signal at δ_P = 33 ppm was tentatively assigned to the [(PCy₃)Ni(**6f**)] adduct. After 2 h, a small signal had appeared that was consistent with a dinickel oxidative addition complex (**7f**, 18% yield).
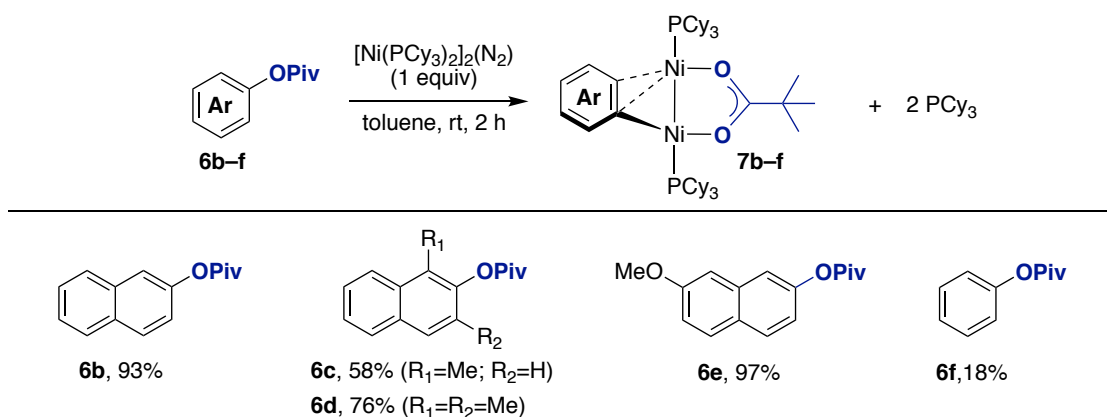
Scheme 2.24. In situ synthesis of dinickel oxidative addition complexes 7b–f.
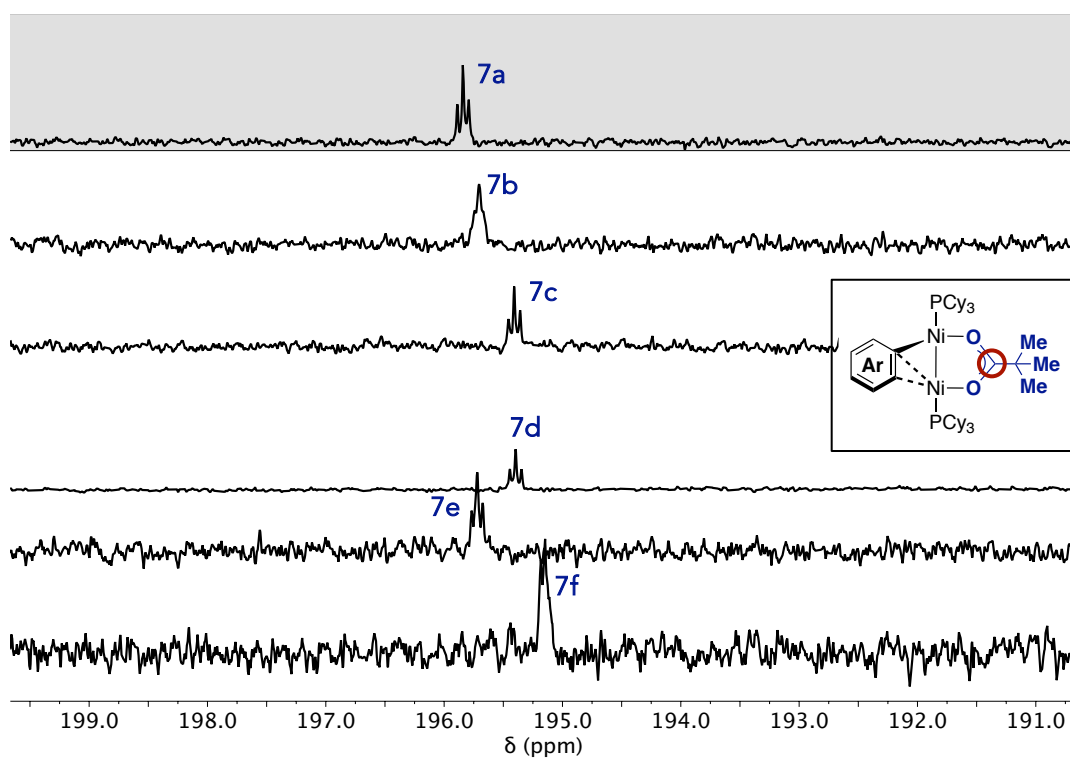
Figure 2.12. Comparison of $^{13}C\{^1H\}$ NMR spectra (191–200 ppm) of Ni–Ni complexes 7a–f derived from aryl pivalates 6a–f (from top to bottom).
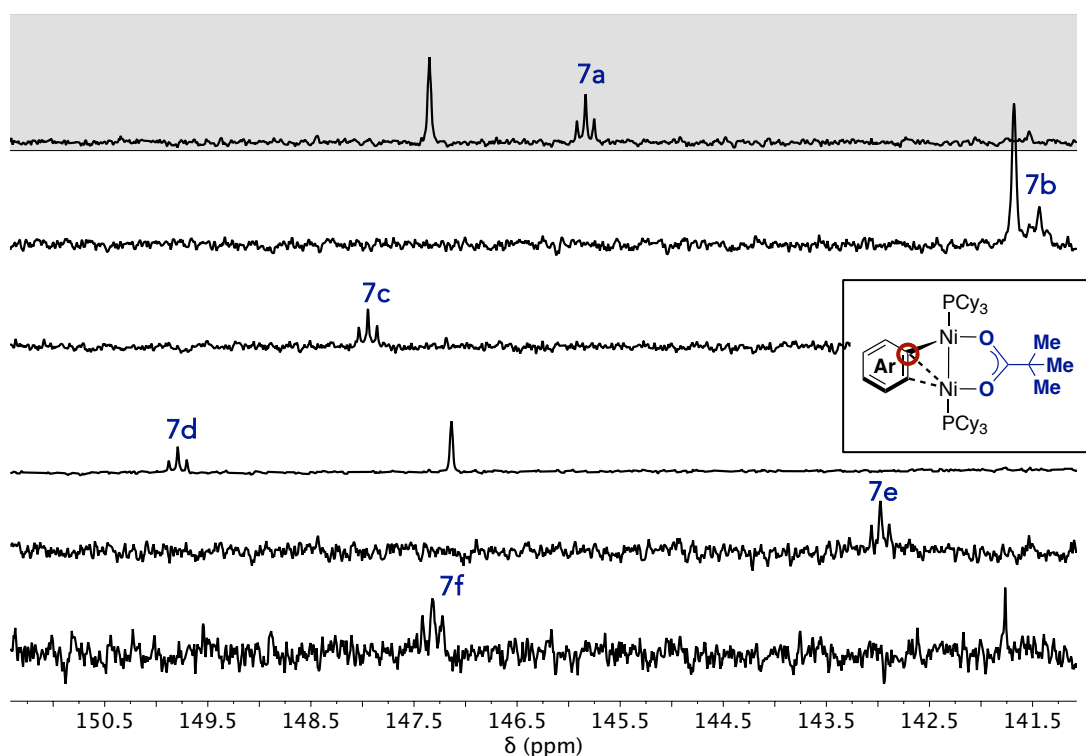
Figure 2.13. Comparison of ¹³C{¹H} NMR spectra (141–151 ppm) of dinickel complexes 7a–f derived from aryl pivalates 6a–f (from top to bottom).

2.4.   Relevance of Ni–Ni complexes in catalytic silylation

The results discussed above demonstrate that direct oxidation addition of a naphthyl pivalate ester to a Ni(0) complex bearing PCy₃ forms an unusual dinickel complex rather than a more "classical" mononickel κ^1- or κ^2-carboxylate complex. This investigation marked the first time that such a complex had been isolated and characterised and therefore was already of interest to the C(*sp²*)–O functionalisation community. Whether it was relevant to a catalytic C(*sp²*)–O functionalisation reaction – specifically, Ni-catalysed silylation – is the subject of the subsequent discussion. The possibility for the formation of **7a** during the reaction and its ability to participate in silylation were both assessed.

First, it was established that **7a** could be used as a precatalyst to give **9a** in a comparable yield to that obtained using either [Ni(COD)₂]/PCy₃ or [Ni(PCy₃)₂]₂N₂ (entries 1–4, Table 2.1). This demonstrated its viability as a Ni(0) source under the reaction conditions and suggested that it may participate in the silylation reaction.

Ni (x mol %)
L (y mol %)
CuF$_2$ (30 mol %)

6a + **Et$_3$Si**Bpin $\xrightarrow{\text{CsF (1 equiv.)}}$ **9a**
toluene, 50 °C, 15 h

entry	Ni (x mol %)	L (y mol %)	9a (%)
1	[Ni(COD)$_2$] (10)	PCy$_3$ (10)	69
2	[Ni(COD)$_2$] (10)	PCy$_3$ (20)	67
3	[Ni(PCy$_3$)$_2$]$_2$(N$_2$) (5)	-	73
4	**7a** (5)	-	72

Ni (x mol %)
L (y mol %)
CuF$_2$ (30 mol %)

6b + **Et$_3$Si**Bpin $\xrightarrow{\text{CsF (1 equiv.)}}$ **9b**
toluene, 50 °C, 15 h

entry	Ni (x mol %)	L (y mol %)	9b (%)
5	[Ni(COD)$_2$] (10)	PCy$_3$ (10)	89
6	[Ni(PCy$_3$)$_2$]$_2$(N$_2$) (5)	-	97
7	dinickel **8** (5)	-	18
8	dinickel **8** (10)	-	22

Table 2.1. Silylation of 6a and 6b employing different Ni sources.

Next, the silylation of **6a** was monitored by multinuclear NMR spectroscopy to investigate whether **7a** (or one of the mononickel oxidative addition complexes from Section 2.3.1) was present during the reaction (Figure 2.14). The CsF and CuF$_2$ additives were omitted resulting in a reduced yield of **9a**. Nevertheless, the formation of **7a** and its persistence during the reaction was evident in both the ^{31}P and ^{1}H NMR spectra collected over almost 17 h (red traces in Figure 2.14). This experiment suggested that dinickel complex **7a** is indeed relevant to the catalytic C(sp^2)–O silylation reaction. Consistent with the decomposition noted during the synthesis of **7a** from [Ni(COD)$_2$]/PCy$_3$, the concentration of **7a** decreased slightly throughout the course of the reaction. This is highlighted in Figure 2.14(b) and is plotted in red alongside the formation of 1,1'-binaphthalene (7.5% at 16.7 h).

OPiv

[Ni(COD)$_2$] (10 mol %)
PCy$_3$ (20 mol %)

+ **Et$_3$Si**Bpin $\xrightarrow{\text{toluene-d}_8, 50 \text{ °C, 16.7 h}}$ **SiEt$_3$**
1.1 equiv

6a **9a**
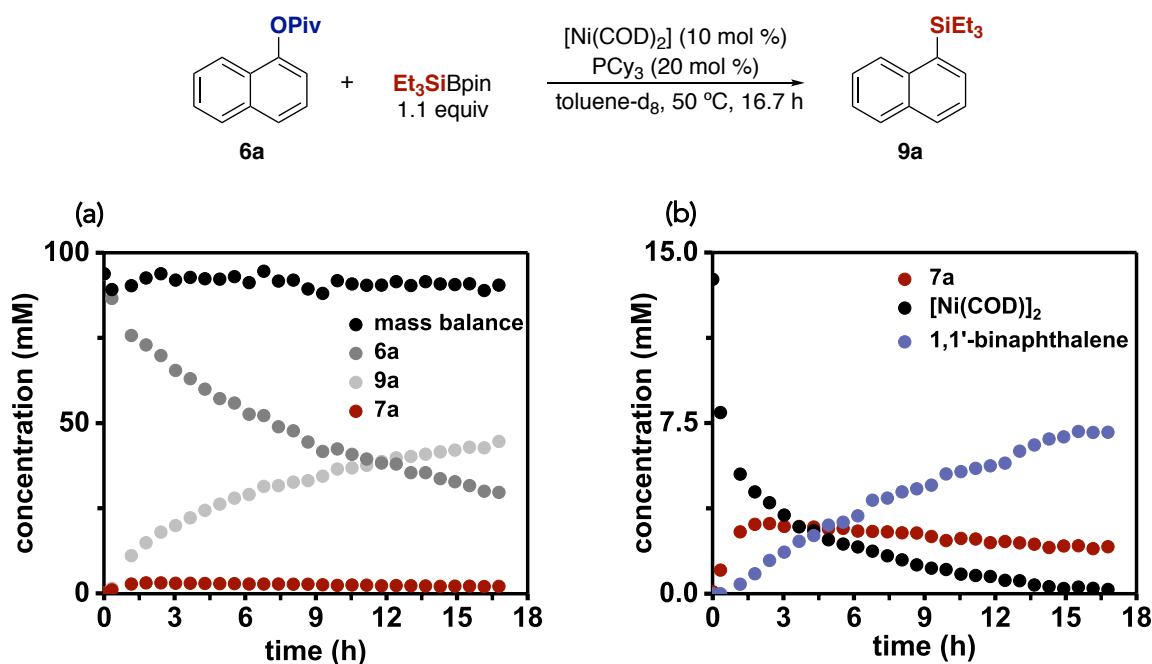
Figure 2.14. ^{1}H NMR monitoring of the CsF/CuF$_2$-free C(sp^2)–O silylation of 6a with Et$_3$SiBpin. Spectra collected every 38 min. [6a]: 0.094 M. (B) is an expansion showing the decrease in the concentration of [Ni(COD)]$_2$ over time, the formation of 1,1'-binaphthalene, and the persistence of 7a.

The same reaction was carried out with isomeric **6b** and it was clear from the ³¹P NMR spectrum that dinickel complex **7b** was present for the duration of the reaction. The ¹H NMR data were not analysed due to the overlap between the signals of **7b**, **6b** and silylated **9b**.

2.5.   Stoichiometric reactivity of 7a

The monitoring experiments described above provide evidence for the presence of dinickel oxidative addition complexes during the reaction. However, they do not directly demonstrate that these complexes take part in productive catalysis. In order to investigate whether this was the case, stoichiometric experiments and, later, kinetic studies were carried out.

2.5.1. Cleavage of the Ni–Ni bond

Preliminary stoichiometric studies were undertaken in order to determine whether reaction of **7a** with Et₃SiBpin can afford silylated **9a**. If so, this would be evidence that the **7a** observed by NMR spectroscopy during catalysis is part of the silylation catalytic cycle. Initially, it was very surprising to observe that stoichiometric reactions between **7a** and Et₃SiBpin did not yield any **9a** at all (Scheme 2.25, top). Even more surprising was that the addition of naphthyl pivalate **6a** to the unsuccessful silylation reactions resulted in the formation of **9a** (Scheme 2.25, bottom).
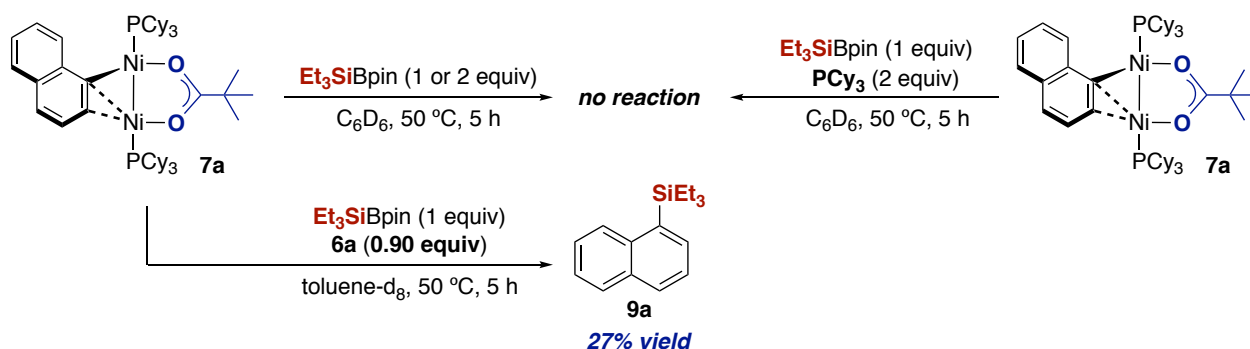
Scheme 2.25. Reactions of 7a with Et₃SiBpin.

The requirement for the presence of **6a** was somewhat intriguing and although it suggested that **7a** was likely to be relevant in catalysis (where there is an excess of **6a** present during most of the reaction) it raised a number of questions. First was obviously why the presence of the substrate unlocks the reactivity of **7a**. Second was how **7a** reacts with **6a** and Et₃SiBpin. Does it react with the Ni–Ni bond intact? Or does the Ni–Ni bond break?

If the Ni–Ni bond breaks, this could occur via three pathways: (a) heterolytic cleavage where two electrons move from one nickel atom to form two charged nickel species (*path 1,* Scheme 2.26); (b) homolytic cleavage of the Ni–Ni bond to give two neutral Ni(I) species (*path 2*); or (c) disproportionation of the Ni–Ni bond giving a Ni(0) and a Ni(II) species (*path 3*).[91,92]
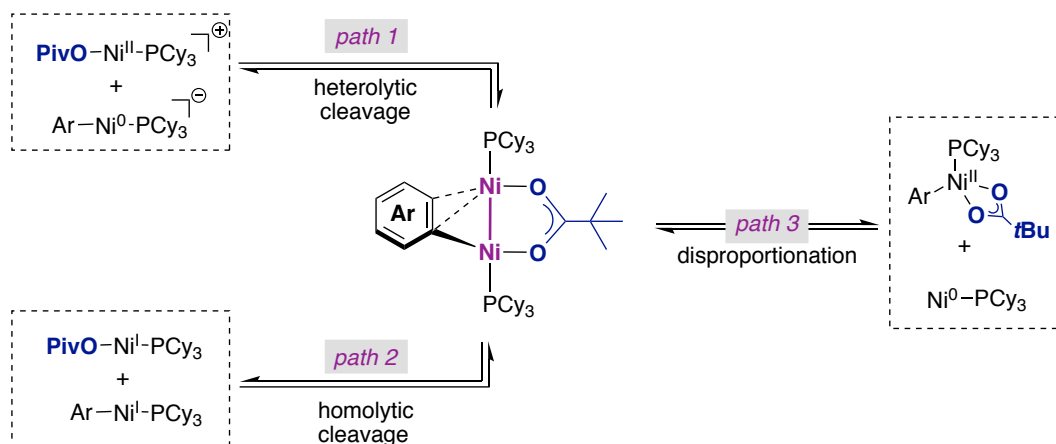
Scheme 2.26. Ni–Ni cleavage pathways.

Knowing that the addition of **6a** to the dinickel oxidative addition complex was necessary for silylation, it is possible to build a hypothesis for how and why **7a** reacts. First, it is important to note that all three cleavage pathways in Scheme 2.26 form Ni species that *might* react with the $C(sp^2)$–O bond. Path 1 forms a Ni(0)-ate complex that might act as a nucleophile; *path 2* forms two complexes that might undergo oxidative addition to **6a** to form Ni(III) species; and finally, *path 3* forms a Ni(0) species that has already been invoked as key to $C(sp^2)$–O bond cleavage.

In reacting with any of these intermediates, **6a** would shift the position of the Ni–Ni cleavage equilibrium. Revisiting the reactions, we see that the first two cleavage pathways form mononickel species that already contain a Ni–Ar bond. Subsequent reaction with **6a** would therefore form Ni(Ar)$_2$ complexes that would likely undergo reductive elimination to form biaryl rather than transmetalation. However, the third pathway – a disproportionation equilibrium – only requires oxidative addition to a Ni(0) complex for the equilibrium to be shifted by added **6a**.

This third pathway therefore became the favoured hypothesis for why the addition of **6a** was necessary (Scheme 2.27). If dinickel complex **7a** exists in equilibrium with Ni(0) and the mononickel oxidative addition complex **3** (with the equilibrium heavily towards **7a**), there will not be a very high concentration of **3** in solution when Et$_3$SiBpin is added. However, if **6a** is added, this will react with Ni(0) and shift the disproportionation equilibrium to increase the concentration of **3**. If mononickel complex **3** is the key intermediate with which transmetalation with Et$_3$SiBpin occurs, then the formation of **9a** would now be possible. Disproportionation reactions for group 10 metal–metal dimers have been reported, supporting this hypothesis. For example, Pfaltz studied Pd–Pd dimers bearing P,N-ligands and demonstrated that their Pd(0) and Pd(II) disproportionation products could be observed by ESI-mass spectrometry.[93]
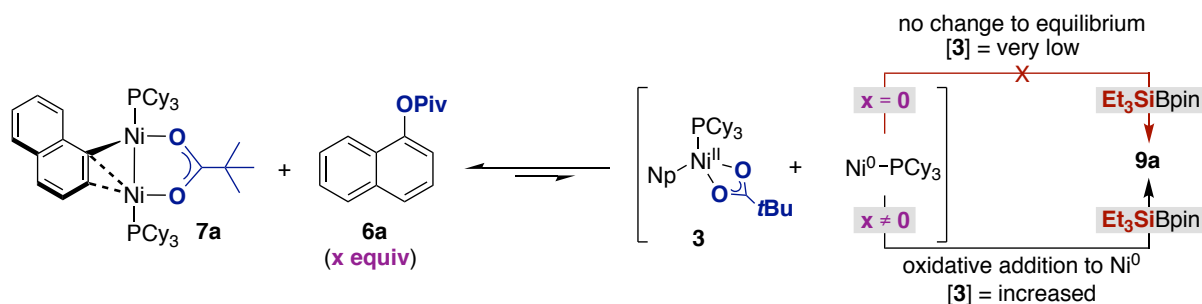
Scheme 2.27. Disproportionation equilibrium and effect of 6a.

To support the hypothesis that disproportionation is the mode of Ni–Ni cleavage, trapping experiments were carried out (Scheme 2.28). It was envisioned that the addition of bidentate dcype would trap the Ni(0) and Ni(II) products of disproportionation as [Ni(0)(dcype)₂] (**10**) and the reported C(*sp²*)– OPiv oxidative addition complex [Ni(σ-2-naphthyl)(κ¹-OPiv)(dcype)] (**1**), respectively.[20] Dinickel complex **7b** was therefore reacted with dcype (3 equiv) at room temperature. After initially turning very dark, the solution lightened over the course of 30 minutes to give a pale orange solution. Analysis by ¹H NMR spectroscopy after 2 h showed full conversion of **7b** and an 83% yield of **1**. As expected, nickel(0) complex **10** was also present.[94,95] Integration of the ³¹P{¹H} NMR spectrum (inverse gated decoupling) gave a 1:2.5 ratio between the signals of **1** and **10** rather than the expected 1:2 ratio. This suggested that some of the Ni–Np bonds originating from the dinickel complex were no longer present and fit with the observation of naphthalene in the ¹H NMR spectrum (not quantified due to overlapping signals). The formation of naphthalene from Ni–(σ-aryl) complexes has been reported.[34] Repeating the trapping experiment with isolated **7a** gave Ni(0) complex **10** and [Ni(σ-1-naphthyl)(κ¹-OPiv)(dcype)] (**11**). Again, naphthalene was formed (30% NMR yield), reducing the amount of **11** relative to **10**. The structure of the isomeric Ni(II) complex was confirmed by X-ray crystallography and NMR spectroscopy (Figure 2.15). The X-ray structure of **11** is similar to that of **1** with Ni–P, Ni–C, and Ni–OPiv distances all comparable.[20] Compared to **1**, the naphthyl and pivalate ligands in **11** point in opposite directions to relieve steric interactions.
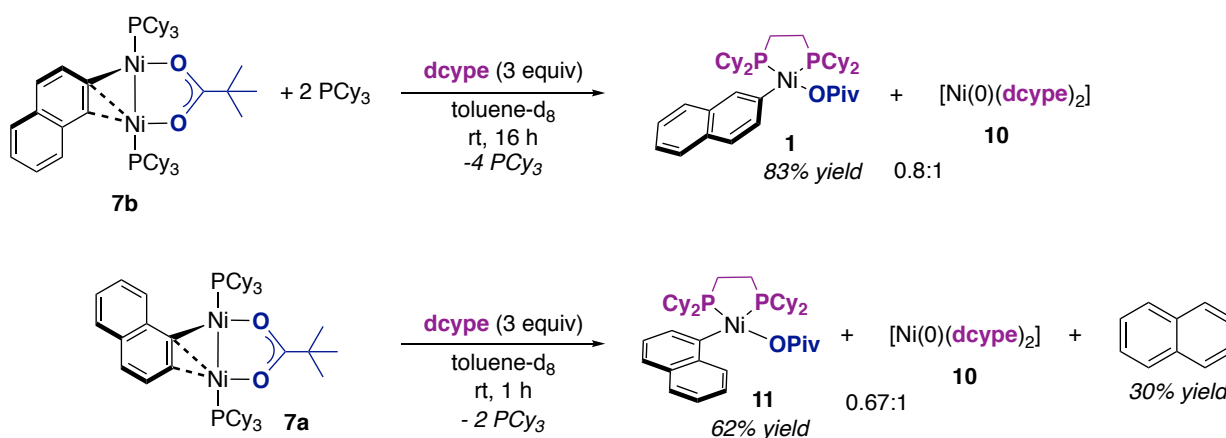
Scheme 2.28. Reactions of dinickel complexes 7a and 7b with dcype.
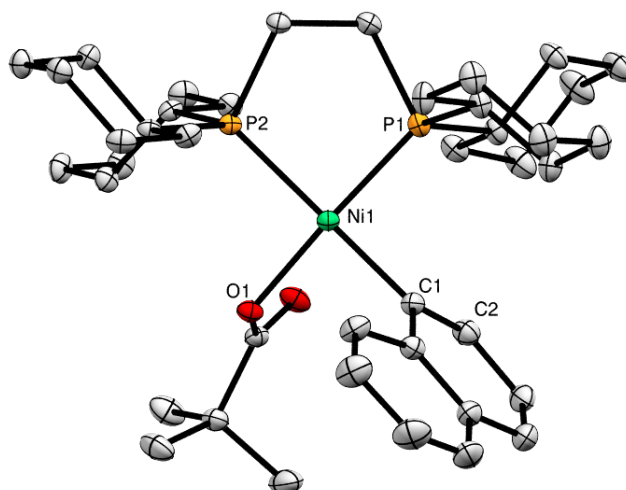
Figure 2.15. ORTEP diagram of 11 (thermal ellipsoids at the 50% probability level). Hydrogen atoms have been omitted. Selected bond distances (Å): Ni1–O1 1.9411(12), Ni1–C1 1.9412(17), C1–C2 1.382(2).

The disproportionation equilibrium was further probed with a crossover experiment (Scheme 2.29). It was hypothesised that if a Ni(0) complex was present during silylation then it could be trapped by a different naphthyl pivalate and form a different dinickel complex that could be identified by NMR spectroscopy. Indeed, when **7a** was reacted with 2-naphthyl pivalate (**6b**) and Et$_3$SiBpin, the isomeric dinickel complex **7b** was observed by NMR spectroscopy alongside silylated products **9a** and **9b** in 25% and 46% yields, respectively.
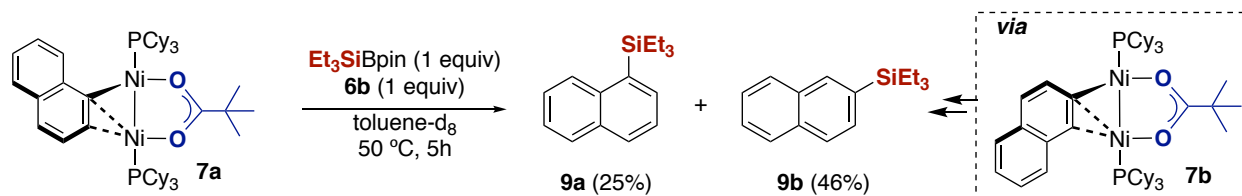
Scheme 2.29. Crossover experiment between 7a and 6b.

Finally, the energy difference between **7a** and the mononickel disproportionation products was calculated (Scheme 2.30).
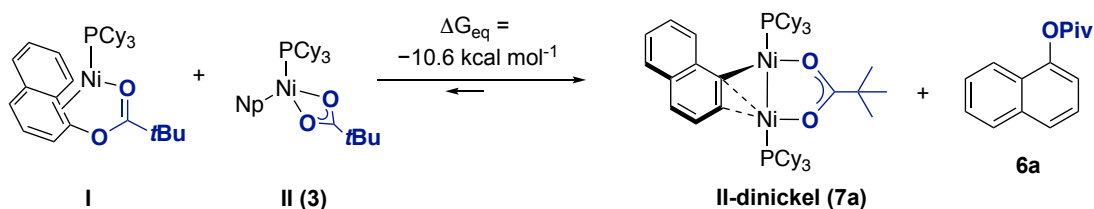
Scheme 2.30. Calculated disproportionation equilibrium.

Overall, stochiometric reactions suggested that disproportionation of the dinickel oxidative addition complex forms the mononickel oxidative addition complex from which transmetalation will occur. The mononickel intermediate was proposed by Liu in the seminal theoretical study of C(sp^2)–OPiv functionalisation with a Ni(0)/PCy$_3$ system.[28]

2.6.   Kinetic Studies

At this point in the mechanistic study, knowledge had been obtained about mononickel and dinickel oxidative addition complexes and stoichiometric experiments had begun to demystify some of the questions about how the dinickel complex is involved in the silylation reaction. However, no overall picture had been obtained. Kinetic studies were therefore called upon to provide this. During the kinetic study, all reactions were carried out in a glovebox and aliquots were periodically removed from the reaction tubes to be analysed by GC-FID.

2.6.1. Same excess experiment

In order to be confident in the results of a kinetic study, it is helpful to determine whether the catalyst is decomposing during the reaction. Thus, "same excess" experiments were carried out with the Ni(0)/PCy$_3$ precatalyst [Ni(PCy$_3$)$_2$]$_2$(N$_2$).[96,97] This experiment compares the concentration vs time profile of the reaction under investigation with a second reaction with identical catalyst loading but with the concentration of the reactants adjusted to an arbitrary conversion (e.g. 50%). Then, if the catalyst does not decompose, the profile of the reaction after 50% conversion should be the same as adjusted "same excess" reaction. If the catalyst had decomposed during the standard reaction, the "same excess" reaction with "fresh" catalyst would reflect this through the absence of overlap between the two reaction profiles. As shown in Figure 2.16, there was no significant difference between the data shown in black – the standard silylation reaction – and those shown in grey. Thus, kinetic data based on the reaction profile will not be drastically affected by any catalyst decomposition.
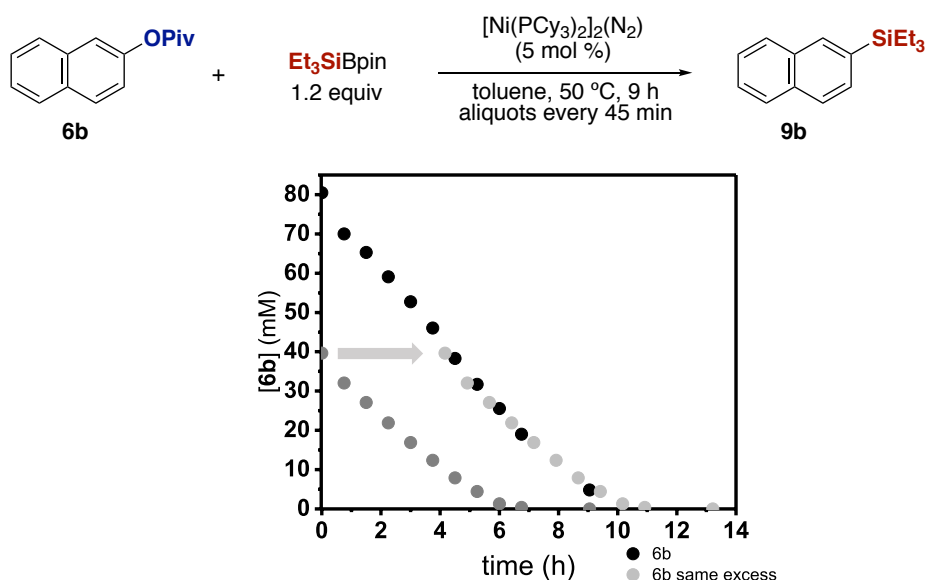
Figure 2.16. Same excess experiments with [Ni(PCy$_3$)$_2$]$_2$(N$_2$) (5 mol%). Standard reaction: [6b]$_i$ = 83 mM; [Si–B] = 100 mM; Same excess: [6b]$_i$ = 42 mM; [Si-B] = 58 mM.

2.6.2. Order in catalyst

Whether the disproportionation pathway supported by stoichiometric experiments is relevant to the catalytic reaction was investigated with kinetic studies. Specifically, the concentrations of **9a** and **9b** were monitored by GC-FID for different reactions then the data subjected to Variable Time Normalisation Analysis (VTNA).[98,99] This analysis offers an alternative method for analysing concentration vs time data to methods such as initial rates or reaction progress kinetic analysis (RPKA). In VTNA the time coordinate of each data point is normalised to remove the influence of the component being analysed (substrate or catalyst concentration, etc). Once normalised, simply visually judging the overlay of the data is enough to obtain an order (or range of orders) for that reaction component. VTNA was developed by Jordi Burés and this section was carried out with his guidance.

If the disproportionation equilibrium is indeed forming the mononickel oxidative species that is the key to reaction with Et$_3$SiBpin, a half order in [catalyst] would be expected. Reactions between **6a** and Et$_3$SiBpin were carried out in the presence of [Ni(PCy$_3$)$_2$]$_2$(N$_2$) (2.08 mM–6.25 mM) and CsF/CuF$_2$. Due to the stirring difficulties that occur after ca. 2 h (see Section 2.7), kinetic orders were obtained using data collected up until this time. As shown in Figure 2.17, when the x axis is normalised to t[cat]$^{0.5}$, the three reaction profiles overlay very well. A half order suggests that the active catalyst is involved in an off-cycle equilibrium. This is consistent with stoichiometric studies and with the observation of **7a** during NMR monitoring experiments. A Ni–Ni cleavage to form the active catalyst contrasts with Matsubara and Kirchner's finding that an NHC-ligated dinickel species (Figure 2.8) maintains the Ni–Ni bond throughout the KTC reaction.[100] Schoenebeck has also reported a number of Pd dimers and trimers where an intact Pd–Pd bond is implicated during catalysis.[101,102]
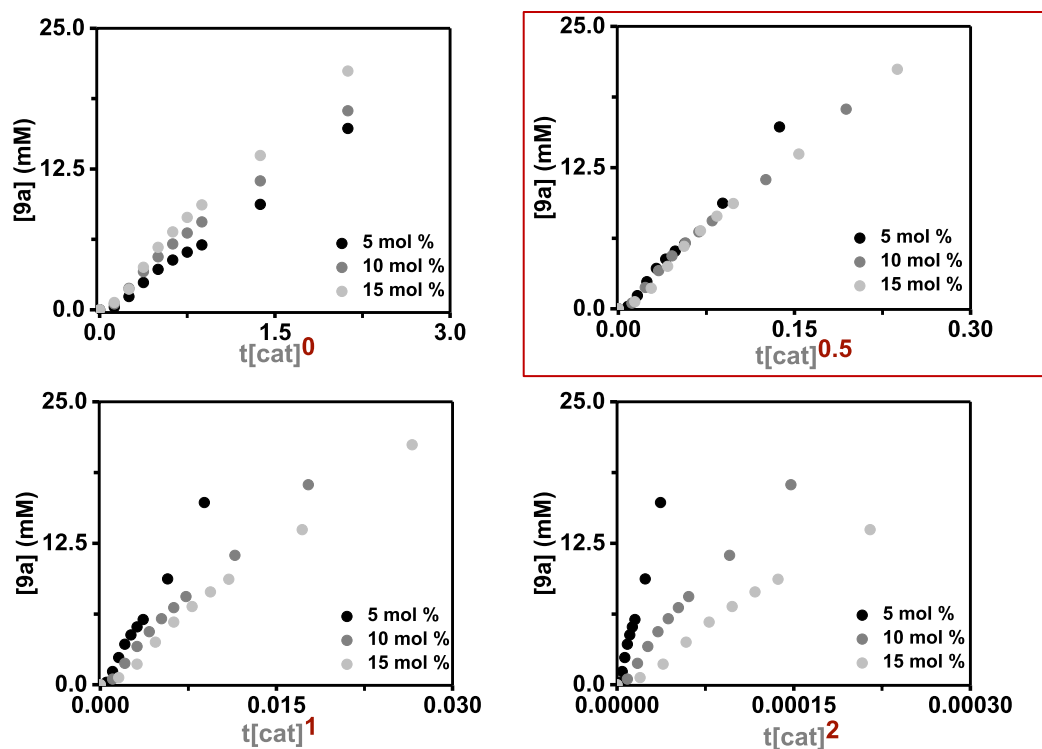
Figure 2.17. Order in catalyst. [Ni(PCy$_3$)$_2$]$_2$(N$_2$) (2.08 mM–6.25 mM).

2.6.3. Order in naphthyl pivalate and Et₃SiBpin

VTNA analysis was not required for the data obtained when the concentration of the naphthyl ester substrate was varied as no change in reaction rate occurred (Figure 2.18). This zero-order dependence is consistent with the low temperature NMR experiment where signals for **7a** were observed at 0 ℃. Significantly, it is also consistent with the conclusion that disproportionation of **7a** to form on-cycle **3** is occurring, as only transmetalation with Et₃SiBpin is required to continue the catalytic cycle from **3**.
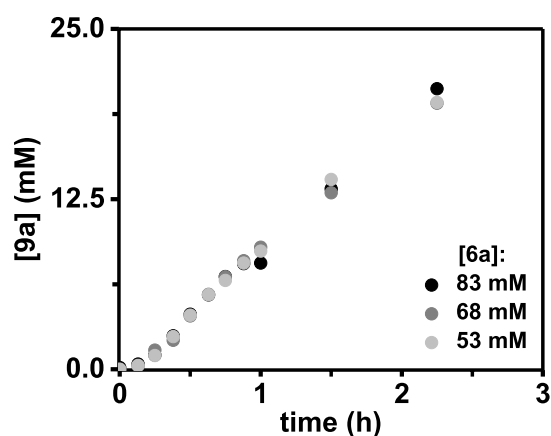
Figure 2.18. Zero-order dependence on [6a].

Consistent with transmetalation being rate-limiting, a positive order in Et₃SiBpin was obtained (Figure 2.19). Unfortunately, application of VTNA was unclear as to the particular numerical order, and a range of orders from 0.4–1 was obtained (Figure 2.20). For example, satisfactory overlay at orders 0.4 and 0.5 is obtained during the first nine points for all three data sets in Figure 2.20. Overlay seems particularly strong between [Et₃SiBpin] = 0.100 M and 0.065 M. However, overlay at this range of orders tends to decrease for the later time periods. When [**9a**] was plotted against $\Sigma[\text{Et}_3\text{SiBpin}]^1 \Delta t$ (Figure 2.20) to test a first order dependence, very good overlay occurred for [Et₃SiBpin] = 0.100 M and 0.087 M.
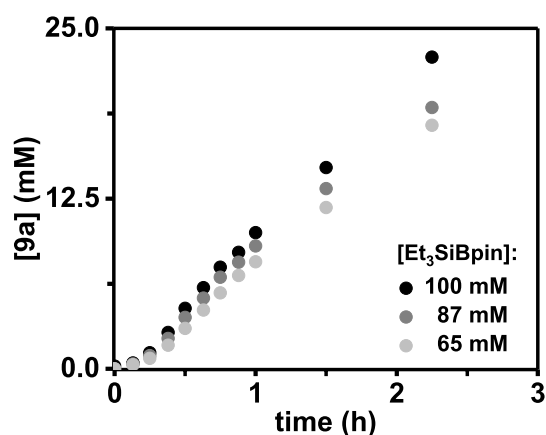
Figure 2.19. Positive order dependence on [Et₃SiBpin].
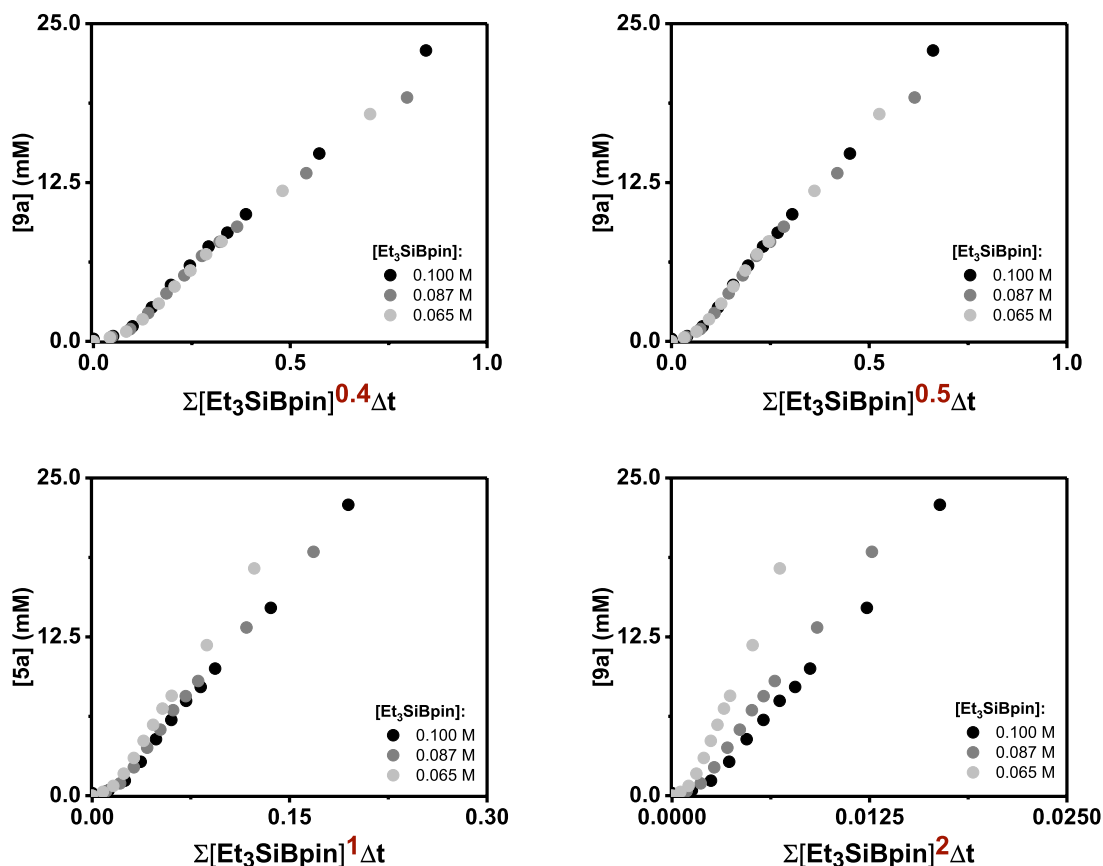
Figure 2.20. VTNA analysis for order in Et₃SiBpin using 6a as substrate.

This range in orders is proposed to be due to two intimately related factors – inefficient stirring over time and additive concentration effects. Stirring of the silylation reactions clearly becomes inefficient after 1.5 h due to the formation of insoluble by-products (vide infra). The second factor – additive effects – is very difficult to quantify as CsF and CuF₂ are sparingly soluble in toluene. Thus, we can be confident only in the positive (and first or less than first) order in [Et₃SiBpin].

2.7.   Role of the CuF₂ and CsF

After determining that oxidative addition of aryl pivalates to Ni(0)/PCy₃ forms dinickel complexes and that disproportionation of these complexes releases on-cycle mononickel complexes, key questions remained regarding the roles of the CuF₂ and CsF in the silylation reaction. Considering that the proposed mechanism shown in Figure 2.21 had invoked a Cu-catalysed transmetalation cycle, a detailed investigation into the effects of the CuF₂ and CsF was an important part of understanding the silylation mechanism. Whereas Cu(I) is involved in the transmetalation step of a number of cross-coupling reactions – particularly, but not limited to, the Sonogashira reaction – C(sp^2)–O silylation reactions are rare and mechanistic studies into the roles of additives or co-catalysts are limited (see Section 2.1.2).[30,63] During

this work, the roles of the CuF_2 and CsF were studied in catalytic and stoichiometric experiments and the reactions analysed by GC-FID and NMR spectroscopy.
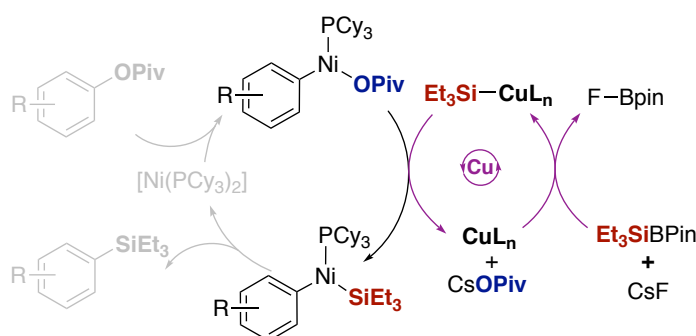
Figure 2.21. Proposed Cu-catalysed transmetalation cycle. Off-cycle dinickel oxidative addition complex not shown for clarity.

In analysing the original report of the silylation reaction it became clear that the silylation reaction still functions in the absence of CsF and CuF_2 but that these additives significantly increase the yield of **9b** (Table 2.2, entry 2). Catalytic formation of a $C(sp^2)$–Si bond is therefore possible in the absence of a Cu cycle. Strikingly, when the CuF_2 was removed completely and the reaction carried out with 1 or 2 equiv CsF, the final yield of **9b** was ca. 80%, significantly more than the 31% provided by the additive-free reaction (entries 3 and 4 compared with entry 2). In fact, when 2 equiv CsF were added, the yield was almost identical to that of the optimised reaction (79% compared to 85%). These results demonstrated that transmetalation through the hypothetical "Cu–SiEt₃" species is not necessary for excellent yields of **9b** to be obtained.
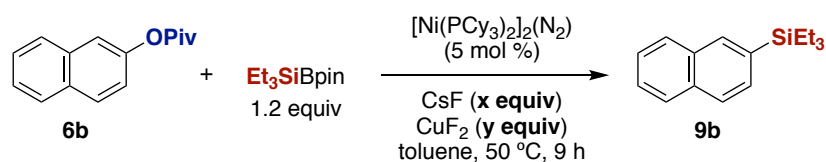
Entry	CsF (x)	CuF₂ (y)	Yield of 9b (%)
1	1	0.3	85
2	0	0	31
3	1	0	69
4	2	0	79

Table 2.2. Effect of CuF₂ and CsF loading on silylation yield.

Although there are similarities in *yield* between entries 1 and 4 in Table 2.2, such data are insufficient to determine whether the presence of Cu has an effect on the reaction rate. Thus, the kinetic profiles of the reactions in Table 2.2 were investigated as for the kinetic studies discussed in Section 2.6. These profiles are displayed in Figure 2.22.
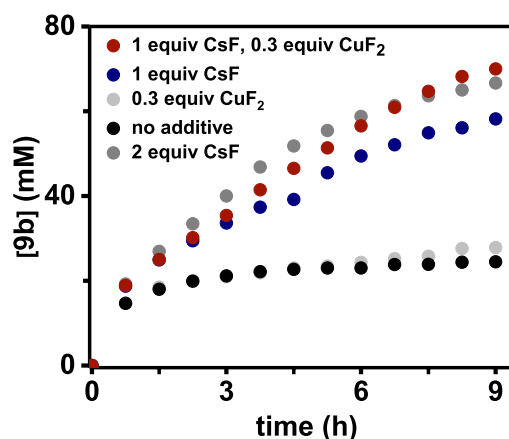
Figure 2.22. Silylation of 6b in the presence of different additives. Reactions were carried out as for kinetic studies and monitored by GC-FID.

Interestingly, there is no significant difference between the reaction profile for the standard CuF_2/CsF reaction (red) and the CsF-only reaction (2 equiv, dark grey). Furthermore, although the reaction with only 1 equiv CsF was lagging behind these reactions after 3–4 hours, after ca. 5 h **9b** was forming at a comparable rate to that of the reaction with 2 equiv CsF. The lack of a dramatic difference in kinetic profile between the Cu-containing and Cu-free reactions lends support to the conclusion that a Cu–SiEt₃ cycle is unnecessary; however, it does not clarify the difference between CuF_2 and CsF in the reaction.

It is important to note that the addition of 0.3 equiv CuF_2 (0.3 equiv Cu^{2+} or 0.6 equiv F^-) does not affect the reaction profile as much as the addition of 1 equiv CsF (light grey and dark blue profiles, respectively). For a better comparison, this experiment should have been carried out with either 0.6 equiv CsF or 0.5 equiv CuF_2 in order to compare reactions with the same nominal fluoride concentration. However, the difference between the reaction profiles is such that this likely would not have changed the conclusion of the experiment. Furthermore, some variability was noted between experiments and it is speculated that solubility differences between CuF_2 and CsF in toluene are responsible for this.

Finally, the reaction profile for the additive-free reaction (black, Figure 2.22) is striking in that formation of **9b** plateaus after 2–3 h. The rate of **9b** formation during the *first 45 minutes* of reaction is not dramatically different between all four reaction profiles, however, suggesting that the amount of deactivation that is occurring increases as **9b** is formed. The proposed origin of this effect and the role of the additives in mitigating it is discussed in the following sections.

2.7.1.1.   Effect of the cation

The addition of CuF_2 or CsF to the reaction provides a source of cations and anions that, as demonstrated above, dramatically affects the final yield and overall reaction profile. There is literature precedent for both cation and anion effects in coupling reactions; however, in the field of C–O functionalisation only cation effects have been investigated.[30] Musaev, Itami and co-workers carried out a computational investigation into the Ni-catalysed C–H arylation of C–OPiv bonds and proposed that the Cs_2CO_3 additive aids in the formation of the Ni–C bond through the formation of a Cs^+ cluster (see Section 2.1.2). In order to determine whether it is the presence of Cs^+ that is necessary to obtain high yields of **9b**,

CsF and CuF$_2$ were replaced with CsBPh$_4$. It was hypothesised that the tetracoordinated borate anion would not be able to bind to any intermediates during the reaction. Indeed, the yield of **9b** for 0.5, 1, or 2 equiv CsBPh$_4$ was almost identical to that obtained without any additives (39–46%). Other Cu salts were not investigated during this work. This was because a range of Cu salts – CuI, CuBr$_2$, Cu(OPiv)$_2$, CuCl$_2$, and Cu(OTf)$_2$ – was screened during the optimisation of the methodology but gave worse results than the optimised conditions.[16] The only Cu salt that gave comparable results was CuSO$_4$, but no explanation can be found for why this particular salt would be beneficial. Overall, investigations to determine whether there is a distinctive cation effect did not shed much light on the role of the additives.

2.7.1.2.   Effect of fluoride anion

With data in hand suggesting that CsBPh$_4$, a salt containing a counteranion that should not coordinate to any key intermediates, does not increase the yield of **9b** more than for the additive-free reaction, focus shifted towards studying the effect of fluoride anions on the reaction. As discussed in Section 2.1.3, fluoride anions have been proposed to activate silylborane reagents by interacting with the Lewis acidic boron atom and increasing the nucleophilicity of the silyl group.[16] To investigate this, Et$_3$SiBpin was stirred with 2 equivalents of CsF for 18 h in either toluene-d$_8$ or THF-d$_8$. This did not result in the appearance of any new signals in the resulting ^{19}F or ^{11}B NMR spectra. When Et$_3$SiBpin was reacted with 1 equivalent of CuF$_2$ and 1.3 equivalents of CsF in C$_6$D$_6$ at 50 ºC for 8 h, no reaction occurred. The possible Si–B activation effect of the CsF or CuF$_2$ was therefore uncertain. However, one effect of CsF and CuF$_2$ on the silylation was not uncertain: when these salts are present the reaction becomes thick and heterogeneous, in striking comparison to the additive-free reaction. A photograph of two silylation reactions after 16 h is shown in Figure 2.23. The effect of the additives on the lower reaction is clearly visible.
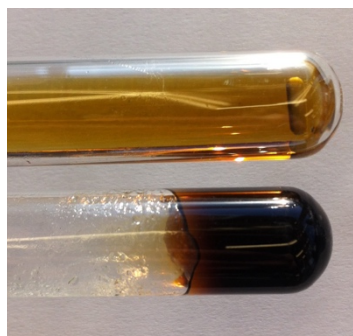
Figure 2.23 CsF/CuF$_2$-free (top) and standard silylation reaction (bottom) after 16 h. A reaction carried out with 2 equiv CsF is indistinguishable from the lower tube.

Filtration of reactions containing either CsF or CuF$_2$ and CsF gave fine off-white powders that are soluble in the polar and highly solvating solvents DMSO and H$_2$O. When the filtrates were analysed by NMR spectroscopy, no fluorine-containing species were identified. Dry DMSO-d$_6$ was chosen for NMR analysis of the solids in order to prevent hydrolysis of any water-sensitive species. Whether CsF or a combination of CuF$_2$ and CsF was present, distinct ^{11}B and ^{19}F NMR signals were obtained. The signals that were present depended on whether 2 equiv CsF or a mixture of CsF and CuF$_2$ (1:0.3 ratio) was utilised

(Figure 2.24). In the case where 2 equiv CsF was added, a well-resolved triplet in the ^{11}B NMR spectrum at δ_B = 4.78 ppm ($^{1}J_{B-F}$ = 21 Hz) and a multiplet in the ^{19}F NMR spectrum due to coupling with quadrupolar (I=3/2) ^{11}B (δ_F = −138.9 ppm ($^{1}J_{B-F}$ = 20.5 Hz)) were observed. These were assigned to the fluoroborate anion [F$_2$Bpin]$^-$. The OPiv$^-$ leaving group was proposed to form CsOPiv. When both CsF and CuF$_2$ were present during the silylation reaction the NMR signals of [F$_2$Bpin]$^-$ were accompanied by a set of broadened signals at a very similar chemical shift (δ_B = 5.34 ppm, δ_F = −138.3 ppm) in a 1:1 ratio. As only 1.6 equivalents of fluoride are available, full conversion of Bpin$^-$ to [F$_2$Bpin]$^-$ is not possible, so this signal was assigned to [F(PivO)Bpin]$^-$.
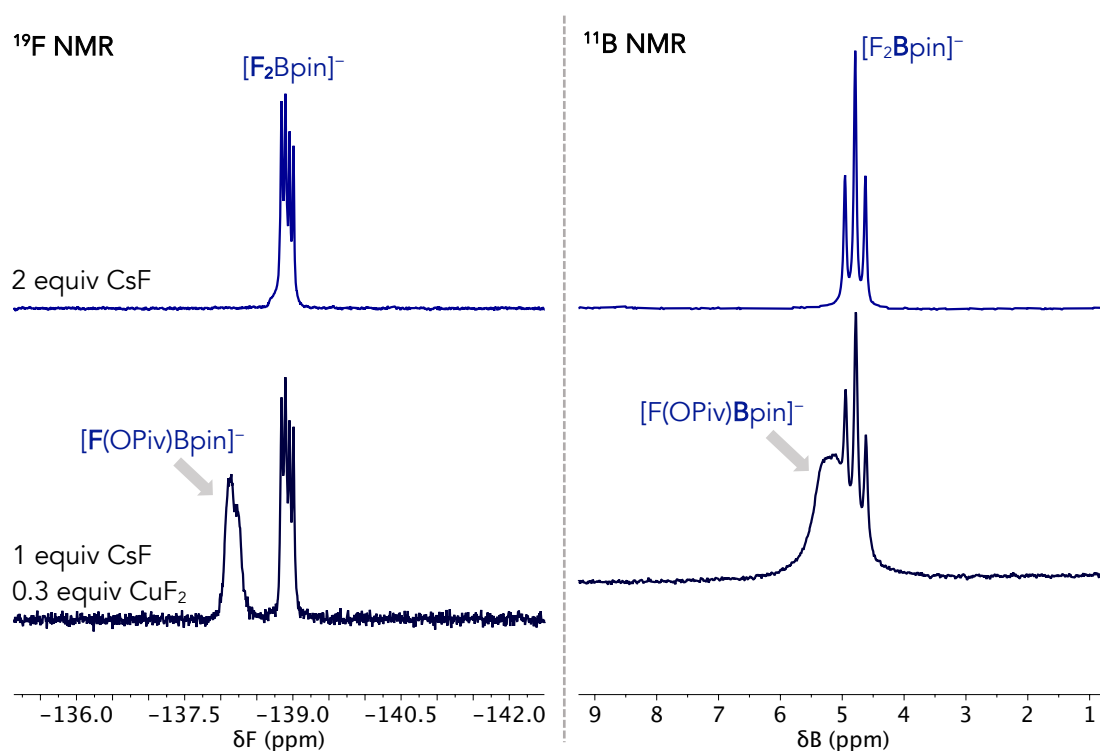
Figure 2.24. ^{19}F and ^{11}B NMR spectra of the toluene-insoluble by-products.

The Cu^{2+}/Cs$^+$ speciation was not determined in this experiment. It was hoped that ^{133}Cs NMR might shed some light on this, as although ^{133}Cs is a quadrupolar nucleus (I = 7/2) line widths are narrow and ^{133}Cs is 100% abundant (4.74% relative to ^{1}H).[103] When ^{133}Cs NMR was run for the by-products of the reaction with CsF/CuF$_2$ only one signal at δ_{Cs} = 70.8 ppm (relative to 0.1 M CsNO$_3$ in D$_2$O) was observed. A single signal for the three proposed species – CsOPiv, Cs[F(PivO)Bpin], and Cs[F$_2$Bpin] – was likely observed due to the extensive solvation of Cs$^+$ in DMSO.[103,104] The broadening of the NMR signals in the case where CuF$_2$ was employed may be due to interaction between paramagnetic Cu(II) and the fluoroborate anion. A reaction where the ratio of CsF/CuF$_2$ was modified could have been carried out to probe this as a different ratio of signals in the ^{19}F and ^{11}B NMR spectra would be expected.

If the mass balance for the silylation reaction in the presence of additives is now considered, all groups are now accounted for: the SiEt₃ and naphthyl groups are coupled in the desired product, the Bpin⁻ group becomes a fluoroborate salt, and the OPiv⁻ anion a Cs⁺ salt (Figure 2.21).
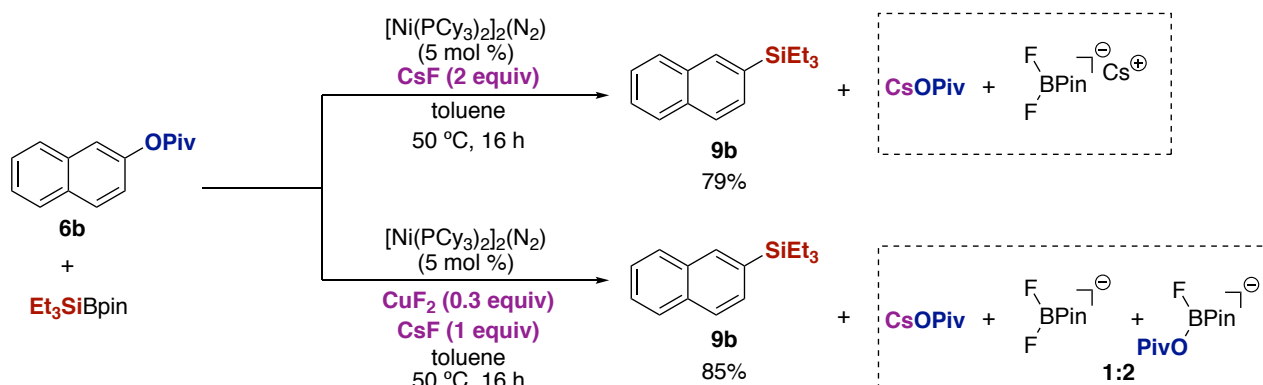
Scheme 2.31. Proposed reaction scheme including fate of OPiv⁻ and Bpin⁻ fragments. Cs⁺ or Cu²⁺ fluoroborate counteranions not included in lower pathway.

The solubility of CsF and CuF₂ in toluene is rather low, so monitoring of the additive-containing reaction by NMR spectroscopy, where stirring is not possible, was not expected to be of use. Surprisingly, however, when the Ni-catalysed silylation of **6a** was monitored by ¹⁹F NMR spectroscopy, two signals appeared over time. The signal at $\delta_F = -151$ ppm was assigned to FBpin based on comparison with the reported chemical shift ($\delta_F = -150.9$ ppm, C₆D₆).[58] The fluoroborates described above are therefore presumably formed upon reaction of FBpin with CsF or CuF₂ but are insoluble in toluene-d₈. Traces of Et₃SiF also appeared over time.
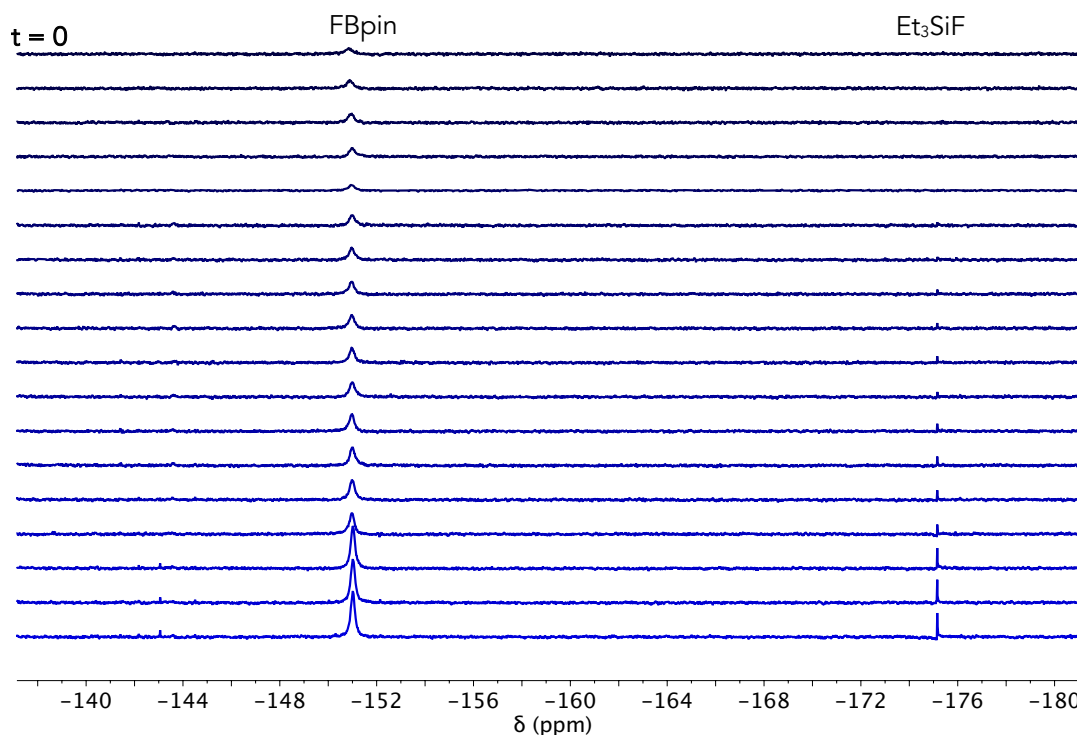
Figure 2.25.¹⁹F NMR showing appearance of FBpin over time (50 °C, spectra collected every 30 min, toluene-d₈).

2.7.1.1.   Catalyst deactivation

The fate of the Bpin⁻ fragment has now been identified based on the experimental evidence discussed above. This is summarised in Scheme 2.31. However, this still does not explain how the formation of fluoroborate salts is involved maintaining productive catalysis. Thus, the additive-free (fluoride-free) reaction was studied. The simplest way to balance the reaction in this case would be for PivOBpin to form following transmetalation. As the rate of naphthyl silane formation decreased over time in the absence of additives, it was thought that the formation of PivOBpin may be interrupting catalysis. With this hypothesis in mind, experiments were designed in order to be able to track the Bpin⁻ and OPiv⁻ fragments.

First, a synthetic route to unreported PivOBpin was planned based on reports of successful dehydrogenative coupling reactions between a dialkylborane and a carboxylic acid.[105–107] Pinacol borane was reacted with dry pivalic acid in toluene and H_2 evolution occurred over 2 h (Scheme 2.32). Upon removal of the solvent, PivOBpin was obtained as a waxy white solid in quantitative yield. A ^{11}B NMR signal at $\delta_B = 23.4$ ppm (C_6D_6) was within the range expected for a three coordinate boronic ester-derived compound. In order to obtain PivOBpin in the highest possible purity (maximum 94–97%), the pivalic acid was dried rigorously and the bottle of pinacol borane was checked for HOBpin prior to use. Purification of impure PivOBpin is very difficult as it is extremely sensitive – its storage in the glovebox freezer was not enough to prevent its slow decomposition to HOBpin and pinB–O–Bpin. A synthesis of PivOBpin from BpinCl and PivOH could also be envisioned, but whereas BpinCl must be synthesised from pinacol and BCl_3 then purified by distillation under an inert atmosphere, high purity pinacol borane is commercially available.
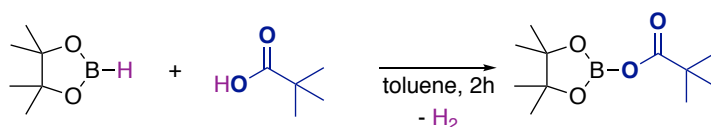
Scheme 2.32. Synthesis of PivOBpin.

With NMR spectral data for PivOBpin in hand, the silylation of **6a** was monitored by ^{11}B NMR spectroscopy in the absence of CuF_2 and CsF. As shown in Figure 2.26, a ^{11}B NMR signal for PivOBpin at $\delta_B = 23$ ppm (toluene-d_8) grew in intensity over time as the signal for Et_3SiBpin decreased in intensity. This experiment confirmed that PivOBpin is produced in the absence of fluoride sources and contrasts with the formation of FBpin (and, subsequently, $[F_2Bpin]^-$) that is produced in the presence of fluoride.
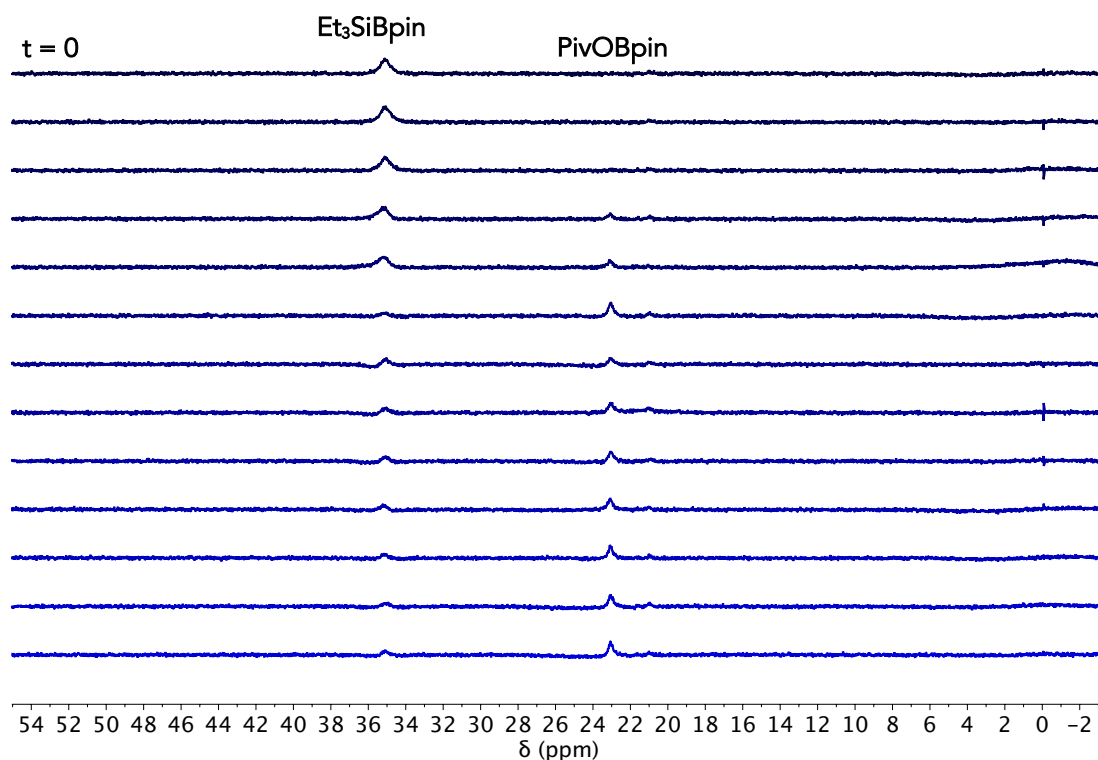
Figure 2.26 ¹¹B NMR monitoring of stoichiometric silylation of 6a at 50 °C showing appearance of PivOBpin. (t=0 at top, spectra collected every 30 minutes).

The results discussed in the previous section indicate that the presence of fluoride, rather than Cs^+ or Cu^{2+}, is the main driver for maintaining active catalysis. This was highlighted visually in Figure 2.22 where in the absence of additives almost all of the product is formed during the first 3 h, and that past this time, a plateau with respect to the formation of **9b** is reached. In order to investigate the mode of this deactivation – and therefore delve deeper into the role of the CsF and CuF_2 – spiking experiments were carried out whereby either CsF or extra catalyst was added once conversion had plateaued. The addition of extra catalyst was carried out in order to determine whether the catalyst is deactivated or poisoned by the build-up of detrimental species. Inhibition by the silylated product had already been ruled out by same excess experiments (Figure 2.16).
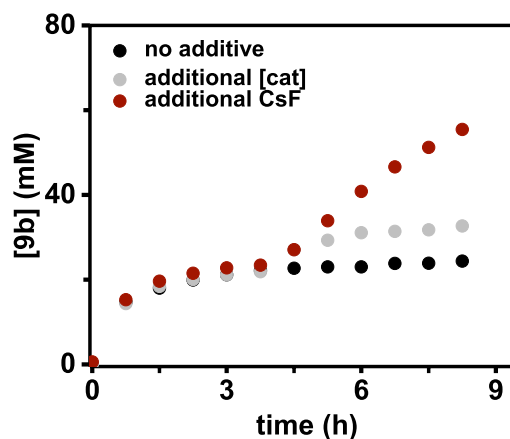
Figure 2.27. Effect of adding [Ni(PCy₃)₂]₂(N₂) (5 mol %) (*grey*), or CsF (2 equiv) (*red*) to the additive-free silylation of 6b. Addition took place at 3.75 h.

As shown in Figure 2.27 above, there was a striking difference between addition of precatalyst and the addition of 2 equiv CsF. Addition of extra Ni(0) precatalyst ([Ni(PCy$_3$)$_2$]$_2$(N$_2$), 5 mol %, grey trace) did result in further product formation, showing that the reaction medium did not instantly decompose the additional Ni(0). However, product formation plateaued after two hours. This supported the hypothesis that turnover of the catalyst resulted in deactivation. Given that a ca. 35% yield of **9b** was obtained with the initial portion of catalyst, a 35% yield of PivOBpin should also be present in the reaction mixture and would continue to be formed by the fresh catalyst. At the point where the new Ni(0) was added this would be in a large excess compared to the Ni(0). The additional Ni(0) was able to catalyse silylation for almost 2 h, indicating that the presence of PivOBpin didn't rapidly deactivate the Ni(0).

When additional CsF was added (red trace), *product formation resumed without any additional catalyst*, and the formation of insoluble fluoroborate salts was observed. This strongly suggested that reactivation of the catalyst occurs when the PivOBpin by-product is removed from solution through the formation of fluoroborates. This investigation was focused on understanding the mechanism of the optimised reaction published by Zarate and Martin;[16] therefore, the experiment was not repeated with anions such as OPiv$^-$ or OMe$^-$ that might also trap PivOBpin as a borate.

To test whether the catalyst is indeed inhibited by PivOBpin, the Ni(0) precatalyst [Ni(PCy$_3$)$_2$](N$_2$) was preincubated with PivOBpin for 1 h at 50 °C before addition of **6b**. When stoichiometric PivOBpin was employed, no **9b** was obtained *after this incubation period*. However, when 0.1 equiv of PivOBpin was used there was a decreased rate of product formation during the first 45 minutes of the reaction (Figure 2.28). This decreased rate is consistent with the decreased rate of product formation when Ni(0) was added to the additive-free reaction once the catalyst had become inactive (Figure 2.27, grey). If this experiment was to be repeated, experiments with stoichiometric PivOBpin and no preincubation would also be carried out.
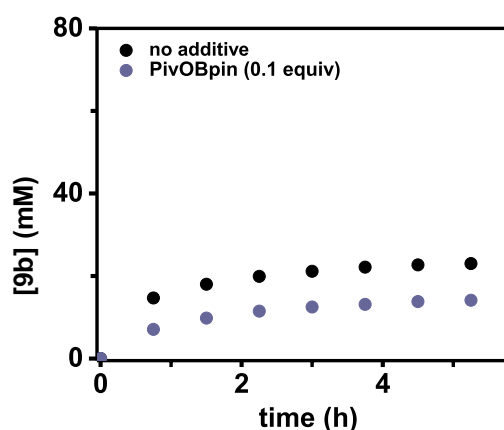
Figure 2.28. Pre-incubation of [Ni(PCy$_3$)$_2$](N$_2$) (5 mol %) with 0.1 equiv PivOBpin (blue) compared with additive-free reaction (black).

Unfortunately, it was difficult to identify the Ni intermediate(s) that interacted with PivOBpin to cause deactivation of the catalyst. Apart from the Ni(0) precatalysts – [Ni(COD)$_2$]/PCy$_3$ or [Ni(PCy$_3$)$_2$]$_2$(N$_2$) – the only isolable intermediate available for a stoichiometric reaction with PivOBpin was dinickel complex **7a**. When this was reacted with PivOBpin for 6 h at 50 ºC, naphthalene was the major product observed by ^{1}H NMR spectroscopy. The ^{11}B NMR spectrum was inconclusive (Figure 2.29-bottom). A broad signal

had appeared at $\delta_B = 75$ ppm. This is in the range of a triarylborane, but the formation of such a compound under these conditions would be rather unlikely. When additive-free reactions with a [Ni(COD)$_2$]/PCy$_3$ precatalyst mixture were monitored by ^{11}B NMR, a signal that was assigned to PivOBpin was the only new signal observed (Figure 2.26 and Figure 2.29-top). Whether some PivOBpin is coordinated to a Ni complex and preventing further reaction could not be determined from the NMR spectrum.
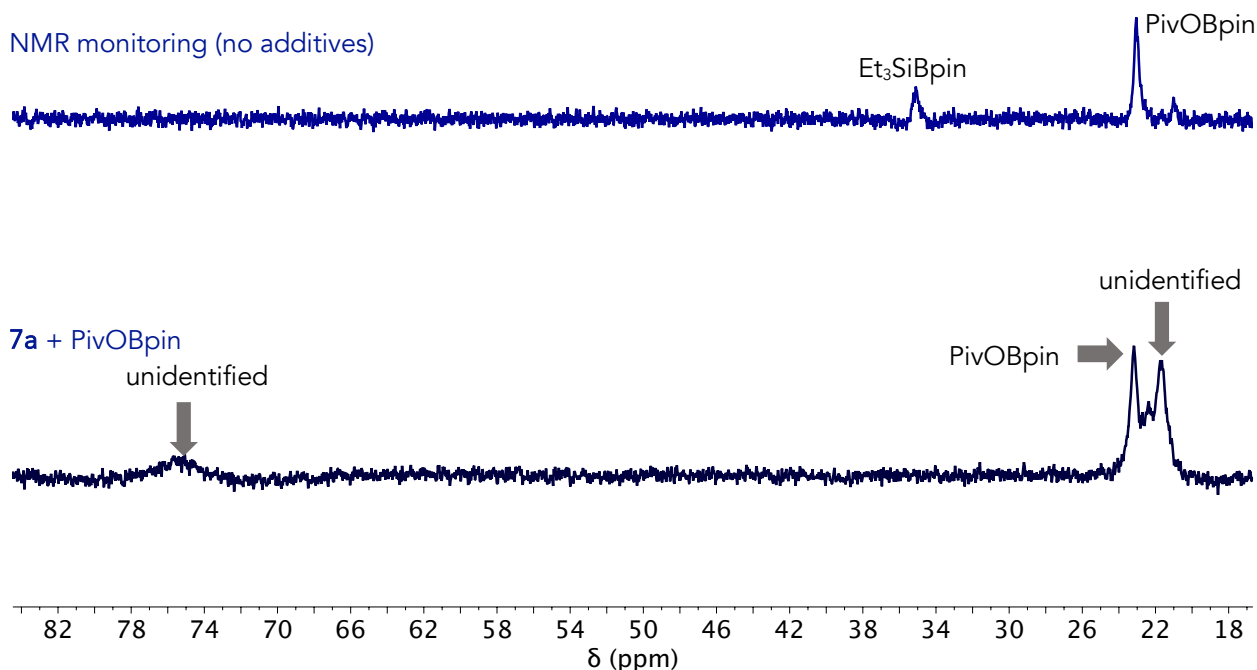
Figure 2.29. Comparison of ^{11}B NMR from monitoring reaction (absence of additives) after 6 h (top) and reaction of 7a with PivOBpin (bottom).

2.7.1.2. Alternative Ni–F mechanism

A mechanism could also be envisioned whereby CsF reacts with [Ni(σ-1-naphthyl)(κ²-OPiv)(PCy$_3$)] (**3**) to first form a Ni–F complex [Ni(σ-1-naphthyl)(F)(PCy$_3$)] from which transmetalation occurs to form Ni–SiEt$_3$ and FBpin (Scheme 2.33). The FBpin byproduct of this proposal was detected in NMR monitoring experiments and would likely go on to react with CsF to form the fluoroborate salt that was also isolated and characterised.

Fluoride complex [Ni(σ-1-naphthyl)(F)(PCy$_3$)$_2$][69] was indeed found to be a modestly competent silylation precatalyst in the presence of CsF and CuF$_2$, giving a 20% yield of **9b**. Interestingly, its chloride congener [Ni(σ-1-naphthyl)(Cl)(PCy$_3$)$_2$] did not catalyse the silylation reaction. This is proposed to be due to the inability of Et$_3$SiBpin to generate Ni(0) from [Ni(σ-1-naphthyl)(Cl](PCy$_3$)$_2$]; in the case of [Ni(σ-1-naphthyl)(F)(PCy$_3$)$_2$], fluoride abstraction by Et$_3$SiBpin might occur to form a cationic Ni(II) naphthyl complex that would lead to Ni(0) via reductive elimination of the naphthyl groups.[108] To test the transmetalation step proposed in Scheme 2.33, [Ni(σ-1-naphthyl)(F)(PCy$_3$)$_2$] was reacted with Et$_3$SiBpin at 50 °C. Interestingly, Et$_3$SiF was detected by ^{19}F NMR ($\delta_F = -175.2$ ppm)[109] rather than the FBpin ($\delta_F = -150.9$ ppm)[58] proposed in Scheme 2.33. No **9b** was observed, even after prolonged heating (60 °C, 24 h).
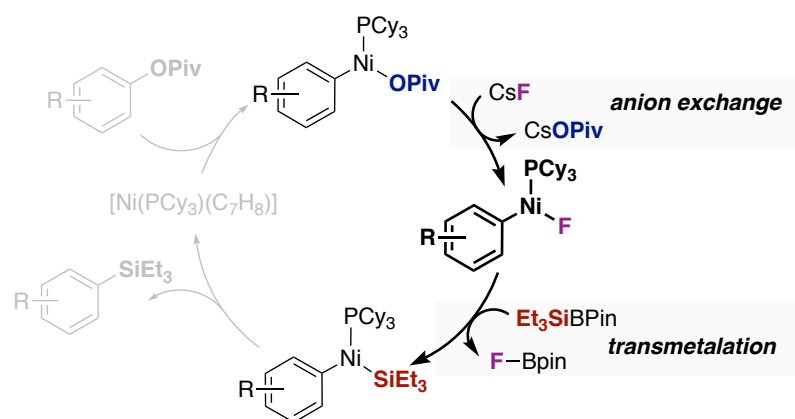
Scheme 2.33. Mechanism via Ni–F intermediate.
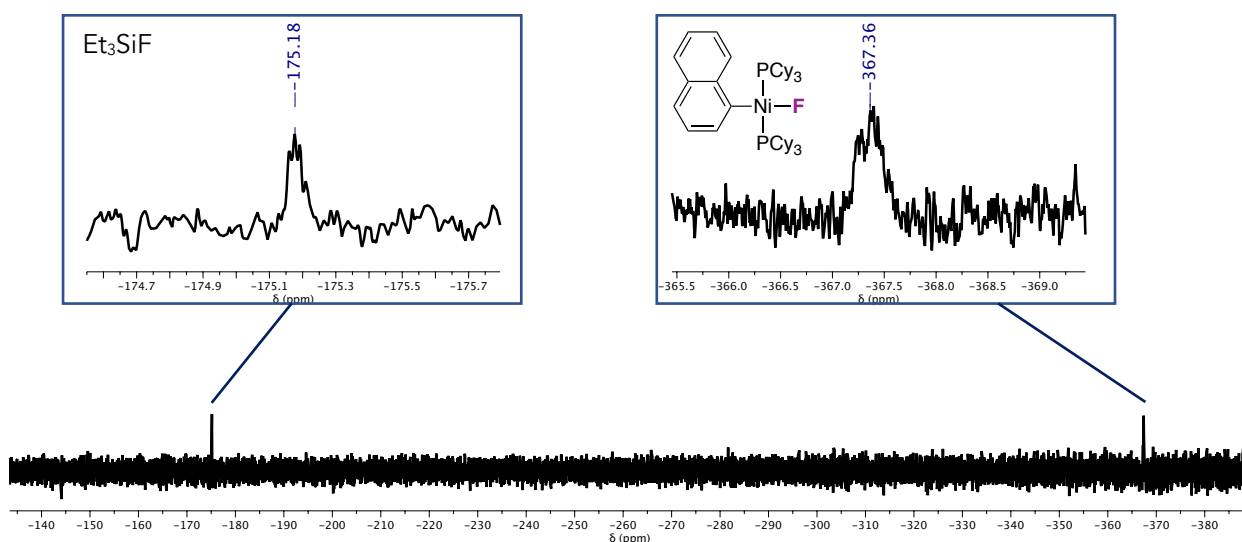
Figure 2.30. Reaction of Et₃SiBpin with [Ni(σ-1-naphthyl)(F)(PCy₃)₂] (¹⁹F NMR, toluene-d₈).

2.8. DFT study

Although analysis of the reaction profiles in the presence and absence of CsF shows that fluoride does not make a significant difference to the rates of silylation in the first hour of reaction, this does not distinguish the two mechanisms. Pivalate-to-fluoride exchange might be fast and transmetalation from the Ni–F and Ni–OPiv complexes might occur via a similar transition state. Thus, DFT studies were carried out at the M06/def2tzvpp level with the inclusion of a solvent model (IEFPCM, dichloromethane, toluene).[110–113] Alongside a study of transmetalation, this allowed the energy profile of the proposed mechanism to be mapped out. To avoid the conformational complexity of the ethyl substituents, Me₃SiBpin was used in place of Et₃SiBpin.

Experimental data provided evidence that an off-cycle dinickel complex forms and that this complex is a catalyst resting state. Experiments also indicated that Et₃SiBpin was involved in the rate-limiting processes of the catalytic cycle and that oxidative addition of the C(sp^2)–O bond was facile. Importantly,

no evidence was obtained for the proposed transmetalation from a Cu–SiEt₃ species. Evidence instead pointed to CuF₂ being a source of fluoride anions alongside CsF. When fluoride was present in the catalytic silylation reaction, FBpin or fluoroborates were observed. When fluoride was absent, PivOBpin was observed. Thus, two cycles were calculated: one without CsF and one with CsF (Figure 2.31 and Figure 2.32, respectively).

The additive-free mechanism is shown below (Figure 2.31). First, π-coordination of the substrate to Ni(0) occurs from [(PCy₃)Ni(toluene)] to form **I**.[85] Next, oxidative addition with a low activation Gibbs free energy of 14.7 kcal mol⁻¹ (**TS_I-II**) leads to [Ni(σ-naphthyl)(κ²-OPiv)(PCy₃)] (**II** or **3**). Coordination of Me₃SiBpin to **II** forms complex **III** from which transmetalation occurs through a six-membered transition state **TS_III-IV** ($\Delta G^{\ddagger}$ **II**-**TS_III–IV** = 22.4 kcal mol⁻¹). Dissociation of PivOBpin from Ni–SiMe₃ complex **IV** forms the overall product of transmetalation, monophosphine complex **V**. Reductive elimination from **V** forms the C(sp²)–Si bond of **9a** (**TS_V-VI**, $\Delta G^{\ddagger}$ = 3.2 kcal mol⁻¹). Ligand exchange with another molecule of **6a** releases **9a** from Ni(0) and recovers **I**. These data support the conclusion that the transmetalation process with the Si–B species and **II** is turnover-limiting during the catalytic reaction (**II**-**TS_III–IV** = 22.4 kcal mol⁻¹). This is consistent with the zero-order dependence in **6a** and the positive-order dependence in Et₃SiBpin obtained from kinetic studies.
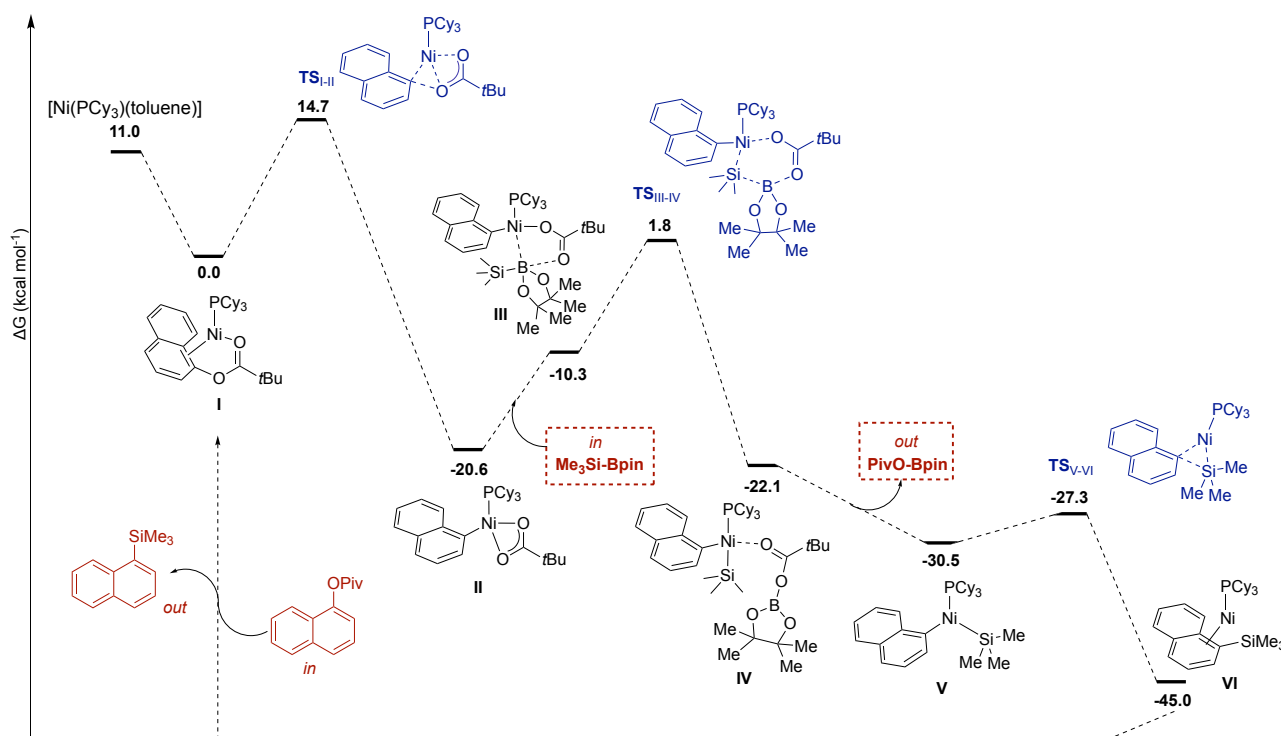
Figure 2.31. Free energy profile for the silylation of 6a calculated in the absence of fluoride sources. Energies are in kcal mol⁻¹.

The overall conclusions from the CsF-free cycle can be translated to the calculated reaction profile that includes CsF (Figure 2.32). Anion exchange between CsF and Ni–OPiv to form a Ni–F complex was *not* found to be favourable. However, a low energy pathway where CsF is involved in transmetalation

was found. Consistent with an NMR monitoring experiment, FBpin is liberated rather than PivOBpin. The presence of CsF lowers the barrier to transmetalation ever so slightly from $\Delta G^{\ddagger} = 22.4$ kcal mol^{-1} (**II** to **TS$_{III–IV}$**) to $\Delta G^{\ddagger} = 21.4$ kcal mol^{-1} (**II** to **TS$_{III-IV\,Cs}$**). The loss of FBpin rather than PivOBpin also adds 20 kcal mol^{-1} to the barrier to the reverse reaction from **IV** to **II**. A transition state for the direct reaction between Et$_3$SiBpin and **7a** could not be located, consistent with the failed stoichiometric experiment between Et$_3$SiBpin and **7a**.
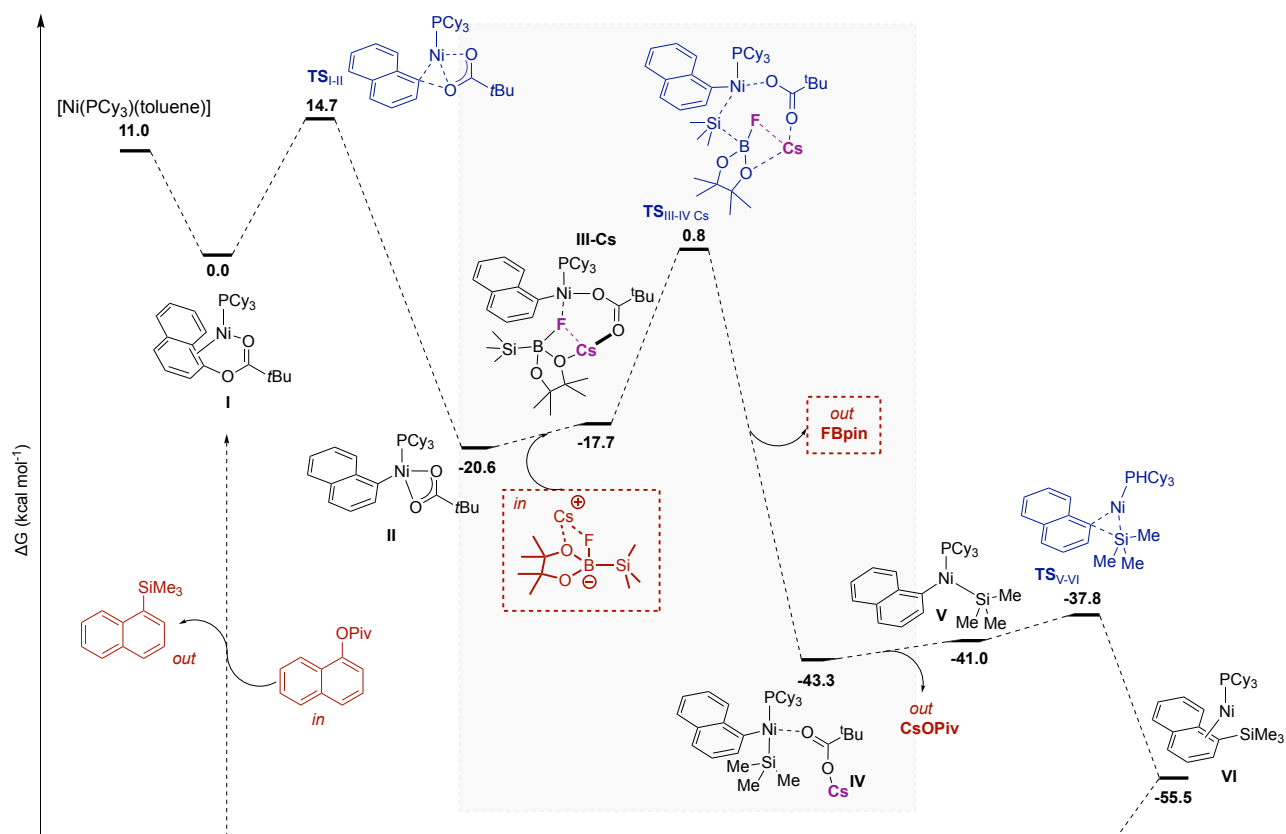
Figure 2.32. Free energy profile for the silylation of 6a calculated in the presence of CsF.

2.9.   Conclusions

Presented in this chapter is the first experimental mechanistic study of a Ni-catalysed C(sp^2)–OPiv functionalisation reaction where a monodentate phosphine is employed. The Ni-catalysed C(sp^2)–O silylation of aryl esters was chosen as a model reaction because (1) it involves the most commonly employed C(sp^2)–OPiv functionalisation catalyst ([Ni(COD)$_2$] and PCy$_3$); (2) the initial study invoked Cu in a transmetalation catalytic cycle; and (3) because there were no computational or experimental studies of any C(sp^2)–OPiv to C(sp^2)–heteroatom transformations. Three main goals were laid out for the investigation: the identification of an oxidative addition complex bearing PCy$_3$, the identification of the role of the CuF$_2$ and CsF, and finally, the proposal of a full mechanism that is consistent with all the experimental data. These three goals were all met.

Initially, the study focused on oxidative addition. Mononickel oxidative addition complexes were first detected by ^{31}P NMR spectroscopy. Next, investigations into direct oxidative addition reactions between Ni(0) sources and naphthyl pivalate substrates showed that unusual dinickel oxidative addition complexes [{Ni(PCy₃)}₂(μ,η²-aryl)(μ-OPiv)] form instead of mononickel complexes. One such complex was isolated and characterised by NMR spectroscopy and X-ray diffraction. Importantly, it was identified as a resting state during the catalytic reaction. These results are noteworthy as they represent long-awaited experimental evidence for aryl pivalate oxidative addition complexes bearing monodentate phosphine ligands.

Stoichiometric experiments and kinetic studies supported the conclusion that the dinickel oxidative addition complex is off-cycle and acts as a reservoir of the mononickel complex. Experimental results were supported by DFT calculations carried out by Enrique Gómez-Bengoa at UPV-EHU. These were consistent with all the experimental evidence and showed that the steps leading from the mononickel oxidative addition complex to transmetalation have the highest overall barrier.

The experiments summarised above demonstrated that Cu–SiEt₃ intermediates are not necessary for the silylation reaction and therefore do not support the original mechanistic proposal of Ni/Cu co-catalysis. Although the precise interaction between PivOBpin and a Ni complex that results in deactivation was not uncovered, the data from NMR monitoring experiments, DFT, and from the isolation of fluoroborate by-products support the conclusion that the additives are necessary to sequester the Bpin$^-$ byproduct as insoluble fluoroborate salts. Whether a similar conclusion is applicable to recent C(sp^2)–O functionalisation reactions between Bpin-containing molecules that employ CuF₂ and a fluoride salt requires further investigation.

Overall, a mechanism is proposed that is consistent with computational studies and omits the Cu cycle that has been favoured (Scheme 2.34).
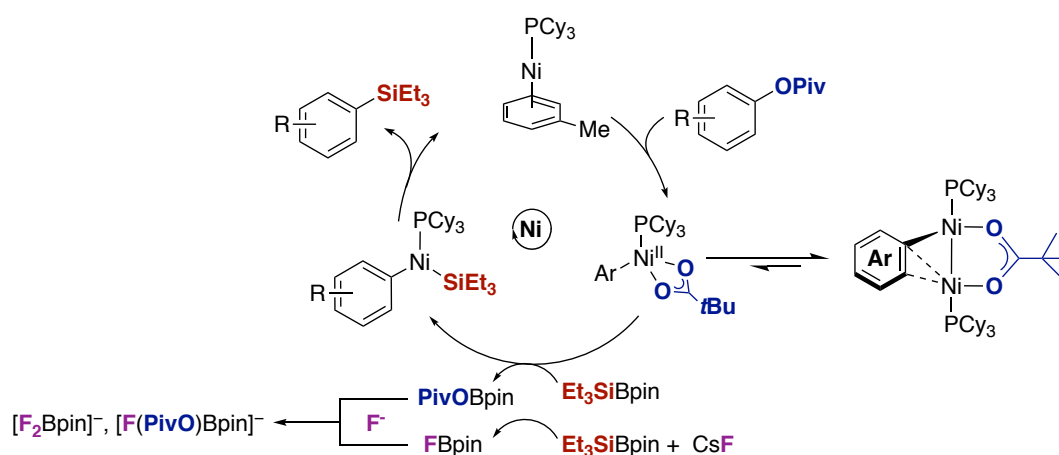
Scheme 2.34. Final mechanistic proposal for the C(sp^2)–O silylation of aryl pivalates.

2.10. References

(1)   Zeng, H.; Qiu, Z.; Domínguez-Huerta, A.; Hearne, Z.; Chen, Z.; Li, C. J. An Adventure in Sustainable Cross-Coupling of Phenols and Derivatives via Carbon-Oxygen Bond Cleavage. *ACS Catal.* **2017**, *7* (1), 510–519.

(2)   Zarate, C.; van Gemmeren, M.; Somerville, R. J.; Martin, R. Chapter Four-Phenol Derivatives: Modern Electrophiles in Cross-Coupling Reactions. *Adv. Organomet. Chem.* **2016**, *66*, 143–222.

(3)   Tobisu, M.; Chatani, N. Cross-Couplings Using Aryl Ethers via C–O Bond Activation Enabled by Nickel Catalysts. *Acc. Chem. Res.* **2015**, *48* (6), 1717–1726.

(4)   Tollefson, E. J.; Hanna, L. E.; Jarvo, E. R. Stereospecific Nickel-Catalyzed Cross-Coupling Reactions of Benzylic Ethers and Esters. *Acc. Chem. Res.* **2015**, *48* (8), 2344–2353.

(5)   Su, B.; Cao, Z.-C.; Shi, Z.-J. Exploration of Earth-Abundant Transition Metals (Fe, Co, and Ni) as Catalysts in Unreactive Chemical Bond Activations. *Acc. Chem. Res.* **2015**, *48* (3), 886–896.

(6)   Cornella, J.; Zarate, C.; Martin, R. Metal-Catalyzed Activation of Ethers via C–O Bond Cleavage: A New Strategy for Molecular Diversity. *Chem. Soc. Rev.* **2014**, *43* (23), 8081–8097.

(7)   Gu, Y.; Martin, R. Ni-Catalyzed Stannylation of Aryl Esters via C−O Bond Cleavage. *Angew. Chem. Int. Ed.* **2017**, *56*, 3187 –3190.

(8)   Guo, L.; Rueping, M. Functional Group Interconversion: Decarbonylative Borylation of Esters for the Synthesis of Organoboronates. *Chem. Eur. J.* **2016**, *22* (47), 16787–16790.

(9)   Quasdorf, K. W.; Tian, X.; Garg, N. K. Cross-Coupling Reactions of Aryl Pivalates with Boronic Acids. *J. Am. Chem. Soc.* **2008**, *130* (44), 14422–14423.

(10)   Huang, K.; Yu, D. G.; Zheng, S. F.; Wu, Z. H.; Shi, Z.-J. Borylation of Aryl and Alkenyl Carbamates through Ni-Catalyzed C–O Activation. *Chem. Eur. J.* **2011**, *17* (3), 786–791.

(11)   Yue, H.; Guo, L.; Liu, X.; Rueping, M. Nickel-Catalyzed Synthesis of Primary Aryl and Heteroaryl Amines via C–O Bond Cleavage. *Org. Lett.* **2017**, *19* (7), 1788–1791.

(12)   MacQueen, P. M.; Stradiotto, M. Nickel-Catalyzed Cross-Coupling of Ammonia or Primary Alkylamines with (Hetero)aryl Sulfamates, Carbamates, or Pivalates. *Synlett* **2017**, *28* (13), 1652–1656.

(13)   Shimasaki, T.; Tobisu, M.; Chatani, N. Nickel-Catalyzed Amination of Aryl Pivalates by the Cleavage of Aryl C–O Bonds. *Angew. Chem. Int. Ed.* **2010**, *49* (16), 2929–2932.

(14)   Yang, J.; Chen, T.; Han, L. B. C–P Bond-Forming Reactions via C–O/P–H Cross-Coupling Catalyzed by Nickel. *J. Am. Chem. Soc.* **2015**, *137* (5), 1782–1785.

(15)   Yang, J.; Xiao, J.; Chen, T.; Han, L. B. Nickel-Catalyzed Phosphorylation of Phenol Derivatives via C–O/P–H Cross-Coupling. *J. Org. Chem.* **2016**, *81* (9), 3911–3916.

(16)   Zarate, C.; Martin, R. A Mild Ni/Cu-Catalyzed Silylation via C–O Cleavage. *J. Am. Chem. Soc.* **2014**, *136* (6), 2236–2239.

(17)   Fahey, D. R. The Reaction of Aryl and Vinyl Halides with Nickel(0) Complexes. *J. Am. Chem. Soc.* **1970**, *92* (2), 402–404.

(18)   Collman, J. P.; Roper, W. R. Preparation and Oxidative Addition Reactions of a Monomeric Ruthenium(0) Complex. *J. Am. Chem. Soc.* **1965**, *87* (17), 4008–4009.

(19)   Desnoyer, A. N.; Love, J. A. Recent Advances in Well-Defined, Late Transition Metal Complexes That Make And/or Break C–N, C–O and C–S Bonds. *Chem. Soc. Rev.* **2017**, *46* (1), 197–238.

(20)   Muto, K.; Yamaguchi, J.; Lei, A.; Itami, K. Isolation, Structure, and Reactivity of an Arylnickel(II) Pivalate Complex in Catalytic C–H/C–O Biaryl Coupling. *J .Am. Chem. Soc.* **2013**, *135* (44), 16384–16387.

(21)   Takise, R.; Muto, K.; Yamaguchi, J.; Itami, K. Nickel-Catalyzed α-Arylation of Ketones with Phenol Derivatives. *Angew. Chem. Int. Ed.* **2014**, *53* (26), 6791–6794.

(22)   Desnoyer, A. N.; Friese, F. W.; Chiu, W.; Drover, M. W.; Patrick, B. O.; Love, J. A. Exploring Regioselective Bond Cleavage and Cross-Coupling Reactions Using a Low-Valent Nickel Complex. *Chem. Eur. J.* **2016**, *22* (12), 4070–4077.

(23)   Batten, M. P.; Canty, A. J.; Cavell, K. J.; Rüther, T.; Skelton, B. W.; White, A. H. Synthesis of nickel(II) Complexes Containing Neutral N,N⁻ and Anionic N,O⁻ Bidentate Ligands, and Their Behaviour as Chain-Growth Catalysts; Structural Characterisation of Complexes Containing (mim)₂CO, mimCO₂⁻, and mimCPh₂O⁻ (Mim = 1-Methylimidazol-2yl). *Inorg. Chim. Acta* **2006**, *359* (6), 1710–1724.

(24)   Desjardins, S. Y.; Cavell, K. J.; Hoare, J. L.; Skelton, B. W.; Sobolev, A. N.; White, A. H.; Keim, W. Single Component N–O Chelated Arylnickel(II) Complexes as Ethene Polymerisation and CO/Ethene Copolymerisation Catalysts. Examples of Ligand Induced Changes to the Reaction Pathway. *J. Organomet. Chem.* **1997**, *544* (2), 163–174.

(25)   Isaeva, L. S.; Drogunova, G. I.; Peregudov, A. S.; Petrovskii, P. V; Kravtsov, D. N. Aryl Bis(tricyclohexylphosphine)nickel Carboxylates. *Organomet. Chem. USSR* **1988**, *1* (4), 482–485.

(26)   Isaeva, L. S.; Drogunova, G. I.; Peregudov, A. S.; Kravtsov, D. N. Arylbis(triphenylphosphinyl)nickel

Carboxylates. *B Acad Sci Ussr Ch+* **1988**, *37* (1), 153–157.

(27) Bajo, S.; Laidlaw, G.; Kennedy, A. R.; Sproules, S.; Nelson, D. J. Oxidative Addition of Aryl Electrophiles to a Prototypical Nickel(0) Complex: Mechanism and Structure/Reactivity Relationships. *Organometallics* **2017**, *36* (8), 1662–1672.

(28) Li, Z.; Zhang, S. L.; Fu, Y.; Guo, Q. X.; Liu, L. Mechanism of Ni-Catalyzed Selective C–O Bond Activation in Cross-Coupling of Aryl Esters. *J. Am. Chem. Soc.* **2009**, *131* (25), 8815–8823.

(29) Hong, X.; Liang, Y.; Houk, K. N. Mechanisms and Origins of Switchable Chemoselectivity of Ni-Catalyzed C(aryl)–O and C(acyl)–O Activation of Aryl Esters with Phosphine Ligands. *J. Am. Chem. Soc.* **2014**, *136* (5), 2017–2025.

(30) Xu, H.; Muto, K.; Yamaguchi, J.; Zhao, C.; Itami, K.; Musaev, D. G. Key Mechanistic Features of Ni-Catalyzed C–H/C–O Biaryl Coupling of Azoles and Naphthalen-2-yl Pivalates. *J. Am. Chem. Soc.* **2014**, *136* (42), 14834–14844.

(31) Kozuch, S. Steady State Kinetics of Any Catalytic Network: Graph Theory, the Energy Span Model, the Analogy between Catalysis and Electrical Circuits, and the Meaning of "Mechanism." *ACS Catal.* **2015**, *5* (9), 5242–5255.

(32) Kozuch, S.; Shaik, S. How to Conceptualize Catalytic Cycles? The Energetic Span Model. *Acc. Chem. Res.* **2010**.

(33) Solel, E.; Tarannam, N.; Kozuch, S. Catalysis: Energy Is the Measure of All Things. *Chem Commun* **2019**, *55*, 5306–5322.

(34) Yamamoto, T.; Ishizu, J.; Kohara, T.; Komiya, S.; Yamamoto, A. Oxidative Addition of Aryl Carboxylates to Ni(0) Complexes Involving Cleavage of the Acyl–O Bond. *J. Am. Chem. Soc.* **1980**, *102* (11), 3758–3764.

(35) Ishizu, J.; Yamamoto, T.; Yamamoto, A. Selective Cleavage of C–O Bonds in Esters Through Oxidative Addition To Nickel(0) Complexes. *Chem. Lett.* **1976**, *5* (10), 1091–1094.

(36) Li, B.; Li, Y.; Lu, X.; Liu, J.; Guan, B.; Shi, Z. Cross-Coupling of Aryl/Alkenyl Pivalates with Organozinc Reagents through Nickel-Catalyzed C–O Bond Activation under Mild Reaction Conditions. *Angew. Chemie Int. Ed.* **2008**, *47*, 10124–10127.

(37) Guan, B. T.; Wang, Y.; Li, B. J.; Yu, D. G.; Shi, Z. J. Biaryl Construction via Ni-Catalyzed C–O Activation of Phenolic Carboxylates. *J. Am. Chem. Soc.* **2008**, *130* (44), 14468–14470.

(38) Muto, K.; Yamaguchi, J.; Itami, K. Nickel-Catalyzed C–H/C–O Coupling of Azoles with Phenol Derivatives. *J. Am. Chem. Soc.* **2012**, *134* (1), 169–172.

(39) Guo, L.; Rueping, M. Decarbonylative Cross-Couplings: Nickel Catalyzed Functional Group Interconversion Strategies for the Construction of Complex Organic Molecules. *Acc. Chem. Res.* **2018**, *51* (5), 1185–1195.

(40) Dzik, W. I.; Lange, P. P.; Gooßen, L. J. Carboxylates as Sources of Carbon Nucleophiles and Electrophiles: Comparison of Decarboxylative and Decarbonylative Pathways. *Chem. Sci.* **2012**, *3* (9), 2671–2678.

(41) Komiyama, T.; Minami, Y.; Hiyama, T. Recent Advances in Transition-Metal-Catalyzed Synthetic Transformations of Organosilicon Reagents. *ACS Catal.* **2016**, *7* (1), 631–651.

(42) Oestreich, M.; Hartmann, E.; Mewald, M. Activation of the Si–B Interelement Bond: Mechanism, Catalysis, and Synthesis. *Chem. Rev.* **2013**, *113* (1), 402–441.

(43) Cuenca, A. B.; Shishido, R.; Ito, H.; Fernández, E. Transition-Metal-Free B–B and B–interelement Reactions with Organic Molecules. *Chem. Soc. Rev.* **2017**, *46* (2), 415–430.

(44) Ohmura, T.; Suginome, M. Silylboranes as New Tools in Organic Synthesis. *Bull. Chem. Soc. Jpn.* **2009**, *82* (1), 29–49.

(45) Lee, S.-C.; Guo, L.; Yue, H.; Liao, H.-H.; Rueping, M. Nickel-Catalyzed Decarbonylative Silylation, Borylation, and Amination of Arylamides via a Deamidative Reaction Pathway. *Synlett* **2017**, *28* (19), 2594–2598.

(46) Vyas, D. J.; Oestreich, M. Copper-Catalyzed Si–B Bond Activation in Branched-Selective Allylic Substitution of Linear Allylic Chlorides. *Angew. Chem. Int. Ed.* **2010**, *49* (45), 8513–8515.

(47) Yamamoto, E.; Izumi, K.; Horita, Y.; Ito, H. Anomalous Reactivity of Silylborane: Transition-Metal-Free Boryl Substitution of Aryl, Alkenyl, and Alkyl Halides with Silylborane/Alkoxy Base Systems. *J. Am. Chem. Soc.* **2012**, *134* (49), 19997–20000.

(48) Zarate, C.; Nakajima, M.; Martin, R. A Mild and Ligand-Free Ni-Catalyzed Silylation via C–OMe Cleavage. *J. Am. Chem. Soc.* **2017**, *139* (3), 1191–1197.

(49) Gu, Y.; Shen, Y.; Zarate, C.; Martin, R. A Mild and Direct Site-Selective Sp² C–H Silylation of (Poly)Azines. *J. Am. Chem. Soc.* **2019**, *141* (1), 127–132.

(50) Gu, Y.; Duan, Y.; Shen, Y.; Martin, R. Stereoselective Base-Catalyzed 1,1-Silaboration of Terminal Alkynes. *Angew. Chemie Int. Ed.* **2019**, 10.1002/anie.201913544.

(51) Nöth, H.; Höllerer, G. Verbindungen Mit Silicium-Bor-Bindung. *Angew. Chemie* **1962**, *74* (18), 718.

(52) Nöth, H.; Höllerer, G. Beiträge Zur Chemie Des Bors, XXXVI. Organylsilyl-borane. *Chem. Ber.* **1966**, *99* (7), 2197–2205.

(53) Suginome, M. Convenient Preparation of Silylboranes. *Organometallics* **2000**, *19* (22), 4647–4649.

(54) Boebel, T. A.; Hartwig, J. F. Iridium-Catalyzed Preparation of Silylboranes by Silane Borylation and Their Use in the Catalytic Borylation of Arenes. *Organometallics* **2008**, *27* (22), 6013–6019.

(55) Buynak, J. D.; Geng, B. Synthesis and Reactivity of Silylboranes. *Organometallics* **1995**, *14* (6), 3112–3115.

(56) Vyazankin, N. S.; Razuvaev, G. A.; Gladyshev, E. N.; Korneva, S. P. The Synthesis of Triethylsilyllithium and Triethylgermyllithium and the Investigation of Some of Their Reactions. *J. Organomet. Chem.* **1967**, *7* (2), 353–357.

(57) Cirriez, V.; Rasson, C.; Hermant, T.; Petrignet, J.; Díaz Álvarez, J.; Robeyns, K.; Riant, O. Copper-Catalyzed Addition of Nucleophilic Silicon to Aldehydes. *Angew. Chem. Int. Ed.* **2013**, *52* (6), 1785–1788.

(58) Braun, T.; Salomon, M. A.; Altenhöner, K.; Teltewskoi, M.; Hinze, S. C–F Activation at Rhodium Boryl Complexes: Formation of 2-Fluoroalkyl-1,3,2-Dioxaborolanes by Catalytic Functionalization of Hexafluoropropene. *Angew. Chem. Int. Ed.* **2009**, *48* (10), 1818–1822.

(59) Huheey, J. E.; Keiter, E. A.; Keiter, R. L. *Inorganic Chemistry: Principles of Structure and Reactivity*; Harper Collins College Publishers: New York, 1993.

(60) Uematsu, R.; Yamamoto, E.; Maeda, S.; Ito, H.; Taketsugu, T. Reaction Mechanism of the Anomalous Formal Nucleophilic Borylation of Organic Halides with Silylborane: Combined Theoretical and Experimental Studies. *J. Am. Chem. Soc.* **2015**, *137* (12), 4090–4099.

(61) Vyas, D. J.; Fröhlich, R.; Oestreich, M. Activation of the Si–B Linkage: Copper-Catalyzed Addition of Nucleophilic Silicon to Imines. *Org. Lett.* **2011**, *13* (8), 2094–2097.

(62) Wang, X.; Wang, Z.; Nishihara, Y. Nickel/Copper-Cocatalyzed Decarbonylative Silylation of Acyl Fluorides. *Chem. Commun.* **2019**, *55* (71), 10507–10510.

(63) Guo, L.; Chatupheeraphat, A.; Rueping, M. Decarbonylative Silylation of Esters by Combined Nickel and Copper Catalysis for the Synthesis of Arylsilanes and Heteroarylsilanes. *Angew. Chem. Int. Ed.* **2016**, *55* (39), 11810–11813.

(64) Pu, X.; Hu, J.; Zhao, Y.; Shi, Z. Nickel-Catalyzed Decarbonylative Borylation and Silylation of Esters. *ACS Catal.* **2016**, *6* (10), 6692–6698.

(65) Niwa, T.; Ochiai, H.; Watanabe, Y.; Hosoya, T. Ni/Cu-Catalyzed Defluoroborylation of Fluoroarenes for Diverse C–F Bond Functionalizations. *J. Am. Chem. Soc.* **2015**, *137* (45), 14313–14318.

(66) Nelson, D. J.; Nolan, S. P. Hydroxide Complexes of the Late Transition Metals: Organometallic Chemistry and Catalysis. *Coord. Chem. Rev.* **2017**, *353*, 278–294.

(67) Christian, A. H.; Müller, P.; Monfette, S. Nickel Hydroxo Complexes as Intermediates in Nickel-Catalyzed Suzuki-Miyaura Cross-Coupling. *Organometallics* **2014**, *33* (9), 2134–2137.

(68) Zhou, L. I.; Feng, X.; He, R.; Bao, M. X-Ray Structure of Trans-Chloro(1-Naphthyl) bis(triphenylphosphine)nickel(II) and Its Application for Catalytic Dehalogenation of Aryl Chlorides. *J. Coord. Chem.* **2009**, *62* (17), 2824–2831.

(69) Jover, J.; Miloserdov, F. M.; Benet-Buchholz, J.; Grushin, V. V.; Maseras, F. On the Feasibility of Nickel-Catalyzed Trifluoromethylation of Aryl Halides. *Organometallics* **2014**, *33* (22), 6531–6543.

(70) LaBerge, N. A.; Love, J. A. Nickel-Catalyzed Decarbonylative Coupling of Aryl Esters and Arylboronic Acids. *Eur. J. Org. Chem.* **2015**, *2015* (25), 5546–5553.

(71) Jezorek, R. L.; Zhang, N.; Leowanawat, P.; Bunner, M. H.; Gutsche, N.; Pesti, A. K. R.; Olsen, J. T.; Percec, V. Air-Stable Nickel Precatalysts for Fast and Quantitative Cross-Coupling of Aryl Sulfamates with Aryl Neopentylglycolboronates at Room Temperature. *Org Lett* **2014**, *16* (24), 6326–6329.

(72) Li, T.; García, J. J.; Brennessel, W. W.; Jones, W. D. C−CN Bond Activation of Aromatic Nitriles and Fluxionality of the η²-Arene Intermediates: Experimental and Theoretical Investigations. *Organometallics* **2010**, *29* (11), 2430–2445.

(73) Garcia, J. J.; Brunkan, N. M.; Jones, W. D. Cleavage of Carbon-Carbon Bonds in Aromatic Nitriles Using Nickel(0). *J. Am. Chem. Soc.* **2002**, *124* (32), 9547–9555.

(74) Cruickshank, D. W. J.; Sparks, R. A. Experimental and Theoretical Determinations of Bond Lengths in Naphthalene, Anthracene and Other Hydrocarbons. *Proc. R. Soc. London. Ser. A. Math. Phys. Sci.* **1960**, *258* (1293), 270–285.

(75) Pal, S.; Uyeda, C. Evaluating the Effect of Catalyst Nuclearity in Ni-Catalyzed Alkyne Cyclotrimerizations. *J. Am. Chem. Soc.* **2015**, *137* (25), 8042–8045.

(76) Pal, S.; Zhou, Y. Y.; Uyeda, C. Catalytic Reductive Vinylidene Transfer Reactions. *J. Am. Chem. Soc.* **2017**, *139* (34), 11686–11689.

(77) Wu, J.; Hazari, N.; Incarvito, C. D. Synthesis, Properties, and Reactivity with Carbon Dioxide of (Allyl) ₂ Ni(L) Complexes. *Organometallics* **2011**, *30* (11), 3142–3150.

(78) Velian, A.; Lin, S.; Miller, A. J. M.; Day, M. W.; Agapie, T. Synthesis and C–C Coupling Reactivity of a Dinuclear NiI–NiI Complex Supported by a Terphenyl Diphosphine. *J. Am. Chem. Soc.* **2010**, *132* (18), 6296–6297.

(79) Beck, R.; Johnson, S. A. Mechanistic Implications of an Asymmetric Intermediate in Catalytic C–C Coupling by a Dinuclear Nickel Complex. *Chem. Commun.* **2011**, *47* (47), 9233–9235.

(80) Wu, J.; Nova, A.; Balcells, D.; Brudvig, G. W.; Dai, W.; Guard, L. M.; Hazari, N.; Lin, P. H.; Pokhrel, R.; Takase,

M. K. Nickel(I) Monomers and Dimers with Cyclopentadienyl and Indenyl Ligands. *Chem. Eur. J.* **2014**, *20* (18), 5327–5337.

(81) Beck, R.; Johnson, S. A. Mechanistic Implications of an Asymmetric Intermediate in Catalytic C–C Coupling by a Dinuclear Nickel Complex. *Chem. Commun.* **2011**, *47* (32), 9233–9235.

(82) Beck, R.; Johnson, S. A. Structural Similarities in Dinuclear, Tetranuclear, and Pentanuclear Nickel Silyl and Silylene Complexes Obtained via Si–H and Si–C Activation. *Organometallics* **2012**, *31* (9), 3599–3609.

(83) Eisch, J. J.; Piotrowski, A. M.; Han, K. I.; Krüger, C.; Tsay, Y. H. Oxidative Addition of Nickel(0) Complexes to Carbon–Carbon Bonds in Biphenylene: Formation of Nickelole and 1,2-Dinickelecin Intermediates. *Organometallics* **1985**, *4* (2), 224–231.

(84) Matsubara, K.; Yamamoto, H.; Miyazaki, S.; Inatomi, T.; Nonaka, K.; Koga, Y.; Yamada, Y.; Veiros, L. F.; Kirchner, K. Dinuclear Systems in the Efficient Nickel-Catalyzed Kumada-Tamao-Corriu Cross-Coupling of Aryl Halides. *Organometallics* **2017**, *36* (2), 255–265.

(85) Zhu, S.; Shoshani, M. M.; Johnson, S. A. Versatile (η⁶-arene)Ni(PCy₃) Nickel Monophosphine Precursors. *Chem. Commun.* **2017**, *53* (98), 13176–13179.

(86) Beromi, M. M.; Nova, A.; Balcells, D.; Brasacchio, A. M.; Brudvig, G. W.; Guard, L. M.; Hazari, N.; Vinyard, D. J. Mechanistic Study of an Improved Ni Precatalyst for Suzuki-Miyaura Reactions of Aryl Sulfamates: Understanding the Role of Ni(I) Species. *J. Am. Chem. Soc.* **2017**, *139* (2), 922–936.

(87) Perdriau, S.; Chang, M.; Otten, E.; Heeres, H. J.; de Vries, J. G. Alkene Isomerisation Catalysed by a Ruthenium PNN Pincer Complex. *Chem. Eur. J.* **2014**, *20* (47), 15434–15442.

(88) Nett, A. J.; Montgomery, J.; Zimmerman, P. M. Entrances, Traps, and Rate-Controlling Factors for Nickel-Catalyzed C–H Functionalization. *ACS Catal.* **2017**, *7* (10), 7352–7362.

(89) Cornella, J.; Gómez-Bengoa, E.; Martin, R. A Combined Experimental and Theoretical Study on the Reductive Cleavage of Inert C–O Bonds with Silanes: Ruling out a Classical Ni(0)/Ni(II) Catalytic Couple and Evidence for Ni(I) Intermediates. *J .Am. Chem. Soc.* **2013**, *135* (5), 1997–2009.

(90) Ogoshi, S.; Kamada, H.; Kurosawa, H. Reaction of (η²-arylaldehyde)nickel(0) Complexes with Me₃SiX (X=OTf, Cl). Application to Catalytic Reductive Homocoupling Reaction of Arylaldehyde. *Tetrahedron* **2006**, *62* (32), 7583–7588.

(91) Inatomi, T.; Koga, Y.; Matsubara, K. Dinuclear Nickel(I) and Palladium(I) Complexes for Highly Active Transformations of Organic Compounds. *Molecules* **2018**, *23* (1), 140.

(92) Powers, I. G.; Uyeda, C. Metal-Metal Bonds in Catalysis. *ACS Catal.* **2017**, *7* (2), 936–958.

(93) Markert, C.; Neuburger, M.; Kulicke, K.; Meuwly, M.; Pfaltz, A. Palladium-Catalyzed Allylic Substitution: Reversible Formation of Allyl-Bridged Dinuclear Palladium(I) Complexes. *Angew. Chem. Int. Ed.* **2007**, *46* (31), 5892–5895.

(94) Castellanos-Blanco, N.; Arévalo, A.; García, J. J. Nickel-Catalyzed Transfer Hydrogenation of Ketones Using Ethanol as a Solvent and a Hydrogen Donor. *Dalton Trans.* **2016**, *45* (34), 13604–13614.

(95) Bennett, M. A.; Johnson, J. A.; Willis, A. C. Synthesis and Reactions of Nickel(0) H²-Cyclohexyne Complexes and X-Ray Crystal Structure of Ni(η²-C₆H₈)((C₆H₁₁)₂PCH₂CH₂P(C₆H₁₁)₂). *Organometallics* **1996**, *15* (1), 68–74.

(96) Blackmond, D. G. Reaction Progress Kinetic Analysis: A Powerful Methodology for Mechanistic Studies of Complex Catalytic Reactions. *Angew. Chem. Int. Ed.* **2005**, *44* (28), 4302–4320.

(97) Baxter, R. D.; Sale, D.; Engle, K. M.; Yu, J. Q.; Blackmond, D. G. Mechanistic Rationalization of Unusual Kinetics in Pd-Catalyzed C–H Olefination. *J. Am. Chem. Soc.* **2012**, *134* (10), 4600–4606.

(98) Burés, J. A Simple Graphical Method to Determine the Order in Catalyst. *Angew. Chem. Int. Ed.* **2016**, *55* (6), 2028–2031.

(99) Burés, J. Variable Time Normalization Analysis: General Graphical Elucidation of Reaction Orders from Concentration Profiles. *Angew. Chem. Int. Ed.* **2016**, *55*, 16084.

(100) Matsubara, K.; Fukahori, Y.; Inatomi, T.; Tazaki, S.; Yamada, Y.; Koga, Y.; Kanegawa, S.; Nakamura, T. Monomeric Three-Coordinate N-Heterocyclic Carbene Nickel(I) Complexes: Synthesis, Structures, and Catalytic Applications in Cross-Coupling Reactions. *Organometallics* **2016**, *35* (19), 3281–3287.

(101) Sperger, T.; Stirner, C. K.; Schoenebeck, F. Bench-Stable and Recoverable Palladium(I) Dimer as an Efficient Catalyst for Heck Cross-Coupling. *Synth.* **2017**, *49* (1), 115–120.

(102) Diehl, C. J.; Scattolin, T.; Englert, U.; Schoenebeck, F. C−I-Selective Cross-Coupling Enabled by a Cationic Palladium Trimer. *Angew. Chem. Int. Ed.* **2019**, *58* (1), 211–215.

(103) Popov, A. I. Multi Nuclear NMR Studies of Alkali Ions in Non Aqueous Solvents. *Pure Appl. Chem.* **1979**, *51* (1), 101–110.

(104) Dijkstra, G.; Kruizinga, W. H.; Kellogg, R. M. An Assessment of The Causes of The "Cesium Effect." *J. Org. Chem.* **1987**, *52* (19), 4230–4234.

(105) Wrackmeyer, B.; Khan, E.; Kempe, R. Protodeborylation of Triorganoboranes. *Zeitschrift fur Naturforsch. B* **2008**, *63* (3), 275–279.

(106) Product Subclass 9: Acyloxyboranes. In *Science of Synthesis, 6: Category 1, Organometallics*; Kaufmann, D. E.,

Matteson, D. S., Schaumann, E., Regitz, M., Eds.; Science of Synthesis; Georg Thieme Verlag: Stuttgart, 2004; Vol. 6.

(107) Lang, A.; Nöth, H.; Schmidt, M. Synthesis of Structures of (Acyloxy)boranes. *Chem. Ber.* **1995**, *128* (8), 751–762.

(108) Standley, E. A.; Jamison, T. F. Simplifying Nickel(0) Catalysis: An Air-Stable Nickel Precatalyst for the Internally Selective Benzylation of Terminal Alkenes. *J. Am. Chem. Soc.* **2013**, *135* (4), 1585–1592.

(109) Wozniak, M.; Braun, T.; Ahrens, M.; Braun-Cula, B.; Wittwer, P.; Herrmann, R.; Laubenstein, R. Activation of SF_6 at a Xantphos-Type Rhodium Complex. *Organometallics* **2018**, *37* (5), 821–828.

(110) Zhao, Y.; Truhlar, D. G. The M06 Suite of Density Functionals for Main Group Thermochemistry, Thermochemical Kinetics, Noncovalent Interactions, Excited States, and Transition Elements: Two New Functionals and Systematic Testing of Four M06-Class Functionals and 12 Other Functionals. *Theor. Chem. Acc.* **2008**, *120* (1–3), 215–241.

(111) Cossi, M.; Barone, V.; Mennucci, B.; Tomasi, J. Ab Initio Study of Ionic Solutions by a Polarizable Continuum Dielectric Model. *Chem. Phys. Lett.* **1998**, *286* (3–4), 253–260.

(112) Cances, E.; Mennucci, B.; Tomasi, J. A New Integral Equation Formalism for the Polarizable Continuum Model: Theoretical Background and Applications to Isotropic and Anisotropic Dielectrics. *J. Chem. Phys.* **1997**, *107* (8), 3032–3041.

(113) Tomasi, J.; Mennucci, B.; Cances, E. The IEF Version of the PCM Solvation Method: An Overview of a New Method Addressed to Study Molecular Solutes at the QM Ab Initio Level. *J. Mol. Struct. THEOCHEM* **1999**, *464* (1–3), 211–226.

(114) Evans, D. F. 400. The Determination of the Paramagnetic Susceptibility of Substances in Solution by Nuclear Magnetic Resonance. *J. Chem. Soc.* **1959**, 2003–2005.

(115) Sur, S. K. Measurement of Magnetic Susceptibility and Magnetic Moment of Paramagnetic Molecules in Solution by High-Field Fourier Trasform NMR Spectroscopy. *J. Magn. Reson.* **1989**, *82*, 169–173.

(116) Mazzini, F.; Salvadori, P. An Easy Two-Step Reduction of Salicylic Acids and Alcohols to 2-Methylphenols. *Synthesis (Stuttg).* **2005**, No. 15, 2479–2481.

(117) Oguma, T.; Katsuki, T. Iron-Catalyzed Dioxygen-Driven C–C Bond Formation: Oxidative Dearomatization of 2-Naphthols with Construction of a Chiral Quaternary Stereocenter. *J. Am. Chem. Soc.* **2012**, *134* (49), 20017–20020.

(118) Ishihara, K.; Kubota, M.; Kurihara, H.; Yamamoto, H. Scandium Trifluoromethanesulfonate as an Extremely Active Lewis Acid Catalyst in Acylation of Alcohols with Acid Anhydrides and Mixed Anhydrides. *J. Org. Chem.* **1996**, *61*, 4560–4567.

(119) Cortijo, M.; Delgado-Martinez, P.; Gonzalez-Prieto, R.; Herrero, S.; Jimenez-Aparicio, R.; Perles, J.; Priego, J. L.; Torres, M. R. Microwave and Solvothermal Methods for the Synthesis of Nickel and Ruthenium Complexes with 9-Anthracene Carboxylate Ligand. *Inorg. Chim. Acta* **2015**, *424*, 176–185.

(120) Lee, C.; Yang, W.; Parr, R. G. Development of the Colle-Salvetti Correlation-Energy Formula into a Functional of the Electron Density. *Phys. Rev. B* **1988**, *37* (2), 785.

(121) Becke, A. D. A New Mixing of Hartree–Fock and Local density-Functional Theories. *J. Chem. Phys.* **1993**, *98* (2), 1372–1377.

(122) Dolg, M.; Wedig, U.; Stoll, H.; Preuss, H. Energy-Adjusted Abinitio Pseudopotentials for the First Row Transition Elements. *J. Chem. Phys.* **1987**, *86* (2), 866–872.

(123) Andrae, D.; Haeussermann, U.; Dolg, M.; Stoll, H.; Preuss, H. Energy-Adjustedab Initio Pseudopotentials for the Second and Third Row Transition Elements. *Theor. Chim. Acta* **1990**, *77* (2), 123–141.

(124) Gonzalez, C.; Schlegel, H. B. Reaction Path Following in Mass-Weighted Internal Coordinates. *J. Phys. Chem.* **1990**, *94* (14), 5523–5527.

2.11.   Experimental section

2.11.1.   General Considerations

Reagents. [Ni(COD)$_2$] and PCy$_3$ were purchased from Strem Chemicals. CuF$_2$ (99.5%) was purchased from Alfa Aesar. CsF (99%) was purchased from Aldrich. Pivalic acid was purchased from Fluorochem and dried by azeotropic distillation with benzene. Triethylsilane was deoxygenated prior to its use in the synthesis of Et$_3$SiBpin. All other reagents were purchased from commercial sources and used without further purification. 1-naphthyl pivalate (**6a**),[16] 2-naphthyl pivalate (**6b**),[48] 7-methoxynaphthalen-2-yl pivalate (**6e**),[16] and phenyl pivalate (**6f**)[7] were synthesised according to literature procedures. (1-triethylsilyl)naphthalene (**9a**),[48] (2-triethylsilyl)naphthalene (**9b**),[48] and **9e**,[16] were previously reported.

Solvents. Toluene, pentane, toluene-d$_8$, and DMSO-d$_6$ were degassed by the appropriate method (sparging or freeze-pump-thaw cycles) then dried over 4Å molecular sieves and stored in the glovebox. Triethylsilane was degassed and stored under argon. Benzene-d$_6$, THF, cyclohexane, and Et$_2$O were degassed by the appropriate method (sparging or freeze-pump-thaw cycles) and dried over Solvona (sodium adsorbed on an inorganic support).

Analytical methods. Flash chromatography was performed with Sigma Aldrich technical grade silica gel 60 (230-400 mesh). Thin layer chromatography was carried out using Merck TLC Silica gel 60 F254. NMR spectra were recorded on Bruker Avance Ultrashield 300, 400, or 500 MHz spectrometers, with chemical shifts reported in parts per million (ppm) and coupling constants, *J*, reported in hertz. Melting points were measured using open glass capillaries in a Mettler Toledo MP70 apparatus. Gas chromatographic analyses were performed on an Agilent 6890N gas chromatograph with a FID detector. IR spectra were obtained with a Bruker FT-IR Alpha spectrometer.

Evans method[114,115] solution magnetic susceptibility measurements were performed for **7a**. Magnetic susceptibility data for **7a** and **8** were obtained with a Quantum Design MPMS-XL SQUID magnetometer and analysed by Dr Cristina Sáenz de Pipaón and Prof José Ramón Galán-Mascarós.

All air-sensitive manipulations were carried out under an atmosphere of nitrogen in an MBraun UNIlab plus glovebox or using standard Schlenk techniques.

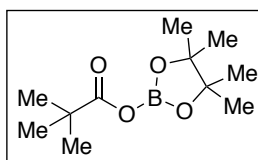## 2.11.2. Synthesis and characterisation of precursors and products

Et$_3$SiBpin
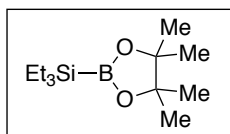
This compound was synthesised following a reported procedure.[16,48,54]

^{1}H NMR (300 MHz, CDCl$_3$): δ 1.23 (s, 12H, CH$_3$ Bpin), 0.97 (t, $^3J_{\text{H-H}}$ = 7.9 Hz, 9H, CH$_3$), 0.59 (q, $^3J_{\text{H-H}}$ = 7.9 Hz, 6H, CH$_2$).

^{11}B NMR (128 MHz, CDCl$_3$): δ 35.18.

^{13}C{^{1}H} NMR (101 MHz, C$_6$D$_6$): δ 83.0 (s, C$_{\text{(Bpin)}}$), 25.2 (s, CH$_{3\text{(OPiv)}}$), 8.5 (s, CH$_3$), 3.1 (s, CH$_2$).

PivOBpin

Inside the glovebox, a toluene solution of dry pivalic acid (172 mg in 1 mL, 1.68 mmol, 1 equiv) was added portion-wise to a toluene solution of pinacolborane (0.25 mL in 0.5 mL toluene, 1.7 mmol, 1.01 equiv) at room temperature over 45 minutes. Hydrogen evolution was observed as the reaction progressed. After 2.5 hours of stirring, volatiles were removed under vacuum to give PivOBpin as a white oil in approximately quantitative yield (estimated 94–97% pure by NMR). PivOBpin was stored in the glovebox freezer at −25 ºC as a soft white solid.

NOTE: This compound is extremely moisture sensitive. Pivalic acid must be dried carefully, and PivOBpin should be stored appropriately (preferably inside a glovebox).

^{1}H NMR (400 MHz, C$_6$D$_6$): δ 1.10 (s, 9H, *t*Bu), 1.05 (s, 12H, CH$_3$).

^{11}B NMR (128 MHz, C$_6$D$_6$): δ 23.39.

^{13}C{^{1}H} NMR (101 MHz, C$_6$D$_6$): δ 175.8 (s, C=O), 84.1 (s, C$_{\text{(Bpin)}}$), 39.6 (s, C$_{\text{(OPiv)}}$), 26.9 (s, CH$_{3\text{(OPiv)}}$), 24.6 (s, CH$_{3\text{(Bpin)}}$).

2.11.3.   Syntheses of aryl pivalates

1,3-dimethyl-naphthalen-2-yl pivalate (6d)
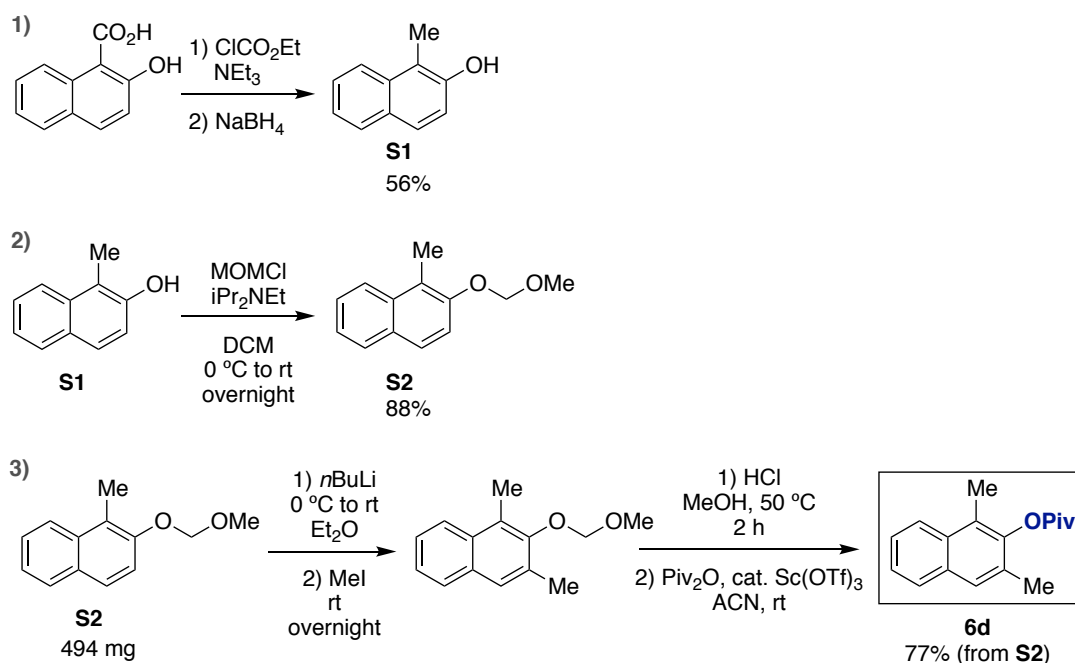
Scheme S2.1. Synthetic route to 6d.

S1 was synthesised in 56% yield following a literature procedure.[116] This was then converted into MOM-protected 1,3-dimethyl-naphthalen-2-ol following a procedure reported by Oguma et al.[117] After deprotection,[117] crude 1,3-dimethyl-naphthalen-2-ol was submitted to the scandium-catalysed esterification conditions reported by Yamamoto et al:[118] Crude 1,3-dimethyl-naphthalen-2-ol (approximately 2.4 mmol) and excess pivalic anhydride (743 µL, 3.66 mmol, 1.5 equiv) were combined in 9 mL acetonitrile under argon. In a separate flask, $Sc(OTf)_3$ (12 mg, 0.024 mmol, 0.1 equiv) was dissolved in 250 µL acetonitrile. This solution was then added slowly to the room temperature alcohol solution. After 20 hours of stirring, the reaction was quenched with saturated $NaHCO_3$ solution, washed with 3 x 10 mL saturated NaCl solution, then dried over $MgSO_4$. Crystallisation from cold pentane gave three crops of a **6d** as a white crystalline solid (487 mg, 77% from **S2**)

¹H NMR (400 MHz, CDCl$_3$): δ 7.94 (m, 1H), 7.75 (m, 1H), 7.55 (s, 1H), 7.44 (m, 2H), 2.44 (s, 3H, CH$_3$), 2.30 (s, 3H, CH$_3$), 1.47 (s, 9H, tBu).
¹³C{¹H} NMR (101 MHz, CDCl$_3$): δ 176.50 (C=O), 146.39, 132.20, 132.00, 129.64, 127.89, 127.40, 125.48, 125.31, 124.68, 124.09, 77.48, 77.16, 76.84, 39.56, 27.57, 17.48, 11.71.
IR (ATR, neat, cm^{-1}): 3074 (medium, Ar); 2978 (strong, CH); 1738 (C=O stretch, strong); 1118 (C-O stretch, strong); 740 (=CH bends, medium).
HRMS (ESI) [C$_{17}$H$_{20}$NaO$_2$] (M+Na) *calcd* 279.1356, *found* 279.1352.
Melting point: 61.2–62 ºC.

1-methyl-naphthalen-2-yl pivalate (6c)
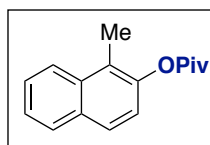
    1-methyl-2-naphthol (**S1**, 109 mg, 0.69 mmol) and NEt$_3$ (91 μL, 0.65 mmol, 1 equiv) were combined in 2 mL dichloromethane and the solution cooled to 0 ºC. PivCl (81 μL, 0.65 mmol, 1 equiv) was added with stirring, then the solution allowed to warm to room temperature. Stirring was continued for 7 hours. The yellow reaction mixture was washed with 2 M HCl (3 x 10 mL), water (1 x 10 mL), saturated NaHCO$_3$ solution (1 x 10 mL), then dried over MgSO$_4$ and concentrated to give an off-white solid. Purification by column chromatography (20:1 hexane/ethyl acetate, Rf = 0.61) gave **6c** as a white solid (97 mg, 61%).

^{1}H NMR (300 MHz, CDCl$_3$): δ 8.01 (d, J = 8.5 Hz, 1H), 7.87–7.82 (m, 1H), 7.72 (d, J = 8.8 Hz, 1H), 7.59–7.50 (m, 1H), 7.50–7.44 (m, 1H), 7.12 (d, J = 8.8 Hz, 2H), 2.49 (s, 3H), 1.45 (s, 9H).

^{13}C{^{1}H} NMR (75 MHz, CDCl$_3$): δ 177.2, 146.6, 133.5, 131.8, 128.6, 127.3, 126.4, 125.3, 124.6, 124.2, 121.5, 39.4, 27.4, 11.5.

IR (ATR, neat, cm^{-1}): 2975 (medium, CH); 1747 (C=O stretch, strong); 1113 (C-O stretch, strong); 800, 768, 746 (=CH bends, medium).

**HRMS** (ESI) [C$_{16}$H$_{18}$NaO$_2$] (M+Na) *calcd* 265.1199, *found* 265.1201.

Melting point: 66.9–68.6 ºC.

2.11.4.   General procedure for silylation reactions
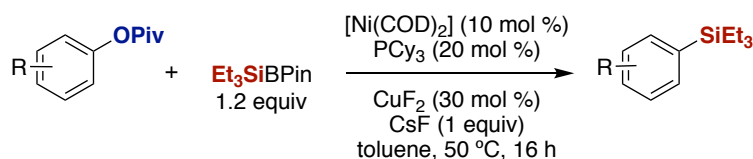
Scheme S2.2. General scheme for Ni-catalysed silylation of aryl pivalates.

This procedure follows that described in the original paper by Zarate and Martin:[16] In the glovebox, an oven-dried 15 mL screw cap reaction tube equipped with a stir bar was charged with CsF (38.0 mg, 0.25 mmol, 1 equiv), CuF_2 (7.6 mg, 0.075 mmol, 0.3 equiv), aryl pivalate (0.25 mmol, 1 equiv), and 1 mL toluene. Solutions of PCy_3 (14.0 mg, 0.050 mmol, 0.2 equiv) and [Ni(COD)₂] (6.9 mg, 0.025 mmol, 0.1 equiv) were then added to give an orange reaction mixture. *It is important to add the PCy₃ solution before the [Ni(COD)₂] solution.* Et₃SiBpin (72.6 mg, 0.3 mmol, 1.2 equiv) and internal standard (decane, 35.6 mg, 0.25 mmol, 1 equiv) were then added, followed by enough toluene to make up the volume to 3 mL. The tubes were then sealed, removed from the glovebox, and heated in a pre-heated (50 °C) aluminium block for 16 hours. After cooling to room temperature, 5 mL ethyl acetate was added to the reaction mixture and an aliquot analysed as required (TLC and/or GC-MS, NMR). The reaction mixture was then transferred to a flask with ethyl acetate and evaporated to give a residue ready for column chromatography.

(1-methyl-2-triethylsilyl)naphthalene (9c)
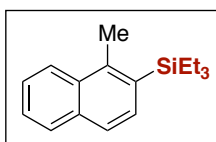
The **general procedure** detailed above was followed using **6c** (60.6 mg, 0.25 mmol, 1 equiv). Purification by flash chromatography on silica gel (100% pentane, Rf = 0.70) gave **9c** as a colourless oil in 64% yield (41.0 mg).

¹H NMR (400 MHz, CDCl₃): δ 8.16–8.03 (m, 1H), 7.87–7.78 (m, 1H), 7.69 (d, *J* = 8.35 Hz, 1H), 7.53 (d, *J* = 8.10 Hz, 1H), 7.57–7.44 (m, 2H), 2.82 (s, 3H, CH₃), 1.12–0.82 (m, 15H, SiEt₃).
¹³C{¹H} NMR (101 MHz, CDCl₃): δ 141.2, 133.9, 132.9, 132.7, 131.7, 128.5, 126.0, 125.8, 125.2, 124.2, 19.6, 7.9, 4.9.
**IR** (ATR, neat, cm⁻¹): 3051 (medium, Ar); 2951, 2873 (strong, CH); 1458 (C=C stretch, weak); 1031, 1014, 809, 728, 706 (=CH bends, strong).
HRMS (ESI) [C₁₆H₁₈NaO₂] (M+Na) *calcd* 265.1199, *found* 265.120.

1,3-dimethyl-2-triethylsilyl naphthalene (9d)
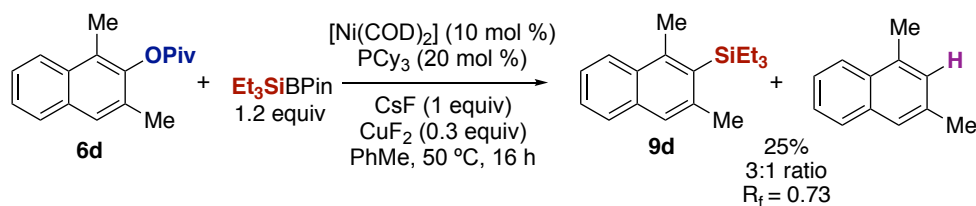
Scheme S2.3. Silylation of hindered naphthyl pivalate 9d.

The **general procedure** detailed above was followed using **6d** (64.6 mg, 0.25 mmol, 1 equiv). Purification by flash chromatography on silica gel (100% pentane, Rf = 0.73) gave a colourless oil (17 mg). NMR analysis showed this to be a 3.3:1 mixture of the desired product **9d** and the reduced product.
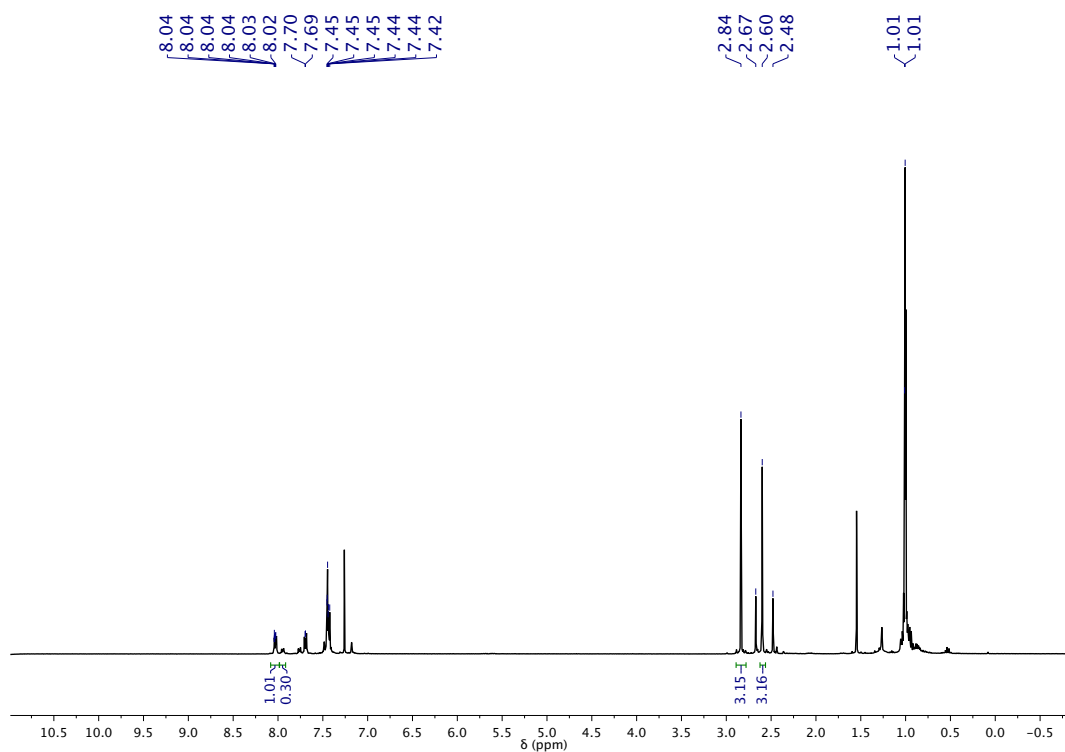
Figure S2.1 Mixture of 9d and 1,3-dimethyl naphthalene obtained from silylation of 6d under the general conditions.

2.11.5. Reaction monitoring (NMR)

2.11.5.1. Silylation of 6a
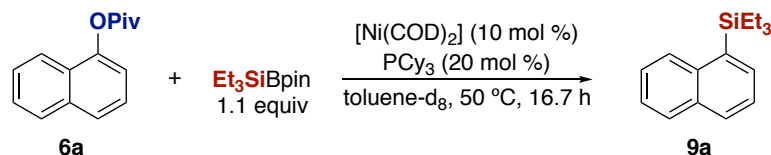
Scheme S2.4. CuF₂/CsF-free silylation of 6a for NMR monitoring.

A vial was charged with **6a** (8.55 mg, 0.0375 mmol, 1 equiv), 271 μL toluene-d₈, and PCy₃ (29.2 μL, 0.257 M toluene-d₈ solution, 0.2 equiv), followed by [Ni(COD)₂] (100 μL, 0.036 M toluene-d₈ solution, 0.1 equiv), and Et₃SiBpin (10.0 mg, 0.041 mmol, 1.1 equiv). The orange solution was transferred to a J Young NMR tube and a capillary containing maleic acid/D₂O was added as an internal standard. After collection of room temperature ³¹P{¹H} and ¹H NMR spectra, NMR spectra were collected at 50 °C every 38 minutes for 17 h, and the resulting integrals plotted as shown in the text.
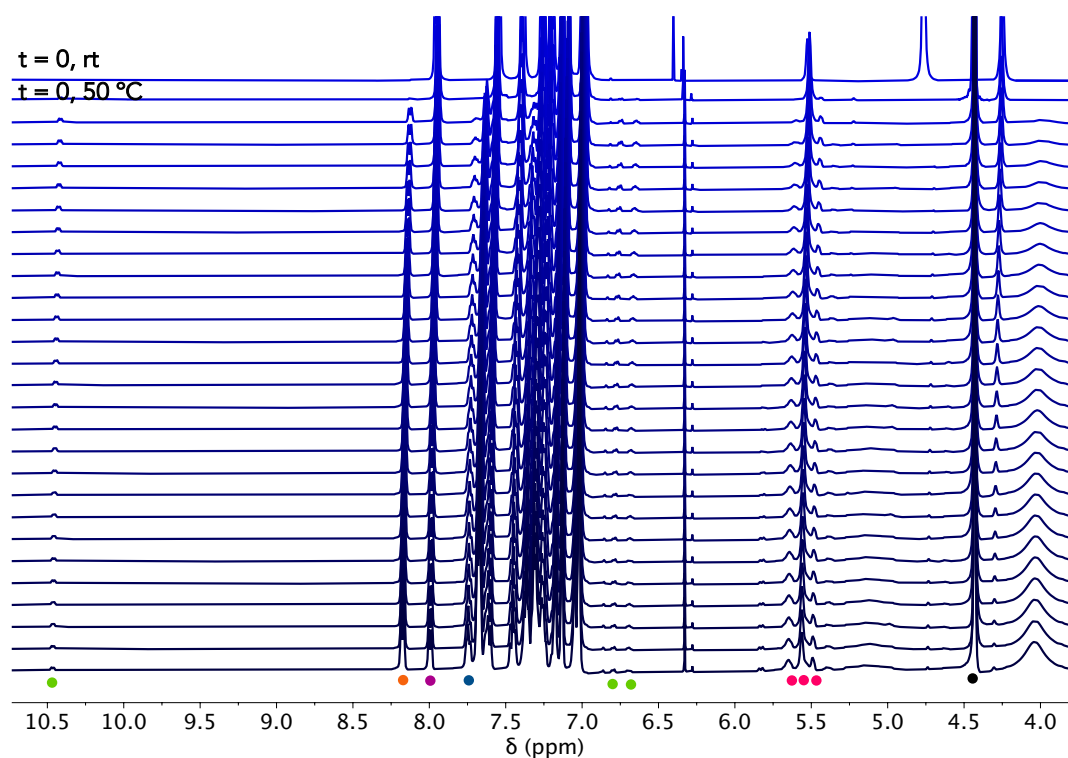
Figure S2.2. Expansion of ¹H NMR monitoring experiment (t=0 from top [*top*: room temperature spectrum, followed by t=0 at 50 °C, spectra collected every 38 minutes]. Peaks for complex 7a (green circles), silylated product (9a, orange), starting material (6a, purple), and COD isomers (pink) are labelled with coloured circles alongside internal standard (capillary of maleic acid/D₂O, black) and 1,1'-binaphthalene (blue).
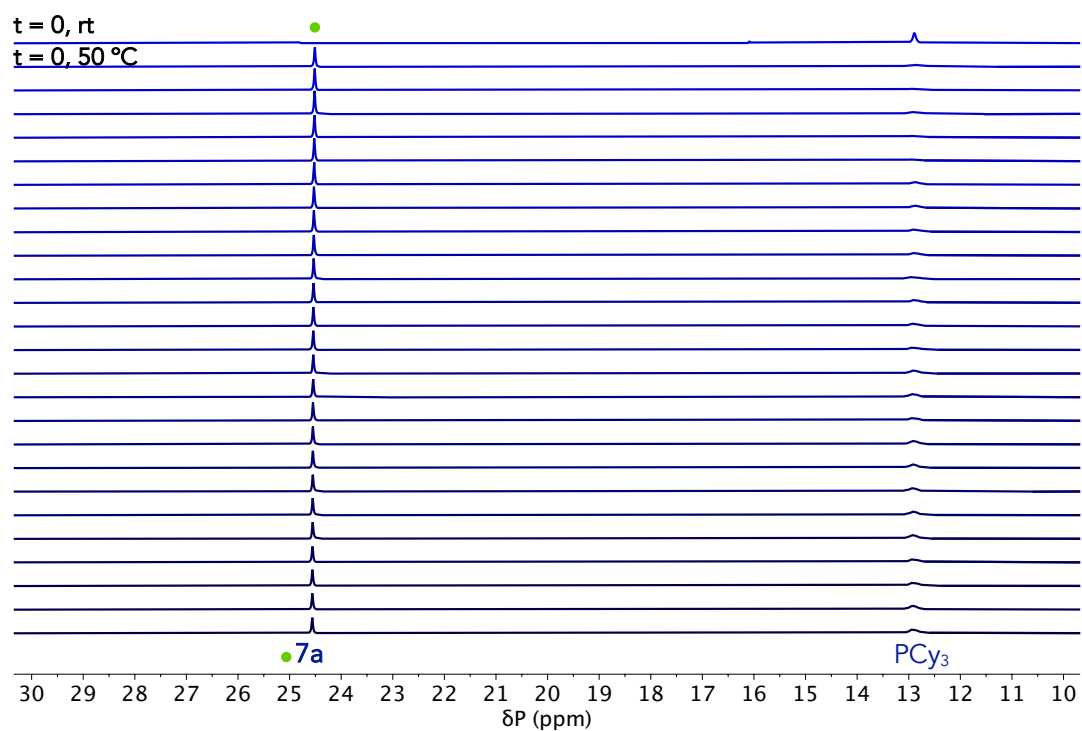
Figure S2.3. Expansion of corresponding $^{31}P\{^{1}H\}$ IGD (integrable) NMR monitoring experiment (t=0 at top, spectra every 38 minutes).

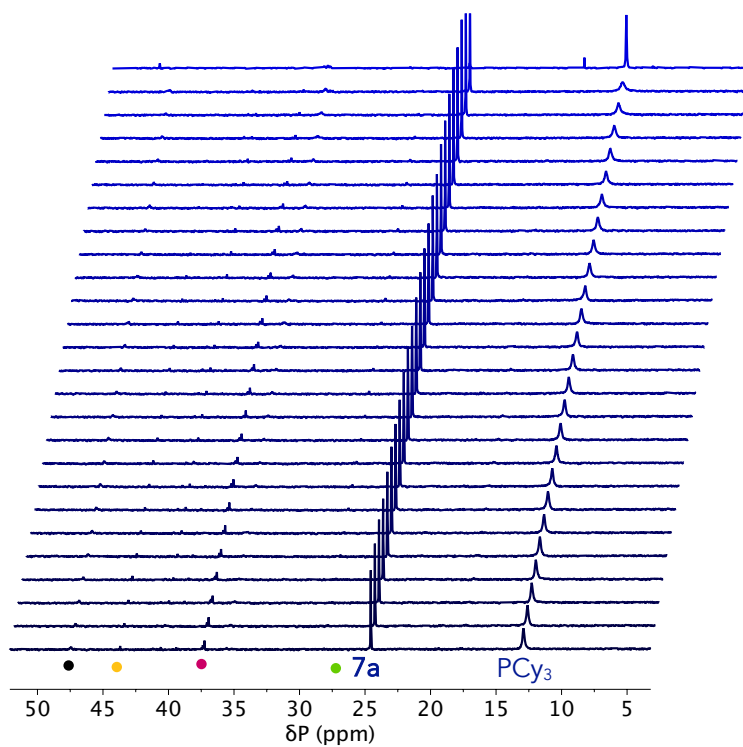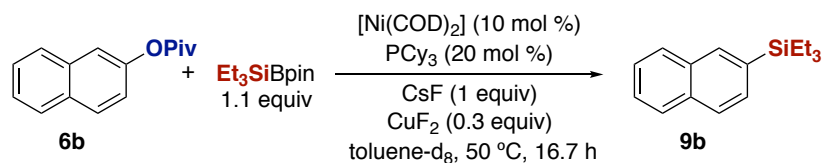**Figure S2.4.** Expansion of corresponding $^{31}P\{^{1}H\}$ IGD (integrable) NMR monitoring experiment in order to show minor signals that appear during reaction. Black circle = unknown; yellow circle assigned to [NiO(PCy$_3$)]$_4$; pink circle assigned to Ni–CO complexes.

2.11.5.2. Silylation of 6b

Scheme S2.5. Silylation of 6b for NMR monitoring.

A vial was charged with **6b** (27 mg, 0.118 mmol, 1 equiv), 0.6 mL toluene-d8, and PCy3 (6.7 mg, 0.024 mmol, 0.2 equiv), followed by [Ni(COD)2] (3.3 mg, 0.012 mmol, 0.1 equiv), and Et3SiBpin (41 μL, 0.130 mmol, 1.1 equiv). The orange solution was transferred to a J Young NMR tube pre-filled with CsF (18.2 mg, 0.118 mmol, 1 equiv) and CuF2 (3.66 mg, 0.035 mmol, 0.3 equiv). After collection of room temperature ³¹P{¹H} and ¹H NMR spectra, NMR spectra were collected at 50 ºC every 30 minutes for 15.5 h. The CsF and CuF2 remained at the bottom of the NMR tube. Quantitative data were not obtained from the resulting NMR spectra as overlap precluded integration of **6b** and **9b**. However, a ¹H NMR spectrum is provided for reference (Figure S2.5). This shows formation of complex **7b** and conversion of **6b** to **9b**, naphthalene, and 1,1'-binaphthalene.
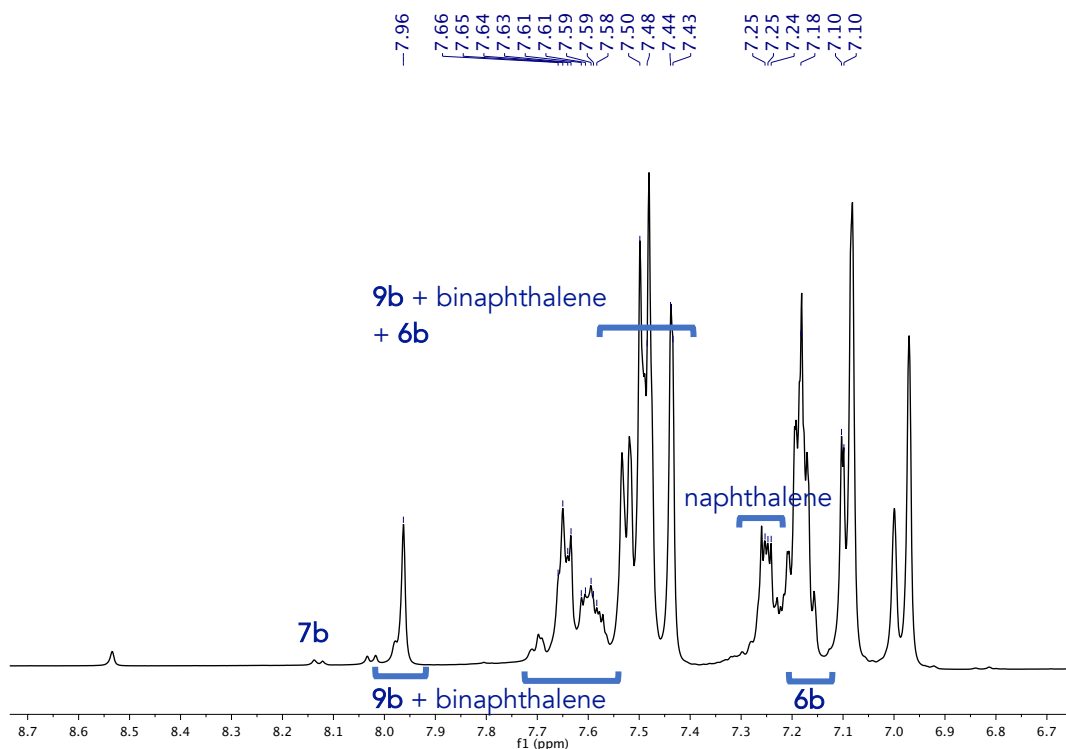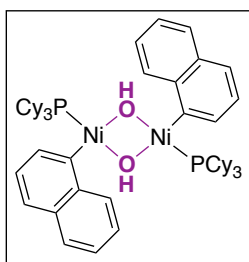

Figure S2.5. ¹H NMR monitoring experiment of 6b silylation: sample spectrum (ca. 7.5 h) indicating occurrence of overlap of product 9b, naphthalene, 1,1'-binaphthalene, and 6b. A small amount of oxidative addition complex 7b was also observed.

2.11.6. Preparation of nickel complexes

[Ni(σ-1-naphthyl)(μ-OH)-(PCy₃)]₂ (4)

Synthesised based on a reported procedure.[67]

[Ni(σ-1-naphthyl)(Cl)(PCy₃)₂] (114 mg, 0.146 mmol, 1 equiv) was weighed into a round bottom flask fitted with an argon inlet then suspended in 6 mL THF. Gentle warming gave an orange solution. Excess CsOH·H_2O (245 mg, 1.46 mmol, 10 equiv) was then added followed by 0.2 mL water. The orange reaction mixture was stirred for 18 h then filtered through a small plug of celite in a glass pipette. The orange solution was dried to give **4** as a yellow powdery solid (70.6 mg, 85%).

Complex **4** exists as two isomers (1:0.3 ratio). As such, the NMR signals were not fully assigned as for the other complexes in this Chapter.

¹H NMR (500 MHz, C_6D_6): δ 11.24 (d, ³J_{H-H} = 8.2 Hz, 2H, H8-1), 11.03 (d, ³J_{H-H} = 8.2 Hz, 0.6H, H8-2), 8.41 (d, ³J_{H-H} = 6.9 Hz, 0.6H, H2-2), 8.21 (d, ³J_{H-H} = 6.8 Hz, 2H, H2-1), 7.84 (t, ³J_{H-H} = 7.5 Hz, 0.7H, H7-2), 7.79 (t, ³J_{H-H} = 7.5 Hz, 2H, H7-1), 7.62 (d, ³J_{H-H} = 8.2 Hz, 0.6H, H5-2), 7.59 (d, ³J_{H-H} = 8.0 Hz, 2H, H5-1), 7.45–7.33 (m, 6H, H6, H3), 7.28–7.19 (m, 4H, H4), 2.35 (m, 4H, Cy-1), 2.22 (s, 2H, Cy-2), 1.88 (m, 6H, Cy), 1.78–0.65 (m, 82H, Cy + OPiv), 0.49 (s, 10H, Cy), −3.51 (s, 2H, OH-1), −3.72 (s, 0.6H, OH-2).

³¹P NMR (121 MHz, C_6D_6): δ 32.76 (1), 31.16 (2).

¹³C NMR (126 MHz, C_6D_6): δ 156.5 (m, 1), 156.2 (m, 2), 143.1 (s, 1), 136.0 (overlap), 133.5 (s), 129.0 (s), 124.9 (s), 123.6 (overlap), 122.6 (s, 1), 122.4 (s, 2), 33.5 (overlap), 30.7 (s, Cy-1), 30.4. (s, Cy-2), 29.4 (s, Cy-2), 29-3 (s, Cy-1), 27.9 (m), 27.4 (m), 26.6 (s, Cy-1), 26.5 (s, Cy-2).

[Ni₂(PCy₃)₂(μ-OPiv)₄] (8)
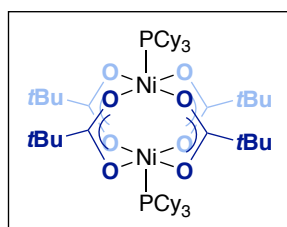
From 6a: [Ni(COD)₂] (25.7 mg, 0.0936 mmol), PCy₃ (52.3 mg, 0.186 mmol), and **6a** (42.5 mg, 0.186 mmol) were weighed into a Schlenk tube then dissolved in 1 mL toluene. This was then removed from the glovebox and placed in a 100 ºC sand bath for 18 h. The reaction was carried out without stirring. After cooling to room temperature, large dark green crystals were obtained. These were filtered, washed

with EtOAc (5 mL), then dried to give **8** (35 mg, 69% yield). The filtrate was purified by column chromatography (hexane, R_f = 0.34) to yield 1,1'-binaphthalene as a white solid (16.7 mg, 70%). NMR spectra of 1,1-binaphthelane match previously reported data.[14]

From 6b: [Ni(COD)$_2$] (21.0 mg, 0.076 mmol), PCy$_3$ (42.7 mg, 0.152 mmol), and **6b** (34.8 mg, 0.152 mmol) were weighed into a Schlenk tube then dissolved in 1 mL toluene. This was then removed from the glovebox and placed in a 100 ºC sand bath for 18 h. The reaction was carried out without stirring. After cooling to room temperature, dark blocks of **8** were obtained (7 mg, 17% yield). *Higher yields are obtained following the method above with a 1:1 ratio of Ni/ligand and a more concentrated solution (0.55 M). For example, large dark blocks of* **8** *(e.g. 79% yield, from 0.277 mmol [Ni(COD)$_2$]) could be obtained in this manner.*

Due to the paramagnetic nature of **8** and its low solubility in all NMR solvents tested, a $^{13}C\{^1H\}$ NMR spectrum was not obtained. The ^{31}P NMR spectrum did not contain any signals. X-ray quality crystals were obtained upon cooling the unstirred reaction mixture (toluene).

IR (ATR, powder, cm^{-1}): 2921 (strong, CH); 1614 (C=O stretch, strong); 1416 (C-O stretch, medium).
HRMS (MALDI): Calcd. for C$_{51}$H$_{93}$O$_8$P$_2$Ni$_2^+$ (M−OPiv+O2)$^+$: 1011.5047; found: 1011.5000. Pyrene in toluene.
Elemental analysis: Calcd. C = 62.12; H = 9.50; Found. C = 61.13, H = 8.83.

SQUID magnetometry:

Measurements were made on a solid sample (13.85 mg) that was sealed in a gelatine capsule. Diamagnetic corrections were estimated using Pascal's constants. The magnetic moment of **8** at room temperature is 0.78 emu K mol^{-1}. This is lower than that expected for a spin only value (2 emu K mol^{-1}), indicating the presence of strong antiferromagentic interactions between the spin carriers. The thermal dependence of the $\chi_M T$ product was fitted to the Hamiltonian: $H = -2J(s_1\ s_2)$, where $s_1 = s_2 = 1$. The fitting parameters in Figure S2.6 agree with values in the literature (see for example Jiménez-Aparicio et al. and references therein).[119]
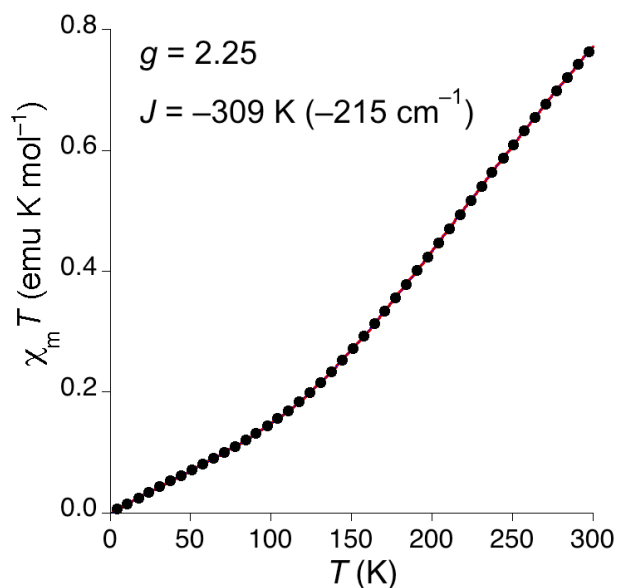
Figure S2.6. Thermal dependence of $\chi_M T$ for 8.

[Ni(OPiv)(σ-1-naphthyl)(dcype)] (11)
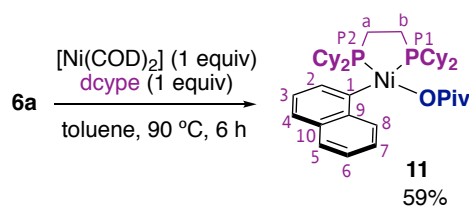

Scheme S2.6. Synthesis of 11.

[Ni(COD)$_2$] (78.3 mg, 0.284 mmol) and dcype (120 mg, 0.284 mmol) were dissolved in 5 mL toluene. After 10 min, **6a** (64.8 mg, 0.284 mmol) was added, then the sealed reaction vessel was transferred from the glovebox to an oil bath pre-heated to 90 °C. After 6 h at 90 °C, volatiles were removed to give an orange oil. Addition of 3 mL pentane followed by 5 minutes of stirring and the removal of volatiles gave a dark yellow residue. This was taken up in 3 mL pentane and placed in the glovebox freezer at −35 °C. After 16 h the solid was filtered, washed with 3 mL pentane, then dried to give **11** as a yellow powder (120 mg, 59%). X-ray quality crystals were obtained by slow evaporation of an acetone solution of **11** (ambient laboratory conditions ca. 20 °C).

^{1}H NMR (500 MHz, toluene-d$_8$): δ 9.71 (d, $^3J_{\text{H-H}}$ = 8.3 Hz, 1H, H8), 7.89 (vt, $|^4J_{\text{Ptrans–H}} + {}^4J_{\text{Pcis–H}}|$ = 13.3 Hz, 1H, H2), 7.64 (d, $^3J_{\text{H-H}}$ = 8.1 Hz, 1H, H5), 7.50 (t, $^3J_{\text{H-H}}$ = 7.7 Hz, 1H, H7), 7.41 (d, $^3J_{\text{H-H}}$ = 7.9 Hz, 1H, H4), 7.30 (t, $^3J_{\text{H-H}}$ = 7.4 Hz, 1H, H6), 7.26 (t, $^3J_{\text{H-H}}$ = 7.3 Hz, 1H, H3), 3.57 (m, 1H, Ha-1), 2.91 (m, 1H, Hb-1), 2.39 (m, 1H, Cy-P1), 2.34 (m, 1H, Ha-2), 2.22 (m, 1H, CH-CyP2), 2.01 (m, 1H, CH-CyP1), 1.96 (m, 1H, CH-CyP1), 1.79–1.50 (Cy), 1.36 (m, 1H, Hb-2), 1.33 (CH, CH-CyP2), 1.20–1.15 (Cy), 1.13 (m, 1H, CH-CyP2), 1.03 (Cy-P2), 0.91 (s, 9H, *t*Bu), 0.82 (m, 1H, Cy-P2), 0.69 (m, 1H, Cy-P2), 0.64 (m, 1H, Cy-P2), 0.47 (m, 1H, Cy-P2), −0.12 (m, 1H, Cy-P2).

³¹P NMR (203 MHz, toluene-d_8): δ 64.44 (d, $^2J_{P-P}$ = 13.1 Hz, P2), 61.93 (d, $^2J_{P-P}$ = 12.6 Hz, P1) (s) ppm.

¹³C NMR (126 MHz, toluene-d_8) δ 182.5 (m, $C_{carbonyl}$), 160.4 (dd, $^2J_{Ptrans-C}$ = 86.71 Hz, $^2J_{Pcis-C}$ = 39.71 Hz, C1), 143.0 (d, $^3J_{Ptrans}$ = 2.7 Hz, C9), 134.7 (d, $^4J_{Ptrans-C}$ = 2.1 Hz, C10), 134.6 (vt, $|^4J_{Ptrans-C} + {}^4J_{Pcis-C}|$ = 4 Hz, C8), 134.4 (dd, $^3J_{Ptrans-C}$ = 4.8 Hz, $^3J_{Pcis-C}$ = 2.2 Hz, C2), 128.3 (overlap with residual toluene, C5), 124.3 (dd, $^4J_{Ptrans-C}$ = 6.8 Hz, $^4J_{Pcis-C}$ = 2.2 Hz, C3), 124.0 (s, C6), 122.8 (s, C4), 122.5 (s, C7), 39.7 (d, $^4J_{Ptrans}$ = 3.2 Hz, C), 36.1 (d, $^1J_{P-C}$ = 26.7 Hz, C1-CyP2), 34.9 (d, $^1J_{P-C}$ = 15.0 Hz, C1-CyP1), 33.31 (d, J = 14.3 Hz, C1-CyP1), 32.27 (d, $^1J_{P-C}$ = 24.8 Hz, C1-CyP2), 31.31 (d, $^1J_{P-C}$ = 3.0 Hz, Ca). 29.7 (s, CH_2 Cy), 29.42 (d, $^1J_{P-C}$ = 3.9 Hz, Cb), 28.90 (d, J = 3.1 Hz, CH2-CyP1), 28.6 (s, tBu), 28.4 (d, J = 3.2 Hz, CH_2 Cy), 28.0 (s, CH_2 Cy), 27.9 (s, CH_2 Cy), 27.8 (s, CH_2 Cy), 27.8 (s, CH_2 Cy), 27.7 (s, CH_2 Cy), 27.4 (s, CH_2 Cy), 27.3 (s, CH_2 Cy), 27.3 (s, CH_2 Cy), 27.1 (s, CH_2 Cy), 27.1 (s, CH_2 Cy), 27.0 (s, CH_2 Cy), 26.9 (s, CH_2 Cy), 26.9 (s, CH_2 Cy), 26.7 (s, CH_2 Cy), 26.4 (s, CH_2 Cy), 26.3 (s, CH_2 Cy), 25.8 (s, CH_2 Cy), 24.2 (m, CH_2 Cy), 17.56 (dd, J = 19.8, 10.9 Hz).

HRMS (cryospray ESI) $[C_{36}H_{55}NiP_2]^+$ (M−OPiv) *calcd* 607.31270 *found* 607.3117.

[{Ni(PCy₃)}₂(µ,η²-1-naphthyl)(µ-OPiv)] (7a)
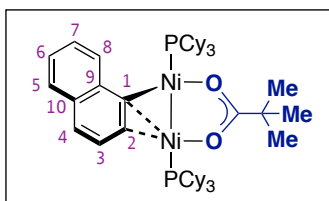
[Ni(COD)₂] (48.6 mg, 0.176 mmol) and PCy₃ (148.5 mg, 0.529 mmol) were dissolved in 6 mL toluene. After 10 min, **6a** (20.1 mg, 0.088 mmol) was added, then the sealed reaction vessel transferred from the glovebox to an oil bath pre-heated to 50 ºC. After 3 h at 50 ºC, volatiles were removed to give a dark green residue. Addition of 3 mL pentane, followed by 5 minutes of stirring and the removal of volatiles gave a dark green residue. A second trituration with pentane gave a green suspension. This was filtered in the glovebox, washed with 3 x 2 mL pentane, then dried to give **7a** as a bright olive-green powder (37.3 mg, 46%).

- *Any solid **7a** that is removed from the glovebox will extremely rapidly decompose to give a pale brown solid.*
- ***7a** synthesised in this way is sparingly soluble in room temperature toluene and benzene (1-2 mg/0.5 mL, slightly higher in benzene). In-situ synthesis without drying (see below) allows higher concentrations to be obtained.*

X-ray quality crystals were obtained from a toluene-pentane mixture at −25 ºC.

In-situ synthesis:

[Ni(PCy₃)₂]₂(N₂) (10 mg, 0.0078 mmol, 1 equiv) and **6a** (1.76 mg, 0.0077 mmol, 1 equiv) were combined in 0.5 mL C₆D₆. After approximately 15 minutes at room temperature, [Ni(PCy₃)₂]₂(N₂) will have undergone conversion to **7a** + 2 PCy₃.

^{1}H NMR (500 MHz, C$_6$D$_6$): δ 10.48 (d, $^3J_{H-H}$ = 7.97 Hz, 1H, H8), 7.65 (m, 1H, H7), 7.39 (m, 2H, H6 & H5), 6.85 (d, $^3J_{H-H}$ = 8.44 Hz, 1H, H4), 6.76 (dd, $^3J_{H-H}$ = 8.50, 6.03 Hz, 1H, H3), 5.60 (d, $^3J_{H-H}$ = 6.01 Hz, 1H, H2), 1.93 (m, CH$_2$ PCy$_3$, 12H), 1.65 (m, PCy$_3$, 24 H), 1.48 (m, PCy$_3$, 12 H), 1.14–1.20 (m, PCy$_3$, 18H (overlap with ^{t}Bu)), 1.21 (s, 9H, tBu).

^{31}P NMR (C$_6$D$_6$, 121 MHz): δ 24.88 (s).

^{13}C{^{1}H} NMR (126 MHz, C$_6$D$_6$): δ 195.8 (t, $^3J_{P-C}$ = 6.03 Hz, C$_{carbonyl}$), 147.4 (vt, $|^3J_{P-C} + {}^3J_{P-C}|$ = 3 Hz, C9), 145.8 (t, $^2J_{P-C}$ = 10.3 Hz, C1), 134.8 (s, C8), 132.6 (s, C10), 130.7 (s, C3), 127.4 (s, C5), 125.6 (s, C6), 125.4 (s, C7), 123.0 (s, C4), 84.9 (s, C2), 39.9 (s, C), 32.7 (vt, $|^1J_{P-C} + {}^4J_{P-C}|$ = 11.85 Hz, C1 Cy), 30.1 (s, C2 Cy), 30.0 (s, C2' Cy), 28.7 (s, tBu), 28.2 (vt, $|^2J_{P-C} + {}^5J_{P-C}|$ = 4.0 Hz, C3 Cy), 27.0 (s, C4 Cy).

Magnetic measurements

μ_{eff} (Evans method, C$_6$D$_6$): 0.

### 2.11.7.   In-situ generated dinickel oxidative addition complexes from aryl pivalates

Experimental details:
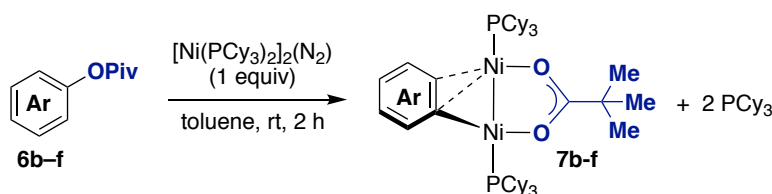
Scheme S2.7 General scheme for the synthesis of dinickel oxidative addition complexes from aryl pivalates.

NMR yields reported in the text are based on the following experiments. However, internal standard-free NMR spectra are provided in Section 2.11.15.1; thus, yields/conversions/NMR solvent may differ slightly.

[{Ni(PCy$_3$)}$_2$(μ,η^2-2-naphthyl)(μ-OPiv)] (7b)
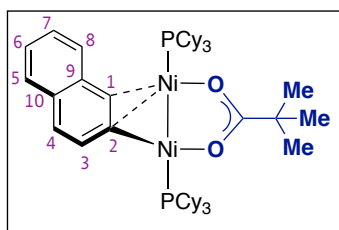
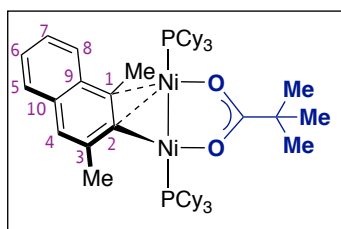Aryl pivalate **6b** (2.34 mg, 0.0103 mmol, 1 equiv) and 1,3,5-trimethoxybenzene (5.98 mg, 0.0356 mmol, internal standard) were pre-weighed using a microbalance. In the glovebox, [Ni(PCy$_3$)$_2$]$_2$(N$_2$) (13.0 mg, 0.0103 mmol, 1 equiv) was added, then the solids dissolved in 0.45 mL toluene-d$_8$. After 2 h at room temperature, ^{1}H NMR spectroscopy (d1 = 5 s) revealed a 93% yield of complex **7b**.

¹H NMR (500 MHz, toluene-d$_8$): δ 8.15 (d, $^3J_{\text{H–H}}$ = 8.54 Hz, 1H, H8), 7.58 (d, $^3J_{\text{H–H}}$ = 7.90 Hz, 1H, H5), 7.33 (d, $^3J_{\text{H–H}}$ = 7.70 Hz, 1H, H3), 7.14 (d, $^3J_{\text{H–H}}$ = 7.58 Hz, 1H, H7), 7.08–7.02 (m, 2H, H4 & H6), 5.62 (s, 1H, H1), 1.99–1.02 (m, PCy$_3$, 66H overlap with PCy$_3$, *t*Bu), 1.17 (s, 9H, *t*Bu).

³¹P NMR (121 MHz, toluene-d$_8$): δ 26.75 (s).

¹³C{¹H} NMR (126 MHz, toluene-d$_8$): δ 195.7 (m, C$_{\text{carbonyl}}$), 141.7 (s, C8), 141.4 (t, $^2J_{\text{P–C}}$ = 10 Hz, C2), 139.4 (s, C9), 132.8 (s, C10), 128.2 (s, C3), 126.7 (s, C5), 124.7 (s, C6), 123.4 (s, C4), 121.1 (s, C7), 84.4 (s, C1), 40.0 (s, C), 28.7 (s, *t*Bu). PCy$_3$: signals 33.2–27.0 ppm.

[{Ni(PCy₃)}₂(μ,η²-2-(1-methyl)naphthyl)(μ-OPiv)] (7c)
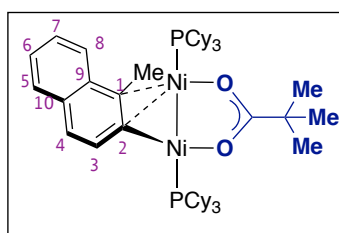
6c (1.92 mg, 0.0079 mmol, 1 equiv) and 1,3,5-trimethoxybenzene (2.53 mg, 0.0150 mmol, internal standard) were pre-weighed using a microbalance. In the glovebox, [Ni(PCy$_3$)$_2$]$_2$(N$_2$) (10.0 mg, 0.0079 mmol, 1 equiv) was added, then the solids dissolved in 0.45 mL toluene-d$_8$. After 2 h at room temperature, ¹H NMR spectroscopy (d1 = 5 s) revealed a 58% yield of complex **7c**.

¹H NMR (500 MHz, C$_6$D$_6$): δ 8.56 (d, $^3J_{\text{H–H}}$ = 8.54 Hz, 1H, H8), 7.78 (d, $^3J_{\text{H–H}}$ = 8.15 Hz, 1H, H5), 7.40 (d, $^3J_{\text{H–H}}$ = 7.45 Hz, 1H, H4), 7.20 (m, 1H, H7), 7.15 (m, 1H H6), 7.09 (t, $^3J_{\text{H–H}}$ = 7.30 Hz, 1H, H3), 4.18 (s, 3H, CH$_{3\,\text{C1}}$), 1.92–1.11 (m, PCy$_3$, 66H overlap with PCy$_3$, *t*Bu), 1.20 (s, 9H, CH$_{3\,\text{(OPiv)}}$).

³¹P NMR (C$_6$D$_6$, 121 MHz): δ 23.35 (s).

¹³C{¹H} NMR (126 MHz, C$_6$D$_6$): δ 195.4 (t, $^3J_{\text{P–C}}$ = 6.20 Hz, C$_{\text{carbonyl}}$), 148.0 (t, $^2J_{\text{P–C}}$ = 11.0 Hz, C2–Ni), 140.6 (s, C8), 138.6 (s, C9), 132.6 (s, C10), 128.0 (s, C4), 124.9 (s, C6), 123.4 (s, C3), 122.6 (s, C5), 120.7 (s, C7), 94.7 (s, C1), 39.9 (s, C$_{\text{OPiv}}$), 32.7 (vt, $|^1J_{\text{P–C}} + ^4J_{\text{P–C}}|$ = 11.83 Hz, C1 Cy), 30.2 (s, C2 Cy), 30.1 (s, C2' Cy), 28.7 (s, CH$_{3\,\text{(OPiv)}}$), 28.1 (m, C3 Cy), 27.0 (s, C4 Cy & CH$_{3\,\text{(C1)}}$).

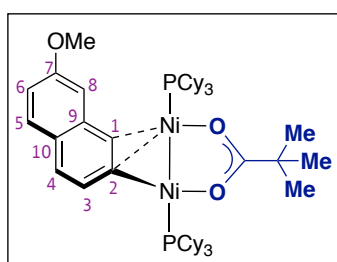## [{Ni(PCy₃)}₂(μ,η²-2-(1,3-dimethyl)naphthyl)(μ-OPiv)] (7d)

6d (1.75 mg, 0.0068 mmol, 1 equiv) and 1,3,5-trimethoxybenzene (2.66 mg, 0.0158 mmol, internal standard) were pre-weighed using a microbalance. In the glovebox, [Ni(PCy$_3$)$_2$]$_2$(N$_2$) (8.65 mg, 0.0068 mmol, 1 equiv) was added, then the solids dissolved in 0.45 mL toluene-d$_8$. After 2 h at room temperature, ¹H NMR spectroscopy (d1 = 5 s) revealed a 76% yield of complex **7d**.

^{1}H NMR (500 MHz, C$_6$D$_6$): δ 7.82 (d, $^3J_{\text{H–H}}$ = 7.17 Hz, 1H, H8), 7.42 (d, $^3J_{\text{H–H}}$ = 7.11 Hz, 1H & H5), 7.17 (m, 1H, H7), 7.11 (m, 1H, H6), 7.08 (s, 1H, H4), 4.40 (s, 3H, CH$_{3\,(C1)}$), 4.29 (s, 3H, CH$_{3\,(C1)}$), 1.93–1.10 (m, PCy$_3$, 66H overlap with PCy$_3$, ^{t}Bu), 1.18 (s, 9H, CH$_{3\,(OPiv)}$).

^{31}P NMR (C$_6$D$_6$, 121 MHz): δ 23.62 (s).

^{13}C{^{1}H} NMR (126 MHz, C$_6$D$_6$): δ 195.4 (t, $^3J_{\text{P–C}}$ = 6.13 Hz, C$_{\text{carbonyl}}$), 149.8 (t, $^2J_{\text{P–C}}$ = 11.11 Hz, C2–Ni), 147.1 (s, C3), 136.9 (s, C9), 134.0 (s, C10), 127.7 (s, C5), 124.2 (s, C7), 123.4 (s, C6), 122.5 (s, C8), 119.97 (s, C4), 96.0 (s, C1), 39.8 (s, tBu), 32.7 (vt, $|^1J_{\text{P–C}} + {}^4J_{\text{P–C}}|$= 11.67 Hz, C1 Cy), 30.1 (s, C2 Cy), 28.6 (s, CH$_{3\,(C3)}$), 28.2 (s, tBu), 28.1 (m, C3 Cy), 27.0 (s, C4 Cy), 26.9 (s, CH$_{3\,(C1)}$).

[{Ni(PCy$_3$)}$_2$(μ,η^2-2-(7-methoxy)naphthyl)(μ-OPiv)] (7e)

6e (2.15 mg, 0.0083 mmol, 1 equiv) and 1,3,5-trimethoxybenzene (4.18 mg, 0.0248 mmol, internal standard) were pre-weighed using a microbalance. In the glovebox, [Ni(PCy$_3$)$_2$]$_2$(N$_2$) (10.5 mg, 0.0083 mmol, 1 equiv) was added, then the solids dissolved in 0.45 mL toluene-d$_8$. After 2 h at room temperature, ^{1}H NMR spectroscopy (d1 = 5 s) revealed a 97% yield of complex **7e**.

**^{1}H NMR** (500 MHz, toluene-d$_8$): δ 8.05 (d, $^3J_{\text{H–H}}$ = 8.64 Hz, 1H, H4), 7.23 (d, $^3J_{\text{H–H}}$ = 8.54 Hz, 1H, H5), 7.08 (m, 2H, H3 & H8), 6.80 (m, 1H, H6), 5.64 (s, H1), 3.51 (s, CH$_{3\,(OMe)}$), 2.00–1.0 (m, PCy$_3$, 66H overlap with PCy$_3$, ^{t}Bu), 1.17 (s, 9H, CH$_{3\,(OPiv)}$).

^{31}P NMR (121 MHz, toluene-d$_8$): δ 26.16 (s).

^{13}C{^{1}H} NMR (126 MHz, toluene-d$_8$): δ 195.6 (t, $^3J_{\text{P–C}}$ = 5.85 Hz, C$_{\text{carbonyl}}$), 157.5 (s, C7), 143.0 (t, $^2J_{\text{P–C}}$ = 10.71 Hz, C2), 140.5 (s, C9), 139.5 (s, C4), 129.4 (s, C5), 127.2 (s, C10), 120.1 (C3), 113.0 (s, C6), 108.5 (s, C8), 84.1 (s, C1), 54.7 (s, CH$_{3\,(OMe)}$), 40.0 (s, C$_{\text{OPiv}}$), 32.9 (vt, $|^1J_{\text{P–C}} + {}^4J_{\text{P–C}}|$ = 11.57 Hz, C1 Cy), 30.3 (m, C2 Cy), 28.1 (m, C3 Cy), 27.1 (s, C4 Cy).

[{Ni(PCy₃)}₂(μ,η²-phenyl)(μ-OPiv)] (7f)
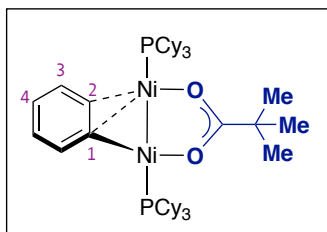
1,3,5-trimethoxybenzene (0.65 mg, 0.00386 mmol, internal standard) was weighed using a microbalance. Inside the glovebox, **6f** (1.1 mg, 0.0062 mmol) was added to the internal standard, followed by 0.2 mL toluene-d_8. [Ni(PCy₃)₂]₂(N₂) (8.1 mg, 0. 0062 mmol, 1 equiv) was then added, followed by 0.25 mL toluene-d_8. After 2 h at room temperature, ^{1}H NMR spectroscopy (d1 = 5 s) revealed a 18% yield of complex **7f**.

^{1}H NMR (500 MHz, C₆D₆): 7.26 (m, 1H, H4), 6.84 (m, 2H, H3), 6.45 (m, 2H, H2), 1.99–1.20 (m, PCy₃, 66H overlap with many signals including free PCy₃, ^{t}Bu), 1.18 (s, 9H, CH₃ (OPiv)).

^{31}P NMR (C₆D₆, 121 MHz): δ 23.32 (s).

^{13}C{^{1}H} NMR (126 MHz, C₆D₆): δ 195.2 (br, C$_{carbonyl}$), 147.3 (t, $^2J_{P–C}$ = 12.2 Hz, C1—Ni), 127.4 (s, C3), 121.6 (s, C2), 120.3 (s, C4), 39.9 (s, C$_{(OPiv)}$), 28.3 (s, CH₃ (OPiv)). PCy₃: br signals 33.2–27.0 ppm.

2.11.8. Stoichiometric experiments: Disproportionation

2.11.8.1. Reactions of 7a with dcype
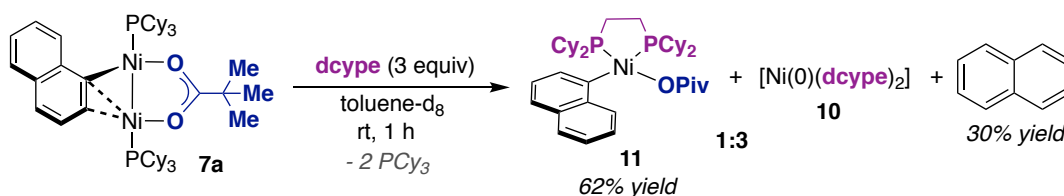
Scheme S2.8. Stoichiometric reaction of 7a with dcype.

Complex **7a** (7.9 mg, 0.087 mmol), dcype (11.1 mg, 0.026 mmol), and 1,3,5-trimethoxybenzene (2.44 mg, 0.0145 mmol, internal standard) were dissolved in 0.45 mL toluene-d_8. The green suspension was agitated until the solids had dissolved, with a concomitant colour change to orange being observed. NMR spectra were collected after 1 h and 12 h at room temperature. NMR spectroscopy after 1 h showed a 62% yield of [Ni(1-naphthyl)(κ^1-OPiv)(PCy$_3$)] (**11**) and a 30% yield of NpH (naphthalene). Integration of the ^{31}P{^{1}H} (IGD) NMR spectrum gave a 1:3 ratio between **11** and **10**,[94,95] which is higher than expected (1:2) (Figure S2.8). This confirmed that some of the Ni–Np bonds originating from the dinickel complex were no longer present following reaction with dcype and fits with the observation of naphthalene.

*See above for preparation and characterisation details of complex **11**, and below for X-ray data.*
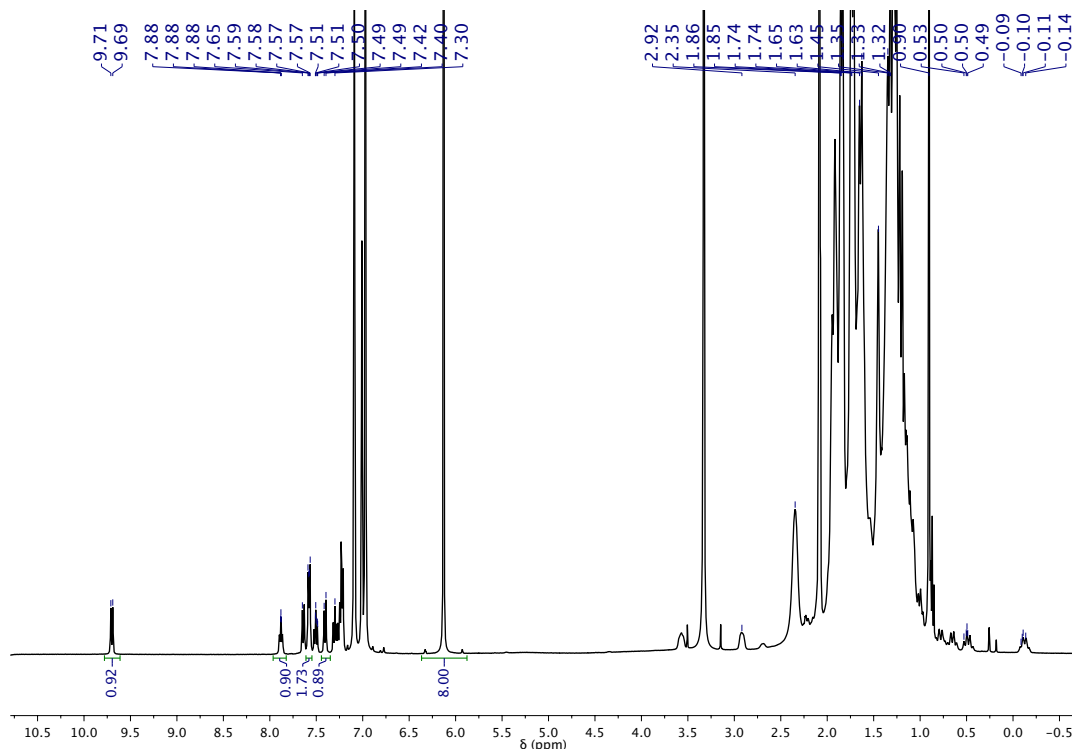
Figure S2.7. ^{1}H NMR spectrum after reaction of 7a with 3 equiv dcype. Internal standard (1,3,5-trimethoxybenzene) visible at 6.13 and 3.13 ppm.
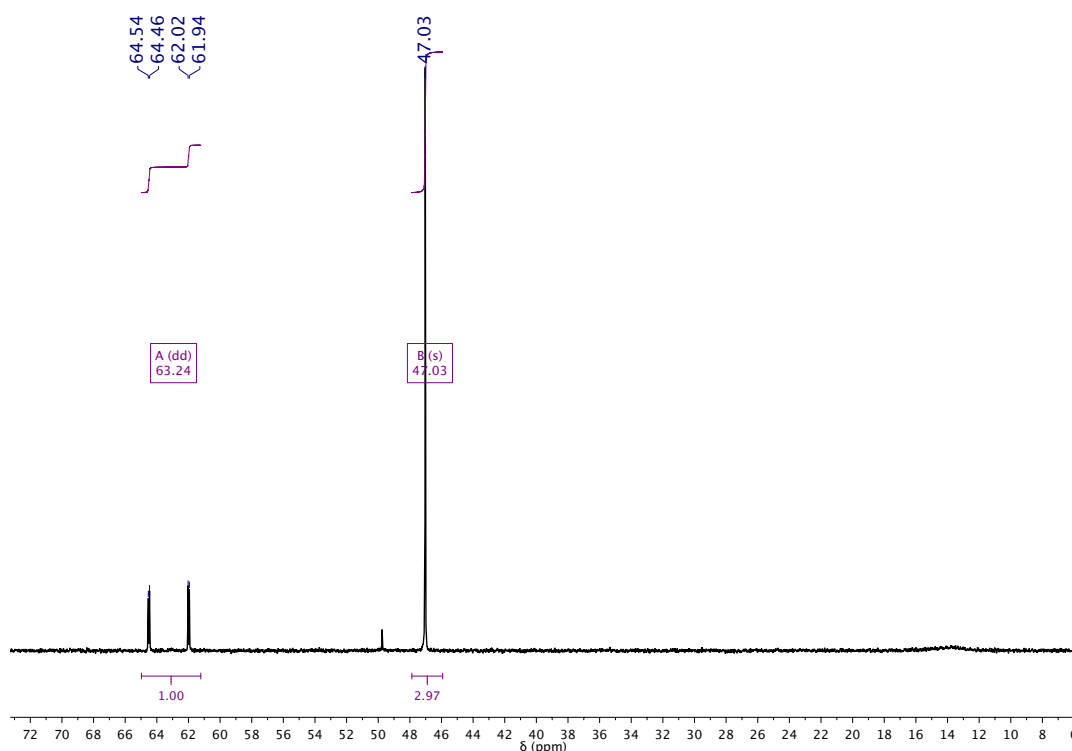
Figure S2.8. ³¹P{¹H} (IGD) NMR spectrum after reaction of 7a with 3 equiv dcype. δ_P = 64.5 (d, ²J_P–P = 13.1 Hz) and 61.97 (d, ²J_P–P = 12.6 Hz) (11). δ_P = 47 ppm (10), broad signal at ca. δ_P = 14 ppm: PCy₃.

2.11.8.2. Reactions of 7b with dcype
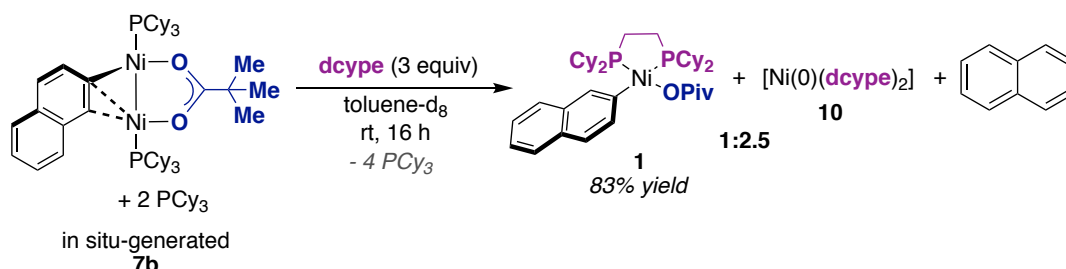
Scheme S2.9. Stoichiometric reactions of in situ formed 7b with dcype. The ratio of 1:10 was 1:2.5.

6b (2.20 mg, 0.0096 mmol), 1,3,5-trimethoxybenzene (2.37 mg, 0.014 mmol, internal standard), and [Ni(PCy₃)₂]₂(N₂) (12.2 mg, 0.0096 mmol) were dissolved in 0.45 mL toluene-d₈. After 16 h at room temperature, conversion was checked by NMR spectroscopy, then the solution was combined with dcype (12.2 mg, 0.029 mmol, in 0.1 mL toluene-d₈). After initially turning almost black in colour, the solution lightened over the course of 30 minutes to give a pale orange solution. NMR spectroscopy after 2 h showed 100% conversion of **6b** and an 83% yield of **1** based on the initial yield of **7b**. Complex **1** has been reported previously by Itami.[20] Integration of aromatic signals suggested naphthalene had formed, but overlap prevented quantification. The presence of naphthalene was confirmed by GC-FID. Integration of the ³¹P{¹H} NMR spectrum (inverse gated decoupling) gave a 1:2.5 ratio between **1** and **10**, which is

slightly higher than expected (1:2) (Figure S2.9). This confirmed that some of the Ni–Np bonds originating from the dinickel complex were no longer present and fits with the observation of naphthalene.
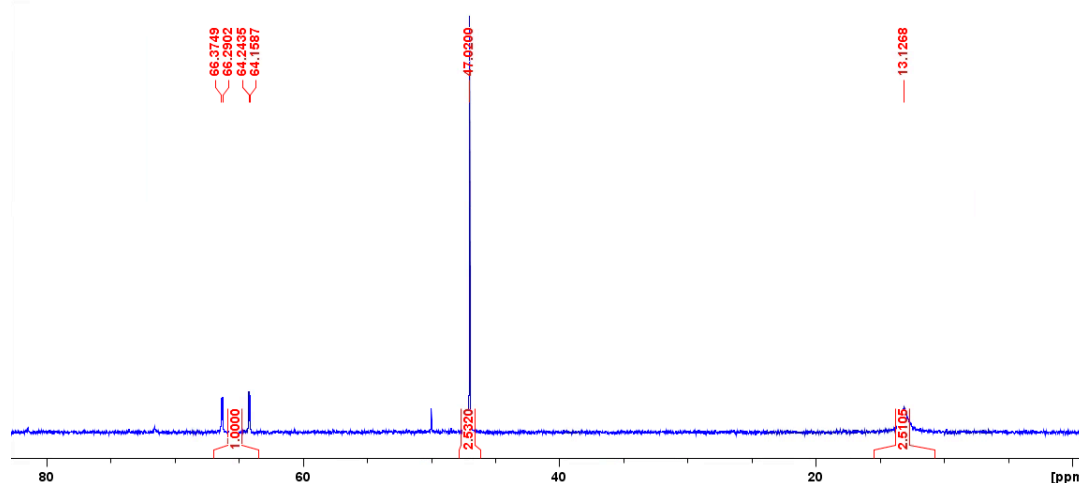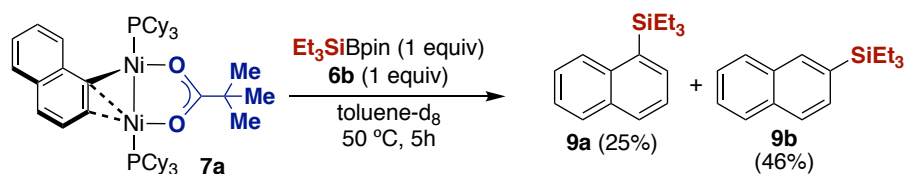

Figure S2.9. ^{31}P{^{1}H} NMR (IGD) spectrum upon addition of dcype to in situ-generated **7b**. δ_P = 66.3 (d, $^2J_{P–P}$ = 14.1 Hz) and 61.97 (d, $^2J_{P–P}$ = 13.9 Hz) (Ni-1). δ_P = 47 ppm (**6**), δ_P = 13.1 ppm (PCy$_3$).

2.11.9. Crossover experiments

Scheme S2.10. Crossover experiment with **7a** (derived from **6a**) and **6b**. NMR yields are given. Crossover complex **7b** and 1,2'-binaphthalene were also identified.

    6b (0.65 mg, 0.0029 mmol), 1,3,5-trimethoxybenzene (1.33 mg, 0.0079 mmol, internal standard), and complex **7a** (2.6 mg, 0.0029 mmol) were dissolved in 0.45 mL toluene-d$_8$. Next, 16 µL of an Et$_3$SiBpin solution (1 equiv, 0.18 M, toluene-d$_8$) was added. An initial ^{1}H NMR spectrum was collected. After 5 h at 50 ºC, the clear brown solution was analysed by NMR spectroscopy. This showed a 39% recovery of **7a**, a 46% yield of **9b**, and 8% 1,2'-binaphthalene. The signals for silylated product **9a** and dinickel complex **7b** overlap in the ^{1}H NMR spectrum, so the yield of **9a** was estimated to be circa 25%. Other binaphthalene isomers may also be present but could not be clearly identified in the ^{1}H NMR spectrum.
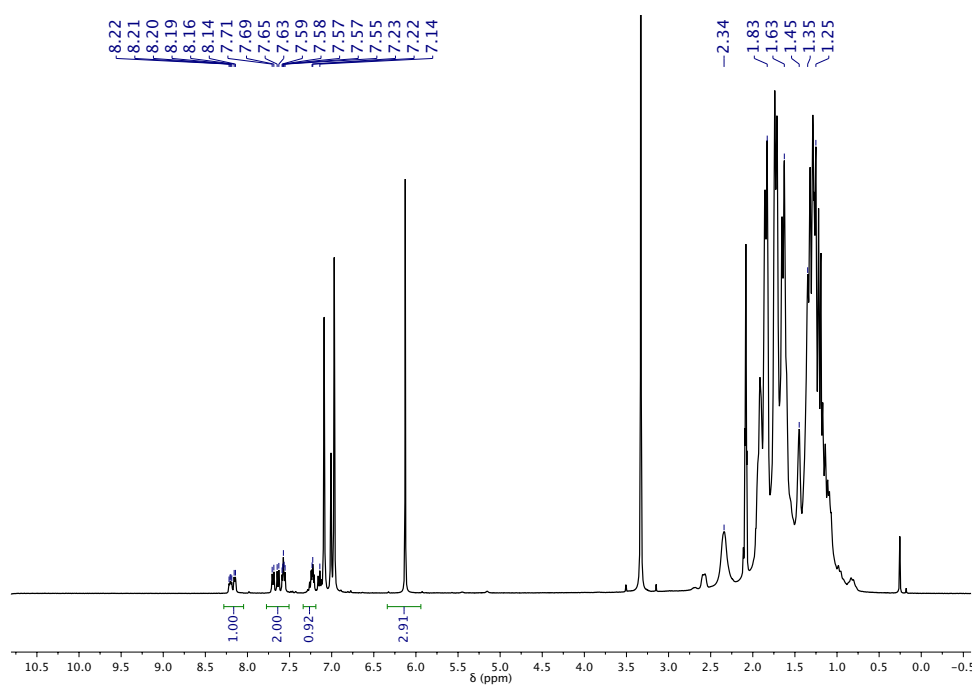
Figure S2.10. ¹H NMR spectrum upon addition of dcype to in situ-generated 7b. Internal standard (1,3,5-trimethoxybenzene) visible at 6.13 and 3.13 ppm.

2.11.10.   Role of CuF$_2$ and CsF

2.11.10.1. Reaction with Et$_3$SiBpin and CsF/CuF$_2$

CuF$_2$ (16.6 mg, 0.16 mmol, 1 equiv), Et$_3$SiBpin (41.9 mg, 0.16 mmol, 1 equiv), and CsF (30.3 mg, 0.20 mmol, 1.2 equiv) were combined in 0.6 mL C$_6$D$_6$ and heated at 50 ºC in a J Young NMR tube for 18 h. No reaction was observed.

2.11.10.2. Isolation of Bpin-containing by-products

2 equivalents of CsF
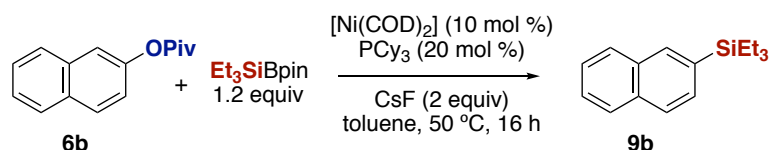
Scheme S2.11. Cu-free silylation.

In the glovebox, an oven-dried 15 mL screw cap reaction tube equipped with a stir bar was charged with CsF (76 mg, 0.5 mmol), **6b** (57 mg, 0.25 mmol), and 1 mL toluene. Et$_3$SiBpin (72.6 mg, 0.3 mmol), internal standard (decane, 35.6 mg, 0.25 mmol) were then added, followed by a freshly prepared toluene solution of [Ni(PCy$_3$)$_2$](N$_2$) (ca. 0.02 M, 0.0125 mmol), and enough toluene to make up the final reaction to 3 mL.

The tubes were then capped and heated in a pre-heated (50 ºC) aluminium block in the glovebox for 9 hours. Samples of approximately 40 µL were removed every 45 minutes in order to study the reaction profile. After cooling to room temperature, the reaction mixture was filtered and the solid residue washed with pentane. The resulting hygroscopic white solid was dried, then dissolved in DMSO-d$_6$ to give a mixture of CsOPiv and Cs[F$_2$Bpin] by NMR spectroscopy (vide infra). Analysis of the solution by GC-FID gave an 83% yield of **9b**.

^{1}H NMR (400 MHz, DMSO-d$_6$): δ 0.93 (s, 9H, *t*Bu (overlap with 0.91)), 0.91 (s, 12H, CH$_3$(Bpin) (overlap with 0.93)). **^{11}B NMR** (128 MHz, DMSO-d$_6$): δ 4.79 (t, $^1J_{F\text{-}B}$ = 22 Hz).
^{19}F NMR (376 MHz, DMSO-d$_6$): −138.93 (m, $^1J_{B\text{-}F}$ = 20.5 Hz, 2F).
^{13}C{^{1}H} NMR (101 MHz, DMSO-d$_6$): δ 180.6 (s, C$_{carbonyl}$), 76.8 (s, C$_{Bpin}$), 29.1 (br s, CH$_3$ $_{(Bpin)}$), 25.5 (s, CH$_3$).

2.11.10.3. Standard additive combination of CuF₂/CsF: isolation of fluoroborates
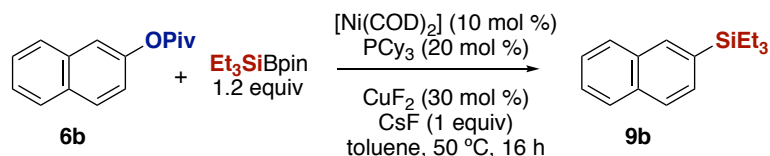
Scheme S2.12. Standard silylation reaction.

In the glovebox, an oven-dried 15 mL screw cap reaction tube equipped with a stir bar was charged with CsF (38 mg, 0.25 mmol), CuF₂ (7.6 mg, 0.075 mmol), **6b** (57 mg, 0.25 mmol), and 1 mL toluene. Et₃SiBpin (72.6 mg, 0.3 mmol), internal standard (decane, 35.6 mg, 0.25 mmol) were then added, followed by a freshly prepared toluene solution of [Ni(PCy₃)₂](N₂) (ca. 0.02 M, 0.0125 mmol), and enough toluene to make up the final reaction to 3 mL. The tubes were then capped and heated in a pre-heated (50 °C) aluminium block in the glovebox for 9 hours. Samples of approximately 40 μL were removed every 45 minutes in order to study the reaction profile. After cooling to room temperature, the reaction mixture was filtered and the solid residue washed with pentane. The resulting hygroscopic white solid was dried, then dissolved in DMSO-d₆ to give a mixture of CsOPiv, Cs[F₂Bpin], and [F(OPiv)Bpin]⁻. Analysis of the solution by GC-FID gave an 89% yield of **9b**. Assignment of all NMR data is difficult due to the many signals of very similar species. Traces of toluene are visible at circa 128 ppm in the ^{13}C{^{1}H} NMR spectrum.

¹H NMR (500 MHz, DMSO-d₆): δ 1.01, 0.98, 0.96, 0.96, 0.92, 0.91.
**¹¹B NMR** (128 MHz, DMSO-d₆): δ 5.16 (br), 4.79 (t, $^1J_{B-F}$ = 22 Hz).
¹⁹F NMR (376 MHz, DMSO-d₆): δ −137.94 (br), −138.60 (m).
¹³C{¹H} NMR (126 MHz, DMSO-d₆) δ 179.6 (s, C_carbonyl), 177.4, 81.2 (s, C_Bpin), 77.0 (s, C_Bpin), 76.6 (s, C_Bpin), 28.8 (s, CH₃), 28.6 (s, CH₃), 27.5 (s, CH₃), 25.5 (s, CH₃), 25.3 (s, CH₃), 25.1 (s, CH₃), 24.9 (s, CH₃), 24.4 (s, CH₃).

2.11.10.4. Formation of PivOBpin during stoichiometric silylation

[Ni(PCy₃)₂]₂(N₂) (13 mg, 0.0103 mmol, 1 equiv), and **6a** (0.0103 mmol, 93 μL of a 0.11 M toluene-d₈ solution) were combined in toluene-d₈ (0.3 mL) and stirred for 10 minutes. Next, a further 93 μL of **6a** solution, and 2.9 μL Et₃SiBpin (0.0103 mmol, 1 equiv) were added. The solution was transferred to a J Young NMR tube, then heated at 50 °C in the NMR spectrometer. After 80 minutes, approximately 1/3 of the **6a** had converted to **9a**. The resulting ¹¹B NMR spectra can be found in the main text (Figure 2.26). PivOBpin is visible at δ_B = 23 ppm.

2.11.10.5. Addition of fresh Ni(0) or CsF to additive-free reaction
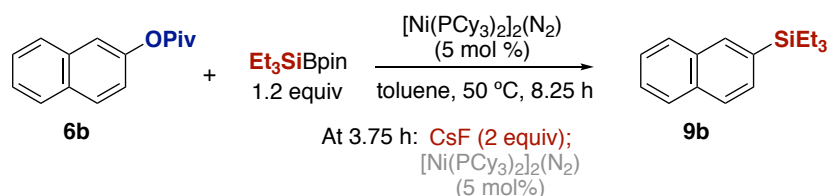
Scheme S2.13. Spiking of additive-free reaction with Ni(0)/PCy$_3$ or CsF.

In the glovebox, an oven-dried 15 mL screw cap reaction tube equipped with a stir bar was charged with **6b** (57 mg, 0.25 mmol, 1 equiv), and 1 mL toluene. Et$_3$SiBpin (72.6 mg, 0.3 mmol, 1.2 equiv), internal standard (decane, 35.6 mg, 0.25 mmol, 1 equiv) were then added, followed by a freshly prepared toluene solution of [Ni(PCy$_3$)$_2$](N$_2$) (ca. 0.02 M, 0.0125 mmol, 10 mol % Ni(0)/20 mol % PCy$_3$), and enough toluene to make up the final reaction to 3 mL. The tubes were then capped and heated in a pre-heated (50 ºC) aluminium block in the glovebox. Samples of approximately 40 µL were removed every 45 minutes in order to study the reaction profile. After 3.75 h, CsF (76 mg, 0.50 mmol, 2 equiv) was added. Sampling continued until 8.25 h had elapsed. See Figure 2.27.

2.11.10.6. PivOBpin inhibition experiments

1 equivalent PivOBpin, [Ni(PCy$_3$)$_2$]$_2$(N$_2$) precatalyst:

The precatalyst ([Ni(PCy$_3$)$_2$]$_2$(N$_2$) (15.8 mg, 0.012 mmol, 0.05 equiv)), PivOBpin (57 mg, 0.25 mmol, 1 equiv), and decane (35.6 mg, 0.25 mmol, 1 equiv) were combined in 2 mL toluene and heated together at 50 ºC for 1 h (we were unsure of the rate of the inhibition process). Next, Et$_3$SiBpin (72.6 mg, 0.3 mmol, 1.2 equiv), **6b** (57 mg, 0.25 mmol), and 1 mL toluene were added. Aliquots were removed from the reaction every 45 minutes for 3.75 h, but no **9b** was observed.

1 equivalent PivOBpin, [Ni(PCy$_3$)$_2$]$_2$(N$_2$) + 6b precatalyst:

The precatalyst ([Ni(PCy$_3$)$_2$]$_2$(N$_2$) (15.8 mg, 0.012 mmol, 0.05 equiv)) was combined with **6b** (0.025 mmol, 0.1 equiv) in 2 mL toluene in order to form dinickel oxidative addition complex **7b** in situ. Next, PivOBpin (57 mg, 0.25 mmol, 1 equiv), and decane (35.6 mg, 0.25 mmol, 1 equiv) were added and the reaction mixture heated at 50 ºC for 1 hour (we were unsure of the rate of the inhibition process). Next, Et$_3$SiBpin (72.6 mg, 0.3 mmol, 1.2 equiv), **6b** (57 mg, 0.25 mmol, 1 equiv), and 1 mL toluene were added. Aliquots were removed from the reaction every 45 minutes for 3.75 h, but no **9b** was observed.

0.1 equivalents PivOBpin, [Ni(PCy$_3$)$_2$]$_2$(N$_2$) + 6b precatalyst:

The precatalyst ([Ni(PCy$_3$)$_2$]$_2$(N$_2$) (15.8 mg, 0.012 mmol, 0.05 equiv)) was combined with **6b** (0.025 mmol, 0.1 equiv) in 2 mL toluene in order to form dinickel oxidative addition complex **7b** in situ. Next, PivOBpin (5.7 mg, 0.025 mmol, 1 equiv), and decane (35.6 mg, 0.25 mmol, 1 equiv) were added and the reaction mixture heated at 50 ºC for 1 hour (we were unsure of the rate of the inhibition process). Next, Et$_3$SiBpin (72.6 mg, 0.3 mmol, 1.2 equiv), **6b** (57 mg, 0.25 mmol, 1 equiv), and 1 mL toluene were added.

Aliquots were removed from the reaction every 45 minutes for 5.25 h. The data are displayed in Figure 2.28.

2.11.11.   Kinetic Studies

Silylation of 1-naphthyl pivalate (6a) with [Ni(PCy$_3$)$_2$]$_2$(N$_2$) catalyst and CsF/CuF$_2$ additives:

In the glovebox, stock solutions of 1-naphthyl pivalate (**6a**) (circa 1.1 M, depending on the run) and catalyst (a *1:1 mixture of [Ni(PCy₃)₂]₂(N₂) and **6a*** (circa 0.02 M, depending on the run)) were prepared in toluene. The catalyst solution was not stored between experiments. An oven-dried 15 mL screw cap reaction tube equipped with a stir bar was charged with CsF (38 mg, 0.25 mmol), CuF$_2$ (7.6 mg, 0.075 mmol), **6a** (0.2375 mmol), and 1 mL toluene. Et$_3$SiBpin (72.7 mg, 0.3 mmol), internal standard (decane, 35.6 mg, 0.25 mmol) were then added, followed by enough toluene to reach the final reaction volume (3 mL). After 30–35 minutes from addition of toluene to the catalyst solution, the required amount of catalyst solution was added to the reaction tube via pipette. A 40 µL aliquot was removed prior to heating and transferred to a GC vial (t = 0 min). Once the reaction tube was placed in the heating block, timing began and aliquots were obtained at 7.5-minute intervals for 1 hour, then sampled after 1.5 hours and 2.25 hours. Each aliquot was diluted with EtOAc and passed through a silica plug into a GC vial. The aliquots were analysed by GC-FID.

2.11.11.1. Order in 1-naphthyl pivalate (6a):

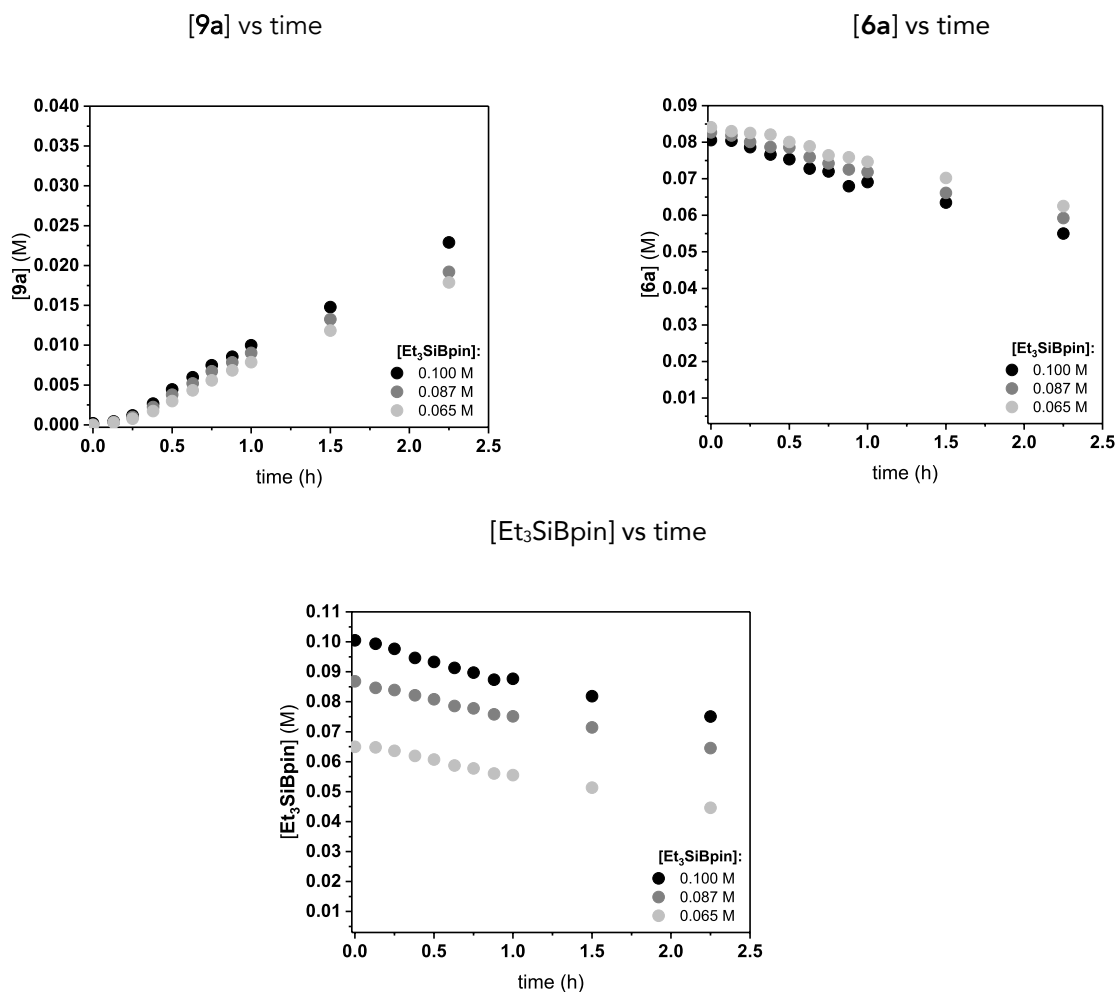Conclusion: zero order in [6a].

[9a] vs time
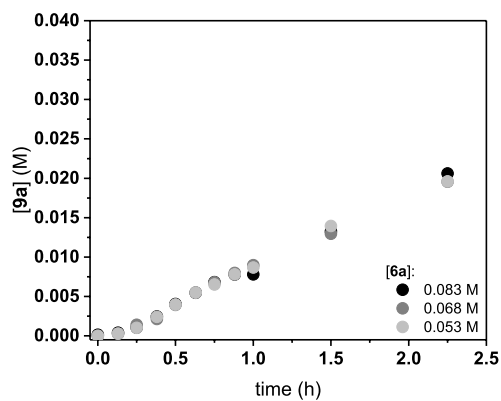
[6a] vs time
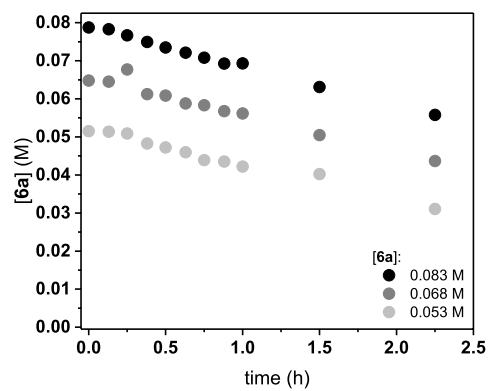
[Et₃SiBpin] vs time
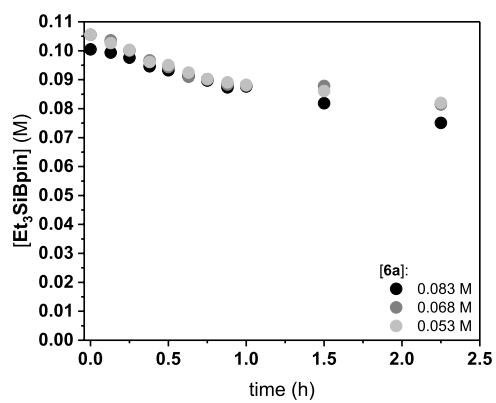
2.11.11.2. Order in Et₃SiBpin (6a):

Conclusion: positive order in Et₃SiBpin.

[**9a**] vs time   [**6a**] vs time

[Et₃SiBpin] vs time

Application of VTNA to the order in Et₃SiBpin is less straightforward than to [cat], and a range of orders from 0.4 to 1 is possible. This is demonstrated below with the [**9a**] data obtained by monitoring the silylation of **6a** (above).
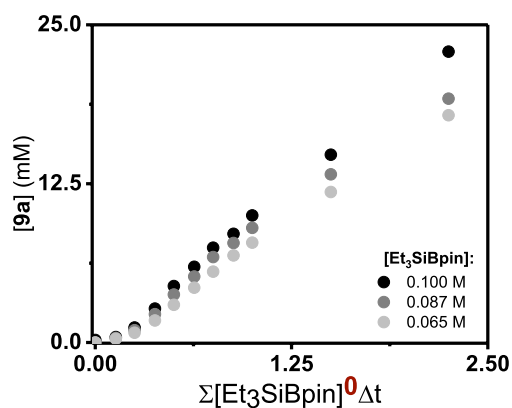
Figure S2.11. Plot of concentration of 9a vs Σ[Et₃SiBpin]⁰Δt (time) for three different concentrations of Et₃SiBpin (the identical graph was shown above as 9a vs time).
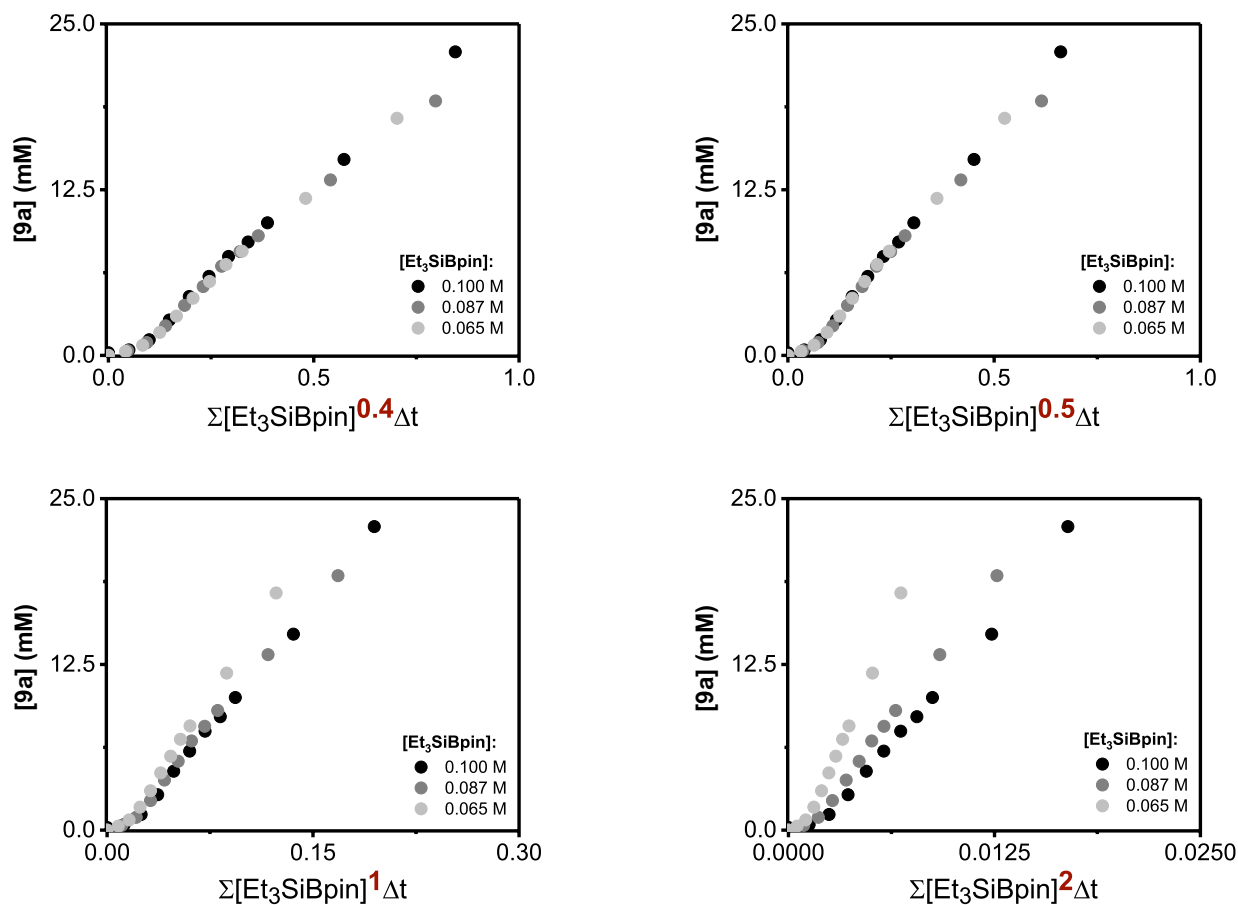
Figure S2.12. VTNA analysis for order in Et₃SiBpin using 6a as substrate.

As shown in Figure S2.12, satisfactory overlay is obtained for all three curves during the first nine points for orders 0.4 and 0.5. In particular, good overlay occurs between [Et₃SiBpin] = 0.100 M and 0.065 M. However, at longer time periods, overlay at this range of orders tends to decrease. When [**9a**] is plotted against Σ[Et₃SiBpin]$^1\Delta$t, good overlay occurs between [Et₃SiBpin] = 0.100 M and 0.087 M. The difficulty in obtaining a numerical order for Et₃SiBpin may be due to CsF/CuF₂ effects that are difficult to measure or to model.

2.11.11.3. Order in catalyst (6a):

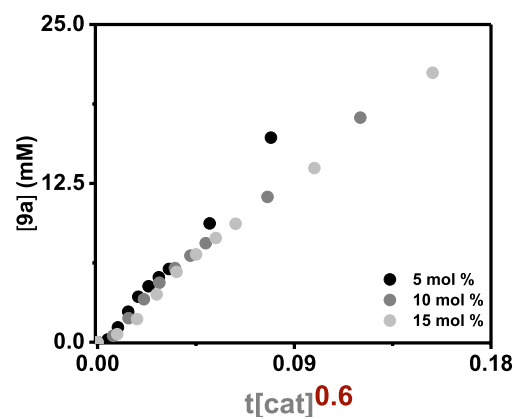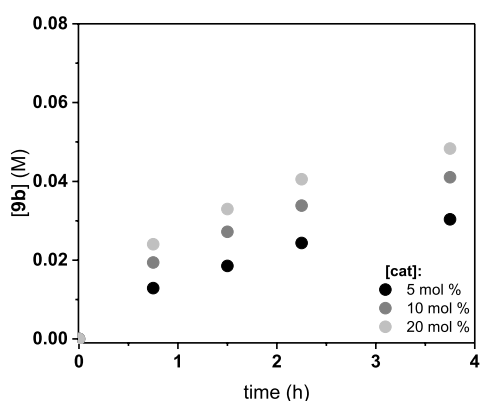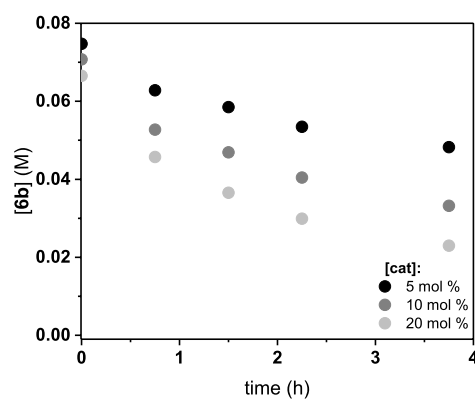[**9a**] vs time
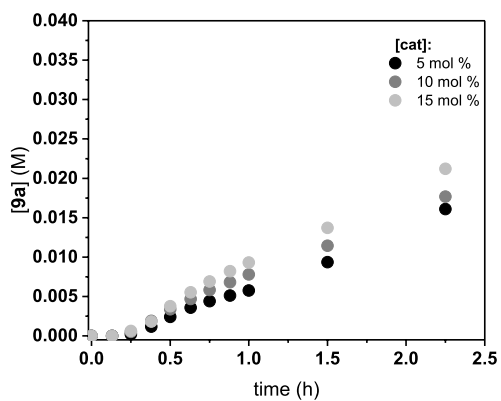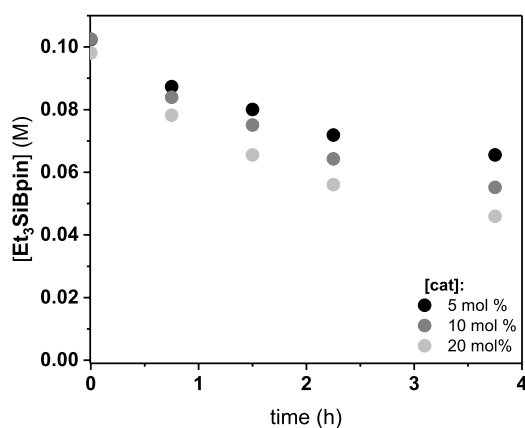

[**6a**] vs time
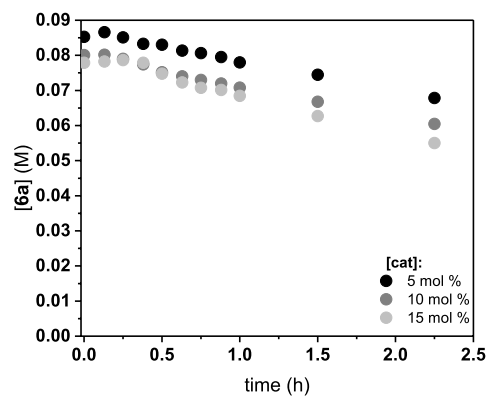
[Et₃SiBpin] vs time
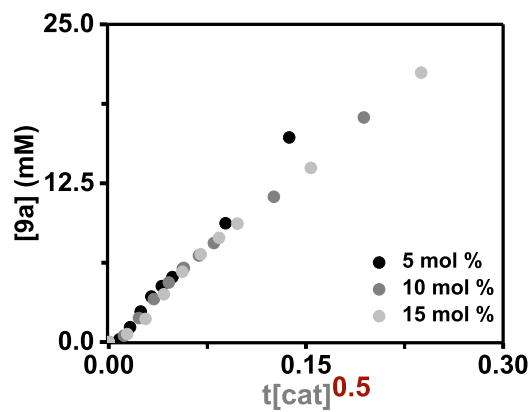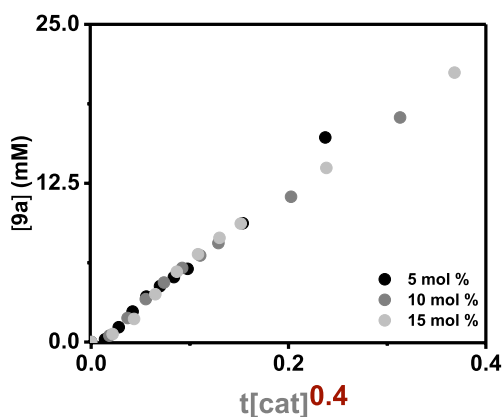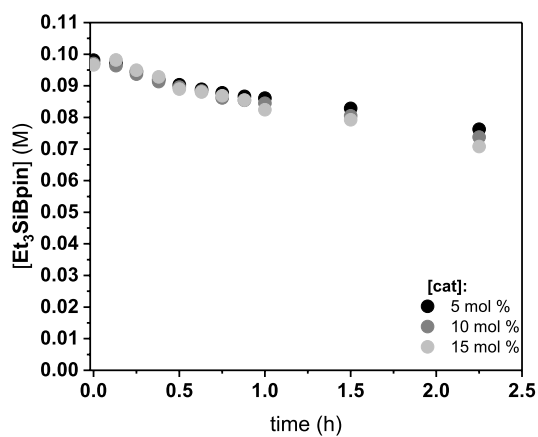
Figure S2.13. VTNA analysis for order in catalyst: comparison of overlay for a range of orders centred on 0.5.

Silylation of 2-naphthyl pivalate (6b) with [Ni(PCy₃)₂]₂(N₂) catalyst and CsF/CuF₂ additives:

In the glovebox, a stock solution of catalyst ([Ni(PCy₃)₂]₂(N₂), circa 0.02 M) was prepared in toluene. An oven-dried 15 mL screw cap reaction tube equipped with a stir bar was charged with **6b** (57 mg, 0.25 mmol), CsF (38 mg, 0.25 mmol), CuF₂ (7.6 mg, 0.075 mmol), and 1 mL toluene. [Ni(PCy₃)₂]₂(N₂) solution (5 mol%, circa 620 µL) was then added, followed by Et₃SiBpin (72.7 mg, 0.3 mmol), internal standard (decane, 35.6 mg, 0.25 mmol), and enough toluene to reach the final reaction volume (3 mL). A 40 µL aliquot was removed prior to heating and transferred to a GC vial (the t = 0 min sample). Once the reaction tube was placed in the heating block, timing began and aliquots were obtained at 45-minute intervals until 2.25 h, then sampled once more after 3.75 h. Each aliquot was diluted with EtOAc and passed through a silica plug into a GC vial. The aliquots were analysed by GC-FID.
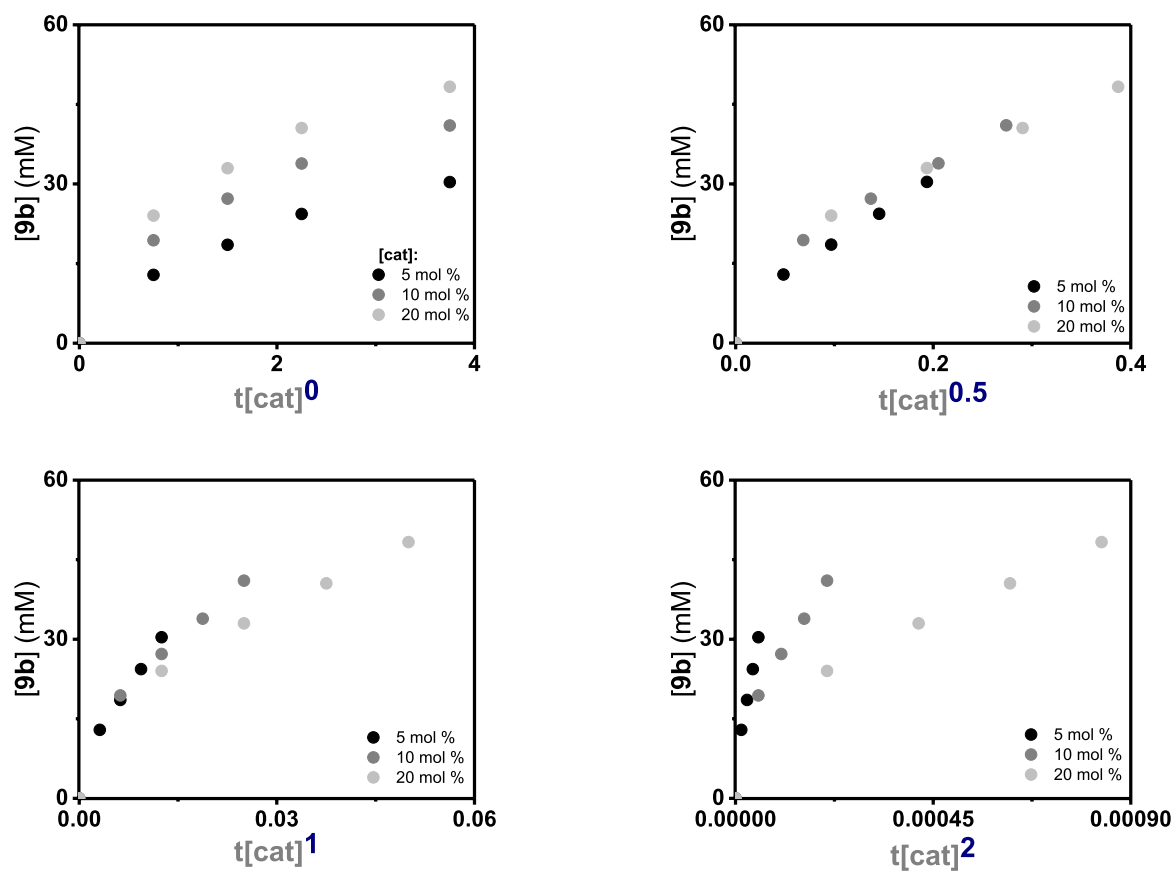
2.11.12.   Order in catalyst (6b):

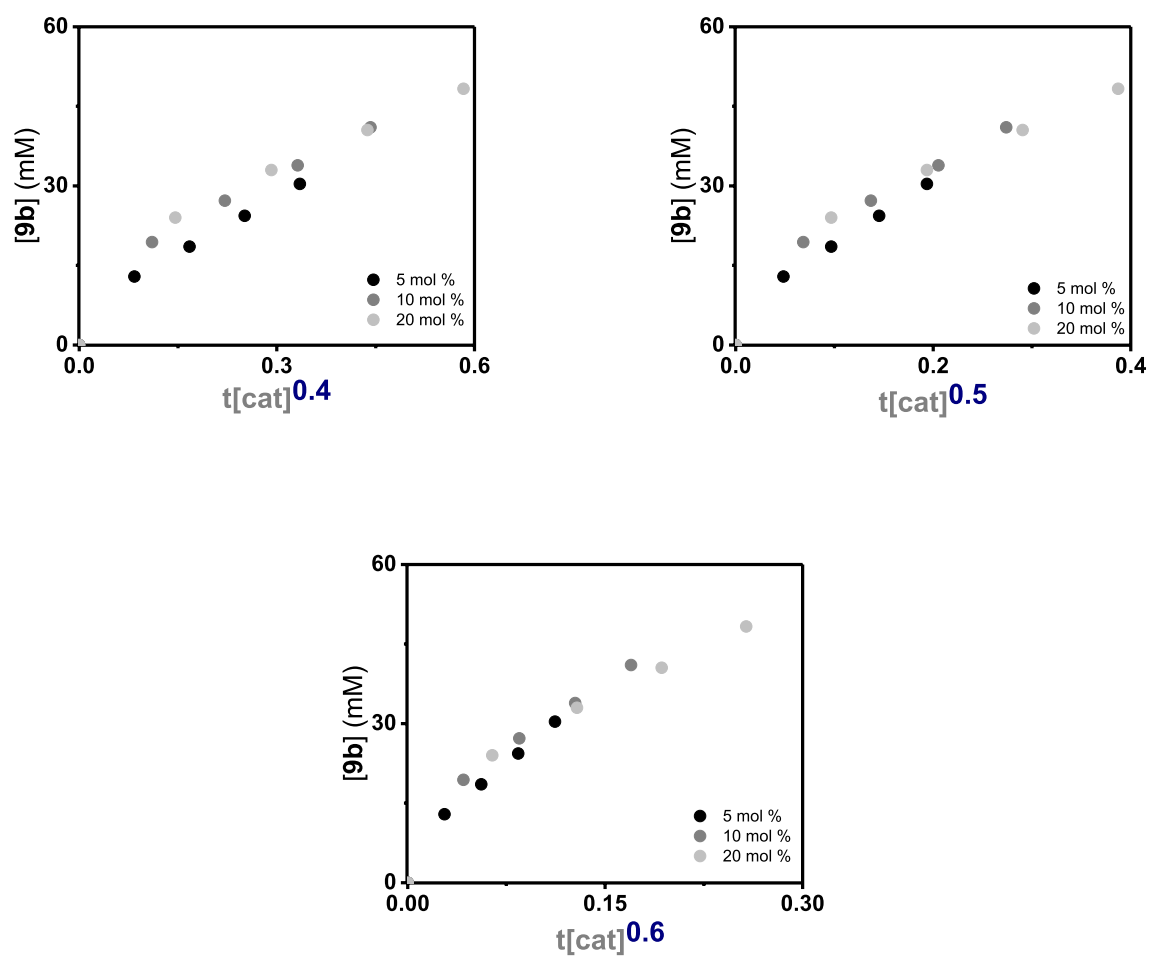**Figure S2.14. VTNA analysis for order in catalyst using 6b as substrate.**

Figure S2.15. VTNA analysis for order in catalyst – comparison of overlay for a range of orders centred on 0.5.
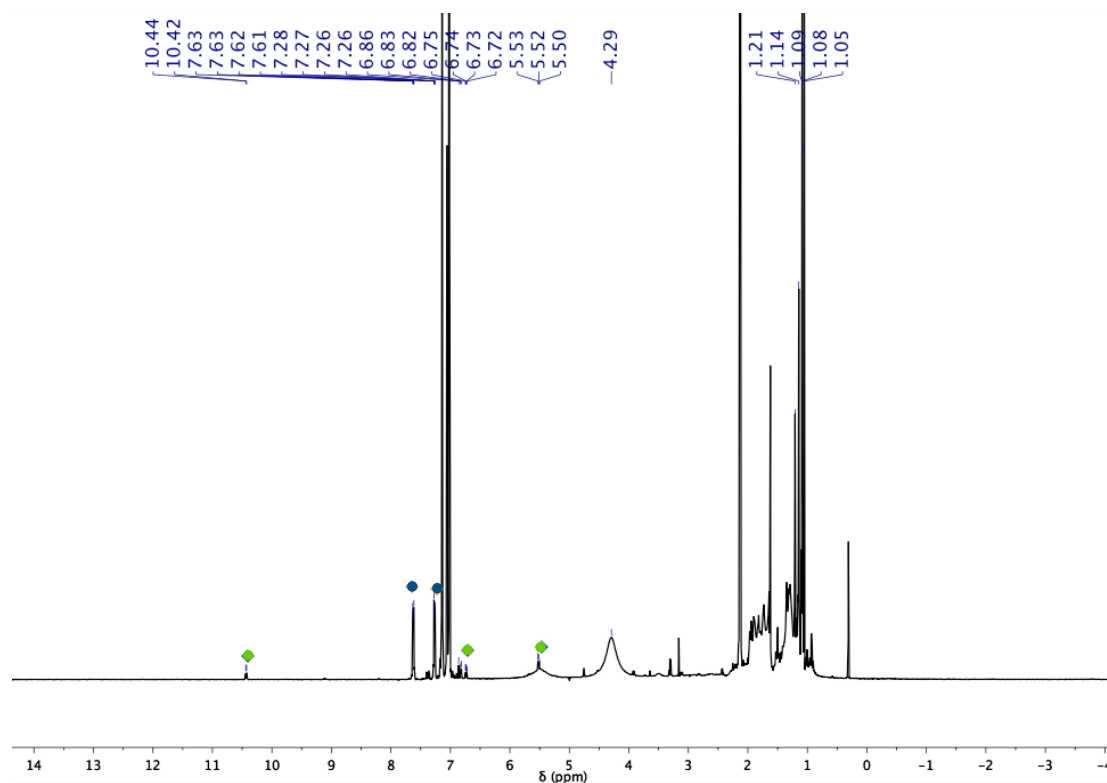
2.11.13. Catalyst deactivation

Figure S2.16. Reaction of 7a (green circles) with PivOBpin (toluene-d8, 6 h, 50 °C). Naphthalene identified and marked with blue circles.

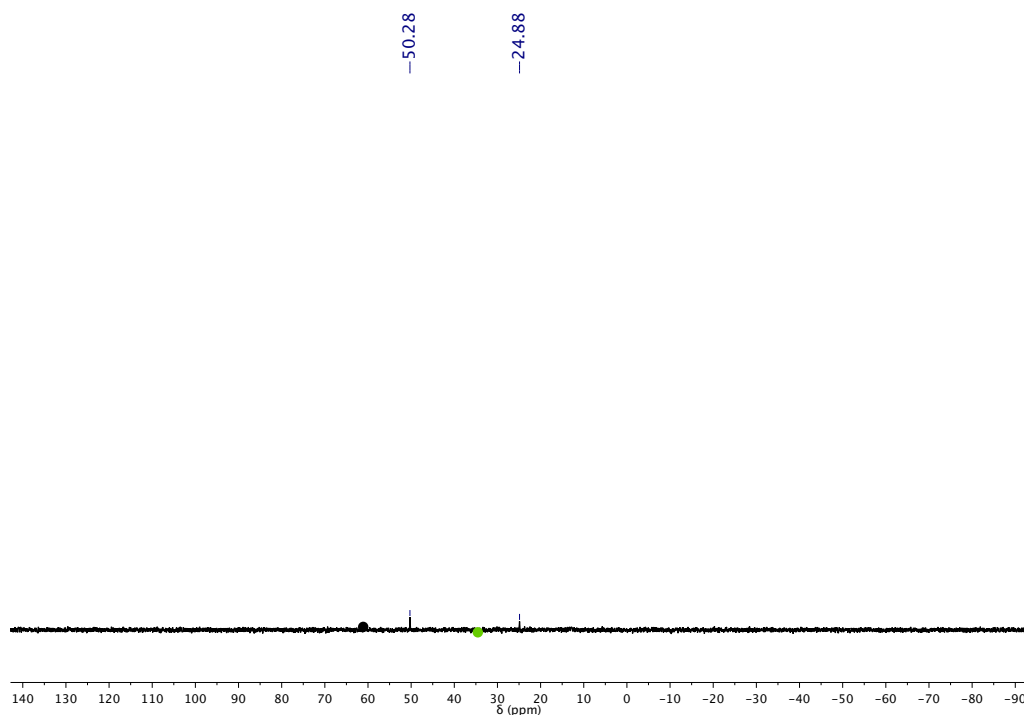Figure S2.17. ^{31}P{^{1}H} NMR from reaction of 7a (green circle) with PivOBpin (toluene-d$_8$, 6 h, 50 °C). Signal at δ_P = 50.28 not identified.

2.11.14. NMR spectra of organic molecules and selected starting materials

Et₃SiBpin and PivOBpin
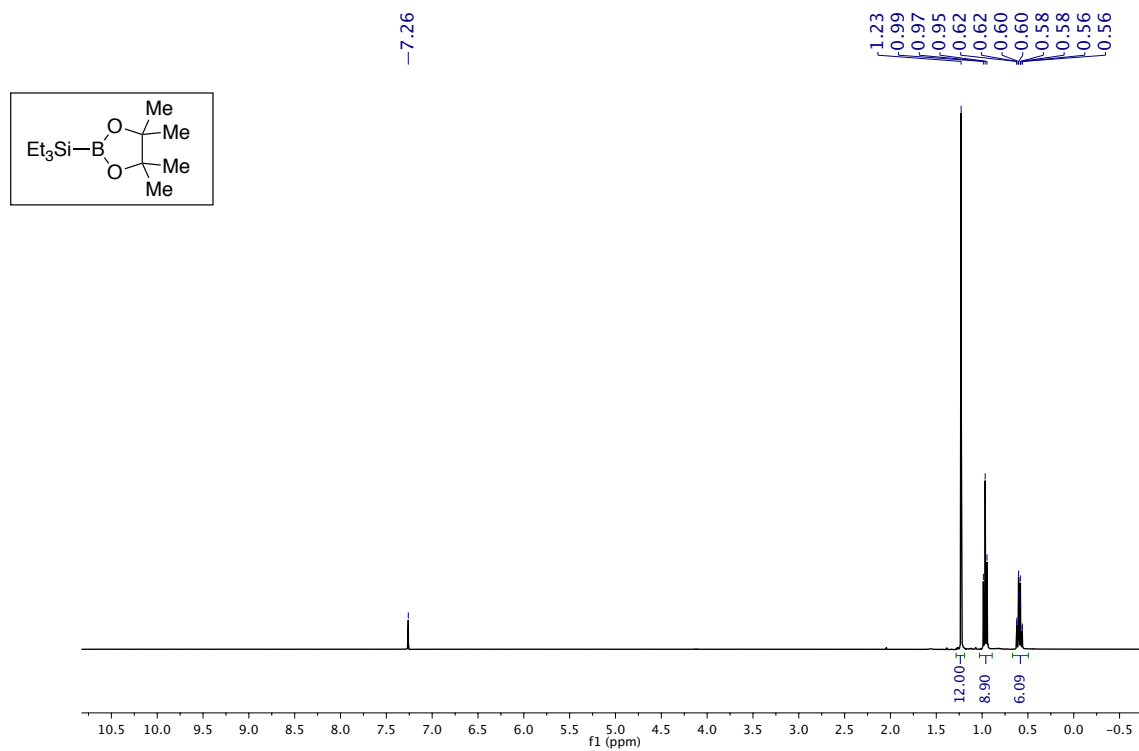
Figure S2.18. ¹H NMR (300 MHz, CDCl₃) of Et₃SBpin.
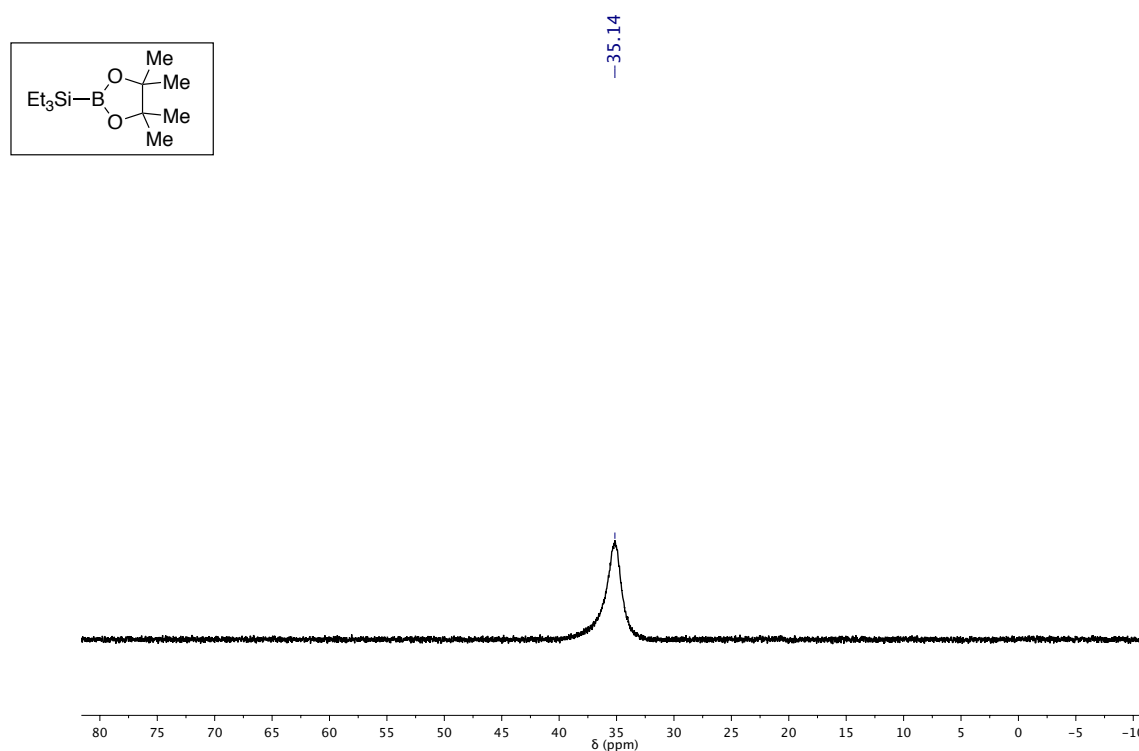
Figure S2.19. ¹¹B NMR (128 MHz, CDCl₃) of Et₃SiBpin.
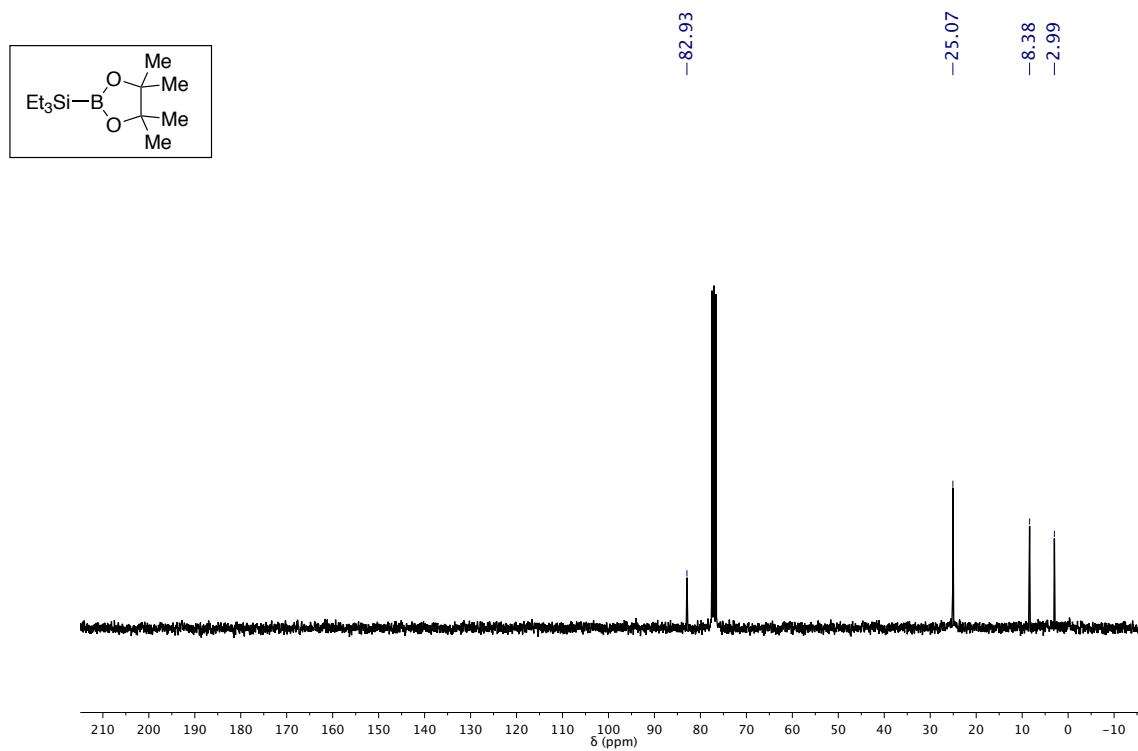
Figure S2.20. $^{13}C\{^1H\}$ NMR (101 MHz,CDCl$_3$) of Et$_3$SiBpin.
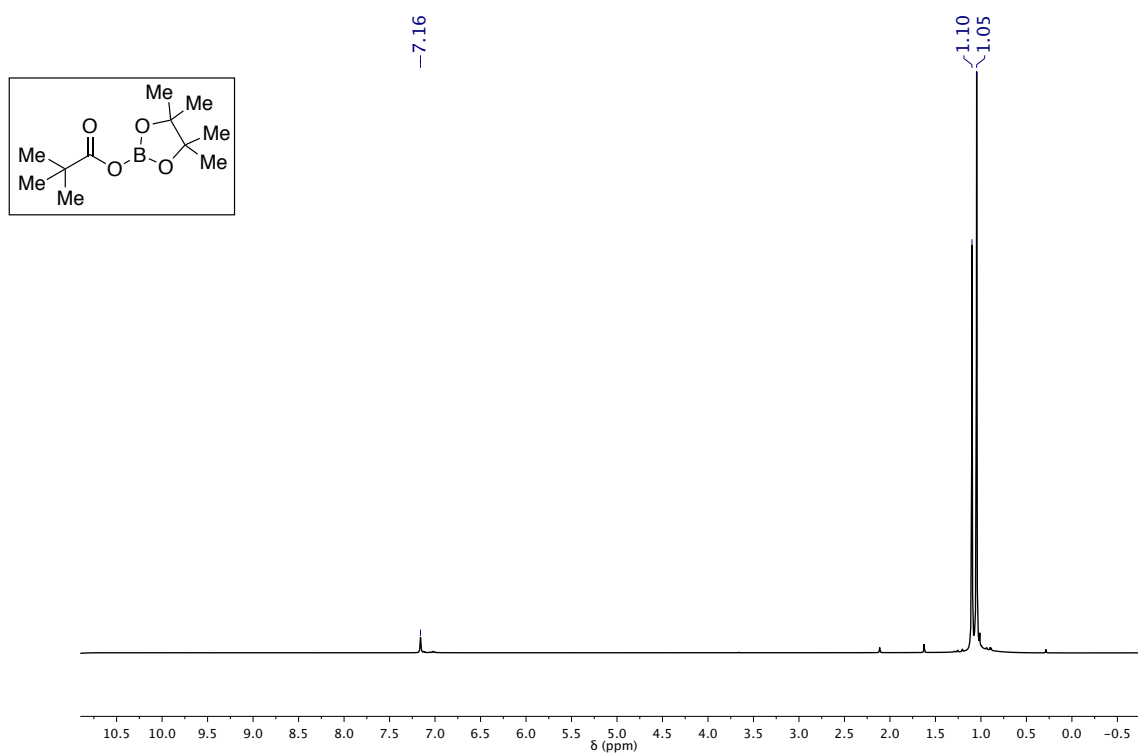
Figure S2.21. ^{1}H NMR (400 MHz, C$_6$D$_6$) of PivOBpin.
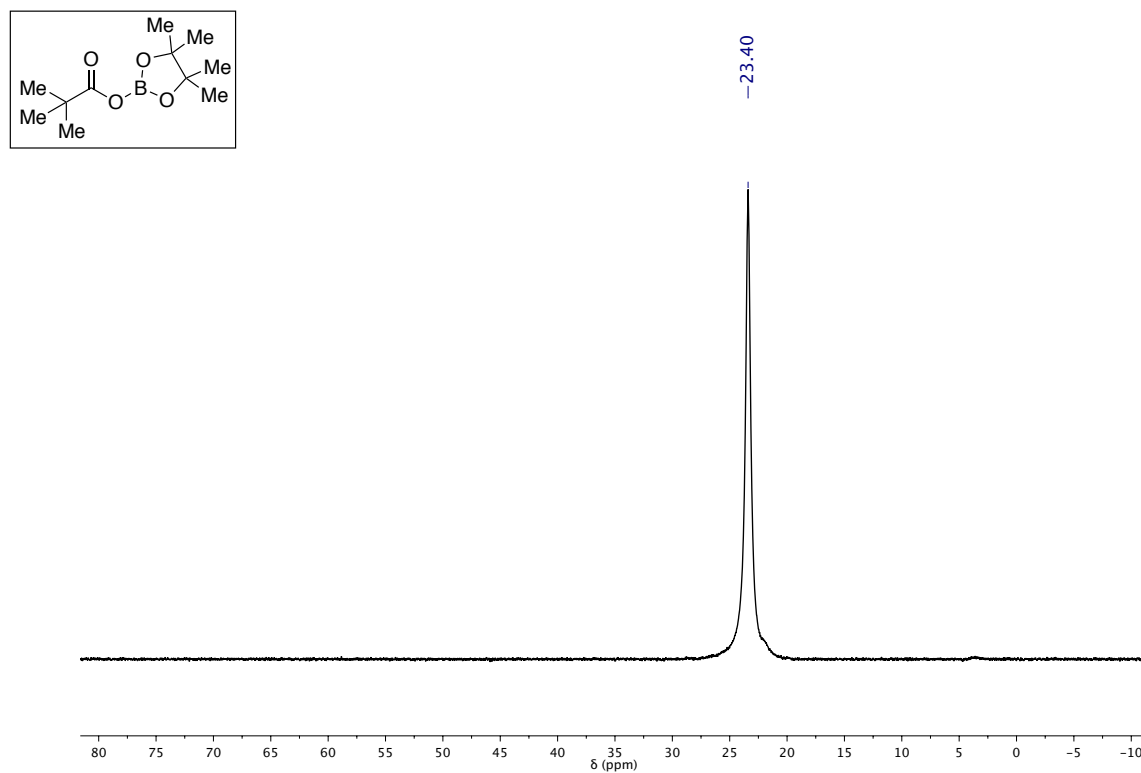
Figure S2.22. ¹¹B NMR (128 MHz, C₆D₆) of PivOBpin.
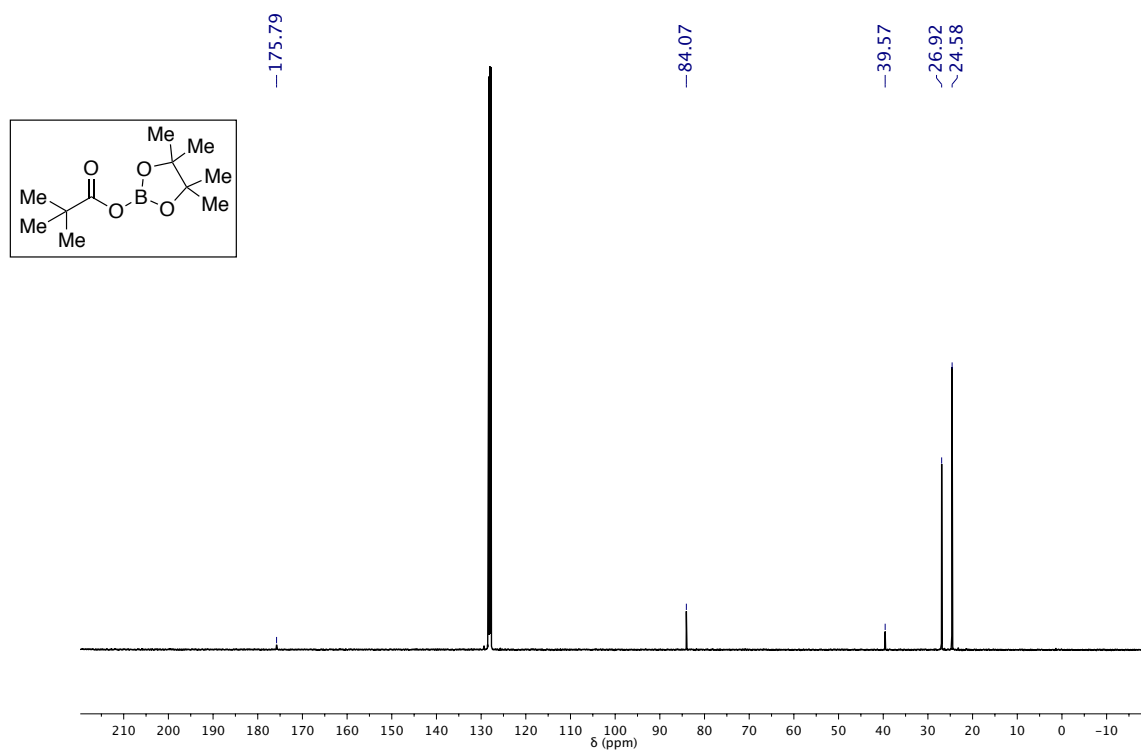
Figure S2.23. ¹³C{¹H} NMR (101 MHz, C₆D₆) of PivOBpin.

2.11.14.1. Naphthyl pivalates
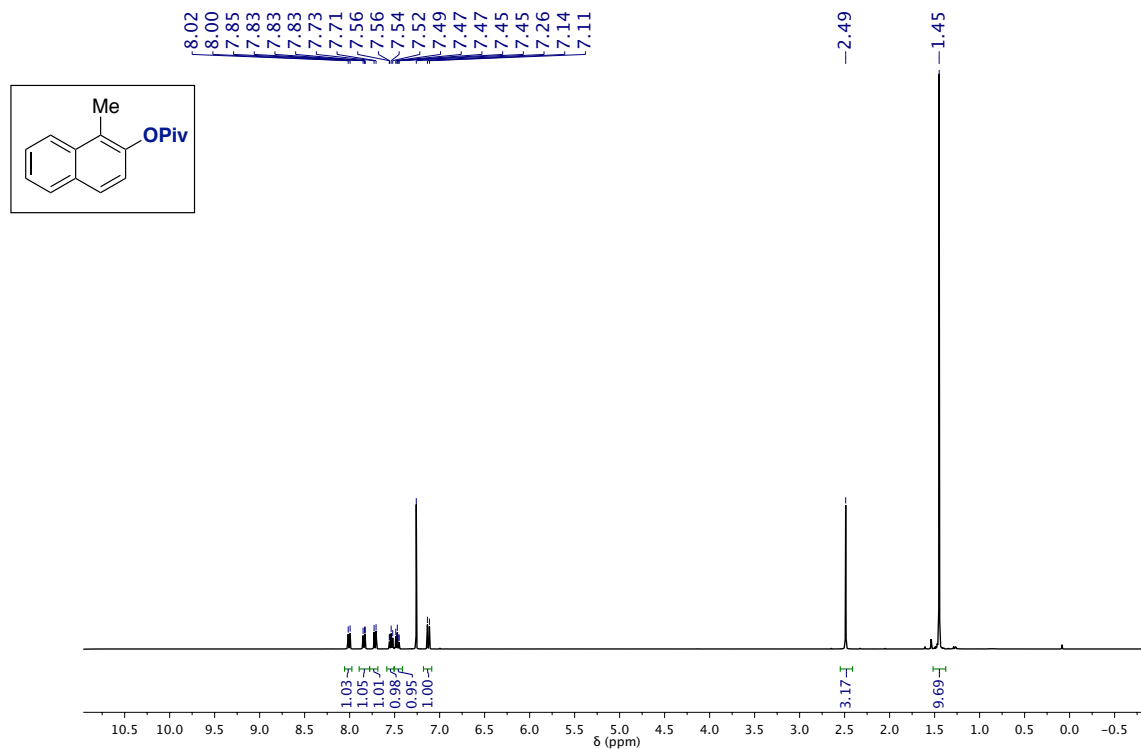
Figure S2.24. ¹H NMR (300 MHz, CDCl₃) of 6c.
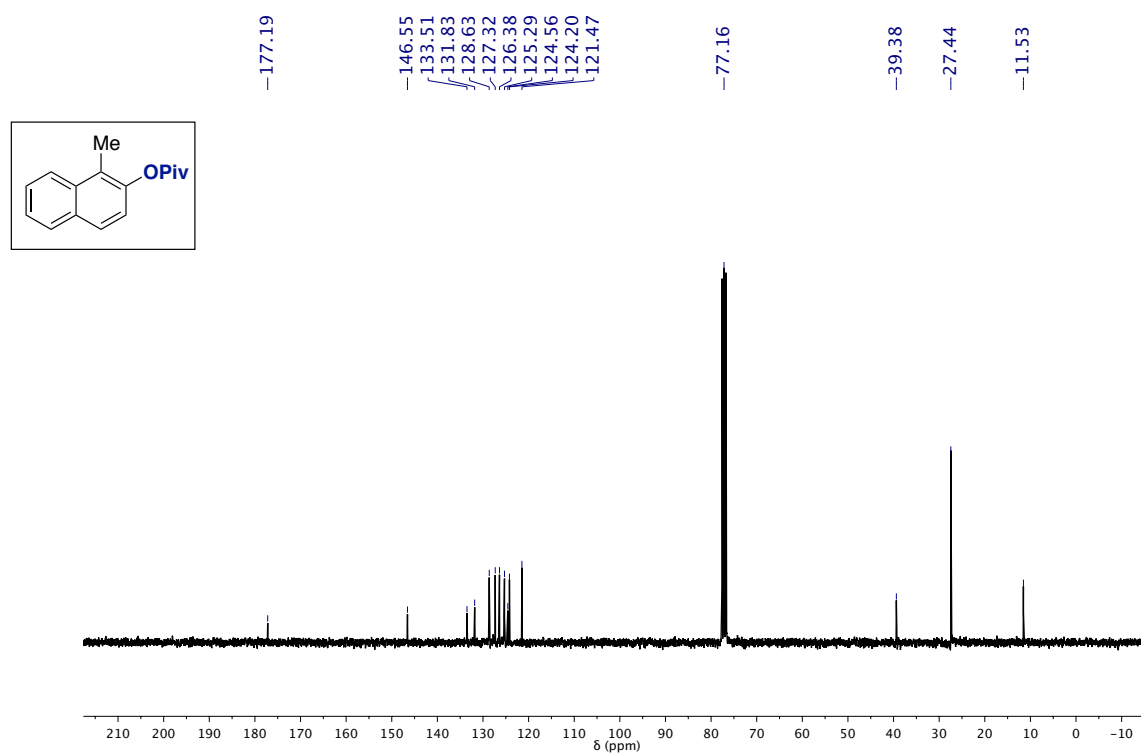
Figure S2.25. ¹³C{¹H} NMR (75 MHz, CDCl₃) of 6c.
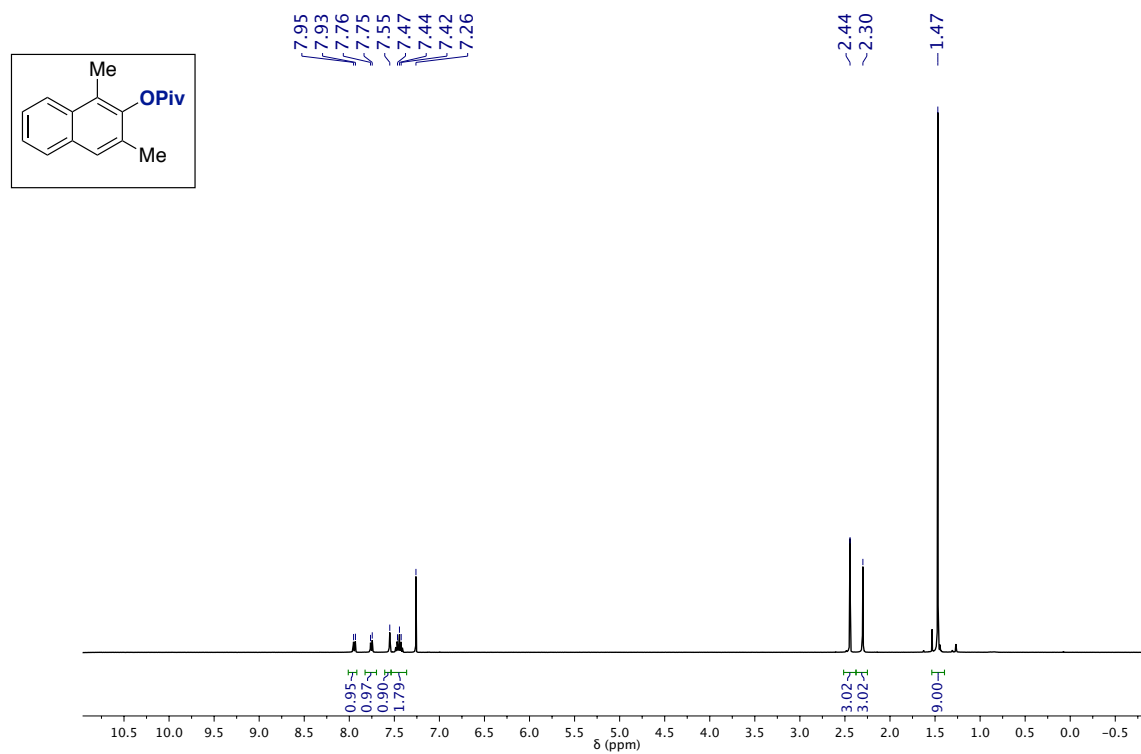
Figure S2.26. ¹H NMR (400 MHz, CDCl₃) of 6d.
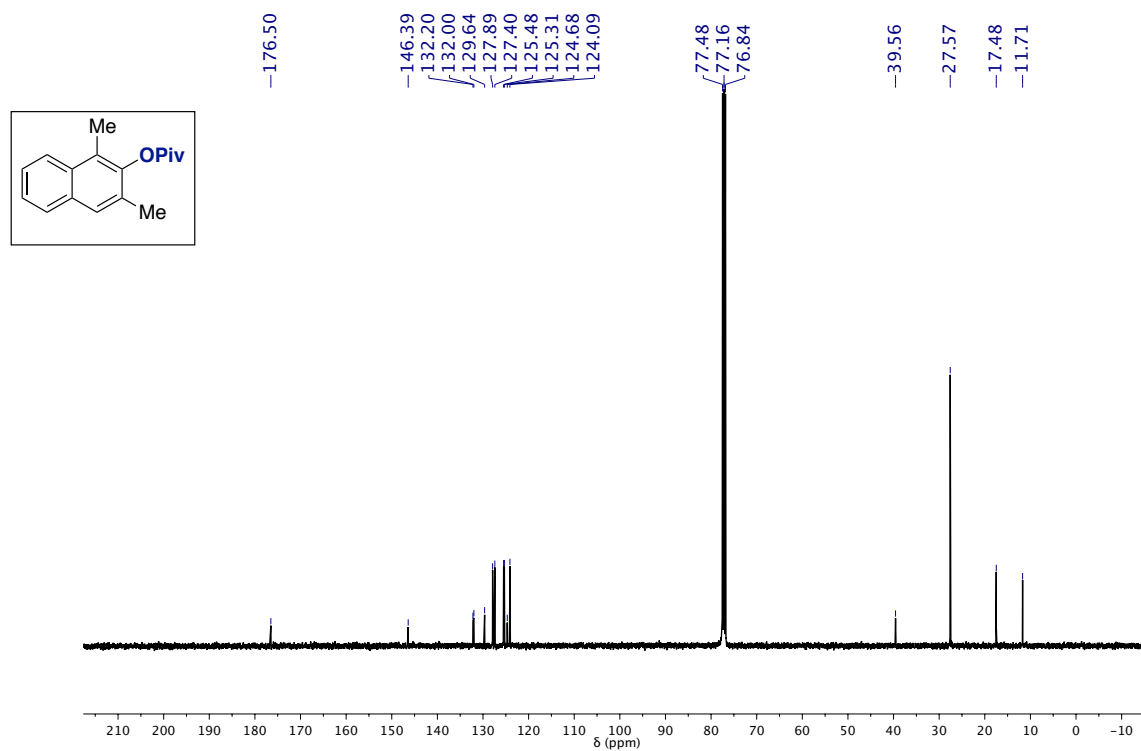
Figure S2.27.¹³C{¹H} NMR (101 MHz, CDCl₃) of 6d.

2.11.14.2. Naphthyl silanes
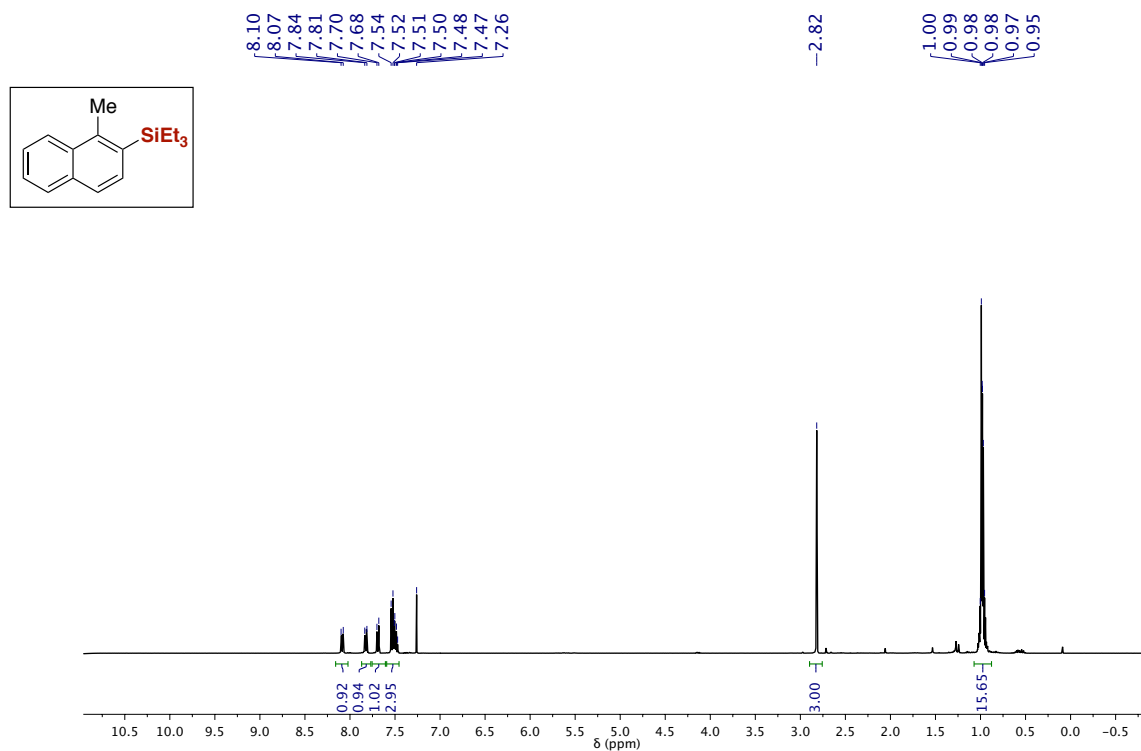
Figure S2.28. ^{1}H NMR (400 MHz, CDCl$_3$) of 9c.
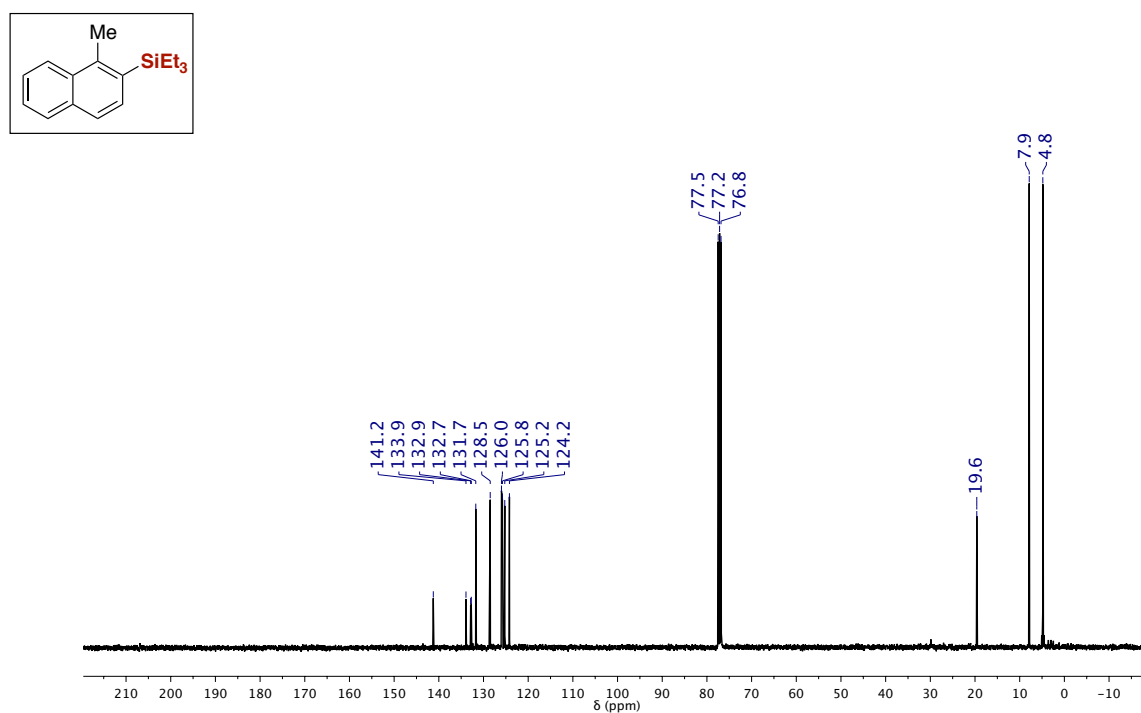
Figure S2.29. ^{13}C{^{1}H} NMR (101 MHz, CDCl$_3$) of 9c.

2.11.15. NMR spectra of isolated nickel complexes

[Ni(σ-1-naphthyl)(µ-OH)-(PCy₃)]₂ (4)
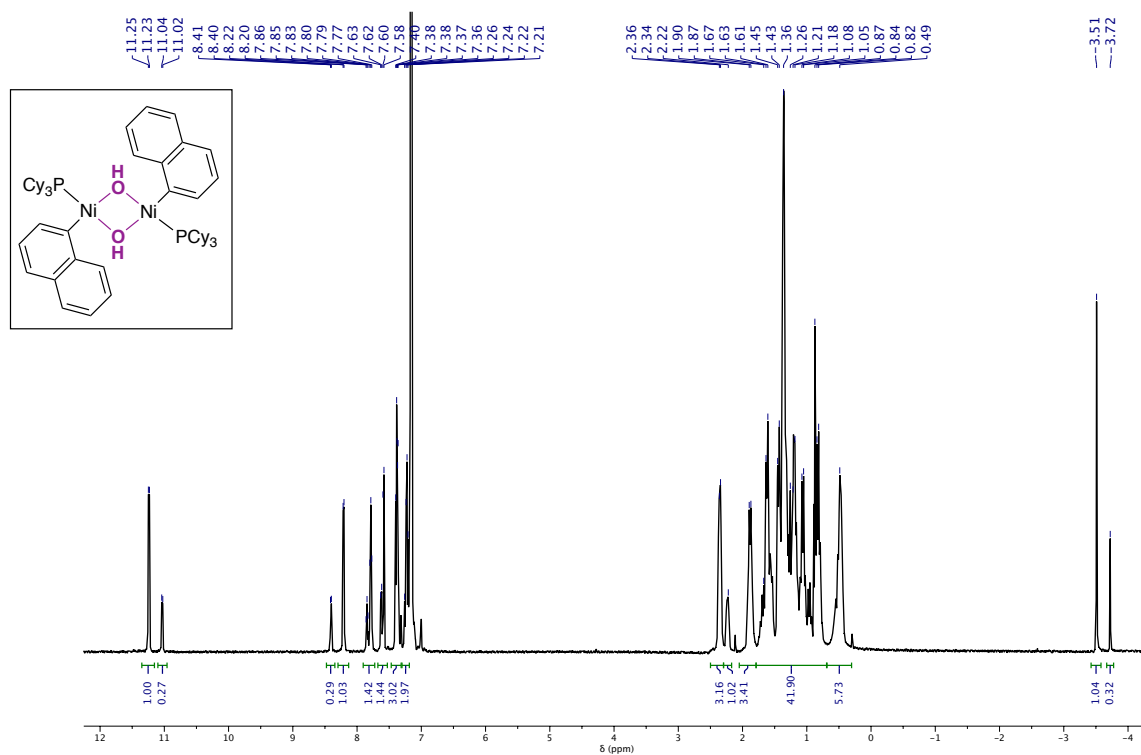
Figure S2.30. ¹H NMR (500 MHz, C₆D₆) [Ni(σ-1-naphthyl)(µ-OH)-(PCy₃)]₂ (4).
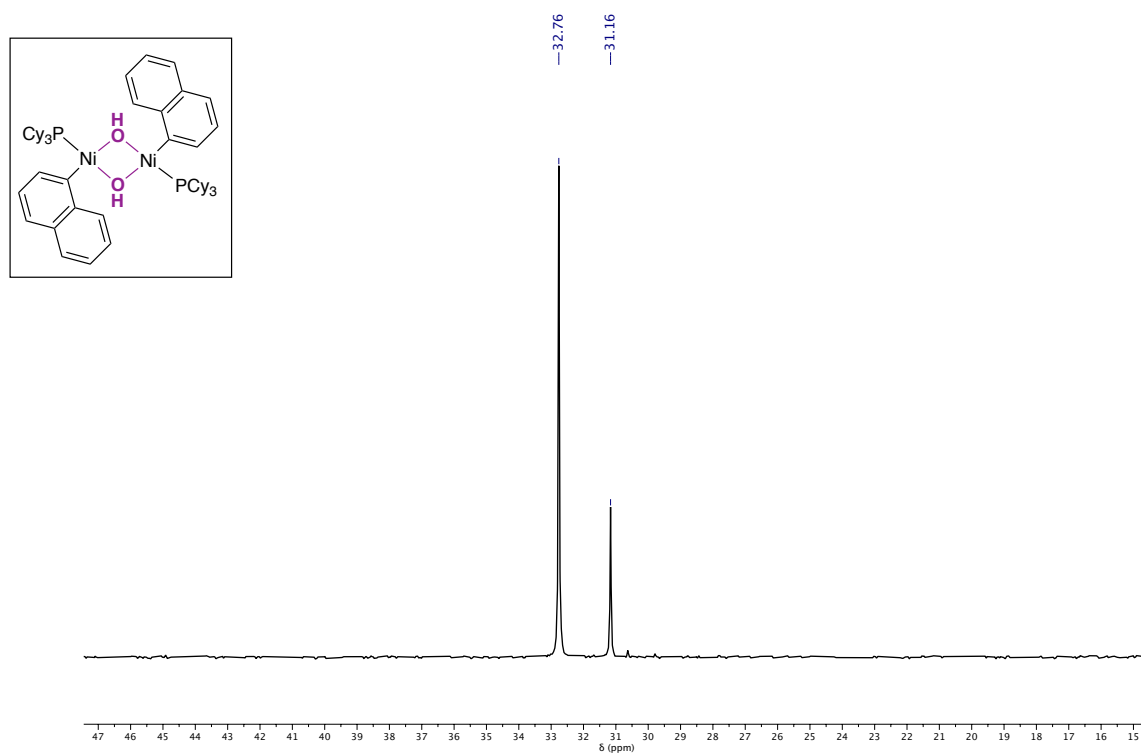
Figure S2.31. ³¹P{¹H} NMR (162 MHz, C₆D₆) [Ni(σ-1-naphthyl)(µ-OH)-(PCy₃)]₂ (4).
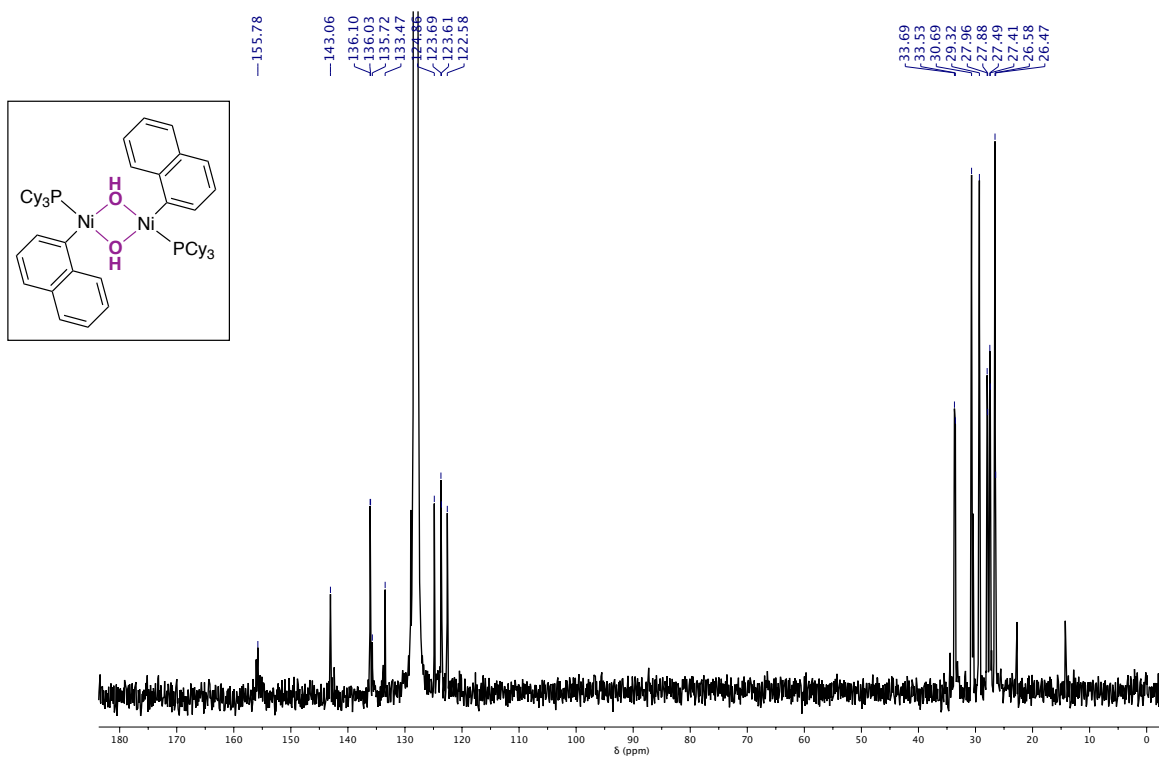
Figure S2.32. ^{13}C{^{1}H} NMR (126 MHz, C$_6$D$_6$) [Ni(σ-1-naphthyl)(μ-OH)-(PCy$_3$)]$_2$ (4).

[Ni$_2$(PCy$_3$)$_2$(μ-OPiv)$_4$] (8)
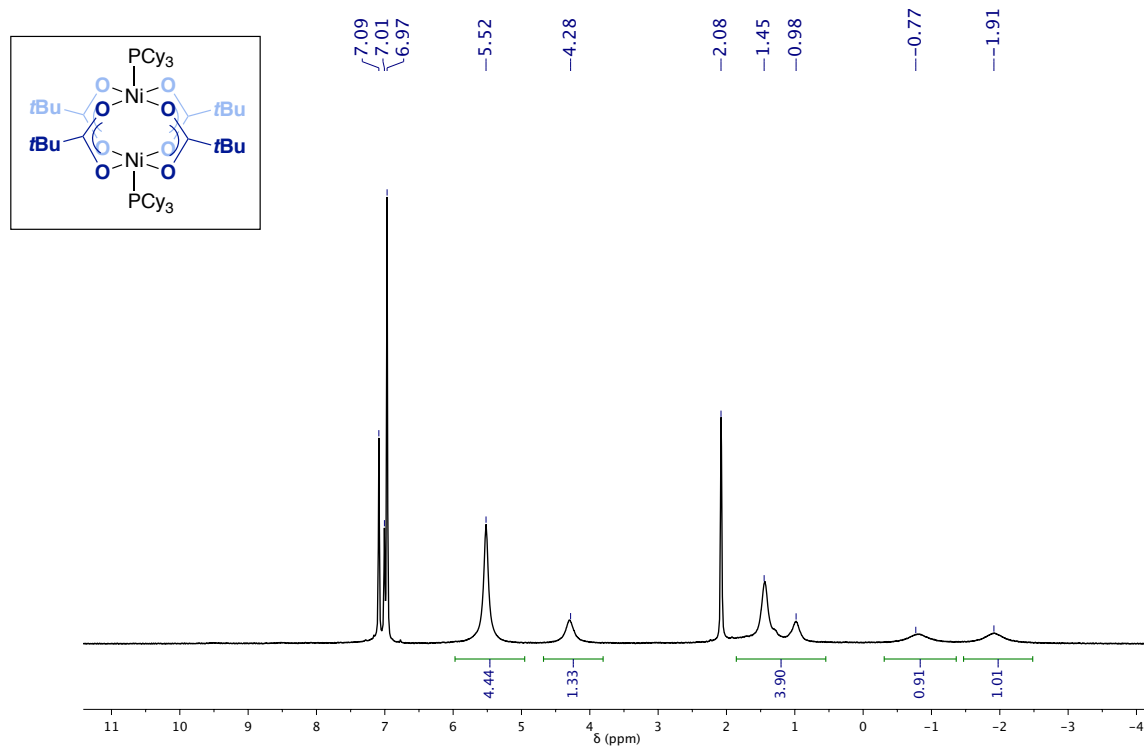
Figure S2.33. ^{1}H NMR (400 MHz, toluene-d_8) [Ni$_2$(PCy$_3$)$_2$(μ-OPiv)$_4$] (8).
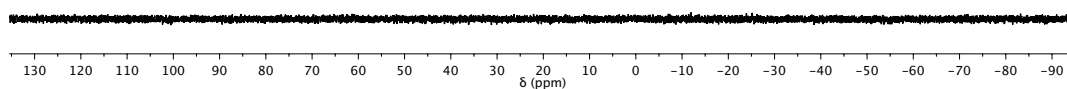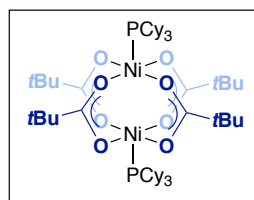
Figure S2.34. ³¹P NMR (162 MHz, toluene-d_8) [Ni$_2$(PCy$_3$)$_2$(μ-OPiv)$_4$] (8).

[Ni(dcype)(σ-1-naphthyl)(κ¹-OPiv)] (11)
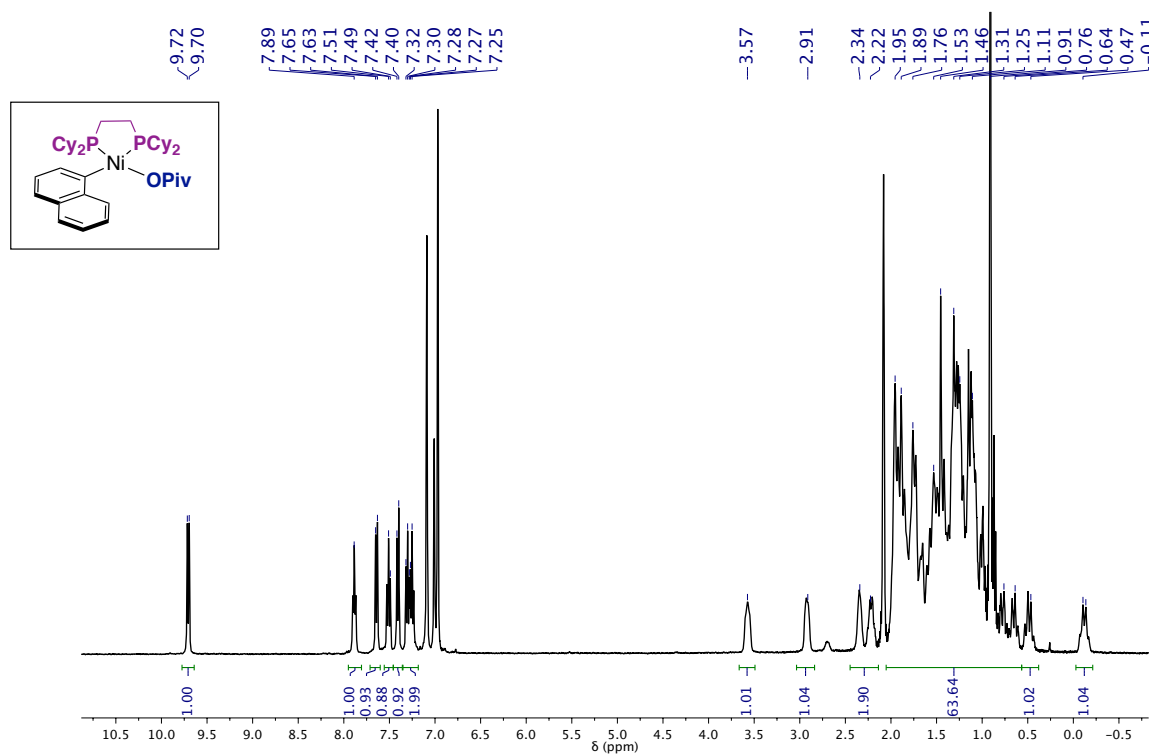
Figure S2.35. ¹H NMR (500 MHz, toluene-d$_8$) [Ni(dcype)(σ-1-naphthyl)(κ¹-OPiv)] (11).
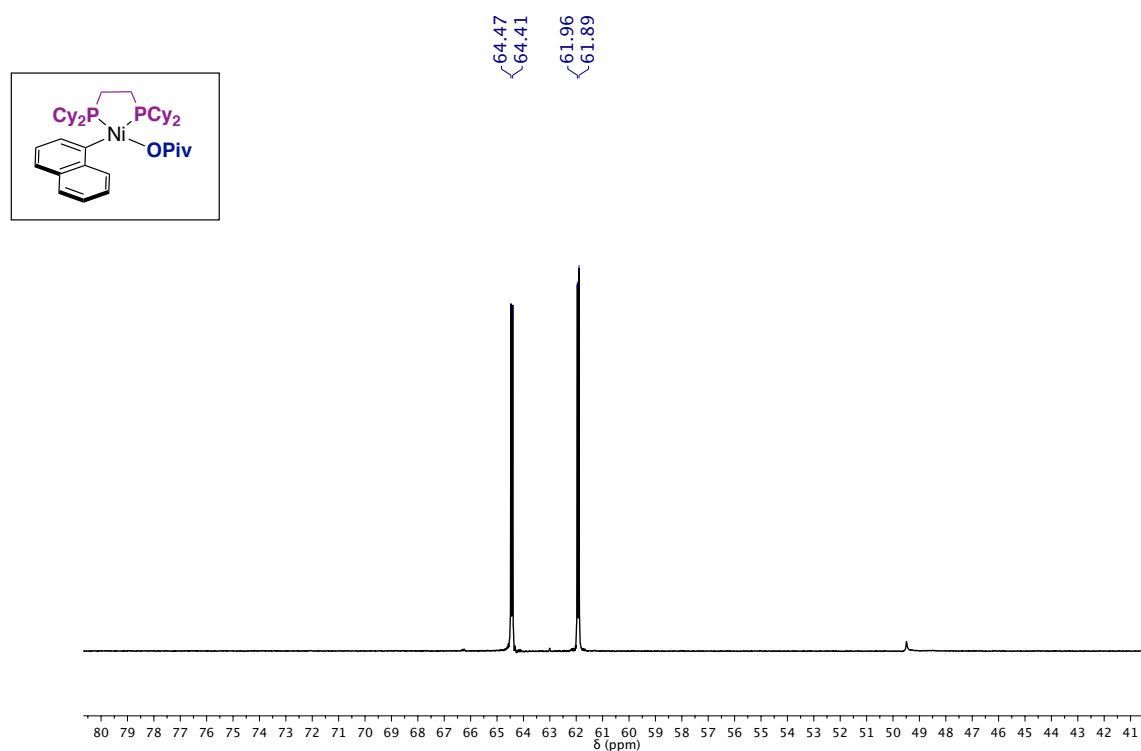
Figure S2.36. ³¹P{¹H} NMR (162 MHz, toluene-d₈) [Ni(dcype)(σ-1-naphthyl)(κ¹-OPiv)] (11).
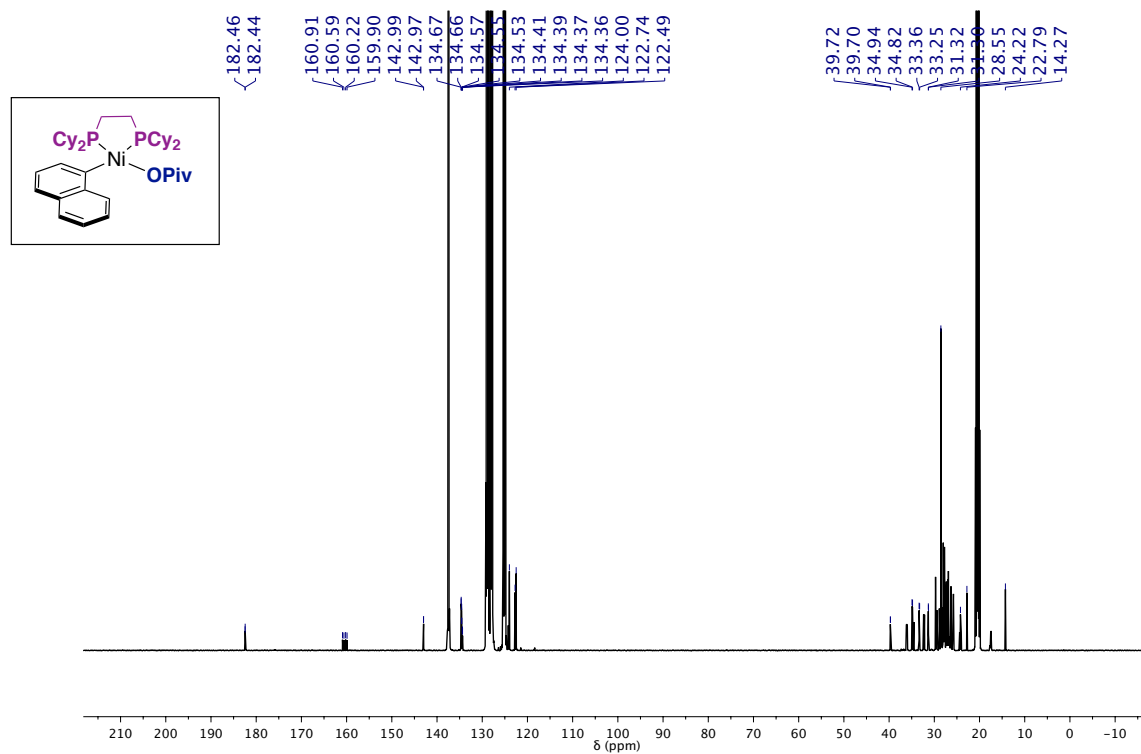
Figure S2.37. ¹³C{¹H} NMR (126 MHz, toluene-d₈) [Ni(dcype)(σ-1-naphthyl)(κ¹-OPiv)] (11).
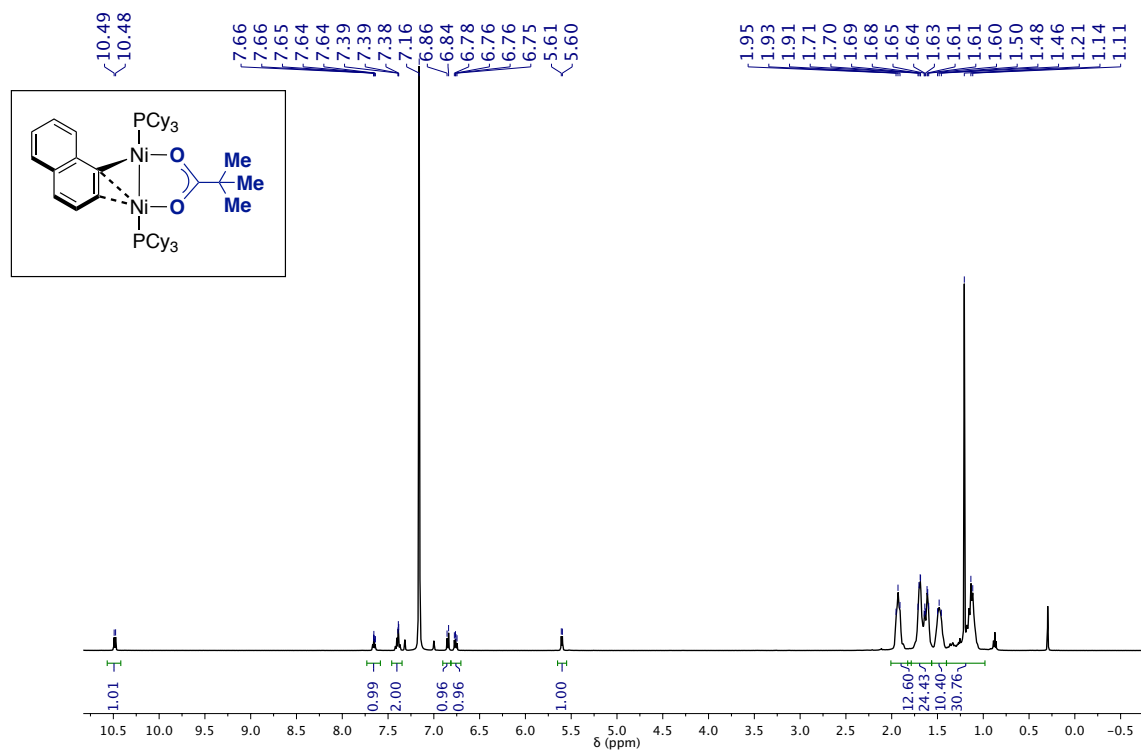
Figure S2.38. ^{1}H NMR (500 MHz, C$_6$D$_6$) [{Ni(PCy$_3$)}$_2$(μ,η^2-1-naphthyl)(μ-OPiv)] (7a).
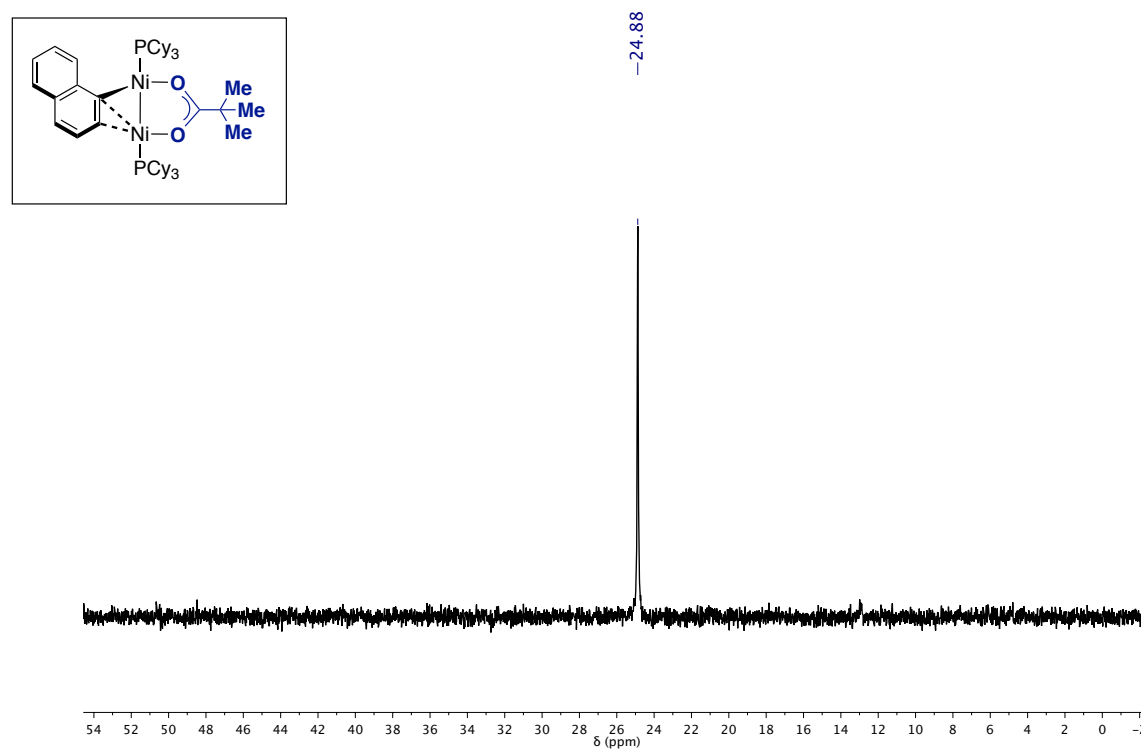
Figure S2.39. ^{31}P{^{1}H} NMR (162 MHz, toluene-d$_8$) [{Ni(PCy$_3$)}$_2$(μ,η^2-1-naphthyl)(μ-OPiv)] (7a).
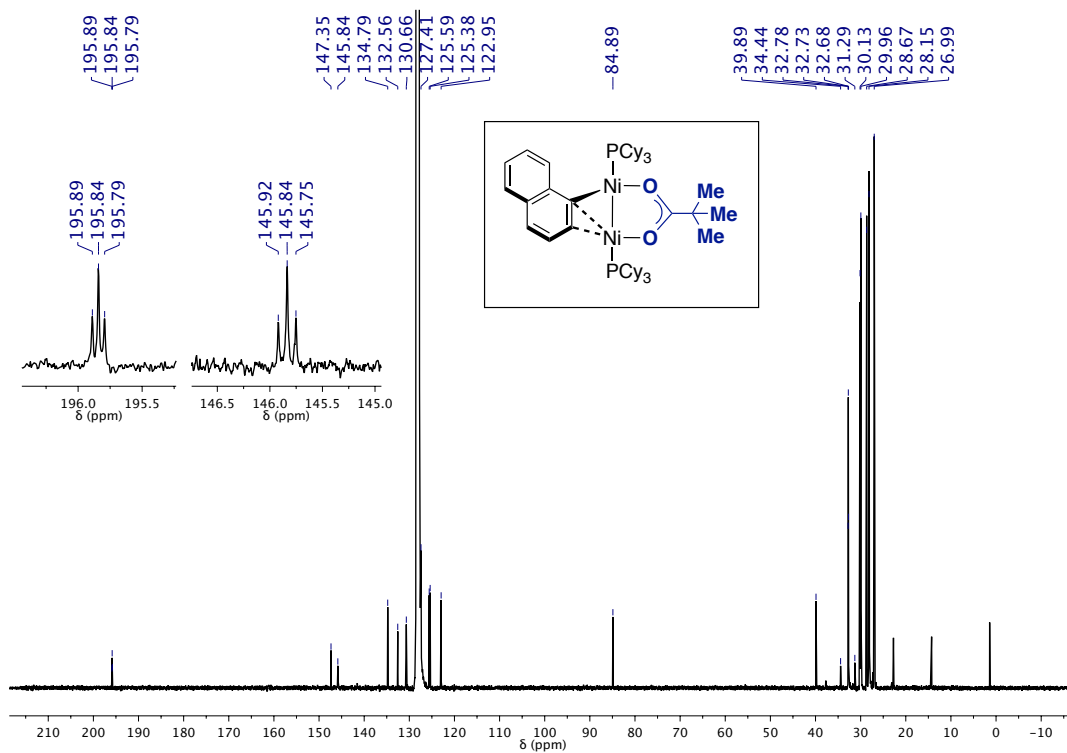
Figure S2.40. ^{13}C{^{1}H} NMR (126 MHz, C$_6$D$_6$) [{Ni(PCy$_3$)}$_2$(μ,η^2-1-naphthyl)(μ-OPiv)] (7a).
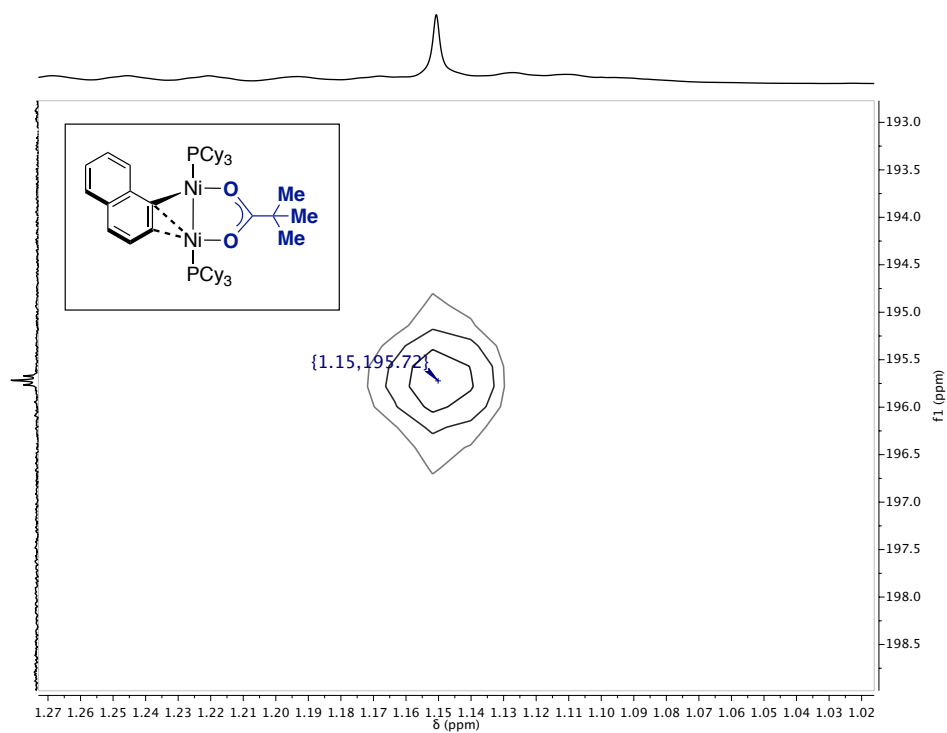
Figure S2.41. Expansion of the ^{1}H–^{13}C HMBC spectrum of 7a showing the correlation between the OPiv carbonyl triplet at δ$_C$ = 195 ppm and the *tert*-butyl singlet at δ$_H$ = 1.14 ppm (toluene-d$_8$).
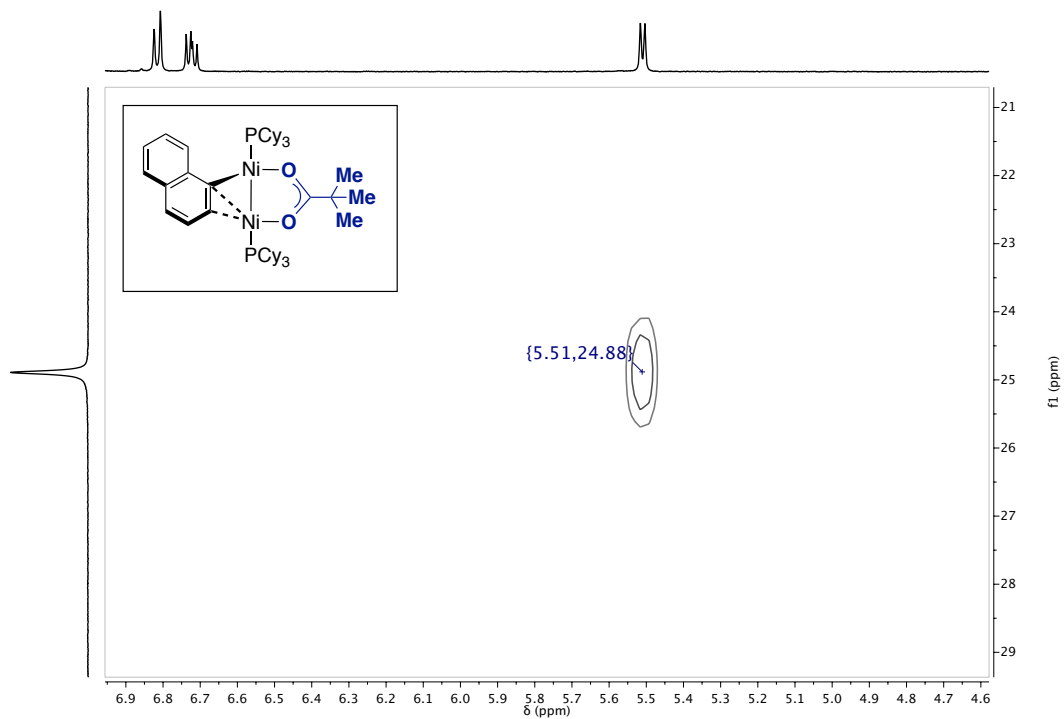
Figure S2.42. Expansion of the room temperature ¹H–³¹P HMBC spectrum of 7a showing the correlation between the single phosphorus environment at δ$_P$ = 24.88 ppm in 7a and the proton in the 2-position of the naphthyl ligand (δ$_H$ = 5.51 ppm).

2.11.15.1. In-situ generated dinickel oxidative addition complexes 7b–f from 6b–f:

[{Ni(PCy₃)}₂(μ,**η**²-2-naphthyl)(μ-OPiv)] (7b)
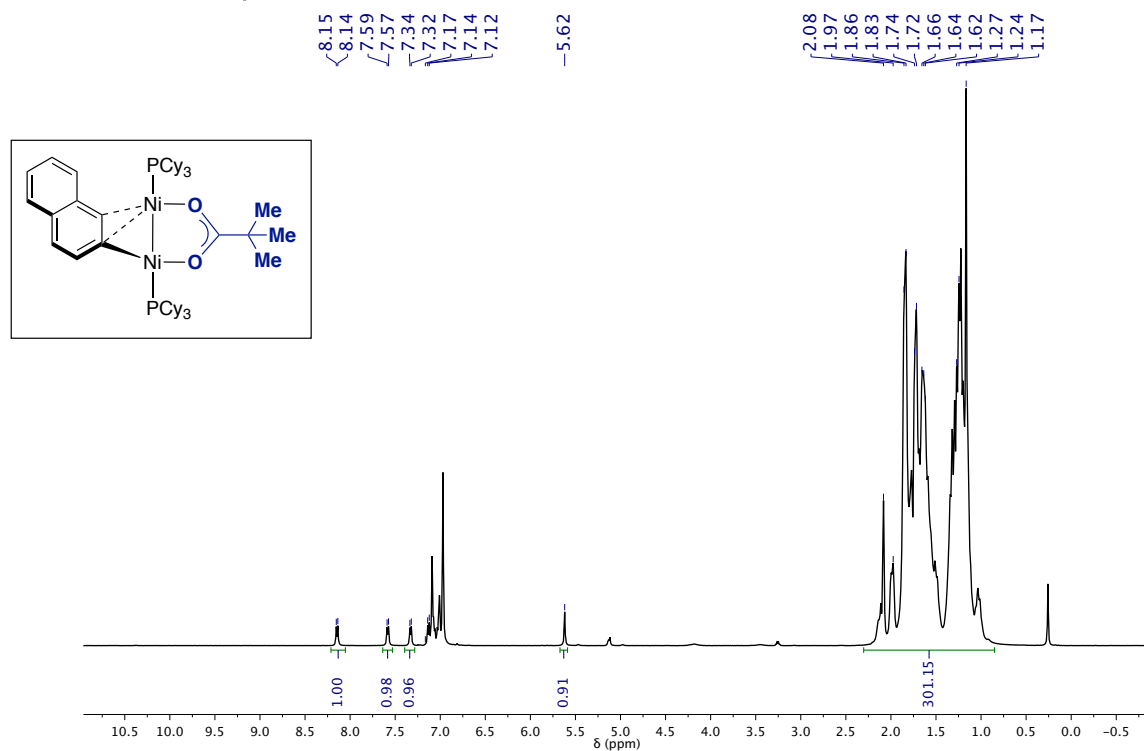
Figure S2.43. ¹H NMR (500 MHz, toluene-d₈) of 7b (in situ synthesis from 6b and [Ni(PCy₃)₂]₂(N₂)).
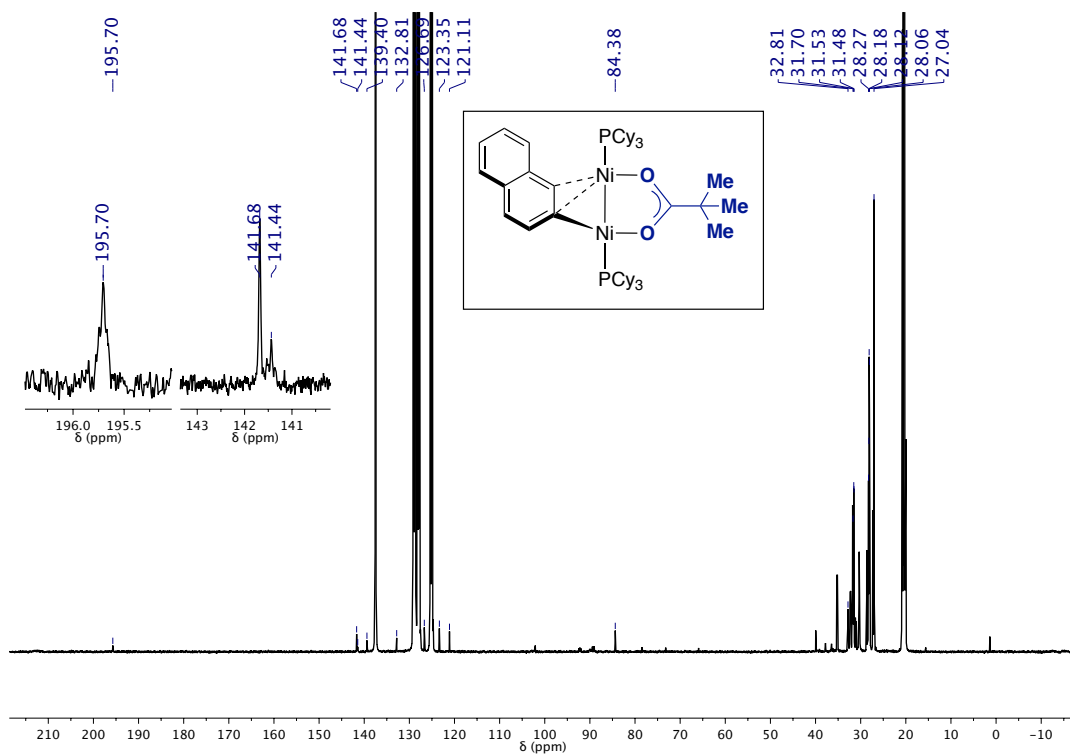
Figure S2.44. ¹³C{¹H} NMR (126 MHz, toluene-d₈) of 7b (in situ synthesis from 6b and [Ni(PCy₃)₂]₂(N₂)).
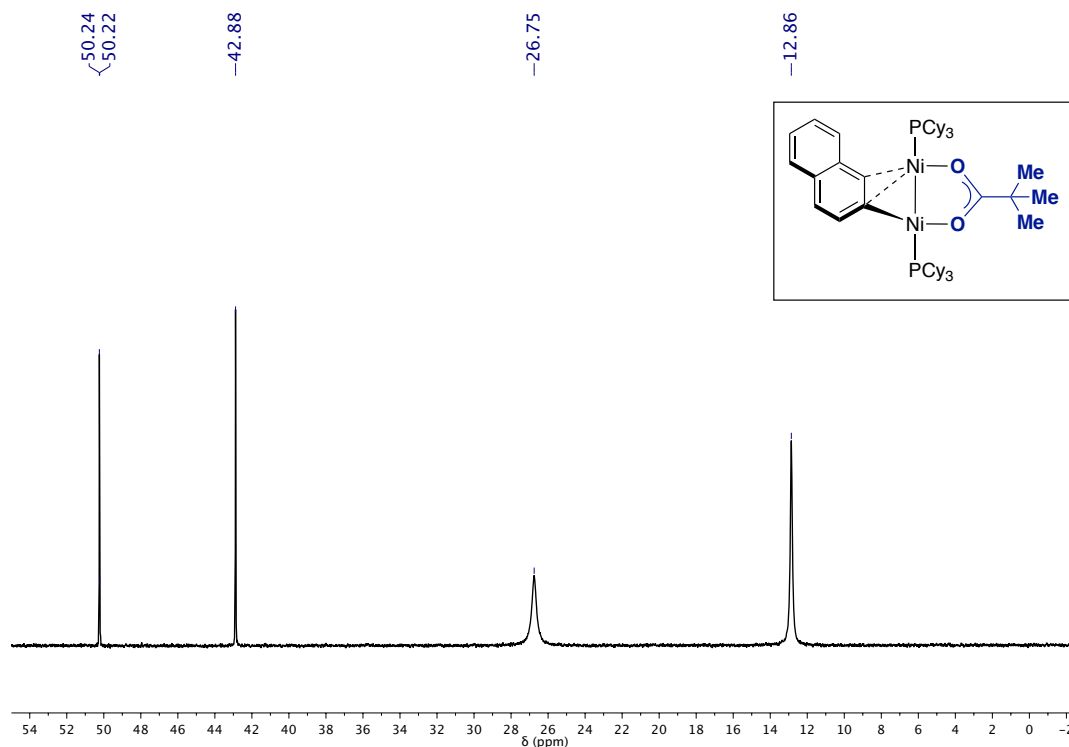
Figure S2.45. ³¹P{¹H} NMR (203 MHz, toluene-d₈) of 7b (δ_P = 26.75 ppm). δ_P = 50.2 ppm [(PCy₃)Ni(η⁶-C₇D₈)] (in situ synthesis from 6b and [Ni(PCy₃)₂]₂(N₂)).
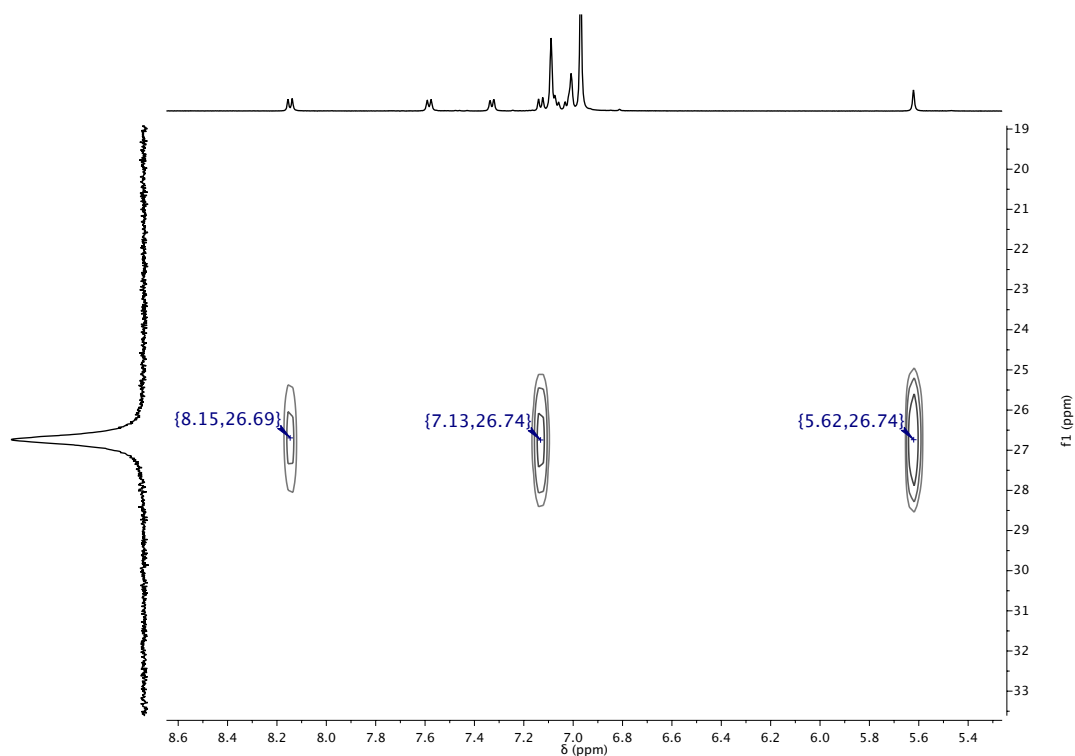
Figure S2.46. Expansion of the room temperature ¹H–³¹P HMBC spectrum of 7b showing the correlation between the single phosphorus environment at δ_P = 26.75 in 7b and H1 (δ_H = 5.62 ppm), H7 (δ_H = 7.13 ppm), and H8 (δ_H = 8.15 ppm) of the naphthyl ligand.

[{Ni(PCy₃)}₂(μ,η²-2-(1-methyl)naphthyl)(μ-OPiv)] (7c)
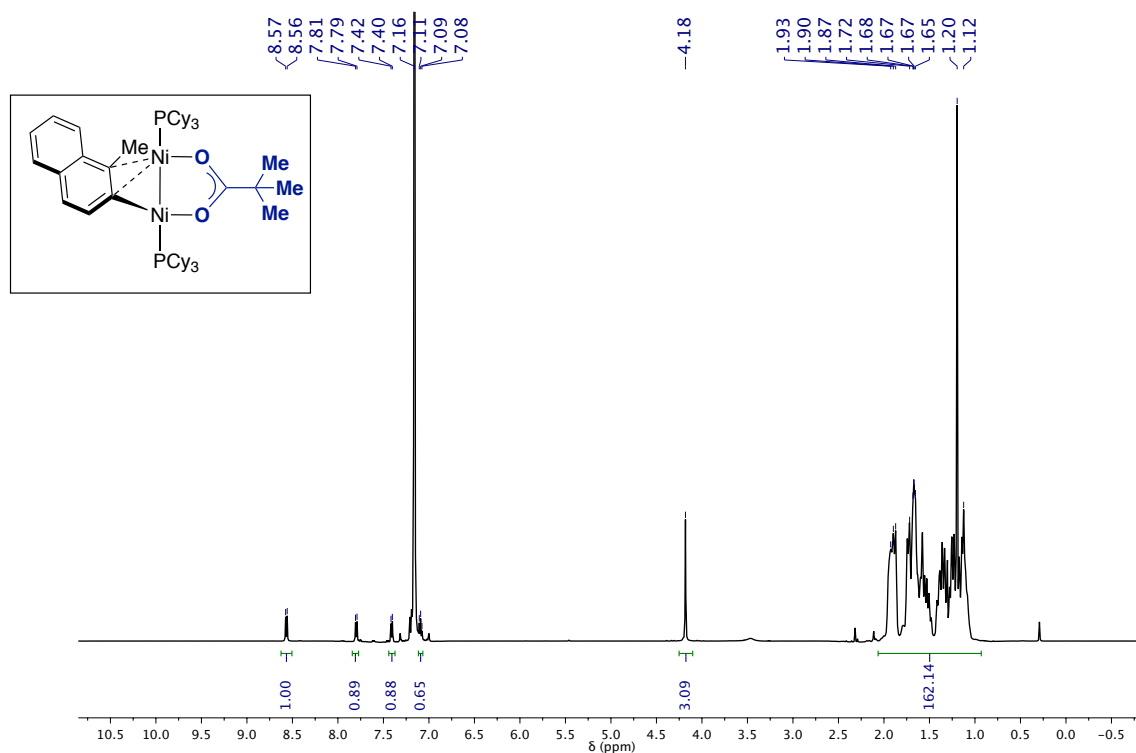
Figure S2.47. ^{1}H NMR (500 MHz, C$_6$D$_6$) of **7c** (in situ synthesis from **6b** and [Ni(PCy$_3$)$_2$]$_2$(N$_2$), NMR spectrum collected after 16 h at 25 °C).
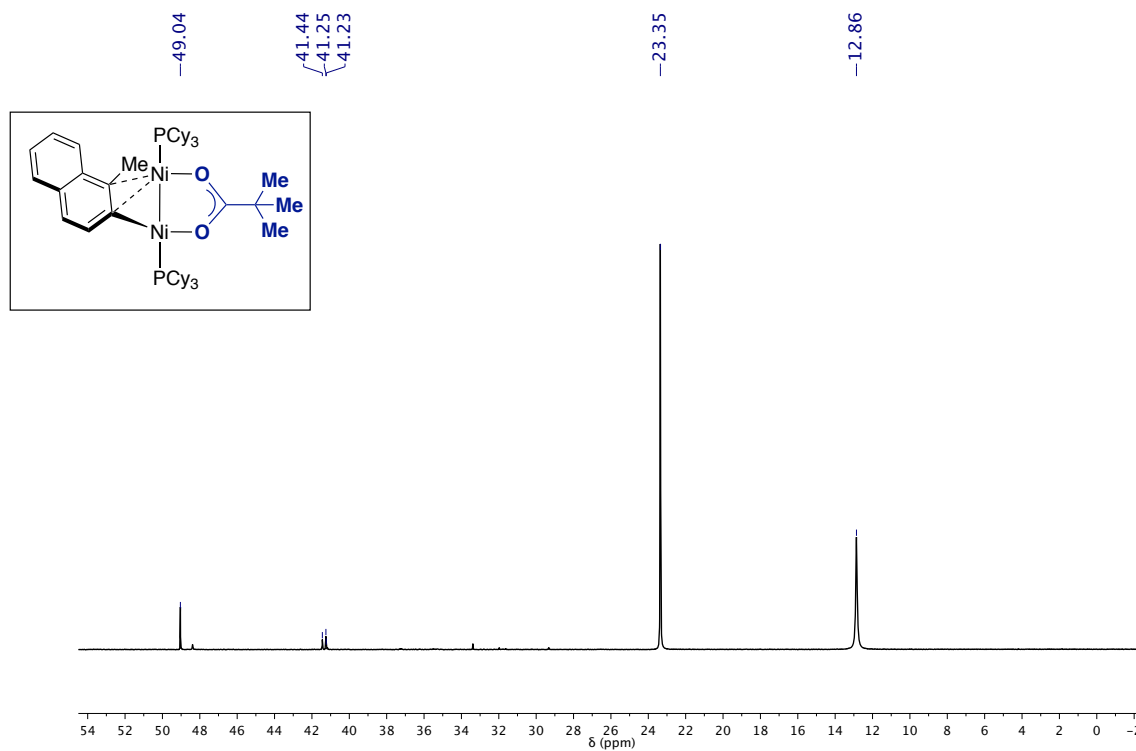
Figure S2.48. ^{31}P{^{1}H} NMR (203 MHz, C$_6$D$_6$) of **7c** (δ_P = 23.35 ppm) δ_P = 49.0 ppm [(PCy$_3$)Ni(η^6-C$_6$D$_6$)]; δ_P = 12.9 (PCy$_3$) ppm. δ_P = 41.0 ppm (unidentified) (in situ synthesis from **6c** and [Ni(PCy$_3$)$_2$]$_2$(N$_2$), NMR spectrum collected after 16 h at 25 °C).
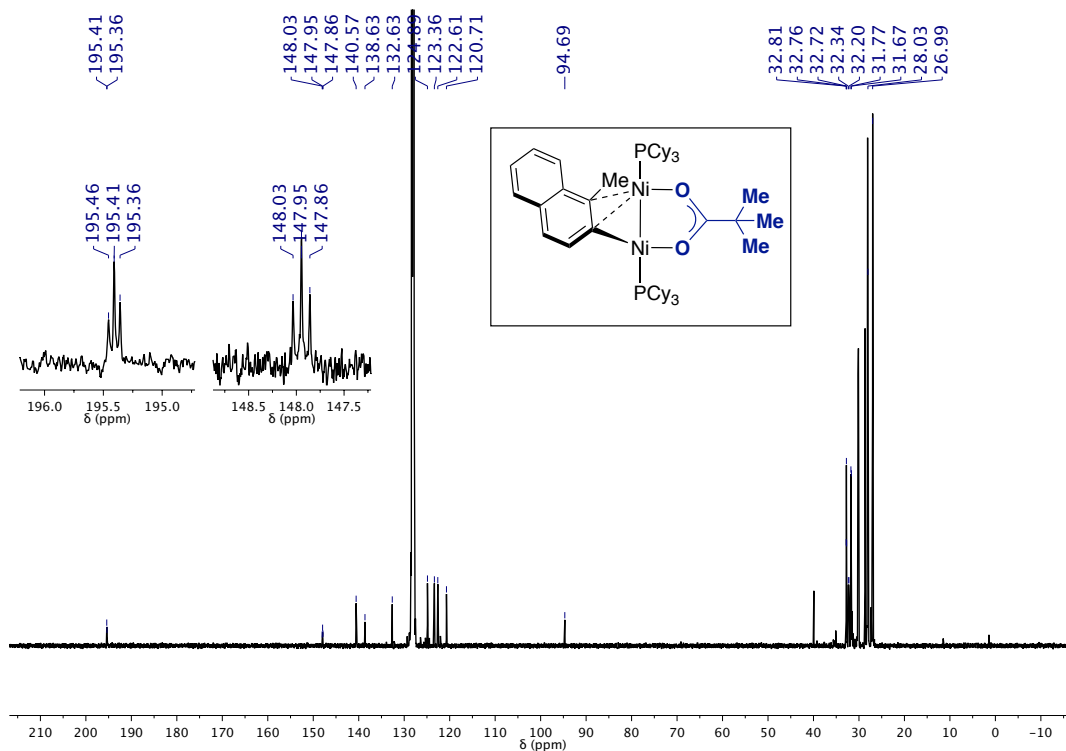
Figure S2.49. $^{13}C\{^1H\}$ NMR (126 MHz, C_6D_6) of **7c** (in situ synthesis from **6c** and [Ni(PCy$_3$)$_2$]$_2$(N$_2$), NMR spectrum collected after 16 h at 25 °C).
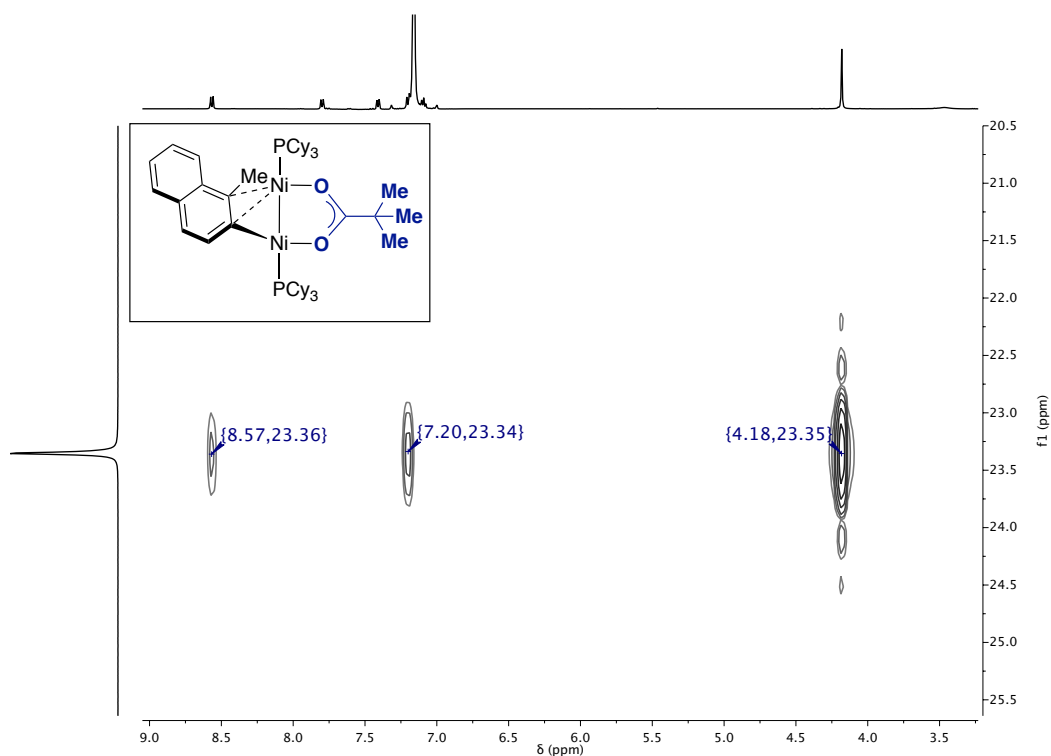
Figure S2.50. Expansion of the room temperature ^1H–^{31}P HMBC spectrum of **7c** showing the correlation between the single phosphorus environment at δ_P = 23.35 ppm in **7c** and the C1 methyl signal (δ_H = 4.18 ppm), H7 (δ_H = 7.20 ppm), and H8 (δ_H = 8.57 ppm) of the naphthyl ligand.

[{Ni(PCy₃)}₂(μ,η²-2-(1,3-dimethyl)naphthyl)(μ-OPiv)] (7d)
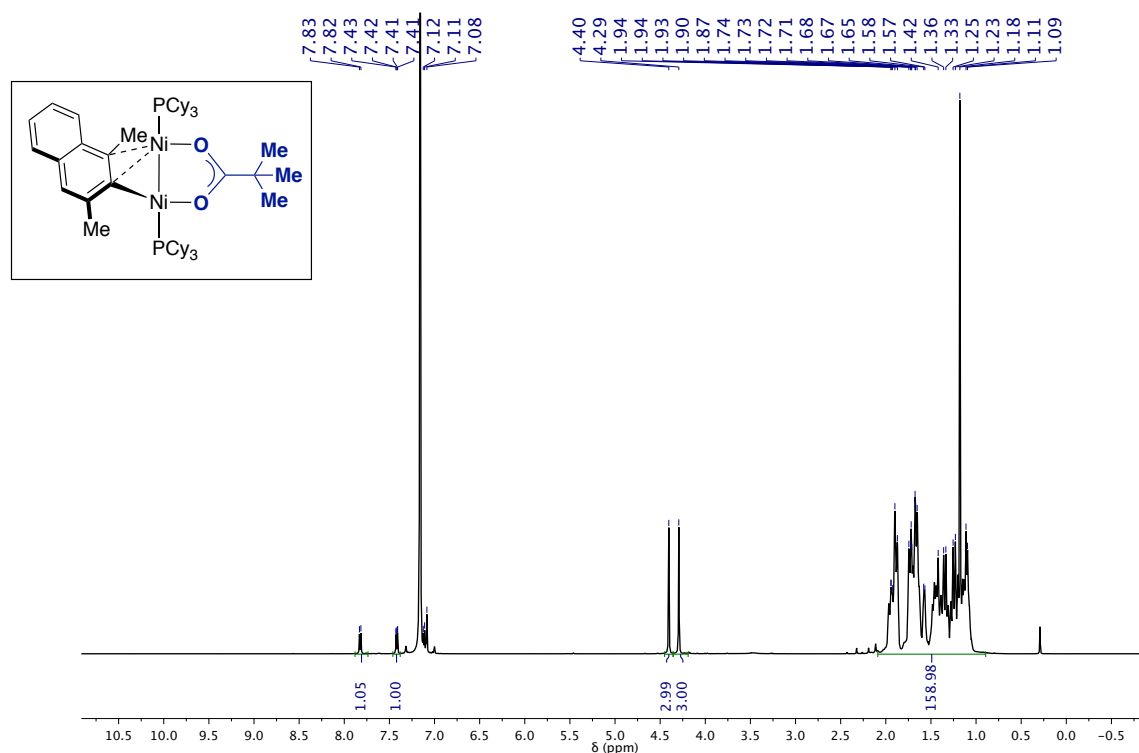
Figure S2.51. ¹H NMR (500 MHz, C₆D₆) of 7d. (in situ synthesis from 6d and [Ni(PCy₃)₂]₂(N₂), NMR spectrum collected after 16 h at 25 °C).
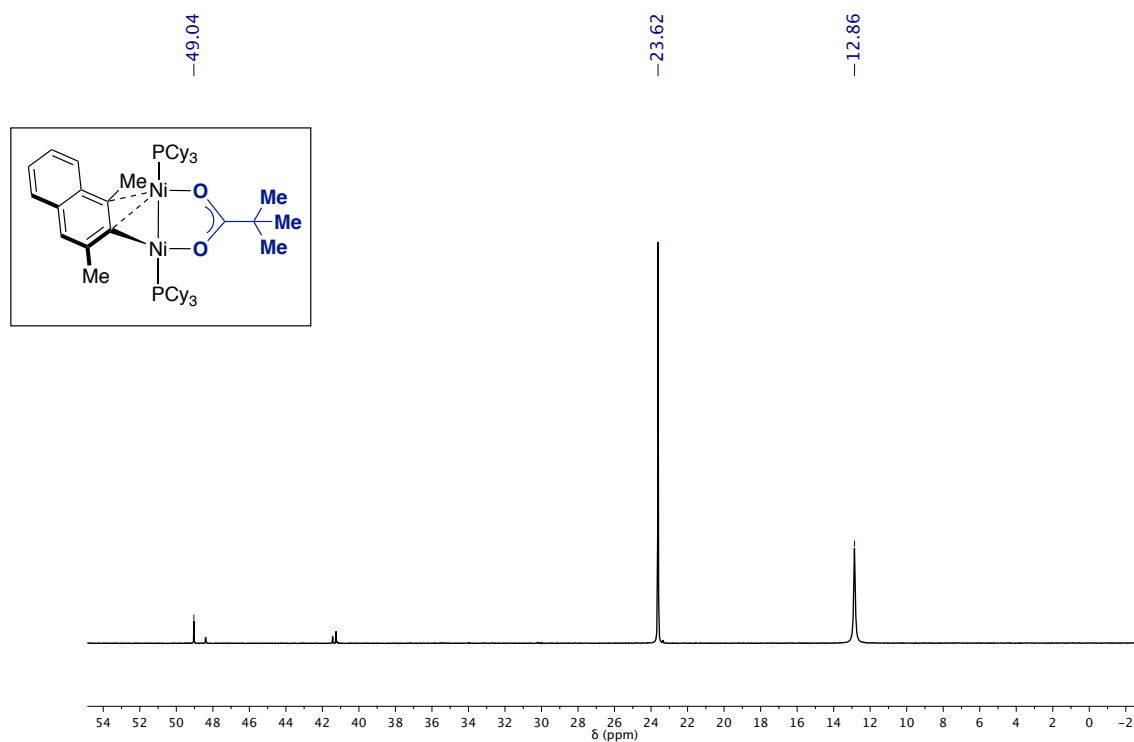
Figure S2.52. ³¹P{¹H} NMR (203 MHz, C₆D₆) of 7d (δ_P = 23.62 ppm). δ_P = 49.0 ppm [(PCy₃)Ni(η⁶-C₆D₆)]; δ_P = 12.9 (PCy₃) ppm (in situ synthesis from 6d and [Ni(PCy₃)₂]₂(N₂), NMR spectrum collected after 16 h at 25 °C).
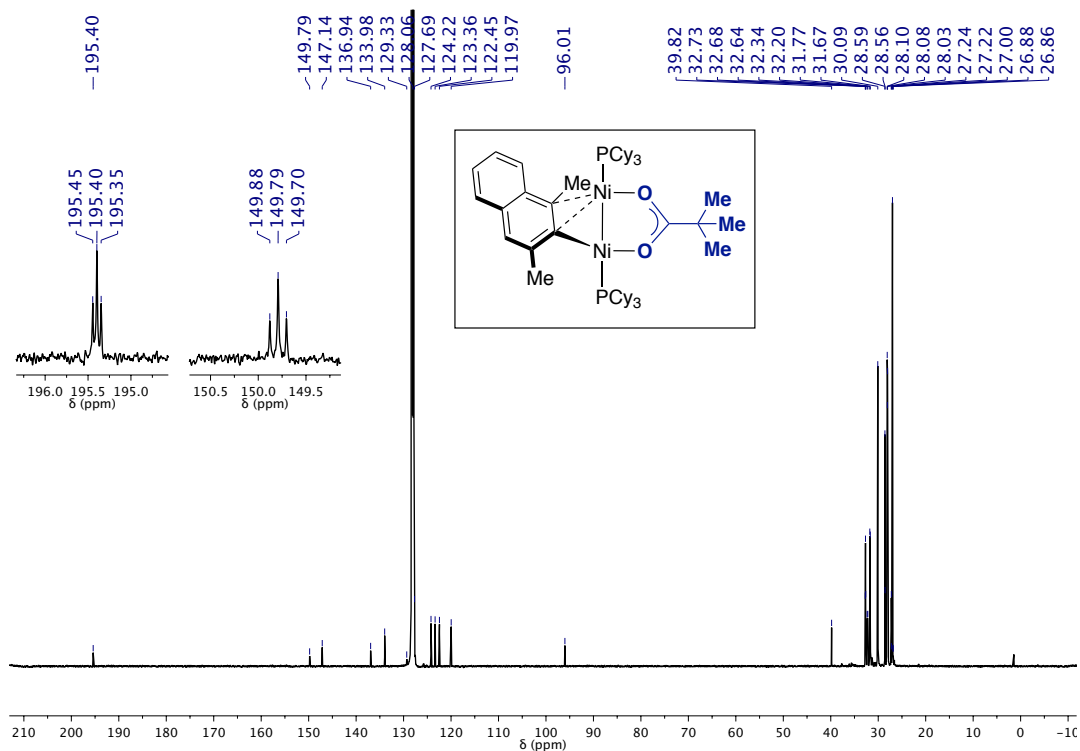
Figure S2.53. $^{13}\text{C}\{^1\text{H}\}$ NMR (126 MHz, C_6D_6) of 7d. (in situ synthesis from 1d and $[\text{Ni}(\text{PCy}_3)_2]_2(\text{N}_2)$, NMR spectrum collected after 16 h at 25 °C).
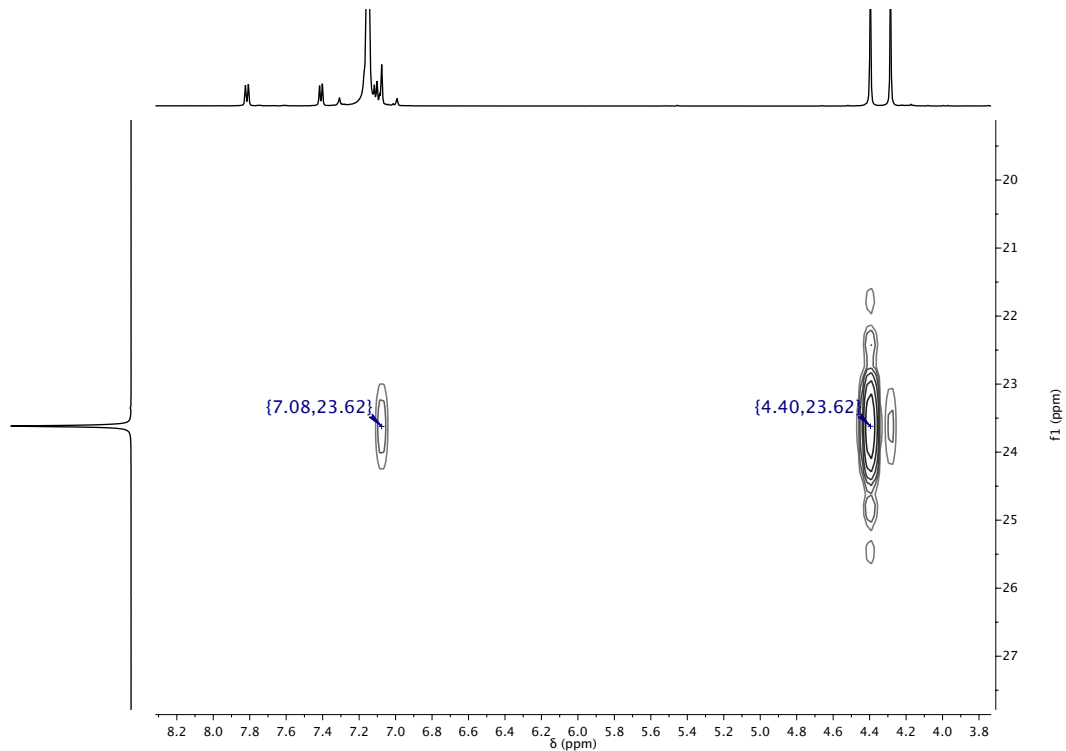
Figure S2.54. Expansion of the room temperature ^1H–^{31}P HMBC spectrum of 7d showing the correlation between the single phosphorus environment at δ_P = 23.62 ppm in 7d and both the C1 methyl signal (δ_H = 4.40 ppm) and H4 of the naphthyl ligand (δ_H = 7.08 ppm).

[{Ni(PCy₃)}₂(μ,η²-2-(7-methoxy)naphthyl)(μ-OPiv)] (7e)
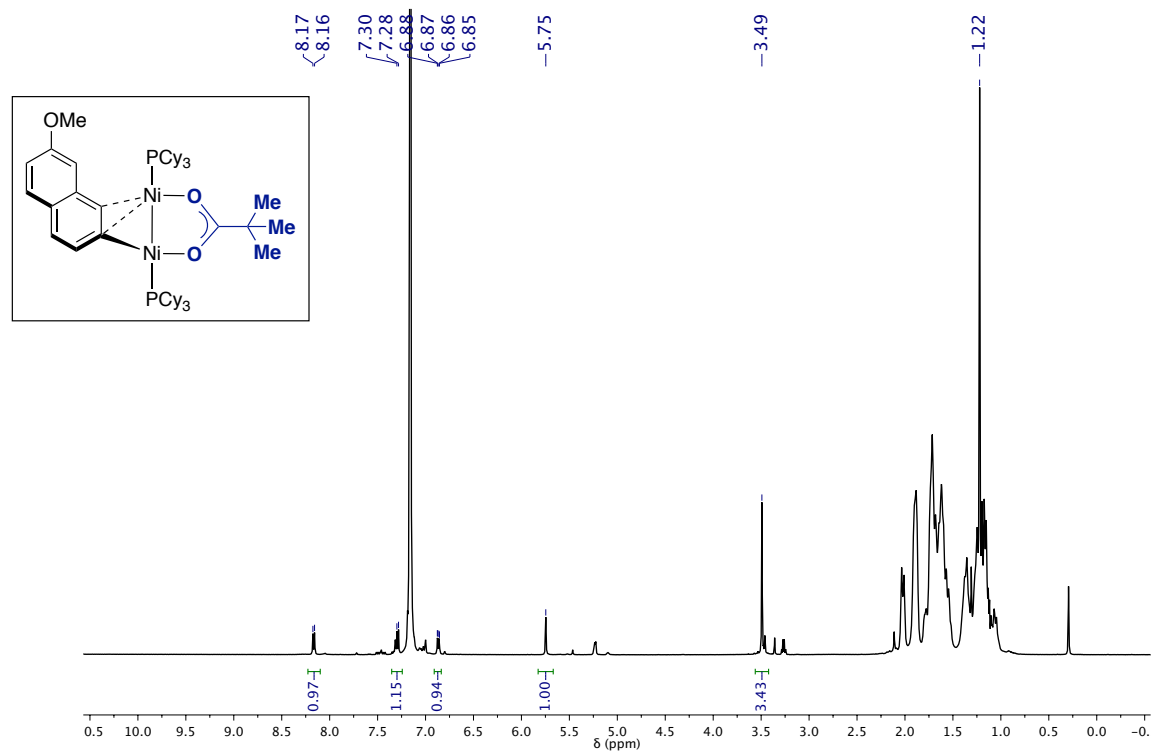
Figure S2.55. ¹H NMR (500 MHz, C₆D₆) of 7e. Includes signals of [Ni(PCy₃)₂]₂(N₂), free PCy₃, unreacted 6e, [(PCy₃)Ni(η⁶-C₆D₆)] (δ_H = 5.25 ppm) (in situ synthesis from 6e and [Ni(PCy₃)₂]₂(N₂), room temperature NMR spectrum collected after 30 minutes heating at 50 °C).
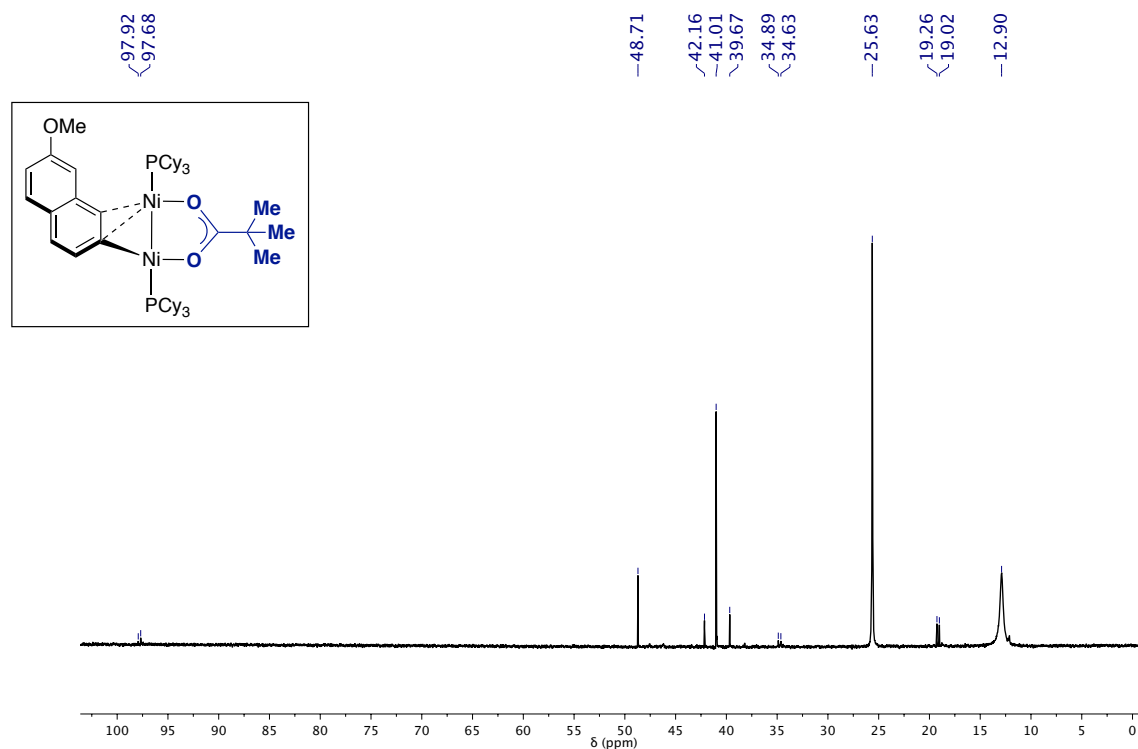
Figure S2.56. ^{31}P{^{1}H} NMR (203 MHz, C$_6$D$_6$) of 7e (δ_P = 25.63 ppm). Remaining signals: δ_P = 97.8 (t, $J_{P\text{-}P}$ = 48 Hz) and 19.1 (d, $J_{P\text{-}P}$ = 48 Hz) (unidentified); δ_P = 48.7 ppm [(PCy$_3$)Ni(η^6-C$_6$D$_6$)]; δ_P = 42.2, 41.0, 39.7 ppm (unidentified); δ_P = 12.9 ppm (PCy$_3$) (in situ synthesis from 6e and [Ni(PCy$_3$)$_2$]$_2$(N$_2$), room temperature NMR spectrum collected after 30 minutes heating at 50 °C).
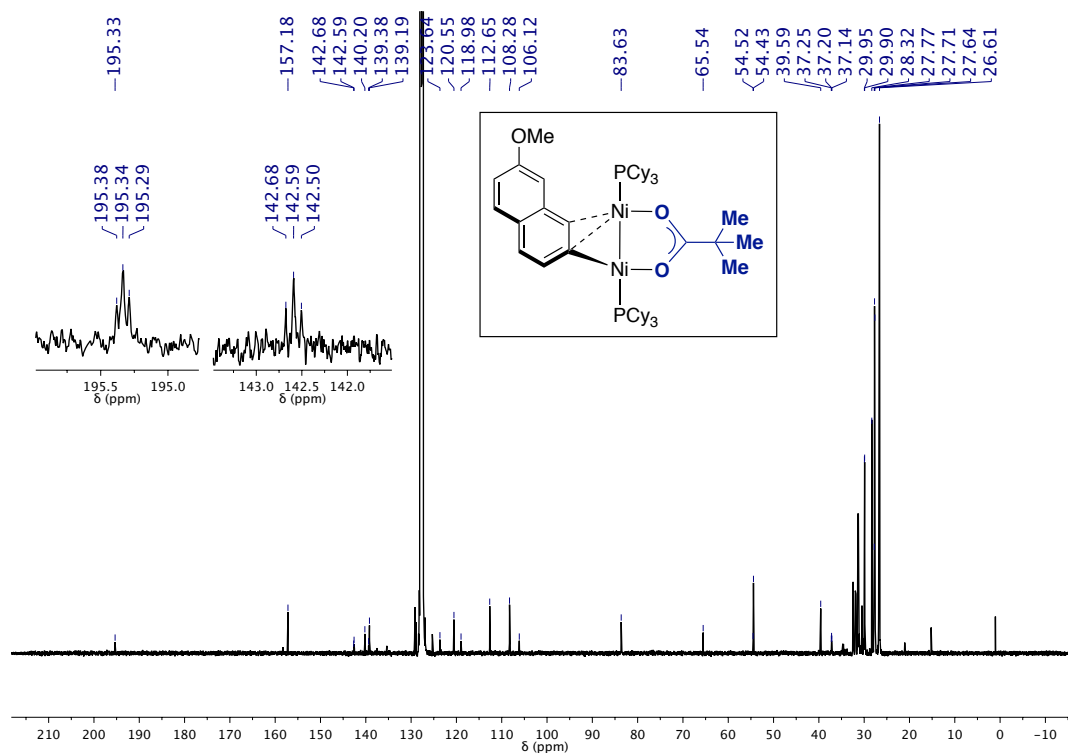
Figure S2.57. ^{13}C{^{1}H} NMR (126 MHz, C$_6$D$_6$) of 7e.

[{Ni(PCy₃)}₂(μ,**η**²-phenyl)(μ-OPiv)] (7f)
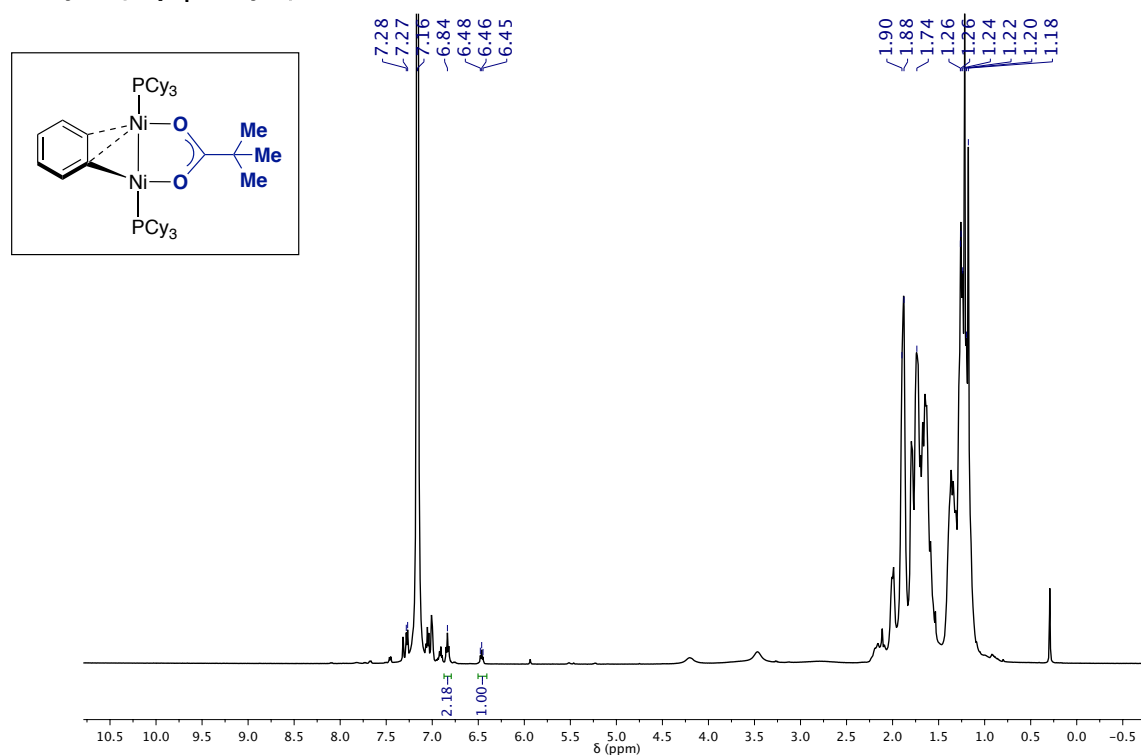
Figure S2.58. ¹H NMR (500 MHz, C₆D₆) of 7f (in situ synthesis from 6f and [Ni(PCy₃)₂]₂(N₂), room temperature NMR spectrum collected after 2 h at room temperature).
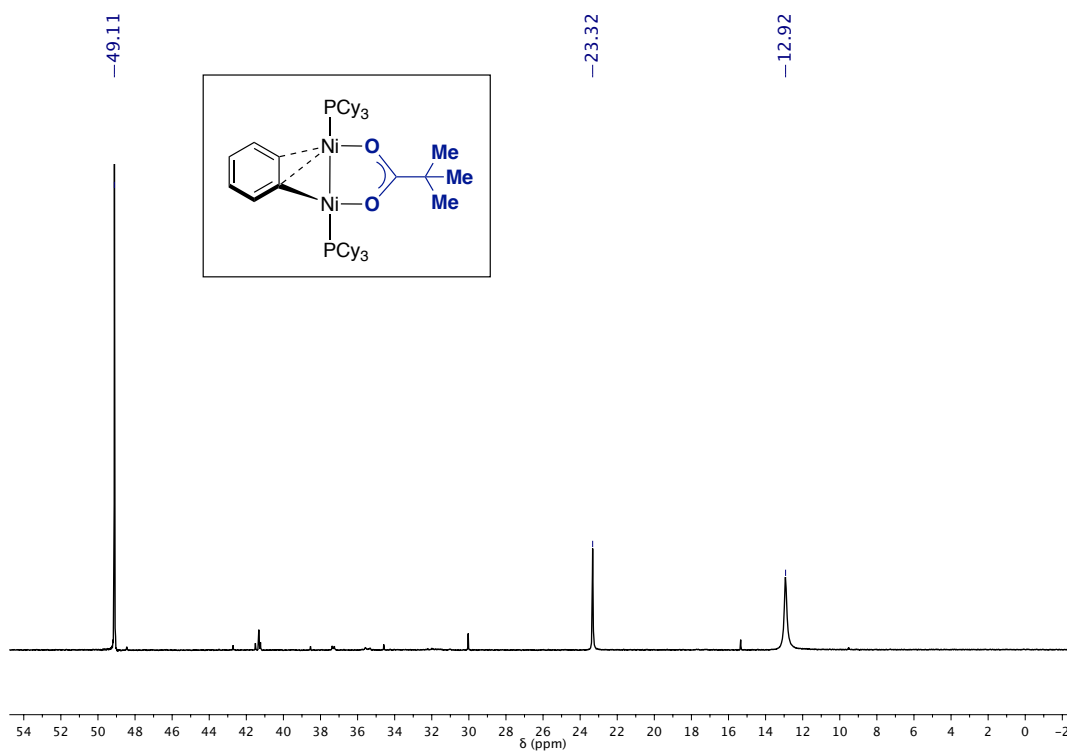
Figure S2.59. ³¹P{¹H} NMR (203 MHz, C₆D₆) of 7f (δ_P = 23.32 ppm). δ_P = 49.1 ppm [(PCy₃)Ni(η⁶-C₆D₆)], δ_P = 12.9 ppm (PCy₃). (in situ synthesis from 6f and [Ni(PCy₃)₂]₂(N₂), room temperature NMR spectrum collected after 2 h at room temperature).
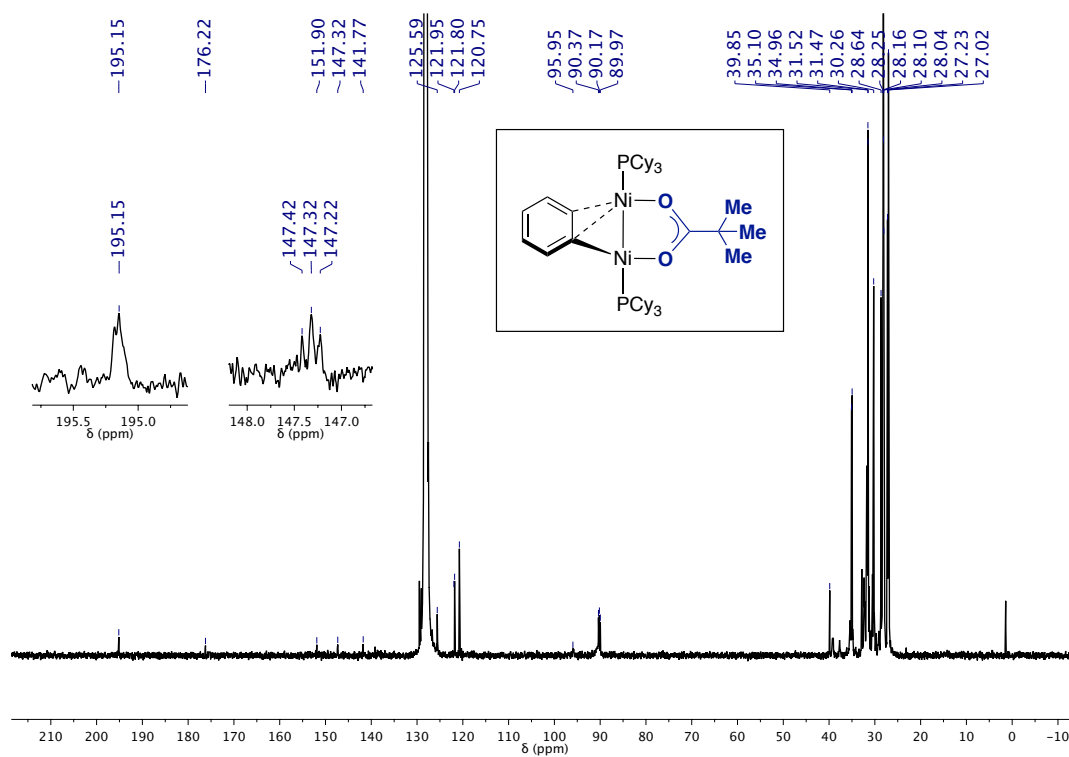
Figure S2.60. ¹³C{¹H} NMR (126 MHz, C₆D₆) of **7f** (in situ synthesis from **6f** and [Ni(PCy₃)₂]₂(N₂), room temperature NMR spectrum collected after 2 h at room temperature).

2.11.16. Fluoroborate by-products

2 equivalents of CsF
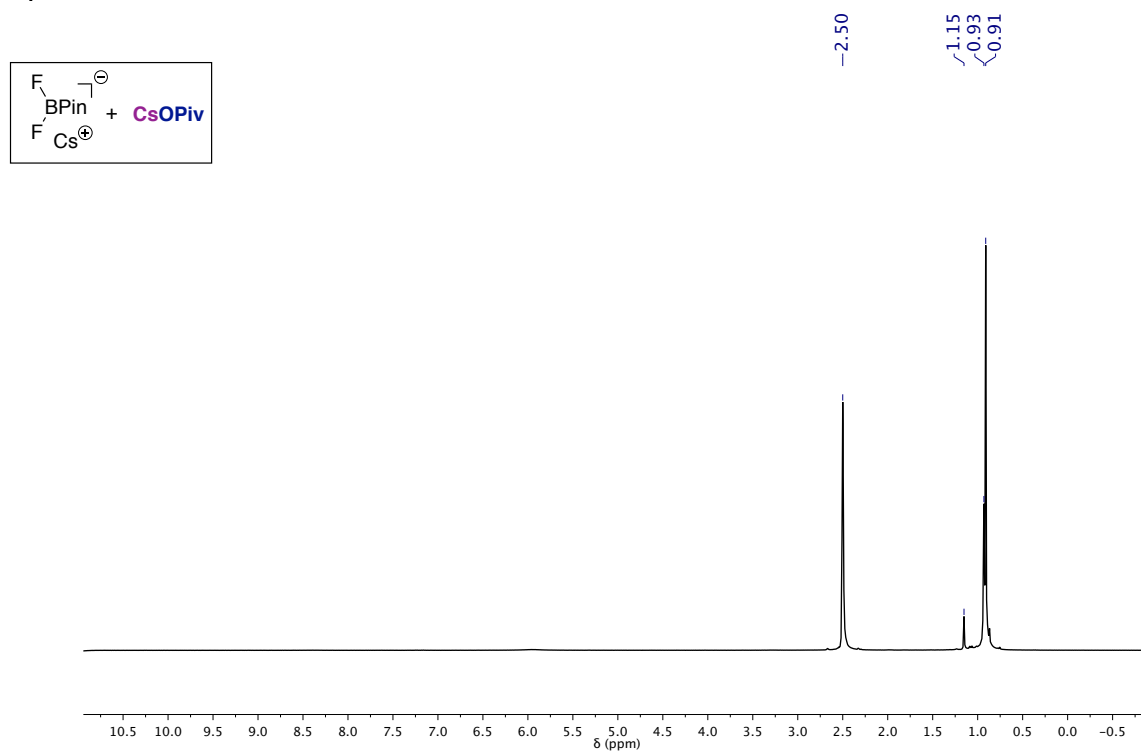
Figure S2.61. ¹H NMR (400 MHz, DMSO-d₆) of by-products with 2 equiv CsF as the additive.
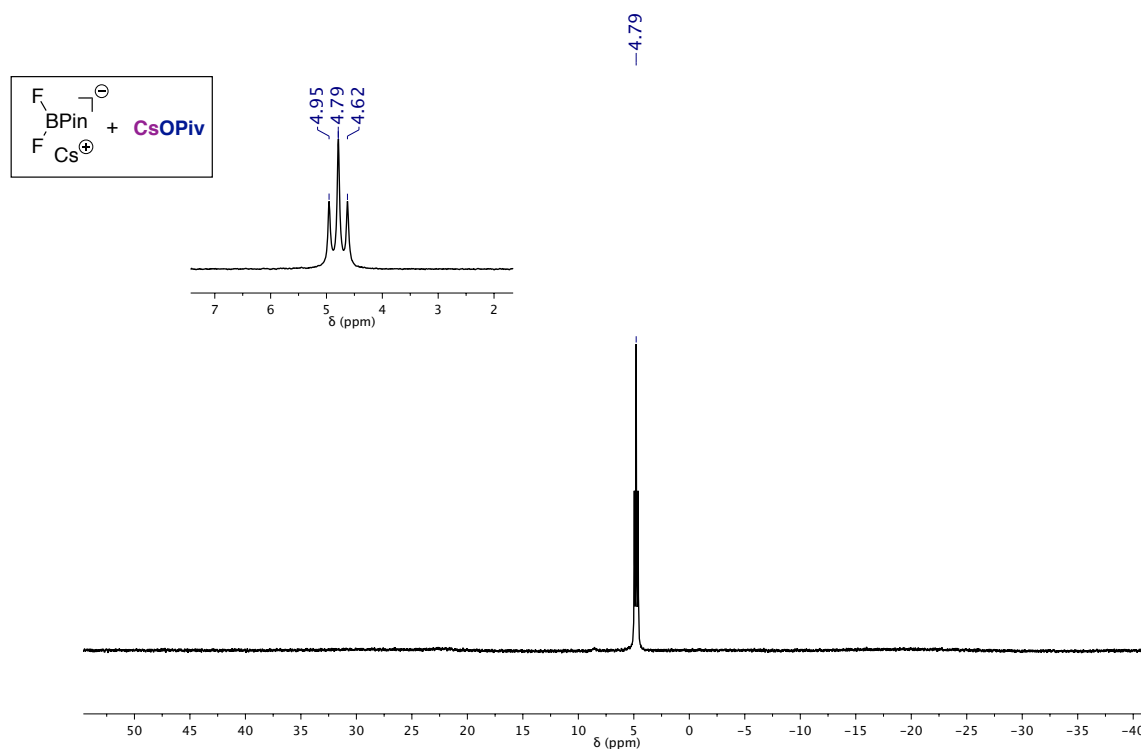
Figure S2.62. ¹¹B NMR (128 MHz, DMSO-d₆) of by-products with 2 equiv CsF as the additive.
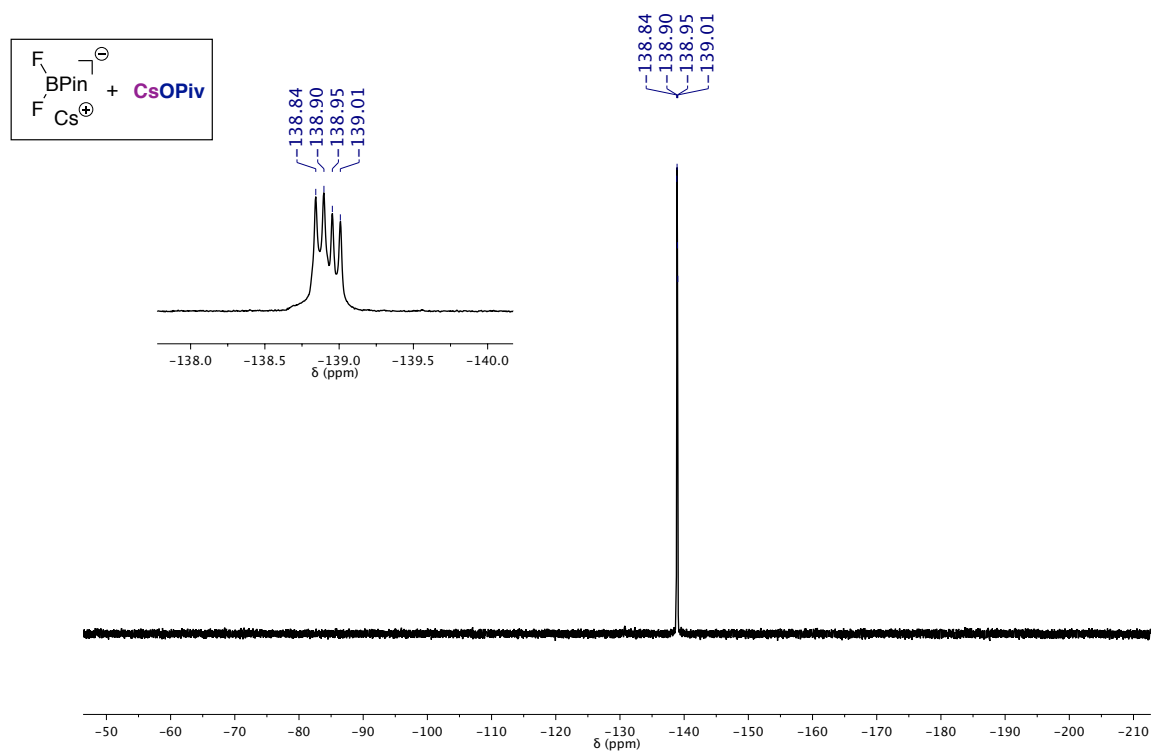
Figure S2.63. ¹⁹F NMR (376 MHz, DMSO-d₆) of by-products obtained from the use of 2 equiv CsF as the additive.
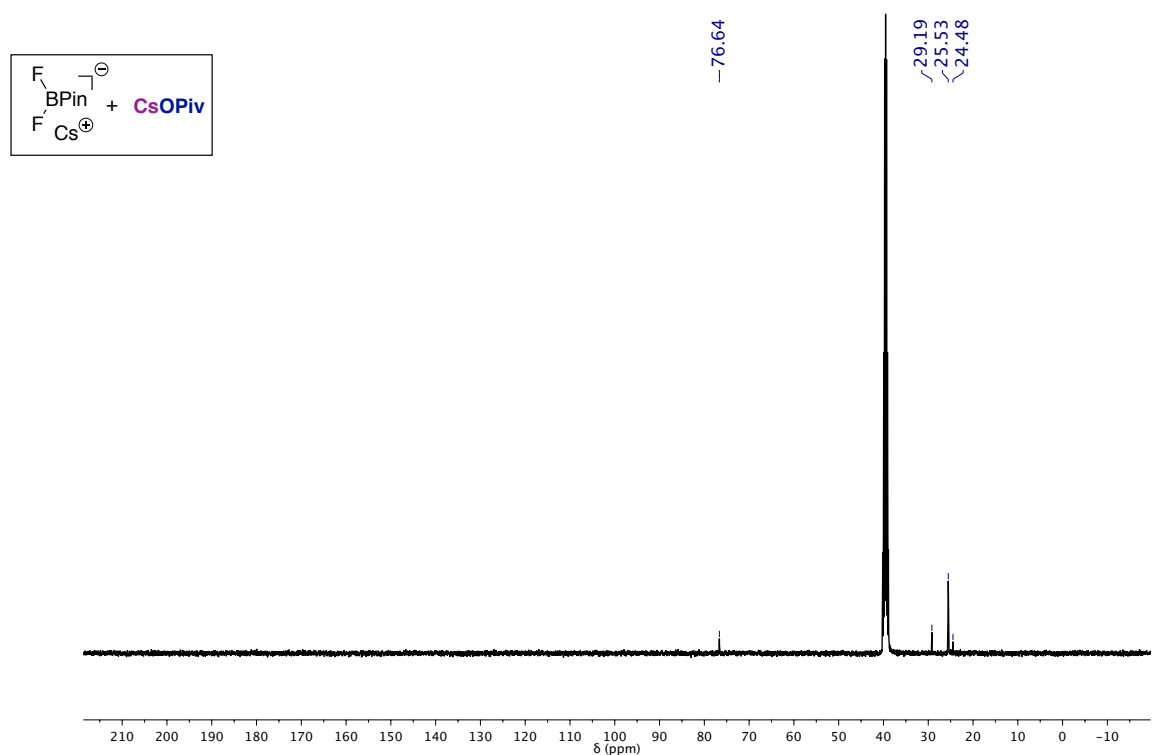
Figure S2.64. ¹³C{¹H} NMR (101 MHz, DMSO-d₆) of by-products obtained from the use of 2 equiv CsF as the additive.

2.11.16.1. 1 equivalent of CsF/0.3 equivalents CuF$_2$
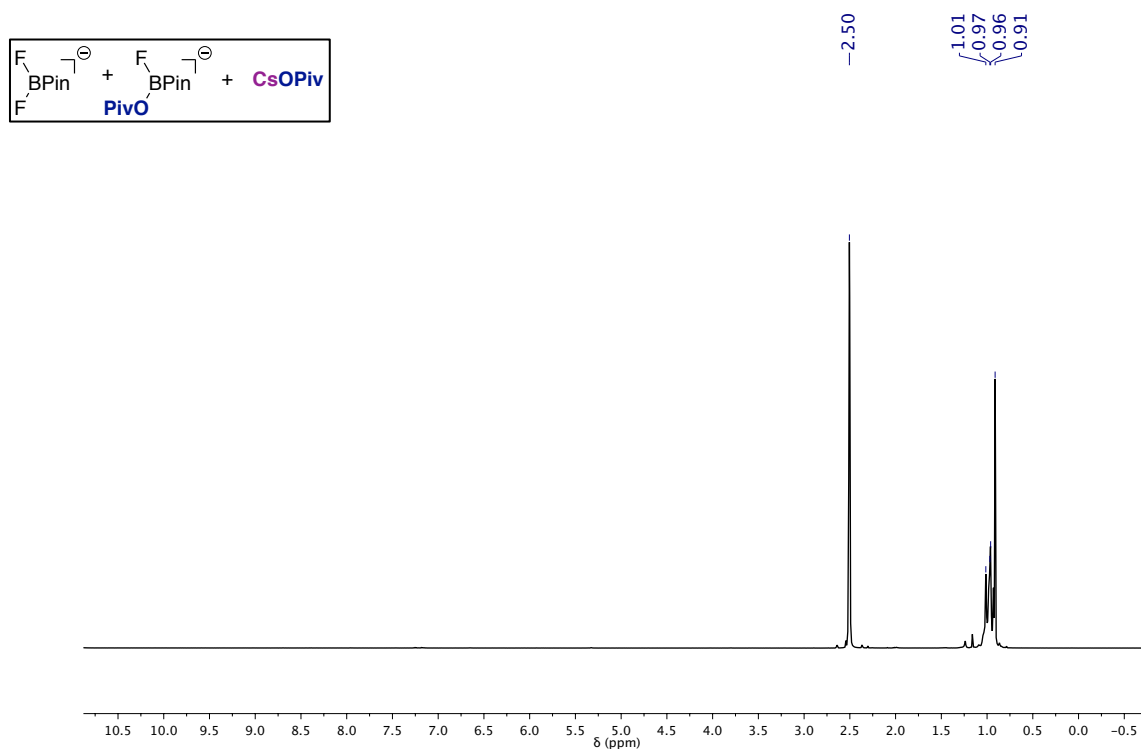
Figure S2.65. ^{1}H NMR (400 MHz, DMSO-d$_6$) of by-products obtained with 1 equiv CsF/0.3 equiv CuF$_2$.
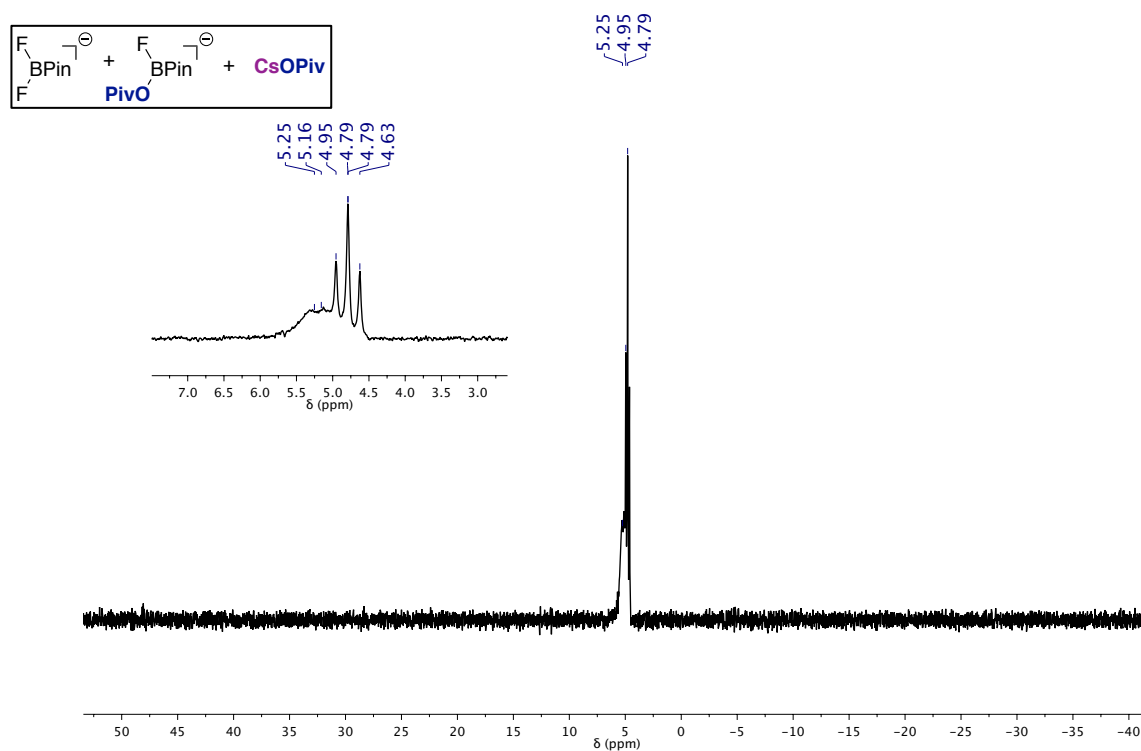
Figure S2.66. ^{11}B NMR (128 MHz, DMSO-d$_6$) of by-products obtained with 1 equiv CsF/0.3 equiv CuF$_2$.
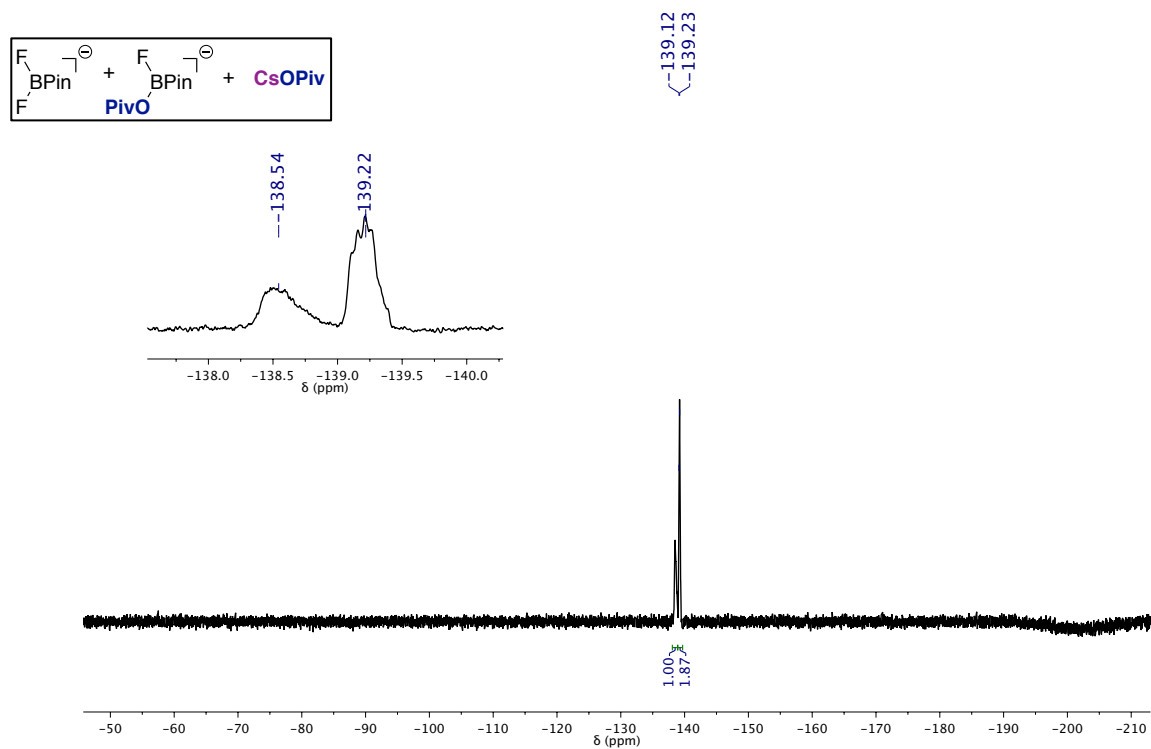
Figure S2.67. ¹⁹F NMR (376 MHz, DMSO-d₆) of by-products obtained from the use of 1 equiv CsF/0.3 equiv CuF₂.
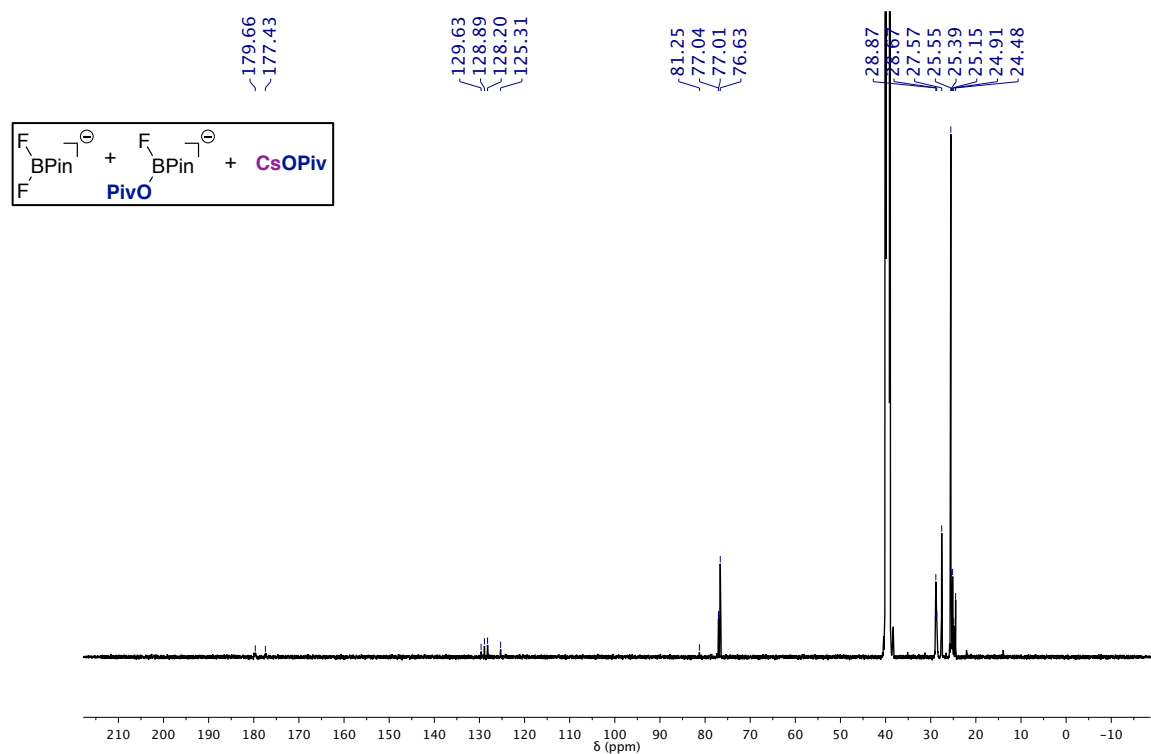
Figure S2.68. ¹³C{¹H} NMR (101 MHz, DMSO-d₆) of by-products obtained from the use of 1 equiv CsF/0.3 equiv CuF₂.

2.11.17.   DFT

DFT calculations were carried out by Enrique Gómez-Bengoa at UPV-EHU.

Computational Methods:

All structures were initially optimised using density functional theory (DFT) by using the B3LYP functional[120,121] as implemented in Gaussian 09. Optimisations were carried out in a solvent model (IEFPCM, solvent = toluene)[111–113] by using the 6-31G** basis set for non-metallic atoms and Stuttgart/Dresden (SDD)[122,123] effective core potential for nickel. The critical stationary points were characterised by frequency calculations in order to verify that they have the right number of imaginary frequencies, and the intrinsic reaction coordinates (IRC)[124] were followed to verify the energy profiles connecting the key transition structures to the correct associated local minima.

Energies were refined by single-point calculations with the M06[110] functional and def2tzvpp basis set on the previously optimised structures. The values correspond to Gibbs free energies and are given in kcal mol^{-1}. These energies are relative to the [Ni(0)(PCy$_3$)(naphthyl pivalate)] complex **I**, marked as G = 0.0 kcal mol^{-1} in the Figures.

Gaussian 09, Revision D.01;
M. J. Frisch, G. W. Trucks, H. B. Schlegel, G. E. Scuseria, M. A. Robb, J. R. Cheeseman, G. Scalmani, V. Barone, B. Mennucci, G. A. Petersson, H. Nakatsuji, M. Caricato, X. Li, H. P. Hratchian, A. F. Izmaylov, J. Bloino, G. Zheng, J. L. Sonnenberg, M. Hada, M. Ehara, K. Toyota, R. Fukuda, J. Hasegawa, M. Ishida, T. Nakajima, Y. Honda, O. Kitao, H. Nakai, T. Vreven, J. A. Montgomery, Jr., J. E. Peralta, F. Ogliaro, M. Bearpark, J. J. Heyd, E. Brothers, K. N. Kudin, V. N. Staroverov, T. Keith, R. Kobayashi, J. Normand, K. Raghavachari, A. Rendell, J. C. Burant, S. S. Iyengar, J. Tomasi, M. Cossi, N. Rega, J. M. Millam, M. Klene, J. E. Knox, J. B. Cross, V. Bakken, C. Adamo, J. Jaramillo, R. Gomperts, R. E. Stratmann, O. Yazyev, A. J. Austin, R. Cammi, C. Pomelli, J. W. Ochterski, R. L. Martin, K. Morokuma, V. G. Zakrzewski, G. A. Voth, P. Salvador, J. J. Dannenberg, S. Dapprich, A. D. Daniels, O. Farkas, J. B. Foresman, J. V. Ortiz, J. Cioslowski, and D. J. Fox, Gaussian, Inc., Wallingford CT, **2013**.

2.11.18.   Crystallographic data

CCDC deposition numbers

8: 1839593; [{Ni(PCy₃)}₂(μ-η²-1-naphthyl)(μ-OPiv)] (**7a**): 1839592.

[Ni(σ-1-naphthyl)(OPiv)(dcype)] (**11**): 1839591.

Table S2.1. Crystallographic data.

	8	**7a**	**11**
Formula	$C_{56}H_{102}Ni_2O_8P_2$	$C_{51}H_{82}Ni_2O_2P_2$	$C_{41}H_{64}NiO_2P_2$
Formula weight	1082.73	906.52	709.57
T (K)	100(2)	100(2)	100(2)
Wavelength (Å)	0.71073	0.71073	0.71073
Crystal system	Triclinic	Orthorhombic	Monoclinic
Space group	P-1	Pbcn	P2(1)/c
a (Å)	10.9948(5)	32.625(2)	10.289(2)
b (Å)	11.8656(5)	9.9735(7)	37.957(6)
c (Å)	12.9686(6)	28.5895(14)	9.791(2)
α (deg)	67.3623(9)	90	90
β (deg)	76.2290(10)	90	99.355(9)
γ (deg)	70.3121(11)	90	90
V (Å³)	1458.77(11)	9302.7(10)	3772.9(13)
Z	1	8	4
Density (calcd.) (Mg/cm⁻³)	1.232	1.295	1.249
μ (mm⁻¹)	0.749	0.917	0.633
F(000)	588	3920	1536
Crystal size (mm³)	0.40 x 0.30 x 0.20	0.050 x 0.03 x 0.01	0.20 x 0.10 x 0.05
Theta range for data collection (deg)	1.715 to 33.814	1.894 to 26.024	2.077 to 31.687
Index ranges	-12<=h<=16, -17<=k<=18, -20<=l<=20	-23<=h<=40, -12<=k<=9, -34<=l<=24	-15<=h<=7 -40<=k<=55 -12<=l<=14
Reflections collected	19035	26815	31091
Independent reflections	10496 [R(int) = 0.0199]	8958 [R(int) = 0.1555]	12316 [R(int) = 0.0393]
Completeness to theta	89.3% (33.814º)	97.7% (26.024º)	96.4% (31.687º)
Absorption correction	Empirical	Empirical	Multi-scan
Max. and min. transmission	0.865 and 0.754	0.991 and 0.766	0.969 and 0.745
Refinement method	Full-matrix least-squares on F^2	Full-matrix least-squares on F^2	Full-matrix least-squares on F^2
Data/restraints/parameters	10496/189/362	8958/387/547	12316/0/418
Goodness-of-fit on F^2	1.025	0.936	0.983
Final R indices [I>2sigma(I)]	R1 = 0.0283, wR2 = 0.0702	R1 = 0.0682, wR2 = 0.0982	R1 = 0.0431, wR2 = 0.0850
R indices (all data)	R1 = 0.0337, wR2 = 0.0728	R1 = 0.2040, wR2 = 0.1356	R1 = 0.0670, wR2 = 0.0948
Largest diff. peak and hole	0.657 and -0.331 e.Å⁻³	0.501 and -0.558 e.Å⁻³	0.487 and -0.384 e.Å⁻³

Table S2.2. Crystallographic data of 5.

	5
Formula	$C_{28}H_{44.5}F_{1.5}Ni_{0.5}O_2P$
Formula weight	501.96
T (K)	100(2)
Wavelength (Å)	0.71073
Crystal system	Monoclinic
Space group	P2(1)/m
a (Å)	9.4756(3)
b (Å)	24.7653(8)
c (Å)	11.3522(3)
α (deg)	90
β (deg)	91.2806(11)
γ (deg)	90
V ($Å^3$)	2663.31(14)
Z	4
Density (calcd.) (Mg/cm^{-3})	1.252
μ (mm^{-1})	0.479
F(000)	1084
Crystal size (mm^3)	0.15 x 0.15 x 0.10
Theta range for data collection (deg)	1.794 to 31.402
Index ranges	-13<=h<=13, -34<=k<=36, -13<=l<=16
Reflections collected	37784
Independent reflections	8789 [R(int) = 0.04711]
Completeness to theta	98.0% (31.402°)
Absorption correction	Empirical
Max. and min. transmission	0.954 and 0.899
Refinement method	Full-matrix least-squares on F^2
Data/restraints/parameters	8789/1387/544
Goodness-of-fit on F^2	1.025
Final R indices [I>2sigma(I)]	R1 = 0.0496, wR2 = 0.1127
R indices (all data)	R1 = 0.0700, wR2 = 0.01203
Largest diff. peak and hole	0.669 and -0.638 e.Å^{-3}

Chapter 3.

Understanding Ni(I)–alkyl complexes in reductive carboxylation

3.1.   Introduction

The conversion of CO_2 into valuable products is an important and interesting challenge for synthetic chemists. Carbon dioxide is an abundant and renewable chemical making it an attractive alternative to other single carbon atom sources such as carbon monoxide, phosgene, and cyanide.[1–5] Its kinetic and thermodynamic inertness notwithstanding, carboxylation methods to form a new C–C bond to CO_2 have existed in some form or another since the late 1800s. These methodologies began with a focus on CO_2 reduction ($E^o = -2.2$ V vs SCE),[6–9] attack on the electrophilic carbon atom of CO_2 by strong nucleophiles, and on methodologies employing high CO_2 pressures. The investigation of new catalytic carboxylation methods that began in the 1950s aimed to develop alternative transformations that occur under much milder conditions and that are more general than these reactions.[10–16]

3.1.1. Ni-catalysed reductive carboxylation

From the first catalytic carboxylation reactions developed in 1950s to state of the art "chain-walking" carboxylation reactions, a large amount of development has occurred in the field of Ni-catalysed reductive carboxylation.[3,10,11,17] Reactions have been developed that can occur under much milder conditions than the stoichiometric carboxylations mentioned above, that tolerate a broad range of substrates, and that avoid reactive and sensitive organometallic reagents.[10–16] Early successes were achieved in the field of electrochemical synthesis.[8] For example, Fauvarque and colleagues found that the addition of a catalytic amount of a Ni(II) salt and a phosphine ligand (usually PPh$_3$) to the electrochemical carboxylation of aryl halides could improve the substrate scope of the reaction.[18] In the absence of a catalyst, aryl bromides and aryl iodides could only be carboxylated in low yields and aryl chloride substrates were unreactive. Upon addition of a Ni salt, good yields of aryl carboxylic acids were obtained for all substrates. The addition of Ni rather than another metal was based on the success of Ni catalysts in electrocatalytic reductive dimerisation and biaryl-forming reactions.[18–21]

More recently, methodologies have been developed where the two electrons are supplied by Mn or Zn powder rather than an electrode.[22] Photoredox reactions have also been developed where a Hantzsch ester is used as the terminal reductant. This avoids the formation of stoichiometric metal-containing waste that is generated if Zn or Mn is used as the reductant.[23,24] Overall, the scope of these mild and tolerant Ni-catalysed reductive carboxylation reactions now spans a very broad range of substrates including challenging unactivated alkyl chlorides and 1,3-dienes (Figure 3.1).[25,26] Modern reductive carboxylation reactions have even been showcased in applications such as remote functionalisation through "chain walking" of the catalyst or through iterative coupling reactions.[27–29] Chapters 3 and 4 of this Thesis will focus on the carboxylation of the substrates highlighted in Figure 3.1: aryl halides, aryl (pseudo)halides (–OTf, –SMe$_2^+$), and alkyl halides. Specific details about the carboxylation of unsaturated systems or vinylic/benzylic/allylic positions will not be discussed here.
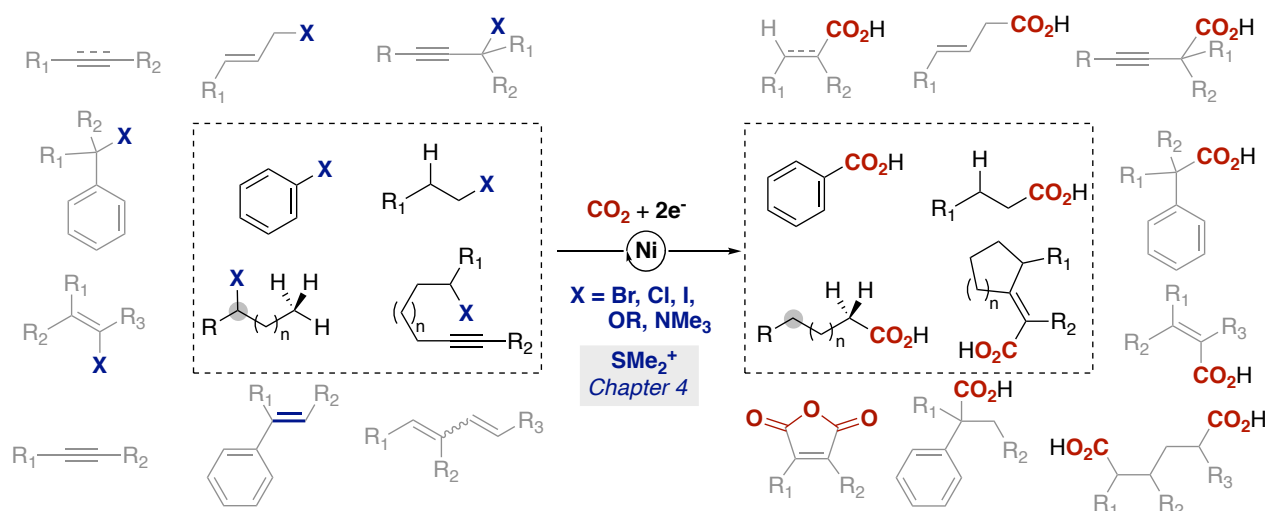
Figure 3.1. Substrate scope of reductive carboxylation reactions. Adapted from ref 59.

3.1.2. Carboxylation of aryl and alkyl halides

In 2008, the Martin group reported the first catalytic reductive carboxylation of aryl halide substrates using a non-electrochemical approach.[30] Although small amounts of the desired carboxylic acids could be obtained with a Ni catalyst, Pd catalysts in combination with an electron-rich phosphine ligand were found to be superior. A drawback of this methodology was the reductant – Et$_2$Zn – as it is air-sensitive and must be handled carefully. This reductant had been employed in the catalytic hydrocarboxylation of numerous unsaturated systems such as styrenes,[31] alkynes,[32] α,β-unsaturated nitriles,[33] allenes,[34] and diynes,[35] and in the Cu-catalysed carboxylation of aryl iodides[36] and the Pd-catalysed carboxylation of allylic alcohols.[37]

Further development of the non-electrochemical reductive carboxylation reaction came when Tsuji and co-workers developed a Ni-catalysed carboxylation of electron-rich C(sp^2)–Cl bonds where air-sensitive Et$_2$Zn was replaced with Mn powder.[38] Attempts to understand mechanistic details of the reaction were carried out (vide infra).
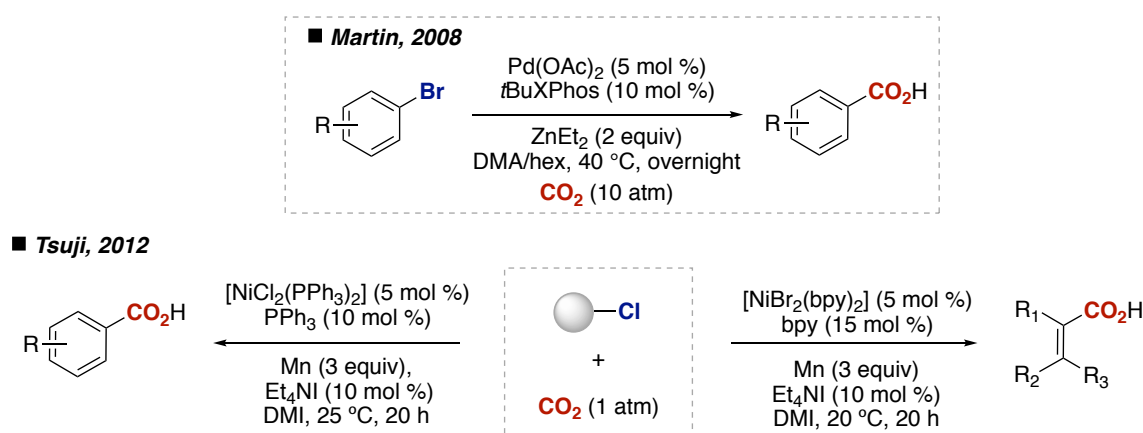
Scheme 3.1. First reports of non-electrochemical reductive C(sp^2)–X carboxylation reactions.

Compared to aryl halides, the use of alkyl halide substrates in carboxylation reactions is a much more challenging goal due to (1) the ability of the substrate to undergo radical oxidative addition pathways that might lead to unwanted side products or decomposition; (2) the difficulty in activating C(sp^3)–X bonds compared to those attached to π systems; and (3) the potential for β-hydride elimination of the Ni–alkyl intermediates. This being said, these challenges have been overcome and the successful carboxylation of many such substrates has been realised.[10]

The first report of the reductive carboxylation of alkyl halides involved the Ni-catalysed carboxylation of unactivated alkyl bromides and alkyl sulfonates using Mn powder as the reductant (Scheme 3.2-left).[39] The choice of ligand had a large influence on the yield of the reaction. When phenanthroline was employed, no carboxylic acid was obtained. However, addition of ethyl substituents in the 2- and 9-positions increased the yield to 76%. The beneficial effect of these substituents was exploited in the optimisation of further reductive carboxylation reactions such as the carboxylation of cyclopropyl bromides (Scheme 3.2-right), and the carboxylation of very challenging unactivated primary, secondary, and tertiary alkyl chlorides.[25]
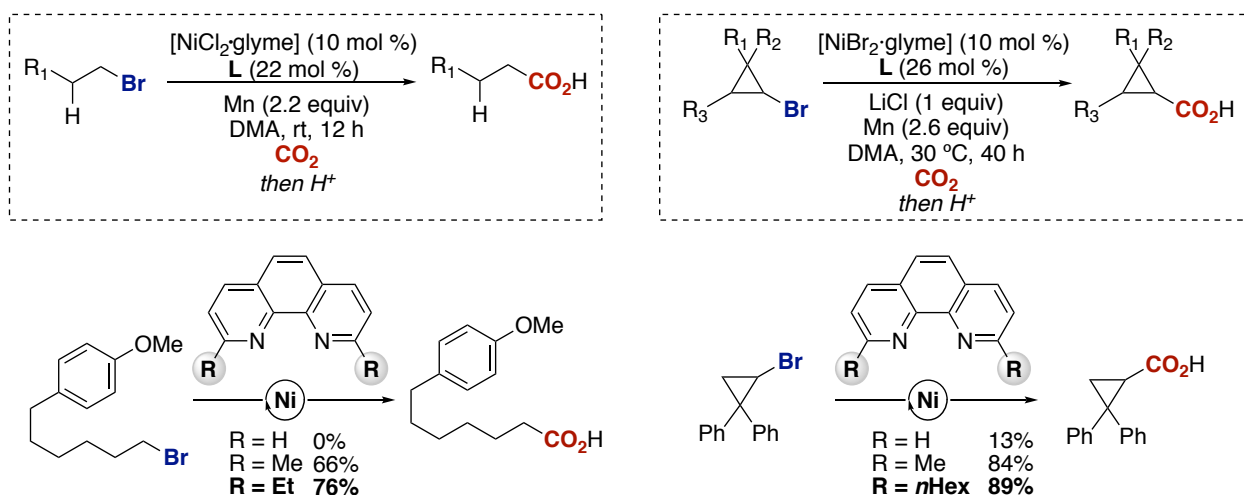
Scheme 3.2. Selected reductive carboxylation reactions of alkyl halides highlighting the ligand effect.

The ability of Ni and Pd to form strong interactions with π bonds and to form weak agostic interactions has allowed "chain-walking" methodologies to be developed.[28,29] In these reactions, the initial insertion of the catalyst at a reactive site is followed by a sequence of olefin isomerisation steps, such as – but not limited to – β-hydride elimination and reinsertion, resulting in a final functionalisation at a distant site.[40] This has recently been applied to the remote C(sp^3)–H carboxylation of alkyl bromides (Scheme 3.3).[27] The potential of this transformation was highlighted in the application of the methodology to a mixture of bromoalkane regioisomers to transform it a single terminal aliphatic carboxylic acid (Scheme 3.3-bottom).
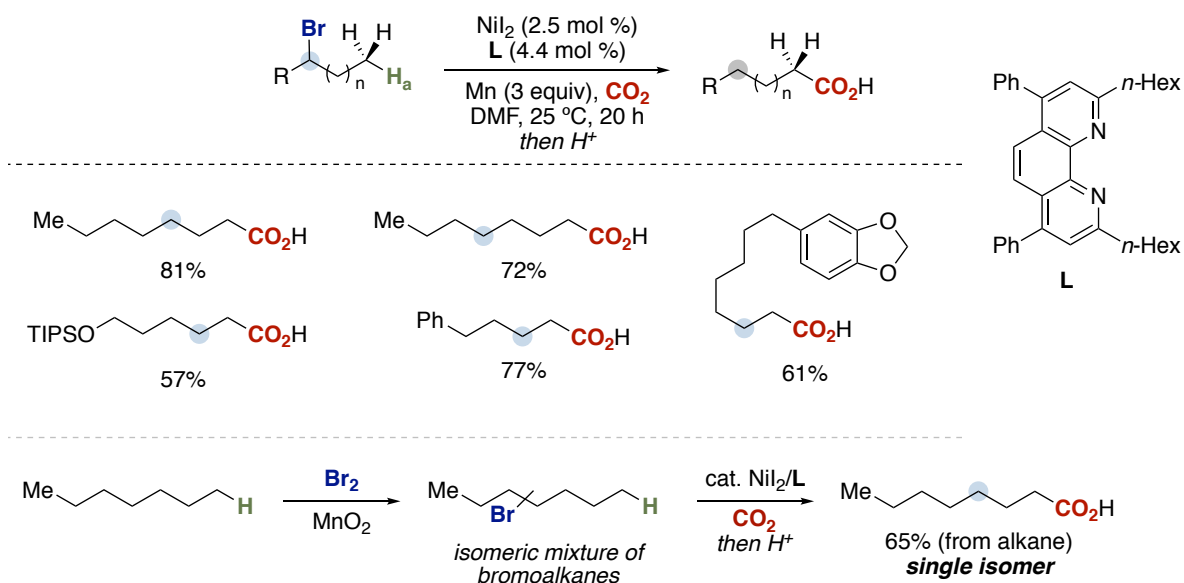
Scheme 3.3. Chain-walking carboxylation of alkyl bromides and application to regioconvergent carboxylation.

3.1.3. Mechanistic understanding

The first mechanistic proposal for a Ni-catalysed reductive carboxylation reaction is shown in Scheme 3.4 and involved generation of a Ni(0) complex *electrochemically*, insertion of this complex into the C–X bond of an aryl halide, and reduction of the resulting Ni(II) complex in the presence of CO_2 to give a complex from which the aryl carboxylate could be obtained.[18] Within this short and straightforward description are almost all the mechanistic questions that linger in the field of Ni-catalysed carboxylation reactions.[41,42] First, it is unclear whether it is possible to predict the mode of Ni insertion into the C–X bond based on the substrate and ligands. Second, a certain ambiguity exists about the identity of the complex that is generated when the Ni(II) complex is reduced in the presence of CO_2. Finally, how catalyst turnover is obtained may depend on the reductant and additives present in the reduction mixture.[43] Further mechanistic details that have arisen as carboxylation has moved from electrochemistry to reductions with metal powders include the role of the reductant as a Lewis acid, roles of the additives that are sometimes required for high yields, and the influence of the ligand on the reaction. In the following sections, the main questions about carboxylation mechanisms will be discussed in the context of the current literature.
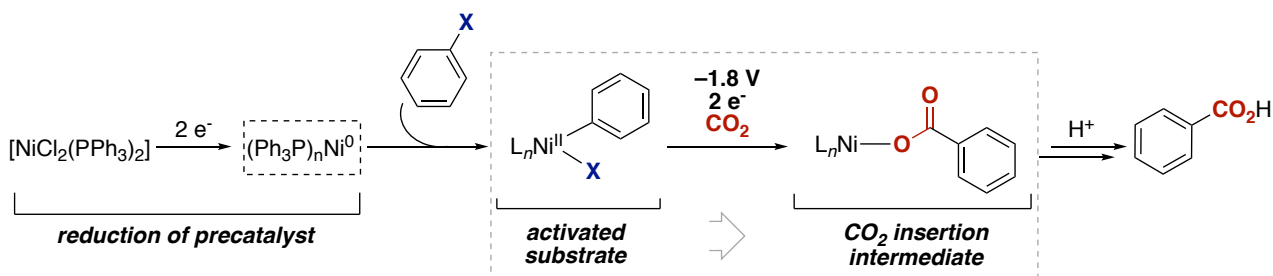
Scheme 3.4. Initial mechanistic sketch for Ni-catalysed reductive carboxylation.

3.1.3.1. Key electrochemical studies

Ni-catalysed electrochemical carboxylation reactions were the first to be developed so it is perhaps unsurprising that the basis for our current mechanistic understanding of reductive carboxylation can be traced back to an electrocarboxylation study. It is also important to note that electrochemical methods sample the rapid processes occurring at the electrode surface from within the diffusion layer. Carboxylation reactions involving heterogeneous Zn and Mn powders can be more difficult to analyse because sampling the bulk solution ignores surface processes.[44]

Amatore, Jutand, and co-workers have carried out important work in the area of electrochemical carboxylation.[44–48] In their seminal mechanistic study, the carboxylation of bromobenzene using a Ni/dppe (dppe = 1,2-bis(diphenylphosphino)ethane) catalyst was investigated (Scheme 3.5). Their interest in the mechanism of this transformation was piqued by the lack of biphenyl formation under these conditions: if CO_2 was absent, nickel-catalysed synthesis of biphenyl from bromobenzene would be expected. The authors were therefore driven to understand how CO_2 could divert the radical chain mechanism of the homodimerisation process.[49–52]

Scheme 3.5 shows the catalytic cycle that was proposed based on electrochemical and kinetic studies. First, cyclic voltammetry showed that, as for homodimerisation, reduction of the Ni(II) precatalyst occurred via two single-electron steps to give [Ni(0)(dppe)].[49] This complex then reacts with bromobenzene to give [Ni(II)(Ph)(Br)(dppe)] (**I**), a key intermediate in both homodimerisation and carboxylation. Cyclic voltammetry showed that this intermediate undergoes further one-electron reduction to [Ni(I)(Ph)(dppe)] (**II**) at −1.8 V vs SCE (THF/HMPA 2:1). The same reaction steps were observed in the presence of CO_2, which ruled out the formation of an Aresta-type complex **1** between [Ni(0)(dppe)] and CO_2.[53]

When CO_2 was present the limiting current for the reduction of **I** to **II** increased two-fold and, more generally, was affected by the concentration of both bromobenzene and CO_2. Oxidative addition complex **I** is common to both the biaryl and carboxylation mechanisms. However, reaction between CO_2 and **I** was ruled out based on experimental data.[54] Attention was therefore focused on its reduction product, the Ni(I)–phenyl complex **II**. Given that electrocarboxylation occurs at the potential at which **I** is reduced to **II** (−1.8 V vs SCE), and that **II** is intercepted by CO_2 faster than it can react with more PhBr, the Ni(I)–aryl complex was invoked as the key intermediate in the electrocarboxylation of aryl halides.

■ *Electrocatalytic carboxylation*
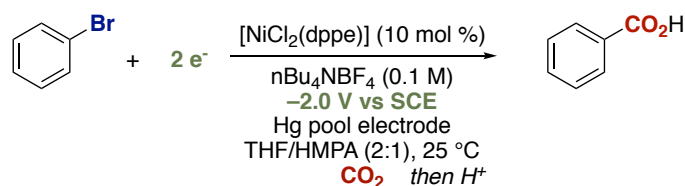
■ *Proposed mechanism*
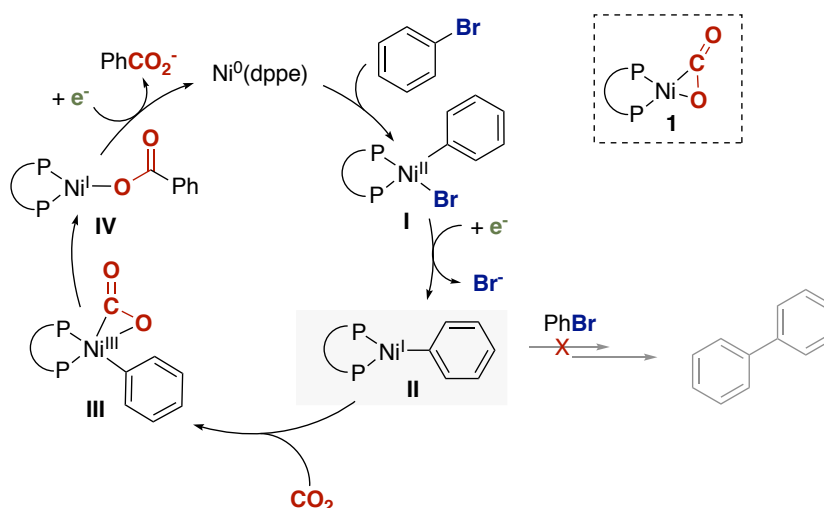
Scheme 3.5. Proposed mechanism for the electrocarboxylation of PhBr.

This study is also noteworthy due to its experimental investigation into CO_2 insertion. Although this is the key step in which the new C–C bond is formed between the substrate and CO_2, very few experimental studies have been carried out on it. Kinetic studies by Amatore et al. and stoichiometric experiments by Diao and Hazari (vide infra) are the only studies of CO_2 insertion specific to reductive carboxylation.[55] The kinetic studies carried out by Amatore suggested that complex **II** underdoes CO_2 insertion in two steps. First, an oxidative cyclisation with CO_2 forms a Ni(III) complex **III**. This is followed by insertion into the Ni–C bond to form the Ni(I)–benzoate complex **IV**. A final one-electron reduction liberates the carboxylate and regenerates Ni(0). The results obtained by Amatore and Jutand form the basis of many carboxylation mechanistic studies that will be discussed below. A particular focus of the following discussion will be on CO_2 insertion at complexes such as **II**.

3.1.3.2. Key DFT studies

Prompted by the seminal work of Amatore and Jutand and by experimental studies that suggested that Ni(I)–aryl complexes were important in Tsuji's Ni/PPh₃-catalysed reductive carboxylation of aryl chlorides (vide infra), Sakaki and colleagues embarked on a computational study of the reaction.[56] Comparison of the energy barriers for the CO_2 insertion pathways from the Ni(II) oxidative addition complex [Ni(II)(Ar)(Cl)(PPh₃)₂] (**V**) (31.7 kcal mol⁻¹) or from the reduced complex [Ni(I)(Ar)(PPh₃)₂] (**VI**) (1.4 kcal mol⁻¹) supported the conclusions of Amatore and Jutand that formation a Ni(I) complex is required prior to CO_2 insertion.[47] As for Amatore and Jutand's work, the proposed catalytic cycle began

with a concerted oxidative addition reaction to form a Ni(II) intermediate **V** that is reduced to Ni(I)–aryl complex **VI** prior to CO_2 insertion. Coordination of CO_2 via one π bond (rather than oxidative cyclisation) and transfer of 0.151 electrons from Ni to form **VII** (no formal oxidation states were invoked) is followed by insertion and isomerisation of the κ^1 complex **VIII** to the 3.0 kcal mol^{-1} more stable κ^2 carboxylate complex **IX**. Reduction by Mn recovers Ni(0) from carboxylate complexes **VIII** and **IX** to form the Mn carboxylate that would be quenched during the acidic workup.
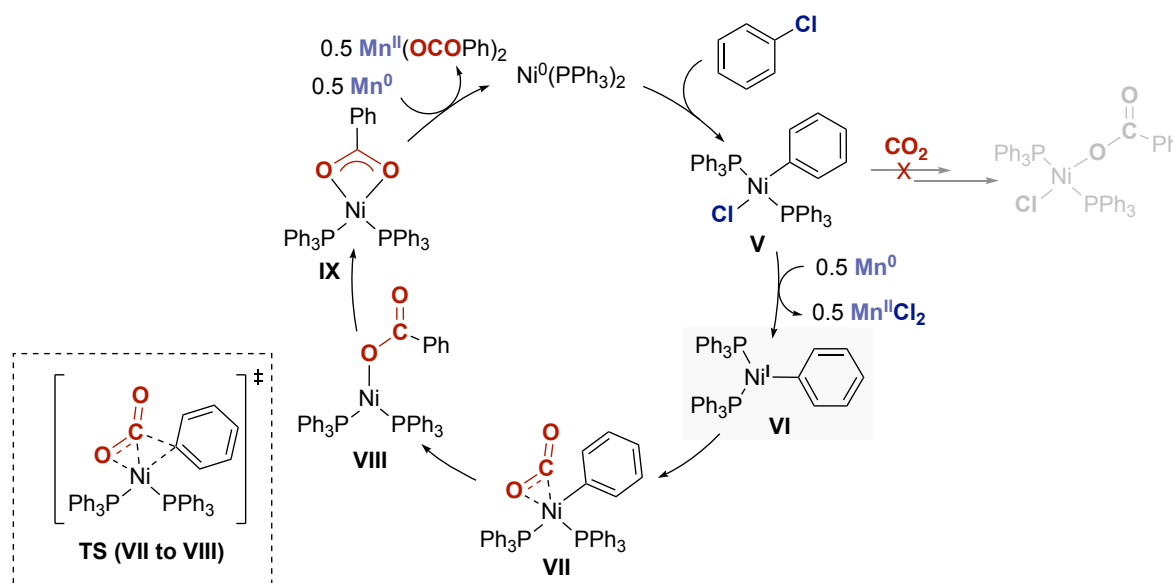
Scheme 3.6. Calculated mechanism for the carboxylation of aryl halides.[56]

The large energy difference between the Ni(II) and Ni(I) pathways was rationalised based on the amount of charge transfer required for the insertion step. Charge is transferred between the anionic phenyl group and the CO_2 molecule. It is also transferred during the cleavage of the Ni–C bond and the formation of Ni–O bond(s). Both steps are favoured by the Ni(I) pathway. First, the strength of the Ni–O bonds in the Ni(I) product is much higher than in the Ni(II) product. Second, the phenyl group in Ni(I) complex **VI** is more negatively charged than in **V**, and this favours attack by the phenyl group on coordinated CO_2.

Durandetti et al. reported a Ni/bipyridine-catalysed carboxylation of aryl and naphthyl tosylates.[57] The electrochemical data obtained in this study showed that a Ni(0) complex generated from reduction of the [NiBr$_2$(bipy)] precatalyst reacted with the C(sp^2)–OTs bond to form an oxidative addition complex which was then reduced to a Ni(I)–Ar species at –1.20 V vs SCE. A small DFT study was carried out on the transformation and showed a lower energy for the interaction of CO_2 with a bipyridine Ni(I)–Ph complex compared to a bipyridine Ni(II)–Ph complex. This was consistent with the experimental findings of Amatore and the computational study of Sakaki. Although there are DFT studies of C(sp^2)–X carboxylation and benzylic carboxylation mechanisms,[58] no similar studies on alkyl C(sp^3)–X carboxylation reactions have been reported.

3.1.3.3. Experimental studies to probe Ni(I) intermediates

As discussed above, computational studies by Sakaki and Durandetti and an electrochemical mechanistic study by Amatore and Jutand make the case for on-cycle Ni(I)–aryl intermediates during carboxylation. These studies set off speculation about whether intermediates in this "unusual" oxidation state are general to all Ni-catalysed reductive carboxylation reactions and prompted a small set of experimental studies.[59] Importantly, these provided evidence for the importance of Ni(I)–Ar complexes.

The first experimental study was reported in Tsuji's seminal work on the carboxylation of aryl halides (Scheme 3.1).[38] The oxidative addition complex [Ni(Ph)(Cl)(PPh$_3$)$_2$] (intermediate **V** in Sakaki's DFT study) was synthesised and exposed to variations of the optimised carboxylation conditions in order to investigate the conditions that lead to CO_2 insertion (Scheme 3.7). First, **V** was reacted with CO_2 in the absence of reductant (Scheme 3.7-*path a*). Under these conditions only traces of the carboxylated product **2** were obtained (esterification can aid in the determination of yields by GC). However, in all cases where Ni(I) was accessible (*paths b–d*), **2** was obtained in good yields. For example, when the Mn reductant and Et$_4$NI were added a 47% yield of **2** was obtained (*path b*). The addition of Et$_4$NI was necessary for **2** to be formed and was proposed to aid outer-sphere electron transfer between the Mn surface and the Ni(II) complex.[60,61] Indeed, when homogeneous reductant CoCp$_2$ was added to the reaction between **V** and CO_2 (E = −0.86 V vs SCE, DME)[62] a 47% yield of **2** was obtained (*path c*). This supported the requirement for reduction prior to CO_2 insertion. Reaction of **V** with [Ni(0)(PPh$_3$)$_4$] was also successful in providing a moderate yield of **2**, presumably due to comproportionation between Ni(II) complex **V** and Ni(0) forming the key Ni(I)–Ph complex (*path d*).
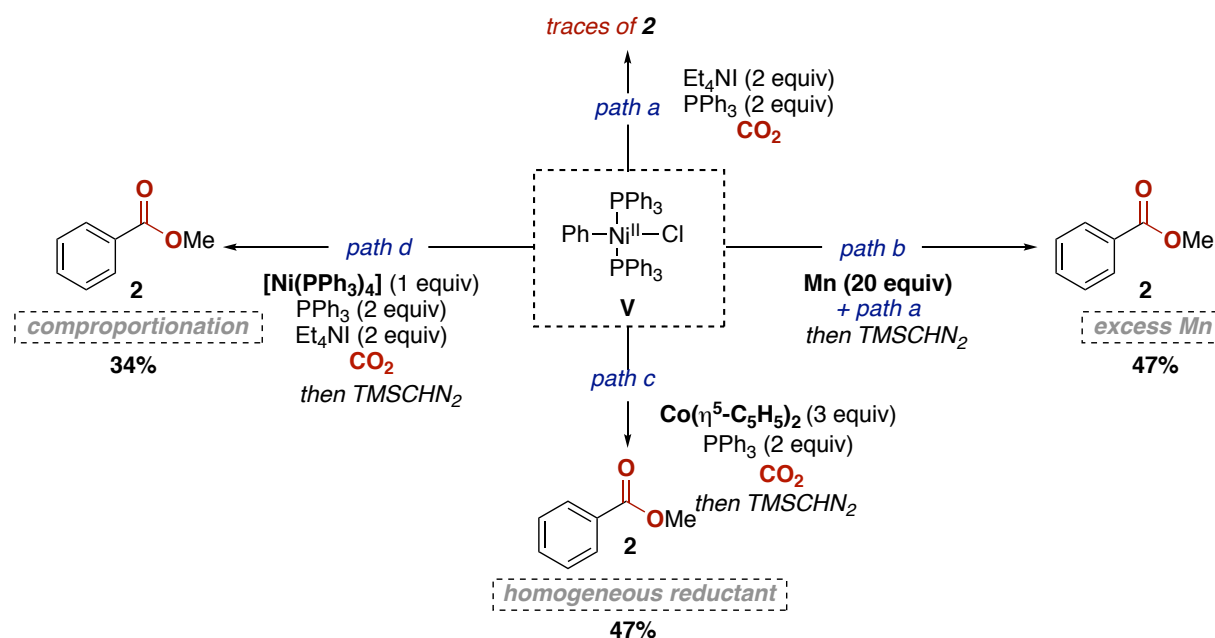
Scheme 3.7. Stoichiometric mechanistic experiments starting from Ni(II) oxidative addition complex V. All reactions carried out in DMI at 25 °C for 20 h.

The mechanisms of aryl halide carboxylation reactions first received attention more than 30 years ago.[18,47] However, when it comes to the carboxylation of alkyl halides, mechanistic knowledge almost completely relies on what has been uncovered for aryl halides. Two stoichiometric experiments have been reported with catalytically relevant ligands. A recent study has reported CO_2 insertion at a (diphosphine)Ni(I)–alkyl complex along with the isolation and characterisation of the resulting carboxylate complex (vide infra).[55]

A common mechanistic experiment in the reductive carboxylation field is the reaction of a $[Ni(L)_2]$ complex (**L** = substituted phenanthroline) with the substrate and CO_2 in the presence and absence of a reductant. The aim of such an experiment is to determine whether oxidative addition of the substrate to the formally Ni(0) complex leads to a Ni(II)–alkyl complex that is able to insert CO_2, or whether the presence of a reductant is necessary because the formation of a Ni(I) intermediate is required. The experiments summarised in Scheme 3.8 for the chain walking carboxylation of alkyl bromides and the carboxylation of cyclopropyl bromides showed that carboxylic acid was not obtained unless Mn powder was present.[27,63]
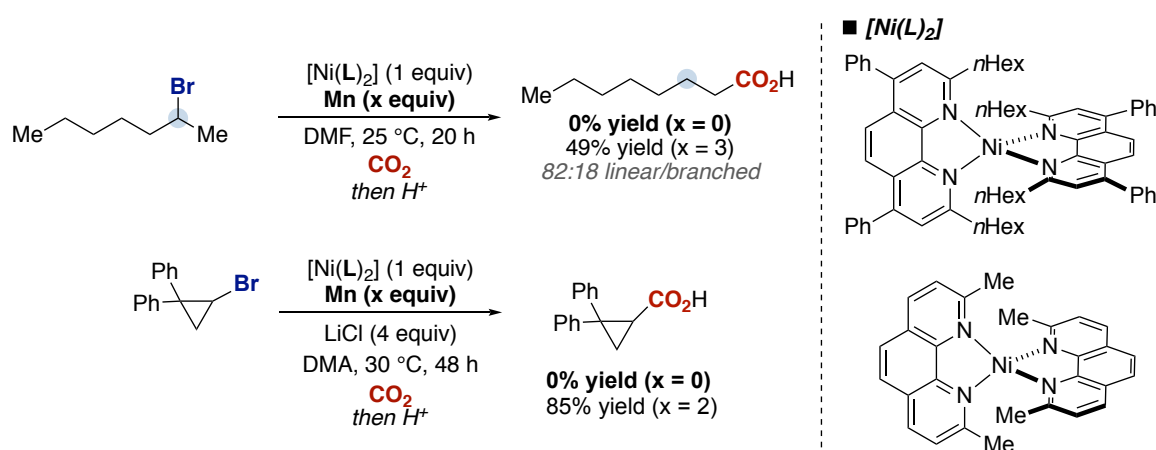
Scheme 3.8. Stoichiometric experiments between formally Ni(0) complexes and alkyl bromides in the presence of CO₂.

When the same experiment was carried out with an alkyl chloride substrate, an unusual product of CO_2 insertion was obtained in the *absence* of Mn powder (Scheme 3.9).[25] Furthermore, carboxylic acid was obtained from the Mn-free carboxylation of a benzyl ammonium salt using 1 equivalent of a similar $[NiL_2]$ complex.[64] These two cases exposed a limitation of this stoichiometric experiment – it could be that substrates to which oxidative addition is slow allow the Ni(II) oxidative addition complex to react with Ni(0) species and generate the key Ni(I) species by comproportionation. This would therefore give a "false positive" to a reductant-free reaction.
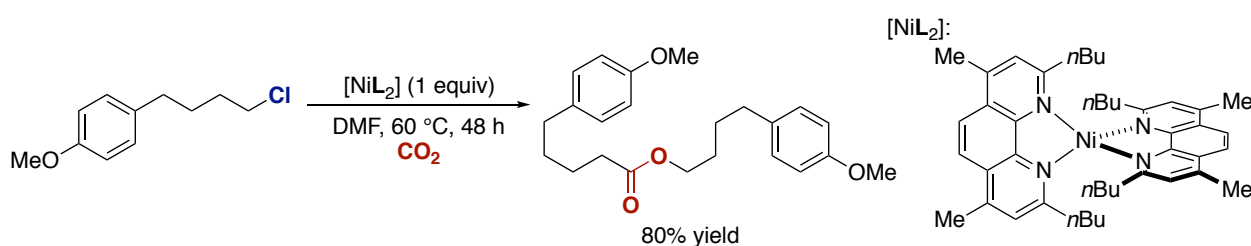
Scheme 3.9. Stoichiometric experiments between Ni(0) complexes and an alkyl chloride in the presence of CO₂.

The formation of carboxylic acid in the absence of Mn prompted the proposal of a catalytic cycle that included a comproportionation step as a possible source of Ni(I) intermediates (Scheme 3.10).
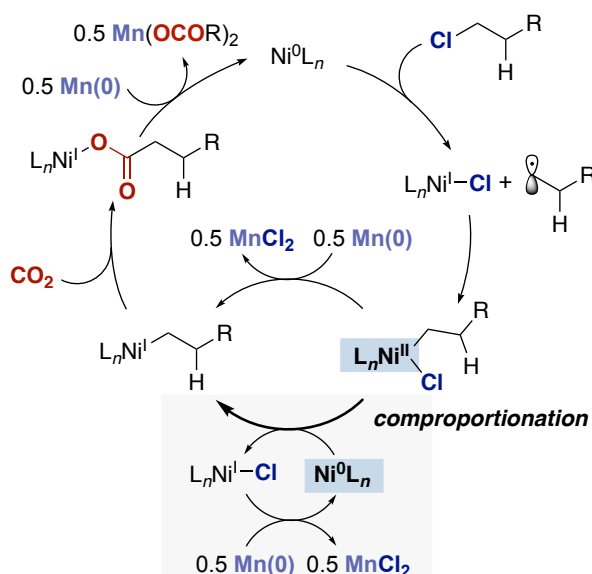
Scheme 3.10. Proposed catalytic cycle for carboxylation of alkyl chlorides including a comproportionation pathway (highlighted in grey).[25]

3.1.3.4.   Insertion of CO₂ into Ni–C bonds

The previous sections of this Chapter detail the computational and experimental evidence for Ni(I) intermediates in the C–C bond forming step of the carboxylation of aryl and alkyl halides. The mechanisms of this step have been investigated computationally for a number of metal-catalysed carboxylation reactions and have been found to vary depending on the specific reaction, the metal, and the nature of the group to which the new C–C bond is formed.[41,59,65]

Scheme 3.11 shows three plausible modes of interaction between a monometallic alkyl or aryl complex and CO_2. Direct interaction is not necessarily required as C–C bond formation can also occur through an outer-sphere pathway.[66] *Path a* in Scheme 3.11 demonstrates a migratory insertion pathway where CO_2 may or may not coordinate to the metal centre prior to the insertion process. *Path b* shows an insertion reaction where CO_2 does not coordinate and is instead attacked by the nucleophilic organometallic group.
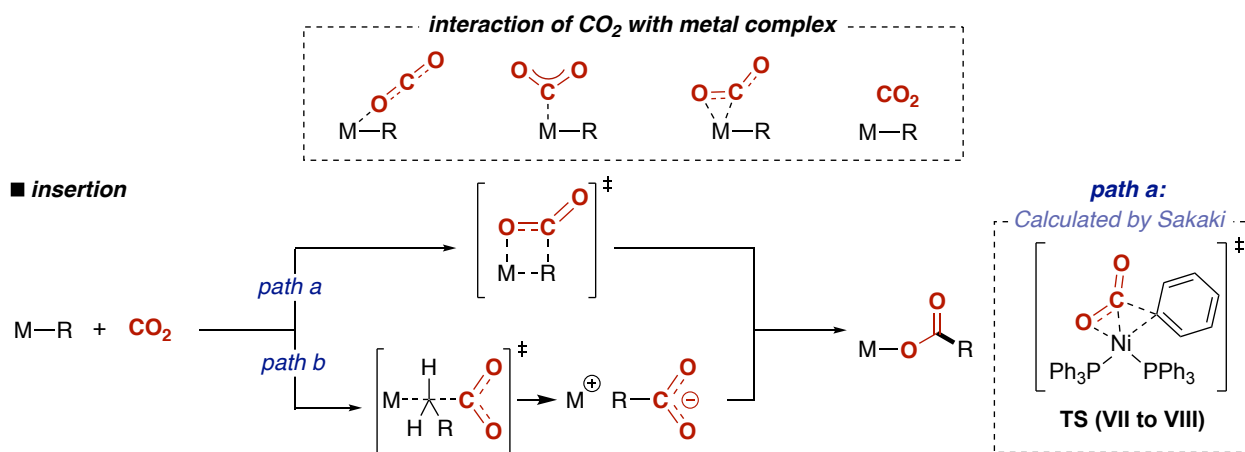
Scheme 3.11. Pathways for CO_2 insertion at a metal–C bond. Top: interaction of CO_2 with a metal centre. Bottom: insertion pathways. Adapted from ref 59.

The computationally determined pathways for CO_2 insertion *at Ni(I)* have only been calculated for Ni–aryl complexes and are proposed to follow *path a*: coordination followed by migratory insertion.[56–58] In general, experimental evidence for this step is very limited. There are only four reports of CO_2 insertion into a Ni–C bond in the literature.[43,55,67,68] Two such studies involve CO_2 insertion at a Ni(II) pincer complex under forcing conditions and are summarised in Scheme 3.12.[67,68] In both cases, the Ni–(η^1-acetate) complexes were also synthesised via anion metathesis with AgOAc to confirm characterisation of the CO_2 insertion product. Infrared spectroscopy was useful in characterising the coordination mode of the carboxylate ligand as η^1 rather than η^2, as the two inequivalent C–O stretches (v_{asym} and v_{sym}) expected for such a binding mode were found to be separated by more than 200 cm^{-1}.[69] A DFT investigation of CO_2 insertion into pincer complex **3** showed that it has a very high barrier (30.2 kcal mol^{-1}) and involves attack of the methyl group on CO_2 without direct involvement of the Ni centre (Scheme 3.11, *path b*).[68]
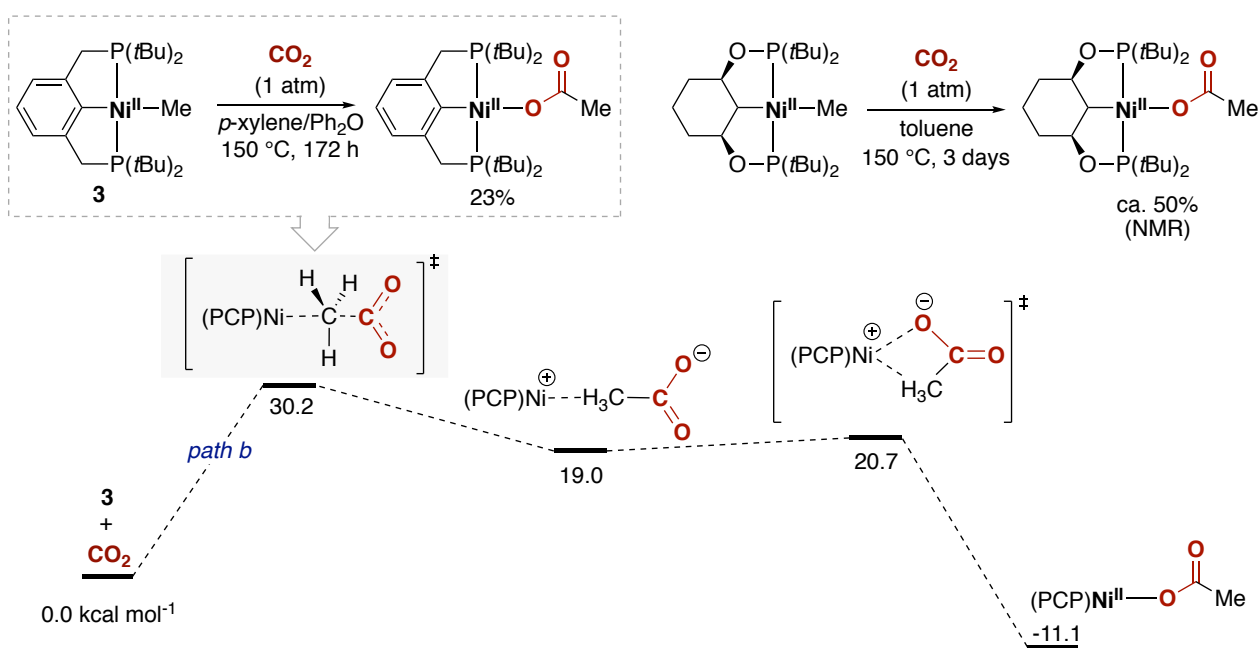
Scheme 3.12. Insertion of CO_2 into Ni(II)–CH$_3$ bonds of isolated complexes.[67,68]

The Hazari group recently reported a detailed experimental study of the Tsuji carboxylation of aryl chlorides discussed in Section 3.1.2.[43] Investigations into the Ni-based elementary steps were carried out alongside a study of the role of the Mn as both a reductant and source of $MnCl_2$. The latter aspects of the study are discussed in detail in Chapter 4. Importantly, investigations into the Ni-based elementary steps involved the synthesis of a Ni(I)–aryl complex [$(PPh_3)_2Ni(I)(2,4,6-iPr_3C_6H_2)$] (**4**) and allowed the key CO_2 insertion step to be probed experimentally for the first time (Scheme 3.13). When **4** was reacted with CO_2 for 5 h, consumption of the Ni complex was observed by ^1H NMR spectroscopy and a 78% yield of the desired acid was obtained after acidic workup. Attempts to isolate the proposed Ni(I)–carboxylate intermediate were not successful. However, reaction of **4** with CO_2 in the presence of a halide source, which would be present during catalysis due to the reductive steps in the reaction, resulted in the formation of the known Ni(I)–Cl complex [$Ni(I)Cl(PPh_3)_3$] in an 83% yield. This finding is important because it suggests that a Ni(I)–carboxylate complex undergoes anion metathesis in the presence of a halide salt. The final step of the carboxylation catalytic cycle – proposed to be reduction of the Ni(I)–carboxylate complex to form Ni(0) and a carboxylate salt – might therefore occur from a Ni(I)–halide species.

■ *Synthesis of Ni(I)-aryl complex*
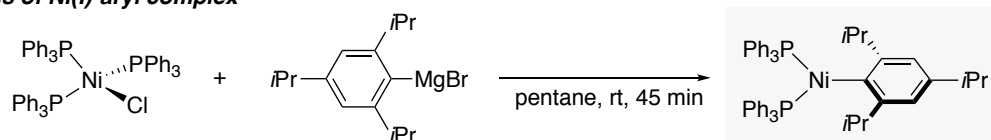
■ *Reactions with CO_2*
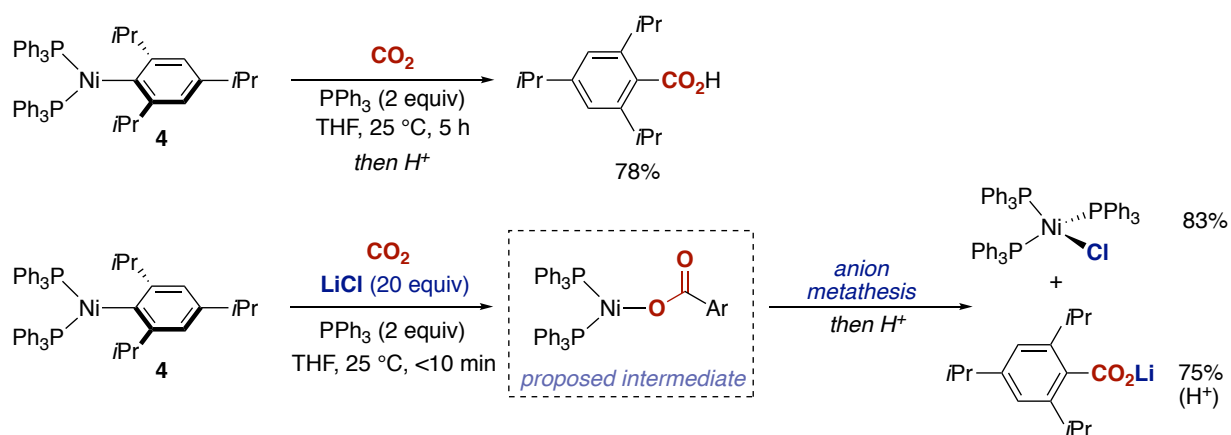
Scheme 3.13. Investigation of CO_2 insertion at an isolated Ni(I)–aryl complex.[43]

Nickel(I) aryl complexes such as **4** are rather rare and usually contain phosphine ligands bearing bulky substituents or a very bulky aryl group (Figure 3.2). The Hillhouse, Diao, and Hazari groups have synthesised aryl complexes by reaction of a Ni(I)–Cl precursor with an organolithium or Grignard reagent.[43,70–73] Johnson et al. isolated the Ni(I)–perfluoroaryl complex shown in Figure 3.2 as a by-product of the C–F cleavage of hexafluorobenzene by Ni(0).[74] Nickel(I)–aryl complexes have also been detected in small amounts during studies of Ni(II) precatalyst activation.[75]

The synthesis of Ni(I)–aryl complexes in the context of reductive carboxylation (vide supra), Suzuki-Miyaura, and cross-electrophile coupling reactions has also been investigated by the Hazari group.[43,72,73] In all cases it was found that bulkier aryl groups dramatically increased the stability of the complexes. The most recent study investigated Ni(I)–aryl complexes bearing phenanthroline-type ligands (highlighted in Figure 3.2).[72] This was important as although these ligands are widely used in reductive coupling reactions, few DFT or experimental studies have been carried out on these systems.
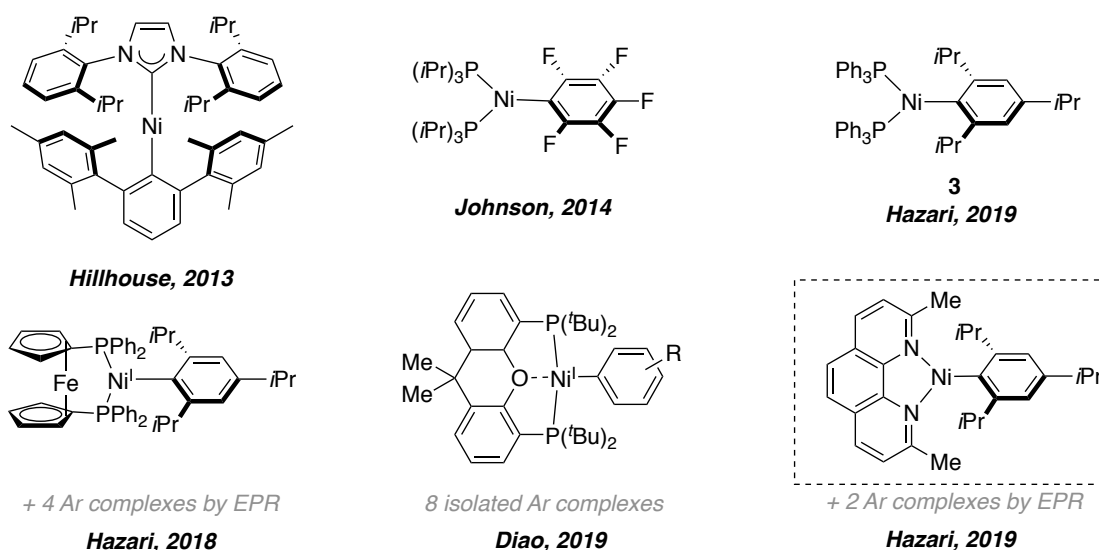
Figure 3.2. Crystallographically characterised Ni(I)–aryl complexes.

In contrast with the experiments using complex **4** described above, the Hazari group did not investigate the reactivity of CO_2 towards Ni(I)–aryl complexes bearing phenanthroline ligands.[76] The only other example of CO_2 insertion to a Ni(I)–C bond was recently reported by the Diao group (Scheme 3.14).[55] During this study, two Ni(I)–alkyl complexes were isolated bearing the bulky diphosphine ligand *t*Bu-Xantphos. The steric bulk of the ligand was important as the use of smaller Ph-Xantphos resulted in decomposition of the alkyl complexes. Reaction of these two complexes with CO_2 (1 atm) at room temperature resulted in the rapid formation of carboxylate complexes that could be isolated and, in the case of the acetate complex, characterised by X-ray crystallography. Although Xantphos has not been employed in any reported carboxylation reactions, this study is important as it is a rare example where an aspect of the mechanism of Ni-catalysed carboxylation of $C(sp^3)$ positions is investigated.
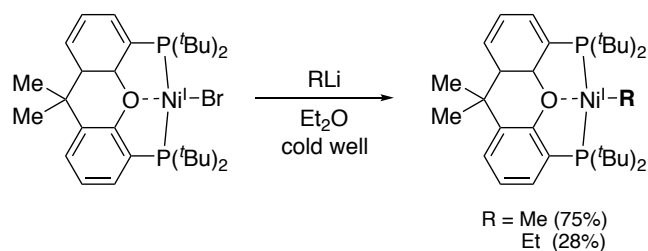
■ Synthesis of Ni(I)–alkyl complexes   **■ CO₂ insertion**
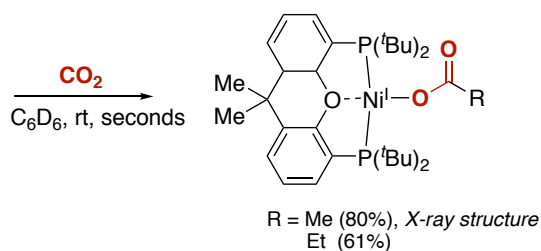
Scheme 3.14. Synthesis and CO₂ insertion reactivity of two Ni(I)–alkyl complexes.

Interestingly, when a previously reported (*t*Bu-Xantphos)Ni(I)–phenyl complex was exposed to CO_2, no carboxylate complex was obtained (Scheme 3.15-left).[71] This contrasted with the successful CO_2 insertion reactions at Ni(I)–alkyl bonds that are summarised in Scheme 3.14. When the *less bulky* (Ph-Xantphos)Ni(I)–phenyl complex was generated in situ from the Ni(I)–Br complex and PhLi, benzoic acid was obtained in 48% yield after workup (Scheme 3.15-right). This suggested that the Ph-Xantphos ligand is small enough to allow the approach of CO_2 that is required for the inner-sphere insertion mechanism proposed for aryl halides.[56] In contrast, the nucleophilic attack mechanism calculated by Hazari for CO_2 insertion at Ni(II)–*alkyl* complexes does not require CO_2 to interact with the metal and would therefore be less affected by the change from Ph-Xantphos to bulky *t*Bu-Xantphos.[68]
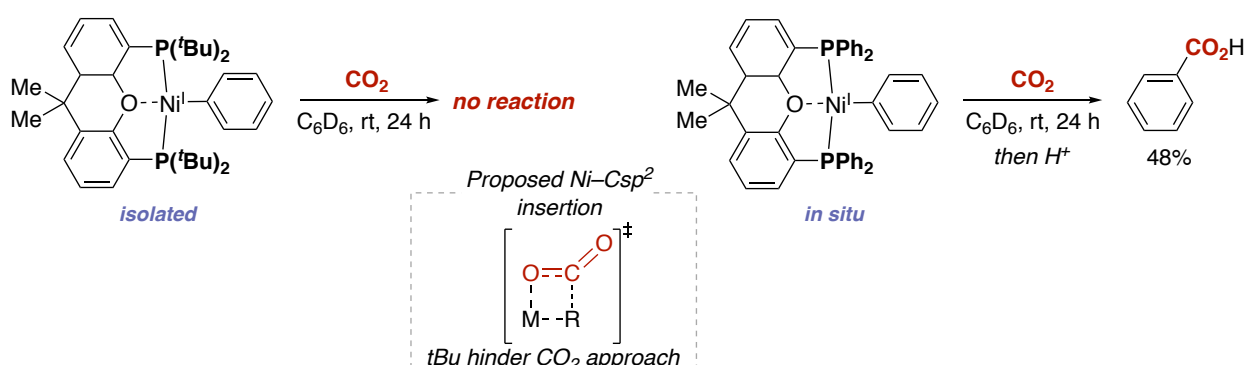
Scheme 3.15. Insertion at Xantphos Ni(I)–phenyl complexes suggesting interplay between proposed migratory insertion mechanism and ligand steric bulk.

As mentioned above, *t*Bu-Xantphos and Ph-Xantphos are not employed in any reported carboxylation reactions. Diao therefore aimed to show that the ligands can be relevant in carboxylation by testing Xantphos complexes as catalysts for the carboxylation of BnZnCl, PhZnCl, and *n*BuZnBr (Scheme 3.16). The bulky *t*Bu-Xantphos complexes did not result in any carboxylation but Ph-Xantphos gave 30–68% yields of the three targeted carboxylic acids. Reductive carboxylation of benzyl bromide was also tested using conditions reported by Martin et al.,[77] and while the use of a *t*Bu-Xantphos complex did not give turnover, a Ph-Xantphos precatalyst gave a modest 32% yield of phenylacetic acid.
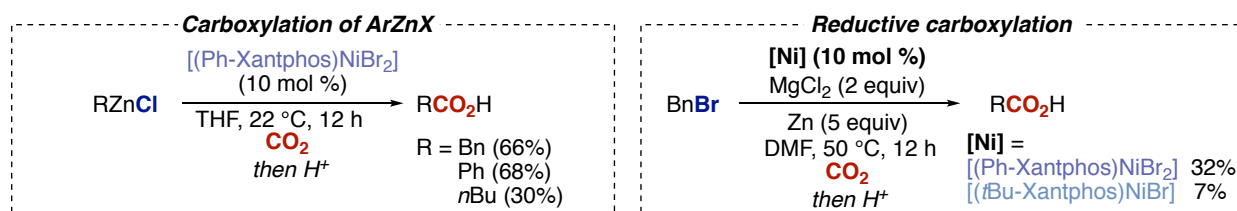
Scheme 3.16. Use of Xantphos complexes in carboxylation reactions by the Diao group.

Given that the carboxylation of arylzinc species was used as a model reaction, it would have been interesting to know whether the methyl and ethyl complexes reported by Diao could also have been formed by reaction of the Xantphos Ni(I)–Br complex with diethylzinc, methylzinc, or an RZnX reagent. It is perhaps important to note that the proposed mechanism for the Ni-catalysed carboxylation of alkylzinc species does not include any Ni(I)–alkyl or –aryl intermediates.[78,79] Instead of the formation of a L_nNi(I)–R complex, a L_nNi–(η^2-CO$_2$) adduct is proposed to form prior to transmetalation of the RZnX (Scheme 3.17). Transmetalation is then proposed to form a *Ni(II)*–acylzinc complex. There is therefore still a large gap in the literature for studies into Ni(I)–alkyl complexes of catalytically relevant ligands in alkyl halide *reductive* carboxylation reactions.
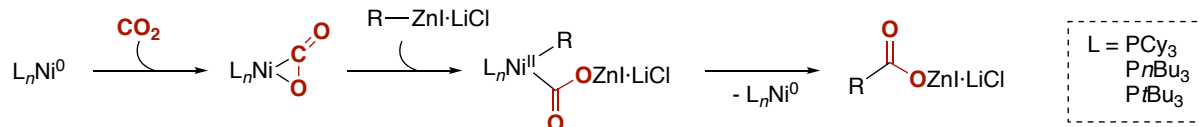
Scheme 3.17. Proposed mechanism for the Ni-catalysed carboxylation of alkylzinc compounds.[78,79]

3.2.   Aims of the project

In recent years, Ni-catalysed cross-coupling reactions have received considerable research attention and new methodologies to form compounds that are inaccessible by two-electron Pd catalysis are routinely reported. Efforts to understand the mechanisms of such reactions must therefore tackle the one-electron reactivity of Ni that is not displayed by Pd. In particular, the role of monovalent nickel halide or organometallic species often receives particular attention.

This project aims to investigate Ni(I)–alkyl complexes in the context of Ni-catalysed reductive carboxylation reactions. Very few studies have addressed the mechanisms of alkyl halide carboxylation reactions, particularly those with ligands that are relevant to a wide range of carboxylation reactions. Furthermore, Ni(I)–alkyl and Ni(I)–carboxylate complexes are extremely rare.

First, the development of synthetic routes to Ni(I)–halide complexes bearing substituted phenanthroline ligands was targeted. Transmetalation with an organolithium or Grignard reagent was then investigated as a means to install the alkyl group. This was expected to be challenging as organonickel(I) complexes are often unstable. Next, insertion of CO$_2$ into the Ni–C bond was to be investigated and the outcome of the reaction probed by a range of spectroscopic techniques. A collaboration with the Hopmann group was also set up in order to use calculations to shed light on CO$_2$ insertion at these Ni(I) complexes.

3.3. Ni(I)–halide complexes

This study began with an investigation into the synthesis of three-coordinate Ni(I)–halide complexes. It was envisioned that these would act as precursors to Ni(I)–alkyl complexes through reaction with an organolithium or a Grignard reagent. If alkyl complexes could indeed be obtained, their reactivity towards CO_2 would then be investigated.
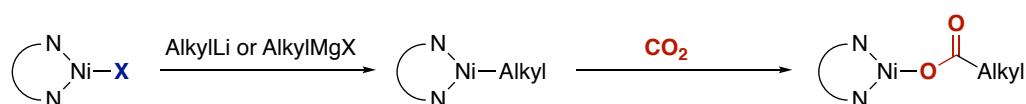
Scheme 3.18. General scheme for the transformation of inner sphere Ni(I)–halide complexes to alkyl and carboxylate complexes.

3.3.1. Ligand synthesis

Two substituted phenanthroline ligands were selected for this project (Scheme 3.19). Such ligands are easy to synthesise, are employed in all Ni-catalysed reductive carboxylations of alkyl halides and, as discussed in Chapter 1, are employed more generally in a range of cross-electrophile coupling reactions. The choice of extremely bulky 2,9-dimesityl-substitued phenanthroline (**L1**) was based on two factors. First, the steric bulk of **L1** might favour the formation of the desired mono-ligated Ni(I)–X complexes rather than the [Ni(**L**)$_2$]X complexes that have been reported for less bulky phenanthroline ligands.[80] Secondly, bulky ligands have been used to stabilise Ni(I)–alkyl complexes. For example, previous work on the synthesis of Ni(I)–alkyl complexes by Hillhouse employed bulky *t*Bu substituents on the diphosphine ligand to shield the Ni–C bond.[81] The second ligand, *n*-hexyl-substituted **L2**, was chosen as it is employed in the optimised conditions for the chain-walking carboxylation of alkyl bromides.[27] Although it was not clear whether the *n*-hexyl chains would provide enough steric bulk to prevent the formation of an [Ni(**L**)$_2$]X complex, it is the bulkiest ligand employed in a reported reductive carboxylation reaction. Long alkyl chains may also lend solubility to **L2** complexes in hydrocarbon solvents such as pentane and hexane. This may aid in the removal of the by-products of the anticipated alkylation reaction, MgX$_2$ or LiX salts.
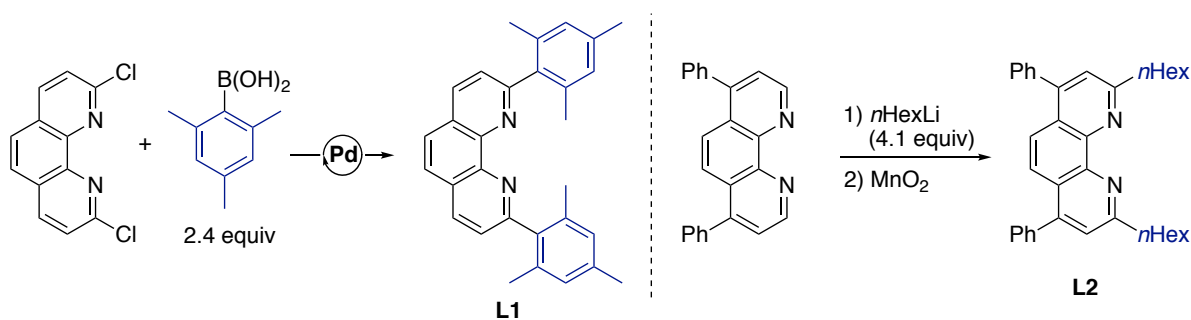
Scheme 3.19. Syntheses of L1 and L2.[82,83]

3.3.2. Synthesis of Ni(I)–halide complexes

Two synthetic routes to the Ni(I)–halide precursors were considered. Oxidation of Ni(0) complexes with a Ag(I) salt has been reported in the synthesis of a number of [Ni(**L**)$_2$]X-type complexes and was employed during work summarised in Chapter 4 for the synthesis of two Ni(I) complexes with *outer sphere* counterions.[25,76,84,64] Comproportionation between a Ni(0) complex and a Ni(II) complex was reported by the Hazari lab for the synthesis of related complex [Ni(**L**)$_2$]Cl (L = 2,9-dimethylphenanthroline).[76] This route circumvents the purification steps required to remove the Ag(0) by-product of oxidation and avoids the overoxidation that is possible with Ag(I).[85] At the time the work described herein was carried out, [Ni(**L**)$_2$]Cl was the only reported Ni(I) halide complex bearing an *N,N'* donor ligand. As mentioned in Chapter 1, Chirik later reported inner-sphere Ni(I)–halide complexes bearing α-diimine ligands that were also synthesised by comproportionation.[86]
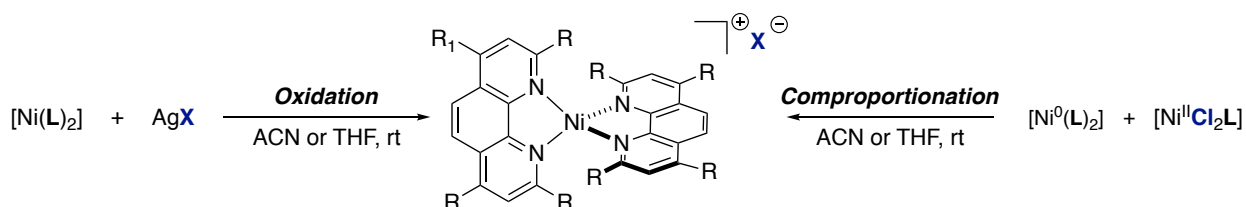
Scheme 3.20. Reported synthetic routes to Ni(I)–halide complexes bearing phenanthroline ligands.

In order to carry out the synthesis of a Ni(I)–halide complex by oxidation or comproportionation, a Ni(0) complex is required. One starting point would be to isolate a formally Ni(0) complex bearing the desired ligand. However, when **L1** was reacted with [Ni(COD)$_2$], equilibrium mixtures of **L1**, [(**L1**)Ni(COD)], and unreacted [Ni(COD)$_2$] were obtained, even after heating or with excess **L1**. In contrast, a Ni(0) complex bearing **L2** – [Ni(**L2**)$_2$] – has been reported, isolated on a 200 mg scale, and employed in stoichiometric studies probing chain-walking carboxylation.[27]

Given the difficulty encountered in obtaining a pure **L1**Ni(0) complex, the synthesis of the Ni(I)-halide complexes in this work was streamlined by employing a simplified comproportionation method where the Ni(0) source was [Ni(COD)$_2$]. The Ni(II) complexes were synthesised with ease by reacting the appropriate ligand with NiBr$_2$·3H$_2$O or NiCl$_2$.glyme. Using this method, the desired Ni(I)–halide complexes **5-Cl**, **5-Br**, **6-Cl**, and **6-Br** were obtained in high yields (77–95%) (Scheme 3.21). All four complexes are paramagnetic and have broadened ^{1}H NMR spectra. Broadening is particularly significant for the protons of the phenanthroline core.

L1: R$_1$ = H, R$_2$ = mesityl
L2: R$_1$ = Ph, R$_2$ = hexyl
X = Cl, Br

L1: 78% **5-Cl**, 77% **5-Cl**
L2: 95% **6-Br**, 78% **6-Br**
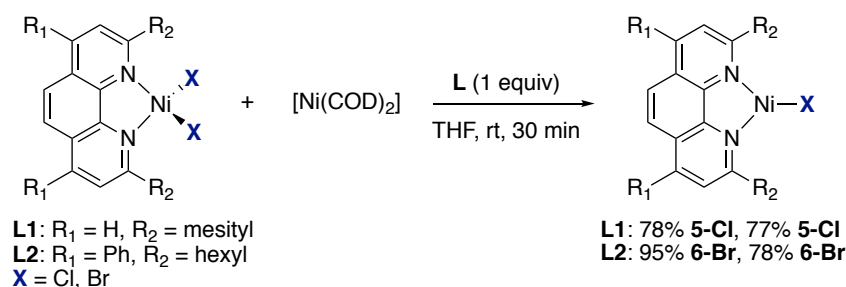
Scheme 3.21. Successful syntheses of Ni(I)–halide complexes bearing phenanthroline ligands.

X-ray structures of [(**L**)NiCl] complexes **5-Cl** and **6-Cl** confirmed the formation of the targeted three-coordinate halide complexes (Figure 3.3 and Figure 3.4). These complexes were the first examples of three-coordinate Ni(I)–halide complexes bearing an N-donor ligand. During the course of this study, Chirik and Diao reported three-coordinate Ni(I)–halide complexes bearing α-diimine and bipyridine ligands, respectively.[86,87]

The X-ray structures of **5-Cl** and **6-Cl** show Ni–Cl bond distances of 2.11 Å (average of the four similar molecules in the asymmetric unit) and 2.1417(9) Å, respectively. Both display distorted trigonal planar Y-shaped geometries with comparable N–Ni–Cl angles. The sum of the angles around the Ni centre at **5-Cl** is 359.5(11)° and **6-Cl** is 359.92(16)° showing that both complexes have an almost planar coordination geometry at the Ni centre. In both complexes there is only a ca. 2–4° angle between the NNNiCl coordination plane and the plane of the ligand backbone. This angle is mentioned as a much larger angle was obtained for a complex described in Section 3.4.3. The length of the central C–C bond in Ni phenanthroline complexes can indicate radical anion character.[88] However, the C71–C72 distance of 1.417(3) Å in the **5-Cl** molecule displayed in Figure 3.3 does not reflect a marked shortening compared to the distance of 1.421(11) Å in a Cu(I) complex [Cu(**L1**)(phen)]PF$_6$.[82] Comparison with Ni(II) complexes of **L1** or **L2** would be more appropriate, but these complexes were not characterised by X-ray crystallography.

Characterisation data for **5-Br** and **6-Br** matched those of the chloride complexes so their structures were assigned as [(**L**)NiBr].
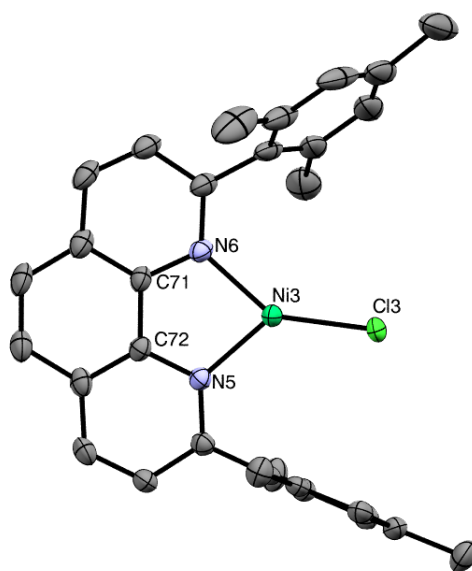
Figure 3.3. X-ray structure of 5-Cl with thermal ellipsoids drawn at 50% probability levels. There are four molecules in the asymmetric unit. The hydrogen atoms are omitted for clarity. Selected distances (Å) and angles (°): Ni3–Cl3 2.1252(6). Ni3–N5 1.9379(18). Ni3–N6 1.9409(18). C71–C72 1.417(3). N5–Ni3–Cl3 130.33(5). N6–Ni3–Cl3 145.34(6). N5–Ni3–N6 83.83(8).
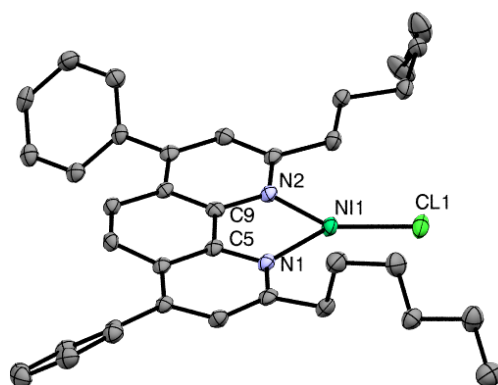
Figure 3.4. X-ray structure of 6-Cl with thermal ellipsoids drawn at 50% probability levels. Hydrogen atoms omitted for clarity. Selected distances (Å) and angles (°): Ni–Cl 2.1417(9). Ni–N1 1.961(3). Ni–N2 1.937(3). C5–C9 1.425(5). N1–Ni–Cl 133.80(8). N2–Ni–Cl 142.61(9). N1–Ni–N2 83.51(11).

The EPR spectra of all four halide complexes are consistent with the presence of a Ni-centred radical due to the deviation of the g values from g_e = 2.002 due to spin-orbit coupling with the Ni nucleus.[89] Spectra of **5-Cl** and **5-Br** are shown in Figure 3.5 for reference. The g values for all four halide complexes are centred on *average* values of g_x = 2.09, g_y = 2.12, and g_z = 2.46 (see the Experimental Section for full details). These were comparable with the g values of the bipyridine Ni(I)–Br complex recently reported by Diao and Lin of [2.103, 2.108, 2.473].[87] Interestingly, neither **5-Br**, **6-Br**, nor Diao's complex displayed hyperfine coupling to bromide (I = 3/2, ^{79}Br and ^{81}Br) or the nitrogen donor atoms (I = 1/2, ^{15}N and I = 1, ^{14}N). One mechanism for the appearance of hyperfine coupling requires the SOMO to have s-character, so this may suggest that the unpaired electron density is mainly located in Ni d orbitals (vide infra). Alternatively, it is known that hyperfine interactions are sometimes difficult to resolve in X-band EPR spectra and that pulsed experiments may be required to observe coupling.[89]
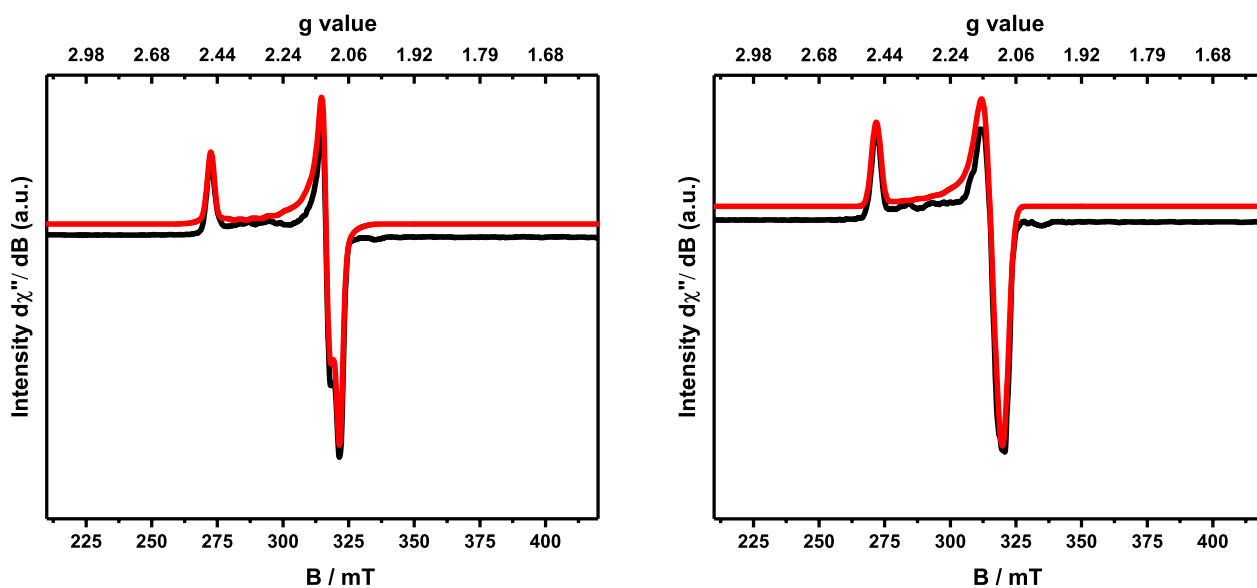
Figure 3.5. EPR spectra of 5-Cl (left) and 5-Br (right) (X-band, 77K, 2-MeTHF). Simulated spectra are shown in red.

With the ability to easily access Ni(I) complexes with inner-sphere halide ligands, it is envisioned that exploiting the general reactivity patterns for Ni–halide bonds in reactions such as anion metathesis will provide routes to new Ni(I) complexes bearing catalytically relevant ligands. Furthermore, as these halide complexes themselves are invoked as intermediates in cross-coupling reactions involving radical processes (Chapter 1, Section 1.3.1.), investigations into their catalytic relevance are now possible. To date, the use of **6-Br** as a precatalyst in the chain-walking carboxylation of alkyl bromides has not been investigated; however, studies along these lines are currently in progress in the Martin laboratory.

3.4.   Ni(I)–alkyl complexes

With Ni(I)–halide complexes in hand, the synthesis of a series of Ni(I)–alkyl complexes was investigated. In order to obtain a picture of whether the synthesis of these potentially unstable complexes would be feasible, exploratory reactions between a range of organometallic reagents and the Ni(I)–halide complexes **5** and **6** were carried out (Scheme 3.22). In all experiments, the halide of the Ni(I) complex was matched with the halide of the organometallic reagent. Analysis of the resulting reaction mixtures was carried out by EPR spectroscopy as the Ni(I) complexes synthesised in this work have broad ^{1}H NMR spectra making it difficult to pinpoint diagnostic signals during preliminary reactions. Furthermore, EPR is much more sensitive than NMR spectroscopy and does not require deuterated solvents.

The resulting alkyl complexes were expected to be rather sensitive, so reaction temperatures and ligand choices were carefully considered. Indeed, bulky **L1** allowed alkylation reactions to be carried out at room temperature (vide infra), whereas reactions carried out with **L2** halide complexes were carried out below −35 °C. If not, the reaction mixtures turned brown and the EPR spectra showed very low intensity signals for a Ni(I) complex, if any, along with a signal for organic radical (isotropic signal, g ca. 2.00).

L1: R_1 = H, R_2 = mesityl **5-Cl,Br**
L2: R_1 = Ph, R_2 = hexyl **6-Cl,Br**
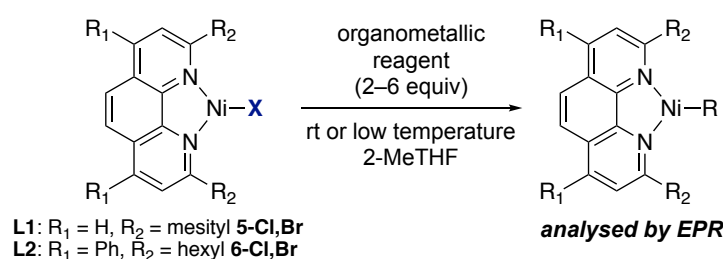
Scheme 3.22. General reaction scheme for alkylation reactions.

3.4.1. Bulky β-hydride-free alkyl groups

Initial screening focused on three alkyl groups lacking β-hydrogen atoms as these groups were expected to give the greatest chance of success. Neopentyl (CH$_2$tBu) and neosilyl (CH$_2$SiMe$_3$) complexes were targeted for comparison with the diphosphine Ni(I)–alkyl complexes reported by Hillhouse.[81] Benzylmagnesium chloride was also tested as the reductive carboxylation of benzylic substrates with a Ni/PCp$_3$/Zn/MgCl$_2$ system has been investigated computationally by Sakaki.[58,77] The EPR spectra

obtained from these six reactions are shown in Figure 3.6 (**L1**) and Figure 3.7 (**L2**). When the reactions were carried out at the appropriate temperature – **L1** reactions at room temperature and **L2** reactions in the cold well – the deep blue colour of the Ni(I)–X solution became emerald green and the resulting EPR spectrum became rhombic. This confirmed the conversion of the halide complex into a different S = 1/2 d^9 species. To demonstrate this, the EPR spectra of **5-Br** and **6-Br** are superimposed in grey on the EPR spectra derived from the neopentylMgBr reactions.

The g values for all five observable Ni(I) complexes **7a–c** and **8a,b** are all extremely similar and the average values are g_x = 2.072, g_y = 2.139, and g_z = 2.515. Full EPR details and simulated spectra can be found in the Supporting Information (Section 3.8.2). As shown in Figure 3.7, the complex formed upon reaction of **5-Cl** with benzylmagnesium chloride (**8c**) was not as stable as the other species and what is assumed to be a carbon-centred organic radical (g ca. 2.00) was present as the major product.
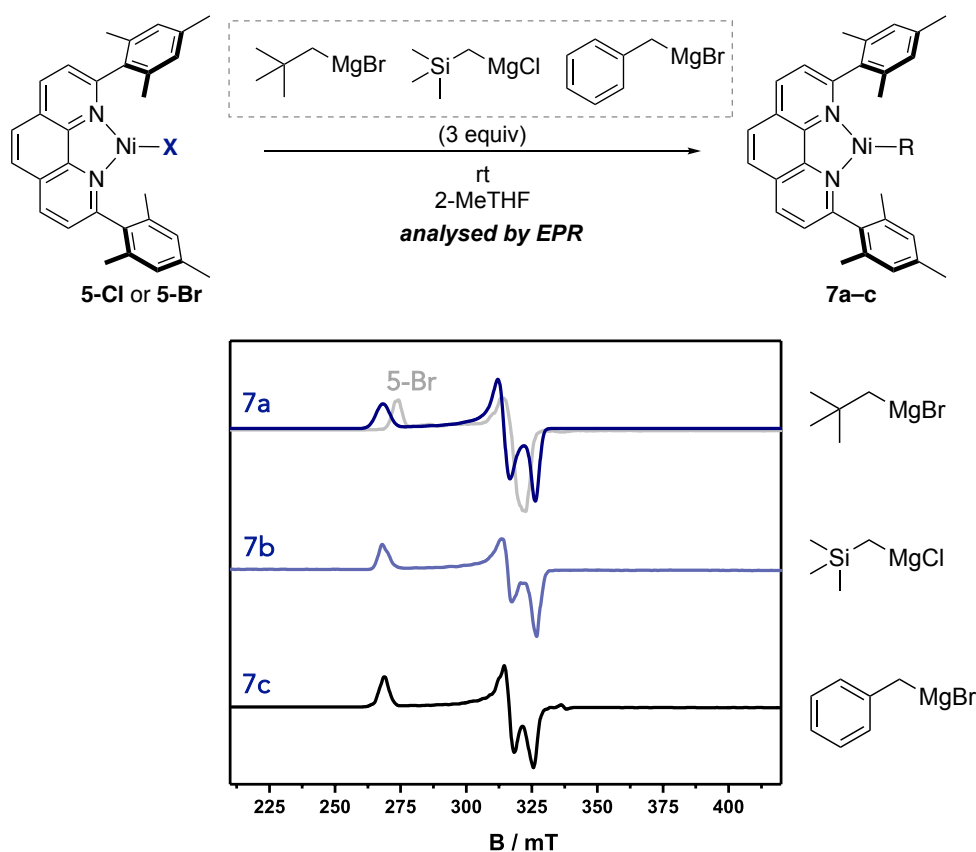
Figure 3.6. X-band EPR spectra (77 K, 2-MeTHF) of Ni(I)–alkyl complexes formed from reactions between [(L1)NiX] and alkyl Grignard reagents.
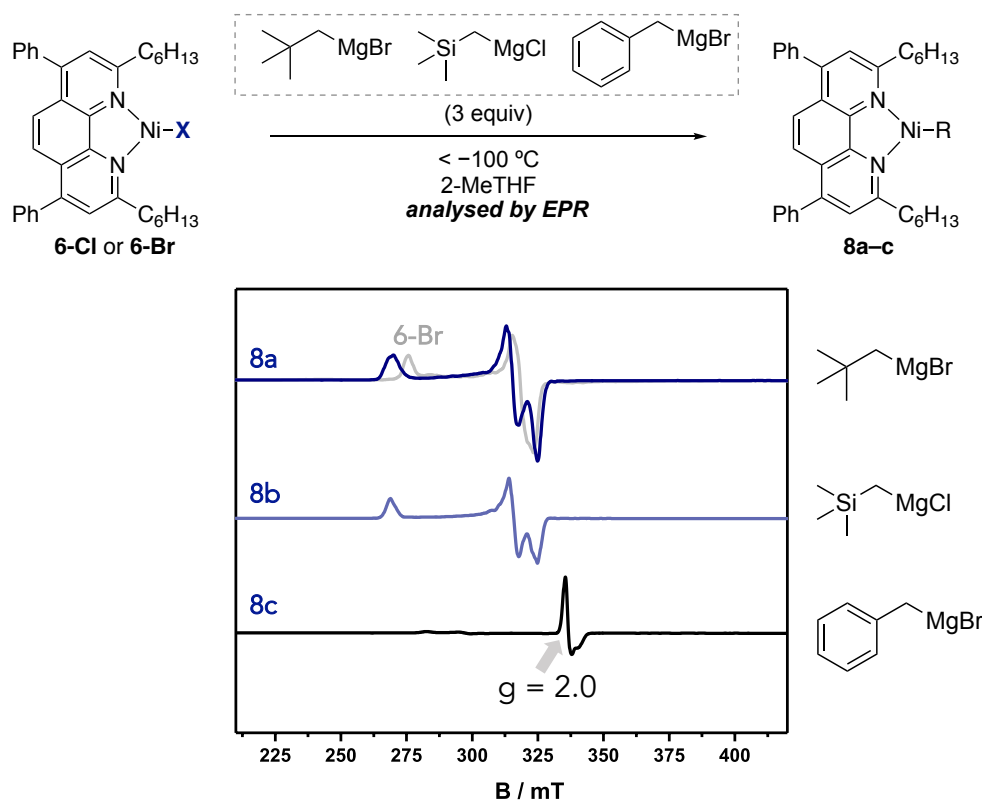
Figure 3.7. X-band EPR spectra (77 K, 2-MeTHF) of Ni(I)–alkyl complexes formed from reactions between [(L2)NiX] and alkyl Grignards.

Low temperature ^{1}H NMR spectroscopic analysis of the alkylation reactions was also carried out. All samples were prepared in the glovebox cold well then transferred to the precooled (−60 ºC) NMR probe. The ^{1}H NMR signals are very broad, but distinct signals for the different ligand backbones were observed at δ_H = 54–57 ppm and δ_H = 44 ppm for **L1** complexes **7a** and **7b**, and 48−51 ppm for **L2** complexes **8a** and **8b**. No signals upfield from 0 ppm were observed.
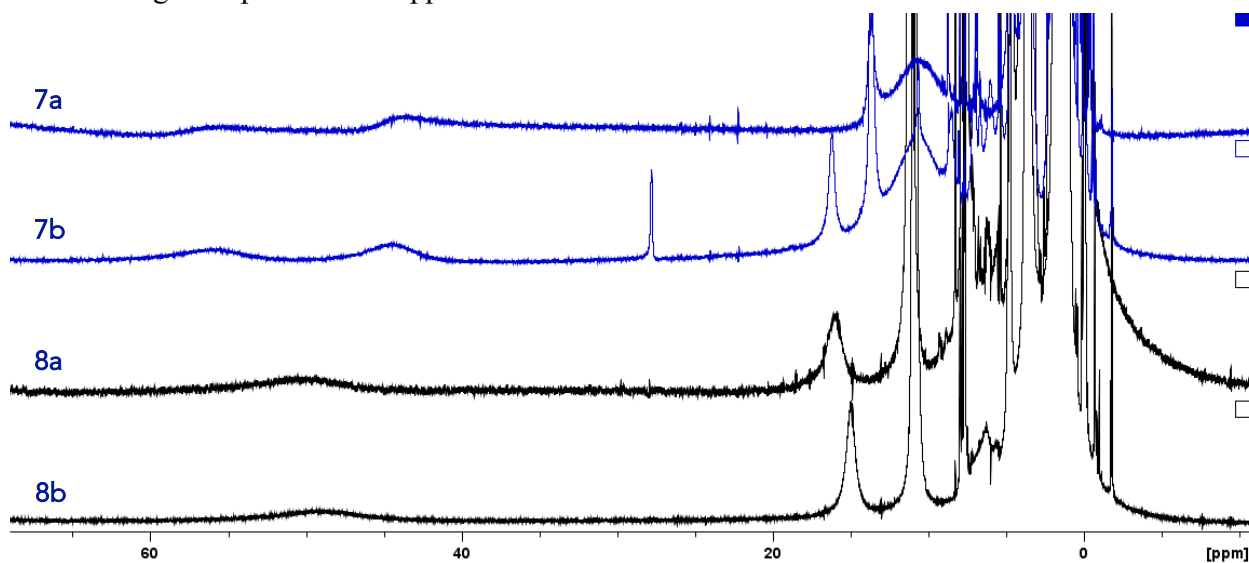
Figure 3.8. ^{1}H NMR spectra (213 K, THF-d$_8$) of [(L)Ni(alkyl)] complexes generated in situ.

3.4.2. Methyl and ethyl groups

The alkylation experiments described above were very promising as the EPR and NMR spectra showed the disappearance of the halide complexes and the formation of new paramagnetic Ni(I) complexes. Particularly promising were reactions involving **L1** complexes as the stability of the resulting complexes was significantly higher than those bearing **L2**.

Next, prompted by the successful synthesis of [(*t*Bu-Xantphos)NiMe] and [(*t*Bu-Xantphos)NiEt] complexes by Diao et al., the synthesis of phenanthroline-ligated methyl and ethyl complexes was attempted.[55] Reactions with **L1** complexes are discussed below because reactions of **L2** complexes resulted in decomposition to a carbon-centred radical and the formation of [Ni(**L2**)$_2$] as judged by EPR and ^{1}H NMR spectroscopy, respectively.[27] Interestingly, whereas Diao was able to isolate and characterise Ni(I)–methyl and –ethyl complexes, none of the reactions carried out in this work produced significant quantities of the analogous **L**Ni(I) species. If two equivalents of MeMgCl or EtMgBr was added to the corresponding Ni(I) halide complex, an EPR spectrum for the starting material was observed (black spectra in Figure 3.9). Further equivalents only produced organic radical as the major product (purple spectra in Figure 3.9).
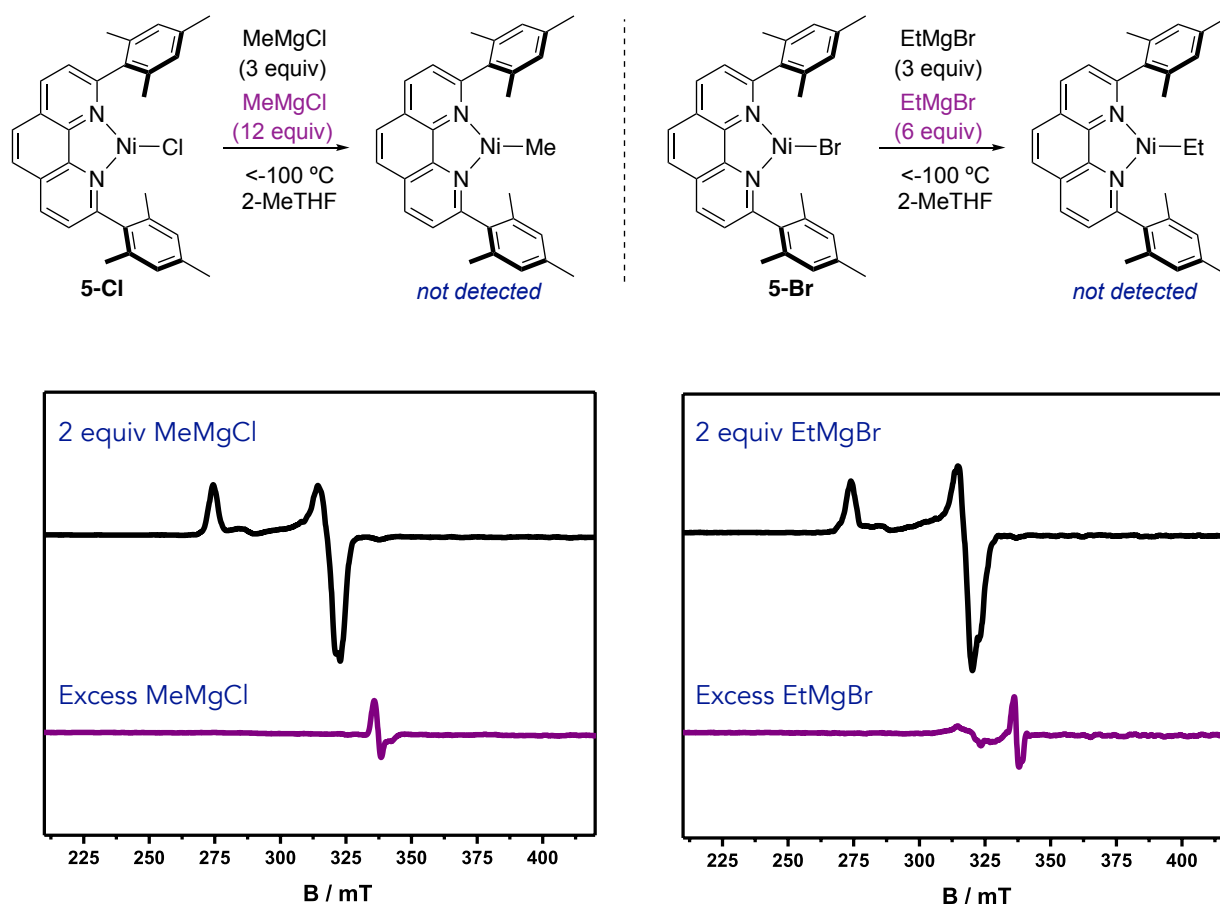
Figure 3.9. X-band EPR spectra (77 K, 2-MeTHF) of reactions between [(L1)NiX] and MeMgCl (left) and EtMgBr (right).

When the reaction of 2 equiv MeMgCl with **5-Cl** was repeated in toluene-d$_8$ and analysed by ^{1}H NMR spectroscopy, no signals for paramagnetic species were observed; however, dark block-shaped crystals were obtained from this solution. Although the crystals diffracted very poorly, an unrefined connectivity structure was obtained. This indicated the formation of a [Ni(**L1**)]$_4$ tetramer where each Ni(**L1**) unit had coordinated to C5–C6 bond of the **L1** backbone of another Ni(**L1**) unit (Figure 3.10)
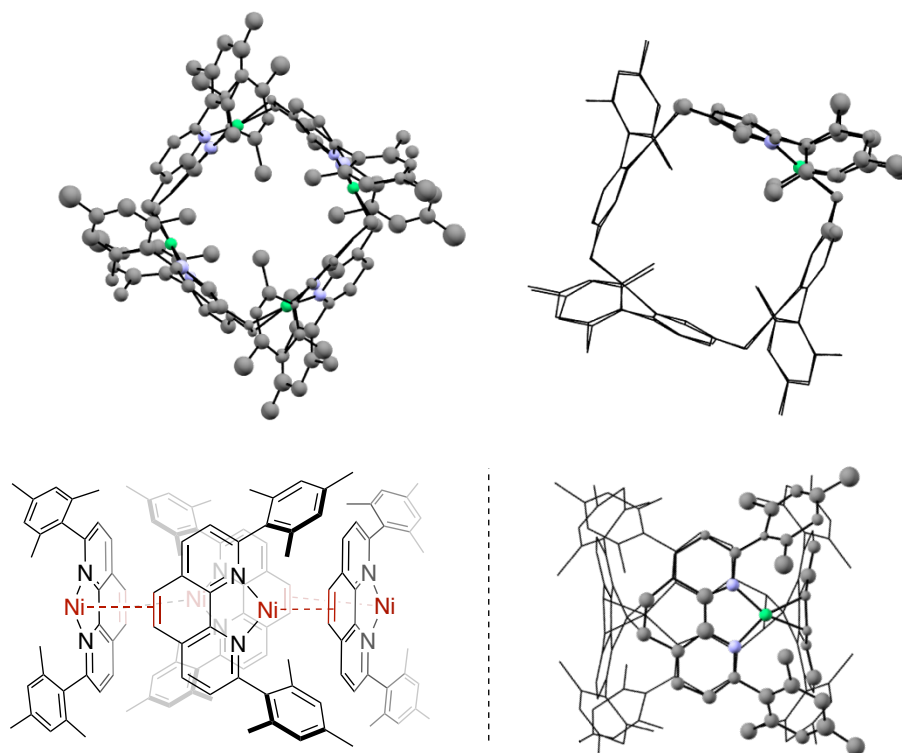
Figure 3.10. Views of the tetramer formed by four Ni(L1) monomers. There are two molecules in the asymmetric unit.

As of January 2020, there are no examples in the Cambridge Structural Database of any complexes where a metal is coordinated to the C5–C6 bond of a phenanthroline ligand. The angle between the (**L1**)Ni unit and the **L1** backbone to which it is coordinated is approximately 105º. This is consistent with reported complexes where a L$_n$Ni(0) group is coordinated to a π system.[90–95] For example, the angle of the Ni(0) group to the anthracene plane in [(*i*Pr$_3$P)$_2$Ni(0)(η^2-anthracene)] is also ca. 105º.[74] The bottom-right view in Figure 3.10 shows the (**L1**)Ni(η^2-**L1**) core from above and from the side. Unlike the planar η^2-anthracene in [(*i*Pr$_3$P)$_2$Ni(0)(η^2-anthracene)], the η^2-mesphen ligand is slightly concave. When **5-Br** was reacted with EtMgBr in THF-d$_8$, dark green single crystals formed inside the NMR tube. Analysis by X-ray diffraction showed the formation of a [Ni(**L1**)]$_3$ trimer (Figure 3.11).
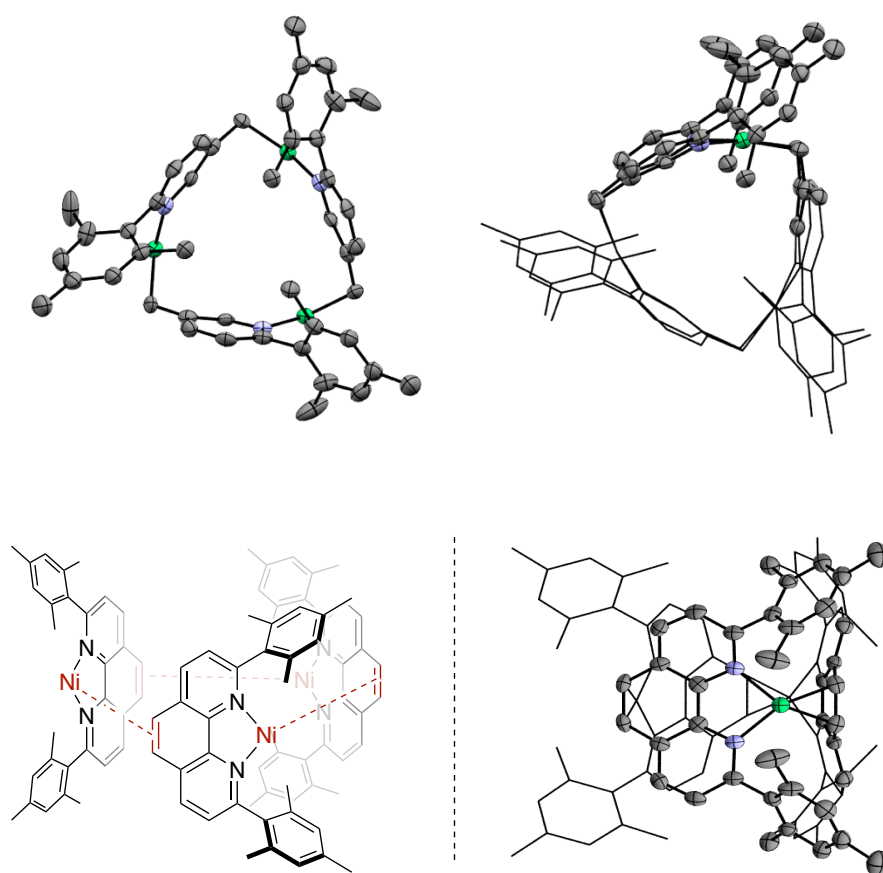
Figure 3.11. Views of the [Ni(L1)]₃ trimer. Hydrogen atoms and two THF molecules of crystallisation hidden.

In the trimer, the (**L1**)Ni–(η^2-**L1**) angle is correspondingly more acute than in the tetramer (98° rather than 105°). The data quality for this complex was higher than that of the tetramer and an approximate C–C π bond distance of 1.43 Å was obtained. This distance is comparable to that in the [(iPr₃P)₂Ni(0)(η^2-anthracene)] complex (1.427(4) Å) and is significantly longer than the analogous C–C distances in **5-Cl** and **6-Cl** of ca. 1.35 Å. Although the C–C bond distances and angles are comparable with Ni(0) η^2-anthracene or η^2-phenanthrene complexes,[91] it is important to note that the concavity of the **L1** backbone in [Ni(**L1**)]₃ and [Ni(**L1**)]₄ is not. The loss of planarity of **L1** is highlighted in Figure 3.12. The four carbon atoms highlighted in grey in Figure 3.12(a) are coplanar and all other **L1** atoms are above the plane. The angle between the two sections of the phenanthroline ligand (highlighted in green and blue in Figure 3.12(b)) is 27°. This angle suggests that the phenanthroline ligand is acting as two separate pyridine ligands with a π-bond spacer to which Ni(**L1**) coordinates.
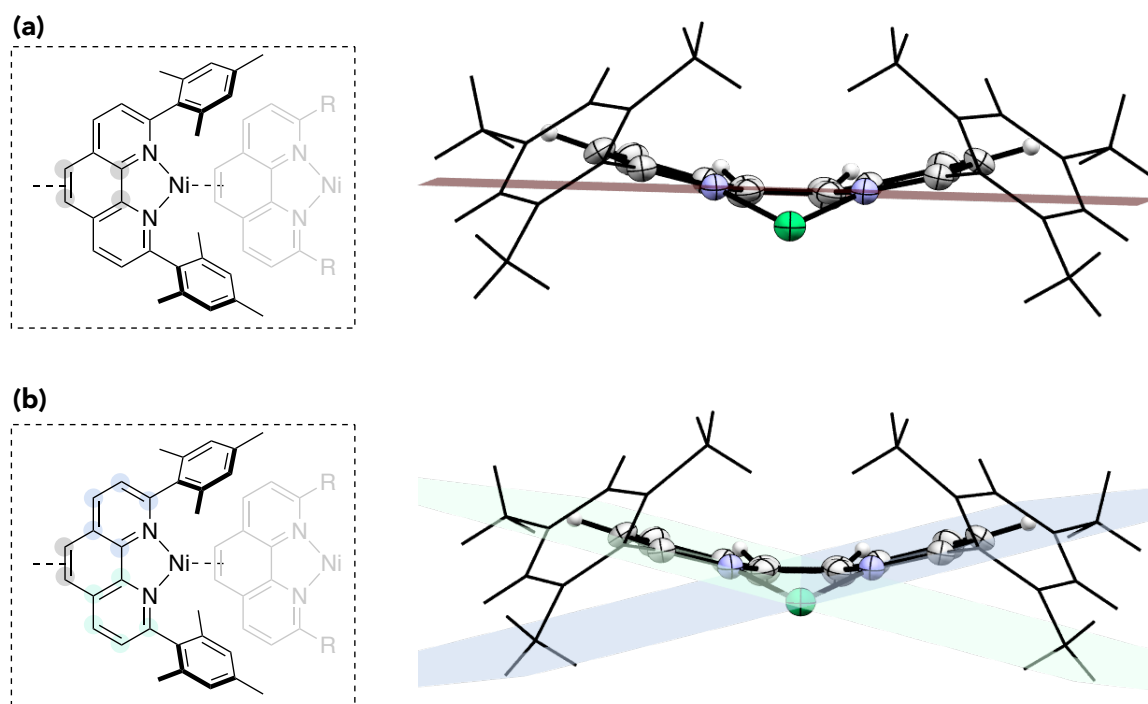
Figure 3.12. Simplified fragment of [Ni(L1)]₃. View along the mean plane of the carbon atoms highlighted in grey the inset figures.

In decomposition reactions of **L2**-containing Ni(I) complexes, the formally Ni(0) complex [Ni(**L2**)₂] was identified by NMR spectroscopy. However, in the case of **L1**, the analogous complex cannot form due to the very large and rigid mesityl substituents. In the absence of a coordinating ligand, it is plausible that the 14-electron complex Ni(**L1**) formed upon decomposition or reduction of, for example, an [(**L1**)Ni(I)Me] complex, is forced to form these unusual Ni(0) trimers and tetramers. The presence of a small alkene such as COD, norbornene, or ethylene during a reaction where a Ni(I)**L1** complex decomposes might allow the Ni(**L1**) fragment to be trapped as a monomer.

3.4.3. Synthesis and isolation of [(L1)Ni(neopentyl)] 7a

The EPR spectra in Figure 3.6 and Figure 3.7 and the NMR spectra in Figure 3.8 summarise a set of exploratory alkylation reactions that reveal the formation of new Ni(I) complexes with similar geometries and spin density distributions. These signals were confirmed as a set of Ni(I) alkyl complexes **7a–c** and **8a,b** after the isolation of deep green single crystals of [(**L1**)Ni(neopentyl)] (**7a**) from a concentrated pentane/diethyl ether solution at –35 °C (Figure 3.13). This structure confirmed the successful synthesis of the first long-sought Ni(I)–alkyl complex bearing a substituted phenanthroline ligand and is a new member of the rare set of Ni(I)–alkyl complexes (Scheme 3.23).
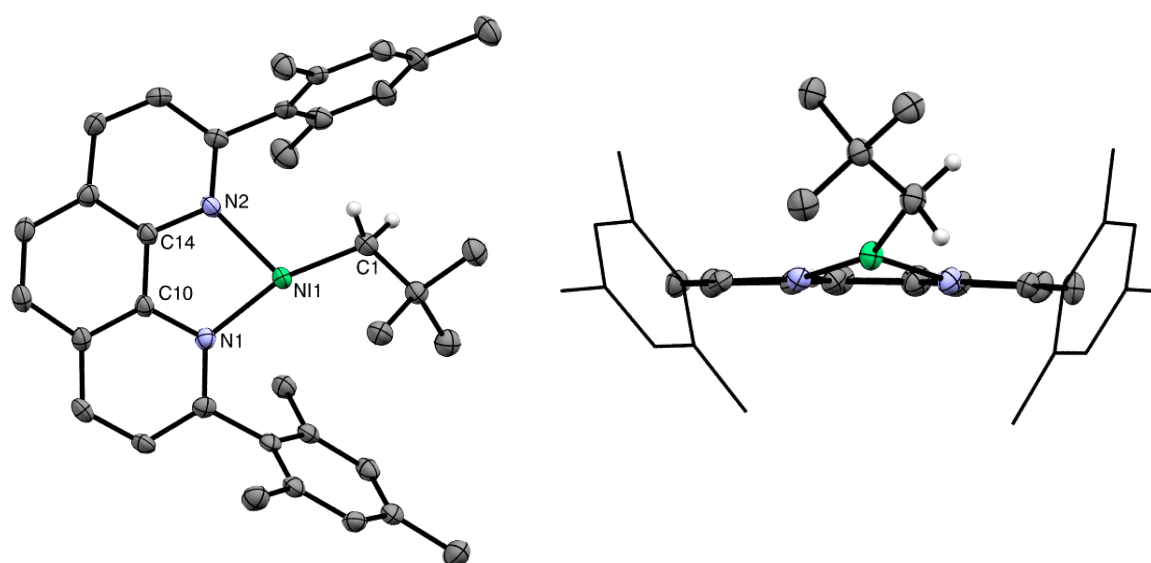
Figure 3.13. X-ray structure of 7a (thermal ellipsoids drawn at 50% probability level). Ligand and *t*Bu hydrogen atoms omitted. Disordered molecule of diethyl ether hidden from view. Bond lengths and angles discussed in the text.

The structural features of solid-state **7a** warrant some discussion. The Ni–C distance of 1.961(3) Å is similar to that of the Ni(I)–alkyl complexes bearing phosphine or NHC ligands reported by Hillhouse and co-workers and slightly shorter than that in the Xantphos complexes reported by Diao (Scheme 3.23).[55,70,81] The coordination geometry at Ni is almost planar (sum of angles = 353.68(22)°); however, the coordination plane is distorted by 23° from the mean plane of the **L1** backbone (Figure 3.13-right). This is significantly more than the 1–4° in **5-Cl** and **6-Cl** and is likely due to the steric demands of the neopentyl group inside the binding pocket delimited by the mesityl substituents. The T-shape geometry of the three-coordinate centre of **7a** compared to the Y-shaped geometry of **5-Cl** and **6-Cl** is characterised by the large N1–Ni–C1 angle of 156.74(14)° and compressed N2–Ni–C1 angle (82.69(11)°). An asymmetric three-coordinate Ni(I) complex with very similar L–Ni–C angles was also observed by Hillhouse in [(dtbpe)Ni(CH₂*t*Bu)] (dtbpe = 1,2-bis(di-tert-butylphosphino)ethane) (Scheme 3.23-box). Depending on the ligands at Ni, T-shape geometry is electronically preferred over Y-shape geometry.[96]

Hillhouse, 2004
P1–Ni–C = 110.97(8)°
P2–Ni–C = 157.82(8)°
Ni–C = 1.982(3) Å

Hillhouse, 2013
Ni–C = 1.910(2) Å

Diao, 2019
R = Me, Et
Ni–Me = 2.055(7) Å
Ni–Et = 2.034(2) Å
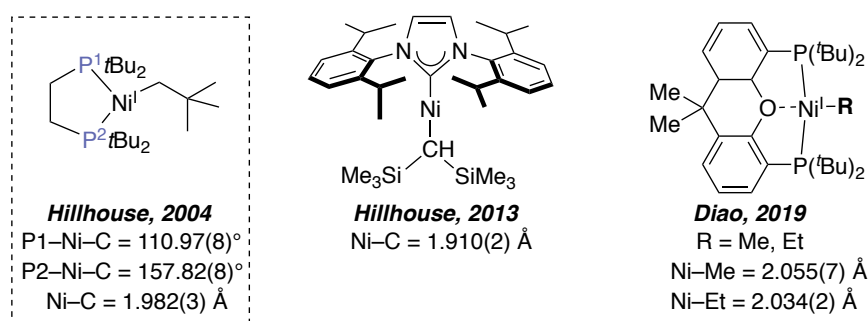
Scheme 3.23. Isolated Ni(I)-alkyl complexes.

The Ni–N2 bond (2.001(3) Å) is significantly longer than the Ni–N1 bond (1.942(3) Å) or the average in **5-Cl** (ca. 1.94 Å). Spin-density plots were calculated for **5-Cl** and **7a**. As expected from the EPR measurements, both complexes had the majority of the spin density localised in d orbitals on the Ni centre. The long Ni–N bond may be due to the antibonding character of the SOMO that is angled along the Ni–N2 bond.
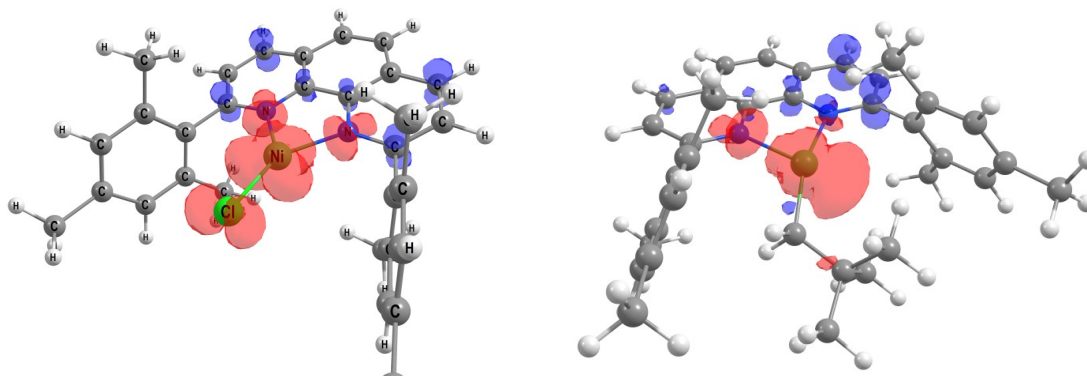
Figure 3.14. Spin density plots for 5-Cl and 7a.

With a number of alkyl complexes generated in situ and crystals of **7a** obtained for X-ray diffraction, investigations turned to isolating a Ni(I)–alkyl complex in larger quantities. Due to time constraints, only neopentyl complexes **7a** and **8a** were targeted; however, the **L1** and **L2** neosilyl complexes synthesised for EPR and NMR experiments seemed of comparable stability and would be an avenue to explore in future work.

Gratifyingly, the isolation of **7a** was indeed achieved, but was only investigated on small scales (ca. 0.02 mmol, 10 mg) and the moderate yield that was obtained was not further optimised (Scheme 3.24). The addition of 1,4-dioxane to the cold diethyl ether solution of **7a** formed upon alkylation of **5-Br** was necessary to remove the MgBr$_2$. Carefully repeating the same procedure for the **L2** analogue in the cold well of the glovebox resulted in decomposition of the alkyl complex **8a** as judged by EPR spectroscopy.
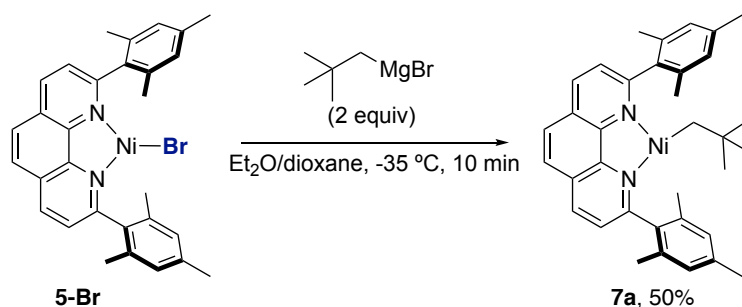
Scheme 3.24. Synthesis of 7a.

3.5.   CO₂ insertion at Ni(I)

3.5.1. Pre-formed carboxylate complex

With Ni(I)–alkyl complexes now able to be isolated or generated in situ, CO_2 insertion was investigated. In order to obtain reference EPR and IR spectra of the proposed CO_2 insertion product, anion metathesis reactions between **5-Cl** and $KOCOCH_2tBu$ (**9**) were carried out (Scheme 3.25). When the reaction was carried out with 1–2 equiv **9** for 30 minutes at room temp, full conversion of **5-Cl** was observed. The EPR spectrum of this new complex **10** was very different to that of the Ni(I)–halide or Ni(I)–alkyl complexes, suggesting a change in ligand and potentially in geometry at the Ni(I) centre. Instead of a rhombic spectrum with $g_z \gg g_y$, g_x, this spectrum was only slightly rhombic with $g_z < g_y$, g_x. As such, **10** was tentatively assigned as the desired carboxylate complex [(**L1**)Ni(OCOCH₂tBu] with κ^1 coordination of the carboxylate ligand as for Diao's Xantphos complex. Unfortunately, **10** seemed to decompose under the anion metathesis conditions after ca. 1 h, with the intensity of the EPR signal decreasing if the reaction was left for longer periods of time.
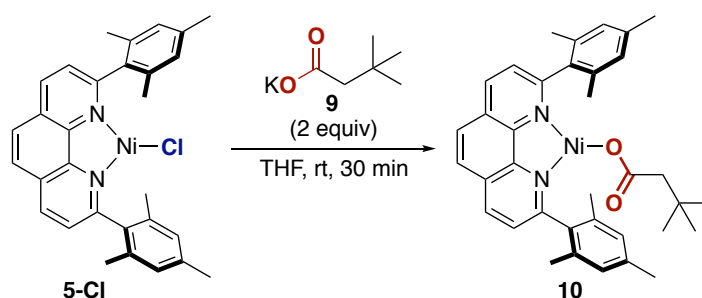
Scheme 3.25. Anion metathesis reaction of 5-Cl with potassium carboxylate 9 to install the carboxylate ligand (*tentative assignment*).
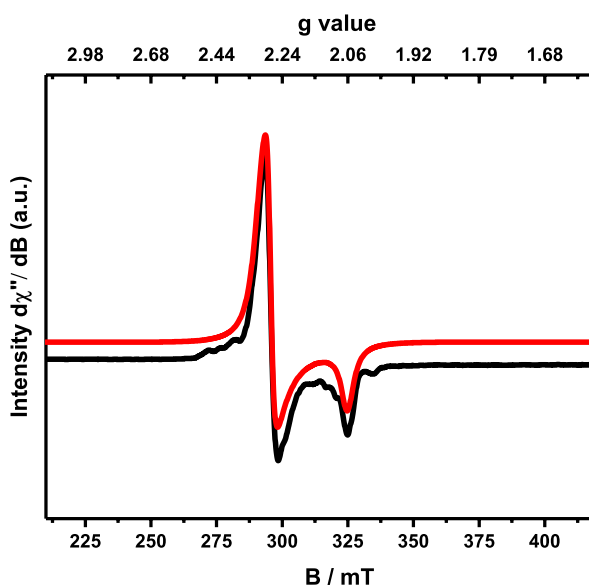
Figure 3.15. EPR spectrum of carboxylate complex 10 synthesised by anion metathesis. *Simulated spectrum shown in red* with: $g_x = 2.299$, $g_y = 2.272$, $g_z = 2.064$ freq: 9.388 GHz. lineshape = 0

Infrared spectroscopy is a useful tool for probing the coordination mode of carboxylate ligands as the C–O stretching frequencies are often distinctive. For a κ^1 carboxylate ligand, the ν_{asym} stretch of the OCO unit is usually found at 1500–1700 cm^{-1}, while the symmetric stretch ν_{sym} is usually found at 1200–1400 cm^{-1}.[69,97] A difference of >200 cm^{-1} between these two frequencies is expected for κ^1 coordination. If the carboxylate ligand is coordinated via both oxygen atoms, the C–O bonds are more equivalent and as a consequence the separation between the frequencies is much lower. Furthermore, the ν_{asym} stretch for κ^2 coordination is typically not found above 1575 cm^{-1}.[69] The IR spectra of **10**, **5-Cl**, and **5-Br** were collected by evaporation of their THF solutions on the window of an ATR-IR spectrometer inside the glovebox. These spectra are shown in Figure 3.16. A distinctive signal at 1542 cm^{-1} appeared in the spectrum of **10** (highlighted in blue) and is absent in those of **5-Cl**, and **5-Br**. This stretching frequency is in the range of ν_{asym} of a carboxylate ligand. Interestingly, no signals in the 1200–1400 cm^{-1} range of a κ^1 coordination mode were obvious in the spectrum of **10**.
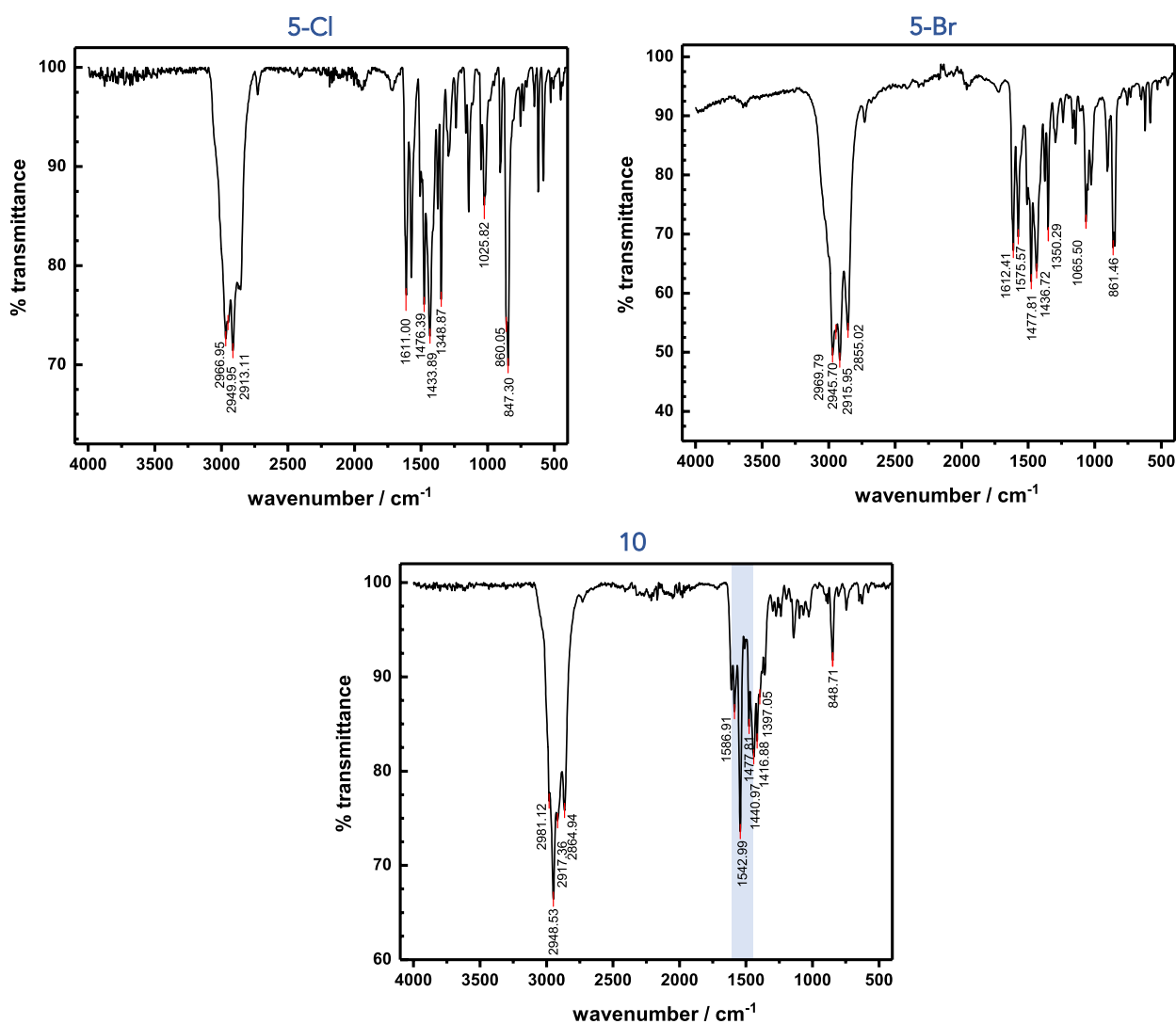
Figure 3.16. IR spectra of 5-Cl and 5-Br (top) and 10 synthesised via anion metathesis.

Efforts were made to crystallise **11** and confirm the presence of a carboxylate ligand by X-ray crystallography. Unfortunately, these have so far been unsuccessful. In order to obtain investigate the binding mode of the carboxylate ligand, complex **10** was therefore modelled by DFT (B3LYP and PBE functionals) (Figure 3.17). Both functionals had produced optimised geometries of **7a** that were in good agreement with the X-ray structure.

The predicted structure of **10** has a *distorted tetrahedral geometry* at Ni and a κ^2 carboxylate ligand. This is characterised by a 48 ° angle between the mean plane of the **L1** and carboxylate chelate rings and the Ni–O distances of 2.12 Å and 2.14 Å (PBE functional). The flattening from an idealised tetrahedron (90º) is rather large and may be due to the steric bulk of the neopentyl group. A dependence of this angle on oxidation state has been observed for a set of Ni complexes, where the angle decreased from Ni(0) (85º) to Ni(I) (62º) to Ni(II) (23º).[98] Whether the oxidation state of the metal centre is relevant to the (predicted) geometry of complex **10** is unknown at this time.
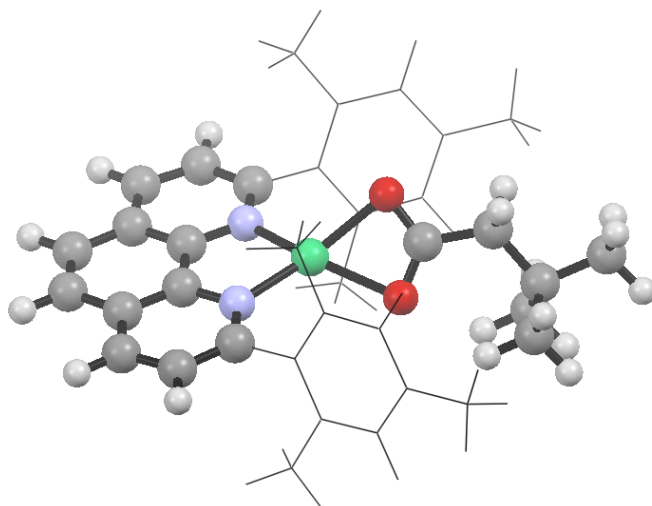
Figure 3.17. Optimised geometry of 10 (PBE). Mesityl substituents shown as wireframe for clarity.

The IR stretch at 1542 cm^{-1} for **10** discussed above was assigned to the ν_{asym} stretch of the OCO unit and is within the range of crystallographically characterised κ^2 carboxylate complexes. For example, ν_{asym} values were in the 1535–1567 cm^{-1} range for cadmium κ^2 arylcarboxylate complexes.[99] The asymmetric stretch of the κ^2 carboxylate ligand in **10** was calculated to be 1482.9 cm^{-1} (PBE functional). Further DFT results are in progress. The optimised geometry of **10** differs from the κ^1 complex isolated by Diao, potentially due to the wide bite-angle Xantphos ligand preventing the second oxygen atom from binding. The Tilley group demonstrated that reaction of CO_2 with a Ni(I)–silyl complex resulted in the formation of a κ^2 silylcarboxylate complex. Unfortunately, ν_{asym} was not assigned.[100]

The difference in EPR spectra between that of **7a** and that of **12** might indeed be explained by the change in coordination geometry from three- to four-coordinate that is proposed by DFT. Whether the **g** tensors of **7a** and **13** can be calculated and rationalised remains a possible route of investigation for future work.

3.5.2. CO_2 insertion

With reference EPR spectra for putative carboxylate complex **10** in hand, CO_2 insertion experiments were performed with neopentyl complex **7a** to investigate whether **10** might be obtained via direct reaction of a Ni(I)–alkyl complex with CO_2. Neopentyl complex **7a** was dissolved in 2-MeTHF, then the solution transferred to a J Young EPR tube and frozen in liquid N_2. After placing the tube under vacuum, the reaction mixture was thawed to ca. −60 ºC, then the tube was pressurised to approximately 0.1 bar CO_2 and briefly agitated. The brown-green solution was then very carefully refrozen and the EPR tube evacuated. Analysis of the frozen reaction mixture by EPR spectroscopy showed the disappearance of **7a** and the appearance of the same signal obtained from anion metathesis reactions (Figure 3.18). This suggested that **10** had been formed. This result is significant as insertion of CO_2 into the pincer Ni(II)–alkyl complexes of the Hazari and Wendt groups occurred at 150 ºC. Furthermore, although CO_2 insertion at Xantphos complexes investigated by Diao was hindered by the steric bulk of the ligands, very bulky **L1** did not seem to cause problems for CO_2 insertion.[55,67,68]
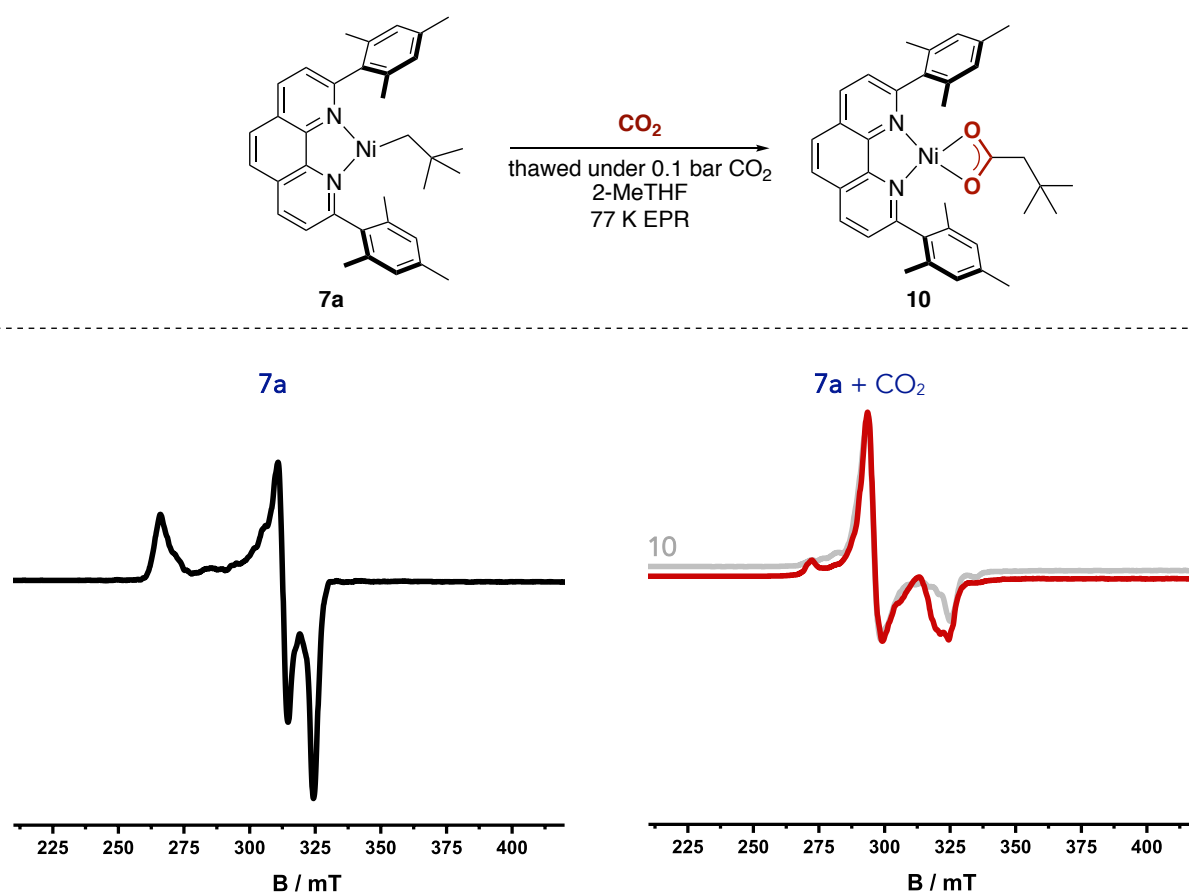
Figure 3.18. Reaction of CO_2 with 7a. Left: 77 K EPR spectrum of 7a; right: after addition of CO_2 (spectrum of 10 superimposed in pale grey).

Carboxylate complex **10** was not obtained when the insertion reaction was carried out in the presence of the $MgBr_2$ by-products of the alkylation reaction. Instead, the green solution of **7a** + $MgBr_2$ rapidly

turned deep blue under 0.1 bar CO_2 and the EPR spectrum of **5-Br** was obtained. This was likely due to rapid anion metathesis between **10** and $MgBr_2$. Indeed, when $ZnCl_2$ was added to a sample of **10** that had been generated from CO_2 insertion, the EPR spectrum showed the formation of **5-Cl**. This finding is relevant to catalysis as metathesis reactions between a Ni(I)–carboxylate complex and M(II) salts have recently been proposed to occur prior to the final reduction of a Ni(I) complex to Ni(0).[43]

The IR spectrum of **10** synthesised by CO_2 insertion was compared to that of **10** synthesised by anion metathesis and to that of **7a**. As shown in Figure 3.19, the anion metathesis and CO_2 insertion spectra are comparable, with both displaying a strong peak at 1543 cm^{-1} (highlighted in blue). This signal is absent in the IR spectrum of **7a**.
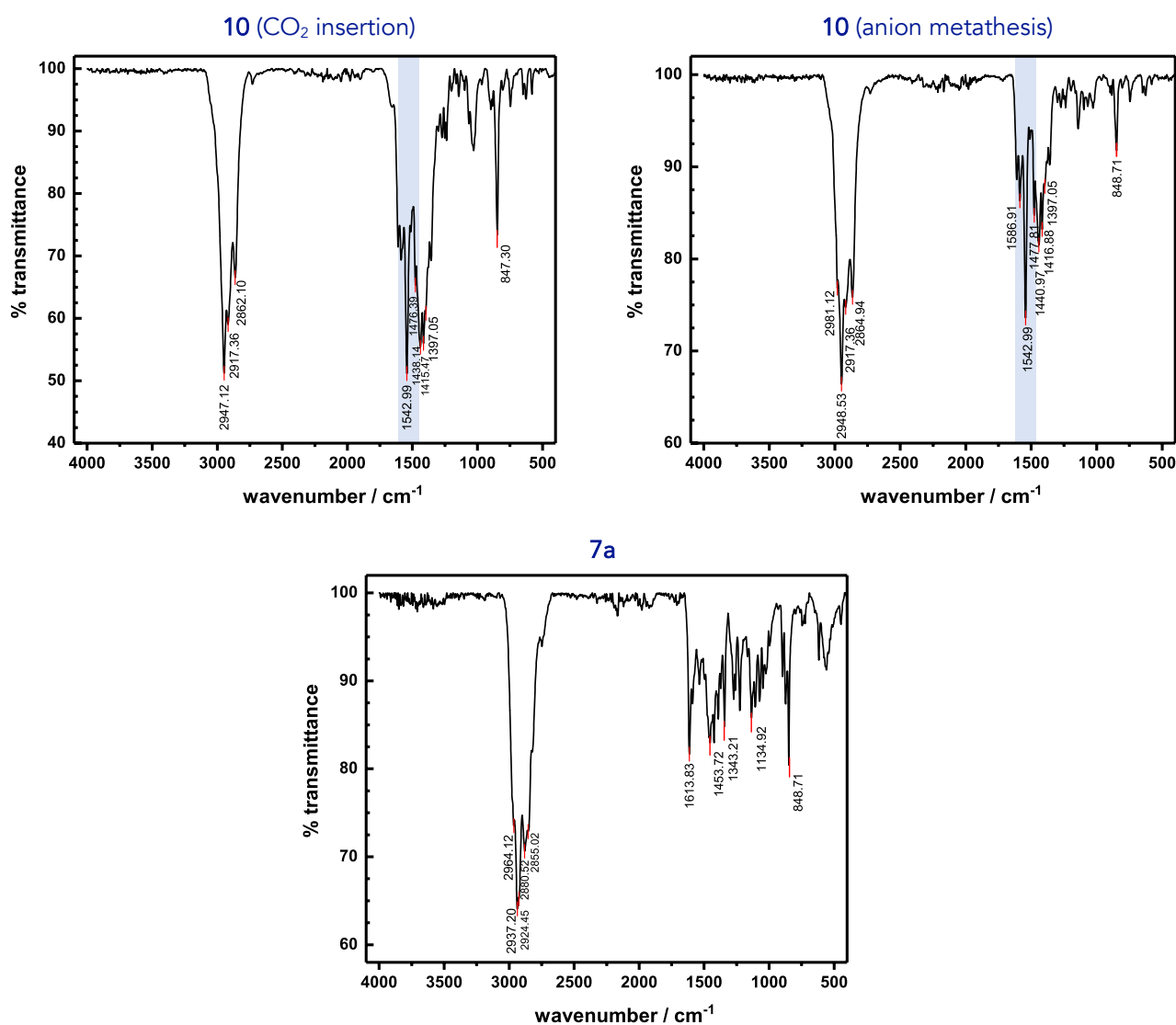
Figure 3.19. Top: IR spectra of 10 synthesised via CO_2 insertion (left) and anion metathesis (right). Bottom: IR spectrum of 7a.

In order to provide further evidence for successful CO_2 insertion, **7a** was reacted with $^{13}CO_2$. It was hypothesised that this would result in disappearance of the stretch at 1543 cm^{-1} and the appearance of lower energy C–O stretches. Figure 3.20 shows a comparison of the IR spectra of the complexes obtained from CO_2 (black) or $^{13}CO_2$ insertion (green). As expected, the ν_{asym} stretch at 1543 cm^{-1} was absent when $^{13}CO_2$ was employed and new signals had appeared at lower wavenumbers.
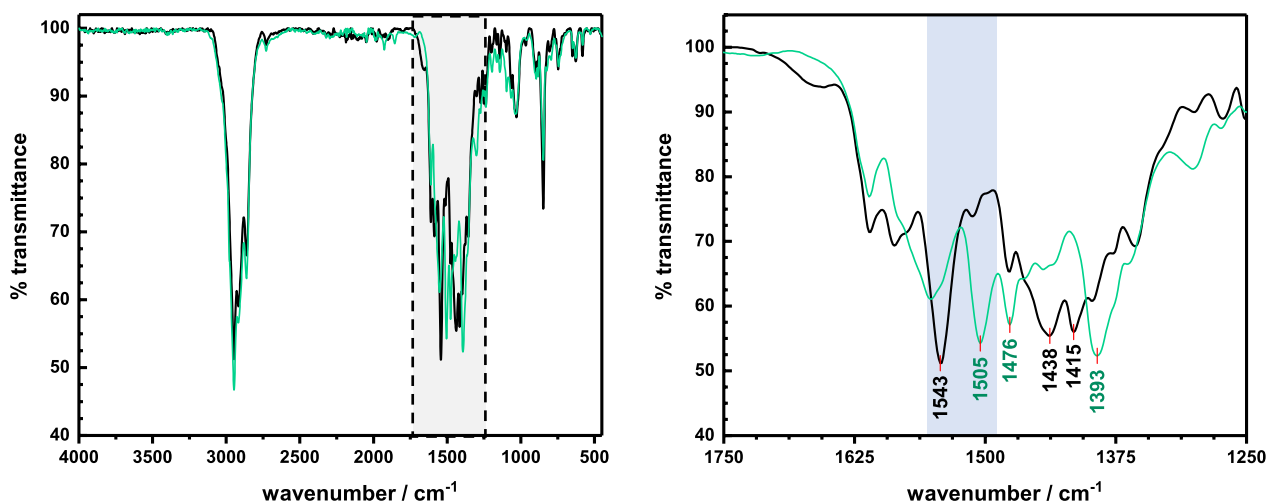
Figure 3.20. Left: comparison of IR spectra from CO_2 insertion with CO_2 (black) and $^{13}CO_2$ (green). Right: expansion of 1250–1750 region showing ν_{asym} stretches.

As shown in Figure 3.21, typical red shifts of ν_{asym} and ν_{sym} upon ^{13}C incorporation are 20–50 cm^{-1}.[68,101,102] These reported shifts are consistent with the calculated frequencies for the optimised geometry of **10-^{13}C**, where a 30 cm^{-1} decrease for ν_{asym} was predicted. This suggested that the stretch at 1505 cm^{-1} in Figure 3.20 – a 38 cm^{-1} decrease – might be the experimental ν_{asym} stretch for **10-^{13}C**. Figure 3.21 also shows reported examples of the small difference between ν_{asym} and ν_{sym} for κ^2 coordination and the much larger difference for κ^1 coordination.

CO₂   **^{13}CO₂**
ν_{asym} = 1616 cm^{-1} —> 1581 cm^{-1} $\Delta\nu$ = 35
ν_{sym} = 1374 cm^{-1} —> 1354 cm^{-1} $\Delta\nu$ = 20

CO₂   **^{13}CO₂**
ν_{asym} = 1514 cm^{-1} —> 1486 cm^{-1} $\Delta\nu$ = 28
ν_{sym} = 1445 cm^{-1} —> 1414 cm^{-1} $\Delta\nu$ = 41

ν_{asym} = 1495 cm^{-1}
ν_{sym} = 1448 cm^{-1}
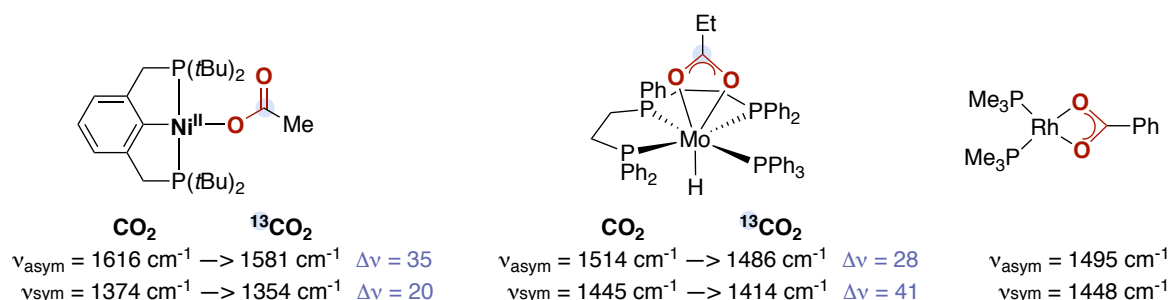
Figure 3.21. Examples of IR data for κ^1 and κ^2 carboxylate complexes formed from CO_2 insertion.[68,101,102]

Overall, these results mark the first observation of CO_2 insertion at a Ni(I)–alkyl complex bearing a substituted phenanthroline ligand. Insertion occurred at very low temperatures and the steric bulk of the mesityl substituents did not seem to affect the insertion reaction.

3.5.3. Reactions with L2 complexes

This project aimed to investigate complexes bearing ligands that are relevant to catalytic carboxylation reactions. Therefore, attempts were made to trap a Ni(I)–carboxylate complex bearing **L2**. However, the neopentyl precursor complex bearing **L2** (**8a**) is extremely temperature-sensitive. Although the purification steps required to rigorously remove $MgBr_2$ after the Grignard reaction (dioxane addition, filtration) were all carried out at very low temperature in the glovebox cold well, decomposition of **8a** occurred as judged by very low intensity EPR signals and a colour change from deep green to brown. Carboxylation was therefore carried out from **8a** that was generated in situ from neopentylMgBr. It was expected that the carboxylate complex would –therefore undergo rapid halide exchange with the $MgBr_2$ to from **6-Br** and $Mg(OCOCH_2tBu)Br$. As expected, when CO_2 was added to the green solution of **8a** + $MgBr_2$ the colour of the solution rapidly changed from green to blue and the EPR spectrum of **6-Br** was observed (Figure 3.22).
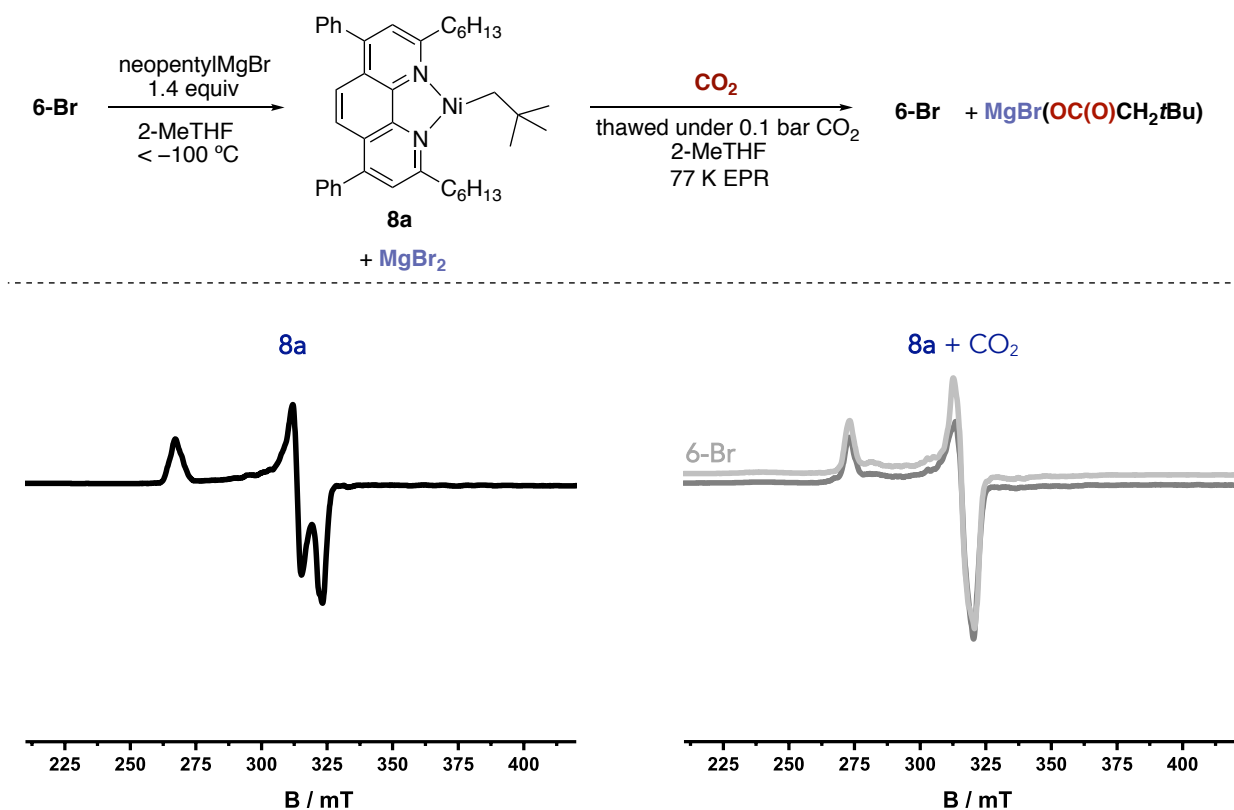
Figure 3.22. Reaction of CO_2 with 8a. Left: 77 K EPR spectrum of 8a synthesised in situ from 6-Br; right: EPR spectrum after addition of CO_2 (spectrum of isolated 6-Br superimposed in pale grey).

A larger scale carboxylation experiment was carried out to probe the fate of the neopentyl group on **8a**. After CO_2 addition, 2 M HCl was added to quench the putative Mg-carboxylate salt. Gratifyingly, a 50% NMR yield of *t*-butylacetic acid was obtained. This experiment marks the first example of CO_2 insertion to a Ni(I)–alkyl complex bearing a catalytically relevant ligand.

3.5.4. Insertion mechanism

A nucleophilic addition mechanism for CO_2 insertion has been proposed by Diao for Xantphos Ni(I)–alkyl complexes,[55] while a migratory insertion mechanism has been proposed by Sakaki.[56] In the case of CO_2 insertion at the Ni(I)–alkyl complexes in this work, DFT calculations (PBE functional) showed that the energy for an *inner-sphere* pathway at **7a** was 7.7 kcal mol^{-1}, significantly lower than that of the outer-sphere pathway calculated by Hazari and proposed by Diao (22.7 kcal mol^{-1}). The inner-sphere transition state for the conversion of **7a** to **10** is shown in Figure 3.23.
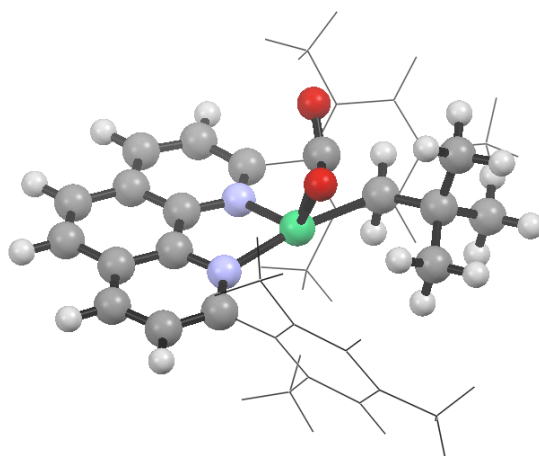
Figure 3.23. Inner-sphere CO_2 insertion transition state. Mesityl substituents shown as wireframe for clarity.

3.6.   Conclusions

This Chapter presents the first experimental study of alkyl carboxylation at the level of the key intermediates proposed to be active during the catalytic cycle. This was carried out in order to increase understanding of the mechanism of Ni-catalysed reductive carboxylation reactions and to fill a large void in the alkyl carboxylation literature. At the outset of this work, three goals were set: the synthesis of inner sphere Ni(I)–halide complexes, the alkylation of these complexes to generate Ni(I)–alkyl complexes, and with these in hand, investigations into their reactivity with CO_2.

The first part of the work concentrated on the synthesis of halide complexes bearing either a very bulky phenanthroline ligand or a ligand that is employed in a reported a reductive carboxylation methodology. Four inner-sphere halide complexes were synthesised via comproportionation in very good yields (>75%). Aside from linking to the second goal of this project, these represent a useful starting point

for the investigation of a diverse range of phenanthroline-bearing aryl, coordinatively unsaturated, or cationic complexes, amongst others.

The synthesis of an elusive Ni(I)–alkyl complex was investigated in the second part of the project. By shielding the Ni centre with bulky mesityl substituents, a neopentyl complex could be synthesised, isolated, and characterised by NMR, EPR, IR, and X-ray crystallography. Four other alkyl complexes of **L1** and **L2** were synthesised and the possibility for a stable neosilyl complex was uncovered. As perhaps to be expected for a ligand that is employed in a catalytic methodology, **L2** led to unstable complexes that could only be handled at low temperature as in situ-generated complexes. Analysis by NMR spectroscopy of unsuccessful alkylation reactions showed the presence of Ni(0) complexes, suggesting alkyl-to-halide exchange, reduction, and homolytic cleavage are some of the decomposition pathways accessible to these complexes.

Finally, CO_2 insertion to the Ni(I)–alkyl complexes was investigated. This was found to occur at cryogenic temperatures, a stark difference from the 150 ºC required for insertion of CO_2 into pincer Ni(II) complexes.[68] It was also found to occur for a catalytically relevant ligand **L2**, and the formation of carboxylic acid observed in a moderate yield after an acidic quench. Infrared spectra were collected and were consistent with calculated stretching frequencies. Initial DFT studies showed that a concerted pathway was found to be more energetically favourable than a previously proposed nucleophilic attack pathway.

This work is the first example of an investigation into Ni(I)–alkyl complexes of a ligand class that is extremely relevant to reductive carboxylation and cross-electrophile coupling. It is also the first example of CO_2 insertion at such complexes. Overall, the Ni(I) complexes synthesised in this project have implications not just in carboxylation reactions but in cross-electrophile couplings more broadly as a starting point for the investigation of insertion, isomerisation, and hydroalkylation reactions.

3.7. References

(1)   Aresta, M. My Journey in the CO_2-Chemistry Wonderland. *Coord. Chem. Rev.* **2017**, *334*, 150–183.

(2)   Liu, Q.; Wu, L.; Jackstell, R.; Beller, M. Using Carbon Dioxide as a Building Block in Organic Synthesis. *Nat. Commun.* **2015**, *6*, 1–15.

(3)   Tsuji, Y.; Fujihara, T. Carbon Dioxide as a Carbon Source in Organic Transformation: Carbon–carbon Bond Forming Reactions by Transition-Metal Catalysts. *Chem. Commun.* **2012**, *48* (80), 9956.

(4)   *Carbon Dioxide as Chemical Feedstock*; Aresta, M., Ed.; Wiley VCH: Weinheim, 2010.

(5)   Sakakura, T.; Choi, J. C.; Yasuda, H. Transformation of Carbon Dioxide. *Chem. Rev.* **2007**, *107* (6), 2365–2387.

(6)   Chaussard, J.; Folest, J.-C.; Nedelec, J.-Y.; Périchon, J.; Sibille, S.; Troupel, M. Use of Sacrificial Anodes in Electrochemical Functionalization of Organic Halides. *Synthesis (Stuttg).* **1990**, *1990* (5), 369–381.

(7)   Matthessen, R.; Fransaer, J.; Binnemans, K.; De Vos, D. E. Electrocarboxylation: Towards Sustainable and Efficient Synthesis of Valuable Carboxylic Acids. *Beilstein J. Org. Chem.* **2014**, *10*, 2484–2500.

(8)   Dubois, D. L. Electrochemical Reactions of Carbon Dioxide. In *Encyclopedia of Electrochemistry*; 2006; pp 202–225.

(9)   Tyssee, D. A.; Wagenknecht, J. H.; Baizer, M. M.; Chruma, J. L. Some Cathodic Organic Syntheses Involving Carbon Dioxide. *Tetrahedron Lett.* **1972**, *13* (47), 4809–4812.

(10)   Tortajada, A.; Juliá-Hernández, F.; Börjesson, M.; Moragas, T.; Martin, R. Transition-Metal-Catalyzed Carboxylation Reactions with Carbon Dioxide. *Angew. Chem. Int. Ed.* **2018**, *57* (49), 15948–15982.

(11)   Burkart, M. D.; Hazari, N.; Tway, C. L.; Zeitler, E. L. Opportunities and Challenges for Catalysis in Carbon Dioxide Utilization. *ACS Catal.* **2019**, *9* (9), 7937–7956.

(12)   Huang, K.; Sun, C. L.; Shi, Z.-J. Transition-Metal-Catalyzed C–C Bond Formation through the Fixation of Carbon Dioxide. *Chem. Soc. Rev.* **2011**, *40* (5), 2435–2452.

(13)   Artz, J.; Müller, T. E.; Thenert, K.; Kleinekorte, J.; Meys, R.; Sternberg, A.; Bardow, A.; Leitner, W. Sustainable Conversion of Carbon Dioxide: An Integrated Review of Catalysis and Life Cycle Assessment. *Chem. Rev.* **2018**, *118* (2), 434–504.

(14)   Yeung, C. S.; Dong, V. M. Making C–C Bonds from Carbon Dioxide via Transition-Metal Catalysis. *Top. Catal.* **2014**, *57* (17–20), 1342–1350.

(15)   Appel, A. M.; Bercaw, J. E.; Bocarsly, A. B.; Dobbek, H.; DuBois, D. L.; Dupuis, M.; Ferry, J. G.; Fujita, E.; Hille, R.; Kenis, P. J. A.; et al. Frontiers, Opportunities, and Challenges in Biochemical and Chemical Catalysis of CO_2 Fixation. *Chem. Rev.* **2013**, *113* (8), 6621–6658.

(16)   Cokoja, M.; Bruckmeier, C.; Rieger, B.; Herrmann, W. A.; Kühn, F. E. Transformation of Carbon Dioxide with Homogeneous Transition-Metal Catalysts: A Molecular Solution to a Global Challenge? *Angew. Chem. Int. Ed.* **2011**, *50* (37), 8510–8537.

(17)   Börjesson, M.; Moragas, T.; Gallego, D.; Martin, R. Metal-Catalyzed Carboxylation of Organic (Pseudo)halides with CO_2. *ACS Catal.* **2016**, *6* (10), 6739–6749.

(18)   Fauvarque, J. F.; Chevrot, C.; Jutand, A.; François, M.; Périchon, J. Electrosynthese Catalytique d'Acides Benzoiques Para-Substitues a Partir Du Derive Halogene Correspondant et de l'Anhydride Carbonique. *J. Organomet. Chem.* **1984**, *264* (1–2), 273–281.

(19)   Troupel, M.; Rollin, Y.; Périchon, J.; Fauvarque, J. F. *Nouv. J. Chim.* **1981**, *5* (12), 621.

(20)   Nédélec, J.; Périchon, J.; Troupel, M. Organic Electroreductive Coupling Reactions Using Transition Metal Complexes as Catalysts. *Top. Curr. Chem.* **1997**, *185*.

(21)   Yan, M.; Kawamata, Y.; Baran, P. S. Synthetic Organic Electrochemical Methods since 2000: On the Verge of a Renaissance. *Chem. Rev.* **2017**, *117* (21), 13230–13319.

(22)   Richmond, E.; Moran, J. Recent Advances in Nickel Catalysis Enabled by Stoichiometric Metallic Reducing Agents. *Synthesis (Stuttg).* **2018**, *50* (3), 499–513.

(23)   Sahoo, B.; Bellotti, P.; Juliá-Hernández, F.; Meng, Q. Y.; Crespi, S.; König, B.; Martin, R. Site-Selective, Remote Sp³ C−H Carboxylation Enabled by the Merger of Photoredox and Nickel Catalysis. *Chem. Eur. J.* **2019**, *25* (38), 9001–9005.

(24)   Meng, Q. Y.; Wang, S.; Huff, G. S.; Konig, B. Ligand-Controlled Regioselective Hydrocarboxylation of Styrenes with CO_2 by Combining Visible Light and Nickel Catalysis. *J. Am. Chem. Soc.* **2018**, *140* (9), 3198–3201.

(25)   Börjesson, M.; Moragas, T.; Martin, R. Ni-Catalyzed Carboxylation of Unactivated Alkyl Chlorides with CO_2. *J. Am. Chem. Soc.* **2016**, *138* (24), 7504–7507.

(26)   Tortajada, A.; Ninokata, R.; Martin, R. Ni-Catalyzed Site-Selective Dicarboxylation of 1,3-Dienes with CO_2. *J. Am. Chem. Soc.* **2018**, *140* (6), 2050–2053.

(27)   Juliá-Hernández, F.; Moragas, T.; Cornella, J.; Martin, R. Remote Carboxylation of Halogenated Aliphatic Hydrocarbons with Carbon Dioxide. *Nature* **2017**, *545* (7652), 84–88.

(28)   Janssen-Müller, D.; Sahoo, B.; Sun, S.-Z.; Martin, R. Tackling Remote Sp³ C−H Functionalization via Ni-

Catalyzed "chain-walking" Reactions. *Isr. J. Chem.* **2019**, *59*, 1–13.

(29) Sommer, H.; Juliá-Hernández, F.; Martin, R.; Marek, I. Walking Metals for Remote Functionalization. *ACS Cent. Sci.* **2018**, *4* (2), 153–165.

(30) Correa, A.; Martin, R. Palladium-Catalyzed Direct Carboxylation of Aryl Bromides with Carbon Dioxide. **2009**, *4645* (entry 8), 4645.

(31) Williams, C. M.; Johnson, J. B.; Rovis, T. Nickel-Catalyzed Reductive Carboxylation of Styrenes Using CO₂. *J. Am. Chem. Soc.* **2008**, *130* (45), 14936–14937.

(32) Li, S.; Yuan, W.; Ma, S. Highly Regio- and Stereoselective Three-Component Nickel-Catalyzed Syn-Hydrocarboxylation of Alkynes with Diethyl Zinc and Carbon Dioxide. *Angew. Chem. Int. Ed.* **2011**, *50* (11), 2578–2582.

(33) Hayashi, C.; Hayashi, T.; Kikuchi, S.; Yamada, T. Cobalt-Catalyzed Reductive Carboxylation on α,β-Unsaturated Nitriles with Carbon Dioxide. *Chem. Lett.* **2014**, *43* (4), 565–567.

(34) Takimoto, M.; Kawamura, M.; Mori, M.; Sato, Y. Nickel-Promoted Carboxylation/cyclization Cascade of Allenyl Aldehyde under an Atmosphere of CO₂. *Synlett* **2011**, No. 10, 1423–1426.

(35) Cao, T.; Ma, S. Highly Stereo- and Regioselective Hydrocarboxylation of Diynes with Carbon Dioxide. *Org. Lett.* **2016**, *18* (7), 1510–1513.

(36) Tran-Vu, H.; Daugulis, O. Copper-Catalyzed Carboxylation of Aryl Iodides with Carbon Dioxide. *ACS Catal.* **2013**, *3* (10), 2417–2420.

(37) Mita, T.; Higuchi, Y.; Sato, Y. Highly Regioselective Palladium-Catalyzed Carboxylation of Allylic Alcohols with CO₂. *Chem. Eur. J.* **2015**, *21* (46), 16391–16394.

(38) Fujihara, T.; Nogi, K.; Xu, T.; Terao, J.; Tsuji, Y. Nickel-Catalyzed Carboxylation of Aryl and Vinyl Chlorides Employing Carbon Dioxide. *J. Am. Chem. Soc.* **2012**, *134* (22), 9106–9109.

(39) Liu, Y.; Cornella, J.; Martin, R. Ni-Catalyzed Carboxylation of Unactivated Primary Alkyl Bromides and Sulfonates with CO₂. *J. Am. Chem. Soc.* **2014**, *136* (32), 11212–11215.

(40) Biswas, S. Mechanistic Understanding of Transition-Metal-Catalyzed Olefin Isomerization: Metal–Hydride Insertion-Elimination vs. π-Allyl Pathways. *Comments Inorg. Chem.* **2015**, *35* (6), 301–331.

(41) Obst, M.; Pavlovic, L.; Hopmann, K. H. Carbon-Carbon Bonds with CO₂: Insights from Computational Studies. *J. Organomet. Chem.* **2018**, *864*, 115–127.

(42) *Reaction Mechanisms in Carbon Dioxide Conversion*; Aresta, M., Dibenedetto, A., Quaranta, E., Eds.; Springer-Verlag, 2016.

(43) Charboneau, D. J.; Brudvig, G. W.; Hazari, N.; Lant, H. M. C.; Saydjari, A. K. Development of an Improved System for the Carboxylation of Aryl Halides through Mechanistic Studies. *ACS Catal.* **2019**, *9* (4), 3228–3241.

(44) Amatore, C.; Jutand, A. Rates and Mechanisms of Electron Transfer/Nickel-Catalyzed Homocoupling and Carboxylation Reactions. An Electrochemical Approach. *Acta Chem. Scand.* **1990**, *44*, 755–764.

(45) Fauvarque, J. F.; De Zelicourt, Y.; Amatore, C.; Jutand, A. Nickel-Catalyzed Electrosynthesis of Anti-Inflammatory Agents. III. A New Electrolyser for Organic Solvents; Oxidation of Metal Powder as an Alternative to Sacrifical Anodes. *J. Appl. Electrochem.* **1990**, *20*, 1–3.

(46) Amatore, C.; Jutand, A. Mechanism of Nickel-Catalyzed Electron-Transfer Activation of Aromatic Halides. Part 2. Electrocarboxylation of Bromobenzene. *J. Electroanal. Chem.* **1991**, *306* (1–2), 141–156.

(47) Amatore, C.; Jutand, A. Activation of Carbon Dioxide by Electron Transfer and Transition Metals. Mechanism of Nickel-Catalyzed Electrocarboxylation of Aromatic Halides. *J. Am. Chem. Soc.* **1991**, *113* (8), 2819–2825.

(48) Amatore, C.; Savéant, J. M. Mechanism and Kinetic Characteristics of the Electrochemical Reduction of Carbon Dioxide in Media of Low Proton Availability. *J. Am. Chem. Soc.* **1981**, *103* (17), 5021–5023.

(49) Amatore, C.; Jutand, A. Rates and Mechanism of Biphenyl Synthesis Catalyzed by Electrogenerated Coordinatively Unsaturated Nickel Complexes. *Organometallics* **1988**, *7* (10), 2203–2214.

(50) Amatore, C.; Azzabi, M.; Calas, P.; Jutand, A.; Lefrou, C.; Rollin, Y. Absolute Determination of Electron Consumption in Transient or Steady-State Electrochemical Techniques. *J. Electroanal. Chem.* **1990**, *288* (1–2), 45–63.

(51) Rollin, Y.; Meyer, G.; Troupel, M.; Fauvarque, J. F. Catalyse Par Des Complexes Du Nickel de l'Electrosynthese de 1,1 Diarylethane a Partir de Halogenures Aromatiques et d'Ethylene. *Tetrahedron Lett.* **1982**, *23* (35), 3573–3576.

(52) Schiavon, G.; Bontempelli, G.; Corain, B. Coupling of Organic Halides Electrocatalyzed by the NiI/NiI/Ni0–PPh₃ System. A Mechanistic Study Based on an Electroanalytical Approach. *J. Chem. Soc., Dalt. Trans.* **1981**, *0* (5), 1074–1081.

(53) Aresta, M.; Nobile, C. F.; Albano, V. G.; Forni, E.; Manassero, M. New Nickel-Carbon Dioxide Complex: Synthesis, Properties, and Crystallographic Characterization of (Carbon Dioxide)-Bis(tricyclohexylphosphine)nickel. *J. Chem. Soc., Chem. Commun.* **1975**, *0*, 636–637.

(54) Behr, A.; Keim, W.; Thelen, G. Stoichiometric Insertion of Carbon Dioxide and Ethylene into Nickel-Carbon Bonds. *J. Organomet. Chem.* **1983**, *249*, 38–40.

(55) Diccianni, J. B.; Hu, C. T.; Diao, T. Insertion of CO_2 Mediated by a (Xantphos)Ni^I–Alkyl Species. *Angew. Chem. Int. Ed.* **2019**, *58* (39), 13865–13868.

(56) Sayyed, F. B.; Tsuji, Y.; Sakaki, S. The Crucial Role of a Ni(I) Intermediate in Ni-Catalyzed Carboxylation of Aryl Chloride with CO_2: A Theoretical Study. *Chem. Commun.* **2013**, *49* (91), 10715.

(57) Rebih, F.; Andreini, M.; Moncomble, A.; Harrison-Marchand, A.; Maddaluno, J.; Durandetti, M. Direct Carboxylation of Aryl Tosylates by CO_2 Catalyzed by In situ-Generated Ni(0). *Chem. Eur. J.* **2016**, *22* (11), 3758–3763.

(58) Sayyed, F. B.; Sakaki, S. The Crucial Roles of $MgCl_2$ as a Non-Innocent Additive in the Ni-Catalyzed Carboxylation of Benzyl Halide with CO_2. *Chem. Commun.* **2014**, *50* (86), 13026–13029.

(59) Somerville, R. J.; Martin, R. Relevance of Ni(I) in Catalytic Carboxylation Reactions. In *Nickel Catalysis in Organic Synthesis*; Ogoshi, S., Ed.; Wiley Online Library, 2019; pp 285–330.

(60) Iyoda, M.; Otsuka, H.; Sato, K.; Nisato, N.; Oda, M. Homocoupling of Aryl Halides Using Nickel(II) Complex and Zinc in the Presence of Et_4NI. An Efficient Method for the Synthesis of Biaryls and Bipyridines. *Bull. Chem. Soc. Jpn.* **1990**, *63* (1), 80–87.

(61) Iyoda, M.; Sakaitan, M.; Otsuka, H.; Oda, M. Reductive Coupling of Benzyl Halides Using nickel(0)-Complex Generated in Situ in the Presence of Tetraethylammonium Iodide, a Simple and Convenient Synthesis of Bibenzyls. *Chem. Lett.* **1985**, *14* (1), 127–130.

(62) Aranzaes, J. R.; Daniel, M. C.; Astruc, D. Metallocenes as References for the Determination of Redox Potentials by Cyclic Voltammetry - Permethylated Iron and Cobalt Sandwich Complexes, Inhibition by Polyamine Dendrimers, and the Role of Hydroxy-Containing Ferrocenes. *Can. J. Chem.* **2006**, *84* (2), 288–299.

(63) Moragas, T.; Martin, R. Nickel-Catalyzed Reductive Carboxylation of Cyclopropyl Motifs with Carbon Dioxide. *Synth.* **2016**, *48* (17), 2816–2822.

(64) Moragas, T.; Gaydou, M.; Martin, R. Nickel-Catalyzed Carboxylation of Benzylic C–N Bonds with CO_2. *Angew. Chem. Int. Ed.* **2016**, *55* (16), 5053–5057.

(65) Fan, T.; Chen, X.; Lin, Z. Theoretical Studies of Reactions of Carbon Dioxide Mediated and Catalysed by Transition Metal Complexes. *Chem. Commun.* **2012**, *48* (88), 10808.

(66) Hazari, N.; Heimann, J. E. Carbon Dioxide Insertion into Group 9 and 10 Metal-Element σ Bonds. *Inorg. Chem.* **2017**, *56* (22), 13655–13678.

(67) Jonasson, K. J.; Wendt, O. F. Synthesis and Characterization of a Family of POCOP Pincer Complexes with Nickel: Reactivity towards CO_2 and Phenylacetylene. *Chem. Eur. J.* **2014**, *20* (37), 11894–11902.

(68) Schmeier, T. J.; Hazari, N.; Incarvito, C. D.; Raskatov, J. A. Exploring the Reactions of CO_2 with PCP Supported Nickel Complexes. *Chem. Commun.* **2011**, *47* (6), 1824–1826.

(69) Deacon, G. B.; Phillips, R. J. Relationships between the Carbon-Oxygen Stretching Frequencies of Carboxylato Complexes and the Type of Carboxylate Coordination. *Coord. Chem. Rev.* **1980**, *33*, 227–250.

(70) Laskowski, C. A.; Bungum, D. J.; Baldwin, S. M.; Del Ciello, S. A.; Iluc, V. M.; Hillhouse, G. L. Synthesis and Reactivity of Two-Coordinate Ni(I) Alkyl and Aryl Complexes. *J. Am. Chem. Soc.* **2013**, *135* (49), 18272–18275.

(71) Diccianni, J. B.; Katigbak, J.; Hu, C.; Diao, T. Mechanistic Characterization of (Xantphos)Ni(I)-Mediated Alkyl Bromide Activation: Oxidative Addition, Electron Transfer, or Halogen-Atom Abstraction. *J. Am. Chem. Soc.* **2019**, *141* (4), 1788–1796.

(72) Mohadjer Beromi, M.; Brudvig, G. W.; Hazari, N.; Lant, H. M.; Mercado, B. Q. Synthesis and Reactivity of Paramagnetic Polypyridyl Ni Complexes Relevant to Csp^2–Csp^3 Coupling Reactions. *Angew. Chem. Int. Ed.* **2019**.

(73) Mohadjer Beromi, M.; Banerjee, G.; Brudvig, G. W.; Hazari, N.; Mercado, B. Q. Nickel(I) Aryl Species: Synthesis, Properties, and Catalytic Activity. *ACS Catal.* **2018**, *8* (3), 2526–2533.

(74) Hatnean, J. A.; Shoshani, M.; Johnson, S. A. Mechanistic Insight into Carbon-Fluorine Cleavage with a ($^iPr_3P)_2Ni$ Source: Characterization of ($^iPr_3P)_2NiC_6F_5$ as a Significant Ni(I) Byproduct in the Activation of C_6F_6. *Inorganica Chim. Acta* **2014**, *422*, 86–94.

(75) Barth, E. L.; Davis, R. M.; Mohadjer Beromi, M.; Walden, A. G.; Balcells, D.; Brudvig, G. W.; Dardir, A. H.; Hazari, N.; Lant, H. M. C.; Mercado, B. Q.; et al. Bis(dialkylphosphino)ferrocene-Ligated Nickel(II) Precatalysts for Suzuki-Miyaura Reactions of Aryl Carbonates. *Organometallics* **2019**, *38* (17), 3377–3387.

(76) Mohadjer Beromi, M.; Brudvig, G. W.; Hazari, N.; Lant, H. M. C.; Mercado, B. Q. Synthesis and Reactivity of Paramagnetic Polypyridyl Ni Complexes Relevant to C(sp^2)–C(sp^3) Coupling Reactions. *Angew. Chem. Int. Ed.* **2019**, *58* (18), 6094–6098.

(77) Leon, T.; Correa, A.; Martin, R. Ni-Catalyzed Direct Carboxylation of Benzyl Halides with CO_2. *J. Am. Chem. Soc.* **2013**, *135* (4), 1221–1224.

(78) Yeung, C. S.; Dong, V. M. Beyond Aresta's Complex: Ni- and Pd-Catalyzed Organozinc Coupling with CO_2. *J. Am. Chem. Soc.* **2008**, *130* (25), 7826–7827.

(79) Ochiai, H.; Jang, M.; Hirano, K.; Yorimitsu, H.; Oshima, K. Nickel-Catalyzed Carboxylation of Organozinc Reagents with CO_2. *Org. Lett.* **2008**, *10* (13), 2681–2683.

(80) Kohler, L.; Hadt, R. G.; Hayes, D.; Chen, L. X.; Mulfort, K. L. Synthesis, Structure, and Excited State Kinetics of Heteroleptic Cu(i) Complexes with a New Sterically Demanding Phenanthroline Ligand. *Dalton Trans.* **2017**, *46* (38), 13088–13100.

(81) Kitiachvili, K. D.; Mindiola, D. J.; Hillhouse, G. L. Preparation of Stable Alkyl Complexes of Ni(I) and Their One-Electron Oxidation to Ni(II) Complex Cations. *J. Am. Chem. Soc.* **2004**, *126* (34), 10554–10555.

(82) Kohler, L.; Hayes, D.; Hong, J.; Carter, T. J.; Shelby, M. L.; Fransted, K. A.; Chen, L. X.; Mulfort, K. L. Synthesis, Structure, Ultrafast Kinetics, and Light-Induced Dynamics of CuHETPHEN Chromophores. *Dalton Trans.* **2016**, *45* (24), 9871–9883.

(83) Sugihara, H.; Okada, T.; Hiratani, K. Lithium Ion-Selective Electrodes Based on 1,10-Phenanthroline Derivatives. *Anal. Sci.* **1993**, *9* (5), 593–597.

(84) Powers, D. C.; Anderson, B. L.; Nocera, D. G. Two-Electron HCl to H_2 Photocycle Promoted by Ni(II) Polypyridyl Halide Complexes. *J. Am. Chem. Soc.* **2013**, *135* (50), 18876–18883.

(85) Callan, B.; Manning, A. R. Silver(I) Salts as One-Electron or Two-Electron Oxidants in Their Reactions with $[Fe_2(\eta\text{-}C_5H_5)_2(CO)_{4-n}(CNMe)_n]$ The Effect of Varying the Reaction Solvent. *J. Chem. Soc. Chem. Commun.* **1983**, 263–264.

(86) Zarate, C.; Yang, H.; Bezdek, M. J.; Hesk, D.; Chirik, P. J. Ni(I)–X Complexes Bearing a Bulky α-Diimine Ligand: Synthesis, Structure, and Superior Catalytic Performance in the Hydrogen Isotope Exchange in Pharmaceuticals. *J. Am. Chem. Soc.* **2019**, *141* (12), 5034–5044.

(87) Lin, Q.; Diao, T. Mechanism of Ni-Catalyzed Reductive 1,2-Dicarbofunctionalization of Alkenes. *J. Am. Chem. Soc.* **2019**, *141* (44), 17937–17948.

(88) Wang, M.; England, J.; Weyhermüller, T.; Wieghardt, K. Electronic Structures of "Low-valent" Neutral Complexes $[NiL_2]^0$ (S = 0; L = Bpy, Phen, Tpy) – An Experimental and DFT Computational Study. *Eur. J. Inorg. Chem.* **2015**, *2015* (9), 1511–1523.

(89) Goswami, M.; Chirila, A.; Rebreyend, C.; de Bruin, B. EPR Spectroscopy as a Tool in Homogeneous Catalysis Research. *Top. Catal.* **2015**, *58* (12–13), 719–750.

(90) Hatnean, J. A.; Beck, R.; Borrelli, J. D.; Johnson, S. A. Carbon-Hydrogen Bond Oxidative Addition of Partially Fluorinated Aromatics to a $Ni(P^iPr_3)_2$ Synthon: The Influence of Steric Bulk on the Thermodynamics and Kinetics of C–H Bond Activation. *Organometallics* **2010**, *29* (22), 6077–6091.

(91) Johnson, S. A.; Huff, C. W.; Mustafa, F.; Saliba, M. Unexpected Intermediates and Products in the C−F Bond Activation of Tetrafluorobenzenes with a Bis(triethylphosphine)Nickel Synthon: Direct Evidence of a Rapid and Reversible C−H Bond Activation by Ni(0). *J. Am. Chem. Soc.* **2008**, *130* (51), 17278–17280.

(92) Li, T.; García, J. J.; Brennessel, W. W.; Jones, W. D. C–CN Bond Activation of Aromatic Nitriles and Fluxionality of the η^2-Arene Intermediates: Experimental and Theoretical Investigations. *Organometallics* **2010**, *29* (11), 2430–2445.

(93) Braun, T.; Cronin, L.; Higgitt, C. L.; McGrady, J. E.; Perutz, R. N.; Reinhold, M. Coordination and Oxidative Addition of Octafluoronaphthalene at a Nickel Centre: Isolation of an Intermediate in C–F Bond Activation. *New J. Chem.* **2001**, *25* (1), 19–21.

(94) Bach, I.; Pörschke, K.-R.; Goddard, R.; Kopiske, C.; Krüger, C.; Rufińska, A.; Seevogel, K. Synthesis, Structure, and Properties of $\{(^tBu_2PC_2H_4P^tBu_2)Ni\}_2(\mu\text{-}\eta^2\text{:}\eta^2\text{-}C_6H_6)$ and $(^tBu_2PC_2H_4P^tBu_2)Ni(\eta^2\text{-}C_6F_6)$. *Organometallics* **1996**, *15* (23), 4959–4966.

(95) Johnson, S. A.; Taylor, E. T.; Cruise, S. J. A Combined Experimental and Computational Study of Unexpected C–F Bond Activation Intermediates and Selectivity in the Reaction of Pentafluorobenzene with a $(PEt_3)_2Ni$ Synthon. *Organometallics* **2009**, *28* (13), 3842–3855.

(96) Eckert, N. A.; Dinescu, A.; Cundari, T. R.; Holland, P. L. A T-Shaped Three-Coordinate Nickel(I) Carbonyl Complex and the Geometric Preferences of Three-Coordinate D^9 Complexes. *Inorg. Chem.* **2005**, *44* (22), 7702–7704.

(97) Nara, M.; Torii, H.; Tasumi, M. Correlation between the Vibrational Frequencies of the Carboxylate Group and the Types of Its Coordination to a Metal Ion: An Ab Initio Molecular Orbital Study. *J. Phys. Chem.* **1996**, *100* (51), 19812–19817.

(98) Niklas, J.; Westwood, M.; Mardis, K. L.; Brown, T. L.; Pitts-McCoy, A. M.; Hopkins, M. D.; Poluektov, O. G. X-Ray Crystallographic, Multifrequency Electron Paramagnetic Resonance, and Density Functional Theory Characterization of the $Ni(P^{Cy}_2N^{tBu}_2)_2^{n+}$ Hydrogen Oxidation Catalyst in the Ni(I) Oxidation State. *Inorg. Chem.* **2015**, *54* (13), 6226–6234.

(99) Kreider-Mueller, A.; Quinlivan, P. J.; Owen, J. S.; Parkin, G. Synthesis and Structures of Cadmium Carboxylate and Thiocarboxylate Compounds with a Sulfur-Rich Coordination Environment: Carboxylate Exchange Kinetics Involving tris(2-Mercapto-1-T-Butylimidazolyl)hydroborato Cadmium Complexes, $[Tm^{Bu^t}]Cd(O_2CR$. *Inorg. Chem.* **2015**, *54* (8), 3835–3850.

(100) Witzke, R. J.; Tilley, T. D. A Two-Coordinate Ni(I) Silyl Complex: CO_2 Insertion and Oxidatively-Induced Silyl Migrations. *Chem. Commun.* **2019**, *55* (46), 6559–6562.

(101) Zhang, Y.; Hanna, B. S.; Dineen, A.; Williard, P. G.; Bernskoetter, W. H. Functionalization of Carbon Dioxide with Ethylene at Molybdenum Hydride Complexes. *Organometallics* **2013**, *32* (14), 3969–3979.

(102) Darensbourg, D. J.; Rheingold, A. L.; Grotsch, G.; Wiegreffe, P. Insertion Reactions of Carbon Dioxide with Square-Planar Rhodium Alkyl and Aryl Complexes. *Inorg. Chem.* **1987**, *26* (22), 3827–3830.

(103) Torker, S.; Müller, A.; Sigrist, R.; Chen, P. Tuning the Steric Properties of a Metathesis Catalyst for Copolymerization of Norbornene and Cyclooctene toward Complete Alternation. *Organometallics* **2010**, *29* (12), 2735–2751.

(104) Saito, T.; Uchida, Y.; Misono, A.; Yamamoto, A.; Morifuji, K.; Ikeda, S. Diethyldipyridylnickel. Preparation, Characterization, and Reactions. *J. Am. Chem. Soc.* **1966**, *88* (22), 5198–5201.

(105) Evans, D. F. 400. The Determination of the Paramagnetic Susceptibility of Substances in Solution by Nuclear Magnetic Resonance. *J. Chem. Soc.* **1959**, 2003–2005.

(106) Sur, S. K. Measurement of Magnetic Susceptibility and Magnetic Moment of Paramagnetic Molecules in Solution by High-Field Fourier Trasform NMR Spectroscopy. *J. Magn. Reson.* **1989**, *82*, 169–173.

3.8.   Experimental section

Reagents. [Ni(COD)$_2$] was purchased from Strem Chemicals. Neocuproine and bathocuproine were purchased from Sigma Aldrich. 2,9-Dichlorophenanthroline was purchased from Fluorochem.

Neopentylmagnesium bromide was synthesised following a reported procedure.[103]

L1[82] and **L2**[27,104] were synthesised according to literature procedures. Potassium carboxylate salt **9** was synthesised by combining 2,3-dimethyl butyric acid with KOH in methanol followed by removal of the volatiles. All other reagents were purchased from commercial sources and used without further purification.

Solvents. Hydrocarbon solvents, 2-MeTHF, toluene-d$_8$, THF-d$_8$ and benzene-d$_6$ were degassed by the appropriate method (sparging or three freeze-pump-thaw cycles) then dried over 4Å molecular sieves and stored in the glovebox. Inhibitor-free THF and Et$_2$O were purified with an Innovative Technologies solvent purification system. CDCl$_3$ was used as received for NMR of air-stable Ni(II) complexes.

Analytical methods. Flash chromatography was performed with Sigma Aldrich technical grade silica gel 60 (230-400 mesh). Thin layer chromatography was carried out using Merck TLC Silica gel 60 F254. NMR spectra were recorded on Bruker Avance Ultrashield 300, 400, or 500 MHz spectrometers, with chemical shifts reported in parts per million (ppm) and coupling constants, *J*, reported in hertz. IR spectra were obtained with a Bruker FT-IR Alpha spectrometer inside the glovebox. UV-vis spectra were obtained with an Agilent Cary 60 spectrophotometer. Samples were contained in Hellma Suprasil quartz cuvettes and sealed with silicon stoppers.

Continuous wave (CW) EPR spectra were obtained using a Bruker EMX Micro X-band spectrometer using a Bruker ER 1164 HS resonator. Spectra were simulated using SpinFit within Xenon. The samples were cooled to 77 K in a Suprasil finger dewar (Wilmad-LabGlass) filled with liquid nitrogen. Spectrometer settings are provided with the EPR data. The spectral data were collected at 77 K with the following spectrometer settings: microwave power = 0.56 mW; centre field = 3250 G, sweep width = 2500 G, sweep time = 35.07 s, modulation frequency = 100 KHz, modulation amplitude = 10 G, power attenuation = 25 dB, time constant = 20.48 ms.
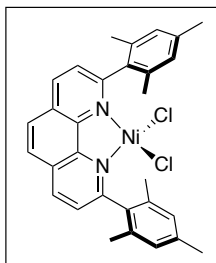
Evans method[105,106] solution magnetic susceptibility measurements were performed for [NiBr$_2$(**L2**)], **5-Cl**, and **5-Br**.

Dr Brandon Q. Mercado (Yale University) collected the X-ray data for **5-Cl** and refined and solved the structure (see Section 3.8.7).

3.8.1. Preparation of nickel complexes

3.8.1.1.   Nickel(II) dihalide precursors

[NiCl₂(L1)]

In a 12 mL vial, **L1** (175.4 mg, 0.421 mmol, 1 equiv) and NiCl₂·DME (92.5 mg, 0.421 mmol, 1 equiv) were combined in 4 mL THF. Stirring at room temperature for 45 minutes followed by sonication for 10 minutes gave a purple suspension. This was combined with 4 mL Et₂O then filtered, washed with further Et₂O (2 x 5 mL), and dried under vacuum to give [NiCl₂(**L1**)] as a pink solid (197 mg, 86% yield).

¹H NMR (500 MHz, CDCl₃ (paramagnetic)): δ 73.78 (s, 2H, **L1**), 25.28 (s, 2H, **L1**), 24.71 (s, 2H, **L1**), 9.63 (s, 4H, **L1**-mes), 5.30 (s, 12 H, *ortho*-CH₃), 4.97 (br, $\Delta v_{1/2}$ = 41 Hz, 6 H, *para*-CH₃).
EA Calcd. C, 65.98; H, 5.17; N, 5.13; Found: C, 65.26; H, 5.40; N, 4.88.

[NiBr₂(L1)]
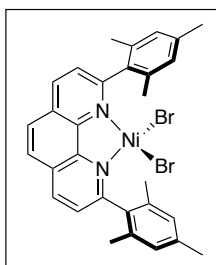
In a 12 mL vial, **L1** (80 mg, 0.192 mmol, 1 equiv) and NiBr₂·DME (59 mg, 0.192 mmol, 1 equiv) were combined in 2 mL THF. Sonication for 10 minutes gave a purple suspension that was filtered, washed with Et₂O, and dried under vacuum to give [NiBr₂(**L1**)] as a dark pink solid.

¹H NMR (500 MHz, CDCl₃ (paramagnetic)): δ 73.78 (s, $\Delta v_{1/2}$ = 60 Hz, 2H, **L1**), 25.28 (s, 2H, **L1**), 24.71 (s, 2H, **L1**), 9.63 (s, 4H, **L1**-mes), 4.94 (s, 12 H, *ortho*-CH₃), 4.33 (br, $\Delta v_{1/2}$ = 70 Hz, 6 H, *para*-CH₃).
EA Calcd. C, 52.69; H, 4.06; N, 4.03; Found: C, 52.31; H, 4.41; N, 4.05.
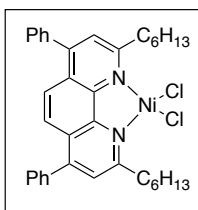
[NiCl₂(L2)]

In a 12 mL vial, **L2** (200.6 mg, 0.401 mmol, 1 equiv) and NiCl₂·DME (88.0 mg, 0.401 mmol, 1 equiv) were combined in 3 mL THF. Stirring at room temperature for 45 minutes followed by sonication for 10 minutes gave a purple suspension. This was combined with 10 mL pentane then filtered, washed with further Et₂O (3 x 5 mL), and dried under vacuum to give [NiCl₂(**L2**)] as a pink solid (234.8 mg, 93% yield).

¹H NMR (400 MHz, CDCl₃): δ 82.40 (s, 2H, **L2**), 30.26 (br, $\Delta v_{1/2}$ = 450 Hz, 4H, CH₂), 28.40 (s, 2H, **L2**), 17.89 (s, 4H) , 9.43 (m, 4H, **L2**-Ph), 8.75 (m, 2H, **L2**-Ph), 7.23 (m, 4H, **L2**-Ph), 7.08 (s, 4H, CH₂), 3.95(s, 4H, CH₂), 2.73 (s, 4H, CH₂), 1.58 (m, 6H, CH₃).
EA Calcd. C, 68.60; H, 6.40; N, 4.44; found: C, 68.09; H, 6.27; N, 4.50.

[NiBr₂(L2)]
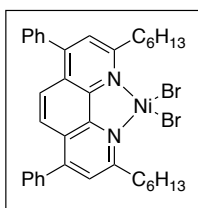
Synthesised following a modified literature procedure.[24]

To a mixture of NiBr₂·3H₂O (99.0 mg, 0.363 mmol, 1 equiv) and **L2** (181.8 mg, 0.363 mmol, 1 equiv) was added 10 mL ethanol. The mixture was stirred under air at 40 °C for 30 minutes, then the purple solid was filtered off and washed with 2 x 10 mL anhydrous ethanol followed by 2 x 10 mL Et₂O. Drying under vacuum gave [NiBr₂(**L2**)] as a pink solid (166.4 mg, 64% yield).

¹H NMR (400 MHz, CDCl₃): δ 80.46 (br, $\Delta v_{1/2}$ = 80 Hz, 2H, **L2**), 29.06 (s, 2H, **L2**), 18.25 (br, $\Delta v_{1/2}$ = 800 Hz, 4H, CH₂), 13.88 (br, $\Delta v_{1/2}$ = 110 Hz, 4H, CH₂), 9.20 (m, 4H, **L2**-Ph), 8.61 (m, 2H, **L2**-Ph), 7.07 (m, 4H, **L2**-Ph), 4.66 (s, 4H, CH₂), 2.74 (s, 4H, CH₂), 2.06 (s, 4H, CH₂), 1.24 (s, 6H, CH₃).
Magnetic susceptibility (Evans method) μ_{eff} = 2.88 μ_B
EA Calcd. C, 60.12; H, 5.61; N, 3.89; Found C: 59.95; H: 5.47; N: 3.99

3.8.1.2. Nickel(I) halide complexes

The four Ni(I)-halide complexes below were synthesised by comproportionation (Scheme S3.1).

L1: R$_1$ = H, R$_2$ = mesityl
L2: R$_1$ = Ph, R$_2$ = hexyl
X = Cl, Br

L1: 78% **5-Cl**, 77% **5-Cl**
L2: 95% **6-Br**, 78% **6-Br**
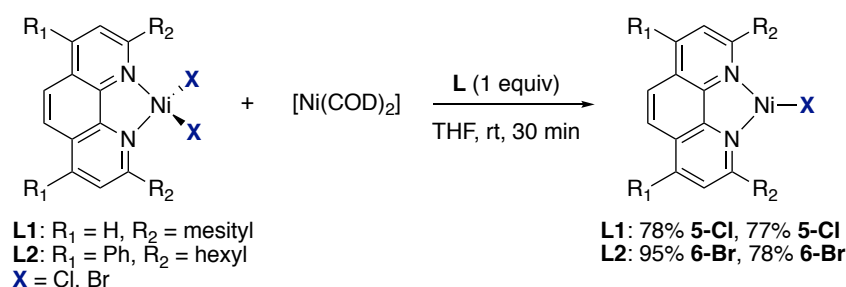
Scheme S3.1. General methods for synthesis of nickel(I) halide complexes.

[(L1)NiCl] (5-Cl)
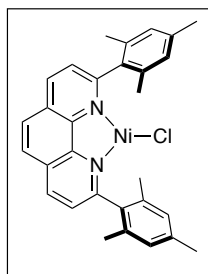
L1 (42.5 mg, 0.102 mmol, 1 equiv), [NiCl$_2$(**L1**)] (55.7 mg, 0.102 mmol, 1 equiv), and [Ni(COD)$_2$] (28.1 mg, 0.102 mmol, 1 equiv) were combined in 2 mL THF. After stirring for 10 min at room temperature, the solution was filtered through glass fibre filter paper. This was washed with an additional 2.5 mL THF. The volatiles were then removed, the solid washed with pentane, then dried under vacuum to give **5-Cl** as a dark blue powder (80 mg, 77%).

^{1}H NMR (500 MHz, toluene-d$_8$): δ 33.38 (br, $\Delta\nu_{1/2}$ = 1200 Hz (approx.), 2H, **L1**), 10.75 (br, $\Delta\nu_{1/2}$ = 300 Hz (approx.), 2H, **L1**), 6.14 (br, $\Delta\nu_{1/2}$ = 850 Hz), 5.03 (br, $\Delta\nu_{1/2}$ = 400 Hz (approx.)), 2.11 (s).
The ^{1}H NMR spectrum is very broad and the signals were not able to be assigned to particular proton environments.
Magnetic susceptibility (Evans method) μ_{eff} = 1.94 μ_B
EPR spectrum simulated with g$_x$ = 2.084, g$_y$ = 2.119, g$_z$ = 2.461. lineshape = 0.8. The continuous wave EPR spectrum was obtained in 2-MeTHF at 9.386 GHz.

Single crystals were grown from toluene/pentane at −35 °C.

Figure S3.1. EPR spectrum of 5-Cl (77K, 2-MeTHF). red = simulated spectrum.

[(L1)NiBr] (5-Br)
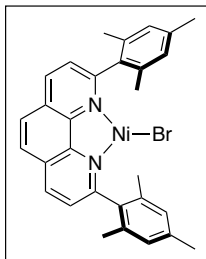
L1 (52.7 mg, 0.127 mmol, 1 equiv), [NiBr$_2$(**L1**)] (80.4 mg, 0.127 mmol, 1 equiv), and [Ni(COD)$_2$] (28.1 mg, 0.127 mmol, 1 equiv) were combined in 4 mL THF. After stirring for 15 min at room temperature, the solution was filtered through glass fibre filter paper. This was washed with an additional 1 mL THF. The volatiles were then removed, the solid washed with pentane, then dried under vacuum to give **5-Br** as a dark blue powder (109.7 mg, 78%).

^{1}H NMR (500 MHz, toluene-d$_8$): δ 33.38 (br, $\Delta v_{1/2}$ = 1400 Hz (approx.), **L1**), 10.75 (br, $\Delta v_{1/2}$ = 255 Hz, **L1**), 6.14 (br s), 5.03 (br, $\Delta v_{1/2}$ = 360 Hz), 2.28 (br s).
The ^{1}H NMR spectrum is very broad and the signals were not able to be assigned to particular proton environments.
Magnetic susceptibility (Evans method) μ_{eff} = 1.87 μ_B
EPR spectrum simulated with g$_x$ = 2.093, g$_y$ = 2.129, g$_z$ = 2.469. lineshape = 1. The continuous wave EPR spectrum was obtained at 9.389 GHz.
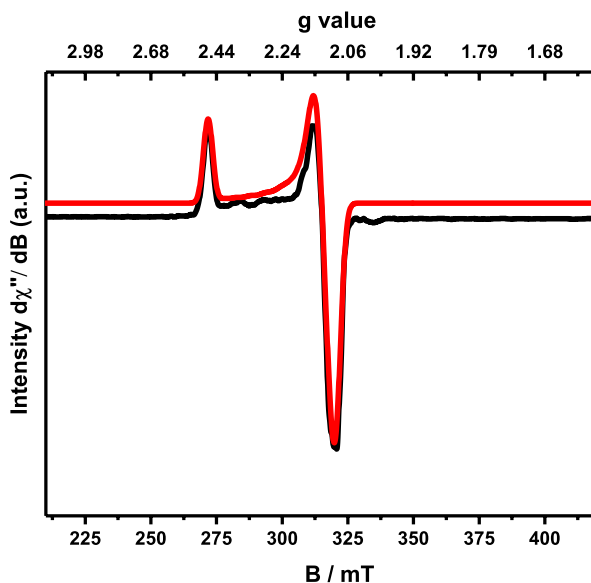
Figure S3.2. EPR spectrum of 5-Br (77 K, 2-MeTHF). red = simulated spectrum.

[(L2)NiCl] (6-Cl)
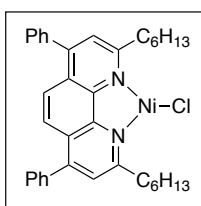
L2 (35.4 mg, 0.0707 mmol, 1 equiv), [NiCl$_2$(**L2**)] (44.6 mg, 0. 0707 mmol, 1 equiv), and [Ni(COD)$_2$] (19.5 mg, 0. 0707 mmol, 1 equiv) were combined in 1 mL THF. After stirring for 1 h at room temperature, the solution was filtered through glass fibre filter paper. This was washed with an additional 1 mL THF. Pentane (2 mL) was then added and the solution placed in the freezer (-35 °C) overnight. The solid was filtered off, washed with cold pentane (2 mL), then dried under vacuum to give **6-Cl** as a deep blue crystalline solid (66.2 mg, 78%).

Crystals suitable for X-ray diffraction were obtained from this THF/pentane mixture at −35 ºC.

^{1}H NMR (400 MHz, toluene-d$_8$): δ 37.07 (br, $\Delta v_{1/2}$ = 1500 Hz (approx.), 2H, **L2**), 12.61 (br, $\Delta v_{1/2}$ = 300 Hz, 2H), 8.74 (s, **L2**-Ph), 8.62 (s, **L2**-Ph) [δ(8.74+8.62) = 10H], 5.72 (s, 6H, hexyl signals), 1.29 (br m, 20 H, hexyl signals).
EPR spectrum simulated with g$_x$ = 2.089, g$_y$ = 2.114, g$_z$ = 2.449. lineshape = 0.9. The continuous wave EPR spectrum was obtained at 9.384 GHz.
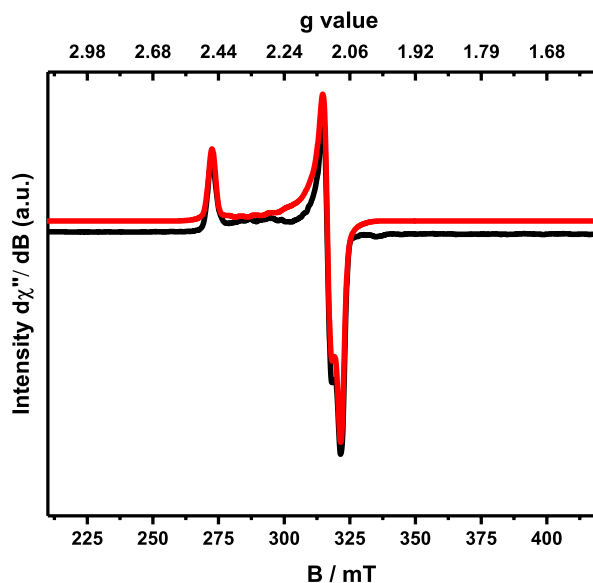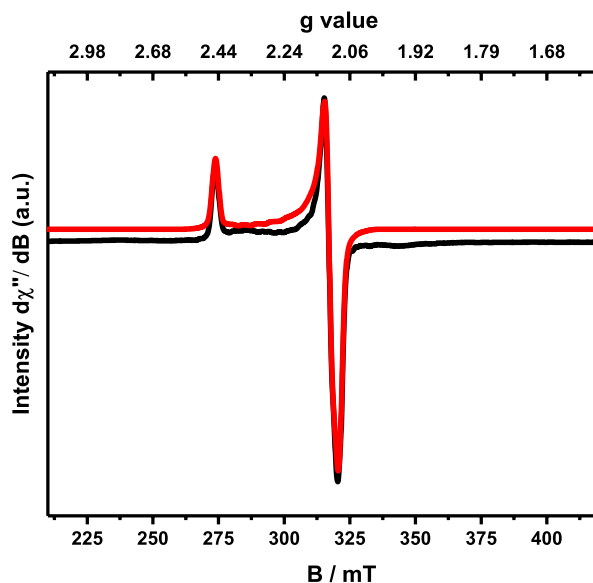
Figure S3.3. EPR spectrum of 6-Cl (77 K, 2-MeTHF). red = simulated spectrum.

[(L2)NiBr] (6-Br)
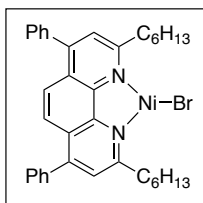
L2 (91.8 mg, 0.183 mmol, 1 equiv), [NiBr$_2$(L2)] (131.9 mg, 0.183 mmol, 1 equiv), and [Ni(COD)$_2$] (50.44 mg, 0.183 mmol, 1 equiv) were combined in 3 mL THF. After stirring for 40 min at room temperature, the solution was filtered through glass fibre filter paper. This was washed with an additional 2 mL THF. The volatiles were then removed, the solid washed with pentane, then dried under vacuum to give 6-Br as a dark blue powder (224 mg, 95%).

^{1}H NMR (400 MHz, toluene-d$_8$): δ 35.81 (very broad s, $\Delta v_{1/2}$ = 1500 Hz (approx.)), 12.40 (br, $\Delta v_{1/2}$ = 215 Hz, 2H, L2), 8.64 (s, L2-Ph), 8.50 (s, $\Delta v_{1/2}$ = 1500 Hz, L2-Ph) [δ(8.74+8.62) = 8H], 5.79 (s, 5H), 1.25 (m). Some signals are extremely broad.

EPR spectrum simulated with g$_x$ = 2.090, g$_y$ = 2.126, g$_z$ = 2.458. lineshape = 1. The continuous wave EPR spectrum was obtained at 9.390 GHz.
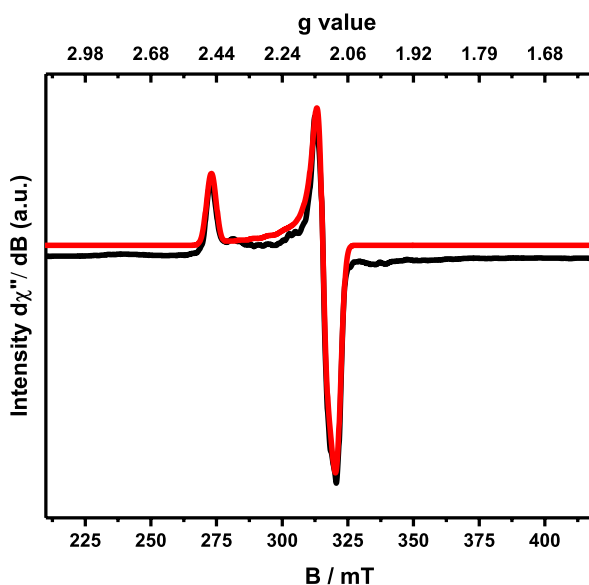
Figure S3.4. EPR spectrum of 6-Br (77 K, X-band, 2-MeTHF). red = simulated spectrum.

3.8.1.3. Nickel(I) alkyl complexes

[(L1)Ni(CH₂tBu)] (7a)
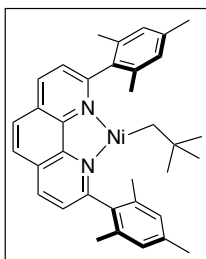
A suspension of **5-Br** (7.8 mg, 0.014 mmol, 1 equiv) in 1.5 mL Et$_2$O was cooled to −35 ºC. A solution of neopentylMgBr (140 μL, 0.2 M in THF, 2 equiv) was then added. The vial was agitated until the dark blue **5-Br** had disappeared. The deep green reaction mixture was filtered through glass fibre filter paper to remove unreacted **5-Br** and some MgBr$_2$, then dioxane (200 μL) was added to precipitate the magnesium salts. The cloudy solution was placed in the glovebox freezer for 10 minutes (−35 ºC) then filtered through 1.5 cm of celite in a pipette. Volatiles were removed then the dark green residue was extracted with 3 mL pentane. The pentane extracts were filtered through celite, then pentane was removed to give **7a** as a dark green solid (3.9 mg, 50%).

Single crystals were obtained from an Et$_2$O/pentane mixture at −35 ºC.

¹H NMR (500 MHz, toluene-d$_8$): δ 55.35 (br, $\Delta v_{1/2}$ = 1500 Hz (approx.), **L1**), 43.97 (br, $\Delta v_{1/2}$ = 1700 Hz (approx.), **L1**), 13.68 (br, $\Delta v_{1/2}$ = 185 Hz), 10.74 (br, $\Delta v_{1/2}$ = 2000 Hz (approx.)), 6.82 (br, $\Delta v_{1/2}$ = 650 Hz (approx.)), 2.06 (br, $\Delta v_{1/2}$ = 250 Hz (approx.)).
The broad and overlapping signals between 0–10 ppm precluded assignment.

EPR spectrum simulated with $g_x = 2.065$, $g_y = 2.145$, $g_z = 2.519$. lineshape = 0.95. The continuous wave X-band EPR spectrum was obtained at 9.390 GHz.

A small amount of **5-Br** is visible as a shoulder on the right-hand side of g_z in the black **7a** spectrum.
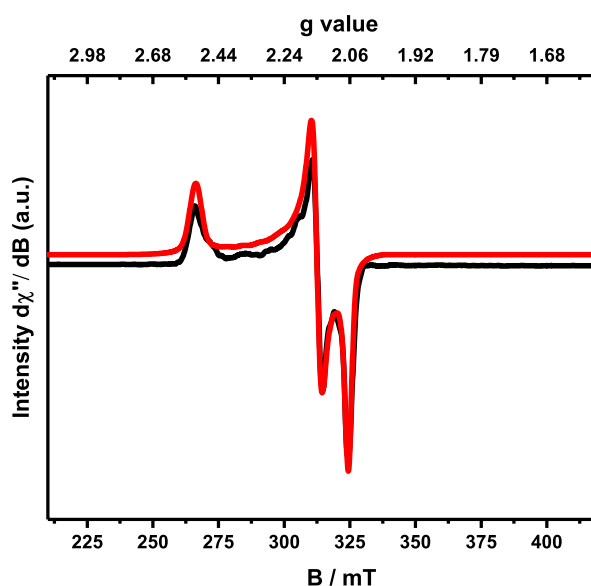
Figure S3.5. EPR spectrum of isolated 7a (77 K, X-band, 2-MeTHF). red = simulated spectrum.

3.8.2. In situ synthesis of Ni(I)-alkyl complexes

3.8.2.1.   **L1** complexes

neopentyl (7a)

5-Br (5.0 mg, 0.0098 mmol, 1 equiv) was suspended in 1 mL 2-MeTHF. A solution of neopentylmagnesium bromide (145 µL, 0.029 mmol, 3 equiv) was then added and the vial agitated briefly to ensure reaction of the **5-Br**. The resulting deep green **7a** solution was transferred to an EPR tube.

EPR spectrum simulated with $g_x = 2.065$, $g_y = 2.145$, $g_z = 2.519$. lineshape = 0.95. The continuous wave X-band EPR spectrum was obtained at 9.385 GHz.

Figure S 3.6. EPR spectrum of in situ generated 7a (77 K, X-band, 2-MeTHF). red = simulated spectrum.

neosilyl (7b)

5-Cl (1.36 mg, 0.0027 mmol, 1 equiv) was suspended in 0.8 mL 2-MeTHF. A solution of neosilylmagnesium chloride (15 μL, 0.0081 mmol, 3 equiv) was then added and the vial agitated briefly to ensure reaction of the **5-Cl**. The resulting deep green **7b** solution was transferred to an EPR tube.

EPR spectrum simulated with $g_x = 2.071$, $g_y = 2.142$, $g_z = 2.526$. lineshape = 1. The continuous wave EPR spectrum was obtained at 9.390 GHz.

Figure S3.7. EPR spectrum of in situ generated 7b (77 K, X-band, 2-MeTHF). red = simulated spectrum.

benzyl (7c)

5-Cl (3.1 mg, 0.0060 mmol, 1 equiv) was suspended in 1 mL 2-MeTHF and cooled for 30 minutes in cold well of the glove box (<-100 ºC). A solution of benzylmagnesium chloride (76 μL, 0.018 mmol, 3 equiv) was then added and the vial agitated briefly to ensure reaction of the **5-Cl**. The resulting deep green solution was transferred to a chilled EPR tube that had been placed inside an aluminium block in the cold well. This was removed from the glovebox and the tube frozen in liquid nitrogen.

EPR spectrum in Figure S3.8 simulated with $g_x = 2.071$, $g_y = 2.133$, $g_z = 2.515$. lineshape = 1. The continuous wave X-band EPR spectrum was obtained at 9.389 GHz.

Figure S3.8. EPR spectrum of in situ generated 7c (77 K, X-band, 2-MeTHF). red = simulated spectrum.

3.8.2.2.   **L2** complexes

neopentyl (8a)

6-Br (3.5 mg, 0.0055 mmol, 1 equiv) was suspended in 1 mL 2-MeTHF and cooled for 30 minutes in cold well of the glove box (<-100 ºC). A solution of neopentylMgBr (81 μL, 0.016 mmol, 3 equiv) was then added, the vial agitated briefly, then the deep green solution was transferred to a chilled EPR tube placed inside an aluminium block that had been kept in the cold well. This was removed from the glovebox then the tube frozen in liquid nitrogen.

EPR spectrum in Figure S3.9 simulated with $g_x = 2.074$, $g_y = 2.138$, $g_z = 2.506$. lineshape = 1. The continuous wave X-band EPR spectrum was obtained at 9.385 GHz.
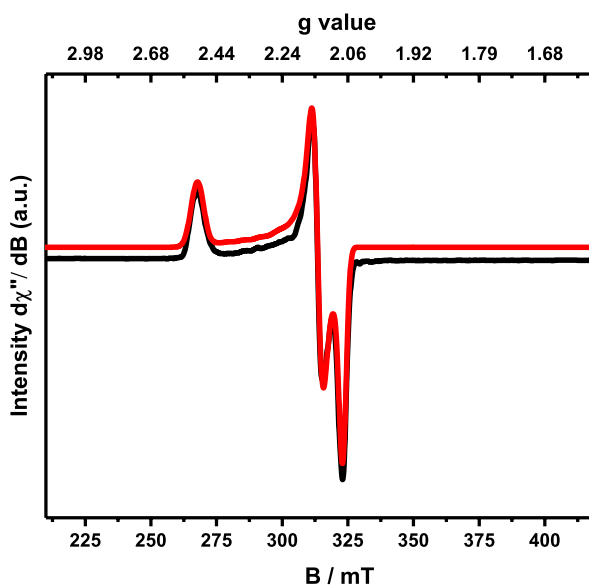
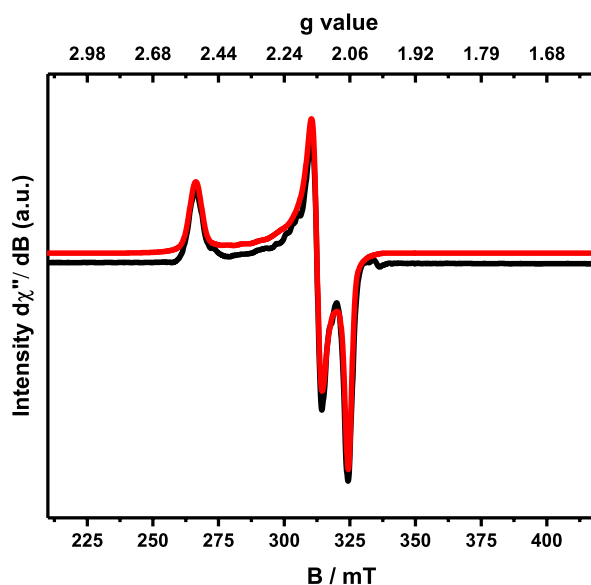**Figure S3.9. EPR spectrum of in situ generated 8a (77 K, X-band, 2-MeTHF). red = simulated spectrum.**

neosilyl (8b)

6-Cl (2.2 mg, 0.0037 mmol, 1 equiv) was suspended in 1 mL 2-MeTHF and cooled for 30 minutes in cold well of the glove box (< −100 ºC). A solution of neosilyllithium (53 μL, 0.011 mmol, 3 equiv) was then added and the vial agitated briefly to ensure reaction of the **6-Cl**. The resulting deep green **8b** solution was transferred to a chilled EPR tube placed inside an aluminium block that had been kept in the cold well. This was removed from the glovebox and the tube frozen in liquid nitrogen.

EPR spectrum in Figure S3.10 simulated with g_x = 2.076, g_y = 2.136, g_z = 2.511. lineshape = 1. The continuous wave X-band EPR spectrum was obtained at 9.387 GHz.
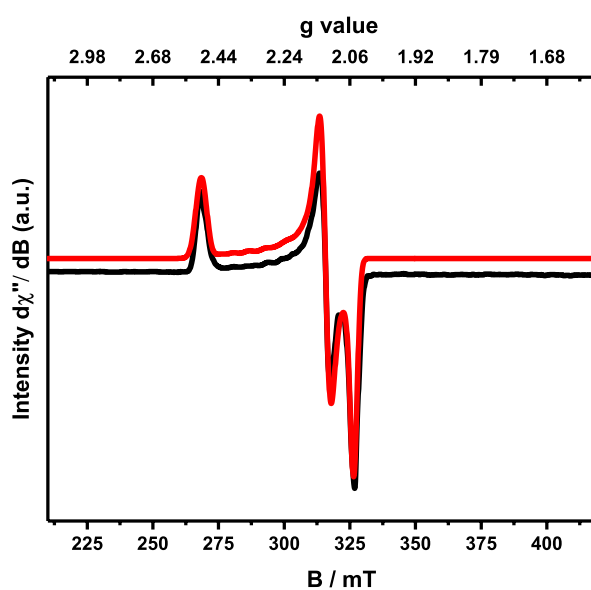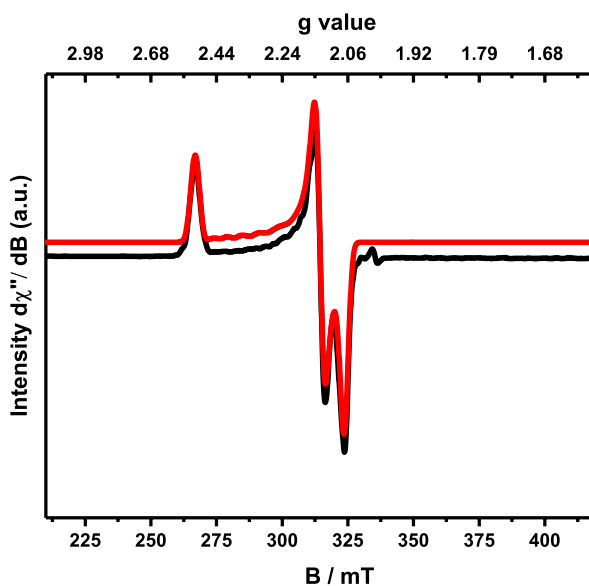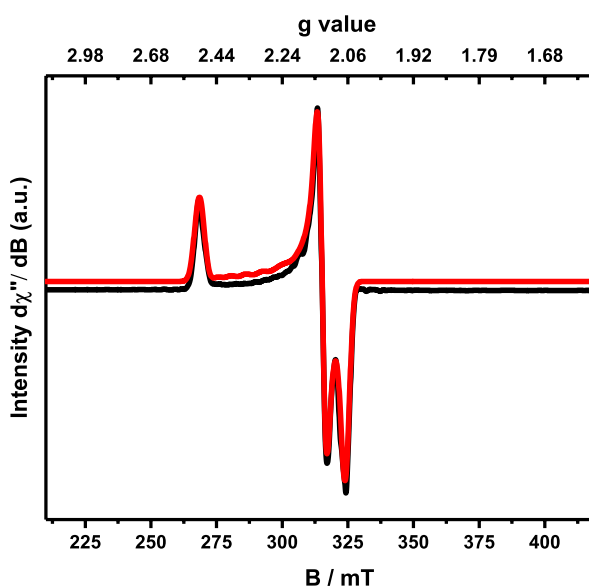

Figure S3.10. EPR spectrum of in situ generated 8b (77 K, X-band, 2-MeTHF). red = simulated.

benzyl (8c)

6-Cl (2.4 mg, 0.0040 mmol, 1 equiv) was suspended in 1 mL 2-MeTHF and cooled for 30 minutes in cold well of the glove box (< -100 ℃). A solution of benzylmagnesium chloride (50 μL, 0.012 mmol, 3 equiv) was then added and the vial agitated briefly to ensure reaction of the **6-Cl**. The resulting deep green solution was transferred to a chilled EPR tube placed inside an aluminium block that had been kept in the cold well. This was removed from the glovebox and the tube frozen in liquid nitrogen.

EPR spectrum in Figure S3.11 was not simulated. The continuous wave X-band EPR spectrum was obtained at 9.387 GHz.
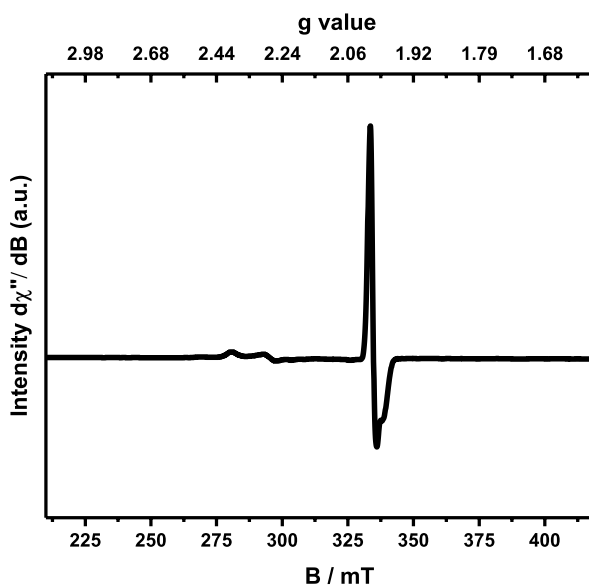
Figure S3.11. EPR spectrum of attempted synthesis of 8c (77 K, X-band, 2-MeTHF).

3.8.3. Nickel(I) carboxylate complexes

Synthesis via anion metathesis

5-Cl (6.2 mg, 0.012 mmol, 1 equiv) and KO_2CCH_2tBu (**9**) (3.74 mg, 0.024 mmol, 2 equiv) were suspended in 2-MeTHF (1 mL) and stirred at room temperature for 30 minutes. After this time, a 0.4 mL aliquot was transferred to an EPR tube. The tube was sealed, taken out of the glovebox and the sample frozen in liquid nitrogen for analysis by EPR spectroscopy (77 K).

When the same reaction was repeated with 3 equiv **9** (45 min) or with 1.5 equiv **9** for 90 min, the resulting EPR signal for **10** was lower in intensity than that of the 2 equiv reaction.

See Figure 3.15 for EPR spectrum simulated with $g_x = 2.062$, $g_y = 2.273$, $g_z = 2.289$. lineshape = 0.9. The continuous wave X-band EPR spectrum was obtained at 9.388 GHz.

3.8.4. Addition of CO_2 to Ni(I)–alkyl complexes

Neopentyl complexes were either generated in situ with 1.3 equiv neopentylMgBr or isolated **7a** was employed. An EPR spectrum of the neopentyl complex was always collected prior to CO_2 addition. Reactions involving **L2** neopentyl complexes were maintained at low temperature by working in the cold well and transferring the EPR tube from the glovebox while it was inside an aluminium block.

Procedure for CO_2 addition

The desired alkyl complex was dissolved in 2-MeTHF or prepared from NiBr and neopentylMgBr inside the glovebox. The solution was then transferred to a resealable EPR tube and frozen in liquid N_2. The atmosphere in the tube was carefully exchanged for 0.1 bar CO_2, then the reaction mixture was thawed to ca. −60 ºC (ethanol dry ice bath, thermometer), briefly agitated, and finally refrozen under vacuum.

Addition of $^{13}CO_2$ was carried out in a similar manner using a 1 L lecture bottle (Sigma Aldrich). Pressure inside the bottle was 1.36 atm.

3.8.5. NMR data of halide complexes
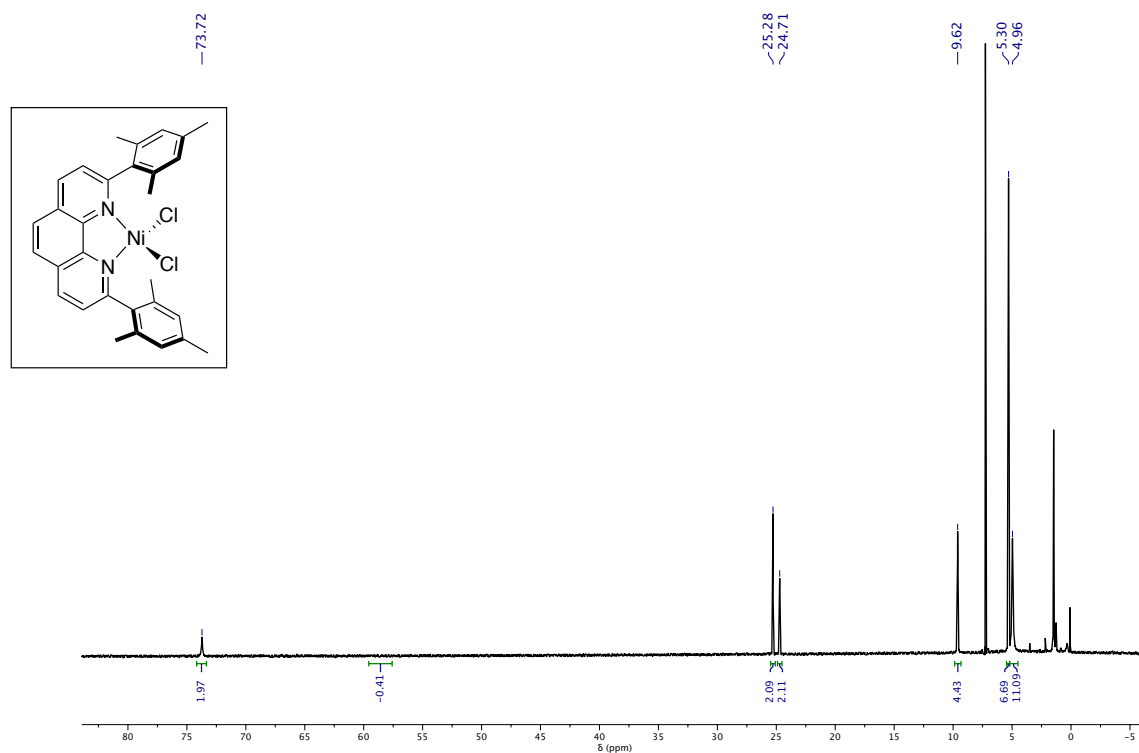
Figure S3.12. ^{1}H NMR (500 MHz, CDCl$_3$) of [NiCl$_2$(L1)].
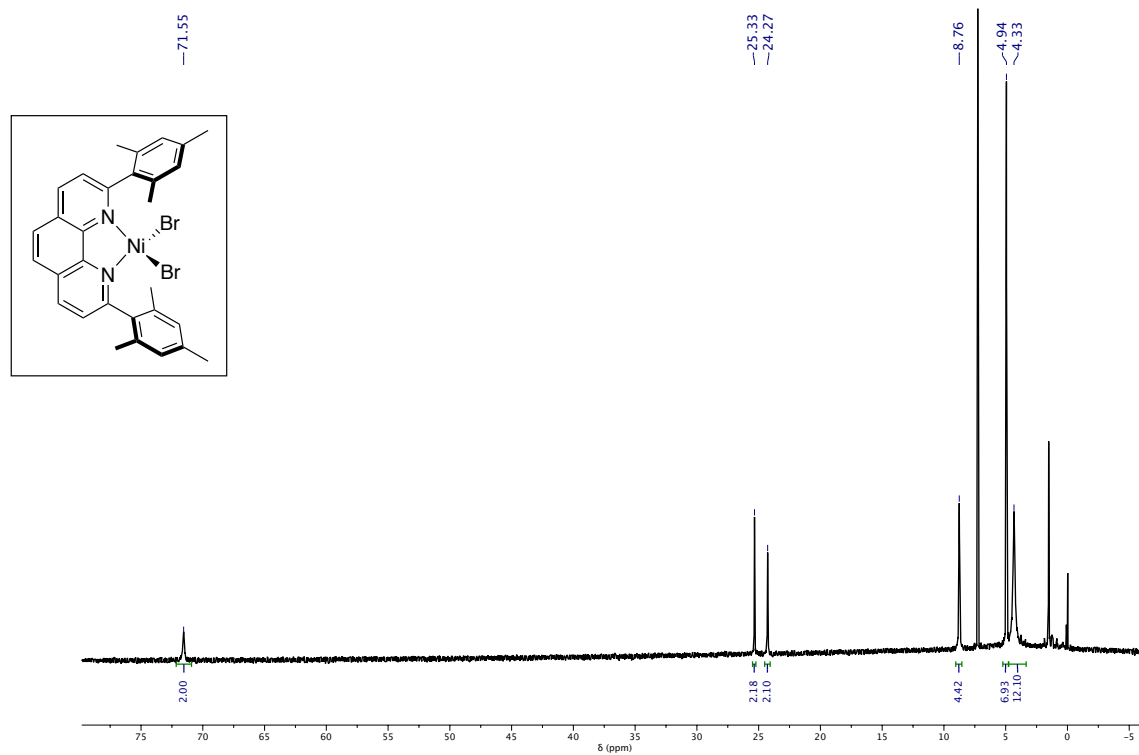
Figure S3.13. ^{1}H NMR (500 MHz, CDCl$_3$) of [NiBr$_2$(L1)].
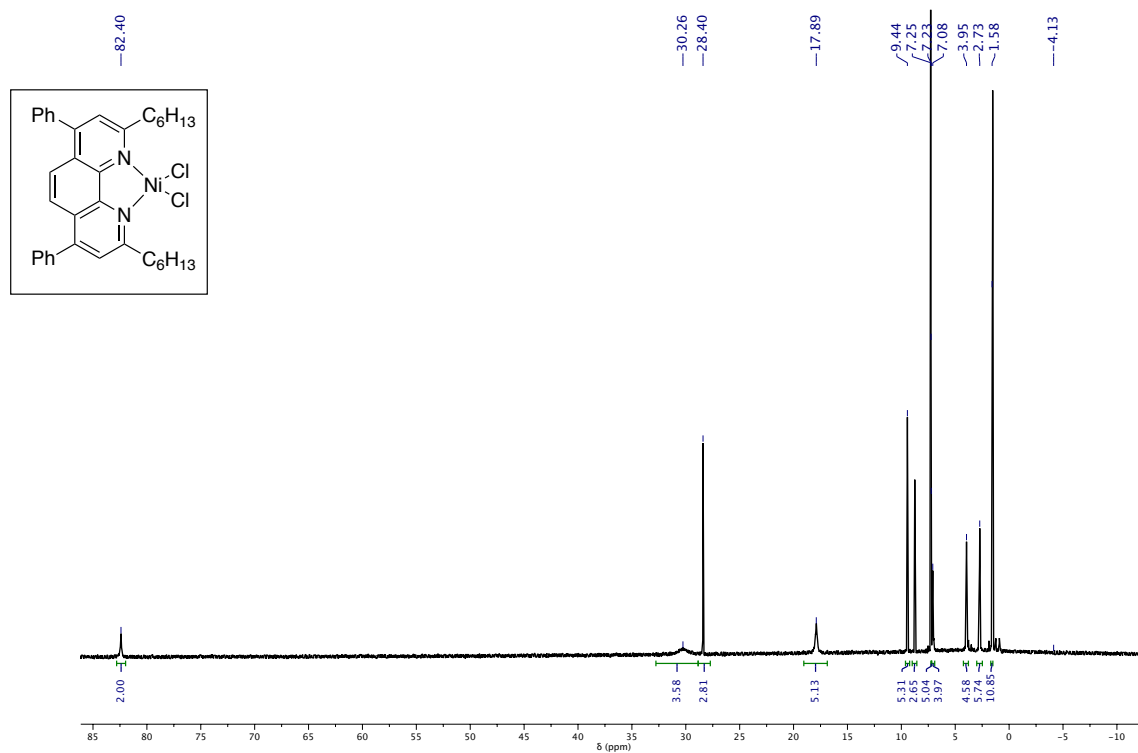
Figure S3.14. ^{1}H NMR (400 MHz, CDCl$_3$) of [NiCl$_2$(L2)].
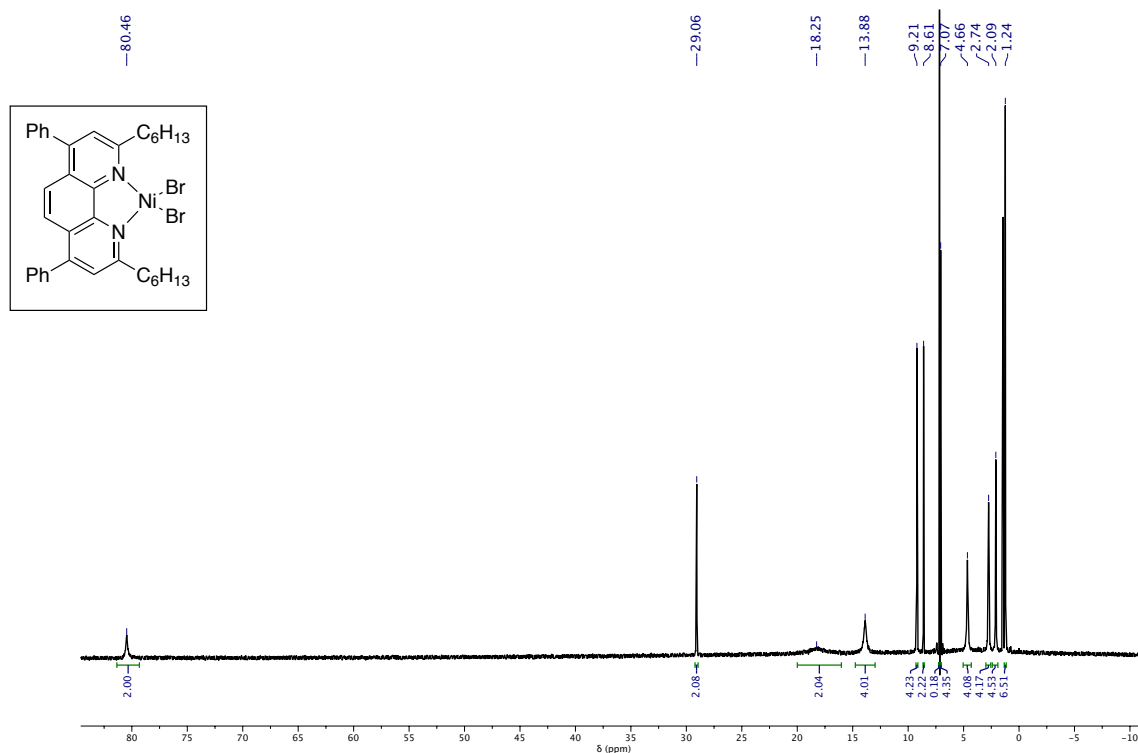
Figure S3.15. ^{1}H NMR (400 MHz, CDCl$_3$) of [NiBr$_2$(L2)].
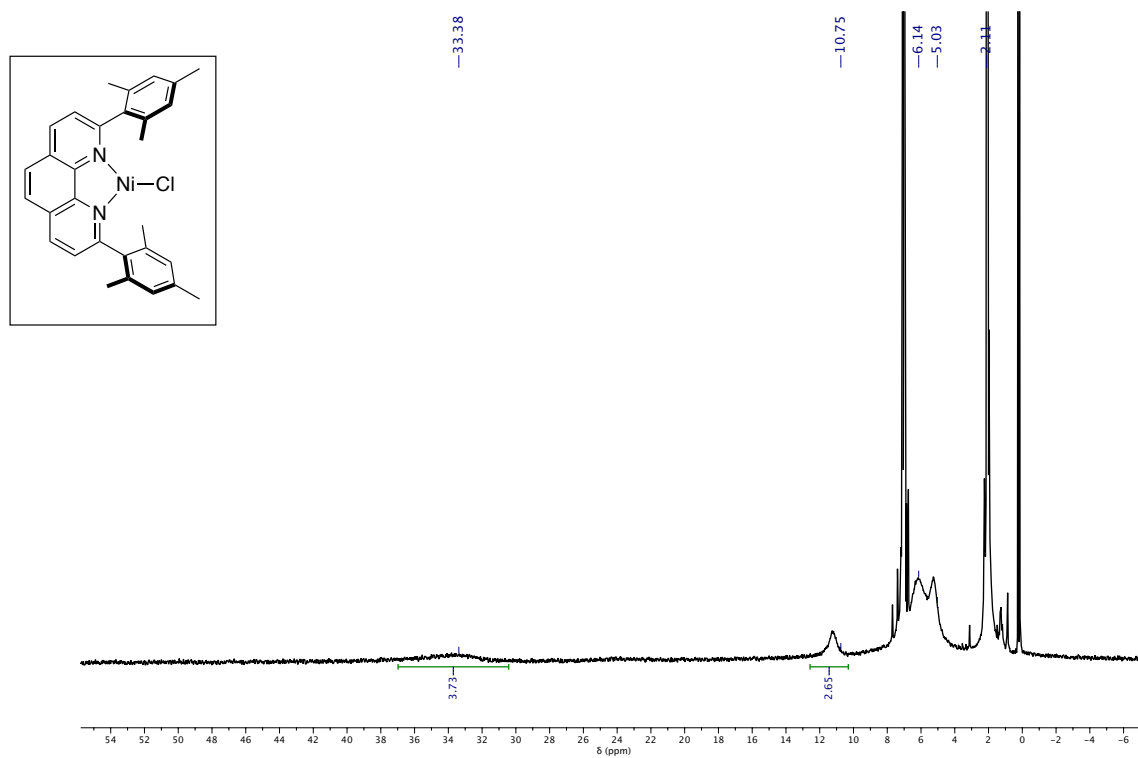
Figure S3.16. ¹H NMR (500 MHz, toluene-d₈) of 5-Cl.
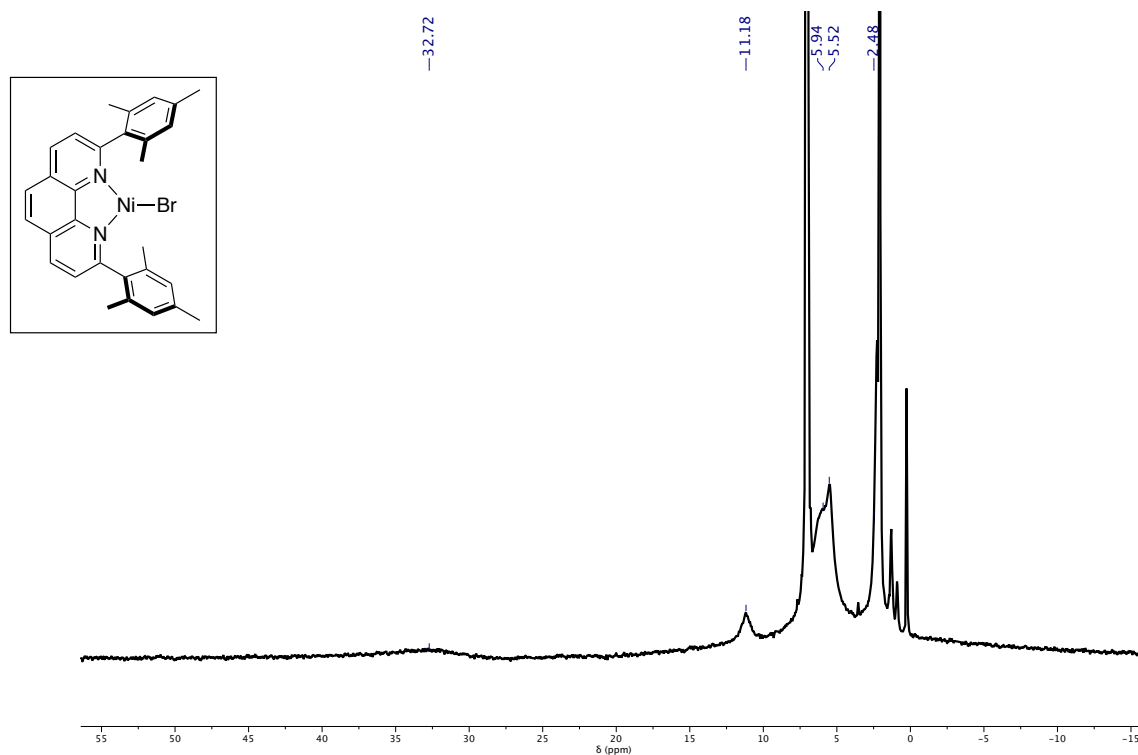
Figure S3.17. ¹H NMR (500 MHz, toluene-d₈) of 5-Br.
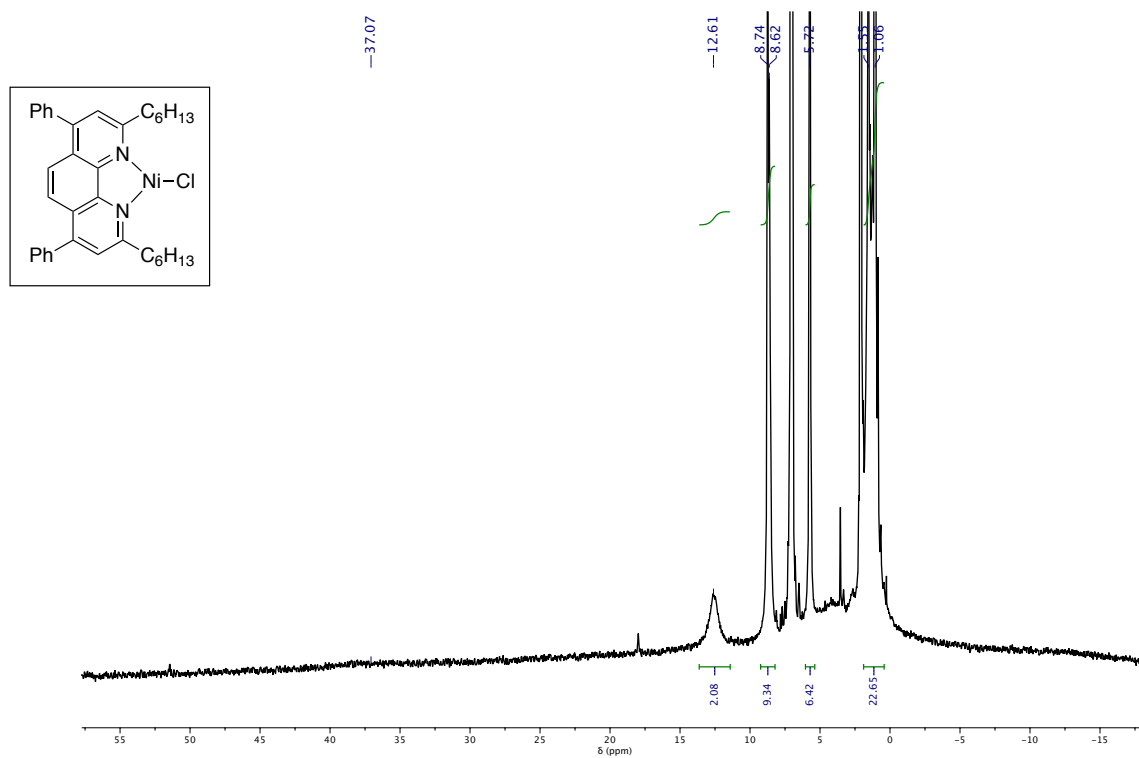
Figure S3.18. ¹H NMR (400 MHz, toluene-d₈) of 6-Cl.
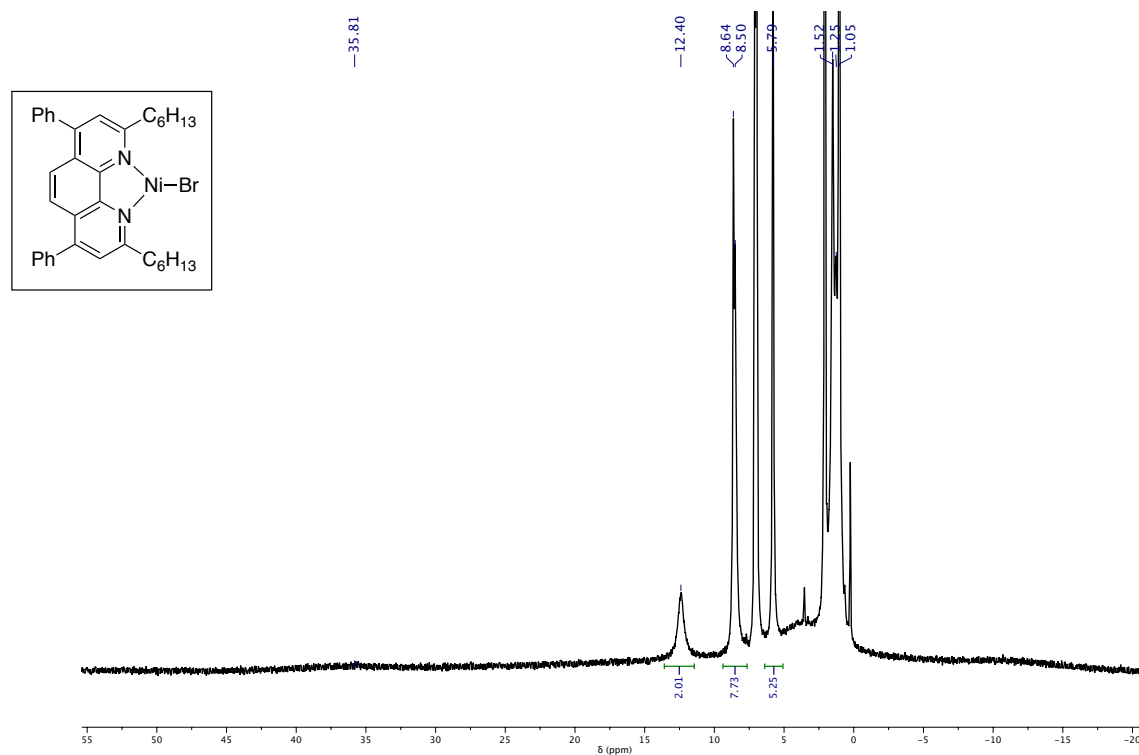
Figure S3.19. ¹H NMR (400 MHz, toluene-d₈) of 6-Br.

3.8.6. NMR data of alkyl complexes
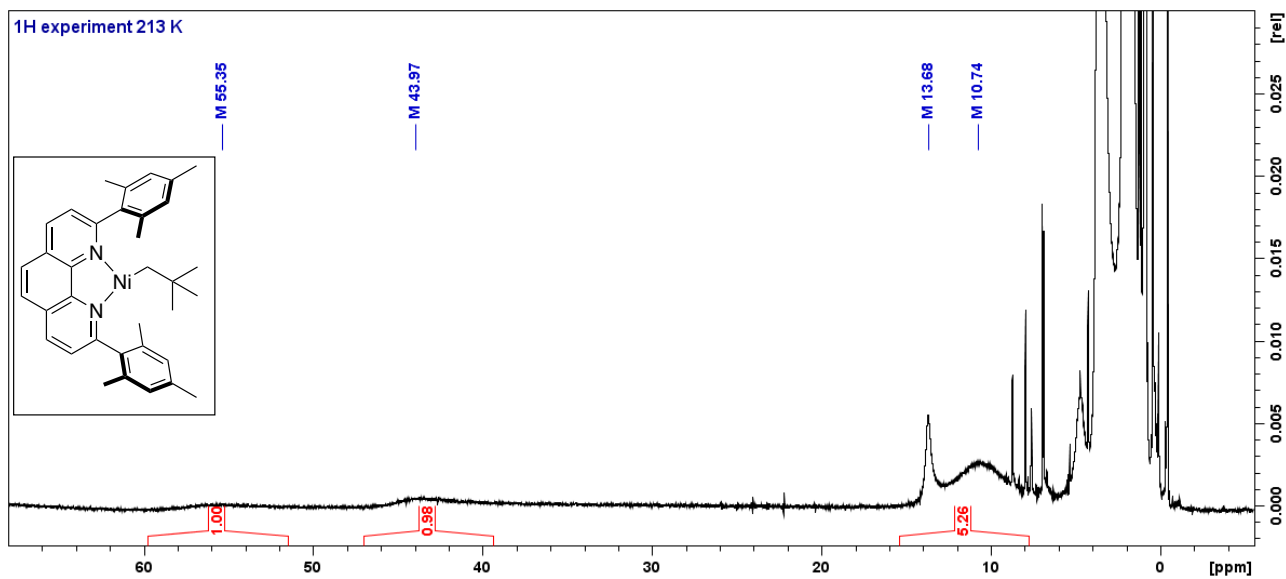
Figure S3.20. ¹H NMR (500 MHz, THF-d₈, 213 K) of 7a.
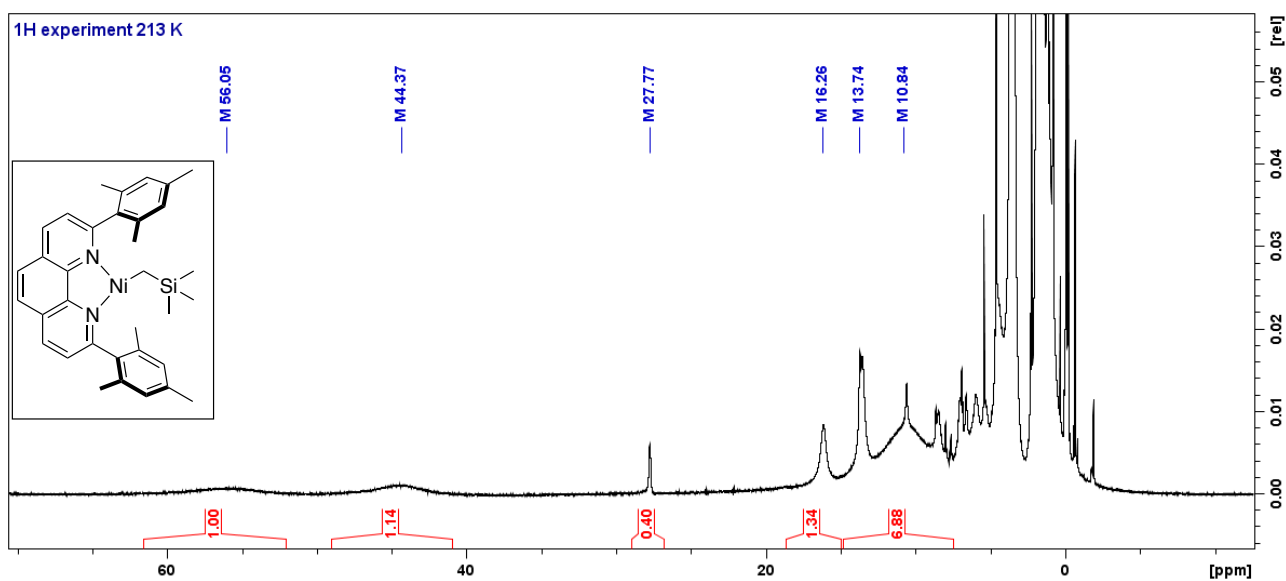
Figure S3.21. ¹H NMR (500 MHz, THF-d₈, 213 K) of 7b.

Figure S3.22. ^{1}H NMR (500 MHz, THF-d$_8$, 213 K) of 8a.

Figure S3.23. ^{1}H NMR (500 MHz, THF-d$_8$, 213 K) of 8b.
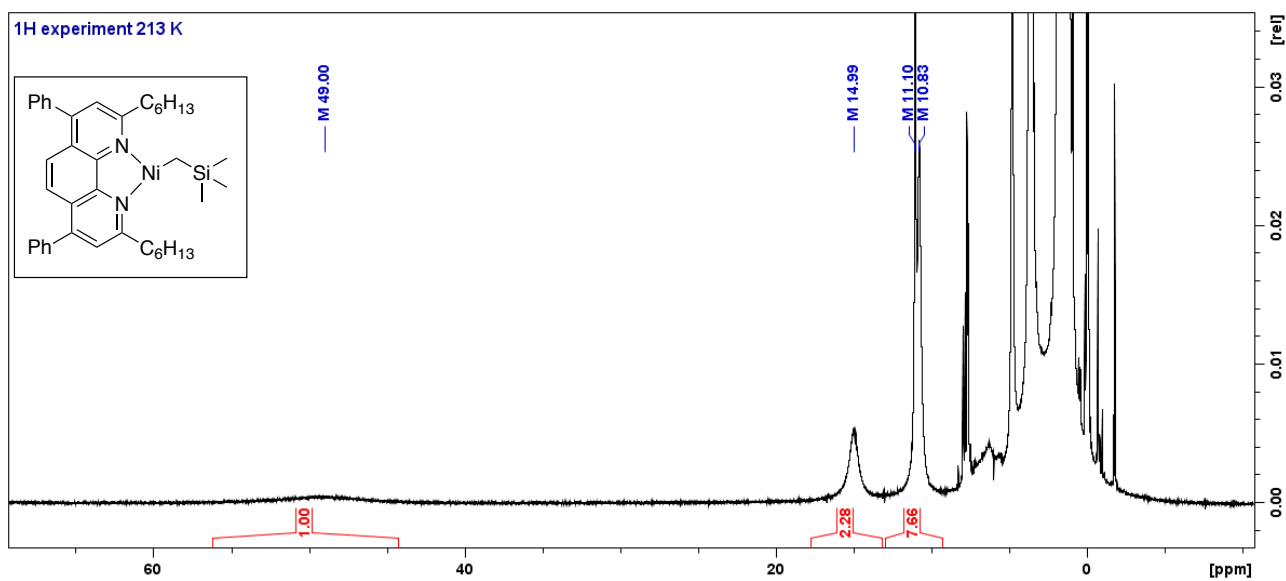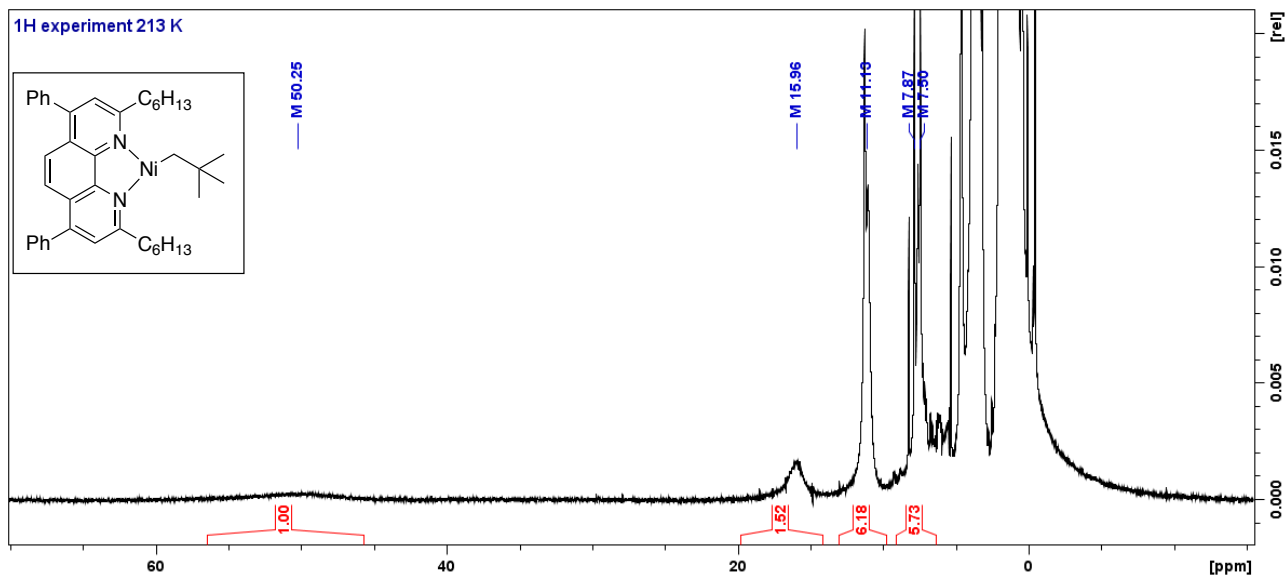
3.8.8. Crystallographic data

Details for 5-Cl (Dr. B. Q. Mercado, Yale University)

Low-temperature diffraction data (ω-scans) were collected on a Rigaku MicroMax-007HF diffractometer coupled to a Dectris Pilatus3R detector with Mo Kα (λ = 0.71073 Å) for the structure of 007c-18081. The diffraction images were processed and scaled using Rigaku Oxford Diffraction software (CrysAlisPro; Rigaku OD: The Woodlands, TX, 2015). The structure was solved with SHELXT and was refined against F^2 on all data by full-matrix least squares with SHELXL (Sheldrick, G. M. Acta Cryst. 2008, A64, 112–122).

All non-hydrogen atoms were refined anisotropically. Hydrogen atoms were included in the model at geometrically calculated positions and refined using a riding model. The isotropic displacement parameters of all hydrogen atoms were fixed to 1.2 times the U value of the atoms to which they are linked (1.5 times for methyl groups). The program SQUEEZE was used to compensate for the contribution of disordered solvents contained in voids within the crystal lattice from the diffraction intensities. This procedure was applied to the data file and the submitted model is based on the solvent removed data. Based on the total electron density found in the voids (325 e/Å^3), it is likely that ~6.5 toluene molecules are present in the unit cell. See "_platon_squeeze_details" in the .cif for more information.

- Sheldrick, G. M. *SHELXTL* Version 2014/7. *http://shelx.uni-ac.gwdg.de/SHELX/index.php*

The crystals of [Ni(**L1**)]$_3$ and [Ni(**L1**)]$_4$ did not diffract well and the data were not of high quality. Further crystallisation attempts are necessary.
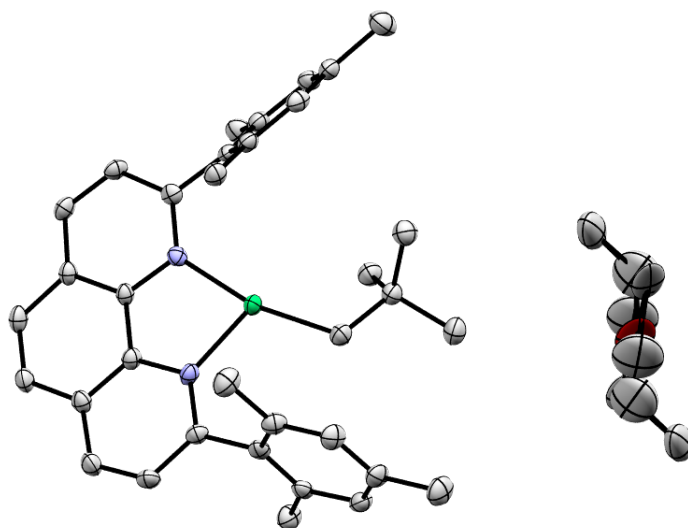
Figure S3.24. ORTEP diagram of 7a showing disordered solvent: 1 molecule of diethyl ether (reflected in data shown in Table S3.1).

Table S3.1. Crystallographic data.

	5-Cl	6-Cl	7a (+Et$_2$O)
Formula	C$_{30}$H$_{28}$ClN$_2$Ni	C$_{36}$H$_{40}$ClN$_2$Ni	C$_{37}$H$_{44}$N$_2$NiO$_{0.5}$
Formula weight	510.70	594.86	583.45
T (K)	93(2)	100(2)	100(2)
Wavelength (Å)	0.71073	0.71073	0.71073
Crystal system	Triclinic	monoclinic	monoclinic
Space group	P-1	P 21/c	P 21/c
a (Å)	18.0288(15)	9.8891(16)	11.0083(6)
b (Å)	18.5080(14)	21.524(3)	32.4592(17)
c (Å)	22.4157(15)	14.620(2)	8.8043(5)
α (deg)	113.701(7)	90	90
β (deg)	90.846(7)	103.029(5)	90.9405(18)
γ (deg)	114.996(8)	90	90
V (Å^3)	6051.7(9)	3031.8(8)	3145.5(3)
Z	8	4	4
Density (calcd.) (Mg/cm^{-3})	1.121	1.303	1.232
μ (mm^{-1})	0.747	0.755	0.646
F(000)	2136	1260	1248
Crystal size (mm^3)	0.200 x 0.150 x 0.070	0.200 x 0.050 x 0.050	0.300 x 0.050 x 0.020
Theta range for data collection (deg)	2.725 to 27.484	2.114 to 26.565	1.954 to 25.076
Index ranges	-21<=h<=23, -24<=k<=24, -28<=l<=29	-12<=h<=12, -26<=k<=26, -18<=l<=13	-12<=h<=13, -38<=k<=37, -10<=l<=8
Reflections collected	116021	19883	41144
Independent reflections	27570 [R(int) = 0.1214]	6057 [R(int) = 0.0687]	5508 [R(int) = 0.1016]
Completeness to theta	99.8% (25.242°)	95.5% (26.565º)	98.7% (25.076)
Absorption correction	Semi-empirical from equivalents	Multi-scan	Multi-scan
Max. and min. transmission	1.00000 and 0.49560	0.74 and 0.49	0.74 and 0.49
Refinement method	SHELXL-2014/7 (Sheldrick, 2014)	Full-matrix least-squares on F^2	Full-matrix least-squares on F^2
Data/restraints/parameters	27570/0/1249	6057/0/363	5508/61/399
Goodness-of-fit on F^2	0.986	1.032	1.055
Final R indices [I>2sigma(I)]	R1 = 0.0452, wR2 = 0.1058	R1 = 0.0526, wR2 = 0.1148	R1 = 0.0521, wR2 = 0.1090
R indices (all data)	R1 = 0.0799, wR2 = 0.1163	R1 = 0.0935, wR2 = 0.1306	R1 = 0.0821, wR2 = 0.1217
Largest diff. peak and hole	0.612 and −0.559 e.Å^{-3}	0.845 and −0.554 e.Å^{-3}	0.556 and -0.439 e.Å^{-3}

Chapter 4.

Ni-catalysed carboxylation of C(sp^2)–S bonds:

Mechanistic studies into C–S cleavage and the role of the Zn.

4.1. Introduction

As discussed in Chapters 1 and 3, mechanistic understanding of Ni-catalysed reductive carboxylation reactions is rather limited. Although employing CO_2 in C–C bond formation is highly attractive due to its abundance and renewability, limitations regarding solvents, catalyst loading, and reductants make obtaining mechanistic understanding important if such reactions are to find widespread use.[1–7] Given mechanistic understanding, improvements to reductive carboxylation systems – such as reducing the amount of Ni required or avoiding toxic solvents – will be possible. With this in mind, a number of mechanistic details of these reactions have been receiving increased attention. In particular, studies are being undertaken into the role of Ni(I) as a key oxidation state,[8–10] and into the interplay between additive, carboxylation, and solvent.[11] An understanding of substrate activation by Ni is also being sought.[12–15] Furthermore, the role of the metal powder reductant, be it Mn(0) or Zn(0), had initially been thought of as just the source of the two electrons necessary for the reductive reaction to occur.[16] However, reports discussed in detail below suggest that it also plays a role as a source of M(II) Lewis acids or even as a source of organometallic species.

This chapter describes a new $C(sp^2)$ carboxylation reaction – the Ni-catalysed reductive carboxylation of arylsulfonium salts shown in Scheme 4.1 – from the perspective of studies that were performed to obtain understanding about some of the questions stated above. The reaction was developed by Tomoyuki Yanagi in the Yorimitsu lab at Kyoto University. Overall, the project has combined the expertise in catalytic C–S functionalisation reactions and carboxylation reactions of the Yorimitsu lab with the Martin lab's expertise in the development of Ni-catalysed reductive carboxylation reactions for a wide variety of substrates.[6,17–20]
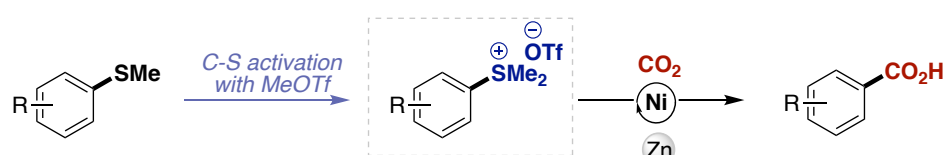
Scheme 4.1. General scheme for the C(sp^2)–S carboxylation reaction studied herein.

4.1.1. Organosulfur chemistry

The development of a reductive carboxylation of arylsulfonium salts is the first link between the rich field of organosulfur chemistry and that of catalytic carboxylation with CO_2. Such a link is attractive for a number of reasons. First, organosulfur compounds are plentiful in nature and therefore lend inspiration (and challenges) to the design of new reactions and biologically active molecules. Sulfur-containing groups are present in enzymes, drugs, in metabolites, fossil fuels, and in natural products such as the marine natural product pateamine (Figure 4.1).[21–23]
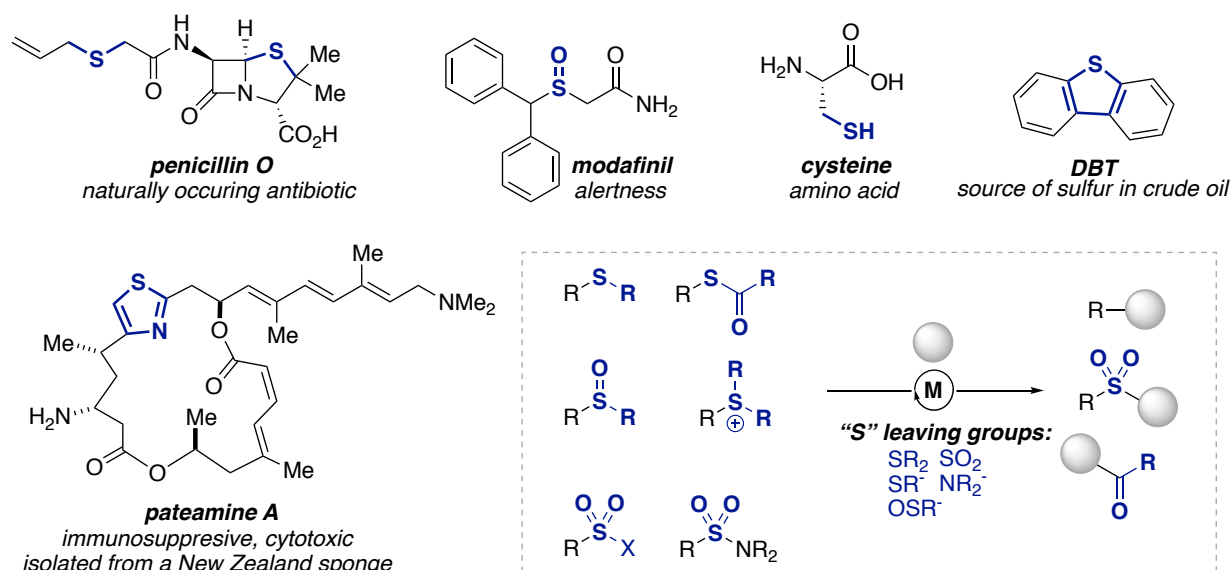
Figure 4.1. Examples of a wide variety of organosulfur groups found in societally-relevant compounds and transition metal-catalysed C–S coupling reactions.

Secondly, sulfur can access a wide range of oxidation states (from −2 to +6) in a variety of functional groups.[24–26] This contrasts with halide atoms, which cannot be transformed in the same way. Thus, the use of organosulfur groups as handles for further functionalisation can open up reactive sites at many locations in molecules. Organosulfur cross-coupling reactions can occur with aryl sulfides, sulfonyl chlorides, sulfones, sulfoxides, thioesters, and sulfonium salts, amongst others.[27]

The Yorimitsu group has extensive experience in organosulfur chemistry, particularly within the area of Pd- and Ni-catalysed C(sp^2)–S functionalisation. Of the coupling partners shown above, the Yorimitsu group has focused the greatest attention on aryl sulfides and arylsulfonium salts.[17–20] Aryl sulfides were the first organosulfur group with which a transition-metal-catalysed C(sp^2)–S functionalisation reaction was reported.[28–30] These two reports were followed within months by the Cu-catalysed coupling of allylic sulfones with Grignard reagents.[31] In 1979, Takei and Wenkert independently reported Ni-catalysed Kumada-Tamao-Corriu (KTC) reactions with substrates containing C(sp^2)–S bonds (Scheme 4.2).[28–30] Takei and co-workers published two reports in the same year regarding the reactions of aryl and allylic sulfides with Grignard reagents in the presence of catalytic amounts of [NiCl₂(PPh₃)₂]. A representative example of this reaction is shown in Scheme 4.2.[29,30] In Wenkert's report – a follow-up to another seminal work on the use of aryl ethers as electrophiles in Ni-catalysed KTC reactions[32] – a range of aryl sulfides, thiols, sulfoxides, and sulfones were reacted with methyl-, phenyl-, and *p*-tolyl-magnesium bromide.[28] Wenkert noted that the aryl sulfide substrates underwent the Ni-catalysed reaction much more readily than aryl ethers, which may be part of the reason why the use of aryl ethers as coupling partners remained rather unexplored for more than two decades, whereas aryl sulfides received somewhat more steady interest after the publication of these reports.[27,33]
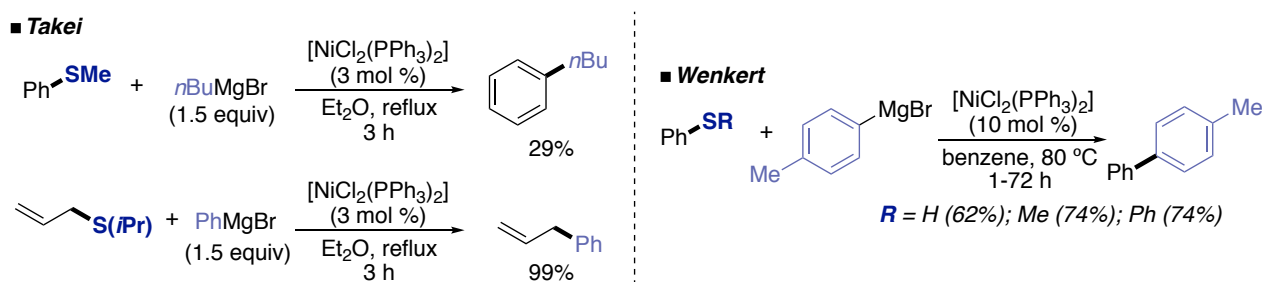
Scheme 4.2. Early examples of Ni-catalysed C(*sp²*)–S functionalisation.[29,30]

Since these reports, organosulfur substrates have been employed in a wide variety of transition metal-catalysed reactions that do not require polar organometallics. For example, Martin developed the Ni-catalysed reduction of aryl sulfides using a silane,[34] Morandi developed Pd- and Ni-catalysed C–S metathesis reactions,[35,36] and Yorimitsu developed the Pd-catalysed borylation of aryl sulfides.[37] During studies to develop aryl sulfide cross-coupling reactions, the Yorimitsu group was puzzled as to why some of these transformations were not generally applicable given that C(*sp²*)–S bond cleavage should not be difficult. The BDE of the C–S bond in thioanisole is 85.3 ± 1.5 kcal mol^{-1}, which is in the range of aryl halides.[38] One hypothesis was that the metal thiolate complex formed after oxidative addition undergoes *slow transmetalation* due to the stability of the M–SR bond. Another hypothesis for the unpredictable success of C(*sp²*)–S functionalisation was that M–SR might form bridging species that are unable to undergo transmetalation.[38] This prompted the Yorimitsu group to investigate the use of arylsulfonium salts as alternative electrophiles. These easy to synthesise and extremely stable salts were first demonstrated in cross-coupling reactions by Liebeskind (Scheme 4.3).[39,40] In this seminal work, Ni- and Pd-catalysed Suzuki, Negishi, and Stille coupling reactions were carried out under mild conditions.[39,41] This set the foundation for the uptake of these substrates as alternative electrophiles in cross-coupling.
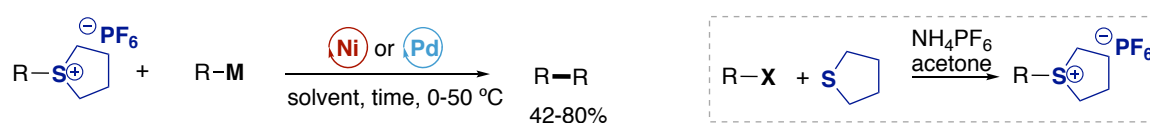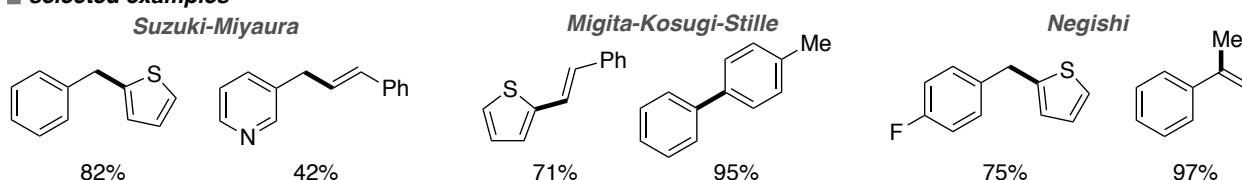
Scheme 4.3. Liebeskind activation of aryl, benzyl, and alkenyl halides to synthesise sulfonium salts, then Suzuki-Miyaura, Migita-Kosugi-Stille, and Negishi coupling reactions.

An activated arylsulfonium group has advantages over the parent sulfide in cross coupling reactions. First, the C–S bond is more electron-poor, facilitating oxidative addition of the metal into this bond. Second, the sulfide leaving group will coordinate much less strongly to the catalyst than the thiolate of a sulfide substrate. These advantages have been exploited by the Yorimitsu group for a number of reactions including the three Pd-catalysed $C(sp^2)$–S functionalisation reactions shown in Scheme 4.4. The use of arylsulfonium salts rather than aryl sulfides in the borylation of $C(sp^2)$–S bonds (Scheme 4.4, middle) allowed the substrate scope to be extended to aldehydes and aryl chlorides, substrates that were not tolerated in the two previously reported aryl sulfide borylation reactions due to the use of a strong base or Rh catalyst.[37,42] In the examples shown in Scheme 4.4, the aryl sulfides were directly converted to sulfonium salts by using a methylating agent. Alternative syntheses include the synthesis used by Liebeskind above,[39] or the conversion of thiols into cyclic phenylsulfonium salts via S_N2 alkylation.[27]
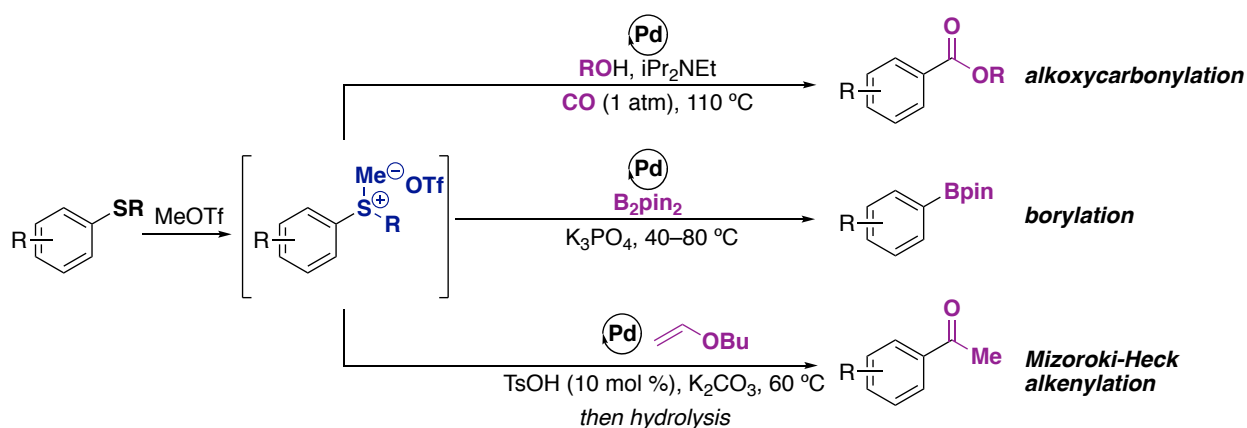
Scheme 4.4. Selected examples of $C(sp^2)$–SR_2^+ functionalisation developed by the Yorimitsu group.[17–19]

Overall, an extension of arylsulfonium salt chemistry to reductive couplings such as reductive carboxylation would not be unexpected given recent interest in broadening the field of cross-electrophile coupling reactions.[43–45] Indeed, although aryl (pseudo)halides have been well-explored in the carboxylation field, no methodologies employing arylsulfonium salts have been reported.

4.1.1. Mechanistic understanding of reductive carboxylation of aryl (pseudo)halides

In Chapter 3, the role of Ni(I) during carboxylation reactions was studied experimentally through the synthesis of Ni(I)–alkyl complexes and their subsequent reactions with CO_2. As already mentioned, Ni(I) is also proposed to be a key oxidation state in the carboxylation of aryl electrophiles and therefore might also be expected to be important in the carboxylation of arylsulfonium salts.[8,10,11,46] During this study, the aim was to investigate the broad mechanistic picture of the C–S carboxylation. Thus, the generally accepted mechanism for the reductive carboxylation of aryl (pseudo)halides shown in Scheme 4.5 was taken as a starting point. Whereas Chapter 3 focused on Ni(I), this chapter will explore C–S cleavage and

the role of the metal powder reductant. The details of the catalytic cycle shown in Scheme 4.5 are discussed in depth in the following sections.
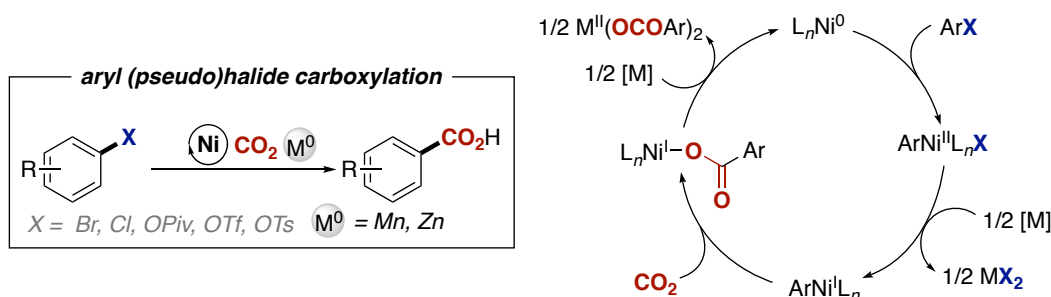
Scheme 4.5. Aryl (pseudo)halide reductive carboxylation and generally accepted catalytic cycle.

4.1.1.1.   Role of Zn(0) and Mn(0) in reductive carboxylation

Although alternatives to Zn(0) or Mn(0) powder reductants, such as organic reductants[11] and photoredox systems,[47–49] now exist, metal powders are still the most commonly employed reductants in reductive carboxylation reactions.[16] Their main task is in forming Ni(0)L_n and Ni(I)L_n species within the catalytic cycle and thereby facilitating the reductive reaction via the overall transfer of two electrons. It should not be overlooked, however, that during reductive steps, Mn(II) or Zn(II) salts are also formed. Whether these are important in facilitating carboxylation has recently begun to attract experimental studies. Reports discussed in detail below suggest that the metal powder also plays a crucial role as a source of M(II) Lewis acids and may even provide a pathway to organometallic RZn or RMn species. Herein, the role of the metal powder in forming Lewis acids, in carrying out anion exchange at M(II), and in forming organometallic species is discussed based on literature evidence.

4.1.1.2.   Lewis acids

Lewis acid additives are often added to catalytic reactions to increase yields and/or selectivities by forming adducts with intermediates in the catalytic cycle.[50] The role of Lewis acids in the insertion of CO_2 into M–C σ bonds has received attention both experimentally and computationally.[11,46,50–52] As mentioned in Chapter 3, Lewis acids are able to facilitate the formation of the new C–C bond in a nucleophilic attack pathway by stabilising the negative charge that builds up on CO_2.

An early DFT investigation into the effect of a Lewis acid on CO_2 insertion that is specific to reductive carboxylation was carried out by Sayyed and Sakaki in 2014.[53] This study focused on the presence of $MgCl_2$ during the carboxylation of benzyl halides.[54] Although some carboxylic acid was obtained in the absence of $MgCl_2$, the yield of the model substrate, *para-t*-butylbenzyl chloride, was boosted from 28% to more than 70% upon addition of this salt.[54] In investigating the role of the $MgCl_2$, the authors took as a starting point the mechanistic proposal for carboxylation that had become accepted by the community: oxidative addition of the benzylic C(sp^3)–Cl bond to form **I**, reduction of the resulting Ni(II) oxidative addition complex to form Ni(I)–benzyl complex **II**, CO_2 insertion at Ni(I), then reduction of the Ni(I)

carboxylate complex **III** with Zn(0) to recover Ni(0) and give a Zn-carboxylate that would be quenched during workup (Scheme 4.6). In both the presence and absence of $MgCl_2$, a mechanistic pathway based on Ni(I) was found to be much lower in energy than that based on Ni(II).[53]
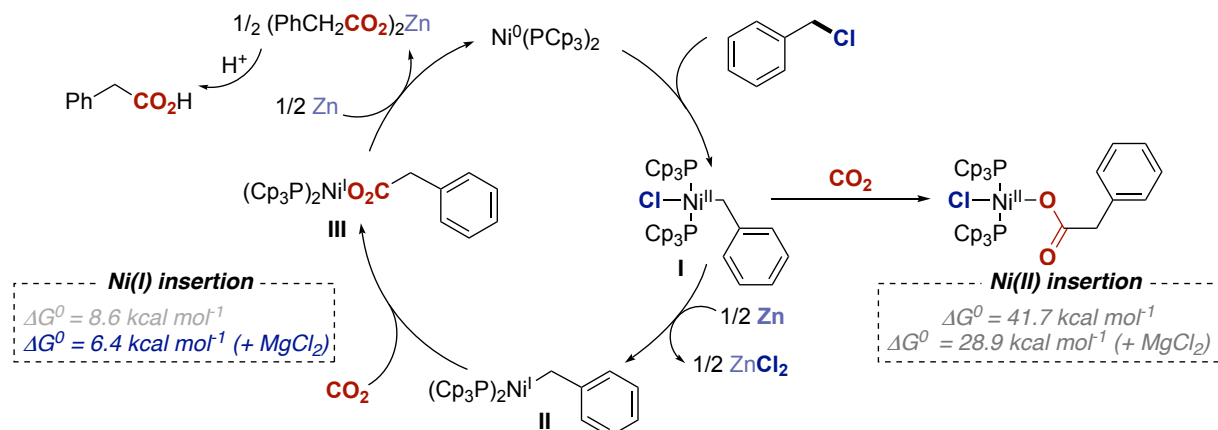
Scheme 4.6. DFT study investigating reductive carboxylation of benzyl halides in the presence and absence of $MgCl_2$.[53]

It is important to highlight the role of the $MgCl_2$ proposed by this study as it might have a bearing on the role of the MX_2 salts that are produced during reduction steps (Scheme 4.7). Upon oxidative addition and one-electron reduction, CO_2 coordinates to the Ni(I)–benzyl species **II** to give a four-coordinate complex. The optimised geometry for the $MgCl_2$ adduct **II-MgCl₂** contained an interaction between one of the O atoms of CO_2 and Mg(II). This interaction was found to be maintained during insertion of the C–O bond into the Ni–C bond and lowered the energy of the insertion transition state by 7.6 kcal mol⁻¹, probably due to the fact that coordination of $MgCl_2$ to CO_2 lowered the energy of the CO_2 π* orbitals. This meant that when charge was transferred from the Ni–benzyl bond in **II-MgCl₂** to the π* orbital during insertion, a smaller overall change in electron density for the benzyl group and for CO_2 resulted. A second aspect to note was that the formation of a Mg(II) carboxylate salt was found to be favoured over the formation of the Zn analogue. The Zn(II) carboxylate is usually invoked during reduction of the Ni(I)–carboxylate by Zn(0) to Ni(0).
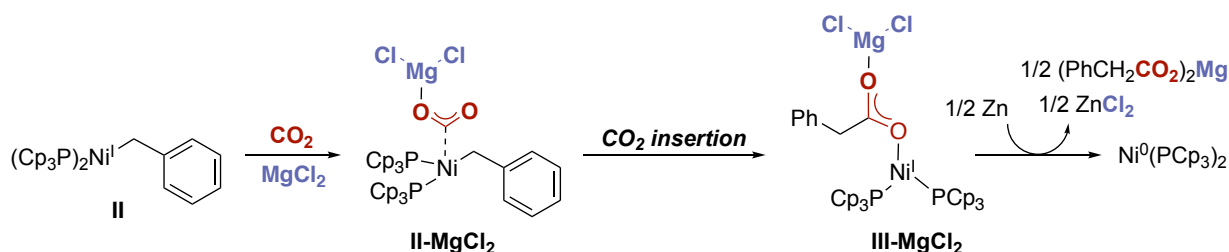
Scheme 4.7. Coordination of $MgCl_2$ aids CO_2 insertion.

The value of obtaining mechanistic information about a transformation is very much on show in a recent report by the Hazari group that probed the Ni-catalysed reductive carboxylation of aryl chlorides reported by Tsuji in 2012.[55,11] Although this reaction had already been studied computationally by Sakaki and co-workers,[8] this was the first detailed experimental study into the role of the reductant, solvent, Ni catalyst, additives, and formation of Ni(I). It resulted in numerous noteworthy findings including lower catalyst loading, the ability to use an organic reductant and the demonstration of a reductive carboxylation reaction in THF rather than an amide solvent (Scheme 4.8).
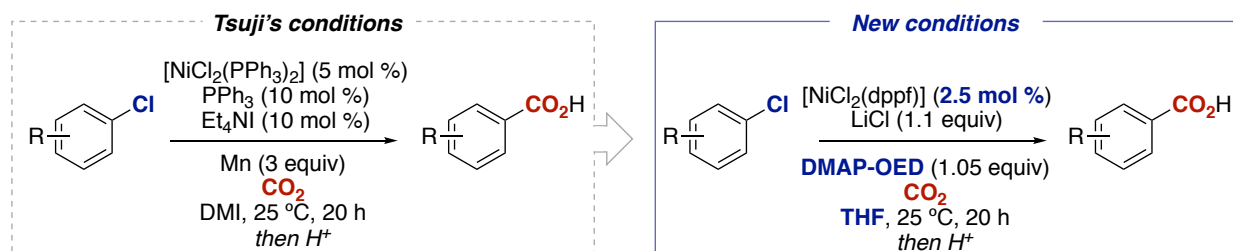
Scheme 4.8. Changes to the original Ar–Cl carboxylation reaction conditions based on mechanistic understanding.

In order to obtain these findings, methodical analysis of all the reaction details was carried out. The first key insight was gained from studying the combination of the precatalyst and reductant (Scheme 4.9). Reduction of a Ni(II) or Ni(I) precatalyst to Ni(0) was assumed to be crucial to activating the substrate and therefore crucial to the beginning of the catalytic cycle. However, when a Ni(0) source was used, the yield dropped from approximately 76% to 51%. This decrease was hypothesised to be due to absence of $MnCl_2$ that would have formed during reduction of the chloride-containing precatalyst. Indeed, using a Ni(0) precatalyst and exogeneous $MnCl_2$ recovered the yield of carboxylic acid (81%). This was the first time that the importance of the MX_2 by-product to catalysis was demonstrated.
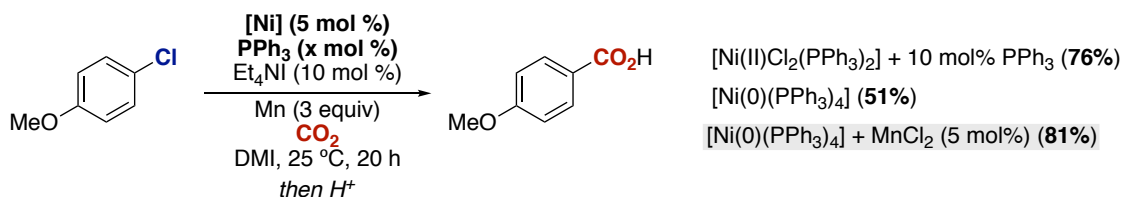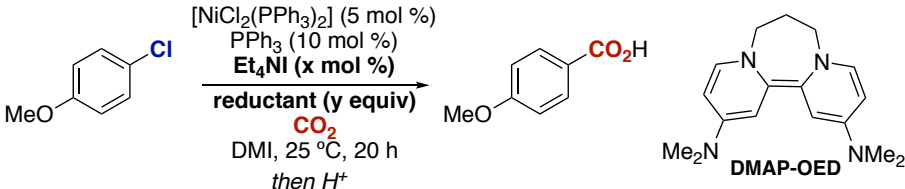
Scheme 4.9. Screening of Ni precatalysts showing beneficial aspect of reduction by-product $MnCl_2$.

Knowing that the Mn powder may be more than just a reductant, the authors moved to investigating different reductants (Table 4.1). Although Zn and Mn powder are typically used with success in cross-electrophile coupling reactions, reductive conditions that do not form stoichiometric amounts of Mn(II) or Zn(II) salts would be attractive for scaled-up reactions. Thus, soluble organic reductants were investigated in the presence and absence of Et$_4$NI (crucial for reduction with heterogeneous reductants).

When DMAP-OED (E = −1.24 V vs SCE[56,57]) and CoCp*$_2$ (E = −1.40 V vs SCE[58]) were employed, no acid was obtained (entries 3 and 4, Table 4.1). However, knowledge about the importance of $MnCl_2$
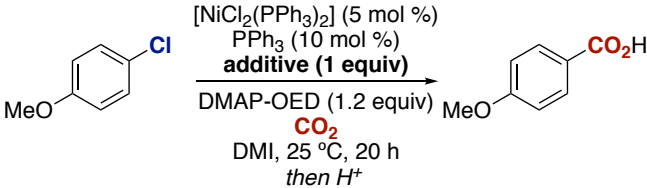
was critical here, as addition of $MnCl_2$ to reactions employing the organic reductant produced the desired carboxylic acid in good yields.

Table 4.1. Screening of reductant showing successful use of DMAP-OED when MgCl₂ was present.

Entry	reductant (y)	x = 0	x = 10	MnCl₂ (1 equiv) (x = 0)
1	Mn (3)	<1	76	86
2	Zn (3)	3	12	35
3	DMAP-OED (1.05)	7	<1	**62**
4	CoCp*₂ (2.1)	36	40	83

With the importance of $MnCl_2$ in mind, other Lewis acids were screened (a selection is shown in Table 4.2). Interestingly, LiCl and LiBr showed excellent activities in promoting the reaction in both DMI and THF. In understanding the interplay between reductant and Lewis acid, the authors were also able to switch the solvent from DMI to THF. This was possible because although it is unable to solubilise $MnCl_2$, THF is able to solubilise the Li^+ salts. Demonstration of successful carboxylation in THF suggests that further screening could allow carboxylic acids to be obtained in solvents that are more attractive in scaled-up processes. By removing Mn/Mn(II) entirely, this experiment also ruled out carboxylation at organomanganese species being an important mechanistic pathway.

Entry	additive	yield (%)
1	MnCl₂	68
2	LiCl	68
3	LiOTf	15
4	LiCl (THF solvent)	77

Table 4.2. Screening of additives and THF.

4.1.1.3. C–S cleavage at group 10 metals

Aside from its relevance to the carboxylation of $C(sp^2)$–S arylsulfonium salts, studying oxidative addition of a C–S bond is of interest to the community due to its industrial and biological relevance. For example, oil refining processes must remove sulfur-containing molecules from crude feedstocks in order

to prevent the formation of SO_2 during their subsequent combustion.[59] The hydrodesulfurisation processes that are employed to do this often involve metal-centred $C(sp^2)$–S cleavage.[60]

Oxidative addition of an aryl sulfide or arylsulfonium salt to Ni has little precedent, contrasting with oxidative addition reactions employing aryl halides that often give predictable reactions and isolable oxidative addition complexes.[61] The first Ni complex derived from $C(sp^2)$–S cleavage and characterised by X-ray diffraction was reported by Wenkert et al. in 1986 (Scheme 4.10-left).[62] This square planar complex was the expected result of two-electron oxidative addition of a $C(sp^2)$–X bond to Ni(0). In the same year, Yamamoto reported the reversible oxidative addition of $C(sp^2)$–SAr bonds to Ni(0) to form a mixture of square planar Ni(II) complexes (Scheme 4.10-right).[63] Recently, this type of reactivity has been harnessed by the Morandi group in Pd- or Ni-catalysed "carbon-sulfur metathesis" reactions, where the reversibility of the $C(sp^2)$–S oxidative addition reaction is key to the efficient formation of the desired C–S-metathesis products.[35,36] Such a reaction allowed the formation of compounds that are difficult to synthesise by other coupling methodologies. In the recent Ni-catalysed example of C–S metathesis, mechanistic studies were carried out and C–S oxidative addition and ligand exchange complexes were synthesised (Scheme 4.10-bottom).[36] The formation of similar C–S oxidative addition complexes can also be carried out by indirect methods such as through reaction of a thiol with a basic Ni–R group or by reaction of a thiolate salt with a Ni–halide bond.[64–66]
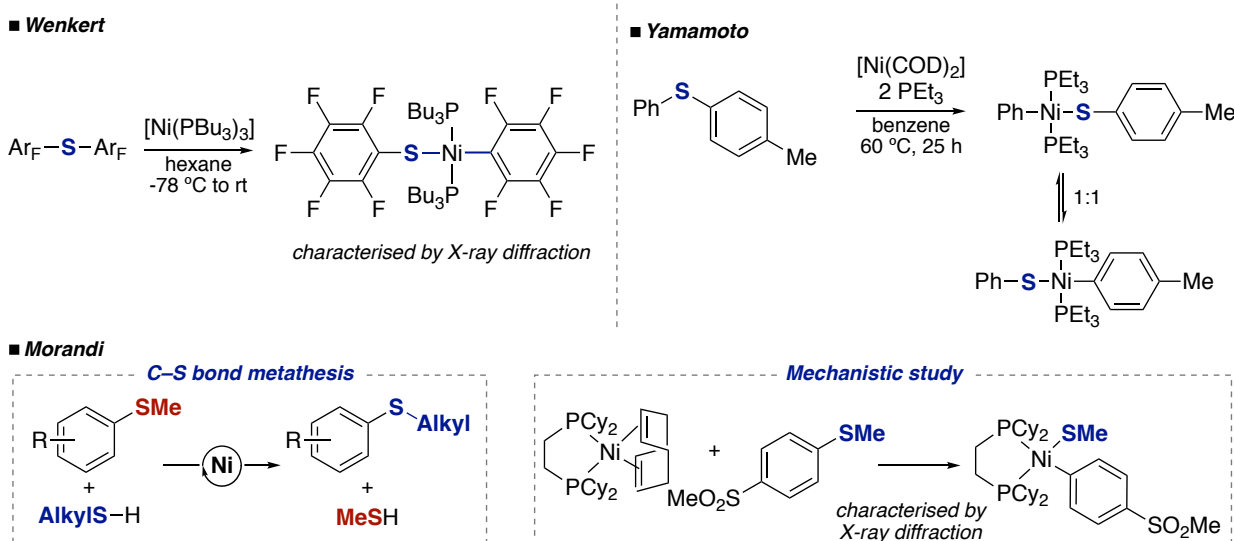
Scheme 4.10. Examples of C–S cleavage of aryl sulfides.[36,62,63]

The majority of investigations into the insertion of Ni(0) into $C(sp^2)$–S bonds have been carried out using phosphine or NHC ligands.[67,60] Oxidative addition reactions involving a low-valent group 10 complex bearing ligands similar to those used for the carboxylation transformation developed by Yorimitsu has only been reported once. Hillhouse demonstrated that cyclic thioethers undergo ring opening with a source of (bipy)Ni(0) (Scheme 4.11).[68] However, a five-membered ring did not possess sufficient ring strain to react with Ni(0).
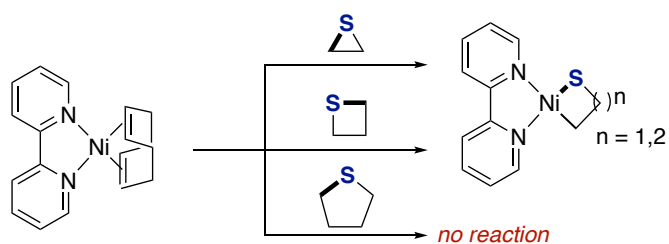
Scheme 4.11. (bipy)Ni(0)-mediated oxidative addition of C–S bonds. Reactions carried out in THF at −5 °C (n=1) or 20 °C (n = 2).

There are no examples of reactions between a group 10 metal complex and an arylsulfonium salt that result in a M–(σ-aryl) bond. In general, the only reported stoichiometric examples of a Ni complex being reacted with a sulfonium salt are when the sulfonium salt is being used an oxidant and source of CF_3^+. In these reactions, the Ni(II) precursor is oxidised to a formally Ni(IV) complex.[69–71] There are also some examples of ylide reactivity.[72,73]

Considering the $C–SR_2^+$ cleavage that presumably occurs in the reductive carboxylation of arylsulfonium salts, and given the small size and lower electronegativity of Ni, the formation of a cationic oxidative addition complex would be expected. There are no reported $Ni–SMe_2$ complexes, but $Pt–SMe_2$ complexes dichlorobis(dimethyl sulfide)platinum(II) and related Pt(II) dimethyl sulfide complexes are stable and widely used Pt(II) precursors.

Although there are no experimental studies of $C(sp^2)–SR_2^+$ cleavage at group 10 metals, there is one DFT study that explores $C(sp^2)–S$ cleavage selectivity in the Pd-catalysed Suzuki-Miyaura coupling of vinyldiphenylsulfonium salts (Scheme 4.12).[74] In this study, it was found that cleavage of the diaryl sulfide always occurred and that coupling between the *vinylic* fragment and the boronic ester was selective (in cases where the *vinyl fragment was bearing a CF₃ group*). In order to rationalise this, the energies of the transition states for the two C–S cleavage pathways – vinyl–S and Ph–S were calculated and compared. In both cases, the Pd(0) was found to coordinate to a π bond – the vinylic alkene or the phenyl ring – prior to insertion. Next, d electrons from Pd are transferred to the π* orbital to begin the formation of the new Pd–C bond. Finally, the $C–SR_2$ bond is weakened as electrons are transferred towards sulfur to form the SR_2 leaving group. The key to $C(sp^2)–S$ cleavage selectivity was therefore the energy of the π* orbital. This was lower for the vinylic substrate and was further lowered by the CF_3 substituent. Overall, insertion of Pd(0) into the Ph–S bond was 11.7 kcal mol^{-1} higher in energy relative to the transition state for favourable vinyl–S insertion.
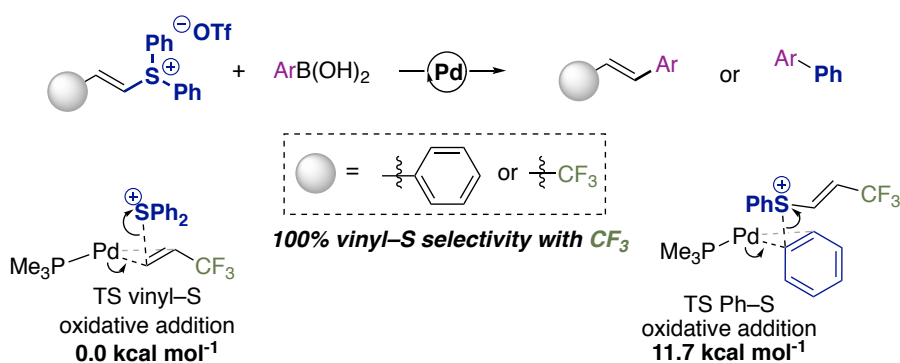
Scheme 4.12. DFT study into C–S cleavage selectivity at a vinyldiphenylsulfonium salt.[74]

4.1.1.4.   Transmetalation and carboxylation of organometallic species

Although no experimental studies have described $C(sp^2)$–SR_2^+ cleavage at Ni(0), a Ni–aryl complex is likely to be formed during the reductive carboxylation of arylsulfonium salts. Most proposed mechanisms (and all DFT studies) have shown that it is at a Ni(I) –aryl complex that CO_2 insertion occurs; however, a few studies have mentioned the transfer of the aryl group from Ni to a Mn(II) or Zn(II) salt.[75] Carboxylation of preformed organomanganese and organozinc species has been reported so it is important to consider the fate of this Ni complex carefully when considering the mechanisms of Ni-catalysed reductive carboxylation reactions.

As mentioned above, M(II) salts are formed during reductive steps and could potentially accept organometallic groups from Ni. These may facilitate the carboxylation reaction by either serving as a reservoir of the organometallic group prior to CO_2 insertion at Ni, or by undergoing carboxylation directly. Carboxylation of organomanganese compounds is much rarer in comparison to organozinc carboxylation.[76] This is at least partially due to the much more developed chemistry of organozincs due to their widespread use in Negishi cross-coupling reactions. There are only two examples of the carboxylation of organomanganese compounds to give isolated carboxylic acids: the carboxylation of alkylmanganese halides reported by Cahiez and the carboxylation of an organomanganese species in the presence of LiCl during the synthesis of α-amino acids reported by Sato and co-workers.[77,78] (Scheme 4.13-left). Hazari ruled out organomanganese species as being important contributors to the Ni-catalysed carboxylation of aryl halides (vide supra).[11] Martin et al. attempted the carboxylation of *n*-butylmanganese bromide and 2-napthylmanganese bromide during investigations into the Ni-catalysed carboxylation of primary alkyl bromides and sulfonates and aryl pivalates, respectively (Scheme 4.13-right).[79,80] No carboxylic acid was obtained under either the Ni-free conditions or the optimised carboxylation conditions.
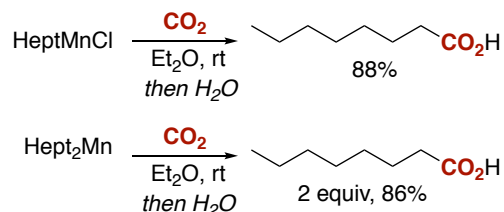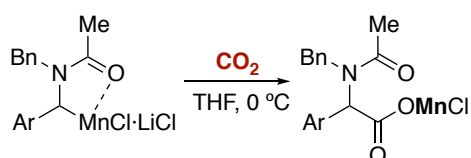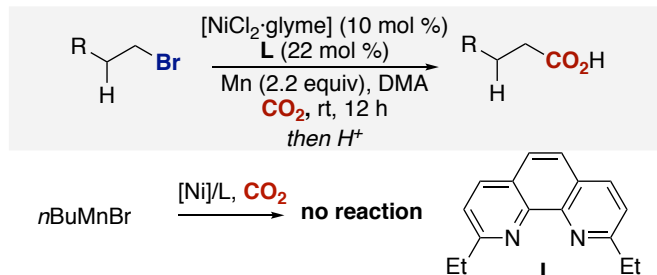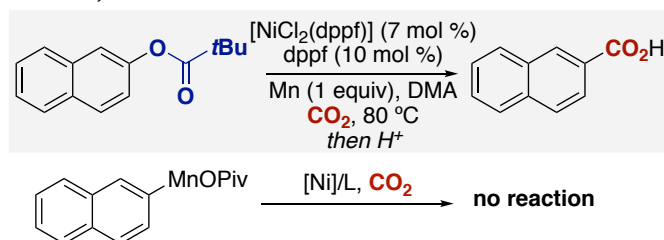
Scheme 4.13. **Carboxylation of organomanganese compounds and investigation of organomanganese intermediates in reductive carboxylation.**[77–79,81]

The first reports of the carboxylation of organozinc species appeared almost simultaneously and have a number of similarities (Scheme 4.14). Both reports took inspiration from Aresta's complex, [(Cy$_3$P)$_2$Ni(η^2-OCO)], a landmark Ni complex in CO_2 functionalisation at transition metals. In 1975, Aresta and co-workers reported that the reaction of a Ni(0) complex bearing electron-rich PCy$_3$ ligands with CO_2 forms a Ni complex bearing reduced CO_2.[82] Although the extent of this reduction is proposed to be one electron and the Ni oxidation state +1, Aresta's complex is also sometimes assigned as Ni(II).[83]

The first example of the Ni-catalysed carboxylation of alkylzinc species was reported by Oshima et al. The presence of LiCl was found to be crucial. This was proposed to be due to its ability to break up organozinc aggregates rather than for reasons related to reactivity of the organozinc with CO_2. The proposed mechanism is shown in Scheme 4.14-right. It involves formation of an electron-rich Cy$_3$P–Ni(0) complex, reaction of electrophilic CO_2 with this complex to form Aresta's complex, then transfer of the alkyl group from the alkylzinc to Ni. Group transfer followed by coordination of Zn(II) to the acyl oxygen that is proposed in this mechanism was also invoked by Rovis in Ni-catalysed coupling reactions involving ZnEt$_2$ as a reductant.[75,84] The C–C bond and zinc carboxylate are subsequently formed upon reductive elimination.[72] This is presumably very rapid as the Ni–alkyl complex might otherwise undergo β-hydride elimination. Dong and Yeung also reported the Ni-catalysed carboxylation of aryl- and alkylzincs.[86] As for Oshima's report, a source of Ni(0) and PCy$_3$ was employed with the aim of forming Aresta's complex. In this report, however, Aresta's complex was also synthesised and reacted with PhZnBr (10 equiv) under CO_2 at room temperature. After 5 h a >95% yield of benzoic acid was obtained. Note that under *Ni-free* conditions *at 65 °C*, benzoic acid was obtained in 25% yield after 5 h. The report by Yeung and Dong left open the question of whether a stoichiometric reaction between Aresta's complex

and the PhZnBr would also result in C–C bond formation. A DFT study on this mechanism supports the mechanistic proposals of Oshima and Dong.[87]
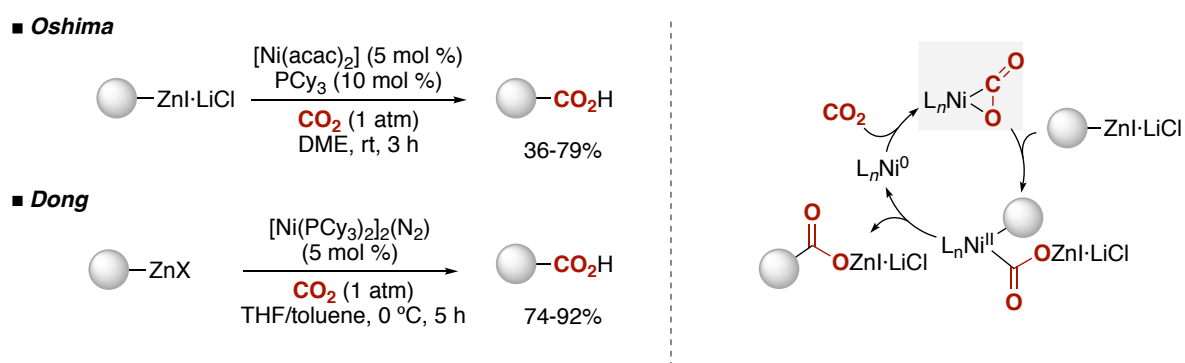
Scheme 4.14. Carboxylation reactions reported by Oshima[85] and Dong.[86]

As described above, Ni-catalysed carboxylation of organozinc compounds is possible. Whether Ni-free carboxylation of organozinc or organomanganese species can occur is important because of the possibility for reverse transmetalation from Ni(II) to M(II) followed by Ni-free carboxylation of the resulting organometallic compound. Cahiez and Sato have shown that Ni-free carboxylation of organomanganese species is possible, and Kondo and Knochel have shown that transition metal-free Lewis acid-mediated carboxylation is possible.[77,78,88,89] Martin also investigated whether organomanganese species could be carboxylated under Ni-free conditions.[79] Whether transmetalation from Ni to Zn is occurring has either not received mention or has been ruled out in the majority of reports of reductive carboxylation reactions.

The first mention of Ni-to-Zn transmetalation in a carboxylation reaction was in the hydrocarboxylation of styrene derivatives reported by Rovis and co-workers (Scheme 4.15).[75] This was invoked because a quenching experiment showed that significant quantities of the protonolysis product (2-ethylnaphthalene) could be obtained when the reaction was quenched after 1 h. The yield of 2-ethylnaphthalene was much higher than the catalyst loading, which suggested that the organometallic ligand was being transferred to the $ZnEt_2$ reductant. A control experiment where an organozinc was reacted with CO_2 showed no carboxylation. Thus, the authors presumed that carboxylation was occurring at Ni after back-transmetalation from Zn. Daugulis also suggested that reversible Cu-to-Zn transfer of the aryl group is occurring during the Cu-catalysed carboxylation of aryl iodides using $ZnEt_2$ as the reductant.[90]

■ *Rovis, 2008*
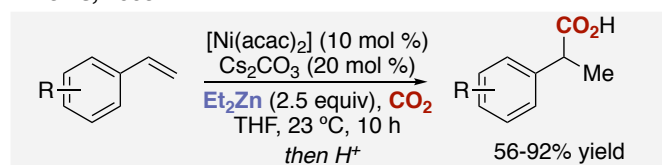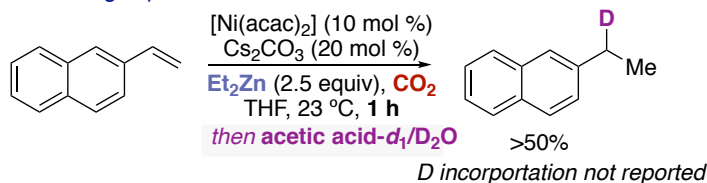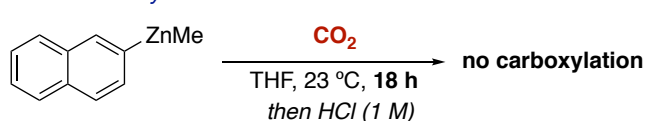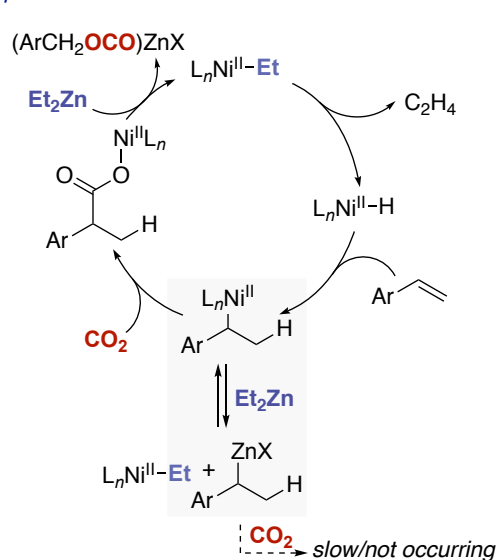
Scheme 4.15. Hydrocarboxylation of styrenes with proposed Ni-to-Zn transmetalation.[75]

Martin and co-workers investigated the potential for organozinc intermediates in the carboxylation of benzyl halides by subjecting benzylzinc chloride to the optimised reaction conditions (Scheme 4.16).[54] As for Rovis' report, no carboxylic acid was obtained upon workup. In this case, it was concluded that benzylzinc intermediates do not form during the reaction. Further support for this conclusion could have come from (1) comparison of the reaction with Mn as reductant and (2) an experiment where a CO_2-free reaction was carried out. Quenching of the resulting reaction mixture with D_2O or I_2 after the optimised time also would have indicated whether significant concentrations of organometallic species in concentration greater than the Ni loading were building up in the reaction mixture.
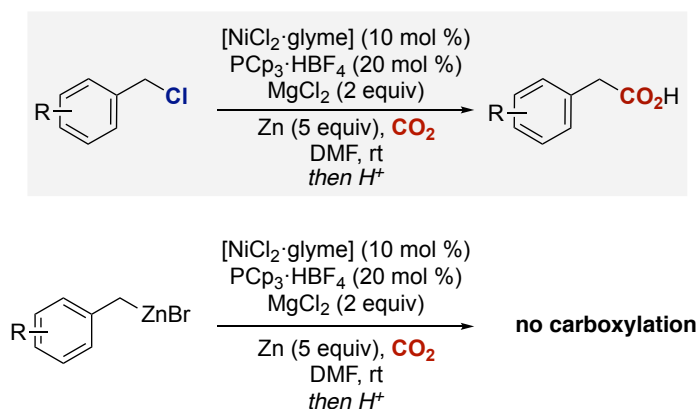
Scheme 4.16. Carboxylation of benzyl halides and failed carboxylation of benzylzinc bromide.[54]

Gosmini discussed the Co-catalysed electrochemical synthesis of arylzincs using $ZnBr_2$ as the Zn source. During studies on the mechanisms of the reaction, transmetalation from Co(II)Ar species to Zn(II) was proposed to explain the electrochemical behaviour of the system.[91,92] Based on this report, the

possibility of transmetalation from Co(II) to Mn(II) was considered by Le Gall and co-workers during the Co-catalysed synthesis of (diarylmethyl)sulfonamides.[93] Nucleophilic organomanganese species would then undergo key C–C formation steps.

4.2.   Aims of this project

Over the last 10 years, the field of Ni-catalysed reductive carboxylation has grown significantly. Part of this growth has involved the extension of the carboxylation reaction to a range of aryl (pseudo)halide electrophiles. Another part has been the increase in mechanistic understanding that is starting to produce results regarding lowered Ni loadings or more optimal solvents. This project aimed to extend the carboxylation reaction to arylsulfonium salt electrophiles – thereby creating the first link from versatile organosulfur chemistry to reductive carboxylation – and to obtain mechanistic information about the new transformation.

First, the development of the Ni-catalysed carboxylation of arylsulfonium salts was targeted by the Yorimitsu group. Second, the knowledge and experience regarding mechanistic studies that was gained from studies described in Chapters 2 and 3 was employed to obtain mechanistic information about the reductive carboxylation reaction.

Taking as a starting point the generally accepted mechanism for reductive carboxylation described in Section 4.1.1, the main goals of this project were to understand activation of the Ni(II) precatalyst, investigate $C(sp^2)$–SMe_2^+ cleavage, investigate the role of the metal powder reductant, and determine whether there were any spectroscopic signatures for Ni(I) intermediates in the catalytic reaction. In order to tackle these questions, catalytic and stoichiometric reactions were combined with NMR and EPR spectroscopy and electrochemical investigations.

4.3.　　Optimisation of the C(*sp²*)–S carboxylation reaction

Investigations into the feasibility of C(sp^2)–S carboxylation began by testing commonly employed carboxylation conditions. Aryl sulfide **1a** was reacted with MeOTf to form arylsulfonium salt **2a**. Although a number of these combinations gave the desired product, it is important to highlight the differences between those that resulted in some carboxylation, those that resulted in none, and those that gave high yields of the desired carboxylic acid. This is important because the optimal conditions for arylsulfonium carboxylation differ somewhat from those of other aryl (pseudo)halide carboxylation reactions.

Initial screening with Ni sources, a substituted phenanthroline ligand (**L1**), and Mn or Zn powder showed that the desired product was indeed being formed. The final optimised conditions are displayed in Table 4.1-entry 1, with an 84% yield of **3a** being obtained without recourse to additives. There was a very strong dependence on the identity of the reductant (Table 4.3). As shown in entry 5, the use of a stronger reductant such as Mn (E = −1.44 V vs SCE compared to −1.02 V for Zn)[16] did not lead to any carboxylic acid.

Entry	Ni	reductant (M)	L1 (%)	Yield of 3a (%)[a]
1	*[NiBr₂L1]*	*Zn*	*3.5*	*87 (84)*
2	[NiBr₂L1]	Zn	-	65
3	[Ni(COD)₂]	Zn	6	86
4	[NiCl₂(PPh₃)₂]	Zn	-	6
5	[NiBr₂L1]	Mn	3.5	0
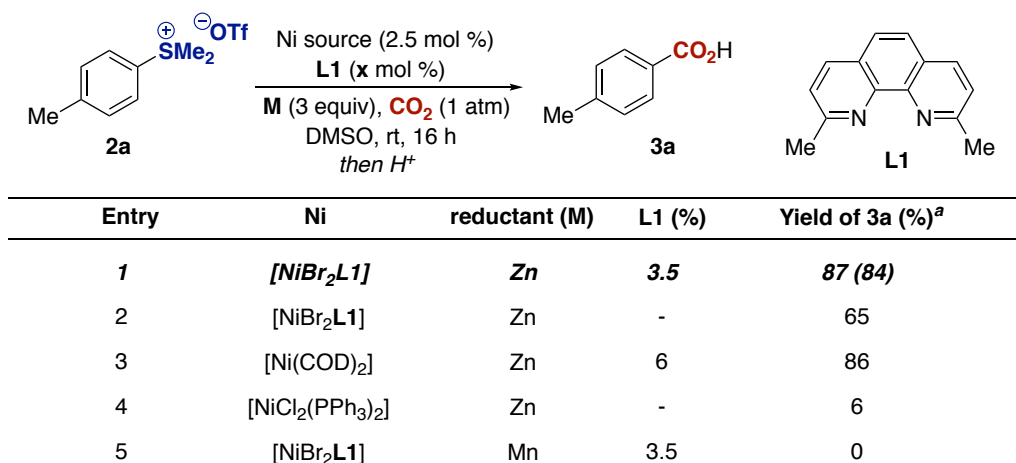
Table 4.3. Initial screening of metal powder reductant and Ni source. [a] **2a** (0.30 mmol), NiBr₂**L1** (2.5 mol %), **L1** (3.5 mol %), Zn powder (0.90 mmol), CO₂ (1 atm), DMSO (1.5 mL) at rt for 16 h followed by acidic workup. Yields are NMR yields using 1,1,2,2-tetrabromoethane as the internal standard. Yield in parentheses = isolated yield.

The use of homogeneous reductants tetrakis(dimethylamino)ethylene (TDAE; E = −0.62 V vs SCE, (DMF))[94,95] and Cp₂Co (E = –0.86 V vs SCE (DME))[58] did not lead to the formation of **3a** after workup (Table 4.4, entries 3–5). Interestingly, addition of 10 mol % Zn(OTf)₂ to the reaction with Cp₂Co reductant gave an 18% yield of **3a** (entry 6). The use of DMAP-OED (E = −1.24 V vs SCE (DMF))[56,57] also failed, even in the presence of ZnBr₂.

Table 4.4. Screening of reductant. [a] Conditions as for Table 4.3.
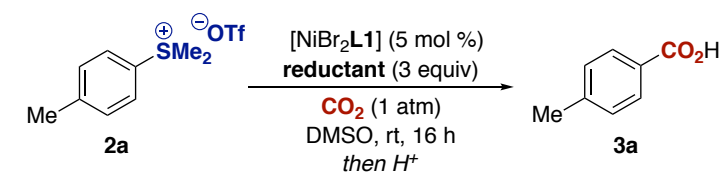
entry	reductant	NMR yield (%)[a]
1	Zn	87
2	Mn	0
3	TDAE	0
4	TDAE/10 mol% Zn(OTf)$_2$	0
5	Cp$_2$Co	0
6	Cp$_2$Co/10 mol% Zn(OTf)$_2$	18

In line with related reductive carboxylation techniques, modification of the substituents in the 2- and 9-positions of the phenanthroline ligand had a strong influence on the yield of the reaction. Unfortunately, the exact nature of this influence was unclear and sometimes seemed counterintuitive (Scheme 4.17). For example, whereas adding consecutive methyl groups to the 2- and 9- positions of phenanthroline increased the yield of **3a** from 33% for phenanthroline up to 85% for **L1**, adding methyl groups in these same positions to a phenanthroline ligand bearing substituents in the 4- and 7- positions *decreased* the yield of **3a**. If a survey of the ligands used in carboxylation reactions is carried out, it is clear that seemingly subtle differences have dramatic influences on yields and that an understanding of which ligand properties influence reactivity would be extremely useful.[6]
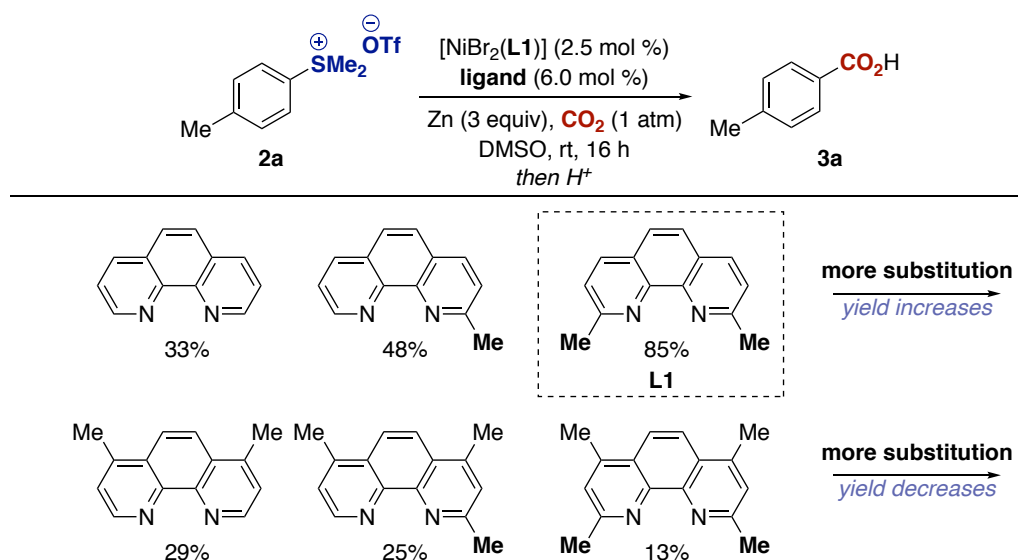
Scheme 4.17. Selection of data from the ligand screening carried out to optimise the reaction.

Solvent choice is also very important in the optimisation of a carboxylation reaction. The above results describe carboxylation reactions that were carried out in DMSO. The use of this solvent is noteworthy because it is rare to find a reductive carboxylation reaction that is not carried out in an amide solvent such as DMF or DMA.[75,90,96,97] DMSO significantly outperformed DMF and DMA (28% and 13% yield under the optimised conditions of Table 4.3, respectively). Hazari recently reported a mechanistic study into a reductive carboxylation reaction where information about the role (and solubility) of the $MnCl_2$ additive allowed DMF to be substituted for THF (see Section 4.1.1.2).[11] In the transformation under study here, the $ZnBr_2$ formed upon reduction of the sulfonium salt should be quite soluble in both DMF and DMSO, suggesting a subtle difference between the aryl chloride and arylsulfonium carboxylation reactions.

Control experiments indicated that all components are necessary (Table 4.5). Specifically, *nickel and Zn are both required* for carboxylation to occur. The remaining mass balance in entries 1–4 was found to be sulfide **1g**. Single electron reduction of dialkylarylsulfonium salts by Zn results in S–Me cleavage and formation of the aryl sulfide.[98] Aryl sulfide **1a** did not undergo any reaction when reacted with stoichiometric Ni/**L1**/Zn (Table 4.5, bottom). This ruled out carboxylation via sulfide intermediates.

Entry	NiBr₂L1/L1	Zn	Additives	3g (%)[a]	2g (%)[a]
1	✓	✓	–	85	0
2	–	✓	–	0	91
3	–	✓	Zn(OTf)₂ (10 mol %)	0	89
4	✓	–	–	0	86
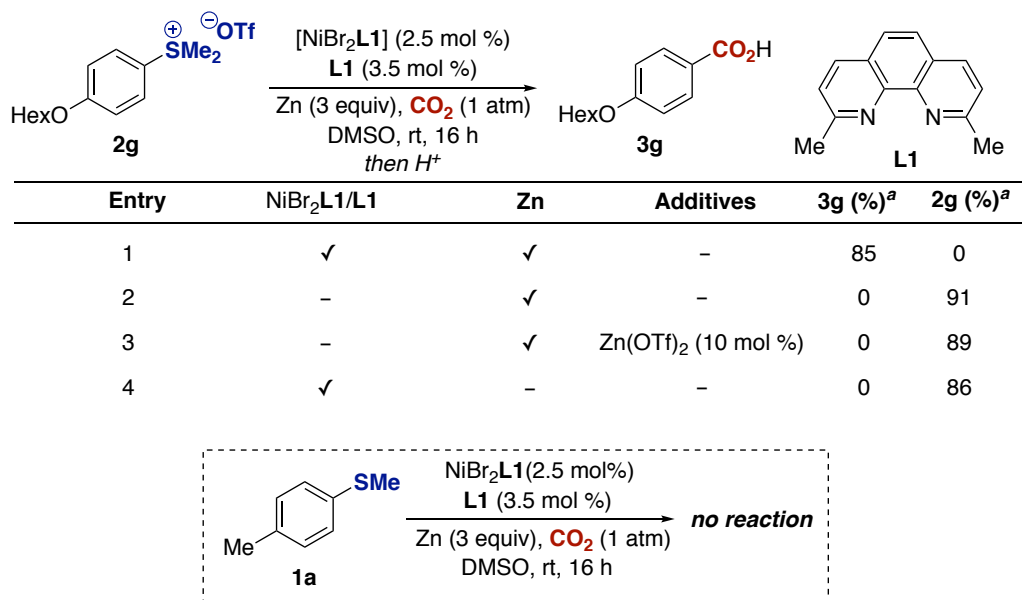
Table 4.5. Summary of control experiments.

When arylsulfonium **2f** was stirred with excess Zn powder for 16 h, a 10:1 ratio of **2f:1f** was visible by ¹H NMR spectroscopy.
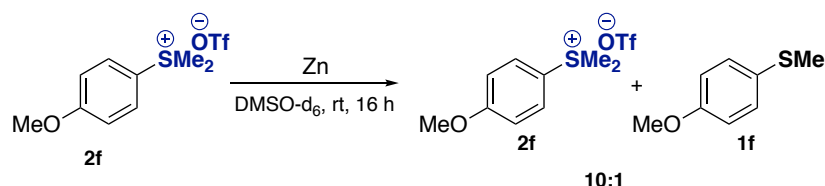
Scheme 4.18. Slow single-electron reduction of the substrate by Zn.

4.4.   Substrate scope

With optimised conditions for the carboxylation of simple arylsulfonium salts **2a** and **2g** in hand, the reaction was tested on substrates bearing different functional groups. Overall, this showed that the reaction has a reasonable amount of generality and is particularly suited to electron-neutral or electron-rich substrates. Electron-poor arylsulfonium salts have a higher reduction potential than electron-rich arylsulfonium salts bringing them closer to that of Zn. Reductive demethylation to form unreactive aryl sulfide may then compete with C(sp^2)–S functionalisation in these reactions.

The reaction could also be carried out in one pot from the aryl sulfide after removal of volatiles from the methylation reaction.
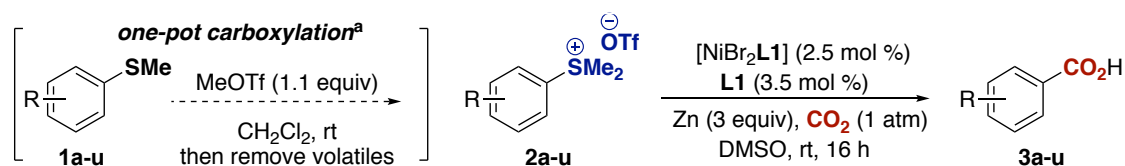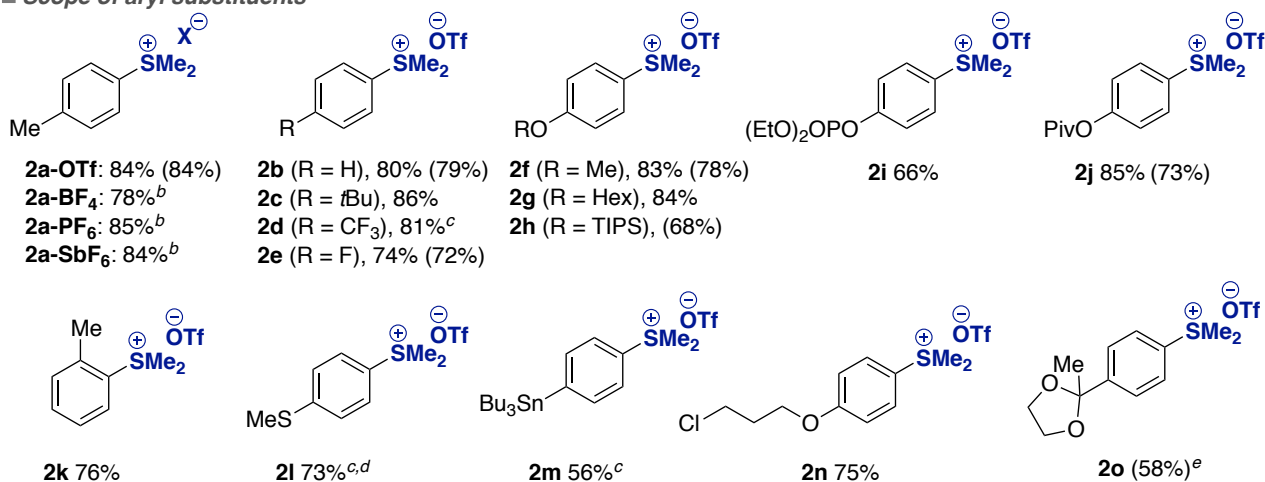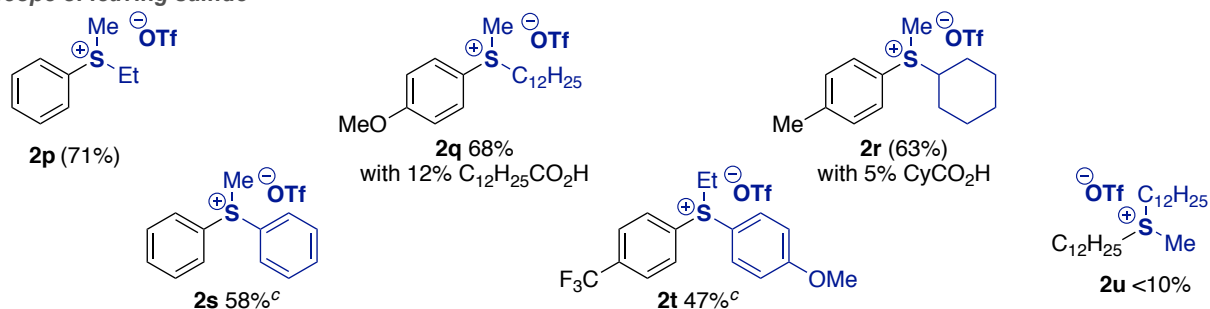
Scheme 4.19. Substrate scope of the arylsulfonium carboxylation reaction. [a] Isolated yield from arylsulfonium salts. Yields in one-pot carboxylation of aryl sulfides are shown in parentheses. [b] Yield was determined by NMR using 1,1,2,2-tetrabromoethane as an internal standard. [c] 5.0 mol % [NiBr$_2$**L1**] and 7.0 mol % **L1** was used. [d] 5% of **2b** was also formed. [e] Obtained as 4-acetylbenzoic acid after acidic workup.

The mild reaction conditions meant that functional groups previously employed in Ni-catalysed coupling reactions, such as esters (**2j**), a stannyl group (**2m**), and an alkyl chloride (**2n**), remained intact after the reaction. Furthermore, a substrate bearing an *ortho*-methyl group underwent carboxylation in good yield (**2k**). Aryl (pseudo)halide carboxylation reactions are often benchmarked against this substrate as the steric bulk introduced by the CH₃ group had previously been shown to hinder reactivity.[55,99] A substrate containing a methyl sulfide group underwent selective carboxylation at the sulfonium group (**2l**).

The sulfide substituents were also investigated. Placing bulkier primary or secondary alkyl substituents on the sulfur atom did not considerably affect the reaction (**2p–r**). Small amounts of alkyl carboxylic acids were also observed for sulfonium substrates bearing long alkyl chains (**2q,r**). Diaryl sulfonium salts (**2s,t**) also underwent carboxylation. Unfortunately, when trialkylsulfonium salt **2u** was subjected to the carboxylation conditions, very little carboxylic acid was obtained. This may be due to the stronger C(sp^3)–S bonds and the lack of a π system to which Ni can bind during oxidative addition. Low-yielding substrates are displayed in Figure 4.2. Attempts to synthesise a pyridylsulfonium salt failed due to competing N-methylation.
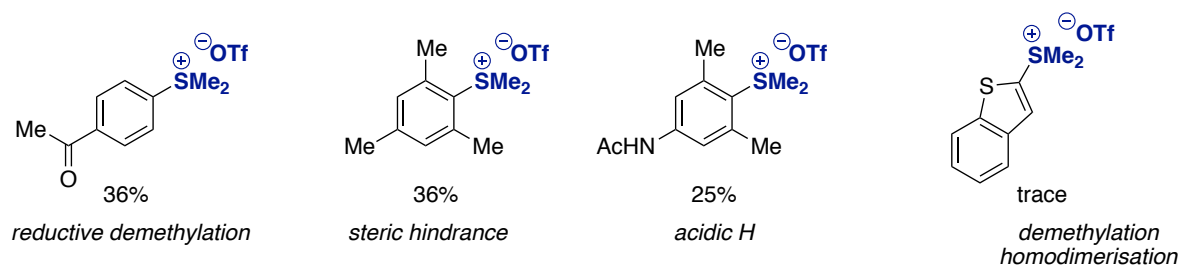
Figure 4.2. Low-yielding substrates.

Overall, the Ni-catalysed reductive carboxylation of arylsulfonium salts developed by the Yorimitsu group can be carried out under very mild conditions, does not require a high catalyst loading, proceeds in DMSO, and does not require any additional additives for excellent yields of **3a** to be obtained. It also displays a reasonable substrate scope that includes potentially reactive stannyl and ester groups.

4.5.　Mechanistic investigations

The main role of this investigation was to obtain mechanistic understanding about the new carboxylation reaction described in Section 4.4. Investigations first focused on the presence of arylzinc intermediates then moved to understanding the reduction of the precatalyst. Finally, stoichiometric experiments were carried out with isolated Ni complexes to investigate C–S cleavage. Experiments focused on (a) identifying important intermediates spectroscopically and (b) stoichiometric reactions between Ni species and the arylsulfonium salt. Kinetic studies were not carried out due to the heterogeneity introduced by the Zn powder.

4.5.1. Arylzinc intermediates

Alongside the control experiments summarised in Table 4.5, an experiment was carried out where the CO_2 atmosphere was replaced with a N_2 atmosphere. The reaction was then quenched after 16 h by the addition of D_2O (Scheme 4.20). After stirring for 1 h a final quench with 2 M HCl was carried out. If the Ni catalyst was the only source of Ni–Ar species a maximum yield of 2.5% of the deuterated product would be expected. However, this experiment gave deuterated aryl ether **4** in a 56% yield (>90% D incorporation). The significant concentration of basic aryl organometallic species suggested that aryl zinc species are formed in the absence of CO_2. A similar quenching experiment was carried out by Rovis and co-workers during the development of a Ni-catalysed hydrocarboxylation of styrenes and a quenching experiment showed a >50% yield of the protonolysis product (see Scheme 4.15).[75]
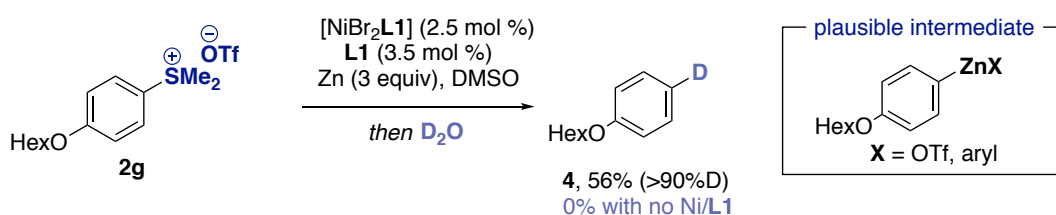
Scheme 4.20. Investigating arylzinc intermediates: quenching experiments.

Given that the products of C–S activation – carboxylic acid, biaryl, or protonolysis product after acidic workup – did not form in the absence of Ni, the isolation of **4** in such a high yield suggests that a Ni-to-Zn transmetalation occurs.[100–103] Whether the so-formed arylzinc species undergo carboxylation directly was investigated by reacting two arylzinc triflates with CO_2 (Table 4.6). The nominally **2b**-derived Zn(p-OMeC$_6$H$_4$)$_2$ was synthesised following a literature procedure and purified by sublimation to ensure the absence of salts that could facilitate Ni-free carboxylation.[88,89] Diphenylzinc was obtained from a commercial supplier.

Low conversions to **3b** and **3f** were observed in the absence of Ni(II) or Zn(0) (entries 2–4). Increasing the reaction time from 40 min to 16 h showed that the Ni-free carboxylation of (p-OMeC$_6$H$_4$)ZnOTf is extremely slow (entry 4). A moderate yield of **3b** was only observed in the presence of *both* the Ni catalyst and Zn(0) (entry 1). Interestingly, addition of **L1** completely shut down carboxylation of both arylzincs (entry 5) (vide infra).
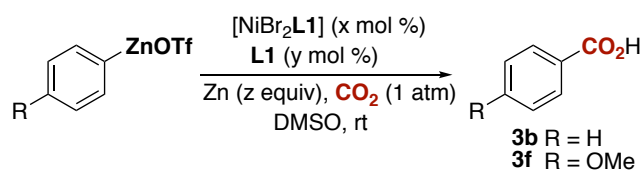
Entry	[Ni] (x)	L1 (y)	Zn (z)	3 (%)[a]
1	2.5	3.5	3	41 (**3b**)
2	2.5	3.5	0	7 (**3b**)
3	0	0	0	11 (**3b**)
4	0	0	0	35 (**3f**)[b]
5	0	100	0	0 (**3b, 3f**)[b]

Table 4.6. Investigating arylzinc intermediates: carboxylation of ArZnOTf. [a] ¹H NMR yields, 1,1,2,2-tetrabromoethane was used as internal standard. [b] 16 h, 1,3,5-trimethoxybenzene internal standard.

These results are consistent with the reports of Ni-catalysed carboxylation of organozincs by Dong and Oshima.[86,85] Specifically, Dong showed that increasing the reaction temperature from 0 ºC to 65 ºC was required for Ni-free carboxylation of phenylzinc bromide to occur.[86] They are also consistent with those obtained by Rovis where Ni-free carboxylation of the organozinc was found to be slow.[75] The carboxylation event was instead proposed to occur at Ni regardless of the formation of arylzinc species.

4.5.2. Reduction of the Ni(II) precatalyst

With knowledge that arylzinc species are forming during the reaction, studies into their origin – presumably transmetalation to Zn(II) from a Ni–aryl complex – were carried out. Prior to beginning these studies, however, the reduction of the Ni(II) precatalyst was investigated. It is important to understand the formation of low-valent Ni as this likely carries out C(sp^2)–S cleavage and forms the Ni–aryl bond.

4.5.2.1. ¹H NMR studies of [NiBr₂L1] reduction

Oxidative addition of the substrate to Ni(0)L$_n$ is the first step of the catalytic cycle in all proposed Ni-catalysed reductive carboxylation mechanisms. Thus, the formation of Ni(0)L$_n$ from [NiBr₂L1] was studied. First, reduction of [NiBr₂L1] with Zn(0) was monitored using ¹H NMR spectroscopy.

The initial spectrum of [NiBr₂L1] in DMSO-d₆ showed multiple paramagnetic species and differed significantly from that of [NiBr₂L1] in CDCl₃ (Figure 4.3). As DMSO is a coordinating solvent, these species were assigned to **L1**Ni(II)-DMSO adducts. X-ray quality crystals of [NiBr₂(DMSO)(**L1**)] were obtained as yellow-brown needles by diffusion of Et₂O into a DMSO solution of [NiBr₂**L1**] (Figure 4.4). This Ni(II) complex has a distorted trigonal bipyramidal geometry with axial bromide ligands. The only similar reported DMSO complex is [NiCl₂(*cis*-DMSO)₂(phen)]DMSO, where two DMSO molecules are coordinated to the Ni centre.[104] The geometry of five-coordinate [Ni(*trans*-Cl₂)(OH₂)(**L1**)] is comparable to that of [NiBr₂(DMSO)(**L1**)] – the effect of the bulkier **L1** is seen in the *trans* disposition of the chloride ligands and the coordination of only one H₂O molecule.[105]

When some of the [NiBr$_2$(DMSO)(**L1**)] crystals were redissolved in DMSO-d$_6$, an almost identical ^{1}H NMR spectrum to that of [NiBr$_2$**L1**] in DMSO-d$_6$ was obtained. This demonstrated that the identity of the Ni(II) complex in solution differed from that of solid state [NiBr$_2$(DMSO)(**L1**)]. Whether bromide displacement occurs as reported for similar complexes that were dissolved in DMF was not determined.[106]
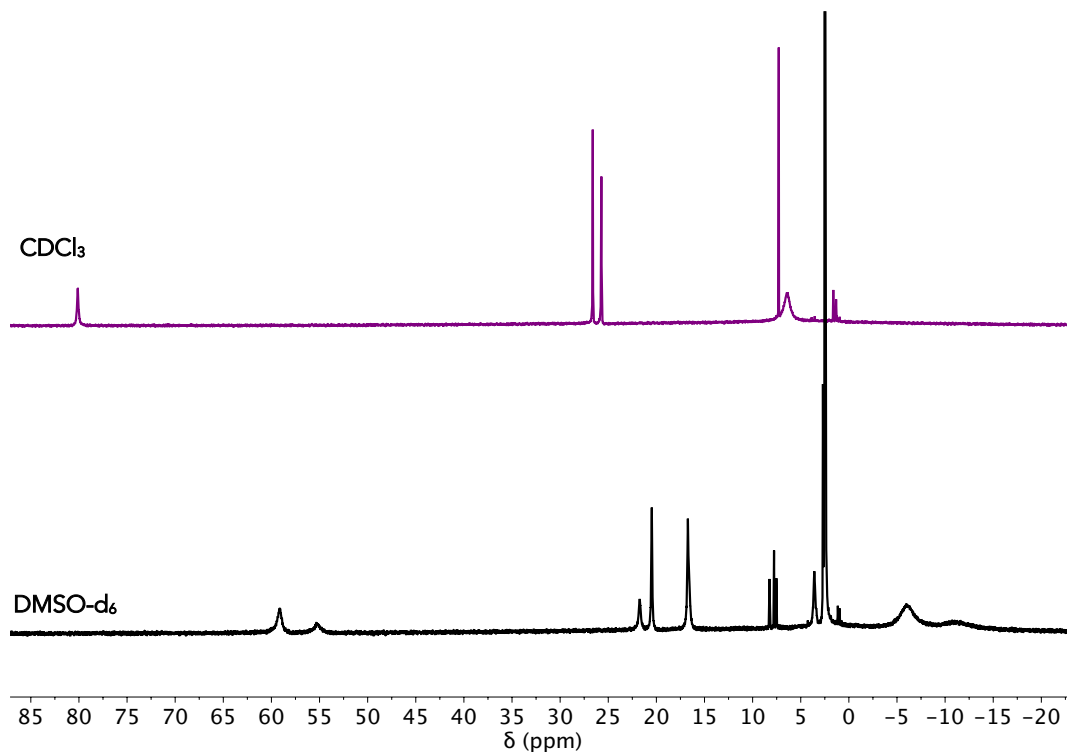
Figure 4.3. Comparison of [NiBr$_2$L1] ^{1}H NMR spectra in CDCl$_3$ (top) and DMSO-d$_6$ (bottom).
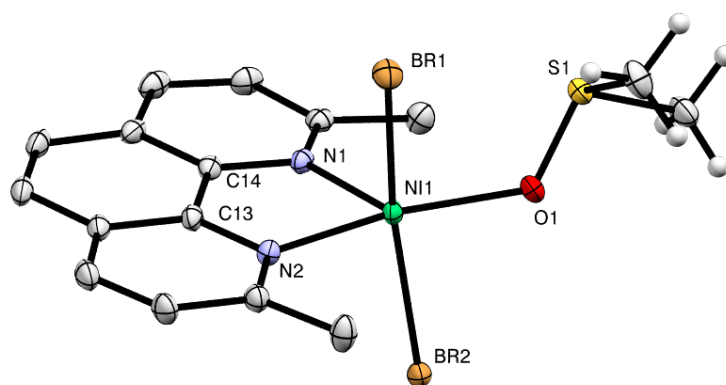
Figure 4.4. X-ray structure of [NiBr$_2$(DMSO)(L1)]. Hydrogen atoms of L1 omitted. Thermal ellipsoids drawn at the 50% probability level. Selected bond lengths (Å): Ni1–O1 2.0294(10), Ni1–N2 2.0375(11), Ni1–N1 2.0466(12), Ni1–Br2 2.4928(3), Ni1–Br1 2.4978(3), S1–O1 1.5385(11), C13–C14 1.441(2). Selected bond angles (°): O1–Ni1–N2 162.62(5), O1–Ni1–N1 115.57(5), Br2–Ni1–Br1 161.725(10), S1–O1–Ni1 125.07(6), N2–Ni1–N1 81.78(5).

In the presence of Zn(0), the pale brown [NiBr₂**L1**] solution rapidly transformed into a deep blue solution. Interestingly, this colour resembled that of the catalytic reactions. After 3 minutes, the NMR yield of this complex was 46% alongside 53% unreacted Ni(II) precatalyst. After 10 minutes, full conversion of [NiBr₂**L1**] was achieved (Figure 4.5). Based on knowledge of Ni(I)**L** complexes gained in Chapter 3, the broadened ¹H NMR signals were quickly identified as being very similar to those of the [Ni(I)(**L1**)₂]⁺ complexes reported by Nocera, Martin, and Hazari.[9,107,108]
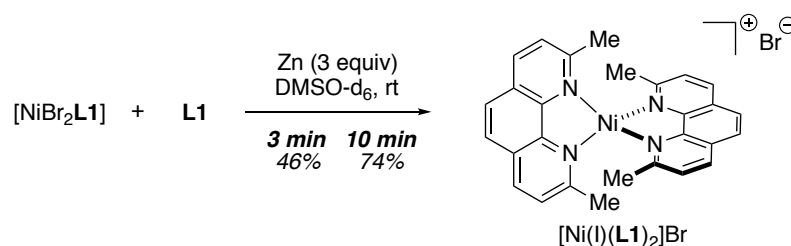
Figure 4.5. Reaction scheme for reduction reactions.

The identity of this complex – [Ni(I)(**L1**)₂]Br (**5-Br**) – was confirmed by X-ray crystallography. The Ni–N bond lengths are comparable to those of the previously reported [Ni(I)(**L1**)₂]⁺ complexes. The central C–C bond lengths of **L1** (C19–C23 and C5–C9) were 1.430(5) Å and 1.440(5) Å, respectively. These are not as short as those in [Ni(**L1**)₂] (1.414(13) Å) where both L1 ligands better described as radical anions coordinated to Ni(II).[109] Complex **5-Br** and its triflate analogue **5-OTf** were synthesised on a 100 mg scale and characterised by NMR and EPR spectroscopy. The syntheses and EPR characterisation are discussed in detail in Section 4.5.3 below.
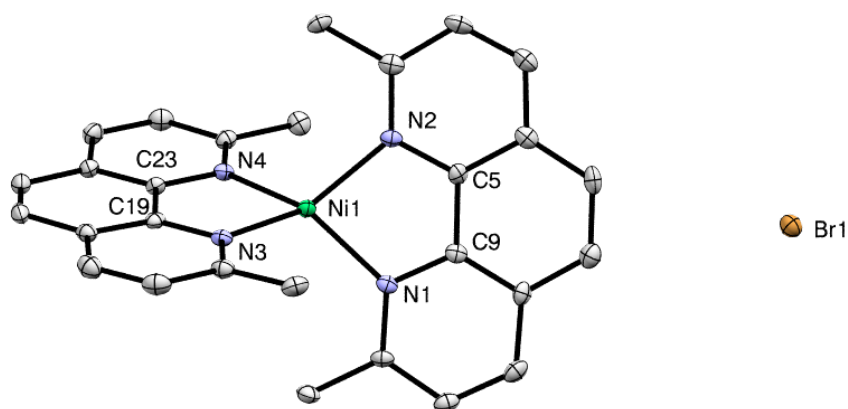
Figure 4.6. X-ray structure of 5-Br. Hydrogen atoms omitted. Thermal ellipsoids drawn at the 50% probability level.

After longer reaction times, the ¹H NMR yield of **5-Br** decreased (Figure 4.7). For example, after 15 h integration of the resulting ¹H NMR spectrum showed only a 16% yield of **5-Br**. The disappearance of **5-Br** suggested the formation of Ni(0)**L1** species. However, the decrease in yield and colour change from

blue to deep brown shown in Figure 4.7-right was not associated with the appearance of any new ^{1}H NMR signals for a Ni complex such as [Ni(**L1**)$_2$]. Two equivalents of **L1** were supplied during reduction reactions, so it is likely that this "Ni(0)" complex is able to form. The absence of new ^{1}H NMR signals may be due to the very poor solubility of [Ni(**L1**)$_2$] in DMSO. When reduction was carried out in THF in order to provide a solvent into which the [Ni(**L1**)$_2$] would dissolve, the product of the first reduction step, **5-Br**, precipitated from solution. The blue suspension was analysed by ^{1}H NMR spectroscopy after 18 h and 2.5 % [Ni(**L1**)$_2$] was visible alongside <10% free **L1**. Although this was evidence for the formation of [Ni(**L1**)$_2$] from [NiBr$_2$**L1**], stronger evidence for the formation of Ni(0) was sought.
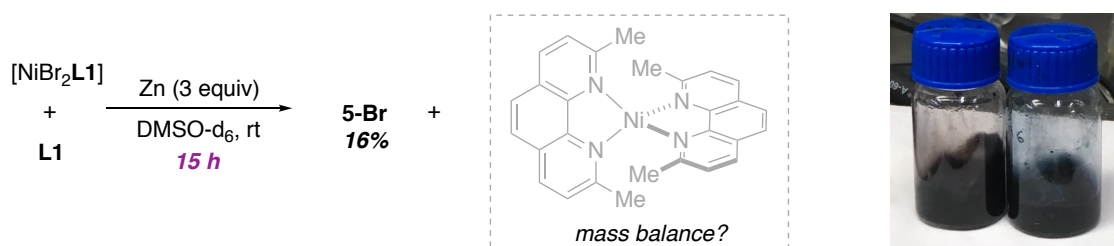
Figure 4.7. Left: Reduction of [NiBr$_2$L1] after 15 h. Right: Comparison of reduction reaction mixtures after 15 h (left), and after ca. 10 minutes (right).

4.5.2.2.   Ni(0) trapping experiments

The absence of ^{1}H NMR signals prompted further investigation into the reduction reaction. In order to try to obtain evidence for Ni(0), trapping experiments were carried out. It was envisioned that coordinatively unsaturated Ni(0) species might react with 1,5-cyclooctadiene to form (**L1**)Ni–COD species with distinctive ^{1}H NMR signals for the coordinated methine protons between 4–5 ppm and that S–S oxidative addition to Ph$_2$S$_2$ might occur to form a well-defined Ni(II) species (Scheme 4.21). [110]
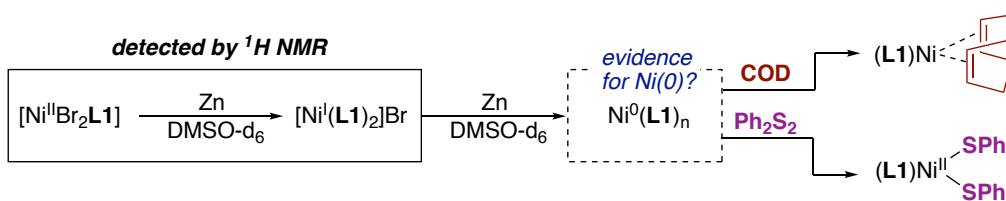
Scheme 4.21. Summary of trapping experiments.

First, an initial experiment was carried out in order to obtain a reference ^{1}H NMR spectrum for the reaction of [Ni(COD)$_2$] with **L1** in DMSO-d$_6$ (Figure 4.8-top). This resulted in a black mixture and the appearance of significant quantities of free COD (δ_H = 5.5 and 2.3 ppm) due to the low stability of [Ni(COD)$_2$] in DMSO. Next, [NiBr$_2$**L1**] was stirred with Zn powder in the presence of COD. Analysis of the black reaction mixture by ^{1}H NMR spectroscopy after 30 min showed the disappearance of [NiBr$_2$**L1**] and a ca. 20% yield of **5-Br**. Signals that matched those of [Ni(COD)$_2$]/**L1** in DMSO-d$_6$ were observed and are highlighted in grey (Figure 4.8-bottom).
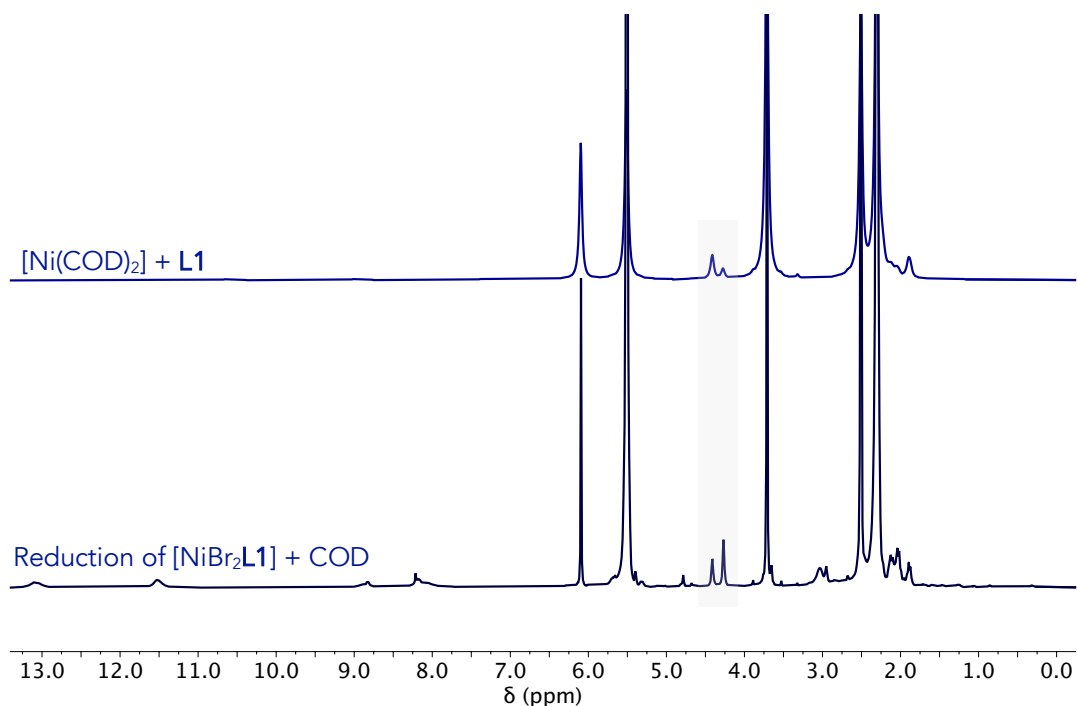
Figure 4.8. Comparison of Ni(COD)₂ + L1 (top) and reduction in presence of COD (bottom). *Note highlighted signals between 4–5 ppm.* 1,3,5-trimethoxybenzene at δ_H = 6.1 and 3.7 ppm.

Next, reactions between [Ni(**L1**)₂] or **5-OTf** and Ph₂S₂ (1 equiv) were carried out in DMSO-d₆ order to obtain reference spectra (Scheme 4.22). The reaction with [Ni(**L1**)₂] was carried out first because it was expected to react as a source of Ni(0) and cleanly provide the S–S oxidative addition product. Indeed, the brown colour of the sparingly soluble Ni(0) precursor became deep red and the resulting NMR spectrum showed a 1:1 ratio between the **L1** signals of a new complex and the equivalent of **L1** that was displaced from the [Ni(**L1**)₂] precursor (Figure 4.9). The chemical shifts of the new **L1** signals were consistent with a d⁸ tetrahedral Ni**L1** complex such as NiBr₂**L1** (compare with Figure 4.3) and the upfield signals near $\delta_H = -30$ ppm were comparable to those of the selenolate ligands of [Ni(SeAr)₂(**L1**)].[111] This suggested that S–S oxidative addition had occurred.
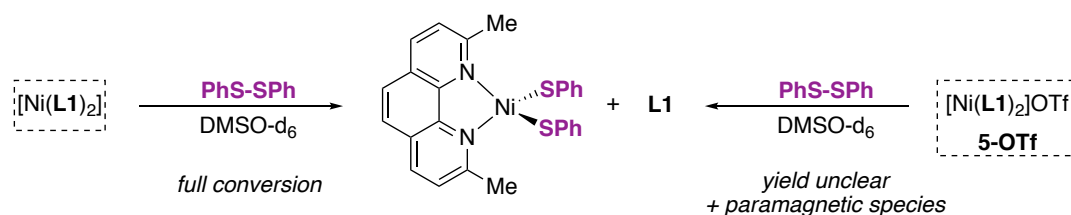
Scheme 4.22. Reactions of Ni complexes with Ph₂S₂.
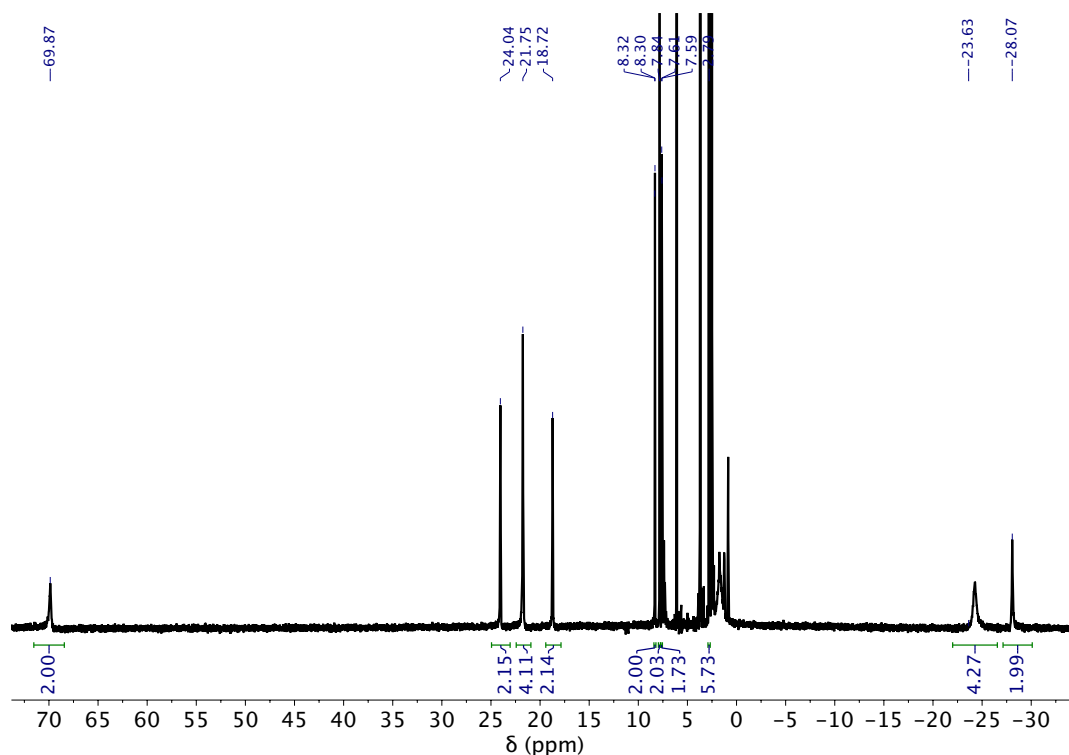
Figure 4.9. ^{1}H NMR (DMSO-d$_6$) of the reaction between **[Ni(L1)$_2$]** with **Ph$_2$S$_2$**. Signals at ca. 8 ppm are from **L1**, demonstrating the 1:1 ratio of Ni(II) complex to **L1**. 1,3,5-trimethoxybenzene at δ_H = 6.1 and 3.7.

Addition of Ph$_2$S$_2$ to a DMSO-d$_6$ solution of **5-OTf** resulted in a colour change from deep blue to red within 5 min. Analysis of the reaction mixture by ^{1}H NMR spectroscopy showed that full conversion of **5-OTf** had been achieved and that 1 equiv of **L1** had been liberated. Although the same Ni(II) complex seemed to have been obtained as for [Ni(**L1**)$_2$], a number of other paramagnetic complexes were present (Figure 4.10). The formation of the S–S oxidative addition complex from **5-OTf** may be due to disproportionation of **5-OTf** to form Ni(II) and Ni(0) complexes. The ability of a related Ni(I) complex to disproportionate in this way was described by Nocera.[107]
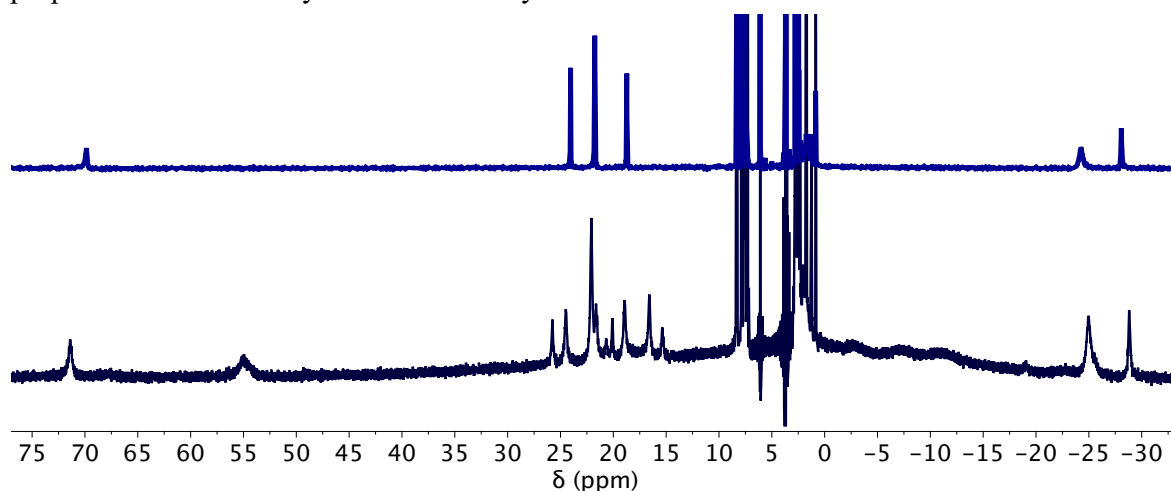
Figure 4.10. ^{1}H NMR (DMSO-d$_6$) of reaction of **[Ni(L1)$_2$]** with **Ph$_2$S$_2$** (top, blue) compared with reaction of **[Ni(L1)$_2$]OTf (5-OTf)** with **Ph$_2$S$_2$**.

Finally, [NiBr$_2$**L1**] was stirred with Zn powder (10 equiv) for 16 h before the reaction was filtered to remove excess Zn and the Ph$_2$S$_2$ added (1 equiv). The dark brown mixture turned red within 2 minutes then turned deep blue-black within another 2 minutes. After 15 minutes, a 10% yield of **5-OTf** was observed by ^{1}H NMR. Interestingly, new **L1** signals had appeared between δ_H = 6–7.7 ppm. The chemical shifts of these signals differed significantly from those of the [Ni(SAr)$_2$(**L1**)] complex discussed above (δ_H = 18–70 ppm). The position of the new aromatic signals and their similarity to those of [ZnBr$_2$(**L1**)] suggested that the presence of Zn(II) might be interfering with the trapping experiment and that transmetalation may be occurring. Zinc thiolate complex [Zn(S(p-OMeC$_6$H$_4$))$_2$(**L1**)] had been synthesised during investigations into the stoichiometric reactivity of **2f** with Ni complexes and Zn(II) salts. The unknown **L1** signals were comparable to those of [Zn(S(p-OMeC$_6$H$_4$))$_2$(**L1**)]. The synthesis of [(**L1**)Zn(SPh)$_2$] or the reaction of [Ni(**L1**)$_2$] with Ph$_2$S$_2$ in the presence of a Zn(II) salt would have provided useful data to support or reject the hypothesis that ligand exchange between Ni(II) and Zn(II) had occurred.

The colour changes occurring during the reduction reaction and during Ph$_2$S$_2$ reactions suggested that UV-vis spectroscopy could be suitable for studying the reactions. First, spectra of [Ni(**L1**)$_2$] and the reduction reaction were compared (Figure 4.11). The intense LMCT bands of **L1** are not shown. Both mixtures were dark brown, and as is visible in the UV-vis spectrum, had strong absorptions in the visible region. The spectra were not completely identical, however.
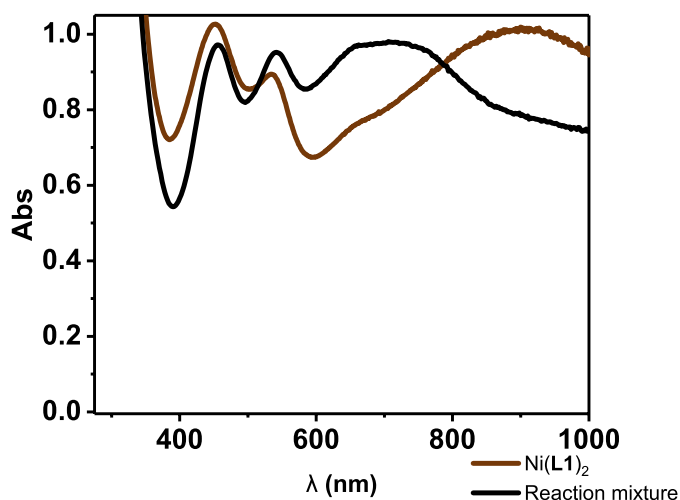
Figure 4.11. Comparison of [Ni(L1)$_2$] (brown trace) and reduction reaction mixture (0.21 mM, black) (DMSO). Ni(L1)$_2$ λ_{max} = 452, 535, 665, 900 nm.

Next, Ph$_2$S$_2$ solution (13 equiv, DMSO) was injected into the cuvette. A UV-vis spectrum was collected as soon as possible after addition (Figure 4.12). Comparison with the UV-vis spectrum of [Ni(**L1**)$_2$]Br (Figure 4.12-right) showed that [Ni(**L1**)$_2$]$^+$ was forming very rapidly. The red colour that was observed during the NMR experiment was not observed this time, potentially due to the very high dilution and the rapidity of the reaction.
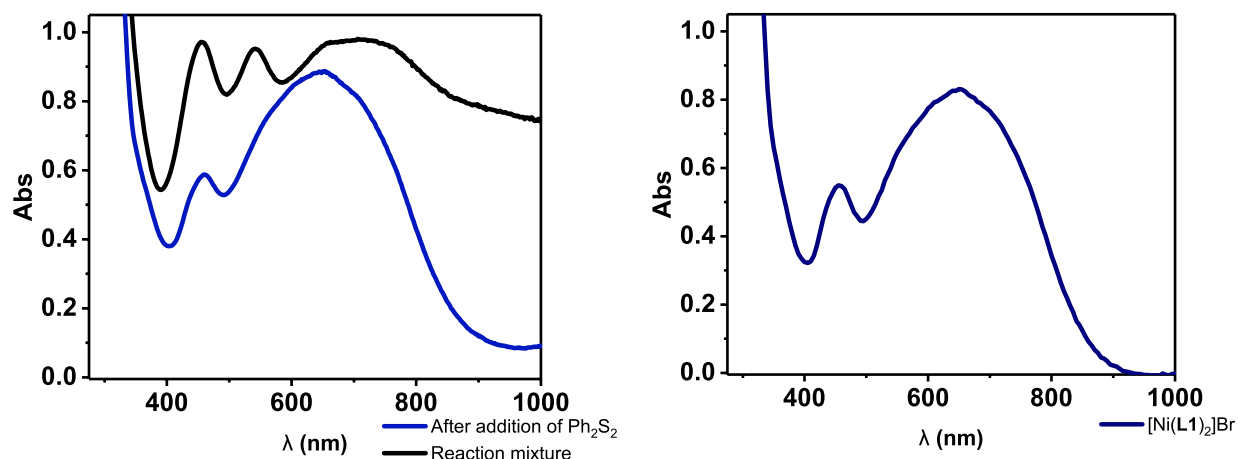
Figure 4.12. Left: Change to UV-vis spectrum obtained from reduction reaction after addition of Ph$_2$S$_2$ solution. Right: 5-Br in DMSO. λ_{max} = 450, 650 nm.

Overall, investigations into the reduction of [NiBr$_2$**L1**] with Zn powder experiments provided indirect evidence for the formation of Ni(0) species. Further experiments to isolate and characterise the brown product that forms after long reaction times might be useful as there is little known about the identities of the Ni(0) complexes that are key to oxidative addition in reductive carboxylation reactions. It is important to note that this result contrasts with a recent report by Diao where single-electron reduction of a Ni(I)(bipyridine) complex by Zn(0) was ruled out.[112]

Electrochemical measurements were also carried out on [NiBr$_2$**L1**] and **5-OTf**. As shown in Figure 4.13, the cyclic voltammograms are almost identical for the two species. A broad reduction from Ni(II)/Ni(I) is followed by a reversible reduction to Ni(0) at ca. -1.5 V vs Fc/Fc$^+$. The reduction potential of Zn/Zn(II) vs SCE is often quoted as -1.02 V in DMF vs SCE. This potential would therefore be close to that of the reduction of **5-OTf** to Ni(0). Further studies would be required to be able to compare these potentials accurately and confirm that Ni(0) is obtained by reduction. It is plausible that **5-OTf** could instead disproportionate to a Ni(II) and a Ni(0) species. If Zn is only able to reduce the Ni(II) species, a build-up of Ni(0) would still be possible.
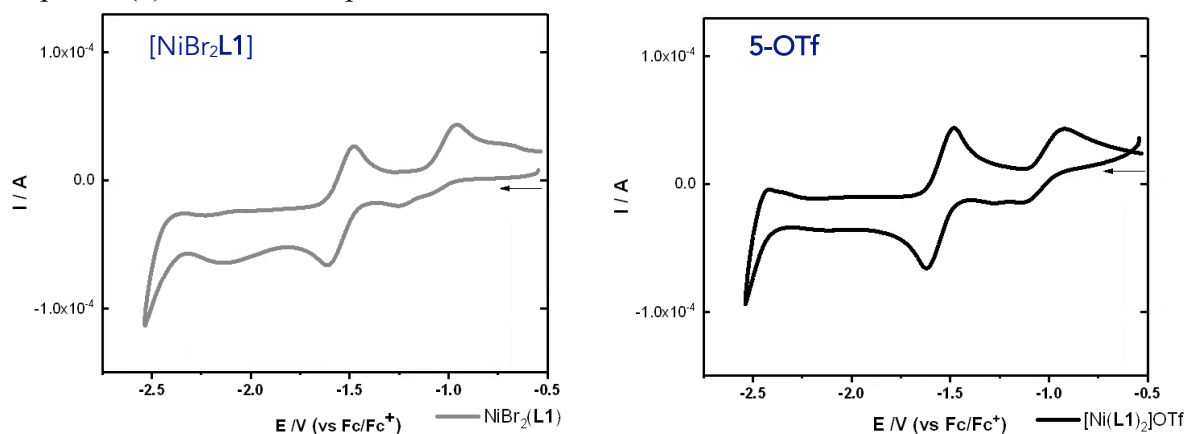
Figure 4.13. Cyclic voltammograms of [NiBr$_2$L1] and 5-OTf (left). Ag/AgCl reference electrode, 0 to -2 V scan at 100 mV s^{-1}, DMSO solvent, 0.1 M Bu$_4$NPF$_6$ electrolyte solution.

4.5.3. Ni(I) complexes

Given that **5-Br** is formed from reduction of [NiBr₂**L1**], the synthesis, isolation, and characterisation of **5-Br** was targeted (Scheme 4.23). Complex **5-Br** and its triflate analogue **5-OTf** were successfully synthesised by following an oxidation route based on that first reported by Nocera.[107] It was found that the Ag⁺ oxidant must be added as a suspension (as reported by Nocera) if the AgX salt has reasonable solubility in the reaction solvent. That is, for reactions with AgCl[9] and AgBr, which have poor solubility in THF or ACN, mixing the two solids then adding solvent will give the desired Ni(I) complex. However, AgOTf is more soluble and reacts very quickly to form unidentified grey solid if it is not added as a suspension. Comproportionation was also used to synthesise **5-Br** in a manner reminiscent to the synthesis of the inner sphere Ni(I)–halide complexes of Chapter 3.
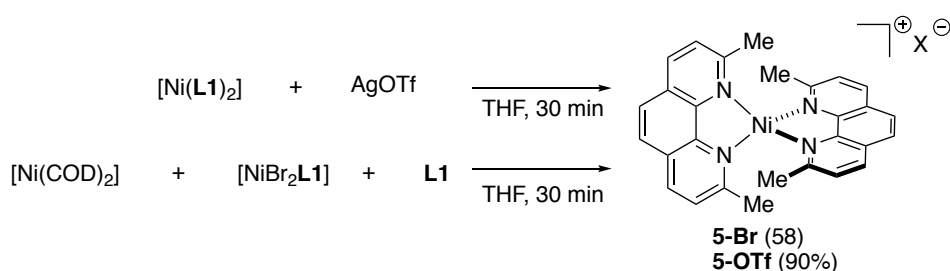
Scheme 4.23. Syntheses of 5-Br and 5-OTf.

Both complexes showed almost identical solution magnetic moments of $\mu_{eff} = 1.65\ \mu_B$ (**5-Br**) and $\mu_{eff} = 1.80\ \mu_B$ (**5-OTf**) (Evans method). These are consistent with the measurements reported by Hazari for [Ni(**L1**)₂]Cl ($\mu_{eff} = 1.73$) and by Scaife for [Ni(bpy)₂]ClO₄ ($\mu_{eff} = 1.99$).[9,113] The EPR spectra of both complexes show axial signals with metal-centred radical character, where the g values are shifted from g_e (2.0023) due to spin-orbit coupling with Ni (Figure 4.14). The EPR spectrum of **5-OTf** shown in Figure 4.14-left matched the axial spectra of reported [Ni(**L1**)₂]⁺ complexes and was easily simulated as a single species shown in red with $g_x = 2.082$, $g_y = 2.117$, $g_z = 2.378$ (lineshape = 1).[9,107]

The EPR spectrum of **5-Br** was more complicated (Figure 4.14-right). The spectrum was best modelled as a mixture of two Ni(I) species without hyperfine coupling. The major species was likely similar to **5-OTf** due to the very similar simulated g values ($g_x = 2.085$, $g_y = 2.148$, $g_z = 2.367$). The second had $g_y > g_x \approx g_z$. This may be due to the better coordination ability of Br⁻ compared to OTf⁻, which might result in equilibrium mixtures of inner- and outer-sphere complexes that are frozen out when the EPR sample is prepared. Indeed, when the spectrum was collected in 1:1 2-MeTHF/ACN rather than 4:1 2-MeTHF/ACN the intensity of the species with $g_y > g_x \approx g_z$ increased.
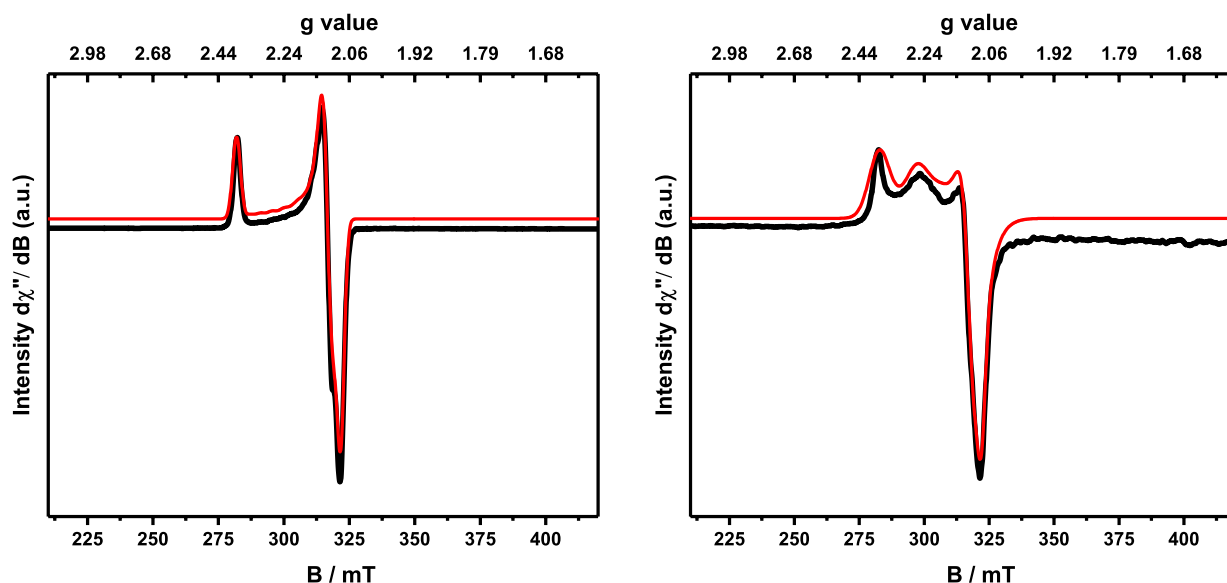
Figure 4.14. EPR spectra (77 K, X-band, 2-MeTHF) of 5-OTf (left) and 5-Br (right). Red = simulated spectra.

Overall, the ^{1}H NMR, EPR, X-ray, and magnetic moment measurements are all consistent with the two $[Ni(\mathbf{L1})_2]^+$ complexes being d^9 Ni(I) complexes with the unpaired electron localised mainly on Ni. A side reaction to note is the slow oxidation of $[Ni(\mathbf{L1})_2]$ in the presence of $Zn(OTf)_2$. When the two were combined in DMSO-d_6 and stirred together for 20 h a 40% yield of **5-OTf** was obtained. Interestingly, the ^{1}H NMR signals of the Ni(I) complexes derived from these experiments were shifted slightly upfield from those of **5-OTf** synthesised from AgOTf oxidation (Figure 4.15). This shift may be due to Zn(II) remaining coordinated to the OTf⁻ counteranion. Lingering Zn(II) salt after reduction was recently reported by Diao, with a Ni–Br--(ZnBr$_2$) interaction captured in an X-ray structure.[114]
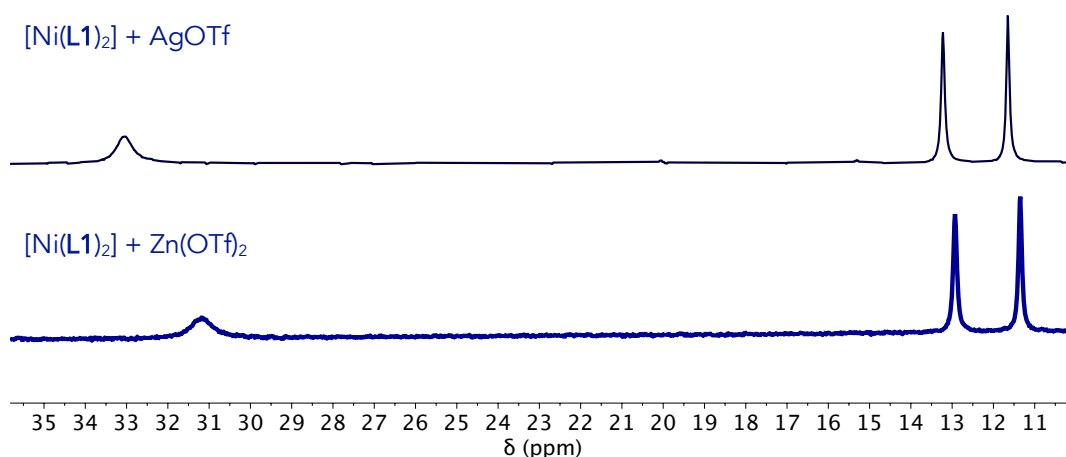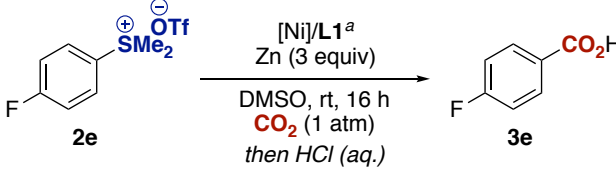
Figure 4.15. Comparison of 5-OTf synthesised by Ag(0) oxidation of [Ni(L1)$_2$] (top) and by oxidation of [Ni(L1)$_2$] by Zn(OTf)$_2$ (bottom, dark blue).

4.5.3.1.   Catalytic relevance of Ni(I) complexes

Given that reduction of [NiBr₂**L1**] rapidly formed **5-Br** and that the carboxylation reaction mixture seemed to be a similar deep blue to **5-Br** and **5-OTf**, the relevance of these Ni(I) complexes to the carboxylation reaction was investigated.

First, their use as precatalysts for the reaction was analysed. As would be expected from the reduction experiments discussed in Section 4.5.2, both were competent precatalysts (entries 2–5, Table 4.7). Interestingly, the addition of 1 equivalent of **L1** relative to the Ni(I) complex increased the yield of **3e** (entries 4,5). The Ni(I) and Ni(II) precatalysts were slightly more active than [Ni(**L1**)₂] (entry 6). This is reminiscent of Hazari's results summarised in Scheme 4.9 where the chloride-free Ni(0) precatalyst gave a reduced yield of acid due to its inability to generate $MnCl_2$.[11]

Entry	Catalyst	Yield 3e (%)[b]
1	[NiBr₂**L1**]/**L1**	70
2	[Ni(**L1**)₂]Br/**L1**	62
3	[Ni(**L1**)₂]OTf/**L1**	65
4	[Ni(**L1**)₂]Br	28
5	[Ni(**L1**)₂]OTf	55
6	[Ni(**L1**)₂]	37

Table 4.7. Precatalyst screening. [a] 2.5 mol % Ni source and 3.5 mol % L1 if added. [b] NMR yields against 1,3,5-trimethoxybenzene.

Next, the catalytic carboxylation of **2f** was analysed by both NMR and EPR spectroscopy in order to investigate the hypothesis that the persistence of deep blue [Ni(**L1**)₂]⁺ complexes was responsible for the deep blue colour of the reaction mixture. First, **2a** was submitted to the optimised reaction conditions and a 0.5 mL aliquot was removed after 1 hour. Signals for [Ni(**L1**)₂]⁺ and [NiBr₂(DMSO)(**L1**)] were clearly visible in the ¹H NMR spectrum. These are marked in blue and red, respectively (Figure 4.16).
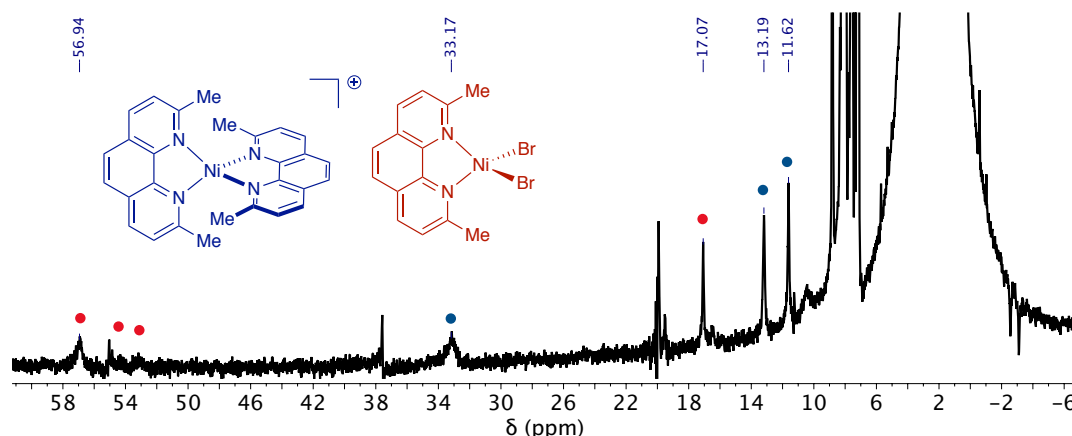
Figure 4.16. ^{1}H NMR analysis of the carboxylation reaction after 1 h showing signals for [Ni(L1)$_2$]$^+$ (blue) and NiBr$_2$L1+DMSO (red). Spikes at ca. 20 and 38 ppm are artefacts.

A second carboxylation reaction of **2f** was sampled after 3 h. The 0.1 mL aliquot was diluted with two parts 2-MeTHF then transferred to an EPR tube and frozen in liquid N$_2$. An axial spectrum was recorded obtained that matched that of **5-OTf** (simulated g$_x$ = 2.082, g$_y$ = 2.117, g$_z$ = 2.378) (Figure 4.17). The approximate yield of the carboxylation reaction at this time – 40% – was obtained by ^{1}H NMR spectroscopy after quenching the remaining solution with 2 M HCl, addition of 1,3,5-trimethoxybenzene, and extraction into Et$_2$O.
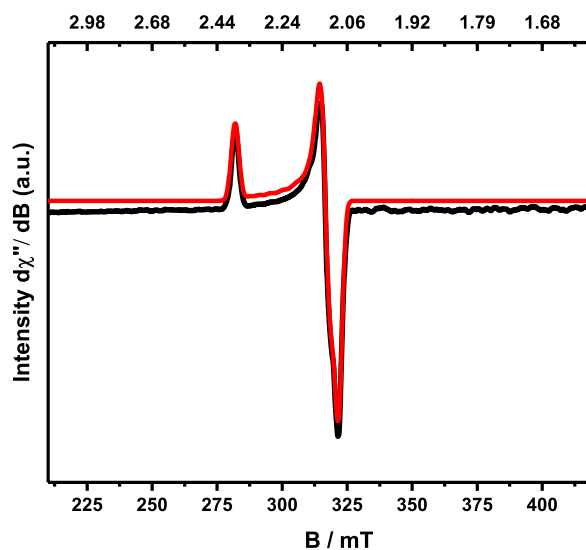
Figure 4.17. Aliquot of reaction mixture (black) compared with simulated spectrum for 5-OTf (red).

Next, the catalytic reaction was sampled after 1 h and 3.5 h and the amount of **5-OTf** quantified against a Cu(II) calibration curve. The catalyst loading was doubled to 5 mol% [NiBr$_2$**L1**]/7 mol% **L1** to decrease weighing error. Of the initial Ni concentration, 60% was **5-OTf** after 1h. This decreased to 44% after 3.5 h. Whether catalyst decomposition is occurring during the reaction was not investigated.

Overall, the detection of **5-OTf** in the reaction mixture is significant as it suggests that **5-OTf** is either a catalyst resting state or an off-cycle complex.

4.5.4. C(*sp²*)–S cleavage

At this point in the mechanistic investigation, evidence for formation of Ni(0) via isolable [Ni(I)(**L1**)$_2$]$^+$ complexes had been obtained. Furthermore, [Ni(I)(**L1**)$_2$]$^+$ complex **5-OTf** had been detected in the catalytic reaction by NMR and EPR spectroscopy. How the Ni(0) and Ni(I) complexes were involved in C(*sp²*)–S bond functionalisation was still unclear: it would not be unreasonable to assume that oxidative addition of Ni(0) to the C(*sp²*)–SMe$_2^+$ bond occurs, but no experimental studies had been carried out into such a reaction. Thus, to investigate whether cleavage of the C(*sp²*)–S bond occurs at Ni(0) and whether an oxidative addition complex could be isolated, NMR-scale reactions in DMSO-d$_6$ were carried out between [Ni(**L1**)$_2$] or **5-OTf** and **2f**.

When **2f** was reacted with [Ni(**L1**)$_2$], small amounts of Me$_2$S and biaryl were observed by ^{1}H NMR spectroscopy (Scheme 4.24-top). These C–S cleavage-derived compounds provide further evidence that Ni(I) needs to be reduced to Ni(0) during the catalytic reaction. Some **5-OTf** was also observed (8%). This could be formed through oxidation of [Ni(**L1**)$_2$] by **2f** giving **1f** (6%) or by comproportionation of the undetected oxidative addition complex with unreacted [Ni(**L1**)$_2$]. Low yields are probably due to the very low solubility of [Ni(**L1**)$_2$]. When Ni(I) complex **5-OTf** was reacted with **2f**, no reaction was observed (Scheme 4.24-bottom). This was further evidence that Ni(0) is needed for C–S cleavage.
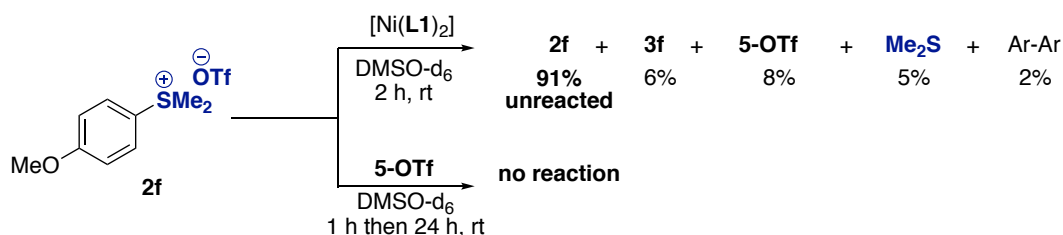
Scheme 4.24. Reactions of arylsulfonium 2f with [Ni(L1)₂] and 5-OTf.

When a source of Zn was added to these reactions, reactivity between the arylsulfonium salt and [Ni(**L1**)$_2$] increased significantly (Scheme 4.25). For example, reaction of **2f** with [Ni(**L1**)$_2$] and Zn(OTf)$_2$ resulted in 50% conversion of **2f**, traces of anisole, and a 44% yield of Me$_2$S. The only Ni species detected by ^{1}H NMR spectroscopy was **5-OTf** (70%). The low conversion of **2f** may be due to the ability of Zn(OTf)$_2$ to slowly oxidise [Ni(**L1**)$_2$] to **5-OTf**. As shown above, this Ni(I) complex does not react with **2f**. When Zn(0) was added to the reaction, full conversion of **2f** was obtained and an 85% yield of Me$_2$S. This indicated that Zn could generate Ni(0) species from the **5-OTf** that was formed under these conditions. Indeed, when **2f** was reacted with **5-OTf** in the presence of Zn powder C–S cleavage products were obtained.
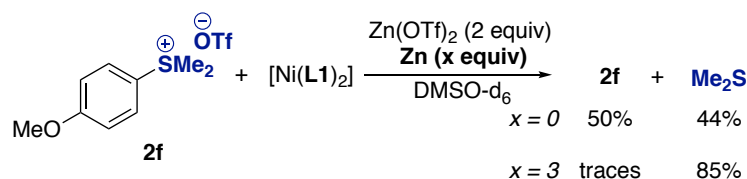
Scheme 4.25. Reactions of 2f with [Ni(L1)₂] in the presence of Zn sources.

4.5.5. Arylzinc species

The stoichiometric experiments described above did not allow for the isolation of an oxidative addition complex of an arylsulfonium salt to [Ni(**L1**)₂]. Indeed, no ¹H NMR signals that could be assigned to a Ni–aryl complex were observed; however, a set of new ¹H NMR signals with the *characteristic pattern of a Zn **L1** complex* appeared in all the experiments where C–S cleavage products were observed. This complex was responsible for the mass balance of the aryl fragment in the reactions summarised in Scheme 4.25 and prompted further investigations into the identity and importance of Zn(II)–aryl complexes during the carboxylation reaction.

The **2f**-derived diarylzinc species Zn(p-OMeC₆H₄)₂ was taken as the starting point in reactions to investigate the identity of the Zn complex formed in the stoichiometric reactions above. This was reacted with Zn(OTf)₂ followed by **L1**. After 3 h the resulting colourless solution was analysed by ¹H NMR spectroscopy. The resulting signals were *identical to those observed in the stoichiometric reactions* above. The Zn species was identified as "[(**L1**)ZnAr]OTf" based on integration of the ¹H NMR signals. Single crystals of this compound were unfortunately not obtained so it was not possible to determine whether "[(**L1**)ZnAr]OTf" is dimeric or an aggregate. Running a DOSY NMR experiment may have provided information in this regard.
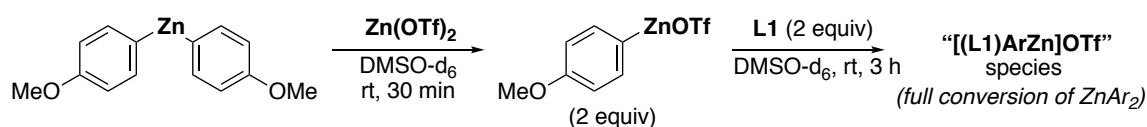
Scheme 4.26. Reaction of (p-OMeC₆H₄)ZnOTf with L1.

Figure 4.18 shows the ¹H NMR spectrum of "[(**L1**)ZnAr]OTf" and the ¹H NMR spectra of the reactions of **2f** with (a) [Ni(**L1**)₂] + Zn; (b) **5-OTf** + Zn; (c) [Ni(**L1**)₂] + Zn(OTf)₂; and (d) Ni(**L1**)₂ + Zn + Zn(OTf)₂. Highlighted in pale grey are the signals of "[(**L1**)ZnAr]OTf" to demonstrate that arylzinc species were formed in all these reactions. Marked with coloured circles are: biaryl (blue), **2f** (red), anisole (green), and 1,3,5-trimethoxybenzene (internal standard, orange).
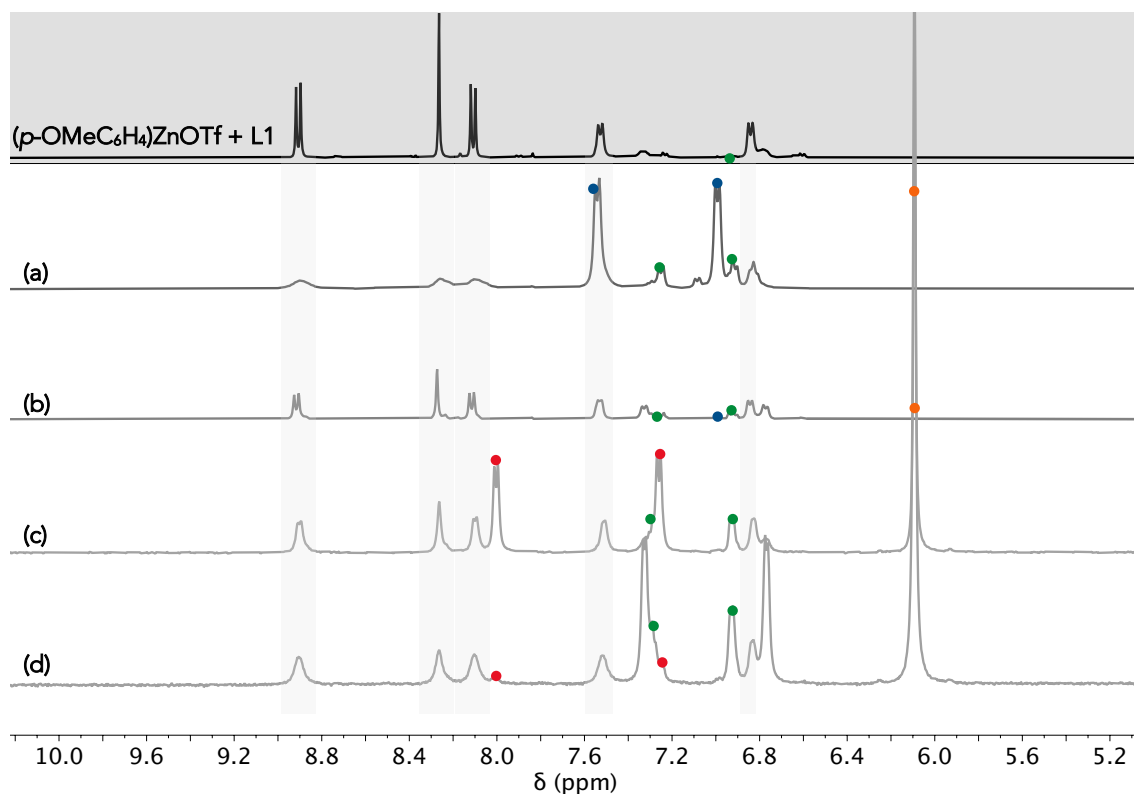
Figure 4.18. Comparison of ¹H NMR spectra of ArZnOTf + L1 (top) with stoichiometric reactions. Red-2f; blue-biaryl; green-anisole; int. std. -orange.

This experiment reinforced the hypothesis that transmetalation from Ni to Zn may occur during the carboxylation reaction. However, as discussed in Section 4.5.1, carboxylation of arylzinc species is very slow in the absence of Ni or LiCl and is shut down when **L1** is added. This suggests that if "[(**L1**)ZnAr]OTf" is formed during the catalytic reaction it only acts as a reservoir of the aryl group rather than as an intermediate at which carboxylation occurs.

4.5.6. Mechanistic proposal

The results discussed above support the C(*sp²*)–S carboxylation mechanism proposed in Scheme 4.27 below. This mechanism is based on the generally accepted reductive carboxylation mechanism discussed in Section 4.1 but includes Ni-to-Zn transmetalation from Ni–aryl intermediates. It is unclear whether the Ni(II) oxidative addition complex **IV** undergoes transmetalation with a Zn(II) salt to give ArZnX and a cationic Ni(II) complex **V** or whether the oxidative addition complex is first reduced to Ni(I) prior to transmetalation. This Ni(I)–Ar species (**VI**) would react with a Zn(II) salt to form ArZnX and Ni(I)X complex **VII**.

Complex **VII** might indeed correspond to isolated Ni(I) triflate complex **5-OTf**. If a Ni-to-Zn transmetalation equilibrium is present and does lead from **VI** to **5-OTf**, slow back-transmetalation from **5-OTf** + ArZnX would explain why **5-OTf** can be identified in the catalytic carboxylation reaction and why quenching experiments show the presence of a significant amount of arylzinc species during the

reaction. Kinetic studies would provide information about whether **5-OTf** is on- or off-cycle. However, whether reliable kinetic studies could be carried out on a reaction that requires both Zn powder and sampling under 1 atm CO_2 is unclear. Diao and Lin found that kinetic data of the bulk solution could be obtained from a Ni-catalysed reductive 1,2-dicarbofunctionalisation reaction if the stirring of the heterogeneous Zn-containing reactions was carefully controlled with an orbital shaker.[112] It would also be interesting to investigate organic reductants more thoroughly. If an organic reductant could be paired with a soluble Zn(II) salt, the heterogeneity problem would be solved.

Insertion of CO_2 at **VI** was proposed based on the literature discussed in Chapters 3 and 4 and the experimental results of Chapter 3. For clarity, the carboxylate complex **VIII** is shown to be reduced by Zn directly. However, anion exchange may with a Zn(II) salts prior to reduction.
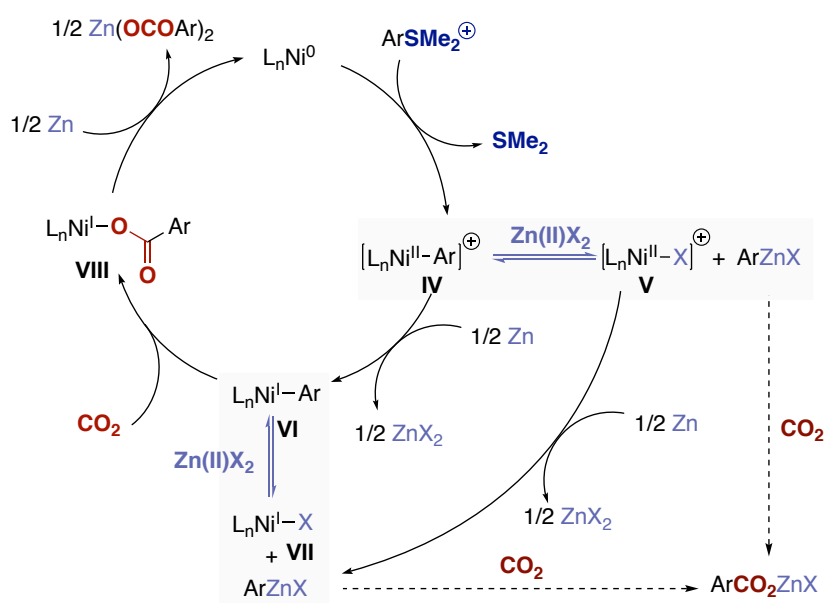
Scheme 4.27. Proposed mechanism for the reductive carboxylation of arylsulfonium salts including Ni-to-Zn transmetalation pathways.

4.6.   Conclusions

This chapter describes the development of a mild Ni-catalysed reductive carboxylation of arylsulfonium salts and the mechanistic studies that were carried out to shed light on key questions in the reductive carboxylation field. Arylsulfonium salts are interesting electrophiles to deploy in reductive carboxylation because they are very stable, they are activated towards oxidative addition, and they provide a link between carboxylic acid synthesis with CO_2 and organosulfur chemistry. Four goals were set at the beginning of the investigation: (1) to develop a reductive carboxylation protocol; (2) to understand $C(sp^2)$–SMe_2^+ cleavage; (3) to understand activation of the Ni(II) precatalyst; and (4) to determine whether there were any spectroscopic signatures of Ni(I) intermediates.

The Yorimitsu group optimised the reaction and investigated the substrate scope. Its mild conditions are underscored by the absence of extra additives and by the solvent. DMSO is a less toxic alternative to the amide solvents that are usually employed in reductive carboxylation reactions with metal powder reducing agents. During optimisation it was found that Zn was the only reductant with which carboxylation reactions would occur. This opened another avenue of investigation during the mechanistic study.

The reduction of the [NiBr$_2$**L1**] precatalyst was investigated and the rapid formation of Ni(I) complex **5-Br** was observed. Its subsequent slower reduction to brown species was investigated by trapping experiments and evidence for the formation of Ni(0) was obtained. This was supported by stoichiometric reactions between isolated Ni complexes [Ni(**L1**)$_2$] and **5-OTf** and an arylsulfonium salt. No C(sp^2)–S cleavage products were obtained when Ni(I) complex **5-OTf** was reacted with the arylsulfonium salt, but when Zn(0) was present or when [Ni(**L1**)$_2$] was employed, Me$_2$S and "[**L1**ZnAr]OTf" were observed.

The observation of ^{1}H NMR signals of "[**L1**ZnAr]OTf" constitutes the first direct evidence for the formation of a Zn–Ar complex after oxidative addition of an aryl (pseudo)halide. Alongside the D$_2$O quenching experiment, this study supports the idea that Ni–aryl complexes can undergo Ni-to-Zn transmetalation during carboxylation reactions when Zn is the reductant. Further studies are required to determine the oxidation state of the Ni–aryl complex that undergoes transmetalation to Zn(II).

Overall, the proposed mechanism reinforces the notion that the role of the metallic reductant might be more complicated than initially anticipated.

4.7.   References

(1)   *Carbon Dioxide as Chemical Feedstock*; Aresta, M., Ed.; Wiley VCH: Weinheim, 2010.

(2)   Sakakura, T.; Choi, J. C.; Yasuda, H. Transformation of Carbon Dioxide. *Chem. Rev.* **2007**, *107* (6), 2365–2387.

(3)   Artz, J.; Müller, T. E.; Thenert, K.; Kleinekorte, J.; Meys, R.; Sternberg, A.; Bardow, A.; Leitner, W. Sustainable Conversion of Carbon Dioxide: An Integrated Review of Catalysis and Life Cycle Assessment. *Chem. Rev.* **2018**, *118* (2), 434–504.

(4)   Cokoja, M.; Bruckmeier, C.; Rieger, B.; Herrmann, W. A.; Kühn, F. E. Transformation of Carbon Dioxide with Homogeneous Transition-Metal Catalysts: A Molecular Solution to a Global Challenge? *Angew. Chem. Int. Ed.* **2011**, *50* (37), 8510–8537.

(5)   Huang, K.; Sun, C. L.; Shi, Z.-J. Transition-Metal-Catalyzed C–C Bond Formation through the Fixation of Carbon Dioxide. *Chem. Soc. Rev.* **2011**, *40* (5), 2435–2452.

(6)   Tortajada, A.; Juliá-Hernández, F.; Börjesson, M.; Moragas, T.; Martin, R. Transition-Metal-Catalyzed Carboxylation Reactions with Carbon Dioxide. *Angew. Chem. Int. Ed.* **2018**, *57* (49), 15948–15982.

(7)   Burkart, M. D.; Hazari, N.; Tway, C. L.; Zeitler, E. L. Opportunities and Challenges for Catalysis in Carbon Dioxide Utilization. *ACS Catal.* **2019**, *9* (9), 7937–7956.

(8)   Sayyed, F. B.; Tsuji, Y.; Sakaki, S. The Crucial Role of a Ni(I) Intermediate in Ni-Catalyzed Carboxylation of Aryl Chloride with CO_2: A Theoretical Study. *Chem. Commun.* **2013**, *49* (91), 10715.

(9)   Mohadjer Beromi, M.; Brudvig, G. W.; Hazari, N.; Lant, H. M.; Mercado, B. Q. Synthesis and Reactivity of Paramagnetic Polypyridyl Ni Complexes Relevant to Csp^2–Csp^3 Coupling Reactions. *Angew. Chem. Int. Ed.* **2019**.

(10)   Diccianni, J. B.; Hu, C.; Diao, T. (Xantphos)Ni(I)-Alkyl Mediated Insertion of CO_2. *Angew. Chemie Int. Ed.* **2019**.

(11)   Charboneau, D. J.; Brudvig, G. W.; Hazari, N.; Lant, H. M. C.; Saydjari, A. K. Development of an Improved System for the Carboxylation of Aryl Halides through Mechanistic Studies. *ACS Catal.* **2019**, *9* (4), 3228–3241.

(12)   Tsou, T. T.; Kochi, J. K. Mechanism of Oxidative Addition. Reaction of Nickel(0) Complexes with Aromatic Halides. *J. Am. Chem. Soc.* **1979**, *101* (21), 6319–6332.

(13)   Diccianni, J. B.; Katigbak, J.; Hu, C.; Diao, T. Mechanistic Characterization of (Xantphos)Ni(I)-Mediated Alkyl Bromide Activation: Oxidative Addition, Electron Transfer, or Halogen-Atom Abstraction. *J. Am. Chem. Soc.* **2019**, *141* (4), 1788–1796.

(14)   Bajo, S.; Laidlaw, G.; Kennedy, A. R.; Sproules, S.; Nelson, D. J. Oxidative Addition of Aryl Electrophiles to a Prototypical Nickel(0) Complex: Mechanism and Structure/Reactivity Relationships. *Organometallics* **2017**, *36* (8), 1662–1672.

(15)   Funes-Ardoiz, I.; Nelson, D. J.; Maseras, F. Halide Abstraction Competes with Oxidative Addition in the Reactions of Aryl Halides with [Ni(PMe$_n$Ph$_{(3-N)}$)$_4$]. *Chem. Eur. J.* **2017**, *23* (66), 16728–16733.

(16)   Richmond, E.; Moran, J. Recent Advances in Nickel Catalysis Enabled by Stoichiometric Metallic Reducing Agents. *Synthesis (Stuttg).* **2018**, *50* (3), 499–513.

(17)   Minami, H.; Nogi, K.; Yorimitsu, H. Palladium-Catalyzed Alkoxycarbonylation of Arylsulfoniums. *Org. Lett.* **2019**, *21*, 2518–2522.

(18)   Uno, D.; Minami, H.; Otsuka, S.; Nogi, K.; Yorimitsu, H. Palladium-Catalyzed Mizoroki–Heck-Type Alkenylation of Monoaryldialkylsulfoniums. *Chem. Asian J.* **2018**, *13* (17), 2397–2400.

(19)   Minami, H.; Otsuka, S.; Nogi, K.; Yorimitsu, H. Palladium-Catalyzed Borylation of Aryl Sulfoniums with Diborons. *ACS Catal.* **2018**, *8* (1), 579–583.

(20)   Kawashima, H.; Yanagi, T.; Wu, C.-C.; Nogi, K.; Yorimitsu, H. Regioselective C–H Sulfanylation of Aryl Sulfoxides by Means of Pummerer-Type Activation. *Org. Lett.* **2017**, *19* (17), 4552–4555.

(21)   Feng, M.; Tang, B.; Liang, S. H.; Jiang, X. Sulfur Containing Scaffolds in Drugs: Synthesis and Application in Medicinal Chemistry. *Curr. Top. Med. Chem.* **2016**, *16*, 1200–1216.

(22)   Northcote, P. T.; Blunt, J. W.; Munro, M. H. G. Pateamine: A Potent Cytotoxin from the New Zealand Marine Sponge, Mycale Sp. *Tetrahedron Lett.* **1991**, *32* (44), 6411–6414.

(23)   *Sulfur Compounds: Advances in Research and Application*; Acton, A. Q., Ed.; Scholarly Eds.: Atlanta, GA, 2012.

(24)   Ruano, J. L. G.; de la Plata, B. C. In *Organosulfur Chemistry I*; Page, P. C. B., Ed.; Springer: Heidelberg, 1999; p 1.

(25)   Furukara, N.; Sato, S. In *Organosulfur Chemistry II*; Page, P. C. B., Ed.; Springer: Heidelberg, 1999; p 89.

(26)   Rayner, C. M. *Advances in Sulfur Chemistry*, Vol. 2.; JAI Press: Greenwich, 2000.

(27)   Dubbaka, S. R.; Vogel, P. Organosulfur Compounds: Electrophilic Reagents in Transition-Metal-Catalyzed Carbon-Carbon Bond-Forming Reactions. *Angew. Chem. Int. Ed.* **2005**, *44* (47), 7674–7684.

(28)   Wenkert, E.; Ferreira, T. W.; Michelotti, E. L. Nickel-Induced Conversion of Carbon-Sulphur into Carbon-Carbon Bonds. One-Step Transformations of Enol Sulphides into Olefins and Benzenethiol Derivatives into Alkylarenes and Biaryls. *J. Chem. Soc. Chem. Commun.* **1979**, No. 14, 637–638.

(29)   Okamura, H.; Takei, H. Cross-Coupling of Allylic Sulfides and Grignard Reagents Catalyzed by Nickel-Phosphine Complex. *Tetrahedron Lett.* **1979**, *4* (36), 3425–3428.

(30)   Okamura, H.; Miura, M.; Takei, H. Nickel-Phosphine Complex Catalyzed Coupling Reaction of Grignard Reagents with Alkenyl or Aryl Sulfides. *Tetrahedron Lett.* **1979**, *20* (1), 43–46.

(31)   Julia, M.; Righini, A.; Verpeaux, J. N. Couplage Des Sulfones Allyliques Avec Des Reactifs de Grignard En Presence de Cuivre Synthese d'Olefines. *Tetrahedron Lett.* **1979**, *20* (26), 2393–2396.

(32)   Wenkert, E.; Michelotti, E. L.; Swindell, C. S. Nickel-Induced Conversion of Carbon-Oxygen into Carbon-Carbon Bonds. One-Step Transformations of Enol Ethers into Olefins and Aryl Ethers into Biaryls. *J. Am. Chem. Soc.* **1979**, *101* (8), 2246–2247.

(33)   Zarate, C.; van Gemmeren, M.; Somerville, R. J.; Martin, R. Chapter Four-Phenol Derivatives: Modern Electrophiles in Cross-Coupling Reactions. *Adv. Organomet. Chem.* **2016**, *66*, 143–222.

(34)   Barbero, N.; Martin, R. Ligand-Free Ni-Catalyzed Reductive Cleavage of Inert Carbon-Sulfur Bonds. *Org. Lett.* **2012**, *14* (3), 796–799.

(35)   Lian, Z.; Bhawal, B. N.; Yu, P.; Morandi, B. Palladium-Catalyzed Carbon-Sulfur or Carbon-Phosphorus Bond Metathesis by Reversible Arylation. *Science* **2017**, *356* (6342), 1059–1063.

(36)   Delcaillau, T.; Bismuto, A.; Lian, Z.; Morandi, B.; Preprint, C. Nickel-Catalyzed Inter-and Intramolecular Carbon-Sulfur Bond Metathesis by Reversible Arylation. **2019**, No. Table 1, 1–7.

(37)   Bhanuchandra, M.; Baralle, A.; Otsuka, S.; Nogi, K.; Yorimitsu, H.; Osuka, A. Palladium-Catalyzed Ipso-Borylation of Aryl Sulfides with Diborons. *Org. Lett.* **2016**, *18* (12), 2966–2969.

(38)   Gao, K.; Otsuka, S.; Baralle, A.; Nogi, K.; Yorimitsu, H.; Osuka, A. Cross-Coupling of Aryl Sulfides Powered by N-Heterocyclic Carbene Ligands. *J. Synth. Org. Chem. Japan* **2016**, *74* (11), 1119–1127.

(39)   Srogl, J.; Allred, G. D.; Liebeskind, L. S. Sulfonium Salts. Participants Par Excellence in Metal-Catalyzed Carbon-Carbon Bond-Forming Reactions. *J. Am. Chem. Soc.* **1997**, *119* (23), 12376–12377.

(40)   Gendreau, Y.; Normant, J. F.; Villieras, J. Action d'Organomagnesiens Sur Des Sulfures et Des Sels de Sulfonium Allyliques Catalysee Par Des Sels Cuivreux. *J. Organomet. Chem.* **1977**, *142* (1), 1–7.

(41)   Zhang, S.; Marshall, D.; Liebeskind, L. S. Efficient Pd-Catalyzed Heterobenzylic Cross-Coupling Using Sulfonium Salts as Substrates and (PhO)₃P as a Supporting Ligand. *J. Org. Chem.* **1999**, *64* (8), 2796–2804.

(42)   Uetake, Y.; Niwa, T.; Hosoya, T. Rhodium-Catalyzed Ipso-Borylation of Alkylthioarenes via C–S Bond Cleavage. *Org. Lett.* **2016**, *18* (11), 2758–2761.

(43)   Goldfogel, M. J.; Huang, L.; Weix, D. J. Cross-Electrophile Coupling. Principles and New Reactions. In *Nickel Catalysis in Organic Synthesis*; Ogoshi, S., Ed.; Wiley Online Books; 2019; pp 183–222.

(44)   Everson, D. A.; Weix, D. J. Cross-Electrophile Coupling: Principles of Reactivity and Selectivity. *J. Org. Chem.* **2014**, *79* (11), 4793–4798.

(45)   Weix, D. J. Methods and Mechanisms for Cross-Electrophile Coupling of Csp² Halides with Alkyl Electrophiles. *Acc. Chem. Res.* **2015**, *48* (6), 1767–1775.

(46)   Obst, M.; Pavlovic, L.; Hopmann, K. H. Carbon-Carbon Bonds with CO₂: Insights from Computational Studies. *J. Organomet. Chem.* **2018**, *864*, 115–127.

(47)   Sahoo, B.; Bellotti, P.; Juliá-Hernández, F.; Meng, Q. Y.; Crespi, S.; König, B.; Martin, R. Site-Selective, Remote Sp³ C−H Carboxylation Enabled by the Merger of Photoredox and Nickel Catalysis. *Chem. Eur. J.* **2019**, *25* (38), 9001–9005.

(48)   Meng, Q. Y.; Wang, S.; Huff, G. S.; Konig, B. Ligand-Controlled Regioselective Hydrocarboxylation of Styrenes with CO₂ by Combining Visible Light and Nickel Catalysis. *J. Am. Chem. Soc.* **2018**, *140* (9), 3198–3201.

(49)   Meng, Q. Y.; Wang, S.; König, B. Carboxylation of Aromatic and Aliphatic Bromides and Triflates with CO₂ by Dual Visible-Light–Nickel Catalysis. *Angew. Chem. Int. Ed.* **2017**, *56* (43), 13426–13430.

(50)   Becica, J.; Dobereiner, G. E. The Roles of Lewis Acidic Additives in Organotransition Metal Catalysis. *Org. Biomol. Chem.* **2019**, *17* (8), 2055–2069.

(51)   Hazari, N.; Heimann, J. E. Carbon Dioxide Insertion into Group 9 and 10 Metal-Element σ Bonds. *Inorg. Chem.* **2017**, *56* (22), 13655–13678.

(52)   Heimann, J. E.; Bernskoetter, W. H.; Hazari, N. Understanding the Individual and Combined Effects of Solvent and Lewis Acid on CO 2 Insertion into a Metal Hydride . *J. Am. Chem. Soc.* **2019**, *141* (26), 10520–10529.

(53)   Sayyed, F. B.; Sakaki, S. The Crucial Roles of MgCl₂ as a Non-Innocent Additive in the Ni-Catalyzed Carboxylation of Benzyl Halide with CO₂. *Chem. Commun.* **2014**, *50* (86), 13026–13029.

(54)   Leon, T.; Correa, A.; Martin, R. Ni-Catalyzed Direct Carboxylation of Benzyl Halides with CO₂. *J. Am. Chem. Soc.* **2013**, *135* (4), 1221–1224.

(55)   Fujihara, T.; Nogi, K.; Xu, T.; Terao, J.; Tsuji, Y. Nickel-Catalyzed Carboxylation of Aryl and Vinyl Chlorides

Employing Carbon Dioxide. *J. Am. Chem. Soc.* **2012**, *134* (22), 9106–9109.

(56) Murphy, J. A.; Gamier, J.; Park, S. R.; Schoenebeck, F.; Zhou, S. Z.; Turner, A. T. Super-Electron Donors: Bis-Pyridinylidene Formation by Base Treatment of Pyridinium Salts. *Org. Lett.* **2008**, *10* (6), 1227–1230.

(57) Garnier, J.; Kennedy, A. R.; Berlouis, L. E. A.; Turner, A. T.; Murphy, J. A. Structure and Reactivity in Neutral Organic Electron Donors Derived from 4-Dimethylaminopyridine. *Beilstein J. Org. Chem.* **2010**, *6*, 4–11.

(58) Aranzaes, J. R.; Daniel, M. C.; Astruc, D. Metallocenes as References for the Determination of Redox Potentials by Cyclic Voltammetry - Permethylated Iron and Cobalt Sandwich Complexes, Inhibition by Polyamine Dendrimers, and the Role of Hydroxy-Containing Ferrocenes. *Can. J. Chem.* **2006**, *84* (2), 288–299.

(59) Stirling, D.; Clark, J. H.; Braithwaite, M. J. *The Sulfur Problem*; RSC Clean Technology Monographs; The Royal Society of Chemistry, 2000.

(60) Vicic, D. A.; Jones, W. D. Modeling the Hydrodesulfurization Reaction at Nickel. Unusual Reactivity of Dibenzothiophenes Relative to Thiophene and Benzothiophene. *J. Am. Chem. Soc.* **1999**, *121* (33), 7606–7617.

(61) Desnoyer, A. N.; Love, J. A. Recent Advances in Well-Defined, Late Transition Metal Complexes That Make And/or Break C–N, C–O and C–S Bonds. *Chem. Soc. Rev.* **2017**, *46* (1), 197–238.

(62) Wenkert, E.; Shepard, M. E.; McPhail, A. T. Oxidative Addition of Aryl Sulphides to Low-Valent Nickel Species. *J. Chem. Soc. Chem. Commun.* **1986**, No. 17, 1390–1391.

(63) Osakada, K.; Maeda, M.; Nakamura, Y.; Yamamoto, T.; Yamamoto, A. Reversible Oxidative Addition and Reductive Elimination of Diaryl Sulphide Involving C–S Bond Cleavage and Formation: Exchange of Two Aryl Groups in Aryl(arylthiolato)nickel Complexes Having Tertiary Phosphine Ligands. *J. Chem. Soc.* **1986**, No. 6, 442–443.

(64) Ito, M.; Matsumoto, T.; Tatsumi, K. Synthesis and Reactions of Mono- and Dinuclear Ni(I) Thiolate Complexes. *Inorg. Chem.* **2009**, *48* (5), 2215–2223.

(65) Desnoyer, A. N.; Friese, F. W.; Chiu, W.; Drover, M. W.; Patrick, B. O.; Love, J. A. Exploring Regioselective Bond Cleavage and Cross-Coupling Reactions Using a Low-Valent Nickel Complex. *Chem. Eur. J.* **2016**, *22* (12), 4070–4077.

(66) Zimmerman, A. C.; Fryzuk, M. D. β-Hydrogen Elimination and Reductive Elimination from a K^3-PPC Nickel Complex. *Organometallics* **2018**, *37* (14), 2305–2318.

(67) Schaub, T.; Marc, B.; Oliver, P.; Radius, U. Facile C–S, S–H, and S–S Bond Cleavage Using a Nickel(0) NHC Complex. *Dalt. Trans.* **2009**, 7071–7079.

(68) Matsunaga, P. T.; Hillhouse, G. L. Thianickelacycles by Ring-Opening Reactions of Cyclic Thioethers and Their Subsequent Carbonylation to Thioesters. *Angew. Chem. Int. Ed. Engl.* **1994**, *33* (17), 1748–1749.

(69) Camasso, N. M.; Sanford, M. S. Design, Synthesis, and Carbon-Heteroatom Coupling Reactions of Organometallic Nickel(IV) Complexes. *Science* **2015**, *347* (6227), 1218–1220.

(70) Bour, J. R.; Camasso, N. M.; Sanford, M. S. Oxidation of Ni(II) to Ni(IV) with Aryl Electrophiles Enables Ni-Mediated Aryl–CF₃ Coupling. *J. Am. Chem. Soc.* **2015**, *137* (25), 8034–8037.

(71) Rovira, M.; Roldán-Gómez, S.; Martin-Diaconescu, V.; Whiteoak, C. J.; Company, A.; Luis, J. M.; Ribas, X. Trifluoromethylation of a Well-Defined Square-Planar Aryl-NiII Complex Involving NiIII/CF₃· and NiIV−CF₃ Intermediate Species. *Chem. Eur. J.* **2017**, *23* (48), 11662–11668.

(72) Serrano, E.; Soler, T.; Navarro, R.; Urriolabeitia, E. P. Different Bonding Modes of Sulfur Bis-Ylides in Pd Complexes: Crystal Structure of [Pd(μ-OAc){μ-[CH(SMe₂)]₂C(O)}(acac-O,O′)₂]ClO₄. *J. Mol. Struct.* **2008**, *890*, 57–62.

(73) Davidson, J. G.; Barefield, E. K.; Van Derveer, D. G. Synthesis and Reactivity of [(Thiomethoxy)methyl]-and [(Dimethylsulfonio)methyl]nickel(II) Complexes. *Organometallics* **1985**, *4* (7), 1178–1184.

(74) Lin, H.; Dong, X.; Li, Y.; Shen, Q.; Lu, L. Highly Selective Activation of Vinyl C–S Bonds over Aryl C–S Bonds in the Pd-Catalyzed Coupling of (E)-(β-Trifluoromethyl)vinyldiphenylsulfonium Salts: Preparation of Trifluoromethylated Alkenes and Dienes. *Eur. J. Org. Chem.* **2012**, No. 25, 4675–4679.

(75) Williams, C. M.; Johnson, J. B.; Rovis, T. Nickel-Catalyzed Reductive Carboxylation of Styrenes Using CO₂. *J. Am. Chem. Soc.* **2008**, *130* (45), 14936–14937.

(76) Cahiez, G.; Duplais, C.; Buendia, J. Chemistry of Organomanganese(II) Compounds. *Chem. Rev.* **2009**, *109*, 1434–1476.

(77) Mita, T.; Chen, J.; Sato, Y. Synthesis of Arylglycines from CO₂ through α-Amino Organomanganese Species. *Org. Lett.* **2014**, *16* (8), 2200–2203.

(78) Friour, G.; Cahiez, G.; Alexakis, A.; Normant, J. F. *Bull. Soc. Chem. Fr. II* **1979**, 515–517.

(79) Liu, Y.; Cornella, J.; Martin, R. Ni-Catalyzed Carboxylation of Unactivated Primary Alkyl Bromides and Sulfonates with CO₂. *J. Am. Chem. Soc.* **2014**, *136* (32), 11212–11215.

(80) Correa, A.; León, T.; Martin, R. Ni-Catalyzed Carboxylation of C(sp²)– and C (sp³)–O Bonds with CO₂. *J. Am. Chem. Soc.* **2014**, *136* (3), 1062–1069.

(81) Correa, A.; León, T.; Martin, R. Ni-Catalyzed Carboxylation of C(sp²)– and C (sp³)–O Bonds with CO₂. *J. Am. Chem. Soc.* **2014**, *136* (3), 1062–1069.

(82) Aresta, M.; Nobile, C. F.; Albano, V. G.; Forni, E.; Manassero, M. New Nickel-Carbon Dioxide Complex: Synthesis, Properties, and Crystallographic Characterization of (Carbon Dioxide)- Bis(tricyclohexylphosphine)nickel. *J. Chem. Soc., Chem. Commun.* **1975**, *0*, 636–637.

(83) Aresta, M. My Journey in the CO₂-Chemistry Wonderland. *Coord. Chem. Rev.* **2017**, *334*, 150–183.

(84) Bercot, E. A.; Rovis, T. Highly Efficient Nickel-Catalyzed Cross-Coupling of Succinic and Glutaric Anhydrides with Organozinc Reagents. *J. Am. Chem. Soc.* **2005**, *127* (1), 247–254.

(85) Ochiai, H.; Jang, M.; Hirano, K.; Yorimitsu, H.; Oshima, K. Nickel-Catalyzed Carboxylation of Organozinc Reagents with CO₂. *Org. Lett.* **2008**, *10* (13), 2681–2683.

(86) Yeung, C. S.; Dong, V. M. Beyond Aresta's Complex: Ni- and Pd-Catalyzed Organozinc Coupling with CO₂. *J. Am. Chem. Soc.* **2008**, *130* (25), 7826–7827.

(87) Wang, J.; Wang, M. Y.; Yin, G.; Jia, R.; Wang, J.; Eglitis, R. I.; Zhang, H. X. Nickel-Catalyzed Carboxylation of Aryl Zinc Reagent with CO₂: A Theoretical and Experimental Study. *J. CO₂ Util.* **2019**, *29*, 262–270.

(88) Kobayashi, K.; Kondo, Y. Transition-Metal-Free Carboxylation of Organozinc Reagents Using CO₂ in DMF Solvent. *Org. Lett.* **2009**, *11* (9), 2035–2037.

(89) Metzger, A.; Bernhardt, S.; Manolikakes, G.; Knochel, P. MgCl-Accelerated Addition of Functionalized Organozinc Reagents to Aldehydes, Ketones, and Carbon Dioxide. *Angew. Chem. Int. Ed.* **2010**, *49* (27), 4665–4668.

(90) Tran-Vu, H.; Daugulis, O. Copper-Catalyzed Carboxylation of Aryl Iodides with Carbon Dioxide. *ACS Catal.* **2013**, *3* (10), 2417–2420.

(91) Seka, S.; Buriez, O.; Nédélec, J.-Y.; Périchon, J. Mechanism of the Electrochemical Conversion of Aryl Halides to Arylzinc Compounds by Cobalt Catalysis in DMF/Pyridine. *Chem. Eur. J.* **2002**, No. 11, 2534–2538.

(92) Seka, S.; Buriez, O.; Périchon, J. Stabilization of CoI by ZnII in Pure Acetonitrile and Its Reaction with Aryl Halides. *Chem. Eur. J.* **2003**, *9* (15), 3597–3603.

(93) Pignon, A.; Le Gall, E.; Martens, T. A New Manganese-Mediated, Cobalt-Catalyzed Threecomponent Synthesis of (Diarylmethyl)sulfonamides. *Beilstein J. Org. Chem.* **2014**, *10*, 425–431.

(94) Wiberg, N. Tetraaminoathylene Als Starke Elektronendonoren. *Angew. Chemie* **1968**, *80* (20), 809–856.

(95) Broggi, J.; Terme, T.; Vanelle, P. Organic Electron Donors as Powerful Single-Electron Reducing Agents in Organic Synthesis. *Angew. Chem. Int. Ed.* **2014**, *53* (2), 384–413.

(96) Sasano, K.; Takaya, J.; Iwasawa, N. Palladium(II)-Catalyzed Direct Carboxylation of Alkenyl C–H Bonds with CO₂. *J. Am. Chem. Soc.* **2013**, *135* (30), 10954–10957.

(97) Ukai, K.; Aoki, M.; Takaya, J.; Iwasawa, N. Rhodium(I)-Catalyzed Carboxylation of Aryl- and Alkenylboronic Esters with CO₂. *J. Am. Chem. Soc.* **2006**, *128* (27), 8706–8707.

(98) Beak, P.; Sullivan, T. A. One-Electron Chemical Reductions of Phenylalkylsulfonium Salts. *J. Am. Chem. Soc.* **1982**, *104* (16), 4450–4457.

(99) Rebih, F.; Andreini, M.; Moncomble, A.; Harrison-Marchand, A.; Maddaluno, J.; Durandetti, M. Direct Carboxylation of Aryl Tosylates by CO₂ Catalyzed by In situ-Generated Ni(0). *Chem. Eur. J.* **2016**, *22* (11), 3758–3763.

(100) Conan, A.; Sibille, S.; Périchon, J. Metal Exchange between an Electrogenerated Organonickel Species and Zinc Halide : Application to an Electrochemical, Nickel-Catalyzed Reformatsky Reaction. *J. Org. Chem.* **1991**, *56*, 2018–2024.

(101) Stüdemann, T.; Knochel, P. New Nickel-Catalyzed Carbozincation of Alkynes: A Short Synthesis of (Z)-Tamoxifen. *Angew. Chem. Int. Ed. Engl.* **1997**, *36* (1-2), 93–95.

(102) Stüdemann, T.; Ibrahim-Ouali, M.; Knochel, P. A Nickel-Catalyzed Carbozincation of Aryl-Substituted Alkynes. *Tetrahedron* **1998**, *54* (7), 1299–1316.

(103) Murakami, K.; Yorimitsu, H. Recent Advances in Transition-Metal-Catalyzed Intermolecular Carbomagnesiation and Carbozincation. *Beilstein J. Org. Chem.* **2013**, *9* (1), 278–302.

(104) Brewer, B.; Brooks, N. R.; Sykes, A. G. Characterization of an Asymmetric M(chelate)₂(μ-Cl)₂MCl₂ Dimer and Isolation of Corresponding DMSO Adducts: X-Ray Crystal Structures of Co(phen)₂(μ-Cl)₂CoCl₂·C₄H₈O and M(chelate)Cl₂(DMSO)ₓ(Co, X = 1 ; Ni , X = 2) Complexes. *J. Chem. Crystallogr.* **2003**, *33* (9), 663–668.

(105) Ding, C. F.; Miao, Y. F.; Tian, B. Q.; Li, X. M.; Zhang, S. S. Aquadichloro(2,9-Dimethyl-1,10-Phenanthroline-κ²N,N′)nickel(II). *Acta Crystallogr. Sect. E* **2006**, *62* (5), 1062–1063.

(106) Klein, A.; Kaiser, A.; Sarkar, B.; Wanner, M.; Fiedler, J. The Electrochemical Behaviour of Organonickel Complexes: Mono-, Di- and Trivalent Nickel. *Eur. J. Inorg. Chem.* **2007**, *2007* (7), 965–976.

(107) Powers, D. C.; Anderson, B. L.; Nocera, D. G. Two-Electron HCl to H₂ Photocycle Promoted by Ni(II) Polypyridyl Halide Complexes. *J. Am. Chem. Soc.* **2013**, *135* (50), 18876–18883.

(108) Börjesson, M.; Moragas, T.; Martin, R. Ni-Catalyzed Carboxylation of Unactivated Alkyl Chlorides with CO₂. *J.*

Am. Chem. Soc. **2016**, *138* (24), 7504–7507.

(109) Wang, M.; England, J.; Weyhermüller, T.; Wieghardt, K. Electronic Structures of "Low-valent" Neutral Complexes [NiL$_2$]^0 (S = 0; L = Bpy, Phen, Tpy) – An Experimental and DFT Computational Study. *Eur. J. Inorg. Chem.* **2015**, *2015* (9), 1511–1523.

(110) Ananikov, V. P.; Gayduk, K. A.; Starikova, Z. A.; Beletskaya, I. P. Ni(acac)$_2$/phosphine as an Excellent Precursor of nickel(0) for Catalytic Systems. *Organometallics* **2010**, *29* (21), 5098–5102.

(111) Baidya, N.; Mascharak, P. K.; Noll, B. C.; Olmstead, M. M. Nickel(II) Complexes with the [NiN$_x$Se$_y$] Chromophore in Different Coordination Geometries: Search for a Model of the Active Site of [FeNiSe] Hydrogenases. *Inorg. Chem.* **1992**, *31* (14), 2999–3000.

(112) Lin, Q.; Diao, T. Mechanism of Ni-Catalyzed Reductive 1,2-Dicarbofunctionalization of Alkenes. *J. Am. Chem. Soc.* **2019**, *141* (44), 17937–17948.

(113) Prasad, R.; Scaife, D. B. Electro-Oxidation and Electro-Reduction of Some iron(II), cobalt(II) and nickel(II) Polypyridyl Complexes in Acetonitrile. *J. Electroanal. Chem. Interfacial Electrochem.* **1977**, *84* (2), 373–386.

(114) Diccianni, J. B.; Hu, C. T.; Diao, T. Insertion of CO$_2$ Mediated by a (Xantphos)Ni^I–Alkyl Species. *Angew. Chem. Int. Ed.* **2019**, *58* (39), 13865–13868.

(115) Khrizanforov, M.; Khrizanforova, V.; Mamedov, V.; Zhukova, N.; Strekalova, S.; Grinenko, V.; Gryaznova, T.; Sinyashin, O.; Budnikova, Y. Single-Stage Synthetic Route to Perfluoroalkylated Arenes via Electrocatalytic Cross-Coupling of Organic Halides Using Co and Ni Complexes. *J. Organomet. Chem.* **2016**, *820*, 82–88.

(116) Liu, C.; Ni, Q.; Bao, F.; Qiu, J. A Simple and Efficient Protocol for a Palladium-Catalyzed Ligand-Free Suzuki Reaction at Room Temperature in Aqueous DMF. *Green Chem.* **2011**, *13*, 1260–1266.

(117) Evans, D. F. 400. The Determination of the Paramagnetic Susceptibility of Substances in Solution by Nuclear Magnetic Resonance. *J. Chem. Soc.* **1959**, 2003–2005.

(118) Buchalski, P.; Pacholski, R.; Shkurenko, A.; Suwińska, K. Novel, Axially Chiral Analogues of Nickelocene with Nickeladibenzofluorenyl Ligand. *J. Organomet. Chem.* **2015**, *785*, 26–31.

(119) Tao, L.; Xie, Y.; Deng, C.; Li, J. Generation of Pd Nanoparticles in Situ from PdCl$_2$ in TBAF : An Efficient and Reusable Catalytic System for the Suzuki-Miyaura Reaction under Ligand- and Solvent-Free Conditions. *Chin. J. Chem.* **2009**, *27*, 1365–1373.

(120) Moragas, T.; Cornella, J.; Martin, R. Ligand-Controlled Regiodivergent Ni-Catalyzed Reductive Carboxylation of Allyl Esters with CO$_2$. *J. Am. Chem. Soc.* **2014**, *136* (51), 17702–17705.

(121) Schley, N. D.; Fu, G. C. Nickel-Catalyzed Negishi Arylations of Propargylic Bromides: A Mechanistic Investigation. *J. Am. Chem. Soc.* **2014**, *136* (47), 16588–16593.

(122) Denmark, S. E.; Cresswell, A. J. Iron-Catalyzed Cross-Coupling of Unactivated Secondary Alkyl Thio Ethers and Sulfones with Aryl Grignard Reagents. *J. Org. Chem.* **2013**, *78*, 12593–12628.

(123) Senoue, M.; Iwaki, T.; Seki, K.; Yagi, M. Counterion and Position-Dependent Methylation Effects on the Excited States of Zinc(II) Complexes with 1,10-Phenanthroline. *J. Photochem. Photobiol. A Chem.* **1996**, *101*, 257–263.

(124) Crosby, G. A.; Jordan, K. J.; Gamble, G. R. Designing Energy Migration Barriers Into Transition-Metal Complexes. *Fluoresc. Detect. II* **1988**, *910* (April 1988), 173.

(125) Korsager, S.; Taaning, R. H.; Skrydstrup, T. Effective Palladium-Catalyzed Hydroxycarbonylation of Aryl Halides with Substoichiometric Carbon Monoxide. *J. Am. Chem. Soc.* **2013**, *135* (8), 2891–2894.

4.8.   Experimental section

4.8.1. General Considerations

Reagents. [Ni(COD)$_2$] was purchased from Strem Chemicals. Neocuproine (**L1**) and MeOTf were purchased from Sigma Aldrich. All other reagents were purchased from commercial sources and used without further purification. [NiBr$_2$**L1**][115] and 4,4'-dimethoxybiphenyl[116] were synthesised following literature procedures. The synthesis and reductive carboxylation of substrates **2a-BF$_4$,PF$_6$,SbF$_6$, 2b–d,f,h–u** was carried out by Tomoyuki Yanagi.

Solvents. Solvents used for air and moisture-sensitive reactions degassed by sparging or freeze-pump-thaw cycles then dried over 4Å molecular sieves and stored in the glovebox.

Analytical methods. Flash chromatography was performed with Sigma Aldrich technical grade silica gel 60 (230-400 mesh). Thin layer chromatography was carried out using Merck TLC Silica gel 60 F254. NMR spectra were recorded on Bruker Avance Ultrashield 300, 400, or 500 MHz spectrometers, with chemical shifts reported in parts per million (ppm) and coupling constants, *J*, reported in hertz. Melting points were measured using open glass capillaries in a Mettler Toledo MP70 apparatus. Gas chromatographic analyses were performed on an Agilent 6890N gas chromatograph with a FID detector. IR spectra were obtained with a Bruker FT-IR Alpha spectrometer.

UV-vis spectra were recorded in quartz cuvettes using an Agilent Cary 60 spectrophotometer. Continuous wave (CW) EPR spectra were obtained using a Bruker EMX Micro X-band spectrometer using a Bruker ER 1164 HS resonator. Spectra were simulated using SpinFit within Xenon. The samples were cooled to 77 K in a Suprasil finger dewar (Wilmad-LabGlass) filled with liquid nitrogen. Spectrometer settings are provided with the EPR data. Evans method solution magnetic susceptibility measurements were performed for **5-Br** and **5-OTf**.[117,118]

All air-sensitive manipulations were carried out under an atmosphere of nitrogen in an MBraun UNIlab plus glovebox or using standard Schlenk techniques.

4.8.2. Preparations and characterisation data for organic molecules

4.8.2.1. Sulfonium salts

Arylsulfonium 2f[18]
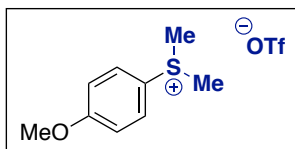
A 50 mL round bottom flask was charged with 4-methoxythioanisole (1.62 g, 10.5 mmol, 1.0 equiv) and put under nitrogen. Dichloromethane (10 mL, undried) was added by syringe, followed by MeOTf (1.38 mL, 12.6 mmol, 1.2 equiv). The resulting solution was stirred at 25 °C for 16 h. Slow addition of Et_2O (10 mL) precipitated the product, which was filtered and washed with 3 × 10 mL Et_2O. Drying under vacuum gave **2f** as a white crystalline solid (3.17 g, 95%).

^{1}H NMR (400 MHz, DMSO-d_6): δ 8.00 (d, $^3J_{H-H}$ = 9.1 Hz, 2H), 7.26 (d, $^3J_{H-H}$ = 9.0 Hz, 2H), 3.87 (s, 3H), 3.21 (s, 6H).

^{19}F NMR (376 MHz, DMSO-d_6): δ −77.83 (s, CF_3).

^{13}C{^{1}H} NMR (101 MHz, DMSO-d_6): δ 163.4 (s, C–OMe), 132.0 (s), 120.7 (q, $^1J_{C-F}$ = 323 Hz, CF_3 OTf), 116.3 (C–SMe_2), 115.9 (s), 56.0 (s, OMe), 28.7 (s).

HRMS (ESI) [$C_9H_{13}OS$]$^+$ (M−OTf) *calcd* 169.0682, *found* 169.0687.

Melting point: 79.9–80.8 °C.

Arylsulfonium 2e
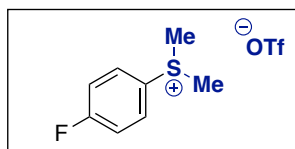
Previously reported compound[18] synthesised from crude 4-fluorothioanisole.[37] Full characterisation data were not available in the literature, so are supplied below.

4-Fluorothiophenol (1.0 mL, 9.4 mmol, 1 equiv) was slowly added to a solution of NaOH (0.563 g, 14 mmol, 1.5 equiv) in dry ethanol (20 mL). After 30 minutes, MeI (0.88 mL, 14 mmol, 1.5 equiv) was added slowly. After 2.5 h, the reaction was cooled in an ice bath. Ice water (15 mL) was added, then the mixture extracted with dichloromethane (2 × 20 mL). After drying over $MgSO_4$ and evaporation of volatiles, the crude oil was filtered through a cotton wool plug. The resulting 969 mg of a pinkish oil was checked by ^{1}H NMR then taken on to the next step.

A 50 mL round bottom flask was charged with 4-fluorothioanisole (0.969 g, 6.8 mmol, 1.0 equiv) and put under nitrogen to protect the reaction from humidity. Dichloromethane (15 mL, undried) was added by syringe, followed by MeOTf (0.894 mL, 8.12 mmol, 1.2 equiv). The resulting solution was stirred at 25 °C for 16 h. The slow addition of Et_2O (10 mL) precipitated the product, which was filtered and washed with 3 × 10 mL Et_2O. Drying under vacuum gave **2e** as a white crystalline solid (2.01 g, 96%).

¹H NMR (400 MHz, DMSO-d_6): δ 8.16 (m, 2H), 7.62 (m, 2H), 3.26 (s, 6H).

¹⁹F NMR (376 MHz, DMSO-d_6): δ −77.83 (s, CF_3), −105.01 (s, F).

¹³C{¹H} NMR (101 MHz, DMSO-d_6): δ 164.9 (d, $^1J_{C\text{-}F}$ = 252.9 Hz, C-F), 133.0 (d, J = 9.9 Hz), 122.5 (d, J = 3.0 Hz), 120.7 (q, $^1J_{C\text{-}F}$ = 323 Hz, CF_3 OTf), 117.7 (d, J = 23.2 Hz), 28.5 (s, SMe_2).

HRMS (ESI) [$C_8H_{10}FS$] (M-OTf) *calcd* 157.0482, *found* 157.0483.

Melting point: 83.8–85.0 °C.

4.8.2.2.   4,4'-Dimethoxybiphenyl
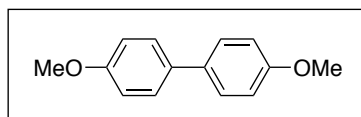
4,4'-dimethoxybiphenyl was synthesised following a literature procedure.[116]

4-bromoanisole (52 μL, 0.42 mmol, 1 equiv), boronic acid (76 mg, 0.48 mmol, 1.1 equiv), and potassium carbonate (115 mg, 0.83 mmol, 2 equiv) were suspended in 2 mL distilled water and 2 mL DMF. Upon addition of $PdCl_2$ (2.2 mg, 0.012 mmol, 0.029 equiv), the reaction was stirred in air for 1 hour. The reaction mixture was then combined with saturated NaCl solution (10 mL), then extracted with Et_2O (3 × 10 mL). After drying and evaporating the crude reaction mixture, column chromatography (9:1 hexane/ethyl acetate) furnished the desired biaryl (74 mg, 83%).

NMR data matched reported data in $CDCl_3$,[119] but ¹H NMR data in DMSO-d_6 are given below for reference with stoichiometric experiments carried out in this work.

¹H NMR (500 MHz, DMSO-d_6): δ 7.53 (d, $^3J_{H\text{-}H}$ = 8.8 Hz, 4H), 6.99 (d, $^3J_{H\text{-}H}$ = 8.7 Hz, 4H), 3.78 (s, 6H).

4.8.3. Preparations and characterisation data for nickel complexes

[NiBr₂L1]
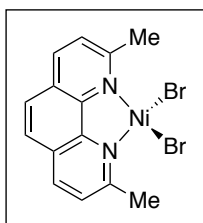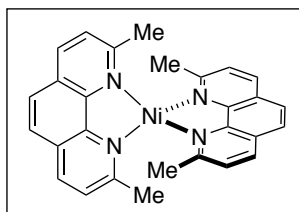

Known compound, synthesised following a literature procedure.[115]
¹H NMR data are provided in CDCl₃ for reference:

¹H NMR (400 MHz, CDCl₃): δ 80.10 (s, 2H), 26.59 (s, 2H), 25.70 (s, 2H), 6.40 (br, $\Delta v_{1/2}$ = 310 Hz, 6H).

[Ni(L1)₂]

[Ni(**L1**)₂] was synthesised following a reported procedure.[120] The method was modified in that filtration through alumina was not carried out before isolation of the dark brown product. This complex is almost completely insoluble in DMSO-d₆, and only low intensity ¹H NMR signals were observed. NMR spectra in C₆D₆ and DMSO-d₆ are provided in Section 3.8.3 for reference.

[Ni(L1)₂]OTf (5-OTf)
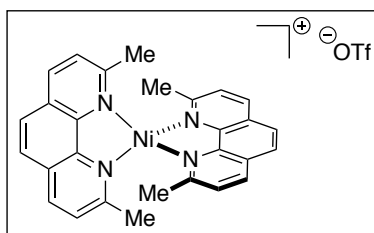
5-OTf was synthesised following a slightly modified literature procedure:[107]

[Ni(**L1**)₂] (99.6 mg, 0.21 mmol, 1 equiv) was dissolved in a mixture of THF (1.5 mL) and ACN (1 mL). Silver triflate (53.8 mg, 0. 21 mmol, 1 equiv) was suspended in a mixture of THF (1.5 mL) and ACN (0.5 mL). *It is important to add the AgOTf as a suspension, as the reaction may otherwise turn grey and precipitate a grey solid.* Upon addition of the AgOTf suspension to the brown [Ni(**L1**)₂] solution, the

reaction mixture became deep blue. After 30 minutes of stirring at room temperature, the solution was passed through a 1 cm celite plug then evaporated to dryness. The residue was washed with pentane (3 × 2 mL), then dried further to give **5-OTf** as a deep blue powder (119 mg, 90%).

¹H NMR (500 MHz, CD₃CN): δ 32.80 (br, $\Delta v_{1/2}$ = 133 Hz, 4H), 13.39 (s, 4H), 11.45 (s, 4H), 0.40 (br, $\Delta v_{1/2}$ = 300 Hz, 12H).

¹⁹F NMR (376 MHz, DMSO-d₆): δ −77.83 (s).

Magnetic susceptibility (Evans method) μ_{eff} = 1.80 μ_{B}

EPR spectrum simulated with g_x = 2.082, g_y = 2.117, g_z = 2.378. lineshape = 1. The continuous wave EPR spectrum was obtained at 9.389 GHz. The spectral data were collected at 77 K with the following spectrometer settings: microwave power = 0.56 mW; centre field = 3250 G, sweep width = 2500 G, sweep time = 35.07 s, modulation frequency = 100 KHz, modulation amplitude = 10 G, power attenuation = 25 dB, time constant = 20.48 ms.

[Ni(L1)₂]Br (5-Br)
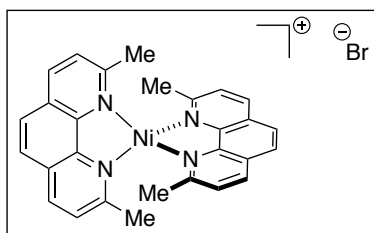
[NiBr₂**L1**] (102.4 mg, 0.24 mmol, 1 equiv), **L1** (50.0 mg, 0.24 mmol, 1 equiv), and Ni(COD)₂ (66.0 mg, 0.24 mmol, 1 equiv) were weighed into an 8 mL vial then suspended in 3 mL THF. Vigorous stirring for 30 minutes gave a dark suspension that was filtered and washed with THF (2 mL), pentane (3 mL), then Et₂O (3 mL). The fine black solid was dried under vacuum to give **5-Br** (156.9 mg, 58%).

¹H NMR (400 MHz, DMSO-d₆): δ 33.13 (br, $\Delta v_{1/2}$ = 230 Hz, 4H), 13.23 (s, 4H), 11.66 (br s, 4H), 0.36 (br, $\Delta v_{1/2}$ = 910 Hz, 12H).

Magnetic susceptibility (Evans method) μ_{eff} = 1.65 μ_{B}

EPR spectra of [Ni(**L1**)₂]Br were more complicated than those of [Ni(**L1**)₂]OTf. Although the presence of a bromine nucleus (I = 3/2) can result in hyperfine coupling being visible in the EPR spectrum, the spectrum was best modelled as a (solvent-dependent) mixture of two Ni(I) species.
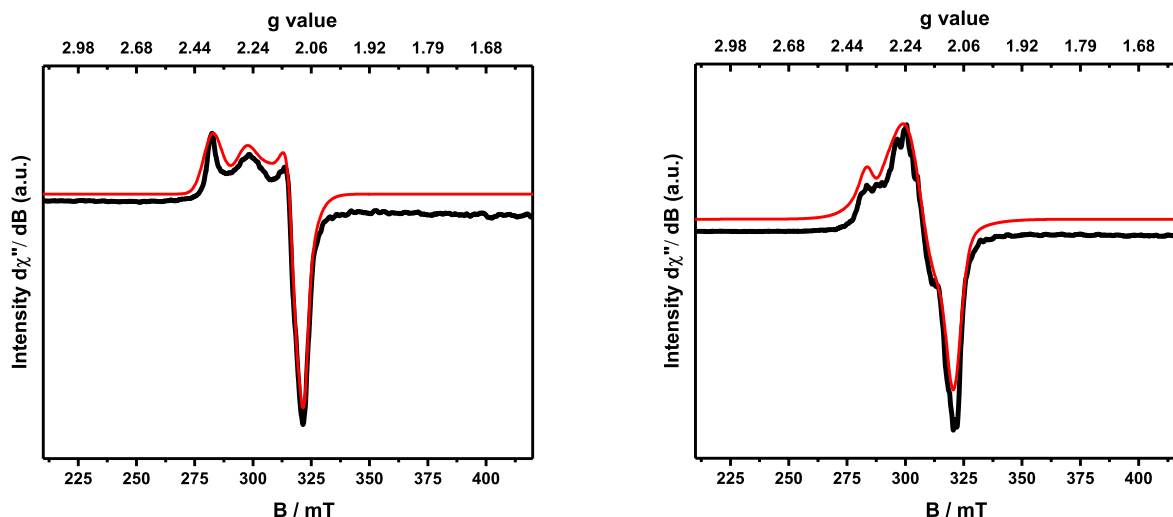
Figure S4.1. Left: EPR spectrum of 5-Br in 2-MeTHF/ACN (4:1) at 77 K; right: 1:1 mixture of 2-MeTHF/ACN.

Left: Simulated spectrum (red) with a 4:1 ratio of two species:

Species 1: $g_x = 2.085$, $g_y = 2.148$, $g_z = 2.367$. lineshape = 1

Species 2: $g_x = 2.099$, $g_y = 2.258$, $g_z = 2.118$. lineshape = 1

**Right:** Simulated spectrum (red) with a 1:1.86 ratio of two species:

Species 1: $g_x = 2.091$, $g_y = 2.189$, $g_z = 2.356$. lineshape = 1

Species 2: $g_x = 2.096$, $g_y = 2.200$, $g_z = 2.254$. lineshape = 1

Continuous wave (CW) EPR spectra were obtained at 9.387 GHz for 4:1 ratio and 9.388 GHz for the 1:1 ratio spectrum. The spectral data were collected at 77 K with the following spectrometer settings: microwave power = 0.56 mW; center field = 3250 G, sweep width = 2500 G, sweep time = 35.07 s, modulation frequency = 100 KHz, modulation amplitude = 10 G, power attenuation = 25 dB, time constant = 20.48 ms.

### 4.8.4. Preparation of Zn species

Zn(*p*-OMeC₆H₄)₂
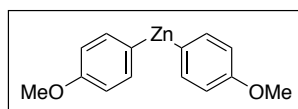
In order to obtain a reference spectrum of a potentially relevant diarylzinc species, the known compound was synthesised following a literature procedure for a diarylzinc with different substituents.[121] The required Grignard reagent was synthesised following a reported procedure.[122]

Dry ZnBr$_2$ (1.37 g, 6.1 mmol, 0.49 equiv) was suspended in 2.2 mL Et$_2$O. Slow addition of 4-methoxyphenylmagnesium bromide (2.49 M) resulted in a colour change to deep brown. The reaction was stirred overnight. The following day, addition of dioxane (2 mL) caused the appearance of a large quantity of white solid and the disappearance of the dark colour. The solid was extracted with diethyl ether (indeed, as noted by Schley and Fu,[121] an excess was required) then the washings transferred to a sublimation flask, evaporated, and the residue purified by sublimation. After washing with hexane (2 × 10 mL) then drying under vacuum, Zn(*p*-OMeC$_6$H$_4$)$_2$ was obtained as a powdery white solid. (0.50 g, 29% yield).

¹H NMR (400 MHz, DMSO-d$_6$): δ 7.44 (d, $^3J_{H-H}$ = 8.13 Hz, 4H), 6.70 (d, $^3J_{H-H}$ = 8.22 Hz, 4H), 3.67 (s, OMe, 6H).
¹³C{¹H} NMR (101 MHz, DMSO-d$_6$): δ 157.1, 151.3, 139.4, 112.1, 54.3.

[ZnBr$_2$L1]
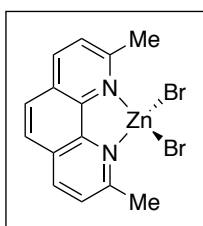
[ZnBr$_2$**L1**] was synthesised following a modified literature procedure:[123]

L1 (42.3 mg, 0.21 mmol, 1 equiv) and ZnBr$_2$ (45.7 mg, 0.21 mmol, 1 equiv) were combined in 3 mL ethanol and the solution stirred until the formation of white solid (approx. 3 min). Filtration of the solid, washing with diethyl ether, and drying under vacuum, gave the desired compound in 82% yield (72.9 mg white solid).

¹H NMR (500 MHz, DMSO-d$_6$): δ 8.90 (d, $^3J_{H-H}$ = 8.4 Hz, 2H), 8.24 (s, 2H), 8.10 (d, $^3J_{H-H}$ = 8.3 Hz, 2H), 3.05 (s, 6H).

## [(L1)Zn(*p*-OMeC$_6$H$_4$)$_2$]
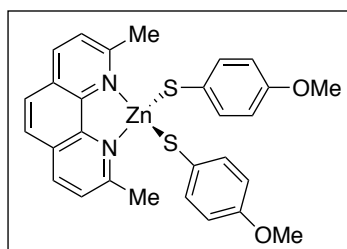
[(**L1**)Zn(*p*-OMeC$_6$H$_4$)$_2$] was synthesised following a reported procedure.[124]

Sodium methoxide (54 mg, 1 mmol, 2 equiv) and 4-methoxythiophenol (123 µL, 2 equiv, 1 mmol) were added to methanol (20 mL) at room temperature under nitrogen. A solution of ZnCl$_2$ (68 mg, 0.5 mmol, 1 equiv) in 10 mL methanol was added via syringe over 1 h. After 1 h stirring at room temperature, a solution of **L1** (104.1 mg, 0.5 mmol, 1 equiv) was added resulting in an instant colour change to bright yellow. The solution was stirred overnight then concentrated carefully (the reaction mixture smells quite strongly) until [(**L1**)Zn(*p*-OMeC$_6$H$_4$)$_2$] began to crystallise. The pale yellow crystalline solid was isolated by filtration and dried under vacuum (132 mg, 48%).

^{1}H NMR (400 MHz, DMSO-d$_6$): δ 8.68 (d, $^3J_{\text{H-H}}$ = 8.4 Hz, 2H), 8.01 (s, 2H), 7.92 (d, $^3J_{\text{H-H}}$ = 8.3 Hz, 2H), 6.63 (d, $^3J_{\text{H-H}}$ = 8.6 Hz, 4H), 6.07 (d, $^3J_{\text{H-H}}$ = 8.5 Hz, 4H), 3.43 (s, 6H, OMe), 3.03 (s, 6H, Me).

4.8.5. General procedure for carboxylation reactions
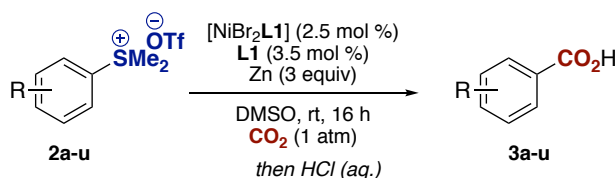
**Scheme S4.1. General scheme for Ni-catalysed carboxylation of aryl sulfonium salts.**

General procedure:

Aryl sulfonium (0.3 mmol, 1 equiv), [NiBr$_2$**L1**] (3.2 mg, 0.0075 mmol, 0.025 equiv), **L1** (2.2 mg, 0.011 mmol, 0.035 equiv) and Zn powder (58.8 mg, 0.9 mmol, 3 equiv) were weighed into an oven-dried Schlenk tube (sealed with a Teflon stopper). The Schlenk tube was placed under CO$_2$ by carrying out three vacuum/CO$_2$ cycles, then the DMSO (1.5 mL) was added under a flow of CO$_2$. The reaction was stirred for 16 h at room temperature (22–27 °C). The reaction was then quenched with 2M HCl. Organic products were extracted into diethyl ether and the yield either measured by ^{1}H NMR against an internal standard (1,3,5-trimethoxybenzene or 1,1,2,2-tetrabromoethane) or by isolation of the pure acid by acid-base extraction of the diethyl ether layer.

The same general procedure was carried out substituting different amounts of Zn/Zn(II) salt/ligand/precatalyst for the optimisation tables presented in the text.

4.8.6. Control experiments

### 4.8.6.1. Slow reduction of aryl sulfonium salt with Zn powder
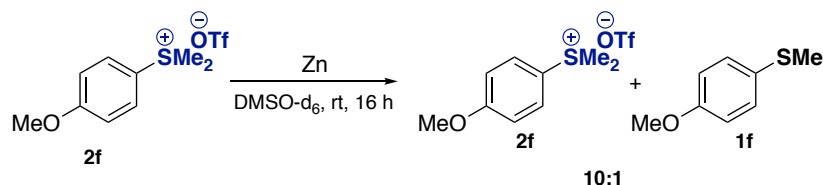
Scheme S4.2. Slow single-electron reduction of 2f by Zn powder.

The reaction of a dialkylarylsulfonium salt with an appropriate reductant is known to produce aryl sulfide upon release of methyl radical.[98] Formation of the aryl sulfide was confirmed in a control experiment:

Arylsulfonium salt **2f** (6.2 mg, 0.019 mmol, 1 equiv) and Zn powder (3.8 mg, 0.058 mmol, 3 equiv) were stirred together in 1 mL DMSO-d_6 for 5 h at room temperature. After this time, no reaction had been observed, so 15 mg (0.23 mmol, 12 equiv) extra Zn powder was added and the reaction stirred for a further 16 h. New signals for aryl sulfide **2f** were detected (1:0.1 ratio). No arylzinc species were formed, as expected.

4.8.6.2. Reaction of aryl sulfide with Ni(0) in the presence of Zn and Zn(OTf)₂
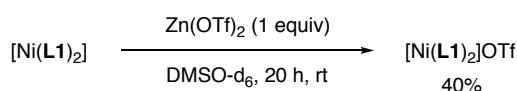
Aryl sulfide **1f** (3.0 mg, 0.0094 mmol, 1 equiv), [Ni(**L1**)₂] (4.5 mg, 0.0094 mmol, 1 equiv), Zn powder (1.9 mg, 0.028 mmol, 3 equiv), Zn(OTf)₂ (6.9 mg, 0.019 mmol, 2 equiv), and 1,3,5-trimethoxybenzene (1.6 mg, 0.0094 mmol, 1 equiv) were dissolved in 0.6 mL DMSO-d_6 and stirred together. The reaction became deep blue-black within 5 minutes. After 16 h stirring at room temperature, the reaction was analysed by ^{1}H NMR spectroscopy. As expected, no reaction of **1f** with [Ni(**L1**)₂] was observed. However, a modest yield of [Ni(**L1**)₂]OTf was observed (35%).
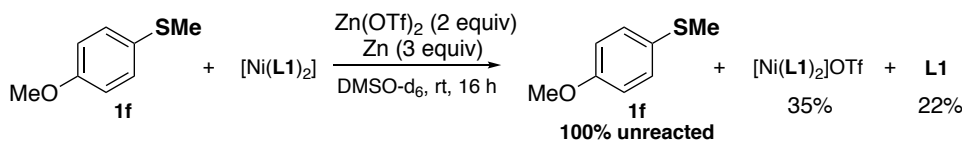
Scheme S4.3. Confirmation of absence of C–S cleavage for aryl sulfides.

This oxidised product was due to reaction between [Ni(**L1**)₂] and Zn(OTf)₂ and was confirmed in an independent reaction:

[Ni(**L1**)₂] (6.7 mg, 0.014 mmol, 1 equiv), and Zn(OTf)₂ (10.3 mg, 0.028 mmol, 2 equiv) were combined in 0.6 mL DMSO-d_6 and stirred at room temperature for 20 h. The dark reaction mixture was analysed by ^{1}H NMR spectroscopy to confirm paramagnetic signals were present. Next, 1,3,5-trimethoxybenzene (2.4 mg, 0.014 mmol, 1 equiv) was added in order to obtain a yield of [Ni(**L1**)₂]OTf (ca. 40%).

$$[Ni(\textbf{L1})_2] \xrightarrow[\text{DMSO-}d_6,\ 20\ \text{h, rt}]{\text{Zn(OTf)}_2\ (1\ \text{equiv})} [Ni(\textbf{L1})_2]OTf$$

40%

Scheme S4.4. Oxidation of [Ni(L1)₂] with Zn(OTf)₂.

4.8.7. Reduction of Ni(II) precatalyst

Effect of solvent

THF

[NiBr₂**L1**] (9.1 mg, 0.021 mmol, 1 equiv), **L1** (4.4 mg, 0.021 mmol), Zn powder (6.7 mg, 0.10 mmol, 4.8 equiv), and 1,3,5-trimethoxybenzene (3.6 mg, 0.021 mmol, 1 equiv) were combined in 0.7 mL THF-d_8. The resulting purple suspension was stirred for 20 h at room temperature.

NMR analysis of the blue suspension showed only 2.5 % [Ni(**L1**)₂] alongside <10% free **L1**.

DMSO

[NiBr₂**L1**] (8.3 mg, 0.019 mmol, 1 equiv), **L1** (4.1 mg, 0.20 mmol, 1 equiv), and Zn powder (5.0 mg, 0.077 mmol, 4 equiv) were combined in 0.7 mL DMSO-d_6 and stirred together for 15 h at room temperature. The resulting brown reaction mixture (which contained some dark solid) was analysed by ^{1}H NMR spectroscopy. A 16% yield of **5-Br** was calculated.

Reaction time

General procedure:

[NiBr₂**L1**] (8–9 mg, approximately 0.020 mmol), **L1** (1 equiv) and 1,3,5-trimethoxybenzene (1 equiv) were combined in 0.7 mL DMSO-d_6. A ^{1}H NMR spectrum was taken of the resulting green solution, then Zn powder (3 equiv) was added and the reaction stirred for **the indicated time** at room temperature. The blue reaction mixture was rapidly filtered through glass fibre filter paper then analysed by ^{1}H NMR.

    3 min: 46% yield of **5-Br**, 53% unreacted Ni(II) precatalyst.

    10 min: 74% yield of **5-Br**.

    2 h: 22% yield of **5-Br**.

4.8.7.1. Trapping experiments

1,5-cycloctadiene (COD)

[Ni(COD)₂] + L1:

- [Ni(COD)₂] (6.6 mg, 0.024 mmol, 1 equiv), **L1** (5.0 mg, 0.024 mmol, 1 equiv), and 1,3,5-trimethoxybenzene (4.0 mg, 0.024 mmol, 1 equiv) were combined in DMSO-d₆ (1 mL). Although [Ni(COD)₂] was not initially soluble in DMSO, the solution rapidly darkened. After stirring for 2 h at room temperature, the dark reaction mixture reaction was analysed by ¹H NMR spectroscopy.

[NiBr₂L1] reduction in the presence of COD:

- [NiBr₂**L1**] (8.5 mg, 0.020 mmol, 1 equiv) and 1,3,5-trimethoxybenzene (3.4 mg, 0.020 mmol, 1 equiv) were combined in DMSO-d₆ (0.6 mL). A ¹H NMR spectrum was collected, then the reaction mixture transferred back to a vial. An excess of COD (12 μL, 0.010 mmol, 5 equiv) and Zn powder (3.9 mg, 0.060 mmol, 3 equiv) was then added and the reaction stirred for 30 minutes. A colour change from deep blue to black was observed. Analysis by ¹H NMR spectroscopy showed the disappearance of [NiBr₂**L1**] and a ca. 20% yield of **5-Br**. Alongside this complex were signals for free COD and s*ignals that matched those obtained when [Ni(COD)₂] was dissolved together with **L1** in DMSO-d₆.*
- When the reduction reaction was carried out for 2 h, the yield of **5-Br** was ca. 35% and the same signals in the region of coordinated COD were observed.

Ph₂S₂

Initial control experiments with [Ni(**L1**)₂] and [Ni(**L1**)₂]OTf:

[Ni(L1)₂]

- [Ni(**L1**)₂] (11.4 mg, 0.024 mmol, 1 equiv), 1,3,5-trimethoxybenzene (4.0 mg, 0.024 mmol, 1 equiv), and Ph₂S₂ (5.3 mg, 0.024 mmol, 1 equiv) were dissolved in DMSO-d₆ (0.6 mL). The initial brown colour of the sparingly soluble Ni(0) precursor became deep red as oxidative addition proceeded. The resulting NMR spectrum showed a 1:1 ratio between the **L1** signals of the new complex and the equivalent of **L1** that was displaced from the [Ni(**L1**)₂] precursor.

5-OTf

- **5-OTf** (5.7 mg, 0.0091 mmol, 1 equiv) and 1,3,5-trimethoxybenzene (1.5 mg, 0.0091 mmol, 1 equiv) were combined in DMSO-d₆. Addition of diphenyl disulfide (2.0 mg, 0.0091 mmol, 1 equiv) resulted in a colour change to red within 5 min.

Ni(II) precatalyst reduction with Zn followed by Ph₂S₂ addition

- [NiBr₂**L1**] (16.8 mg, 0.039 mmol, 1 equiv), **L1** (8.2 mg, 0.039 mmol, 1 equiv), Zn powder (25.7 mg, 0.39 mmol, 10 equiv), and 1,3,5-trimethoxybenzene (6.6 mg, 0.039 mmol, 1 equiv) were combined in 0.6 mL DMSO-d₆ and stirred together for 16 h. Diphenyl disulfide (8.6 mg, 0.040

mmol, 1 equiv) was then added. The dark brown mixture turned red within 2 minutes, and within another 2 minutes had turned deep blue-black. A 10% yield of **5-OTf** was calculated. *New **L1** signals* and broad aryl signals between 6–7.7 ppm also appeared.

4.8.8. Investigations into arylzinc species

Zn(p-OMeC$_6$H$_4$)$_2$

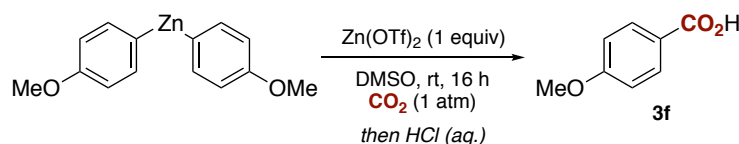**Figure S4.2.** Ni-free carboxylation of Zn(p-OMeC$_6$H$_4$)$_2$

Zn(p-OMeC$_6$H$_4$)$_2$ (12.1 mg, 0.043 mmol, 1 equiv) and Zn(OTf)$_2$ (15.7 mg, 0.043 mmol, 1 equiv) were weighed into a Schlenk tube in the glovebox. The tube was sealed then placed under CO_2 by carrying out three cycles of vacuum/CO_2. Under a flow of CO_2, DMSO (2 mL) was added. After stirring overnight (16 h), the colourless reaction mixture was quenched with 3 mL 5% HCl. Bubbling was observed. Trimethoxybenzene (7.3 mg, 0.043 mmol, 1 equiv) was added as an internal standard, then the organic products extracted into Et$_2$O. Analysis of a portion by ^{1}H NMR spectroscopy showed a 35% yield of **3f**. Signals matched literature data.[125]

When the reaction was repeated with **L1** present (1 equiv), no **3f** was obtained.
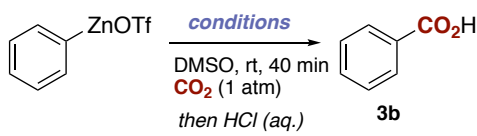
Preparation of PhZnOTf solution

To an oven-dried Schlenk tube, Ph$_2$Zn (132 mg, 0.60 mmol), Zn(OTf)$_2$ (218 mg, 0.60 mmol), and 1,4-dimethoxybenzene (55.3 mg, 0.40 mmol, internal standard) were added. DMSO (4.0 mL) was added, and the resulting solution was stirred at room temperature for 15 min.

Reactions of PhZnOTf with CO$_2$

General procedure:

To a Schlenk tube, [NiBr$_2$**L1**] (3.2 mg, 7.5 μmol), **L1** (2.2 mg, 11 μmol), and Zn (60 mg, 0.90 mmol) were added, then the tube was evacuated and refilled with CO_2 gas three times. DMSO (0.50 mL) was then added, and the resulting mixture was stirred for 1 min. Subsequently, the PhZnOTf solution prepared above (1.0 mL) was added to the tube, and the resulting mixture was stirred vigorously for 40 min. The reaction was quenched with HCl (3 M), and the organic layer extracted with Et$_2$O (3 × 2.0 mL). The combined organic layer was passed through pads of Na$_2$SO$_4$ and silica gel then the volatiles were removed under reduced pressure. The yield was determined by ^{1}H NMR using 1,4-dimethoxybenzene as an internal standard.

Table S4.1. Carboxylation of PhZnOTf in presence or absence of Ni/Zn. [a]1,1,2,2-tetrabromoethane was used as internal standard.

| entry	[NiBr₂**L1**] 2.5 mol%	**L1** 3.5 mol%	**Zn** 3 equiv	**3b** NMR yield[a]
1	✓	✓	✓	41%
2	✓	✓	–	7%
3	–	–	–	11%
4	–	1 equiv	–	0%

4.8.8.1.   D₂O quenching experiment in the absence of CO₂
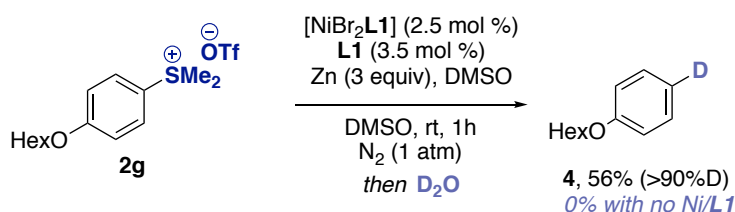
Scheme S4.5. D₂O quenching experiment.

A 20 mL Schlenk tube was charged with (p-hexyloxyphenyl)dimethylsulfonium triflate **2g** (117 mg, 0.30 mmol, 1 equiv), Zn powder (60 mg, 0.90 mmol, 3 equiv), [NiBr₂**L1**] (3.2 mg, 7.5 μmol, 0.025 equiv), and **L1** (2.2 mg, 11 μmol, 0.035 equiv), then the tube was evacuated and refilled with N₂ three times. DMSO (1.5 mL) was then added then the resulting mixture was stirred vigorously for 16 h at room temperature. The reaction was quenched with D₂O (1.0 mL) then stirred for 1 h before the addition of HCl (3 M). The organic layer was extracted with Et₂O (3 × 2.0 mL). The combined organic layers were passed through a pad of Na₂SO₄ then volatiles were removed under reduced pressure. The residue was purified by column chromatography on silica gel (hexane) to afford **4** as a colourless oil (30.1 mg, 0.17 mmol, 56%).

¹H NMR (CDCl₃): δ 7.29 (d, $^3J_{H-H}$ = 8.2 Hz, 2H), 6.94 (t, $^3J_{H-H}$ = 8.2 Hz, 1H × 0.1, minor), 6.92 (d, $^3J_{H-H}$ = 8.2 Hz, 2H), 3.97 (t, $^3J_{H-H}$ = 6.5 Hz, 2H), 1.82–1.77 (m, 2H), 1.51–1.46 (m, 2H), 1.39–1.34 (m, 4H), 0.93 (t, $^3J_{H-H}$ = 6.9 Hz, 3H).
**¹³C NMR** (CDCl₃): δ 159.3, 129.5 (minor), 129.4, 120.6 (minor), 120.3 (t, J = 24.6 Hz), 114.6, 68.0, 31.7, 29.4, 25.9, 22.8, 14.2.
²D NMR (CHCl₃): δ 7.11.

4.8.8.2. Reaction of Zn(*p*-OMeC₆H₄)₂ with **L1** in DMSO.
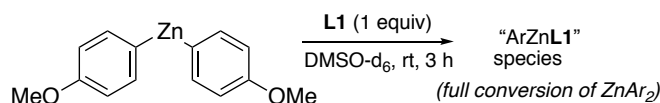
Scheme S4.6. Synthesis of (L1)ZnAr species.

Addition of DMSO-d₆ (0.6 mL) to a mixture of Zn(*p*-OMeC₆H₄)₂ (7.0 mg, 0.025 mmol, 1 equiv) and **L1** (5.21 mg, 0.025 mmol, 1 equiv) resulted in a slight yellowing of the DMSO solution. The reaction mixture was stirred for 3 h at room temperature then the pinkish mixture analysed by ^{1}H NMR spectroscopy. The Zn(*p*-OMeC₆H₄)₂ signals disappeared and new **L1** complexes formed in a 1:0.12 ratio. Traces of anisole and almost negligible amounts of biaryl were also observed. The remainder of the aryl signals were assigned to Zn(II) complexes.

4.8.8.3. Reaction of (*p*-OMeC₆H₄)ZnOTf with **L1** in DMSO.
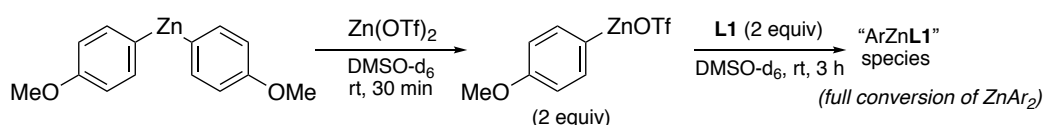
Scheme S4.7. Reaction of (*p*-OMeC₆H₄)ZnOTf with L1

Zn(*p*-OMeC₆H₄)₂ (5.9 mg, 0.021 mmol, 1 equiv) and Zn(OTf)₂ (7.7 mg, 0.021 mmol, 1 equiv) were mixed together in DMSO-d₆ (1 mL) for 3 h, then **L1** (4.4 mg, 0.042 mmol, 1 equiv) was added as a solid. After 5 minutes of stirring, the solution had become homogeneous and pale yellow. Analysis of the reaction mixture by ^{1}H NMR spectroscopy showed one major product, which was assigned as "[(**L1**)ZnAr]OTf" based on integration of the signals.

^{1}**H NMR** (400 MHz, DMSO-d₆): δ 8.90 (d, $^3J_{H-H}$ = 8.4 Hz, 2H, **L1**), 8.26 (s, 2H, **L1**), 8.10 (d, $^3J_{H-H}$ = 8.4 Hz, 2H, **L1**), 7.52 (d, $^3J_{H-H}$ = 7.9 Hz, 2H, Ar), 6.83 (d, $^3J_{H-H}$ = 7.8 Hz, 2H, Ar), 3.70 (s, 3H, OMe), 2.99 (s, 6H, **L1**).

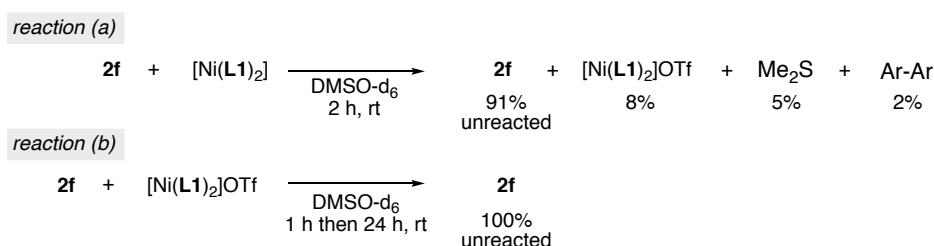## 4.8.9. Reactions with isolated Ni complexes

The following section summarises stoichiometric reactions between arylsulfonium salt **2f** and Ni complexes. The reactions were carried out both in the presence and absence of Zn and/or Zn(II). Results are summarised in Table S4.2.

Table S4.2. Summary of results of stoichiometric experiments.

entry	Ni complex	Zn	Zn(OTf)$_2$	2f	other components	trace components
					observed by ^{1}H NMR:	
1	[Ni(**L1**)$_2$]	–	–	✓	Me$_2$S, Ar-Ar, **1f**	
2	[Ni(**L1**)$_2$]OTf	–	–	✓		L1
3	[Ni(**L1**)$_2$]OTf	✓	–	–	Me$_2$S, "ArZn$_+$"	Ar-H
4	[Ni(**L1**)$_2$]	✓	–	–	Me$_2$S, Ar-Ar, "ArZn$_+$"	Ar-H
5	[Ni(**L1**)$_2$]	–	✓	✓	Me$_2$S, "ArZn$_+$"	Ar-H
6	[Ni(**L1**)$_2$]	✓	✓	–	Me$_2$S, "ArZn$_+$"	

Zn-free reactions

reaction (a)

2f + [Ni(**L1**)$_2$] →(DMSO-d$_6$, 2 h, rt) **2f** (91% unreacted) + [Ni(**L1**)$_2$]OTf (8%) + Me$_2$S (5%) + Ar-Ar (2%)

reaction (b)

2f + [Ni(**L1**)$_2$]OTf →(DMSO-d$_6$, 1 h then 24 h, rt) **2f** (100% unreacted)

Scheme S4.8. Results of stoichiometric reactions between isolated Ni complexes and 2f in the absence of Zn.

a) Reaction of 2f with Ni(0)

Arylsulfonium salt **2f** (8.2 mg, 0.026 mmol, 1 equiv), [Ni(**L1**)$_2$] (12.2 mg, 0.026 mmol, 1 equiv), and 1,3,5-trimethoxybenzene (4.3 mg, 0.026 mmol, 1 equiv) were dissolved in 0.6 mL DMSO-d$_6$ and stirred for 2 h. Results summarised in Scheme S4.8.

b) Reaction of 2f with Ni(I)

Arylsulfonium salt **2f** (2.4 mg, 0.0077 mmol, 1 equiv) and [Ni(**L1**)$_2$]OTf (4.8 mg, 0.0077 mmol, 1 equiv) were combined in DMSO-d$_6$ (0.6 mL) and the blue solution stirred at room temperature. After 1 h, the starting materials were the only species observable by ^{1}H NMR spectroscopy. After approximately 24 h, the only change to the ^{1}H NMR spectrum taken after 1 h was that traces of **L1** were now present.
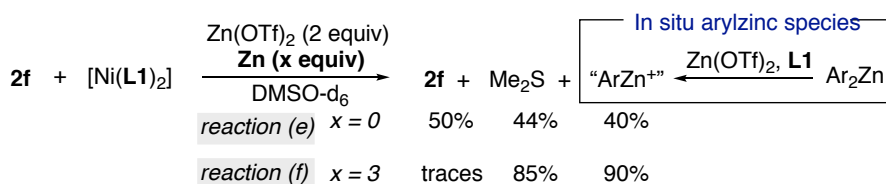
Reactions in the presence of Zn

reaction (c)

$$2f \quad + \quad [Ni(\mathbf{L1})_2] \xrightarrow[\substack{\text{DMSO-}d_6 \\ \text{2 h, rt}}]{\textbf{Zn (3 equiv)}} Ar\text{-}Ar \quad + \quad Me_2S \quad + \quad [Ni(\mathbf{L1})_2]OTf$$
$$+ \quad \text{L1-Zn complex}$$
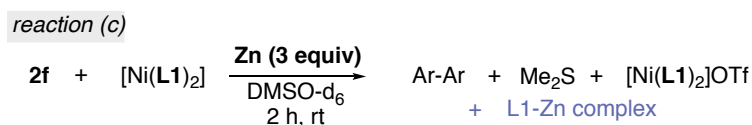
Scheme S4.9. Initial experiment with 2f and [Ni(L1)₂] in the presence of Zn.

c) **Reaction of 2f with Ni(L)₂ and Zn**

Arylsulfonium salt **2f** (8.7 mg, 0.027 mmol, 1 equiv), [Ni(**L1**)₂] (13.5 mg, 0.028 mmol, 1.04 equiv), and Zn powder (5.6 mg, 0.085 mmol, 3 equiv) were combined in DMSO-d_6 (0.6 mL) and stirred together for 16 h at room temperature.

Full conversion of **2f** was observed. The major species to which **2f** was transformed were biaryl and Me₂S, supporting the previous experiment where cleavage at Ni(0) occurred. A small set of new ¹H NMR signals with the *characteristic pattern of a Zn **L1** complex* also appeared between 8–9 ppm.

d) **Reaction of 2f with Ni(I) and Zn**

Arylsulfonium salt **2f** (3.06 mg, 0.0096 mmol, 1 equiv) and [Ni(**L1**)₂]OTf (6.0 mg, 0.0096 mmol, 1 equiv) and Zn powder (1.9 mg, 0.029 mmol, 3 equiv) were combined in DMSO-d_6 (0.6 mL) and the blue solution stirred at room temperature. After approximately 24 h, the disappearance of **2f** was observed. Supporting C–S cleavage at Ni(0) formed by reduction of the Ni(I) starting material was the presence of Me₂S and the absence of **2f** and **1f**. *Unexplained aryl and **L1** signals from arylzinc species were also present in the aromatic region of the ¹H NMR spectrum.*

Reactions in the presence of added Zn(OTf)₂

$$2f \quad + \quad [Ni(\mathbf{L1})_2] \xrightarrow[\substack{\text{DMSO-}d_6}]{\substack{\text{Zn(OTf)}_2 \text{ (2 equiv)} \\ \textbf{Zn (x equiv)}}} 2f \quad + \quad Me_2S \quad + \quad \text{“ArZn}^+\text{”} \xleftarrow[]{\text{Zn(OTf)}_2, \, \mathbf{L1}} Ar_2Zn$$

In situ arylzinc species

		2f	Me₂S	"ArZn⁺"
reaction (e)	x = 0	50%	44%	40%
reaction (f)	x = 3	traces	85%	90%

Scheme S4.10. Summary of reactions between Ni(L1)₂ and Zn(OTf)₂ with or without added Zn. Reaction time: 7h.

e) **Zn(OTf)₂**

Arylsulfonium salt **2f** (3.0 mg, 0.0094 mmol, 1 equiv), [Ni(**L1**)₂] (4.5 mg, 0.0094 mmol, 1 equiv), Zn(OTf)₂ (6.9 mg, 0.019 mmol, 2 equiv), and 1,3,5-trimethoxybenzene (1.6 mg, 0.0094 mmol, 1 equiv) were combined in 0.6 mL DMSO-d_6 and stirred at room temperature. The reaction became deep blue within 10 minutes. This indicated the formation of [Ni(**L1**)₂]OTf. The products of reaction after 7 h are summarised in Scheme S4.10.

f) Zn(OTf)$_2$ + Zn(0)

Arylsulfonium salt **2f** (3.0 mg, 0.0094 mmol, 1 equiv), [Ni(**L1**)$_2$] (4.5 mg, 0.0094 mmol, 1 equiv), Zn powder (1.85 mg, 0.028 mmol, 3 equiv), Zn(OTf)$_2$ (6.9 mg, 0.0188 mmol, 2 equiv), and 1,3,5-trimethoxybenzene (1.58 mg, 0.0094 mmol, 1 equiv) were combined in 0.6 mL DMSO-d$_6$ and stirred for 7 h at room temperature. The reaction also became deep blue within 10 minutes. The products of reaction after 7 h are summarised in Scheme S4.10. Due to overlapping signals, integration of all signals in the 6.8–9 ppm region was not always accurate.

4.8.10. NMR spectra of organic molecules
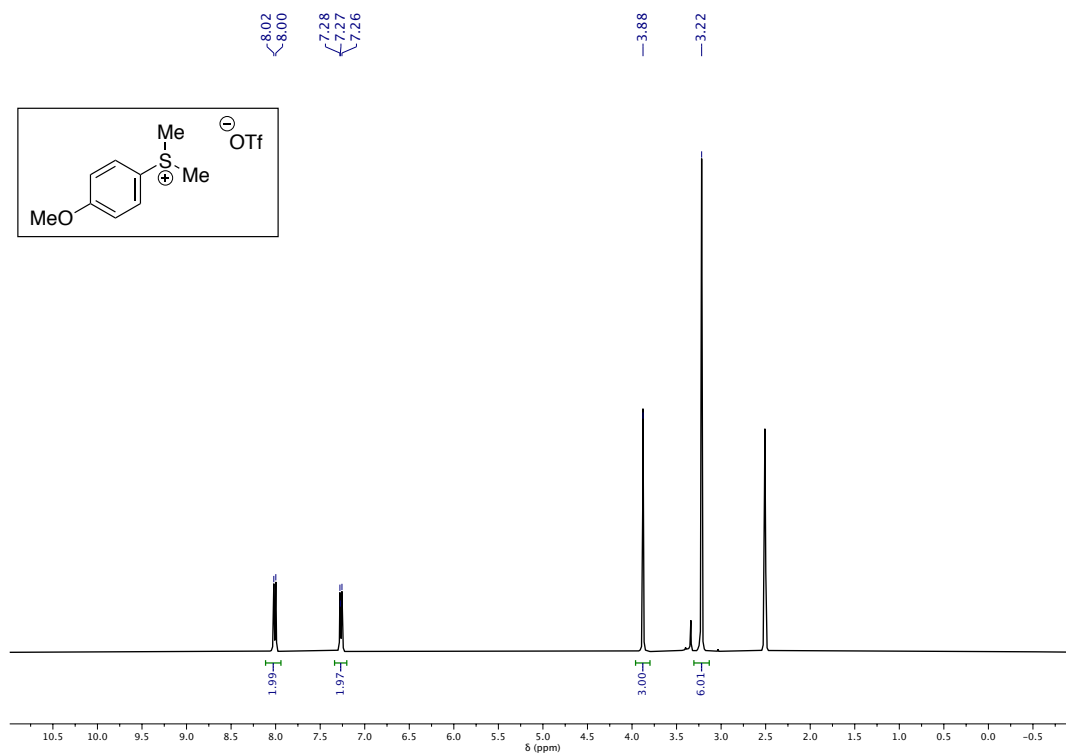
Figure S4.3. ^{1}H NMR (400 MHz, DMSO-d$_6$) of 2f.
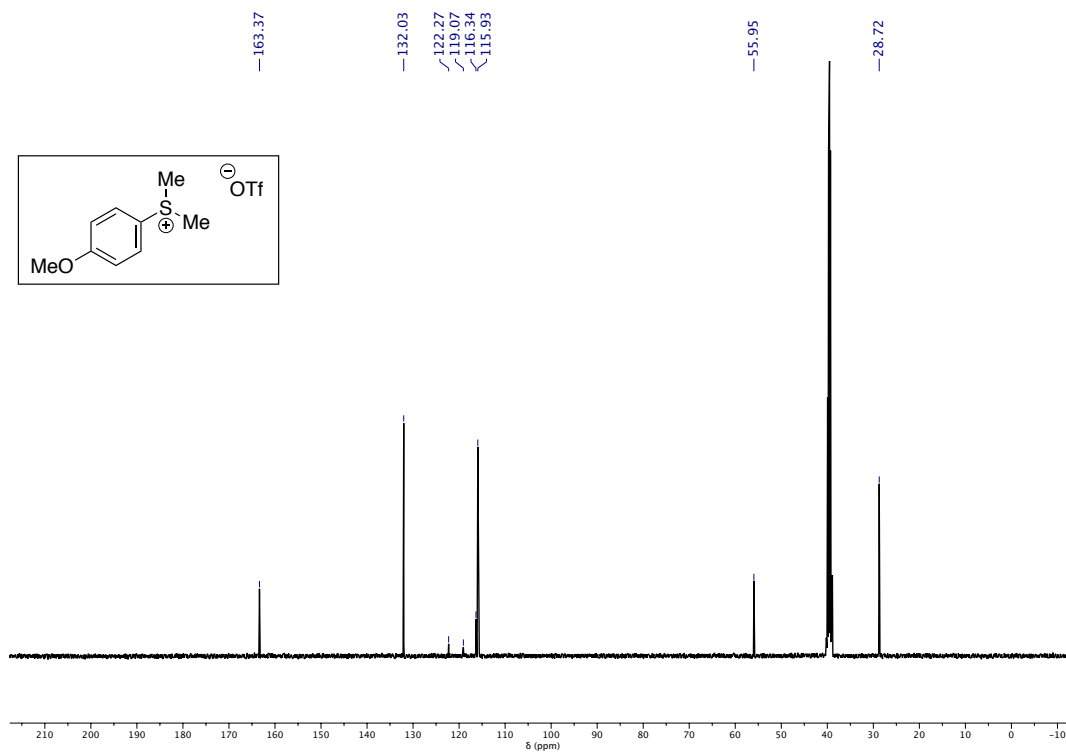
Figure S4.4. ^{13}C NMR (101 MHz, DMSO-d$_6$) of 2f.
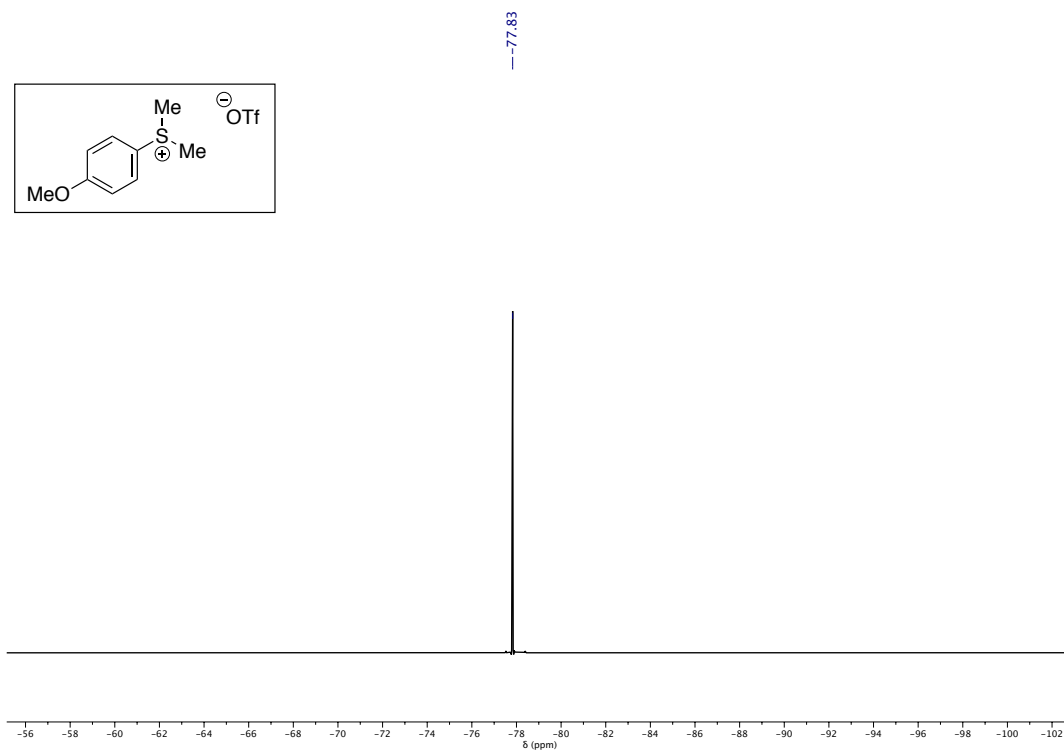
Figure S4.5. ¹⁹F NMR (376 MHz, DMSO-d₆) of 2f.
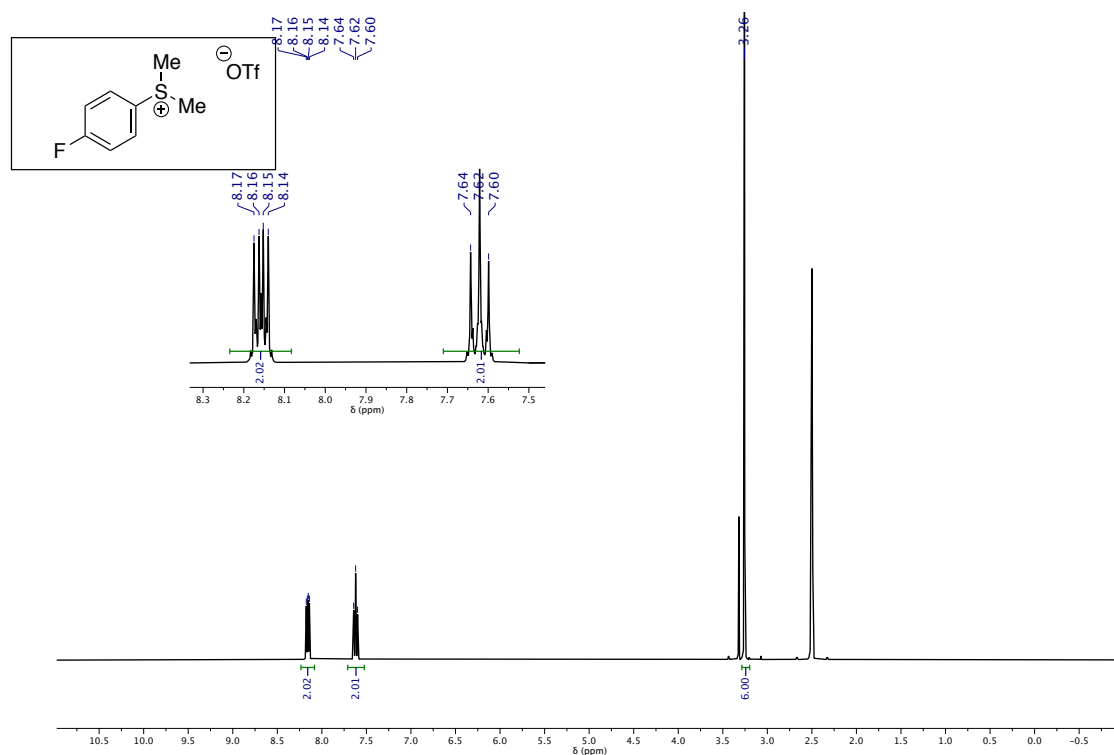
Figure S4.6. ¹H NMR (400 MHz, DMSO-d₆) of 2e. Signal at 3.32 ppm is water in the DMSO-d₆.
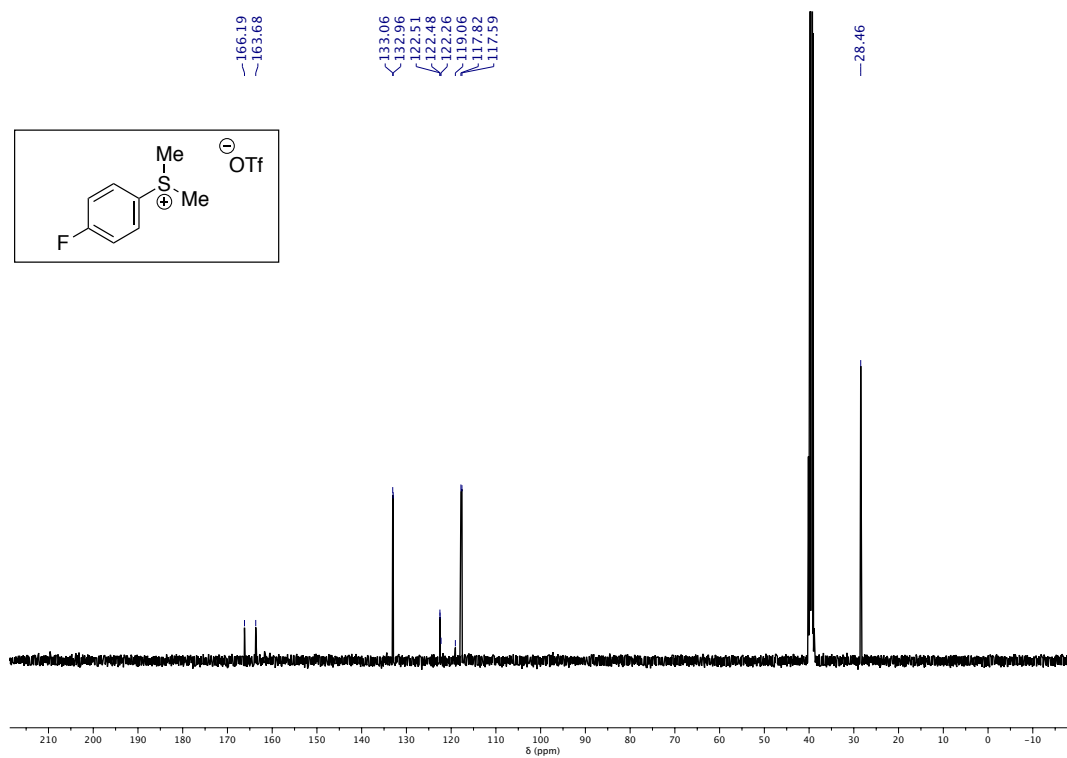
Figure S4.7. ^{13}C NMR (101 MHz, DMSO-d$_6$) of 2e.
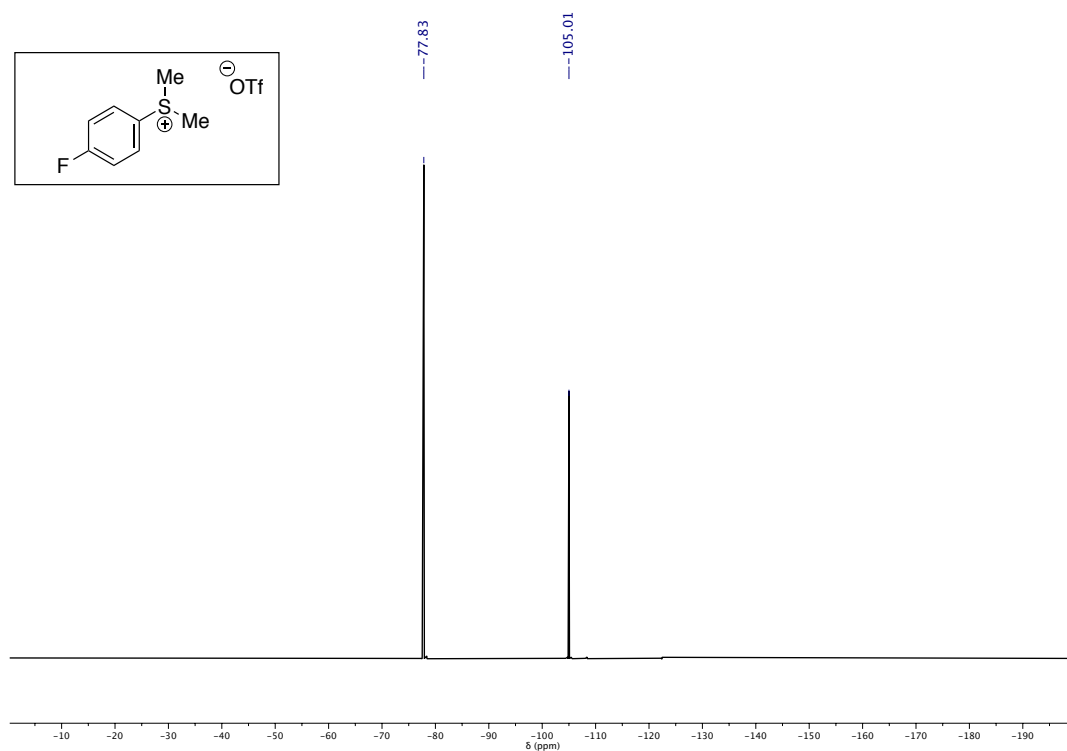
Figure S4.8. ^{19}F NMR (376 MHz, DMSO-d$_6$) of 2e.
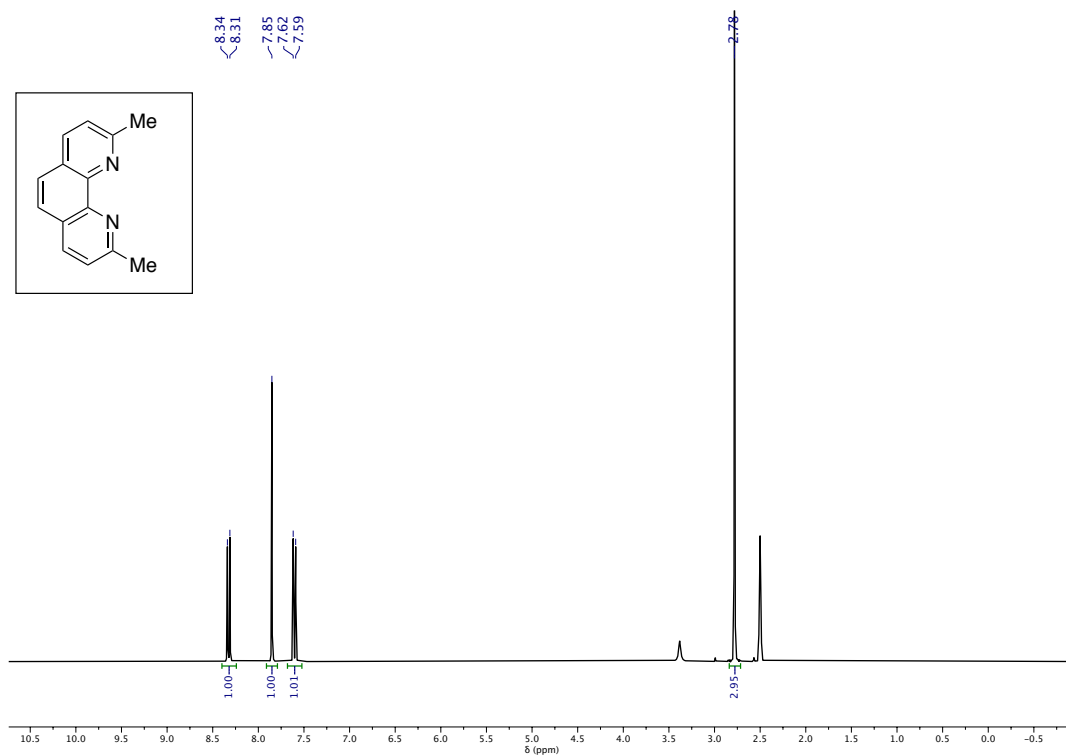
Figure S4.9. ^{1}H NMR (300 MHz, DMSO-d$_6$) of L1 (neocuproine, Sigma Aldrich).
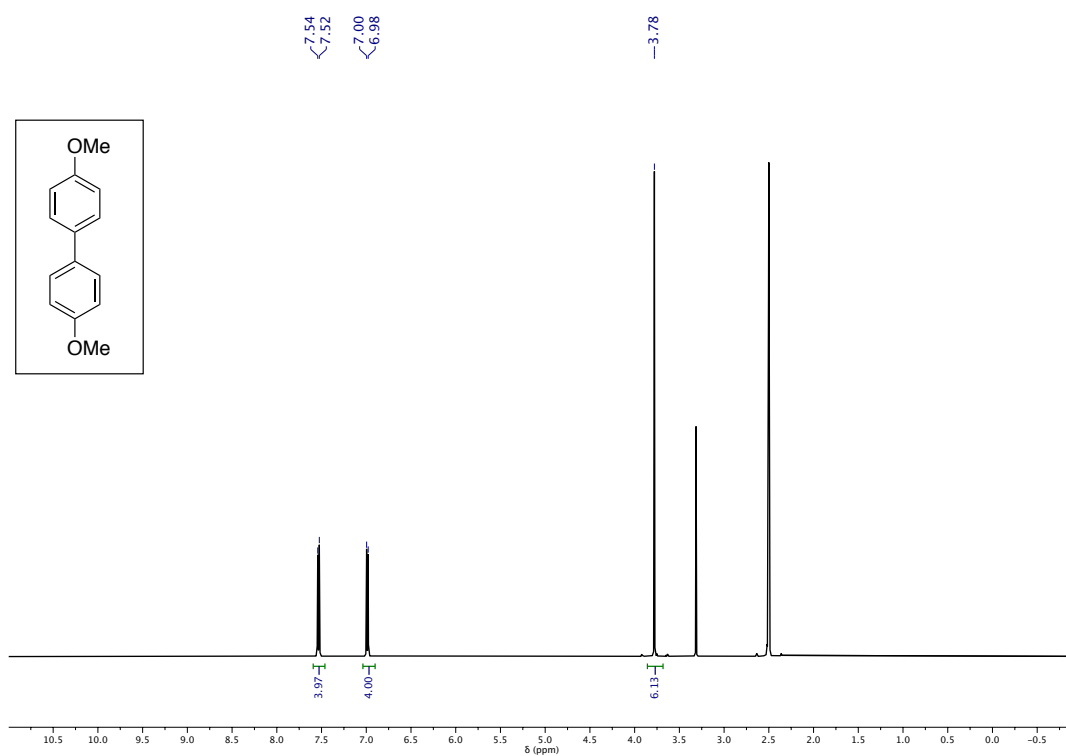
Figure S4.10. ^{1}H NMR (500 MHz, DMSO-d$_6$) of 4,4'-dimethoxybiphenyl.
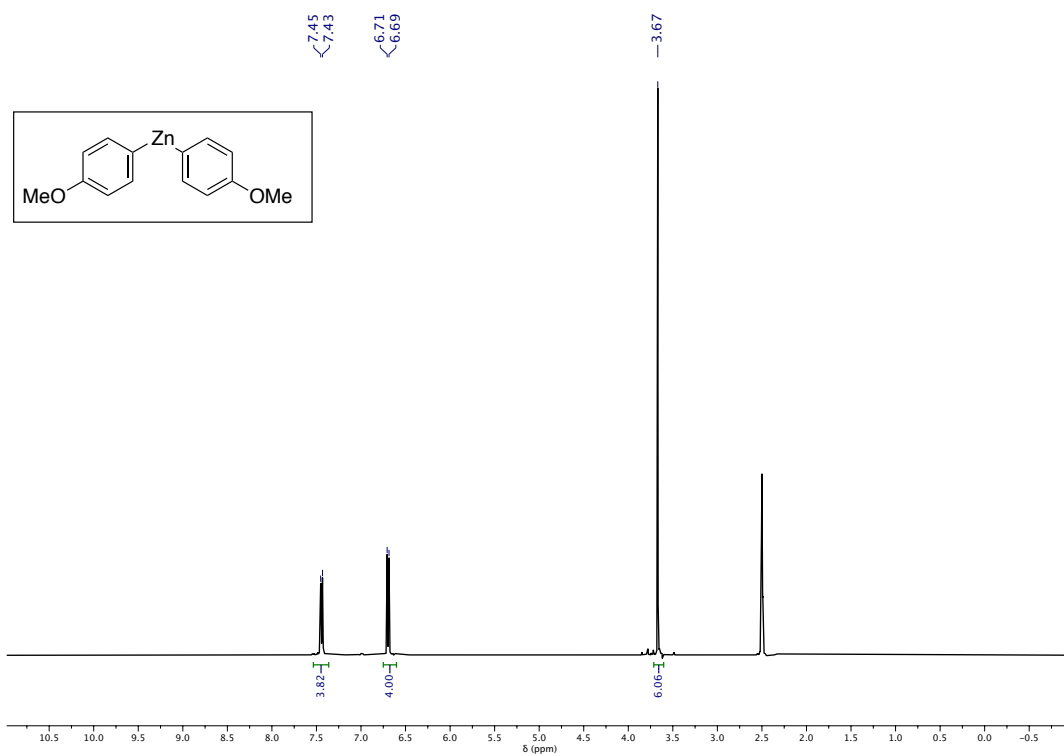
Figure S4.11. ¹H NMR (400 MHz, DMSO-d₆) of Zn(p-OMeC₆H₄)₂.
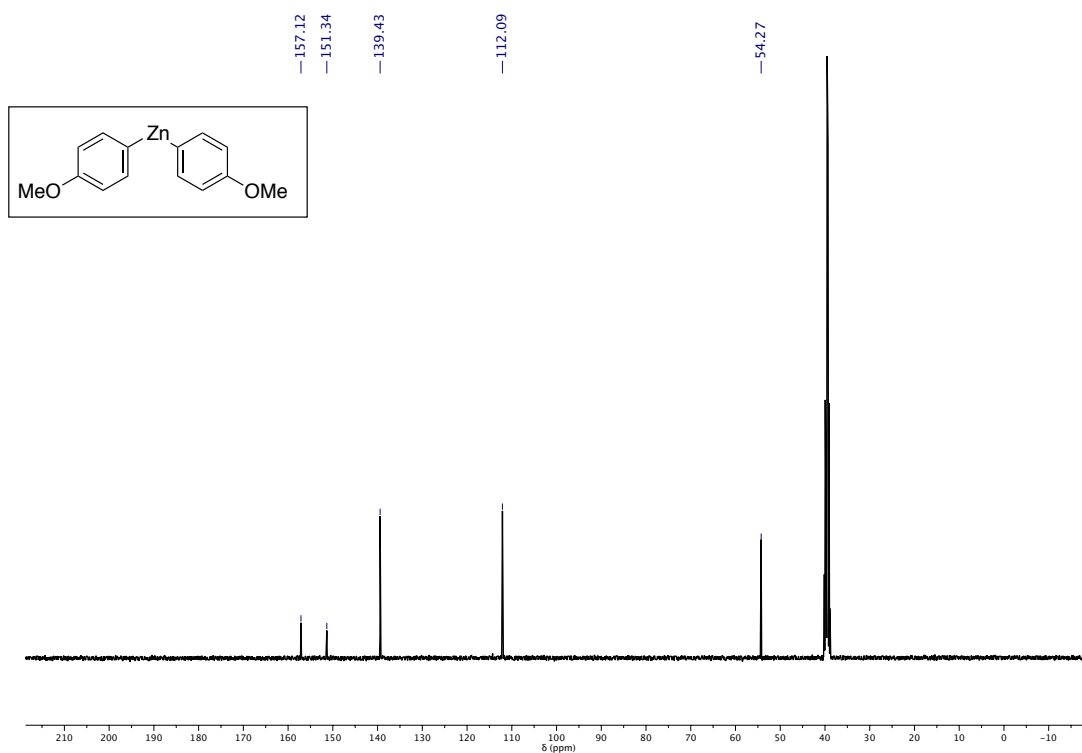
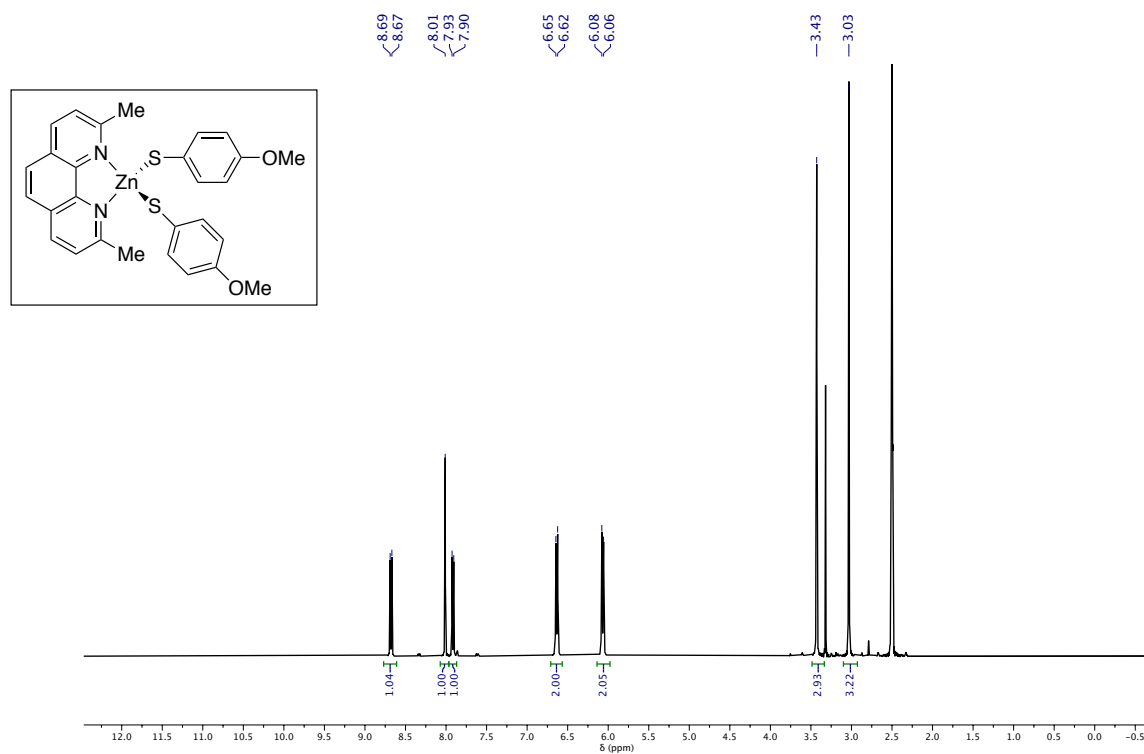**Figure S4.12.** ¹³C NMR (101 MHz, DMSO-d₆) of Zn(p-OMeC₆H₄)₂.

Figure S4.13. ^{1}H NMR (400 MHz, DMSO-d$_6$) of [(L1)Zn(p-OMeC$_6$H$_4$)$_2$].

4.8.11.   NMR spectra of metal complexes
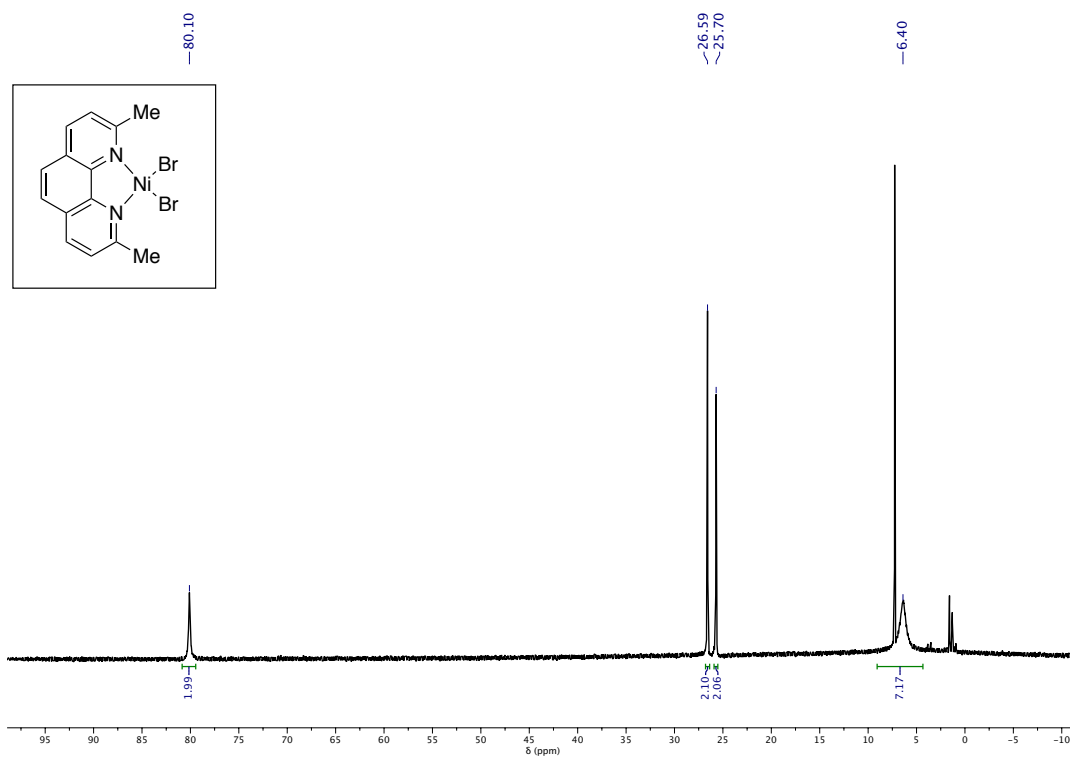
Figure S4.14. ^{1}H NMR (400 MHz, CDCl$_3$) of [NiBr$_2$L1].
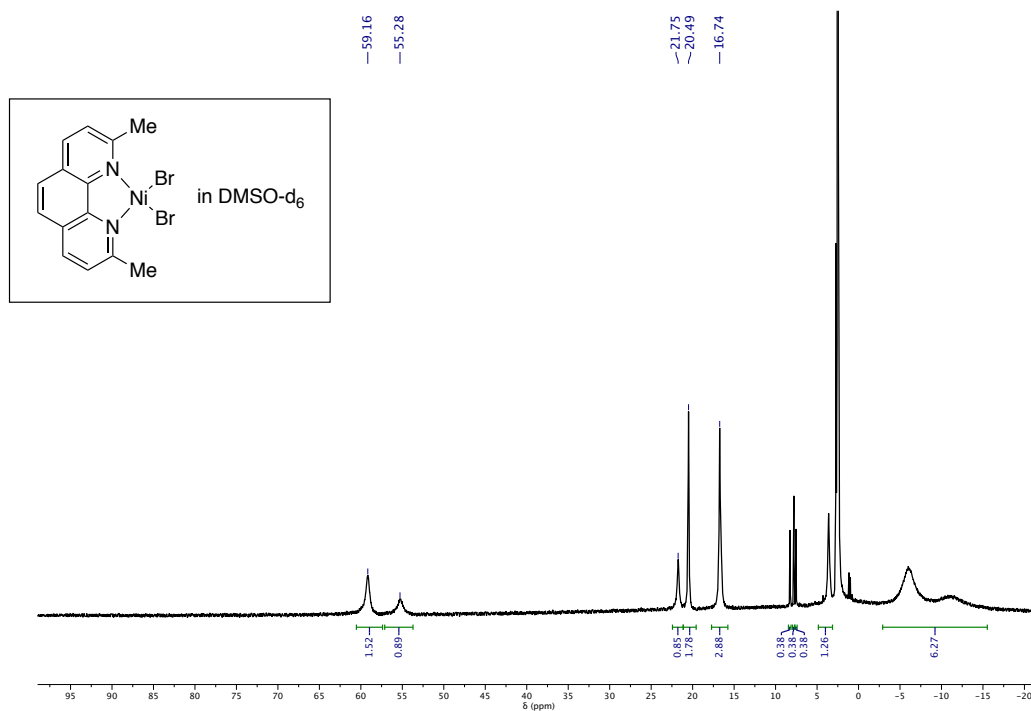
Figure S4.15. ^{1}H NMR (400 MHz, DMSO-d$_6$) of [NiBr$_2$L1]. Free L1 visible between 7.5–8.5 ppm.
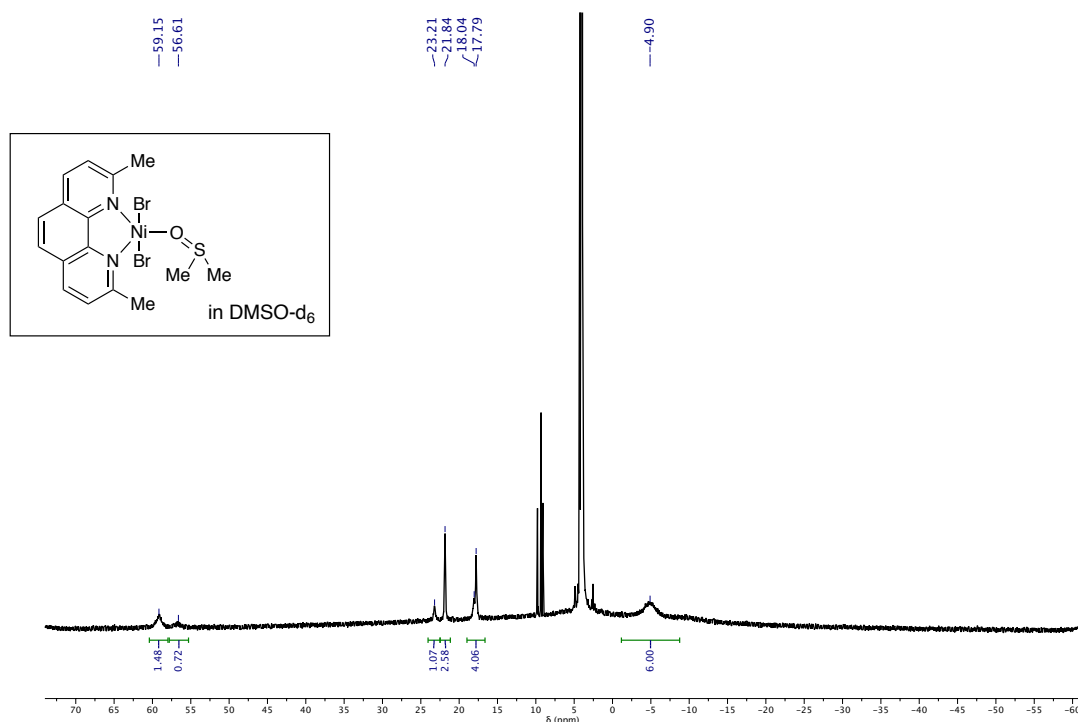
Figure S4.16. ^{1}H NMR (400 MHz, DMSO-d$_6$) of crystals of [NiBr$_2$(DMSO)(L1)]. Free L1 visible between 7.5–8.5 ppm.
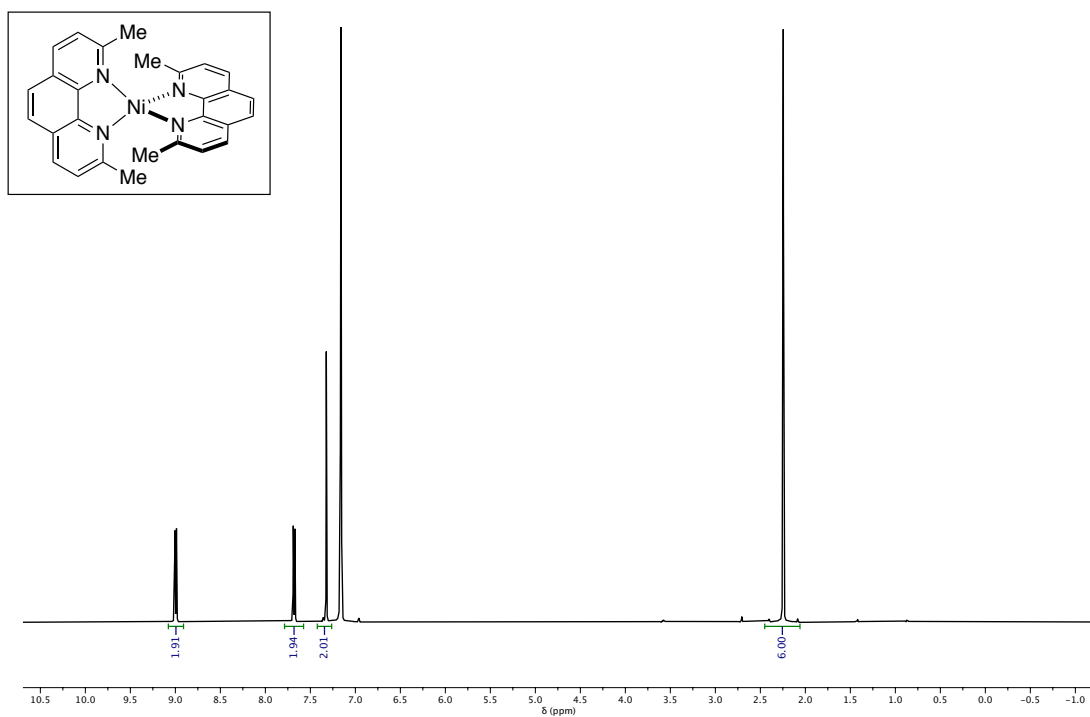
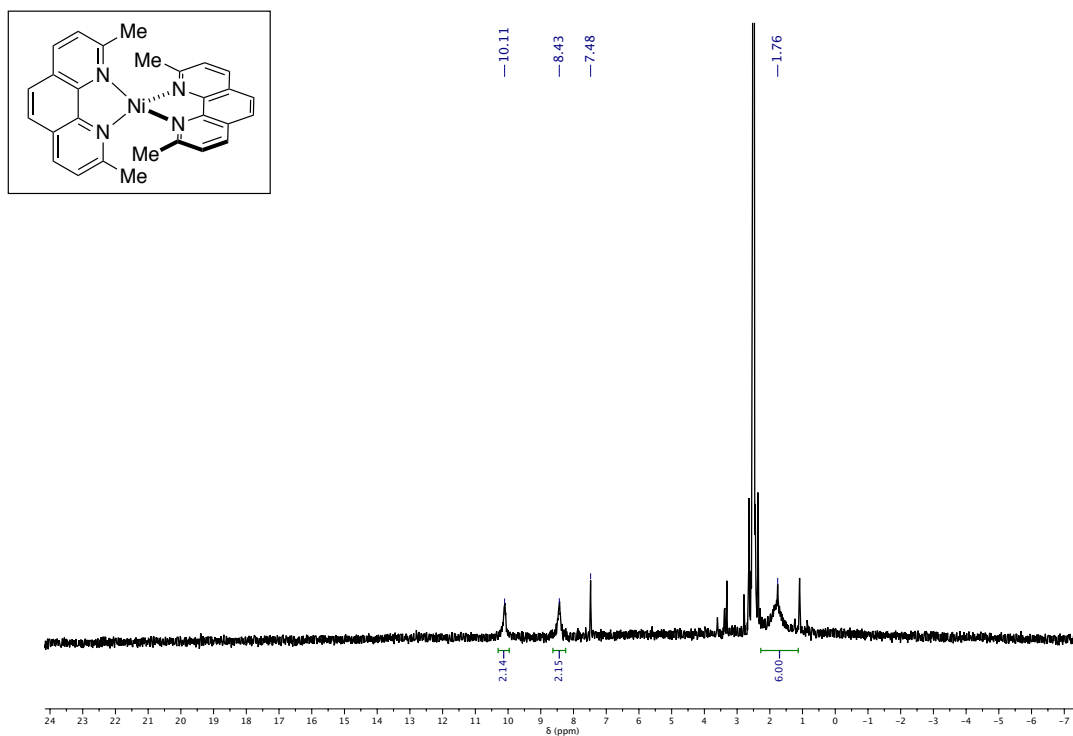**Figure S4.17.** ¹H NMR (400 MHz, C₆D₆) of [Ni(L1)₂].

Figure S4.18. ¹H NMR (500 MHz, DMSO-d₆) of [Ni(L1)₂].
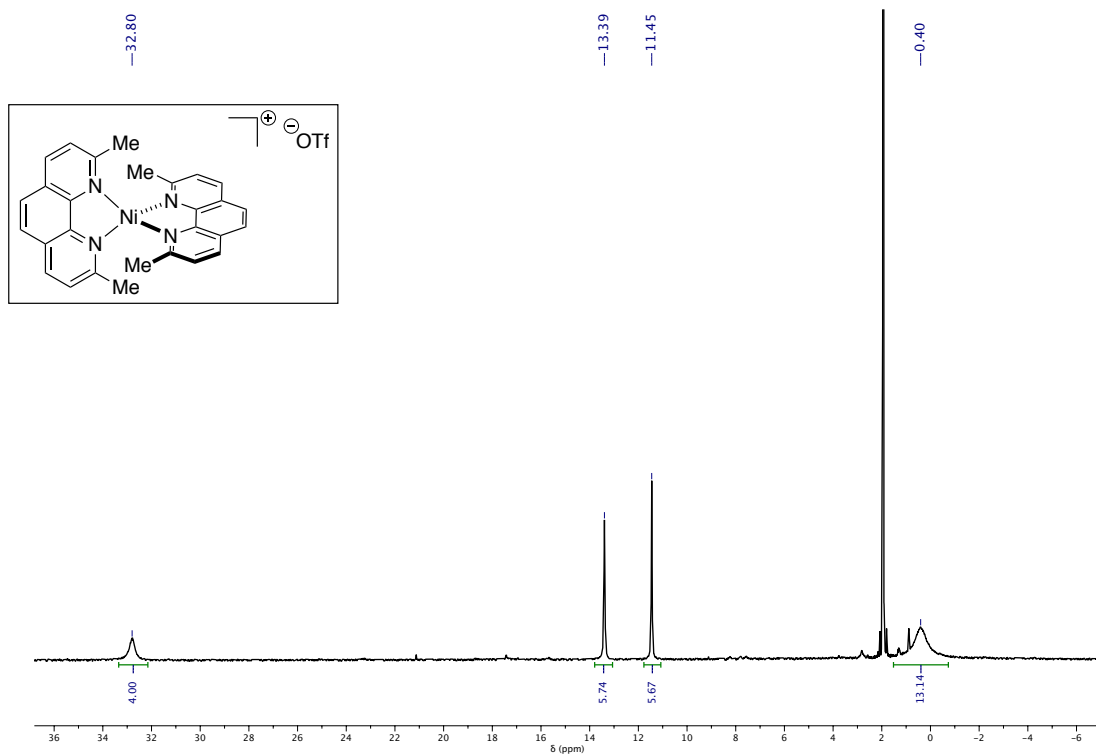
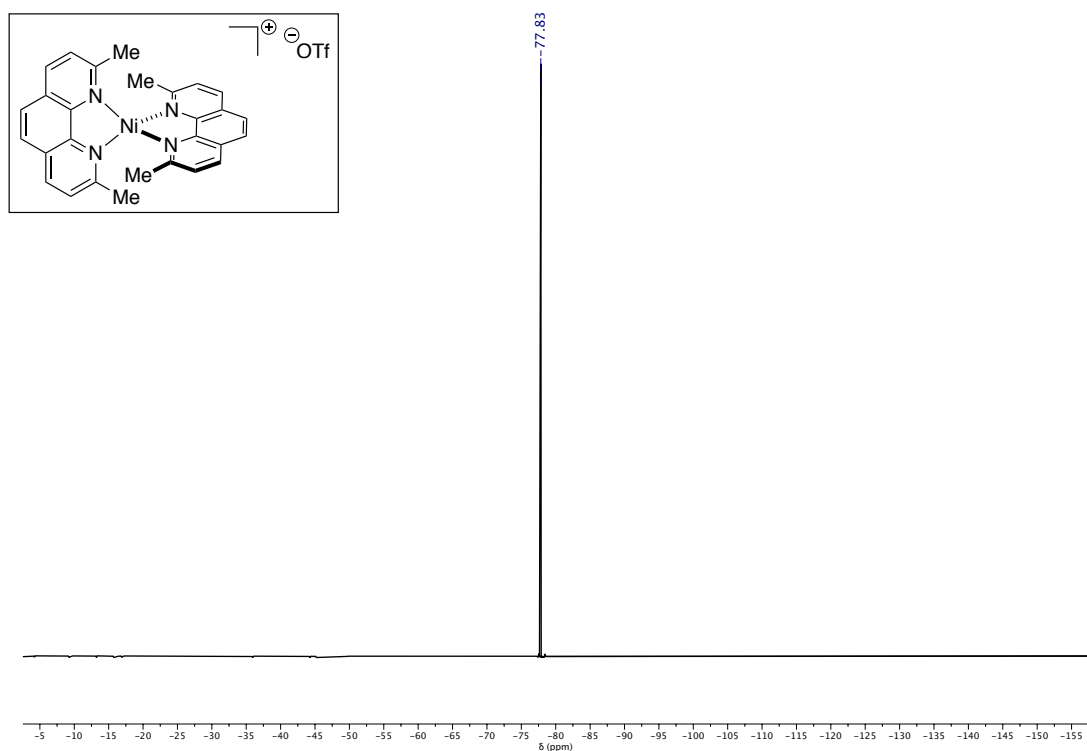**Figure S4.19.** ^{1}H NMR (500 MHz, CD$_3$CN) of 5-OTf.

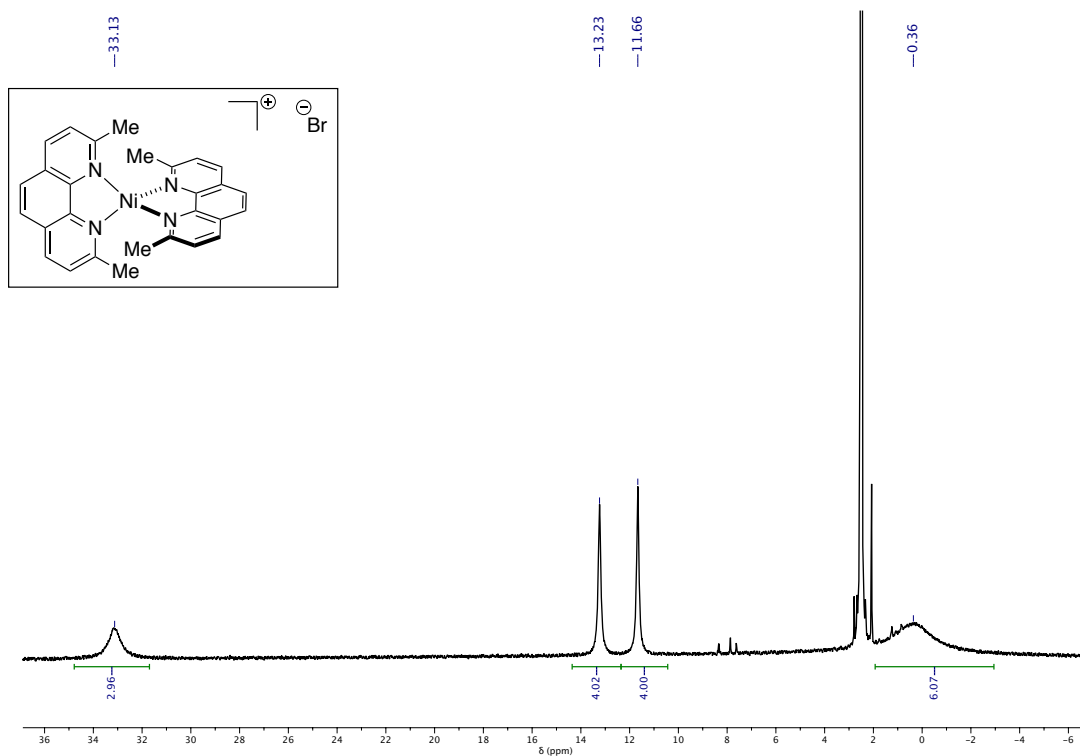**Figure S4.20.** ^{19}F NMR (376 MHz, DMSO-d$_6$) of 5-OTf.

Figure S4.21. ^{1}H NMR (400 MHz, DMSO-d_6) of 5-Br. Traces of L1 (ca. 8 ppm) and acetonitrile (1.94 ppm).

4.8.12. Crystallographic data

CCDC deposition numbers

[NiBr$_2$(DMSO)(**L1**)]: 1966485. [Ni(**L1**)$_2$]Br (**5-Br**): 1966486.

Table S4.3. Crystallographic data.

	[NiBr$_2$(DMSO)(L1)]	[Ni(L1)$_2$]Br (5-Br)
Formula	C$_{16}$H$_{18}$Br$_2$N$_2$NiOS	C$_{28}$H$_{24}$BrN$_4$Ni
Formula weight	504.91	555.13
T (K)	100(2)	100(2)
Wavelength (Å)	0.71073	0.71073
Crystal system	Triclinic	Orthorhombic
Space group	P-1	Pbca
***a* (Å)**	8.3790(7)	12.3683(6)
***b* (Å)**	9.2459(8)	11.2848(5)
***c* (Å)**	12.5657(10)	32.6128(13)
α (deg)	80.0558(19)	90
β (deg)	75.674(2)	90
γ (deg)	72.1841(17)	90
V (Å^3)	893.00(13)	4551.9(3)
Z	2	8
Density (calcd.) (Mg/cm^{-3})	1.878	1.620
μ (mm^{-1})	5.682	2.634
F(000)	500	2264
Crystal size (mm^3)	0.200 x 0.030 x 0.030	0.150 x 0.050 x 0.050
Theta range for data collection (deg)	2.327 to 34.959	2.498 to 32.210
Index ranges	-13<=h<=12, -14<=k<=14, -19<=l<=12	-18<=h<=18, -16<=k<=16, -48<=l<=48
Reflections collected	15108	101654
Independent reflections	6981 [R(int) = 0.0231]	7802 [R(int) = 0.1289]
Completeness to theta	89.1% (34.959°)	97.0% (32.210)
Absorption correction	Multi-scan	Multi-scan
Max. and min. transmission	0.74 and 0.57	1.00 and 0.70
Refinement method	Full-matrix least-squares on F^2	Full-matrix least-squares on F^2
Data/restraints/parameters	6981/0/212	7802/0/311
Goodness-of-fit on F^2	1.056	1.068
Final R indices [I>2sigma(I)]	R1 = 0.0238, wR2 = 0.0537	R1 = 0.0617, wR2 = 0.1337
R indices (all data)	R1 = 0.0323, wR2 = 0.0562	R1 = 0.1232, wR2 = 0.1561
Largest diff. peak and hole	0.701 and -0.489 e.Å^{-3}	1.796 and -0.859 e.Å^{-3}

Chapter 5.

General Conclusions

In conclusion, the studies summarised in this Doctoral Thesis provide mechanistic information about two major research lines in the Martin group: $C(sp^2)$–O functionalisation and reductive carboxylation.

In Chapter 2, the main goal of providing a mechanistic rationale for the $C(sp^2)$–O silylation of aryl esters was met. Furthermore, elusive $C(sp^2)$–OPiv oxidative addition complexes bearing a monodentate phosphine ligand were explored and an unusual dinickel complex was isolated and characterised. The role of the additive, which is often unclear during methodology development, was also investigated. Monitoring experiments and the isolation of fluoroborate by-products showed that fluoride was intercepting the Bpin⁻ fragment and preventing catalyst deactivation. No evidence was obtained for the previous mechanistic hypothesis where Cu played a role as a silyl transfer agent.

In Chapter 3, Ni(I)–alkyl complexes bearing substituted phenanthroline ligands were explored in the context of the reductive carboxylation of alkyl halides. The rather ambitious goal to synthesise and characterise a Ni(I)–alkyl complex from an inner-sphere Ni(I)–halide was achieved, allowing for insertion experiments with CO_2 and $^{13}CO_2$ to be carried out. Comparison of the IR and EPR data of the resulting carboxylate complexes, combined with DFT studies, supported the conclusion that CO_2 insertion at Ni(I)–alkyl complexes occurs and is very rapid. The Ni(I) complexes synthesised in this work will be key starting points for a variety of investigations into key intermediates in cross-electrophile coupling reactions.

In Chapter 4, the mechanism of the reductive carboxylation of arylsulfonium salts newly developed by the Yorimitsu group was probed. It was found that a cationic Ni(I) complex was likely a resting state of the catalyst and that C–S activation occurred at Ni(0). The formation of significant quantities of aryl–Zn species was also observed through quenching and stoichiometric experiments. This was the first time that evidence was obtained for the formation of such species from the Zn powder reductant rather than from $ZnEt_2$.

UNIVERSITAT
ROVIRA i VIRGILI